N° d'ordre : 3700

THESE

Présentée à

L'UNIVERSITE BORDEAUX I

Ecole Doctorale de Sciences et Environnements

Par M^elle^ **Delphine DENIS**

POUR OBTENIR LE GRADE DE

DOCTEUR

Spécialité : SEDIMENTOLOGIE MARINE et PALEOCLIMATS

Variabilité climatique Holocène dans la zone marginale des glaces en Antarctique de l'Est

---

Dirigée par : Xavier CROSTA et Jacques GIRAUDEAU

Soutenue le : 5 décembre 2008

Après avis de :

MASSON-DELMOTTE Valérie, DR CEA, LSCE	Rapporteur
BARCENA PERNIA Angeles, Maitre de Conférence, Université de Salamanque	Rapporteur

Devant la commission d'examen formée de :

MASSON-DELMOTTE Valérie, DR CEA, LSCE	Rapporteur
BARCENA PERNIA Angeles, Maitre de Conférence, Université de Salamanque	Rapporteur
ESCUTIA DOTTI Carlota, Professeur, Université de Grenade	Examinateur
CORREGE Thierry, Professeur, Université Bordeaux 1	Examinateur
GIRAUDEAU Jacques, DR CNRS, Université Bordeaux 1	Directeur de thèse
CROSTA Xavier, CR CNRS, Université Bordeaux 1	Directeur de thèse

~2008~

Remerciements

Bon ben, c'est presque la partie la plus dure à écrire quant on n'est pas très doué pour faire des jolies phrases. On ne peut pas tout dire en quelques mots mais j'espère avoir déjà exprimé à l'orale ma gratitude envers tout les gens que j'ai côtoyé à EPOC mais aussi pendant les congrès dans un anglais approximatif.

Tout d'abord mon grand chef : Xavier. Merci de m'avoir pris en M2 puis en thèse, en me faisant confiance malgré mes notes désastreuses. Merci d'avoir laissé mon côté « non-rigoureux» s'exprimer tout en redressant la barre quand il le fallait. Merci d'avoir toujours considéré le côté humain avant la Science. Merci de m'avoir envoyé et accompagner aux quatre coins du monde où j'ai pu essayer d'améliorer mon anglais et rencontrer plein de personnalité. Enfin, merci de m'avoir apporté tant au niveau scientifique que humain.

Ma deuxième chef « non-officielle » et collègue de salle blanche : Sabine. Merci à toi Sabine pour la cuisine des radio-isotopes qui m'a réconcilié avec la chimie. Merci pour les discussions animées en terrain « stérile » sur les modes de sédimentation qui régissent le bassin de Dumont D'Urville, sur la recherche, les plantes, la vie….prend bien soin de ton avocat !

Mon troisième chef et directeur de thèse officiel : Jacques. Je sais n'avoir pas trop « minaudé » dans ton bureau au cours de ces trois années mais à chaque fois cela a été efficace entre deux bougonnements. Merci de m'avoir éclairé sur le versant Nord de la planète Terre, de m'avoir dépanné en cigarette, et de m'avoir supporté et « drivé » à la fin quand je commençais à péter les boulons.

D. Denis, 2008

Merci à tous les tous les trois d'avoir su composé avec mon sens anarchique de l'organisation et avec mon perpétuel mais néanmoins utopique optimisme en matière de faisabilité temporelle des abstracts, articles, échantillonnage, comptage…..!!

Merci à Hans, Jenny, Anna, Amber, Raja, Damien et Amy, que j'ai connu grâce à Xavier dans les congrès et avec qui j'ai gardé contact au long de ces trois années. Vous avez eu la patience de parler avec moi ou lire mes emails dans mon « bad english » surtout au début, n'est-ce pas Jenny et Anna. Vous m'avez tous apporté : conseils/commentaires scientifiques, corrections d'anglais, encouragements et même des données participant ainsi aux articles de cette thèse. Merci.

Merci au membre du Jury d'être venu et d'avoir eu le courage de lire cette thèse, vous serez peut être les seuls à avoir tout lu! Merci pour les compliments ! Ca fait toujours plaisir surtout dans ce milieu où on ne sait pas trop ce qu'on vaut et ce que l'on peut apporter. Merci pour les remarques constructives dont j'ai essayé de tenir compte au maximum dans ce manuscrit corrigé.

Merci à l'équipe Paléo dans son ensemble, notamment à la sous-partie des compteurs pour les délires musicaux et les goûters gourmands, souvent colorés par les dernières destinations des congrès (Will, Maria, Cons, Jean-Louis, Aurélie, Filipa, Steph, Anne-Laure et Imen), à Isa et Karine pour leur aide et patience au Spectro avec mes échantillons cotonneux pas très réglementaires, à Olivier pour m'avoir appris à monter des lames, à Muriel et Marie Hélène pour leur bonne humeur, à Philippe, Jérôme, et Bruno pour leur gentillesse et leur disponibilité.

Merci à l'équipe Sédimento pour sa convivialité et ses fameux repas de Noël et d'été, notamment à Joël, Bernard, Gérard, Baxou, Seb, Pierrot, Eliane, Messieurs Castaing, Cremer et Jouanneau. Merci à Thierry de m'avoir accepté sur les camps de terrain Sédimento dans les Alpes, ca a été une vraie bouffée d'oxygène et une super expérience…..malgré les aoutas. J'ai presque approché ce que c'est de visualiser les « choses » en 3D.

Merci à l'équipe ECOBIOC, de m'avoir accueillie pendant quelques mois pour mes expérimentations foireuses sur la silice biogène…Merci à Jonathan et Aurélia de m'avoir sortie de ce mauvais pas !! Merci à Domi pour sa bonne humeur et son Pineau ….qui ont égaillé nos soirée thésards.

Un merci aussi à Jean-Michel et plus récemment à Hubert pour l'assistanat sur ordinateur qui est vraiment ma bête noire et pour les intéressantes conversations des pots.

Un grand Merci à tous les thésards, post-docs et autre plus ou moins récents recrutés que j'ai croisé pendant ma thèse et à ceux qui y sont encore. Car sans cet esprit soudé cette expérience ne serait pas aussi belle, alors dans le désordre : Elodie, Samuel, Hanna, Julien, Caro, Aurélia, Aurélie, Loïc, Marion, Emilie, Raphaël, Nico, Jonathan, Pierre, Filipa, Johan, Yannick, Anne-laure, Stéphanie, Elsa, Cédric, Manu, Vincent & Vincent, Tim, Bruno, Sylvain, Gwen, Patrice, Cons, Will et puis les jolie rencontres sur bordeaux : Maud, Aurélie, Hélène, Marine, Fred, Antoine, JC, Guillaume, Christina, Greg & Caro, …..

Enfin, merci à mes parents, de m'avoir permis de faire cette « incursion » dans le monde de la recherche grâce à laquelle j'ai appris des tas de choses dans des tas de domaines et notamment sur l'Antarctique dont je ne savais jamais s'il était au nord ou au sud avant de travailler avec Xavier …

delphine

Table des matières

Liste des Figures :

Liste des tables :

Liste des acronymes utilisés :

AA: Antarctic ou Antarctique
AABW: Antarctic Bottom Water
ACC: Antarctic Circumpolar Current
ACC: Antarctic Coastal Current
ACCbw: Antarctic Circumpolar Current bottom water
ACW: Antarctic Circumpolar Wave
AD: Antarctic Divergence
ADP: Antarctic Dipôle
ALBW: Adelie Land Bottom Water
AO: Antarctic Oscillation
AO: Arctic Oscillation
AP: Antarctic Peninsula
ASSW: Antarctic Summer Surface Water
BSi: Biogenic Silica
CB: Commonwealth Bay
CCSZ: Coastal and Continental Shelf Zone
CDW: Circumpolar Deep Water
CPDW: Circumpolar Deep Water
CRS: *Chaetoceros* resting spores
DDU: Dumont D'Urville
DDUT: Dumont D'Urville Trough
EA: East Antarctic
EAIS: East Antarctic Ice Sheet
EAM: East Antarctic Margin
ENSO: El Niño Southern Oscillation
EWD: East Wind Drift
Fc/Fk: *Fragilariopsis curta*/*Fragilariopsis kerguelensis* ratio
HBi: Highly Branched isoprenoids
HSSW: High Salinity Shelf Water
ITCZ: Inter Tropical Convergence Zone
LSSW: Low Salinity Shelf Water
MCDW: Modified Circumpolar Deep Water
MGT: Mertz Glacier Tongue
MIZ: Marginal Ice Zone
NADW: North Atlantic Deep Water
NAO: North Atlantic Oscillation
PB: Prydz Bay
PDO: Pacific Decadal Oscillation
PE: Productive Event
PF: Polar Front
POOZ: Permanent Open Ocean Zone
PP: Primary Production
PSA: Pacific South America Pattern
RS: Ross Sea
RSBW: Ross Sea Bottom Water
SACC: Southern Front of the Antarctic Circumpolar Current
SAF: Sub Antarctic Front
SAM: Southern Annual Mode
SAT: Surface Atmospheric Temperature
SBACC: Southern Boundary of the Antarctic Circumpolar Current
SIZ: Seasonal Ice Zone
SO: Southern Ocean
SST: Sea Surface Temperature
STF: Sub Tropical Front
THC: Thermohaline circulation
WS: Weddell Sea
WSBW: Weddell Sea Bottom Water
WW: Winter Water
XR: X Ray
XRF: X Ray Fluorescence

Introduction générale

Dans le contexte du réchauffement climatique global, la communauté scientifique emploie toutes ses compétences pour améliorer les modèles prédictifs afin que les populations puissent anticiper les résolutions à prendre en matières environnementales, sociales et économiques (IPCC, 2001). La prédiction du climat futur nécessite une compréhension intégrée de la machine climatique au travers de ses différents compartiments : lithosphère, cryosphère, atmosphère, océan, biosphère, et de leurs interconnections. Pour cela, il est nécessaire d'étudier la climatologie actuelle mais aussi passée à travers une approche couplée modèles-données dans toutes les régions de la Terre pour bâtir des prédictions réalistes et comprendre les processus climatiques.

Actuellement, la paléoclimatologie s'intéresse particulièrement à l'étude du Quaternaire récent (~2 millions d'années) qui présente une répartition des continents et une cyclicité glaciaire/interglaciaire semblable à aujourd'hui. Notamment, les périodes interglaciaires sont devenues rapidement un des champs d'investigation clé pour déchiffrer le climat futur de notre interglaciaire actuel : l'Holocène, qui a débuté il y a 11,7 mille ans. L'étude des périodes interglaciaires passées a mis en évidence d'importantes singularités quant à leur durée, leur climat moyen, la taille des calottes polaires, et la variabilité climatique intrinsèque à ces périodes. L'effort scientifique s'est donc resserré autour des périodes qui présentaient des forçages orbitaux proches de ceux de l'Holocène comme le stade isotopique marin (MIS) 11 (McManus et al., 2003).

L'Holocène a relativement été écarté de ces études du fait de sa courte durée et de son apparente stabilité climatique. Récemment, de nouvelles études suggèrent l'existence

d'une variabilité climatique rapide pendant l'Holocène (Mayewski et al., 2004 et références incluses), inscrivant notre interglaciaire comme un maillon essentiel dans la compréhension de notre climat. Ainsi, de nombreux programmes de recherche internationaux visent actuellement à la collecte d'enregistrements haute-résolution aptes à documenter la variabilité climatique d'ordre millénaire à décennale dans toutes les régions du globe.

Du fait de son éloignement et des conditions climatiques peu clémentes qui y règnent, l'Antarctique et l'Océan Austral qui l'encercle restent à ce jour encore peu étudiés et sont également les maillons « faibles » des modèles prédictifs. Ce continent est peu sensible actuellement au réchauffement climatique du fait de son éloignement, à l'exception de la région Ouest Antarctique qui est proche de l'Amérique du Sud (Steig et al., 2009). L'Antarctique est pourtant un acteur primordial de la machine climatique, intervenant, à l'échelle de l'Holocène, au sein de chacun des sous-systèmes climatiques : cryosphère, atmosphère, océan et biosphère, et entretenant des connections étroites avec les autres régions du globe via les circulations océanique et atmosphérique. Il joue aussi un rôle important sur l'albédo planétaire de part sa couverture englacée. A l'inverse, l'Océan Austral et son immense étendue de banquise hivernale sont particulièrement vulnérables à toute modification de température et des circulations océanique et atmosphérique. C'est pourquoi la communauté internationale a développé ces dernières années de nombreux groupes de recherche (SCAR: Scientific committee on Antarctic Research ; ACE: Antarctic Climate Evolution ; SASSI: Synoptic Antarctic Shelf-Slope Interactions parmi d'autres) qui visent à disséquer l'Antarctique et l'Océan Austral et leurs rôles dans la machine climatique globale.

Cette thèse s'inscrit au sein de ces thématiques de recherche au sein du programme TARDHOL (Tardi-Holocène, financé par l'INSU) et vise à documenter et à appréhender la variabilité climatique Holocène des marges continentales Est antarctiques dans la zone marginale des glaces. Pour cela, nous avons conduit une étude multi-traceurs et multi-échelles afin de documenter tous les compartiments climatiques (cryosphère, atmosphère, océan, biosphère marine) régissant le climat des hautes latitudes Sud et leurs connections respectives. Cette approche nous a permis d'avoir une vision intégrée du climat de l'environnement périantarctique que nous avons comparé avec les enregistrements sédimentaires et de glace voisins mais aussi avec ceux des autres régions du globe, notamment de l'Hémisphère Sud, pour appréhender la cohérence du climat Holocène en Antarctique et plus globalement dans l'hémisphère Sud.

Dans un **premier volet**, nous nous sommes attachés à expliquer les motivations scientifiques de ce travail par une synthèse bibliographique des connaissances actuelles sur le climat Holocène et sur la singularité du Continent et de l'Océan Antarctique. Ensuite, la mise en œuvre dans ce travail est détaillée au travers d'une description des particularités géographiques et climatiques des deux zones d'études et du matériel et des méthodes

utilisés. Ce chapitre 1 constitue un prélude au travail de recherche effectué qui permettra au lecteur de mieux situer la période, les lieux étudiés ainsi que les moyens utilisés dans ce manuscrit.

Dans un **deuxième volet**, nous sous sommes intéressés particulièrement aux compartiments glace-banquise-océan et leurs interconnections de l'échelle plurimillénaire à millénaire au large de la Terre Adélie. Le but était de documenter dans un même enregistrement sédimentaire ces trois compartiments pour voir s'ils réagissaient de manière synchrone ou non et d'identifier les forçages impliqués afin de déterminer si ces compartiments répondent à des changements climatiques locaux, régionaux ou globaux. Pour cela, nous nous somme attachés à bien contraindre les processus de dépôt qui régissent notre site de carottage pour dresser des paléo-reconstructions fiables, notamment à travers la caractérisation des apports latéraux. La comparaison avec des données de modélisation sur notre zone, et sur l'Antarctique en général, a permis de mieux appréhender les forçages responsables. Ce travail a fait l'objet d'une publication scientifique qui constitue le Chapitre 2 sous l'intitulé :

- **Holocene glacier and deep water dynamics, Adélie Land region, Est Antarctica.**

  Denis Delphine, Crosta Xavier, Schmidt Sabine, Carson Damien, Ganeshram Raja, Renssen Hans, Bout-Roumazeilles Viviane, Zaragosi Sebastien, Martin Bernard, Cremer Michel et Giraudeau Jacques.

  Sous-presse à *Quaternary Sciences Reviews*.

Dans un **troisième volet**, nous nous sommes attachés à comprendre les interactions et rétroactions climat-biosphère marine dans la zone marginale des glaces au large de la Terre Adélie et leurs implications dans les cycles biogéochimiques à l'échelle locale. Nous avons essayé de déterminer quels sont les facteurs contrôlant cette variabilité plurimillénaire à millénaire au travers des reconstructions des conditions de vent, d'upwelling, de températures et de banquise. Ces données ont été confrontées avec des données de modélisation pour comprendre la part des forçages externes et internes. Ce travail a fait l'objet d'un article scientifique qui constitue le Chapitre 3 sous l'intitulé :

- **Holocene productivity changes off Adélie Land (East Antarctica).**

  Denis Delphine, Crosta Xavier, Schmidt Sabine, Carson Damien S., Ganeshram Raja S., Renssen Hans, Crespin Julien, Ther Olivier, Billy Isabelle et Giraudeau Jacques.

  En révision à *Paleoceanography*.

Enfin dans un **quatrième volet**, nous avons essayé de comprendre la cohérence spatiale des variations des conditions de surfaces (vents, températures, banquise) en Antarctique de l'Est à travers la comparaison d'enregistrements marins de Terre Adélie et de Baie de Prydz. Ces données sont confrontées avec des données de modèles et à d'autres enregistrements paléoclimatiques des hautes aux basses latitudes Sud afin de documenter le couplage océan-atmosphère dans l'Hémisphère Sud de l'échelle plurimillénaire à millénaire. Ce travail a fait l'objet d'un article scientifique qui constitue le Chapitre 4 sous l'intitulé :

- **Antarctic sea ice and wind variability during the Holocene: Insight on low-high latitudes coupling.**

  Denis Delphine, Crosta Xavier, Barbara Loic, Massé Guillaume, Renssen Hans, Ther Olivier, Leventer Amy et Giraudeau Jacques.

  En préparation pour soumission à *Earth and Planetary Science Letters*.

Le travail effectué pendant cette thèse a contribué à d'autres publications sur des sujets voisins et/ou complémentaires:

- Un article qui s'attache à la variabilité interannuelle et qui constitue un préambule à l'utilisation des diatomées comme traceur des conditions océanographiques et climatiques dans cette région de la zone marginale des glaces (MIZ):

- **Denis D.**, Crosta X., Zaragosi S., Martin B., Mas V. 2006. Seasonal and sub-seasonal climate changes recorded in laminated diatom ooze sediments, Adélie Land, East Antarctica. *The Holocene* 16(8), 1143-1153. **Article complémentaire n°1**.

- Une publication sur les flux biogéniques et l'utilisation de certains proxies biogéochimiques sur le plateau continental au large de la Terre Adélie. Cette étude est un prélude au chapitre 3 et aidera le lecteur à comprendre les proxies utilisés dans ce chapitre (protocole, utilité et limitation):

- Carson D. S., **Denis D.**, Ganeshram R. S., Crosta X., Schmidt S. Reconstructing Paleoproductivity throughout the Holocene: A Case Study from Adélie Land, East Antarctica. Soumis à *Geochimica et Cosmochimica Acta*. **Article complémentaire n°2**.

- Trois publications, qui à l'aide de l'outil diatomée, permettent de reconstruire le couvert de banquise passé et d'identifier ses facteurs forçant à l'échelle régionale de la Terre Adélie. Ces papiers sont préliminaires au chapitre 4:

- Crosta X., Debret M., **Denis D.**, Courty M-A., Ther O. 2007. Holocene long- and short-term climate changes off Adélie Land, East Antarctica. *Geochemistry, Geophysics, Geosystems* 8Q11009, doi:10.1029/2007GC001718.

- Crosta X., **Denis D.**, Ther O. 2008. Sea ice seasonality during the Holocene, Adélie Land, East Antarctica. *Marine micropaleontology* 66, 222-232.

- Pike J., Crosta X., Maddison E. J., Stickley C. E., **Denis D.**, Barbara L., Leventer A., Renssen H. Observations on the relationship between the Antarctic coastal diatoms *Thalassiosira antarctica* Comber and *Porosira glacialis* (Grunow) Jørgensen and sea ice concentrations during the Late Quaternary. Accepté à *Marine Micropaleontology*. **Article complémentaire n°3**.

CHAPITRE 1

Motivations
&
Mise en œuvre

~ Partie 1 : Motivations ~

1. Le climat Holocène : Etat de l'art

L'Holocène est l'interglaciaire actuel qui a débuté il y a environ 11,7 mille ans calendaire avant l'année 1950 (e.g. 11,7 cal ka BP) (IPCC, 2007). Cette période climatique a d'abord été considérée comme stable comparativement à la dernière période glaciaire ou à d'autres interglaciaires (Figure 1).

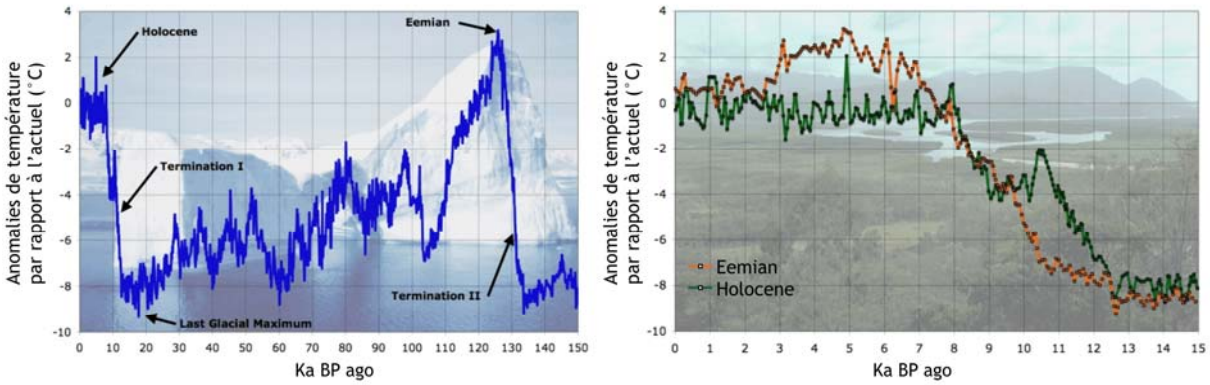

Figure 1. Anomalies de température par rapport à l'actuel estimées à partir des mesures de deutérium sur la carotte de glace de Vostok (Antarctique) : durant les derniers 150 ka BP (courbe bleue), les derniers 15 ka BP (courbe verte) et entre 121 et 136 ka BP (courbe orange), modifié d'après http://www.theoildrum.com/story/2006/. Source: NOAA.

Depuis les années 90, les enregistrements Holocène, issus des carottes de glaces, lacustres, continentales et marines à travers le globe ainsi que des travaux de modélisation numérique ont mis en évidence une variabilité climatique complexe à long et à court terme au travers:

- d'un léger et graduel refroidissement global avec un début d'Holocène ou un milieu d'Holocène plus chaud que le Tardi-Holocène (Masson et al., 2000 ; Hodell et al., 2001 ; Weber et Oerlemans, 2003; Solignac et al., 2004; Andersen et al., 2004 ; Nielsen et al., 2004).

- de variations millénaires à centennales plus ou moins cycliques des températures atmosphériques et océaniques dont les amplitudes peuvent atteindre 1 à 2°C (Bond et al., 1997; de Menocal et al., 2000; Bond et al., 2001; Mayewski et al., 2004; Nielsen et al., 2004; Masson-Delmotte et al., 2004).

1.1. Variabilité climatique plurimillénaire

1.1.1. Variations observées

Le refroidissement Holocène à long terme s'exprime aussi bien dans l'Hémisphère Nord que dans l'Hémisphère Sud. On distingue notamment trois périodes climatiques majeures :

Début de l'Holocène (~12 à 8-6 cal ka BP)

Cette période est appelée « Early Holocene » ou Hypsithermal 1. Située à la fin de la déglaciation du Dernier Maximum Glaciaire, elle correspond au retrait des calottes glaciaires (Lambeck et Chappell, 2001; Anderson et al., 2002; Leventer et al., 2006) et des glaciers continentaux (Grove, 2004; Solomina et al., 2008). Le « timing » et l'intensité du réchauffement postglaciaire sont observés de manières différentes selon les régions et seraient étroitement liés à la position géographique des régions étudiées par rapport aux inlandsis et glaciers (Davis et al., 2003 ; Kaufman et al., 2004; Renssen et al., 2005a) (Figure 2).

Selon la topographie et la climatologie d'une zone, le retrait des glaces va être plus ou moins rapide ce qui peut entraîner une persistance de conditions froides due à l'albédo local et aux circulations atmosphérique et océanique. Ainsi, les conditions chaudes du début de l'Holocène présentent une apparition, une durée et une amplitude différentes suivant les régions (Figure 2).

Milieu de l'Holocène (~ 8-6 à 4-2 cal ka BP)

Cette période est appelée « Mid-Holocene » ou Hypsithermal 2. Elle se distingue de la précédente par l'installation de conditions complètement postglaciaires, dues à la stabilisation des calottes de glace et des glaciers. Une transition climatique abrupte entre le début et le milieu de l'Holocène (EMHT : Early to Mid-Holocene Transition) a été enregistrée aux hautes latitudes Nord et Sud ainsi que dans la Zone Equatoriale (Stager et Mayewski, 1997; Stager et al., 2003) alors qu'elle apparaît plus graduelle aux moyennes latitudes (Davis et al., 2003) (Figure 2). Cette transition peut se caractériser par une augmentation ou une diminution des températures. En effet, l'Optimum climatique Holocène, e.g. la période enregistrant les plus hautes températures estivales de l'Holocène, est documentée soit en début (Petit et al., 1999; Stott et al., 2004; EPICA members, 2004) soit en milieu d'Holocène suivant les régions (Zhao et al., 1995; Davis et al., 2003) (Figure 2).

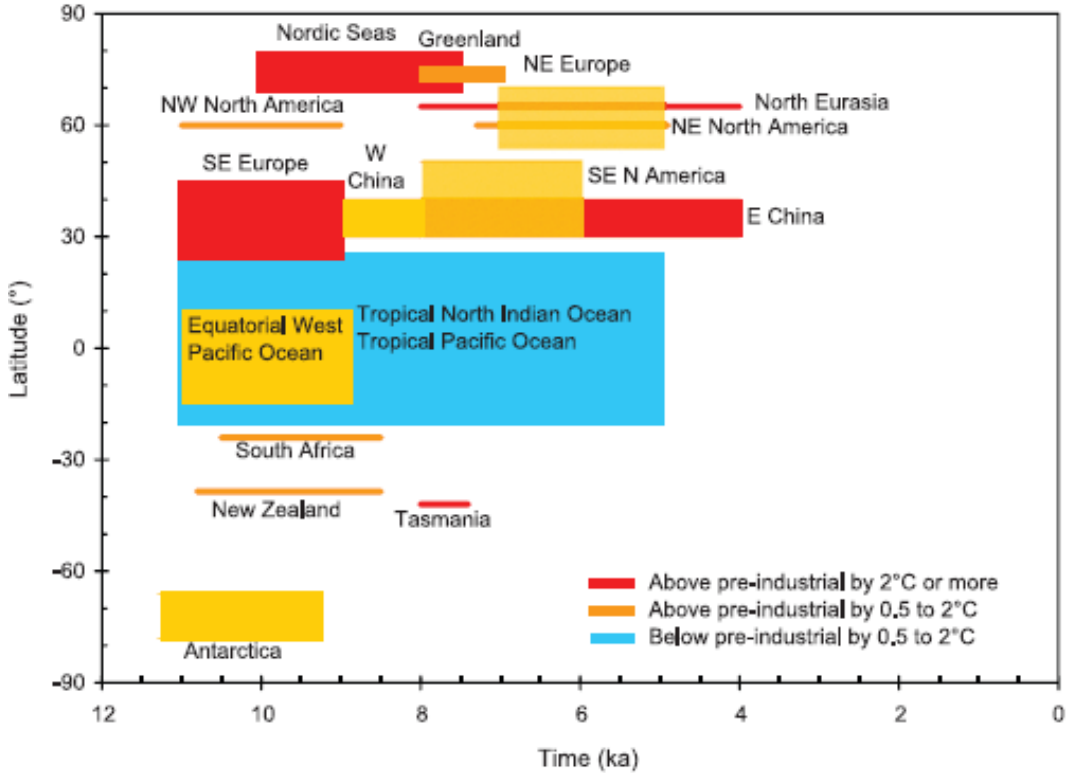

Figure 2. Périodes et intensités des maximas des anomalies de températures par rapport au niveau préindustriel, en fonction de la latitude (axe vertical) et du temps (axe horizontal, en milliers d'années) au cours de l'Holocène. Les températures supérieures de plus de 2°C, de 0.5°C à 2°C et inférieures de 0.5°C à 2°C par rapport au niveau préindustriel apparaissent en rouge, en orange et en bleu, respectivement. Les références des données sont: Mer de Barents (Duplessy et al., 2001), Groenland (Johnsen et al., 2001), Europe (Davis et al., 2003), Amérique du Nord-Est et du Nord-Ouest (MacDonald et al., 2000; Kaufman et al., 2004), Chine (He et al., 2004), océans tropicaux (Rimbu et al., 2004; Stott et al., 2004; Lorenz et al., 2006), Atlantique du Nord (Marchal et al., 2002; Kim et al., 2004), Tasmanie (Xia et al., 2001), Antarctique de l'Est (Masson et al., 2000), Afrique du Sud (Holmgren et al., 2003) et Nouvelle-Zélande (Williams et al., 2004). Source : IPCC, 2007.

Tardi-Holocène (depuis ~4-2 cal ka BP)

Cette période est appelée « Late Holocene Thermal Decline » ou Néoglaciaire. C'est généralement la période la plus froide de l'Holocène, environ 0.5°C de moins qu'à l'actuel. Elle est souvent associée à une ré-avancée des glaciers (Grove, 2004; Solomina et al., 2008) et du couvert de banquise aux deux pôles (Hodell et al., 2001; Nielsen et al., 2004; Crosta et al., 2008). La transition entre le milieu de l'Holocène et le Néoglaciaire peut être abrupte (Stott et al., 2004; Crosta et al., 2008) ou graduelle suivant les régions (Zhao et al., 1995; Petit et al., 1999; Alley, 2000; Hodell et al., 2004).

Ainsi, après un début d'Holocène particulier, influencé par la fonte massive des calottes polaires, la période Holocène expérimente un refroidissement à long terme des températures océaniques et atmosphériques qui culminent au Tardi-Holocène par la ré-avancée des systèmes glaciaires et de la banquise.

1.1.2. Facteurs forçants

Actuellement, les hypothèses invoquées pour expliquer ces tendances holocènes à long terme favoriseraient l'action conjuguée de facteurs externes : variations d'ensoleillement dues aux changements des paramètres orbitaux, et de facteurs internes: albédo et légères variations des concentrations atmosphériques en gaz à effet de serre (Crucifix et al., 2002 ; Renssen et al., 2005a, 2005b). Le premier facteur forçant est appelé « externe » car il est indépendant de la machine climatique terrestre tandis que le deuxième résulte d'effets rétroactifs au sein du système climatique terrestre qui peuvent amplifier ou contrebalancer les forçages externes.

1.1.2.1. Facteur externe : le soleil

Selon la théorie astronomique de Milankovitch (1941), les variations des paramètres orbitaux réguleraient le climat global à long terme, en modulant la quantité de chaleur reçue par la terre (excentricité), sa répartition spatiale (obliquité) et saisonnière (précession) (Figure 3). L'importance de ce forçage orbital est clairement illustré par la relation entre ces périodicités et les cycles glaciaires/interglaciaires de la planète Terre (Hays et al., 1976). Des analyses spectrales réalisées sur l'enregistrement marin du volume de glace (Imbrie et al., 1984) révèle que les cycles glaciaires/interglaciaires varient en fonction des trois périodicités majeures, correspondant aux perturbations orbitales associées à l'excentricité (100 ka), l'obliquité (41 ka) et aux deux cycles de précession identifiés à 23 et 19 ka (21 ka). Les datations radiométriques des massifs de coraux et des inversions magnétiques ont fournies des validations indépendantes de cette échelle de temps astronomique apportant des preuves irréfutables que le climat de la Terre et son orbite sont intimement lié.

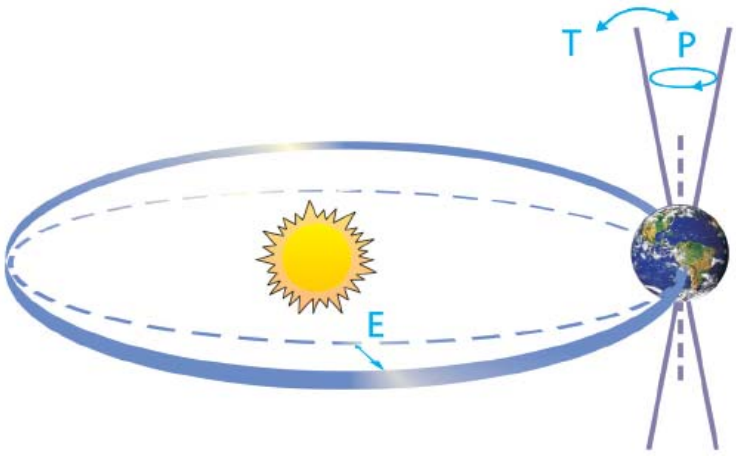

Figure 3. Schéma des changements orbitaux (cycles de Milankovitch) qui sont à l'origine des cycles glaciaires-interglaciaires sur Terre. ''E' figure les variations d'excentricité de l'orbite terrestre, T' montre les changements d'inclinaison de l'axe de rotation de la Terre, e.g. l'obliquité, et 'P' illustre la précession qui est une variation de la direction de l'axe de rotation en un point donné de l'orbite, d'après Rahmstorf et Schellnhuber (2006).

A l'échelle de l'Holocène, c'est majoritairement la précession (~21 ka) et l'obliquité (~41 ka) qui vont agir sur les variations d'ensoleillement reçue par la Terre. La précession des équinoxes est un paramètre orbital qui influe sur l'ensoleillement de chaque hémisphère et sur sa saisonnalité (Figure 4). Un indice de précession élevé (bas) conduit à des saisons très (peu) contrastées dans l'Hémisphère Sud avec un été « chaud » et un hiver « froid » et peu (très) contrastées dans l'Hémisphère Nord avec un été « froid » et un hiver « chaud » (Figure 4). L'obliquité, quant à elle, va surtout moduler l'ensoleillement annuel moyen et le gradient d'ensoleillement latitudinal influençant ainsi les échanges d'énergie entre les basses et les hautes latitudes (Figure 4). Un angle élevé (faible) d'obliquité expose plus (moins) directement les hautes latitudes et donc diminue (augmente) le gradient thermique entre les basses et les hautes latitudes (Figure 4).

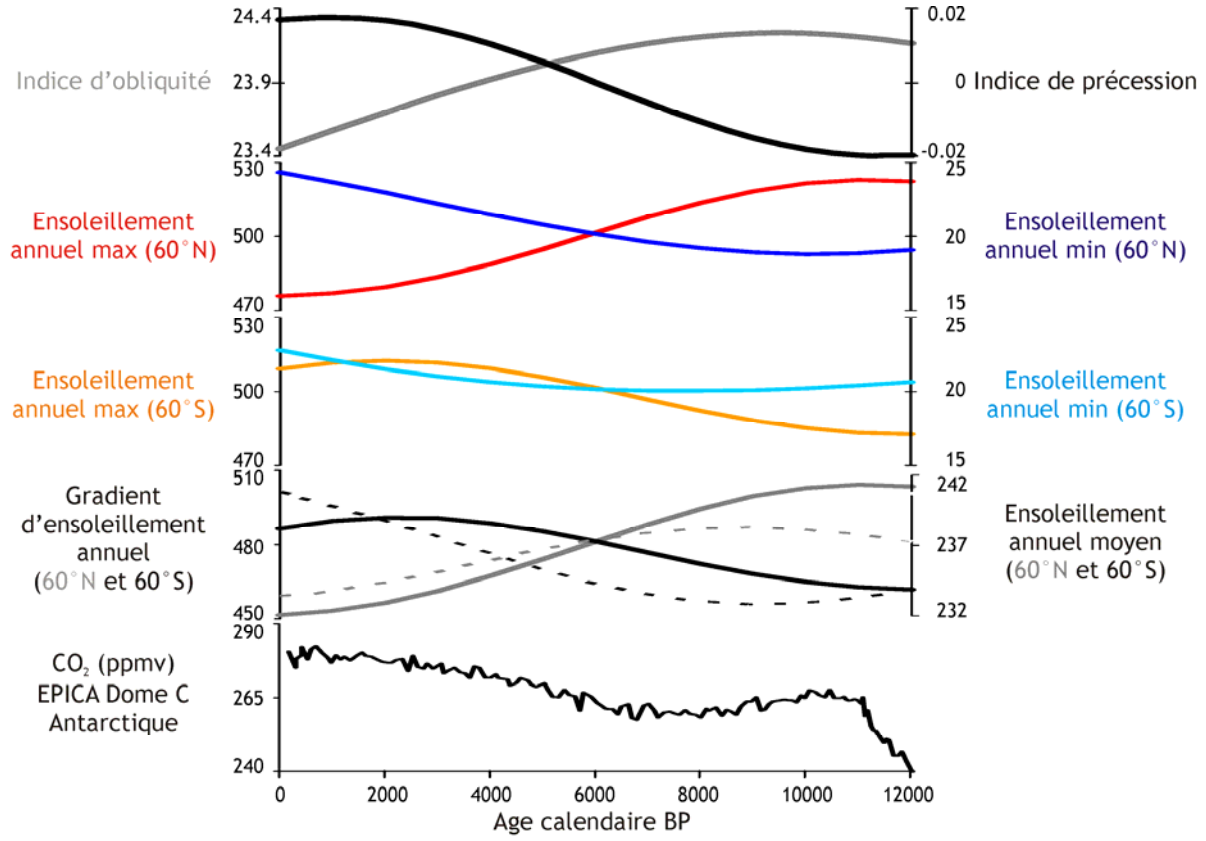

Figure 4. Evolution holocène de l'indice d'obliquité et de précession, de l'ensoleillement annuel maximum et minimum (watt/m²) à 60°N (pendant juin et décembre) et à 60°S (pendant décembre et juin), du gradient d'ensoleillement été-hiver (watt/m²) à 60°N et à 60°S, de l'ensoleillement moyen annuel (pointillé) à 60°N et à 60°S et des concentrations atmosphériques en CO_2 enregistrées à EPICA dôme C, Antarctique, d'après les données astronomiques de Berger et Loutre (1991) et les données de carotte de glace de Monnin et al. (2004).

Ainsi, l'augmentation de l'indice de précession au cours de l'Holocène induit une baisse progressive de l'ensoleillement d'été ainsi qu'une baisse de la saisonnalité dans l'Hémisphère Nord, en accord avec les données de modélisation qui montrent une chute progressive des températures estivales de 1 à 3°C dans aux hautes latitudes Nord (Renssen et al., 2005a). Cette baisse des températures, induite par la précession, serait

contrebalancée en partie (+ 0,5°C) par l'augmentation des concentrations en gaz à effet de serre (Crucifix et al., 2002 ; Renssen et al., 2005a).

Cependant, ce schéma ne peut s'appliquer à l'Hémisphère Sud où la précession devrait induire un réchauffement progressif (e.g. une augmentation de l'ensoleillement d'été) au cours de l'Holocène, en désaccord avec les données géologiques qui indiquent un refroidissement depuis l'Holocène moyen (Alley, 2000 ; Masson et al., 2000 ; Hodell et al., 2001 ; Nielsen et al., 2004 ; Crosta et al., 2008).

Plusieurs hypothèses majeures ont été proposées pour expliquer cet apparent paradoxe :

1) Un contrôle par l'ensoleillement de l'Hémisphère Nord dont les variations sont transportées à l'Hémisphère Sud par la circulation océanique (Hodell et al., 2001 ; Nielsen et al., 2004).

2) Un contrôle par l'obliquité qui surexpose la Zone Equatoriale par rapport aux hautes latitudes au cours de l'Holocène et renforce ainsi les gradients d'ensoleillement entre les hautes et les basses latitudes sud (Masson et al., 2000 ; Lamy et al., 2002 ; Jouzel et al., 2007).

3) Un contrôle par l'ensoleillement saisonnier local, au Sud de 60°S, dont les variations sont déphasées de quelques mois du fait de la grande inertie de l'Océan Austral (très peu de continents par rapport à l'Hémisphère Nord) et du stockage de chaleur en profondeur sous la pycnocline hivernale (Renssen et al., 2005b).

Cette dernière hypothèse implique des forçages identiques locaux aux deux hémisphères mais avec des rétroactions internes différentes du fait de la particularité de chaque Hémisphère.

1.1.2.2. Facteurs internes

La diminution (augmentation) de la saisonnalité au Nord (Sud) peut avoir d'importantes répercutions vis-à-vis des compartiments climatiques. En effet, la saisonnalité joue un rôle important dans la répartition saisonnière des températures, précipitations et pressions, ce qui a un impact majeur sur la dynamique des glaciers (Andrews, 1975), de la banquise (Crosta et al., 2008), sur la formation d'eau profonde (Schmittner, 2003), l'intensité des vents (Lamy et al., 2002) et la biomasse des producteurs primaires terrestres ou marins (Naughton et al., 2007 ; Leventer, 1992). Ainsi, les variations orbitales de la précession peuvent avoir un impact sur la dynamique interne du climat au niveau de ces différents systèmes, ce qui va moduler les effets directs de ces paramètres orbitaux sur la planète au niveau spatial et temporel. Notamment, les compartiments internes de la

machine climatique semblent avoir changé au cours de l'Holocène. On observe notamment des modifications :

- de la circulation océanique thermohaline (THC) qui semblerait diminuer aux hautes latitudes Nord (Oppo et al., 2003 ; Hillaire-Marcel et al., 2004) et augmenter aux hautes latitudes Sud (Sarnthein et al., 1994).

- de la circulation atmosphérique à travers une migration de la zone de convergence intertropicale vers le Sud (ITCZ) (Haug et al., 2001), une augmentation de la force des vents (Haug et al., 2001), une augmentation de la fréquence des tempêtes (Noren et al., 2002), une prépondérance des évènements El Niño sur les évènements La Niña (Rodbell et al., 1999 ; Moy et al., 2002) et une diminution progressive du régime des moussons asiatiques (Wang et al., 2005; Selvaraj et al., 2007) et indiennes (Fleitmann et al., 2003 ; Gupta et al., 2005).

- de la couverture de banquise qui diminue ou augmente aux hautes latitudes Nord après 7-6 ka BP en Mer de Chukchi (de Vernal et al., 2005) et dans l'archipel central canadien (Vare et al., 2009), respectivement, et augmente aux hautes latitudes Sud après 5-4 cal ka BP (Crosta et al., 2008).

- de la biosphère continentale avec une diminution de 7 à 1 cal ka BP de la biomasse terrestre (Blunier et al., 1995 ; Hoelzmann et al., 1998 ; Indermühle et al., 1999).

Ces ajustements des sous-systèmes climatiques internes amplifient ou diffèrent les réponses de chaque région du globe aux changements orbitaux, entraînant les disparités spatio-temporelles documentées dans les études paléoclimatologiques (Figure 2).

1.2. Variabilité climatique millénaire à décennale

1.2.1. Variations observées

Surimposée à ce refroidissement à long terme de l'Holocène, une variabilité climatique millénaire à sub-millénaire a été mise en évidence à travers le globe grâce à de multiples enregistrements climatiques (températures atmosphérique et océanique, précipitations, avancées et reculs de glaciers, productivité marine et terrestre, changements des niveaux lacustres suggérant des variations du rapport évaporation /précipitation, régime des vents) (Mayewski et al., 2004 et références incluses) (Figure 5, bande verte). Le synchronisme et la cohérence de ces évènements climatiques rapides à travers le monde restent cependant discutés.

D'autres événements majeurs de la variabilité climatique millénaire ont été mis en évidence, mais leur extension spatiale est encore à l'étude. Notamment, plusieurs évènements froids semblent ponctuer le début de l'Holocène dans l'Hémisphère Nord à 11,25 cal ka BP (Björck et al., 1996 ; Muscheler et al., 2000), à 10,3 cal ka BP (Muscheler et al., 2000 ; Björck et al., 2001), à 9,2 cal ka BP (Fleitmann et al., 2008) et à 8,2 cal ka BP (Alley et Ágústsdóttir, 2005). Ces évènements froids sont souvent attribués à des débâcles d'icebergs et/ou d'eaux douces, dues à la vidange de lacs pro-glaciaires, qui peuvent stopper ou ralentir la THC (Sarnthein et al., 1994 ; Schroder-Ritzrau et al., 2003 ; Alley et Ágústsdóttir, 2005 ; Stouffer et al., 2007). Des évènements froids ont aussi été répertoriés aux hautes et moyennes latitudes Sud à 10,5-10,3 cal ka BP (Masson et al., 2000 ; Nielsen et al., 2004), à 9,3 cal ka BP (Masson et al., 2000 ; Nielsen et al., 2004) et à 8 cal ka BP (Masson et al., 2000 ; Van Beek et al., 2002 ; Bianchi et Gersonde, 2004 ; Crosta et al., 2005) mais leurs causes restent inconnues.

Le Tardi-Holocène affiche une variabilité millénaire à sub-millénaire prononcée. La Période Chaude Médiévale (WMP) et le Petit Age Glaciaire (LIA), pour les évènements les plus connus, sont documentés en Europe aux alentours de 1,2-0,7 et 0,6-0,1 cal ka BP, respectivement (Mann et Jones, 2003 ; Moberg et al., 2005). Certains enregistrements suggèrent même leurs occurrences plus largement dans l'Hémisphère Nord (Keigwin, 1996 ; Cobb et al., 2003) et en Antarctique (Leventer et al., 1993 ; Mann et Jones, 2003 ; Goosse et al., 2004).

Figure 5. Compilation de séries paléo-climatiques illustrant les changements Holocène de certains facteur forcants, des avancées de glacier à travers le monde et de la circulation atmosphérique des hautes latitudes Nord, d'après Mayewski et al. (2004). Les bandes vertes représentent l'intervalle de temps où des événements climatiques rapides sont observés par rapport à l'échelle de temps de GISP2 (Arctique). (a) Courbe gaussienne (lissée sue 200 ans) de la concentration en ion Na+ (ppb) enregistré à GISP2 comme proxy de l' « Icelandic Low » (Mayewski et al., 1997; Meeker et Mayewski, 2002). (b) Courbe gaussienne (lissée sue 200 ans) de la concentration en ion K+ (ppb) enregistré à GISP2 comme proxy de l' «Siberian High» (Mayewski et al., 1997; Meeker et Mayewski, 2002). (c) Episodes d'avancée de glaciers en Europe, dans le Nord des Etats-Unis et dans l'Hémisphère Sud (Denton et Karlèn, 1973), et dans l'Amérique centrale (Haug et al., 2001). (d) Episodes au cours desquels les glaciers suisses étaient plus restreint qu'aujourd'hui (Hormes et al., 2001). (e) Evénement de vidange des eaux douces du lac pro-glaciaire Agassiz (Barber et al., 1999). (f) Valeur d'ensoleillement d'Hiver (W/m^2) à 60°N (ligne noire) à 60°S (ligne bleue) (Berger et Loutre, 1991). (g) Valeur d'ensoleillement d'été (W/ m^2) à 60°N (ligne noire) à 60°S (ligne bleue) (Berger et Loutre, 1991). (h) $\delta^{14}C$ résiduel (Stuiver et al., 1998): données brutes (ligne fine) et courbe gaussienne moyennée sur 200 ans (ligne en gras). (i) Concentrations en ^{10}Be dans la carotte de glace GISP2 (10^3 atoms/g^1) (Finkel et Nishizumi, 1997). (j) Concentrations atmosphériques en CH_4 (ppbv) dans la carotte de glace GRIP au Groenland, (Chappellaz et al., 1993). (k) Concentrations atmosphériques en CO_2 (ppmv) dans la carotte de glace de Taylor Dome en Antarctique (Indermühle et al., 1999). (l) $SO4^{2-}$ résiduel (ppb) da la carotte de glace GISP2 au Groenland (Zielinski et al., 1996).

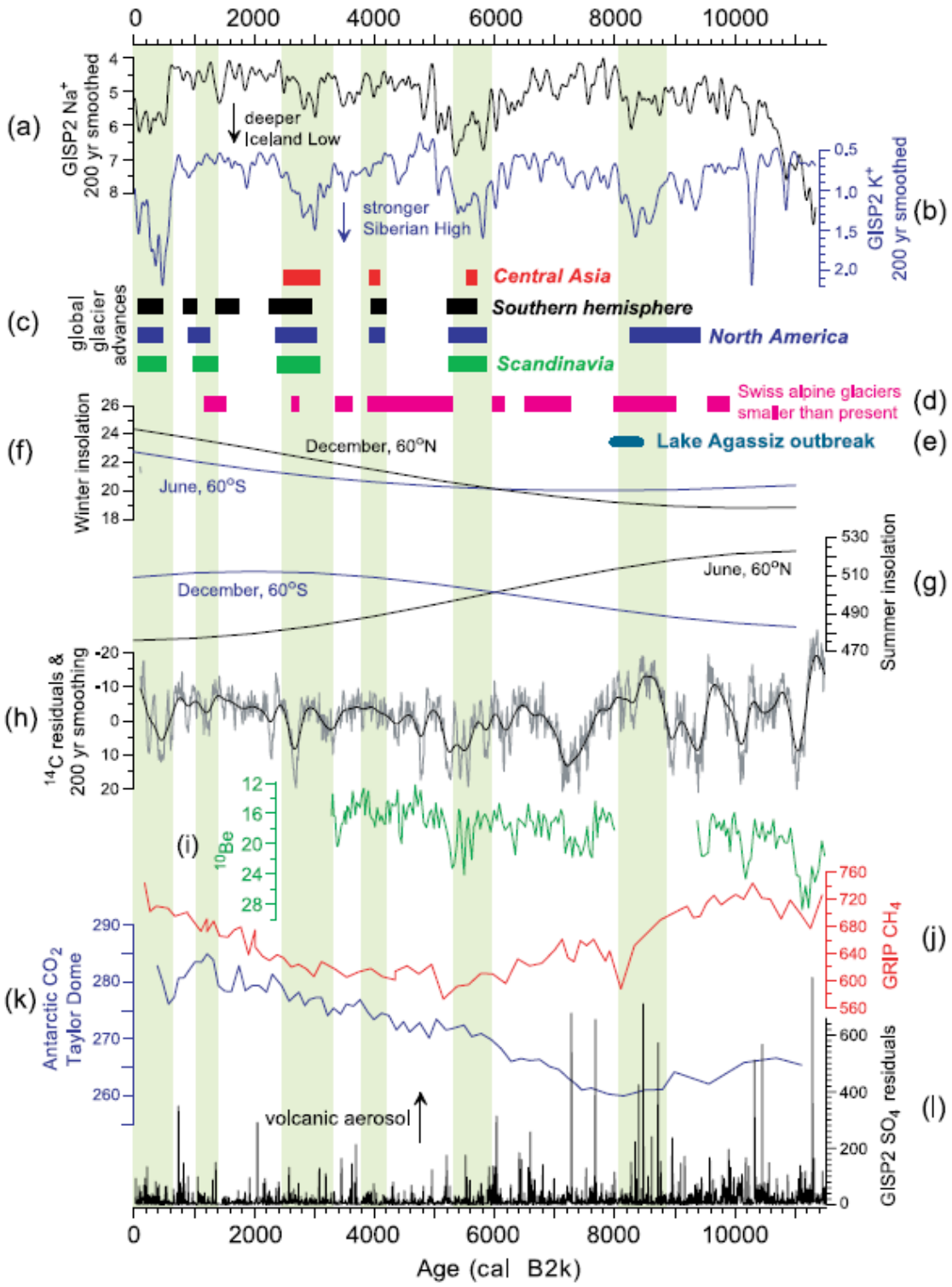

D'autres études montrent localement ou régionalement des variations climatiques récurrentes avec des cyclicités qui varient de l'échelle millénaire à centennale. Par exemple, la THC afficherait une variabilité millénaire plus ou moins cyclique après des variations apériodiques au début de l'Holocène (Broecker, 2000 ; Keigwin et Boyle, 2000 ; Bianchi et McCave, 1999 ; Oppo et al., 2003 ; Marchitto et de Menocal, 2003 ; Weber et al., 2004 ; McManus et al., 2004 ; Stouffer et al., 2007 ; Debret et al., 2007).

L'atmosphère présenterait elle aussi des variations cycliques centennales (Delmonte et al., 2005 ; Lamy et al., 2001 ; Mayr et al., 2007). Des cyclicités du même ordre ont été mises en évidence dans les sédiment marins et impliqueraient des changements océaniques et atmosphériques couplés (Leventer et al., 1996 ; Pike et Kemp, 1997 ; Brachfeld et al., 2002). A l'échelle décennale, les évènements récurrents de type ENSO, Oscillation Nord-Atlantique (NAO), oscillation Arctique (AO), Oscillation Décennale du Pacifique (PDO), Mode Annulaire Austral (SAM), et le Dipôle Antarctique (ADP), dont les périodicités actuelles varient de 3 à 10 ans, se traduisent par un couplage étroit entre l'océan et l'atmosphère (Shiotani et al., 1990 ; White et Peterson, 1996 ; Hurrell et van Loon, 1997 ; Thompson et Wallace, 1998, 2000 ; Rodbell et al., 1999 ; Biondi et al., 2001 ; Silvestri et Vera, 2003 ; Yuan, 2004 ; Yuan et Li, 2008, voir section 2.2.1). Ces périodicités actuelles ont néanmoins pu varier dans le passé.

1.2.2. Facteurs forçants

Les facteurs forçant de la variabilité climatique à court terme sont encore sujets à de nombreux débats. Cependant, il se pourrait que la variabilité climatique rapide résulte de la conjonction de facteurs externes et internes de la machine climatique terrestre (Bond et al., 1997; Bond et al., 2001; van Geel et al., 1999; Mayewski et al., 2004; Debret et al., en révision). Les facteurs prépondérants de la variabilité sub-millénaire à l'Holocène seraient ainsi l'activité solaire, le volcanisme, l'océan et l'atmosphère (Figure 5). La contribution de chacun a vraisemblablement varié au cours de l'Holocène (Debret et al., en révision) (Figure 6).

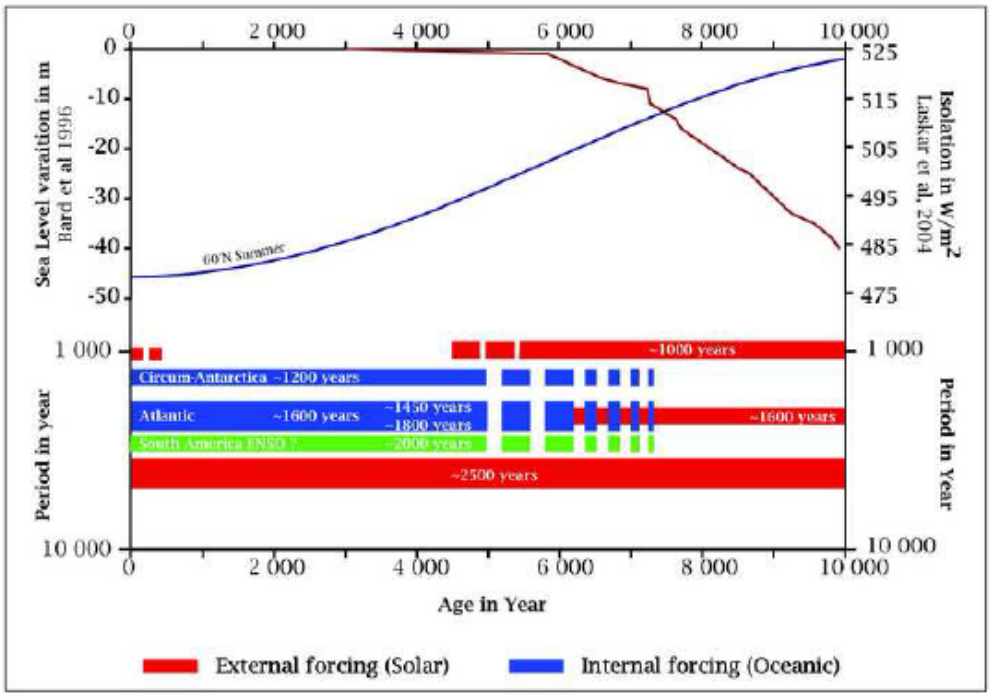

Figure 6. Synthèse des différentes périodes enregistrées au cours de l'Holocène d'après la compilation de plusieurs enregistrements climatiques à travers le globe, d'après Debret et al. (en révision). Il est possible de distinguer les facteurs internes et externes et d'identifier une transition forte entre ces deux types de forçages vers 5 cal ka BP. Les périodes détectées sont basées sur les périodicités identifiées des enregistrements.

1.2.2.1. Facteur externe : l'activité solaire

Le soleil est une étoile qui affiche des variations d'activité allant des échelles temporelles inférieures à la minute à des millions d'années. Parmi ce panel temporel, plusieurs périodes ont été clairement identifiées à 11, 22, 88, 105, 131, 208, 232, 385, 504, 805, 1000, 1450, 1600, 2000, 2241 et 2600 ans pour les plus courtes (qui intéressent l'échelle Holocène) à partir d'observations astronomiques ou de données de ^{14}C et ^{10}Be issus des carottes de glace, des cernes d'arbres et des coraux (Schwabe, 1844 ; Sonett et Suess, 1984 ; Damon et Sonett, 1991 ; Stuiver et Braziunas, 1993 ; Mayewski et al., 1997; Risebrobakken et al., 2003 ; Solanki et al., 2004 ; Vonmoos et al., 2006 ; Muscheler et al., 2004, 2007).

Ces variations du rayonnement émis par le soleil peuvent avoir plusieurs impacts sur le climat. Par exemple, une augmentation de l'activité solaire (maxima solaire) peut entraîner (Figure 7), par effet direct, l'augmentation du rayonnement solaire qui se traduit par une augmentation de l'énergie reçue à la surface de l'atmosphère. Cependant, ces variations sont actuellement encore mal-quantifiées et leurs conséquences en terme de bilan radiatif très débattues (IPCC, 2007). Ainsi, les variations d'activité solaire entre le « Maunder Minimum » et aujourd'hui auraient entraîné une augmentation de l'énergie reçue de moins de 0.68 Watt/m² (IPCC, 2007).

Cette variation directe du rayonnement solaire peut expliquer l'initiation d'un changement climatique, mais elle est souvent trop faible pour expliquer les amplitudes des changements climatiques observés (van Geel et al., 1999 ; Rind, 2002). Malgré cela, de nombreuses études ont montré une claire correspondance à différentes échelles de temps entre :

- les variations d'activité solaire et certains changements climatiques (Muscheler et al., 2000 ; Bond et al., 2001 ; Dergachev et al., 2007).

- les périodicités solaires et certaines cyclicités enregistrées dans les carottes de glace et sédimentaires (van Geel et al., 1999 ; Beer et al., 2000 ; Crosta et al., 2007 ; Debret et al., en révision).

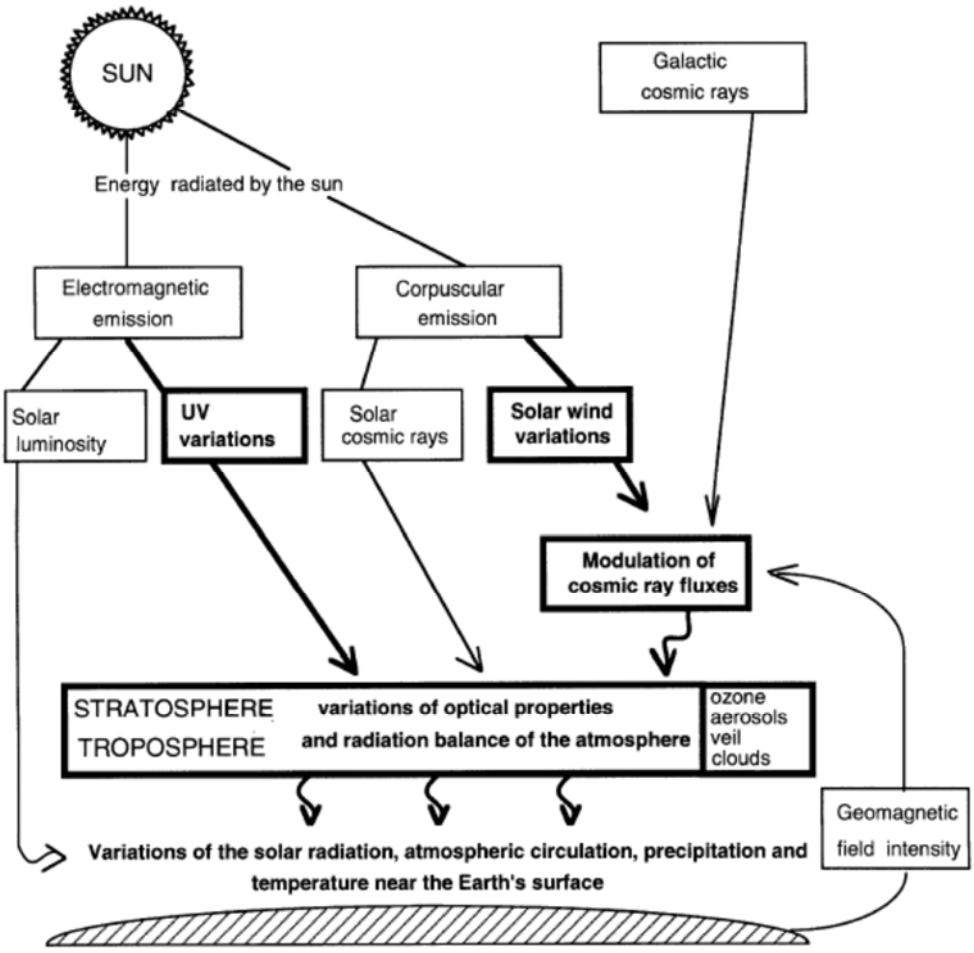

Figure 7. Schéma expliquant les différents facteurs solaires et cosmiques qui affectent le climat de la Terre d'après Van Geel (1999).

Plusieurs effets indirects pourraient moduler l'impact de la variabilité solaire à travers des réactions en chaîne au sein de la machine climatique terrestre. Les maxima solaires provoqueraient (Figure 7):

- une augmentation de l'absorption du rayonnement Ultra Violet (UV), qui transporte une grande partie de l'énergie solaire, par l'O_3 stratosphérique entraînant un réchauffement de la stratosphère et de la troposphère, un renforcement des vents stratosphériques et un déplacement vers les pôles des ceintures de vents troposphériques, et donc des tempêtes et de la chaleur associée (van Geel et Renssen, 1998 ; Shindell et al., 2001).

- une augmentation des vents solaires qui éparpillent les rayons cosmiques et limitent la pénétration des grains cosmiques dans l'atmosphère terrestre. Ces grains servent de noyaux de condensation et donc initient la formation de nuages (Marsh et Svensmark, 2000). La diminution de grains cosmiques entraînerait une baisse de la nébulosité et des aérosols, et donc une augmentation des températures grâce à une plus grande transparence atmosphérique (Raspopov et al., 1998).

Cependant, la relation « soleil actif = peu de nuages et augmentation des températures » et « soleil calme = beaucoup de nuages et diminution des températures » n'est pas aussi simple (Laut, 2003) et les impacts physiques et climatiques de l'activité solaire restent à l'étude. Les variations de l'activité solaire, au travers de ces effets directs et indirects, engendreraient des modifications des températures, précipitations et vents qui affecteraient à leur tour la circulation atmosphérique (régimes de mousson, ENSO…), la THC et la cryosphère à ces différentes échelles de temps (Cubasch et al., 1997 ; Weber et al., 2004 ; Crosta et al., 2007 ; Dergachev et al., 2007).

1.2.2.2. Facteurs internes : océan et atmosphère

Ici, nous développerons deux des facteurs internes impliqués dans la variabilité climatique sub-millénaire naturelle de l'Holocène à savoir l'océan et l'atmosphère car ils seront ensuite abordés dans le cadre de cette étude. Ils en existent d'autres, tout aussi importants, tels que le volcanisme, la végétation et les feux. Ces derniers ont par contre une portée plus régionale. Les données géologiques Holocène et les modèles numériques montrent des oscillations internes des compartiments climatiques océanique et atmosphérique, de l'échelle millénaire à pluriannuelle. Ces oscillations peuvent être initiées/modulées par des forçages externes (paramètres orbitaux et la variabilité solaire) ou peuvent être « auto-entretenus » sans l'aide d'un forçage extérieur. Leur initiation et persistance restent cependant mystérieuses, même si certaines études indiquent qu'elles pourraient résulter de phénomènes de résonance entre ondes internes (Rossby, 1939 ; Gammaitoni et al., 1998).

Océan

De nombreux auteurs ont suggéré des oscillations de la circulation océanique, initiées dans les deux zones polaires. Ces oscillations ont été documentées à l'échelle millénaire et séculaire avec des périodicités autour de 1500-1000 et 400-300 ans, respectivement. Les oscillations, largement documentées pendant les périodes glaciaires dans l'Hémisphère Nord avec une cyclicité de l'ordre de 1500 ans (Dansgaard Oeschger), seraient aussi présentes pendant l'Holocène mais avec des impacts climatiques de plus faibles amplitudes du fait de calottes polaires réduites (Rahmstorf, 2002).

Gammaitoni et al. (1998), puis Alley et al. (2001), ont suggéré l'existence d'une résonance stochastique qui pourrait engendrer ces périodicités de 1500 ans, initiées dans l'Hémisphère Nord et transmises à l'Hémisphère Sud par la THC. La THC est liée à l'entrée des eaux chaudes et salées de la Dérive Nord-Atlantique dans l'Atlantique Nord où elles subissent un refroidissement hivernal, et donc une augmentation de densité qui provoque leur plongée (Figure 8).

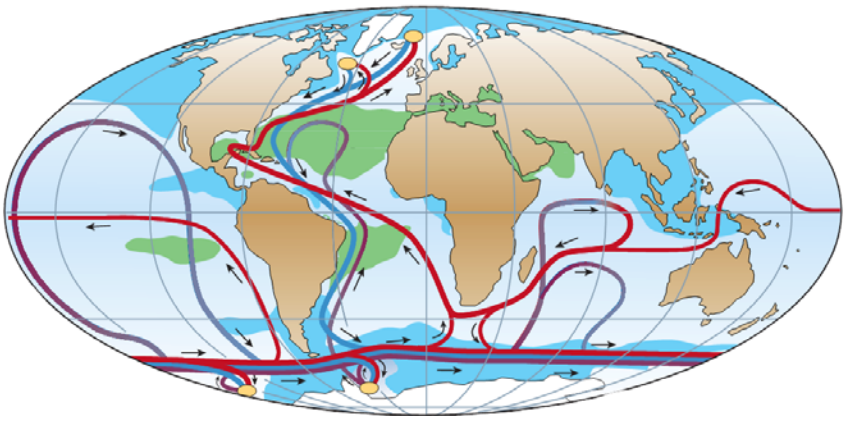

Figure 8. Schéma simplifié de la circulation thermohaline d'après Rahmstorf (2002) (modifié d'après Broecker). Les courants de surface, profonds et de fond sont représentés par les lignes rouges, bleues et violettes, respectivement. Les ronds jaunes symbolisent les sites majeurs dans la formation d'eaux de fonds tandis que les zones bleues et vertes représentent les salinités inférieures à 34 et supérieures à 36.

D'autres auteurs ont évoqué des anomalies de densité initiées dans l'Océan Austral suivant des cycles de 320-360 ans (Pierce et al., 1995; Drijfhout et al., 1996, Osborn, 1997). Cette théorie, appelée le « Southern Ocean Flip Flop », se base sur l'évolution du gradient de densité entre la couche de surface/sub-surface et la couche profonde de l'océan (Figure 9). Cette évolution cyclique résulte (1) du temps nécessaire à la chaleur stockée dans l'océan profond et apportée par la CPDW pour réduire, puis inverser, le gradient de densité entre la couche de surface et la couche profonde (Figure 9, boîtes 1-2-3), et (2) du temps nécessaire à la THC australe pour refroidir l'océan profond et restaurer le gradient de densité (boîtes 2-3-4).

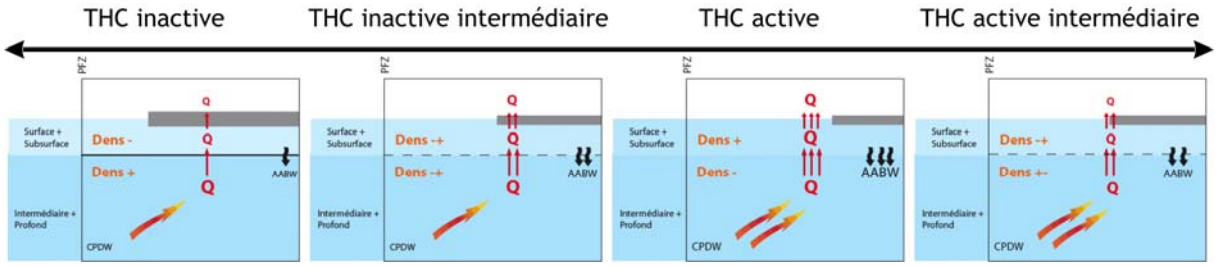

Figure 9. Schéma illustrant le passage d'une THC inactive à une THC active (Pierce et al., 1995; Drijfhout et al., 1996, Osborn, 1997), d'après X. Crosta. PFZ: Polar Frontal Zone, CPDW : CircumPolar Deep Water, AABW : Antarctic Bottom Water, Q : chaleur, Dens : densité.

Ces cycles de 320-360 ans semblent s'auto-amplifier sur un cycle de 1020-1100 ans au cours duquel la perturbation initiée dans l'Océan Austral est transmise à l'Atlantique Nord par la THC, impactant ainsi toutes les régions du globe. En effet, ces oscillations du système océanique influencent le climat global directement en modulant la répartition des apports de chaleur qui régulent le climat régional et la circulation atmosphérique, et indirectement en modifiant les apports de nutriments qui déterminent en partie la productivité primaire.

Atmosphère

Les variations de la circulation atmosphérique de part leur impact sur le transfert de chaleur et d'humidité, sur l'intensité et la direction des vents, et sur le nombre et la force des tempêtes génèrent des perturbations qui modulent spatialement et temporellement le climat (Figure 10).

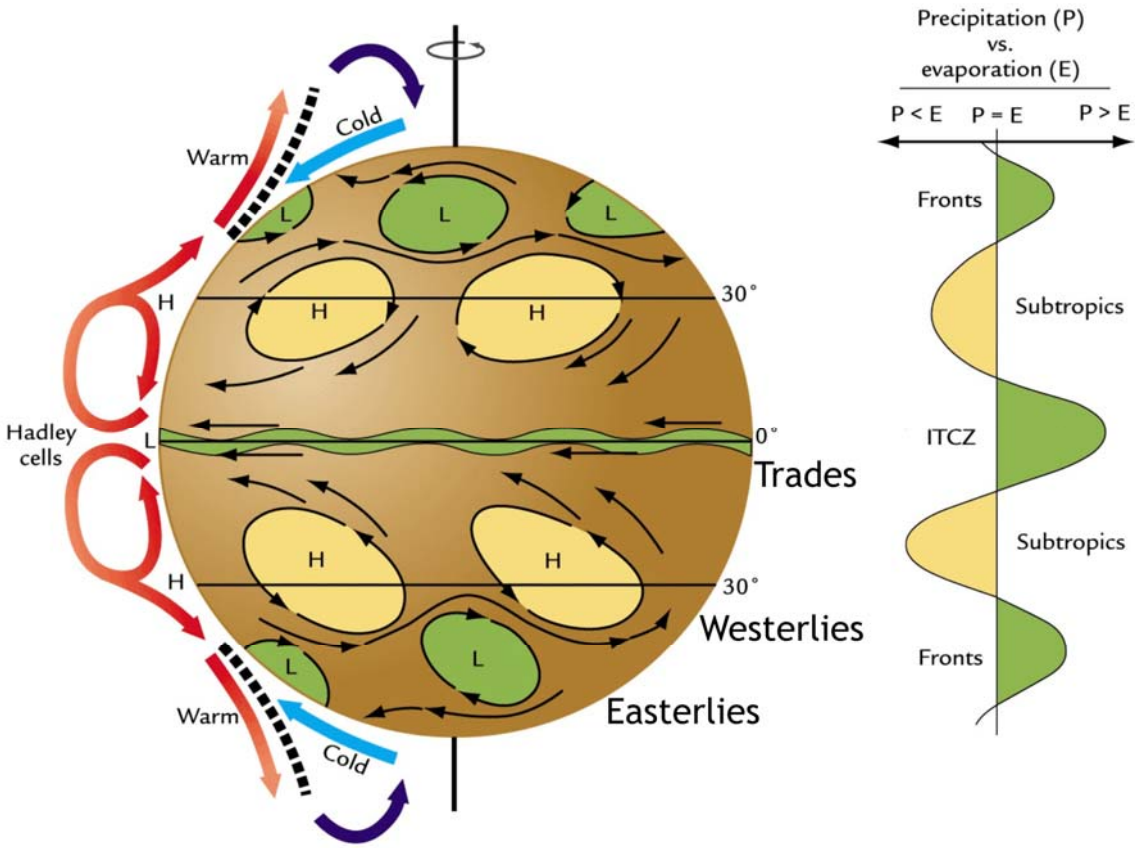

Figure 10. Schéma général de la circulation troposphérique globale d'après Ruddiman (2001). Représentation des cellules de convections (Hadley, polaire), localisation des centres de hautes (H) et basses (L) pressions, des directions des vents dominants et de l'impact sur le régime d'humidité de chaque zone latitudinale.

La dynamique de l'atmosphère est beaucoup plus rapide que la circulation océanique, ainsi les périodicités observées se situent de l'échelle interannuelle à millénaire. Les nombreux modes de variabilité climatique naturelle identifiée de part le monde sont dus à un couplage fort entre l'océan et l'atmosphère. L'initiation et les mécanismes responsables de la durée et de la cyclicité de ces oscillations sont cependant encore relativement mal connus.

L'intensité et la position des vents sont étroitement liées au couplage hautes-basses latitudes de part la distribution des centres de hautes et basses pressions (Figure 10). En effet, l'extension et l'intensité des anticyclones océaniques et continentaux influent sur la circulation atmosphérique et, par conséquent, la circulation océanique, influençant ainsi

la biosphère marine et terrestre en apportant des nutriment par les upwelling et de l'humidité par les vents (Lamy et al., 2002 ; Kim et al., 2002b ; Adkins et al., 2006). De telles variations ont été enregistrées pendant l'Holocène à l'échelle interannuelle au travers de l'ENSO (Yuan et Li, 2008), mais aussi aux échelles centennales (Masson-Delmotte et al., 2005) et millénaires (Mayewski et al., 2006) dont les processus impliqués sont encore mal connus.

Le phénomène ENSO, initié dans le Pacifique et dont les perturbations affectent toutes les régions du globe, présente une périodicité interannuelle, relativement bien connue (Yuan, 2004) qui pourrait aussi engendrer des variations d'ordre séculaire à millénaire (Moy et al., 2002). Ces cyclicités à plus grande échelle temporelle seraient le résultat de forçages orbitaux associés à des rétroactions du couplage océan-atmosphère (Clement et al., 1999). Par exemple, la position de l'ITCZ modulerait à la fois l'intensité des moussons, des vents et la prépondérance des évènements El Niño (ENSO « chaud ») ou La Niña (ENSO « froid ») (Haug et al., 2001 ; Moy et al., 2002) (Figure 11) et serait modulée elle-même par l'extension de banquise (Chiang et Bitz, 2005).

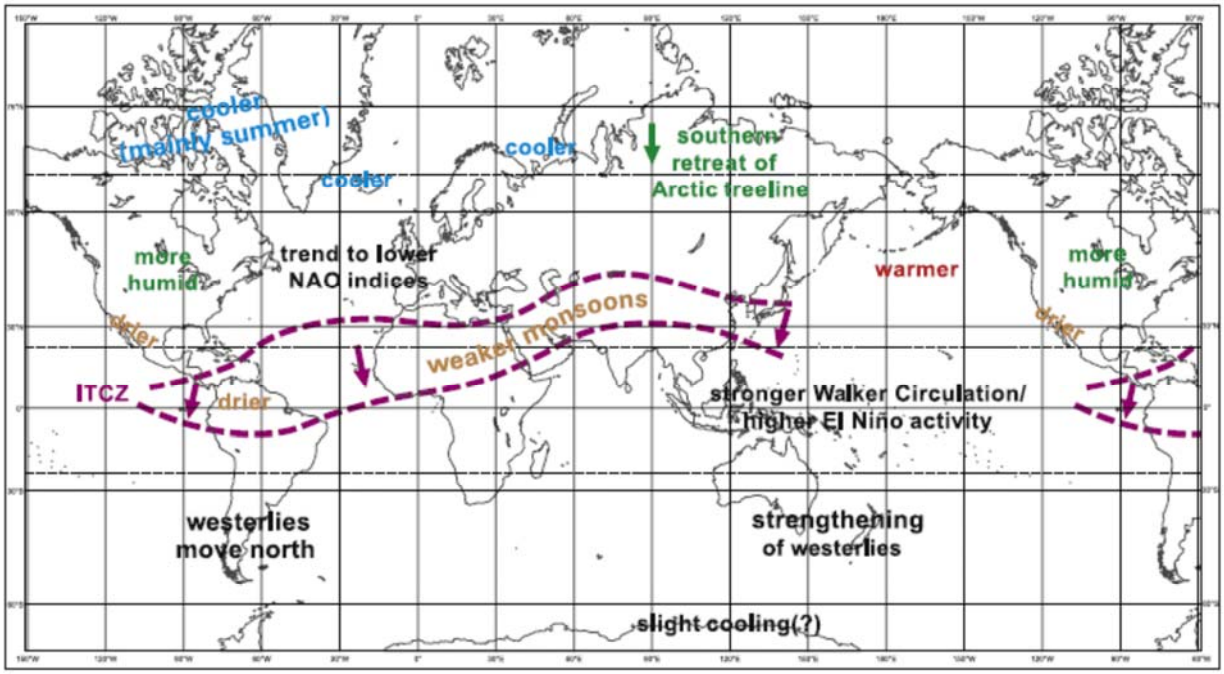

Figure 11. Synthèse spatiale : changement climatique global entre 0 et 6 cal ka BP d'après Wanner et al. (2008).

1.3. Conclusion

En conclusion, les forçages climatiques de la variabilité naturelle Holocène, qu'ils soient externes ou internes, restent peu compris même si les principaux acteurs sont maintenant connus. Leurs interconnections dressent un schéma complexe, avec des rétroactions non-linéaires, difficiles à appréhender. En effet, le climat Holocène affiche de nombreuses disparités inter-régionales quant au « timing » et à l'amplitude des changements climatiques à long- et court terme. Ces disparités peuvent refléter de vrais asynchronismes dus à certaines particularités morpho-géographiques (zone enclavée ou exposée) ou certains effets locaux (albédo, océan, atmosphère, banquise) qui peuvent retarder ou amplifier les réponses des compartiments climatiques considérés. Mais ces disparités régionales peuvent aussi être amplifiées par des biais inhérents aux enregistrements paléoclimatiques, à savoir les problèmes 1) de datation, 2) de comparaison inter-proxies qui tracent des compartiments ayant des dynamiques différentes et/ou (3) des proxies qui peuvent marquer des saisons différentes.

La modélisation se révèle alors un atout majeur dans la compréhension des facteurs forçant et des rétroactions du climat, car elle permet de déconvoluer l'impact de chacun des compartiments climatiques. Or, certaines régions sont encore peu étudiées, notamment dans l'Hémisphère Sud, et donc moins bien paramétrisées dans les modèles. Ainsi, la plupart des anciennes théories plaçaient l'Hémisphère Nord comme le déclencheur et l'acteur principal de nombreux évènements climatiques passés. Cette vision « mono-hémisphérique » du climat est maintenant mise à rude épreuve grâce aux nouveaux jeux de données de l'Hémisphère Sud. Ceux-ci révèlent toute la particularité de cet hémisphère océanique et notamment le rôle prédominant de l'Antarctique et de l'Océan Austral au sein de la machine climatique globale, que se soit en initiant des changement de la THC (Pierce et al., 1995 ; Keeling et Stephens, 2001 ; Clark et al., 2002 ; Shin et al., 2003), de la position et de l'intensité de la circulation atmosphérique (Lamy et al., 2002 ; Chiang et Bitz, 2005) et du contrôle des concentrations atmosphériques en CO_2 (Peacock et al., 2006 ; Toggweiler et al., 2006 ; Arrigo et al., 2008).

2. Continent et Océan Antarctique : Intérêt et contexte?

L'Antarctique (AA) est né il y a au moins 3,8 milliards d'années (Ga). Sa croissance s'est ensuite poursuivie au gré des formations et dislocations des supercontinents que furent le Nuna (1,8 à 1,6 Ga), le Rodinia (1,3 à 0,93 Ga), le Pannotia (0,68 à 0,55 Ga), puis le Gondwana (0,45 à 0,25 Ga). La fragmentation de ce dernier a permis la mise en place des glaciations en AA au milieu du Tertiaire en provoquant l'individualisation progressive du continent et sa dérive vers le Pôle Sud à partir du Paléocène (60 millions d'années (Ma)) (Kennett, 1977). A l'Eocène (30 Ma), l'AA est définitivement isolé et l'ouverture du passage de Drake, au sud du Cap Horn, crée un courant marin circumpolaire qui isole climatiquement l'AA en barrant la route aux influences tempérées des autres océans : Atlantique, Indien et Pacifique (Kennett, 1977). C'est au cours du Miocène (14 Ma) que l'AA devient inlandsis couvert de glace pérenne. Néanmoins, des fluctuations du niveau marin global à la fin du Paléocène (50Ma) pourraient indiquer, dès cette époque, des fluctuations de la calotte interne de l'AA de l'Est (Anderson, 1999).

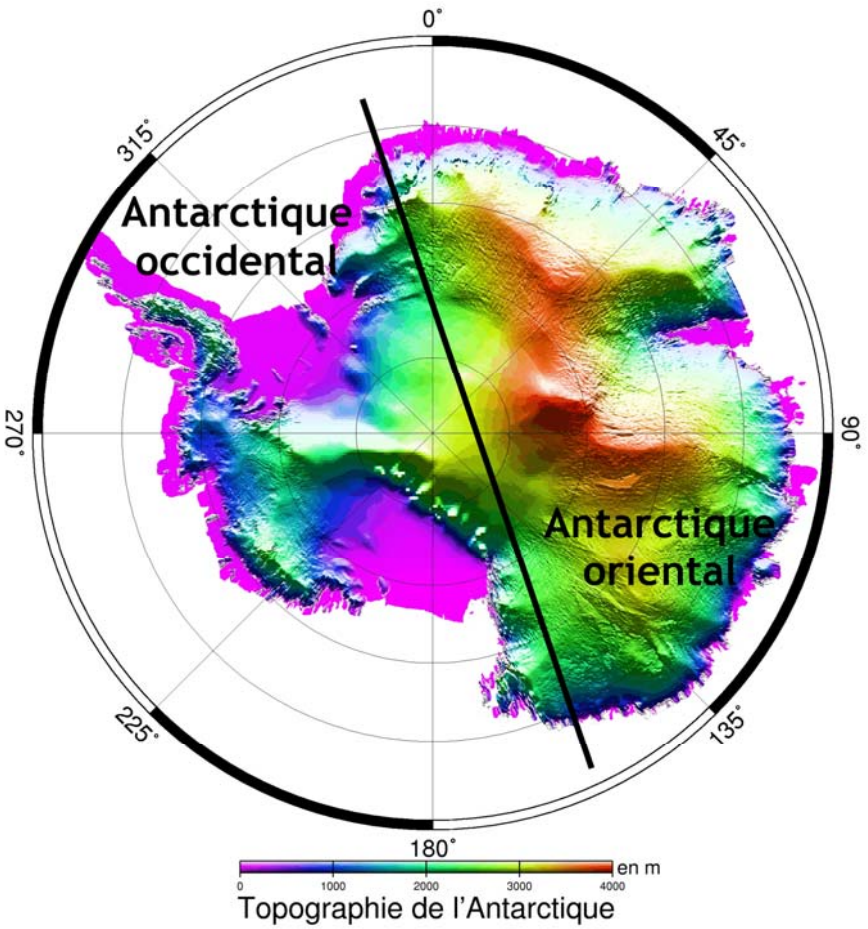

Figure 12. Topographie de l'Antarctique et délimitation des régions Est et Ouest (http://remy.omp.free.fr/FTP/image-satellite-poles/).

L'Antarctique est, depuis, le continent le plus méridional de la Terre. Sa superficie de 13,9 millions de kilomètres carrés est recouverte à 98 % d'une couche de glace faisant en moyenne 1,6 km d'épaisseur (Hambrey et Glasser, 2005). C'est le continent le plus froid (moyenne de -10 à -60°C des côtes à l'intérieur, record : -90°C), le plus sec (- de 200 mm/an de pluie, excepté sur les côtes) et le plus venteux (moyennes de 10 à 70 km/h de l'intérieur vers les côtes, record : 360km/h). Il est divisé en deux principales régions du fait de sa topographie: l'AA de l'Ouest ou AA occidental dont le socle rocheux se situe en dessous du niveau de la mer et l'AA de l'Est ou AA oriental dont le socle rocheux se situe au dessus du niveau de la mer (Figure 12).

2.1. Interconnexion de tous les sous-systèmes climatiques

Les marges AA sont un lieu privilégié pour étudier la variabilité climatique Holocène car tous les sous-systèmes climatiques : cryosphère, atmosphère, océan, et biosphère y sont interconnectés. A travers ces différents compartiments climatiques, les marges AA entretiennent des couplages étroits avec les autres parties du globe, et ce à différentes échelles de temps.

2.1.1. Cryosphère : de la calotte de glace à la banquise

2.1.1.1. Glace

La calotte de glace AA représente 91% du volume mondial de glace, dont 79 % est stocké en AA de l'Est (Wagner et Melles, 2007). L'inlandsis se prolonge dans certains secteurs par d'immenses plateformes de glace, appelées « ice-shelves », et par des langues de glaces, appelées « ice tongues » (Figure 13). En avançant sur l'océan, les « ice-shelves » se fragmentent en blocs qui se décrochent, formant les icebergs qui sont transportés vers le Nord au gré des courants (Figure 13). L'inlandsis et ses terminaisons glacées sont sous l'influence de différents paramètres.

Les températures atmosphériques estivales et les précipitations hivernales sont les facteurs clés qui régulent la croissance ou décroissance de la calotte de glace (Andrews, 1975) (Figure 13). L'océan joue aussi un rôle prépondérant en contrôlant la fonte basale et la stabilité des extrémités de l'inlandsis via les températures océaniques et l'intensité de la circulation océanique (Rignot et Jacobs, 2002) (Figure 13). Enfin, à plus long-terme, le flux géothermique, les variations d'ensoleillement et le niveau marin déterminent les phases de glaciation et déglaciation (Hambrey et Glasser, 2005 ; Bye et al., 2006) (Figure 13).

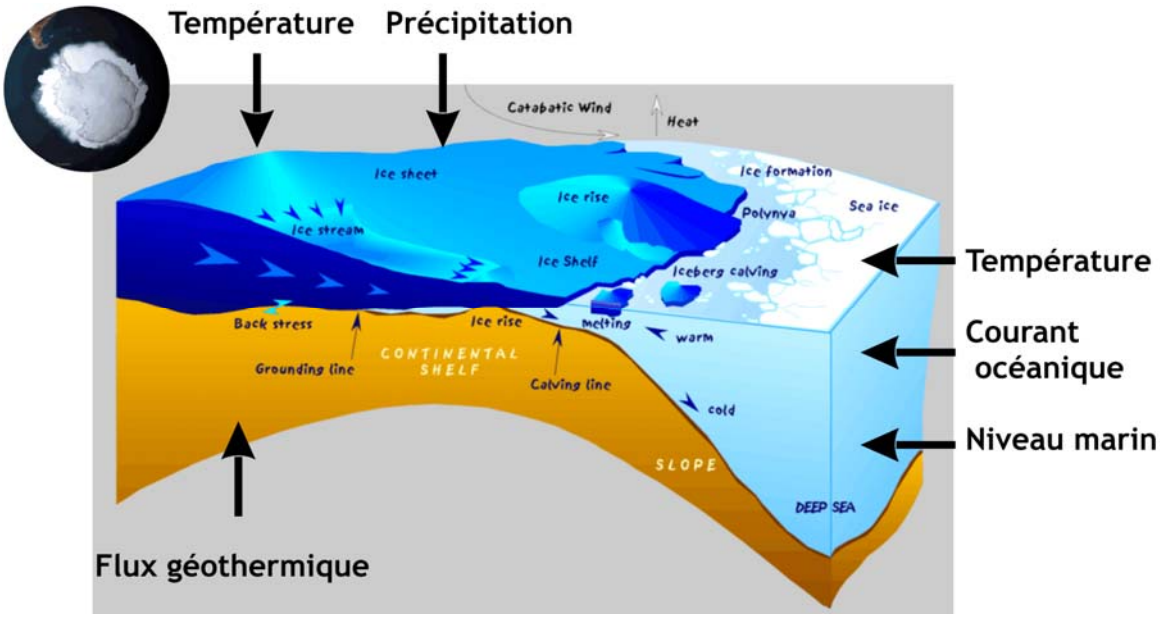

Figure 13. Schéma des différentes parties de la cryosphère d'après Hannes Grobe, (http://www.fr.wikipedia.org/wiki/Ice_stream).

2.1.1.2. Glace de mer

L'eau de mer, du fait de sa salinité, commence à geler en surface à partir de -1,8°C. La banquise, résultant de cette prise en glace hivernale, s'étend dans l'Océan Austral jusqu'à un maximum de 55°S et 65°S dans les secteurs Atlantique et Pacifique, respectivement (Schweitzer, 1995) (Figure 14).

Il existe plusieurs types de banquise :

- la glace de mer, appelée « Fast ice », est attachée au continent. Elle est très compacte et forme un anneau étroit autour du continent (~100 km) qui peut atteindre de 50 cm à 6 m d'épaisseur (Crow et Tucker, 1990). Elle peut être pluriannuelle.

- La glace de mer, appelée « Pack ice », est produite par le transport de cristaux compactés par les vagues et les vents. Son épaisseur est restreinte par rapport à la « Fast ice » et elle est généralement saisonnière.

L'extension nord de la Zone Marginale des Glaces (MIZ), c'est-à-dire la zone de glace non-consolidée, résulte d'un bilan entre advection vers le nord du « Pack ice » et fonte à la marge en raison des températures océanique et atmosphérique plus chaudes (Simmonds et Budd, 1991).

Cycle saisonnier

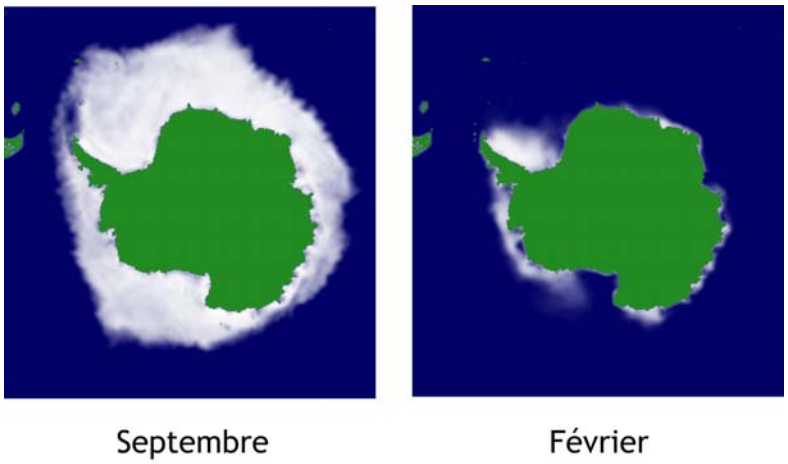

Figure 14. Moyenne mensuelle de l'extension de banquise en septembre et en février au cours de la période 1978-1991 (Schweitzer, 1995).

La glace de mer s'étend lentement de mars à avril. D'abord fragiles, les glaces en formation sont détruites à chaque tempête. Puis, au fur et à mesure que le froid s'intensifie, la glace de mer s'épaissit et s'étend rapidement d'avril à juin pour former la banquise. Au maximum d'extension, en septembre, la surface de la banquise peut atteindre 20 millions de km^2, ce qui double la surface englacée de l'Hémisphère Sud. Puis, elle se retire plus lentement lors de la fonte printanière d'octobre à décembre pour atteindre son extension minimum durant l'été austral. En février, vers la fin de l'été austral, la banquise s'est totalement disloquée et la plupart des côtes sont libres d'accès (Figure 14).

Le cycle saisonnier, la concentration et l'extension de la banquise sont conditionnés par la conjonction de plusieurs facteurs physiques : les températures atmosphériques, océaniques, et la position de la zone de convergence atmosphérique (Enomoto et Ohmura, 1990) liée au couplage entre hautes et basses latitudes de l'Hémisphère Sud (Yuan, 2004 ; Stammerjohn et al., 2003). Régionalement et inter-annuellement, l'extension de la banquise peut varier jusqu'à 5°de latitude (Budd, 1975) et sa persistance jusqu'à 2-3 mois par an suivant les régions (Arrigo et van Dijken, 2003). Cependant, ces importantes variations sont lissées à l'échelle de l'Océan Austral par un effet de compensation d'une région à l'autre (Mullan et Hickman, 1990).

Le rythme annuel de la formation et de la disparition de cette immense quantité de glace de mer a une influence profonde sur la circulation océanique globale, les échanges thermiques entre l'océan et l'atmosphère et la biologie des océans de l'Hémisphère Sud. Notamment, les polynies constituent des zones clés dans tous ces processus car les échanges (chaleur, eau, nutriments) y sont amplifiés (Massom et al., 1998 ; Arrigo et van Dijken, 2003 ; Tamura et al., 2008).

Polynies

Au sein de la banquise hivernale existent, de manière persistante et récurrente, des zones d'eau libre appelées polynies (Figure 15).

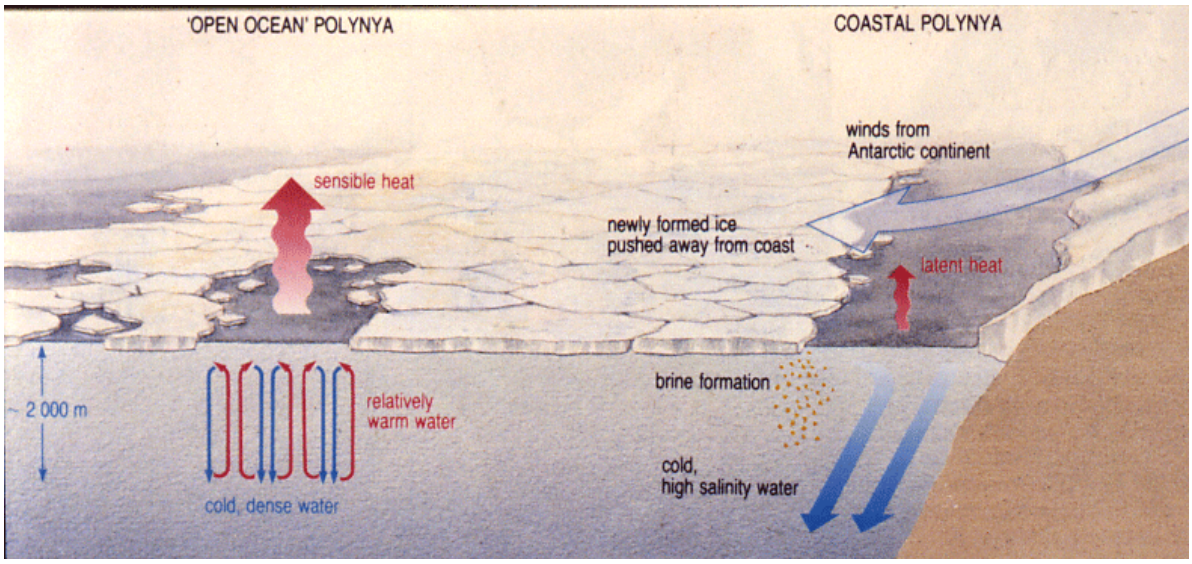

Figure 15. Schéma des deux types de polynies existants (http://www.geology.um.maine.edu).

Différents mécanismes forçants peuvent être à l'origine des polynies et déterminent leur type (Anderson, 1993):

- Les polynies à chaleur sensible sont crées et maintenues par des turbulences océaniques et des résurgences d'eaux plus chaudes dans la couche de surface, via les upwellings ou la pompe tidale, qui inhibent la formation de glace de mer (Davis et McNider, 1997; Polyakov et Martin, 2000). Comme exemple nous pouvons citer la Comonaut Polynya au large de Enderby Land (Comiso et Gordon, 1996) ou la polynie de Maud Rise au Nord-Est de la Mer de Weddell (Gordon et Huber, 1995) (Figure 15-16).

- Les polynies à chaleur latente sont crées et maintenues par les vents synoptiques (Zwally et al., 1985), catabatiques (Adolphs et Wendler, 1995) et les « Easterlies », c'est-à-dire les vents d'Est qui longe les côtes AA (Cavalieri et Martin, 195), et/ou par les courants océaniques de surface. Ce type de polynie résulte d'un équilibre entre formation et export de glace de mer. Elles participent, ainsi, activement à la formation et à la fonte de la banquise. C'est le cas de la Polynie de Mertz en Terre Adélie (Massom et al., 1998) (Figure 15-16).

La distribution spatiale des polynies dépend donc des conditions atmosphériques et océaniques mais aussi de la morpho-bathymétrie des marges continentales qui peut, plus ou moins, faciliter leur établissement (Wright, 1983) (Figure 16).

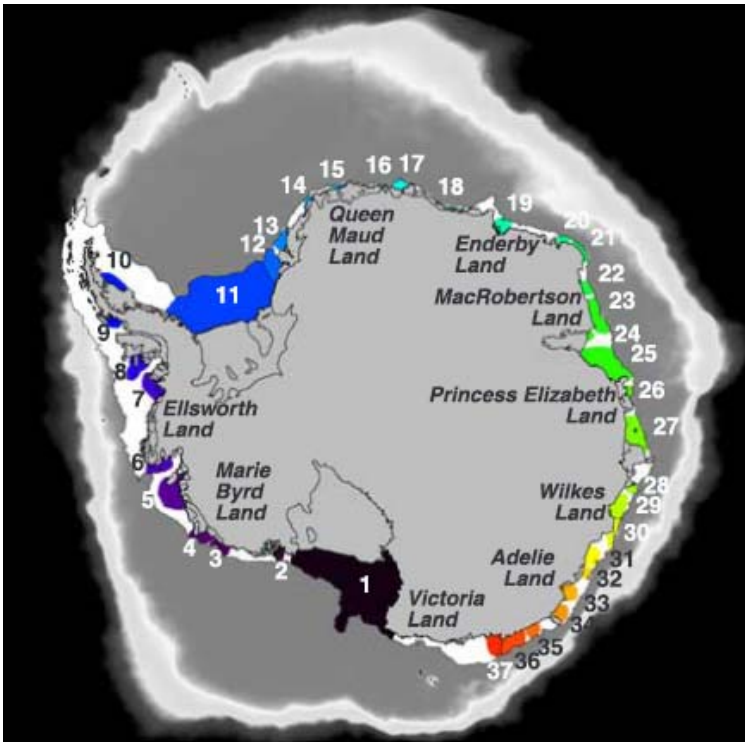

Figure 16. Localisation de 37 polynies, enregistrées au moins une fois autour de l'AA entre 1997 et 2002. Les zones blanches du plateau continental n'ont jamais été associées à une polynie. Le couvert de banquise hivernal moyen au cours de ces 5 ans est représenté (Arrigo et van Dijken, 2003). Le code couleur des polynies aide juste à distinguer les différentes zones régionales. Les couleurs grisée et banche au large du plateau continental figurent la concentration de la banquise (gris : plus épais, blanc : moins épais).

2.1.2. Océan

L'Océan Austral est parcouru par le Courant Circumpolaire Antarctique (ACC) ou « West Wind Drift », qui circule d'Ouest en Est autour du continent AA. Contrairement aux autres océans, qui sont définis comme des étendues d'eau limitées par des continents, l'Océan Austral est le seul à être défini comme une masse d'eau qui encercle un continent. Cet anneau océanique s'étend au sud de 35°S et sur toute la circonférence du globe, avec une superficie de 78 millions de km² (Figure 17). L'Océan Austral est profond de 4 à 5 km tout comme l'étroit plateau continental AA qui atteint 400 à 800 m alors que la moyenne mondiale n'est que de 133 m. La température de la mer varie de -1,8°C à 10°C en hiver et de -1.8°C à 14°C en été. Après une brève présentation des courants et masses d'eaux de l'Océan Austral dans son ensemble, nous nous attarderons plus précisément sur les courants qui gouvernent la circulation océanique des marges AA.

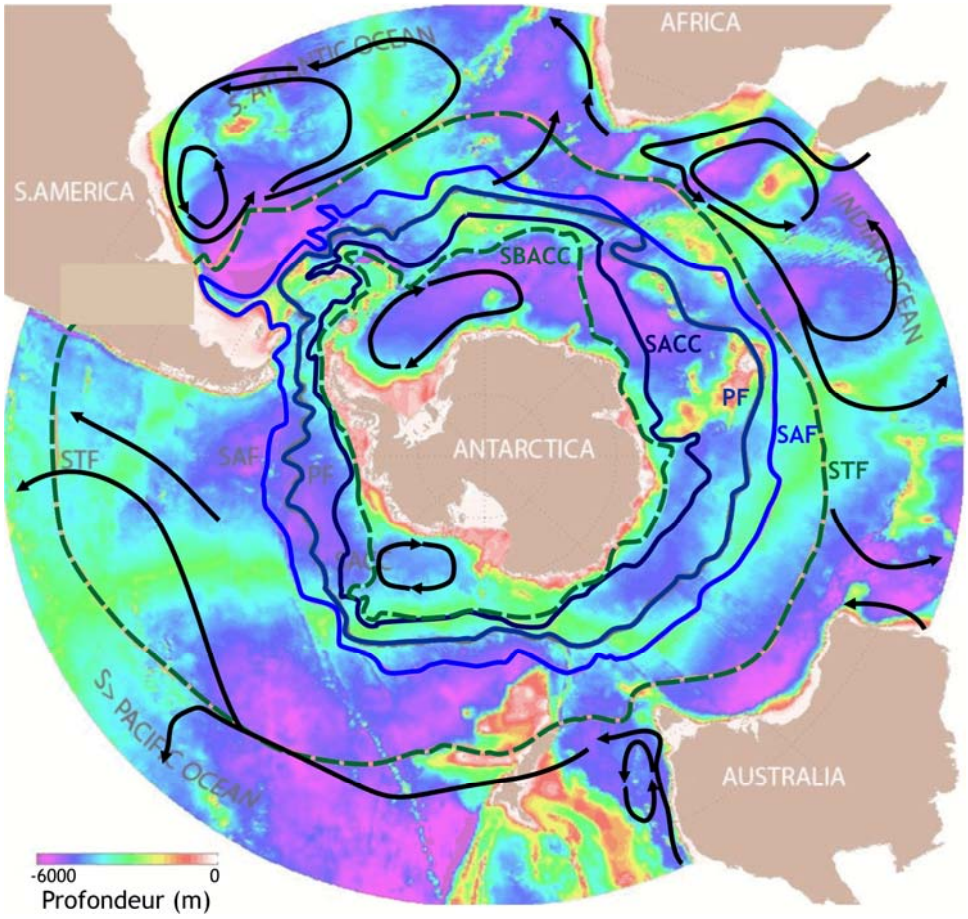

Figure 17. Position des principaux fronts océaniques, des courants océaniques et bathymétrie de l'Océan Austral (GEBCO) au Sud de 30°S (modifiée d'après Orsi et al. (1995) et Rintoul et al. (2001) - (Fond de carte : Hannes Grobe ; http://www. wikipedia.org)). STF: Sub-Tropical Front, SAF: Sub-Antarctic Front, PF: Polar Front, SACC: Southern Front of ACC, SBACC: Southern Boundary of ACC.

2.1.2.1. Circulation océanique de l'océan Austral

La circulation de surface de l'Océan Austral est gouvernée principalement par l'ACC. Ce courant englobe plusieurs fronts créés par des gradients thermohalins. Du Nord au Sud, on retrouve : le Front Sub-tropical (STF), le Front Sub-antarctique (SAF), le Front Polaire (PF) et le front Sud de l'ACC (SACC), (Tchernia, 1978 ; Orsi et al., 1995) (Figure 17). Ces fronts correspondent d'une part à la frontière entre des masses d'eaux de caractéristiques hydrologiques différentes, d'autre part aux puissants jets océaniques composant l'ACC. Le STF et la frontière sud de l'ACC (SBACC) représentent les limite nord et sud de l'ACC, e.g. entre 35-40°S et 60-65°S suivant les bassins de l'Océan Austral (Orsi et al., 1995).

L'ACC s'étend en profondeur jusqu'à 2-3 km, c'est-à-dire la limite inférieure de l' Eau Circumpolaire Profonde (CDW) qui résulte du mélange des Eaux Profondes Nord-Atlantique (NADW) avec les eaux de l'ACC et les eaux profondes des océans Pacifique et Indien (Figure 18). L'ACC s'écoule d'Ouest en Est, sous l'action des Vents d'Ouest (Tchernia, 1978). De plus, l'écoulement de l'ACC est influencé par la force de Coriolis et par la

topographie des fonds sous-marins. En effet, la grande profondeur d'action de l'ACC fait de l'Océan Austral un océan quasi-barotrope. Les fronts de l'ACC sont clairement orientés par les grosses structures bathymétriques (Rintoul, 2001) (Figure 17) et pourraient être ancrés dans leur configuration actuelle par la présence des rides médio-océaniques.

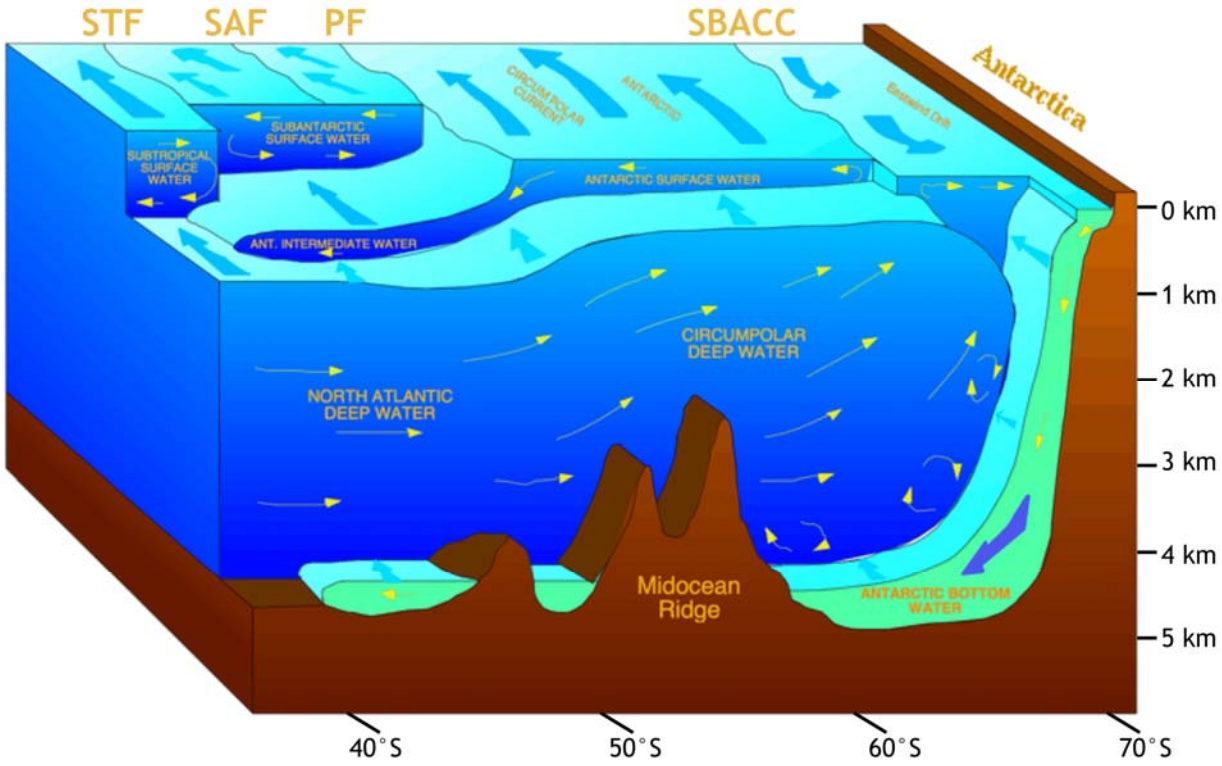

Figure 18. Discontinuités de surface et masses d'eaux de l'Océan Austral (modifiée d'après Matthew England (http://web.maths.unsw.edu.au/~matthew/southern_ocean_variability.htm)). STF: Sub-Tropical Front, SAF: Sub-Antarctic Front, PF: Polar Front, SBACC: Southern Boundary of ACC.

Au Nord de la STF, la circulation est dominée par les gyres subtropicales et anticycloniques et leurs forts courants de bord Ouest (Figure 17). Ces courants permettent l'exportation des masses d'eaux de l'ACC vers la partie Est des bassins tropicaux ainsi que l'advection d'eau subtropicale, chaude et salée, vers l'ACC à travers les courants de bord Ouest (Figure 17).

Au Sud de l'ACC, la Divergence Antarctique (AD) ou la frontière Sud de l'ACC (SBACC) marquent les zones de remontée de la CDW vers le plateau continental AA (Orsi et al., 1995; Heil et Allison, 1999) (Figure 18). Une partie de la CDW, appelée masse d'eau profonde de l'ACC (ACCbw), se densifie au contact de l'Eau Antarctique de Fond (AABW) et est ainsi suffisamment dense pour alimenter la circulation de fond mondiale, et notamment le bassin Atlantique (Orsi et al., 1999). En effet, au niveau du passage de Drake, au Sud de l'Amérique Latine, la topographie très élevée peut restreindre le passage de l'AABW qui est beaucoup plus dense que les masses d'eaux sus-jacentes (détails dans Orsi et al., 1999) (Figure 18).

2.1.2.2. Zoom sur la circulation océanique périantarctique

La circulation océanique des marges AA est très active et grandement affectée par la saisonnalité induite par le cycle de banquise, les polynies, les vents et la proximité du continent. Ces eaux périantarctiques sont plus froides et plus riches en nutriments que les eaux situées au nord de la AD (Orsi et al., 1995).

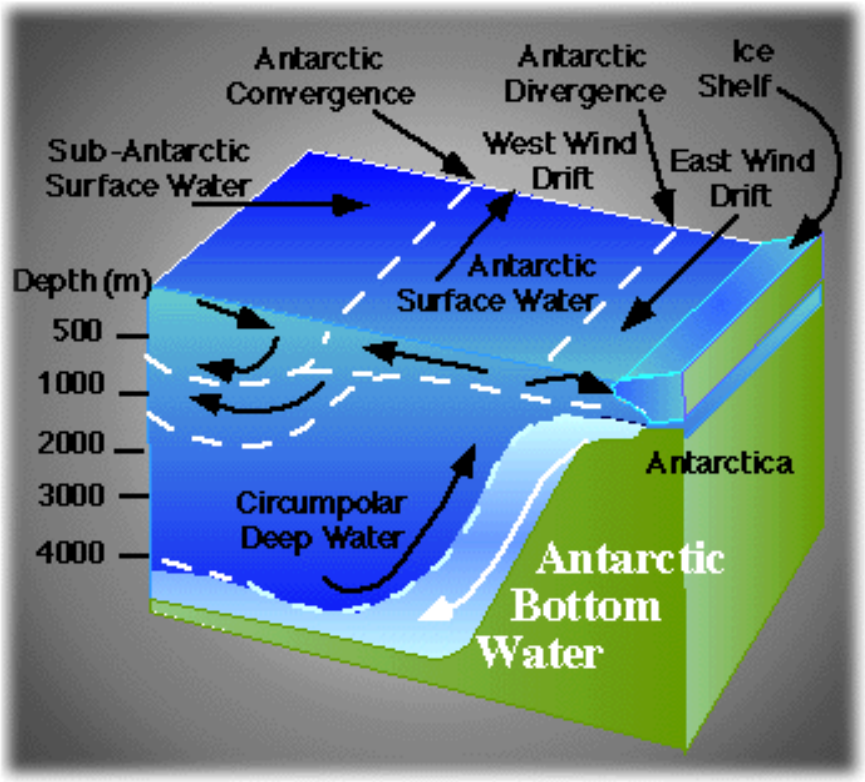

Figure 19. Schéma des principaux courants et masses d'eaux de l'océan périantarctique (http://www.geology.um.maine.edu/ges121/lectures/19-ocean-conveyor/4_antbw.gif).

Courants et masses d'eau de surface

- Un courant opposé au gigantesque ACC circule le long des côtes AA d'Est en Ouest, poussé par les vents d'Est. Ce courant périantarctique est aussi appelé ACC (Antarctic Coastal Current) ou Dérive d'Est « East Wind Drift » (EWD). Nous utiliserons cette dernière appellation dans le manuscrit pour éviter toute confusion (Figure 19).

- L'Eau Antarctique de Surface (AASW) constitue la couche de surface des eaux estivales du plateau continental et rejoint l'EWD vers l'Ouest sous l'influence de Coriolis (Whitworth et al., 1998) (Figure 19).

- Les masse d'eaux de surface hivernales (WW) se modifient soit (Bindoff et al., 2000a, 200b):

- au contact des « Ice Shelf » par un « super » refroidissement et forment ainsi les eaux continentales à faible salinité mais très froides (LSSW), appelées aussi « Ice Shelf Water » (ISW).

- dans les polynies ou zone d'accrétion de la banquise par refroidissement et augmentation de la salinité due au rejet de saumure et forment ainsi les eaux continentales à forte salinité (HSSW).

Upwelling

La CDW remonte au niveau de la AD sous l'effet de la pompe d'Eckman (en relation avec l'opposition des deux systèmes de vents et des deux courants de surface ACC et EWD) et transite le long du talus continental où elle acquiert une nouvelle signature géochimique (Figure 19). Cette nouvelle masse d'eau, appelée Eau Circumpolaire Profonde Modifiée (MCDW), s'écoule alors vers le Sud le long du plateau continental. Ces eaux relativement plus chaudes que les eaux de surface et riches en nutriments participent à la fonte saisonnière de la banquise, à la persistance/récurrence des polynies et à la croissance du phytoplancton.

Courants de fond

Les deux masses d'eaux hivernales de surface, LSSW et HSSW, peuvent acquérir une densité suffisante pour plonger. Elles se mélangent alors avec les eaux de la MCDW pour former l'Eau Antarctique de fond (AABW), qui représente la masse d'eau de fond la plus dense du monde (Orsi et al., 1999) (Figure 19). La contribution de la MCDW à la formation d'AABW pourrait être d'environ 25% (Orsi et al., 1999).

Cependant, ce processus n'est pas actif dans toutes les régions AA (Figure 20) et son efficacité varie selon plusieurs facteurs :

- la présence et la taille des « ice shelves » et « ice tongues » (super-refroidissement).
- l'intensité de formation de la banquise, souvent liée à la présence de polynie (rejet de saumure).
- la forme et la topographie du plateau continental, facilitant ou non l'expulsion de l'AABW hors du plateau continental.
- la pompe tidale, elle-même fortement liée à la morpho-bathymétrie du site, peut favoriser ou non l'expulsion des masses d'eaux de fond.

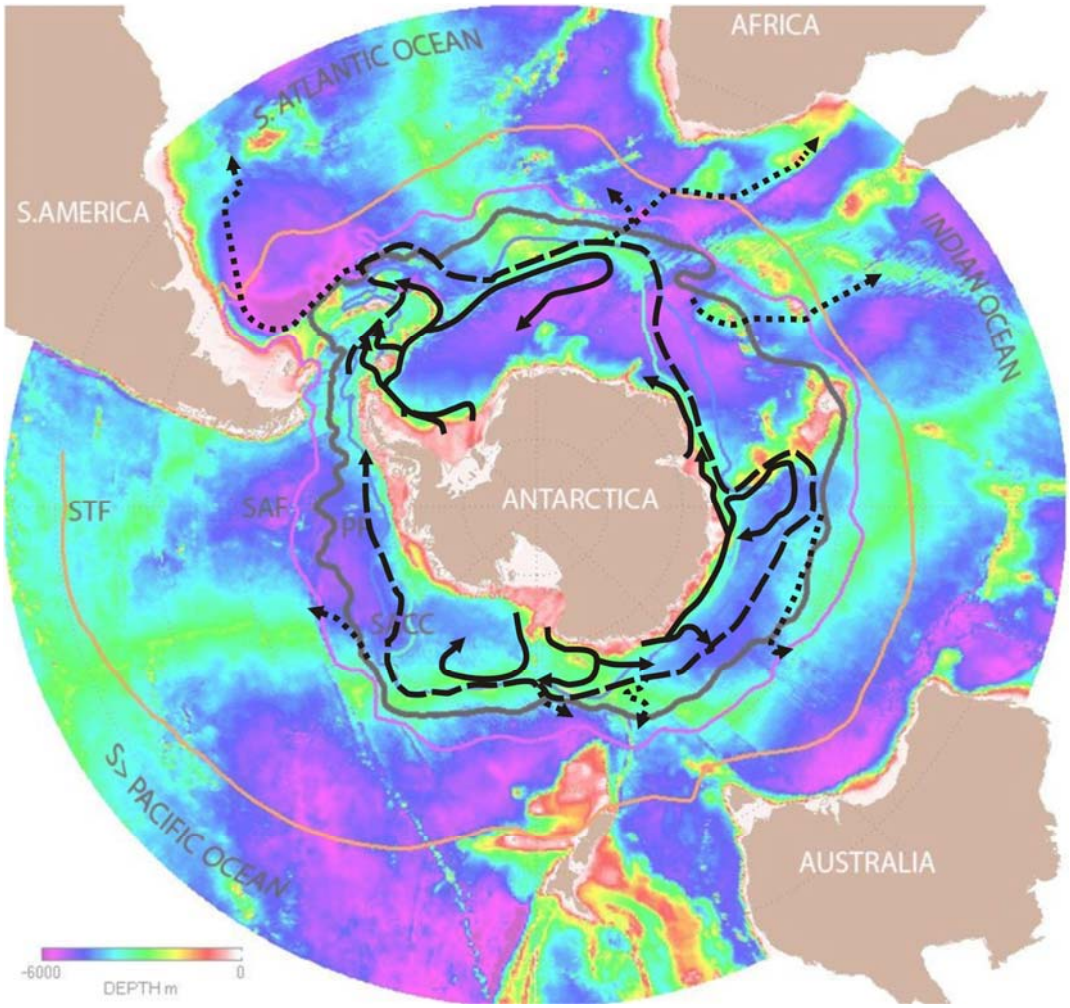

Figure 20. Schéma des eaux profondes sources de l'AABW (ligne noire), de l'AABW (ligne tirée) et du mélange AABW-ACCbw (ligne pointillée), modifiée d'après Orsi et al. (1999)- (Fond de carte : Hannes Grobe ; http://www.wikipedia.org).

Le secteur Atlantique AA, contribuerait à lui seul jusqu'à 60% de la formation d'AABW, notamment via l'eau de fond formée en Mer de Weddell (WSBW) (Orsi et al., 1999) (Figure 20). Les secteurs Pacifique et Indien formeraient les 40 % restant via les eaux de fond formées dans les Mer de Ross (RSBW) et Terre Adélie (ALBW) (Orsi et al., 1999 ; Rintoul, 1998) (Figure 20). Cependant, des travaux de modélisation et d'observations satellitaires suggèreraient une plus grande diversité des sites impliqués dans la formation d'AABW, en lien avec la présence de polynies (Baines et Condie, 1998 ; Tamura et al., 2008). Notamment, la région d'Amery (50-100°E) pourrait être un site important dans la formation d'AABW (Tamura et al., 2008) (Figure 20).

Les eaux denses sources de l'AABW s'écoulent ensuite vers le nord sur le plateau continental AA et rejoignent l'AABW au sein des plaines abyssales qui est ensuite déviée par la force de Coriolis et la morpho-bathymétrie des bassins (Figure 20). Sa forte densité la « colle » aux fonds sous-marins et l'empêche de passer certains haut-fonds marins comme au niveau du Passage de Drake (Orsi et al., 1999). Ainsi, l'exportation de l'AABW

vers les autres bassins océaniques s'effectue par le biais d'un mélange entre l'AABW et l'ACCbw par des phénomènes diffusifs et/ou au moyen de seuils profonds dans les dorsales océaniques (Orsi et al., 1999) (Figure 20).

L'Océan Austral est un maillon clé de la THC via l'exportation de ses eaux profondes (AABW et ACCbw) et de ses eaux de surface et intermédiaires à l'ensemble du globe qui dominent les redistributions globales de chaleur, de salinité, de nutriments (Gordon et al., 2001) (Figure 21). Ainsi, les anomalies climatiques formées dans un bassin austral particulier peuvent avoir des répercussions importantes dans de très lointaines régions (White et Peterson, 1996).

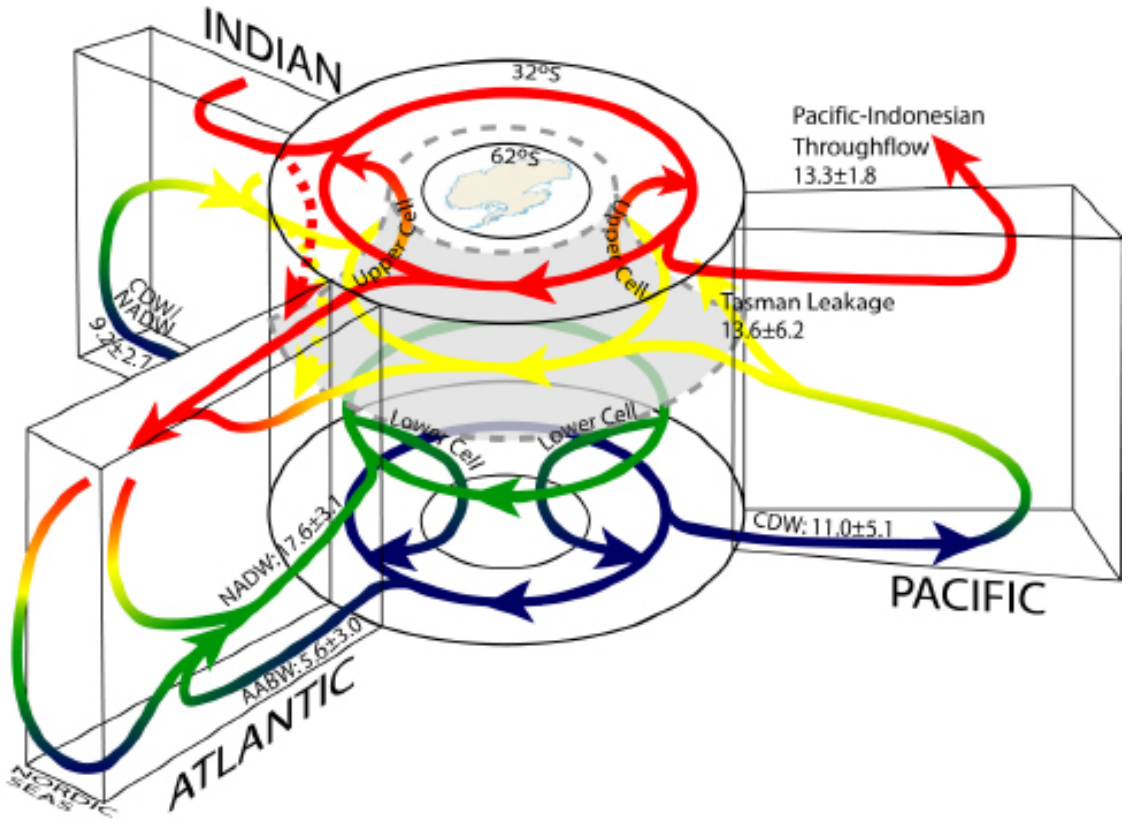

Figure 21. Schéma 3D de la circulation thermohaline globale montrant la position centrale de l'Océan Austral qui modifie et redistribue les masses d'eaux des autres océans (Lumpkin et Speer, 2007).

2.1.3. Atmosphère

Nous allons nous focaliser sur la circulation troposphérique au sud de 30°S, à savoir les « Westerlies » ou vents d'Ouest, les « Easterlies » ou vents d'Est et les vents catabatiques.

2.1.3.1. Westerlies

Les « Westerlies » sont les vents dominants aux moyennes latitudes entre 30°S et 60°S, circulant des zones de hautes pressions des latitudes moyennes vers les pôles. Ces vents proviennent du Nord-Ouest dans l'Hémisphère Sud. Comme, en moyenne, le ruban thermique est orienté Ouest-Est, il en résulte une circulation générale d'Ouest en Est aux latitudes moyennes. Les « Westerlies » peuvent être très forts dans l'Hémisphère Sud où il y a moins de masses continentales causant des frictions et diminuant la vitesse des vents.

Les "Westerlies" jouent un rôle important en transportant la chaleur et l'humidité à l'Océan Austral ainsi qu'en déterminant la circulation du gigantesque ACC autour de l'AA. Les dépressions synoptiques, issues des Westerlies se dirigent du Nord vers le Sud où elles sont généralement récurrentes et plaquées sur les côtes.

2.1.3.2. Easterlies

Les « Easterlies » sont initiés par les cellules de circulation polaire qui échangent l'air plus chaud au nord de 60°S avec l'air froid et sec qui bordent le continent AA. Cette circulation convective fermée induit entre 90 et 60°S un déplacement des masses d'air des zones de hautes pressions AA vers les zones de basses pressions des fronts polaires. Ces masses d'air sont ensuite déviées vers l'Ouest par la force de Coriolis. Ces « Easterlies » sont des vents très froids et très secs, mais, à la différence des « Westerlies », ils sont souvent de faible intensité et irréguliers. Les « Easterlies » sont à l'origine du courant océanique périantarctique « East Wind Drift ».

2.1.3.3. Vents catabatiques

Les vents catabatiques sont définis comme des vents gravitationnels produits par le poids d'une masse d'air froide dévalant un relief géographique (McKnight et Darrel, 2000).

On peut refroidir l'air de deux façons :

- par rayonnement : une masse d'air perd son énergie vers les couches supérieures, comme dans le cas de la température de surface qui descend la nuit lors d'un ciel dégagé.

- par modification par la couche sous-jacente : l'air passe sur une surface plus froide et prendra graduellement la température de celle-ci comme dans le cas de l'air passant sur un glacier.

C'est ce deuxième processus qui est à l'origine de la formation des vents catabatiques. Ceux-ci soufflent du Sud vers le Nord en dévalant le long des glaciers et restent généralement forts toute l'année. Ils peuvent cependant montrer des pics d'intensité en hiver en raison du resserrement des ceintures barométriques dû à une augmentation des écarts de température entre les pôles et l'équateur. La vitesse moyenne du vent est relativement modérée dans les régions centrales (10 à 20 km/h) et plus élevée sur les côtes (30 à 70 km/h) où les rafales peuvent atteindre des vitesses record : 360 km/h enregistrés en Baie de Prydz. Les vents catabatiques peuvent persister durant 9 mois de l'année (Parish, 1988) et étendre leur influence jusqu'à 120 km au large (Adolphs et Wendler, 1995), bien que normalement ils se cantonnent à affecter les quelques dizaines de km au large des côtes (Bromwich et Kurtz, 1984).

2.1.3.4. Influence des régimes de vents

L'intensité des ces trois régimes de vents dépend des gradients de pression et de température entre les pôles et l'équateur. Ainsi, toutes variations des gradients de température équateur-pôle, qu'elles soient saisonnières, interannuelles, milléniales ou orbitales, induisent un déplacement des ceintures barométriques soit par un relâchement de celles-ci (vents moins intenses) soit par un resserrement de celles-ci (vents plus intenses).

Les vents sont impliqués dans la circulation océanique de surface et sub-surface, ainsi que dans la répartition spatiale et la formation du couvert de banquise à ces différentes échelles de temps. Or, l'océan et le couvert de banquise participent aussi à l'intensité du gradient de température équateur-pôle. Ainsi, les trois compartiments climatiques que sont l'océan, l'atmosphère et la cryosphère, sont intimement interconnectés. Notamment sur les marges continentales AA, les vents catabatiques et synoptiques jouent un rôle fondamental sur le couvert de banquise en la compactant et en la fractionnant, sur les upwellings, les polynies et sur la formation d'eaux profondes. De plus, ces vents peuvent brasser la colonne d'eau profondément de manière continue ou épisodique, renouvelant ainsi le stock de nutriments et permettant le développement de la biota.

2.1.4. Biosphère marine

La biosphère marine AA résulte d'une chaîne trophique assez courte, du phytoplancton jusqu'au grands mammifères marins (Figure 22). La communauté phytoplanctonique est largement dominée dans tout l'Océan Austral par les diatomées (Tréguer et Jacques, 1992).

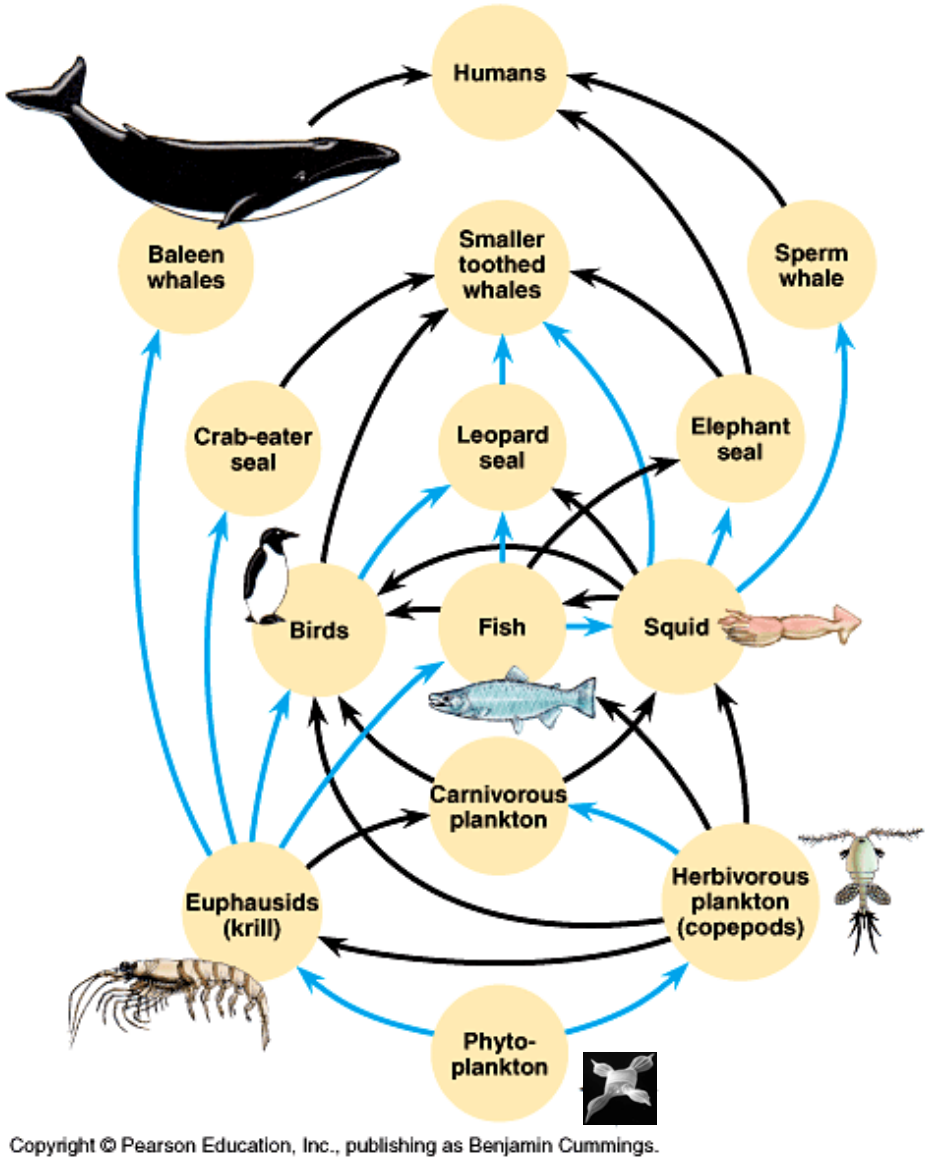

Figure 22. Chaine trophique de l'océan Austral (http://io.uwinnipeg.ca/~simmons/16cm05/1116/16ecosys.htm). Photo de *Chaetoceros Phaeocoeros bulbosom* de *Fiona Scott*.

2.1.4.1. Provinces écologiques

La répartition spatiale et temporelle des biomasses phytoplanctoniques, qui conditionnent celles des maillons trophiques supérieurs, s'organise en fonction des différentes provinces écologiques de l'Océan Austral. Ces provinces écologiques sont définies par rapport à l'influence du couvert de banquise et présentent des superficies et des conditions environnementales très différentes (Figure 23 et table 1) :

- La zone pélagique (POOZ) de l'Océan Austral qui est libre de glace tout au long de l'année.

- La zone marginale des glaces (MIZ) qui est par définition la zone récemment libre de glace (depuis 15 jours à 1 mois) dans la zone saisonnière des glaces (SIZ).

On distingue la :

- la MIZ d'océan ouvert qui est située à l'extérieur du plateau continental
- la MIZ du plateau continental.

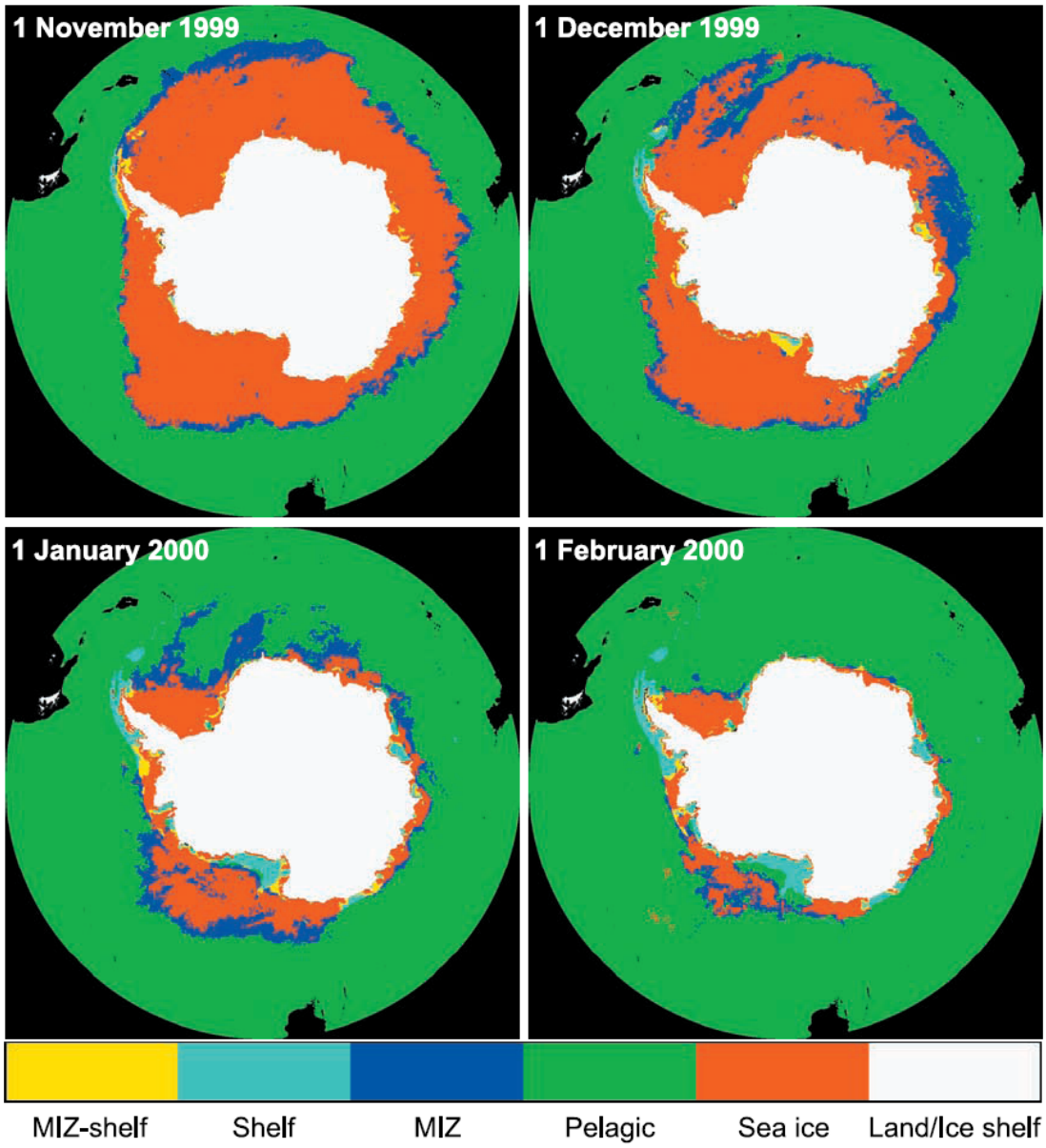

Figure 23. Cartes indiquant les trois provinces écologiques (pélagique, MIZ océan ouvert et MIZ du plateau continentale) et leurs intermédiaires, figurant leur évolution spatiale durant les mois de croissance phytoplanctonique (e.g. printemps/été) (Arrigo et al., 2008).

La zone pélagique de l'Océan Austral est très peu productive par unité de surface bien que la productivité primaire s'y effectue quasiment toute au long de l'année (Table 1). Du fait de son importante superficie, elle représente quand même la zone majeure de production

primaire (PP) de l'Océan Austral (Table 1). Les principales causes de cette faible productivité sont un faible angle solaire incident, une couche de mélange profonde, et une faible abondance en micro-nutriments (Martin et al., 1990 ; Mitchell et Holm-Hansen, 1991 ; Boyd et al., 2000). Cependant, la zone du Front Polaire Antarctique, qui est associée à des résurgences d'eaux profondes chaudes et riches en nutriments, favorise localement des productivités plus importantes (Moore et al., 2000 ; Hense et al., 2000). De même, les zones au large des îles où les micro-nutriments nécessaires au phytoplancton sont remis en suspension par les courants profonds (Korb et Whitehouse, 2004 ; Blain et al., 2007) sont aussi des zones de forte production phytoplanctonique.

La MIZ est beaucoup plus productive que la zone pélagique par unité de surface bien que la production primaire y soit limitée dans le temps (Table 1). En effet, la productivité phytoplanctonique est contrôlée par la dynamique de la banquise et suit son cycle saisonnier (Arrigo et al., 1998). Les plus fortes PP sont dues à l'influence de la banquise qui génère une stratification de la colonne d'eau et apporte des nutriments, créant ainsi des conditions favorables à la croissance du phytoplancton et, notamment, des diatomées (Leventer, 1992).

Dans la MIZ de l'océan ouvert, les apports en nutriments sont toutefois limités, notamment en silicate et en fer, d'où l'apparition épisodique et ponctuelle de conditions co-limitantes (Nelson et al., 2001). De plus, la stratification peut être perturbée par les vents (Fitch et Moore, 2007) d'où des conditions moins favorables au développement de blooms de diatomées (Arrigo et al., 2008).

Dans la MIZ du plateau continental, la stratification de la colonne d'eau est plus forte en relation avec la fonte saisonnière de la banquise et des glaciers. Malgré cela, les nutriments et les métaux traces sont rarement limitants du fait de la multiplicité des sources (fonte de glace et glace de mer, re-suspension par les courants de fond, éolien, upwelling saisonnier) et du renouvellement du stock lors du plongement des eaux hivernales (Leventer, 1992). Ainsi, la MIZ « plateau » montre une très forte productivité printanière mais, du fait de sa faible superficie, sa contribution à l'échelle de l'Océan Austral reste mineure (Table 1).

Provinces écologiques AA	Superficie (%)	PP totale (%)	PP surface ($gC/m^2/a$)	Nb de mois de PP active	Nutriments et métaux traces	Profondeur pycnocline	Stabilité pycnocline
Pélagique	94	90	54	9 à 7	Faible	Importante	Faible
MIZ océan	4	5	57,5	5 à 7	Moyen	Moyenne	Moyenne
MIZ plateau	2	5	88,4	3 à 5	Abondant	Faible	Importante

Table 1. Table des trois provinces écologiques de la biosphère de l'océan Austral et leurs caractéristiques (Arrigo et al., 2008).

2.1.4.2. Pompe biologique

La biomasse marine phytoplanctonique est un acteur majeur des cycles des éléments biogéochimiques tels que le carbone, l'azote, et la silice. Par exemple, l'assimilation par photosynthèse du carbone permet son transfert de l'océan vers le sédiment (Figure 24). Ce transfert peut être direct par sédimentation des producteurs primaires, ou indirect par incorporation de ces éléments le long de la chaîne trophique avant sédimentation par les producteurs secondaires et au-delà. Ce processus biologique, appelé pompe biologique, induit un retrait plus ou moins permanent de ces élément du système climatique par stockage dans les masses d'eaux profondes et/ou enfouissement dans le sédiment. Ainsi, la pompe biologique est un des mécanismes clé dans le cycle du carbone (Figure 24).

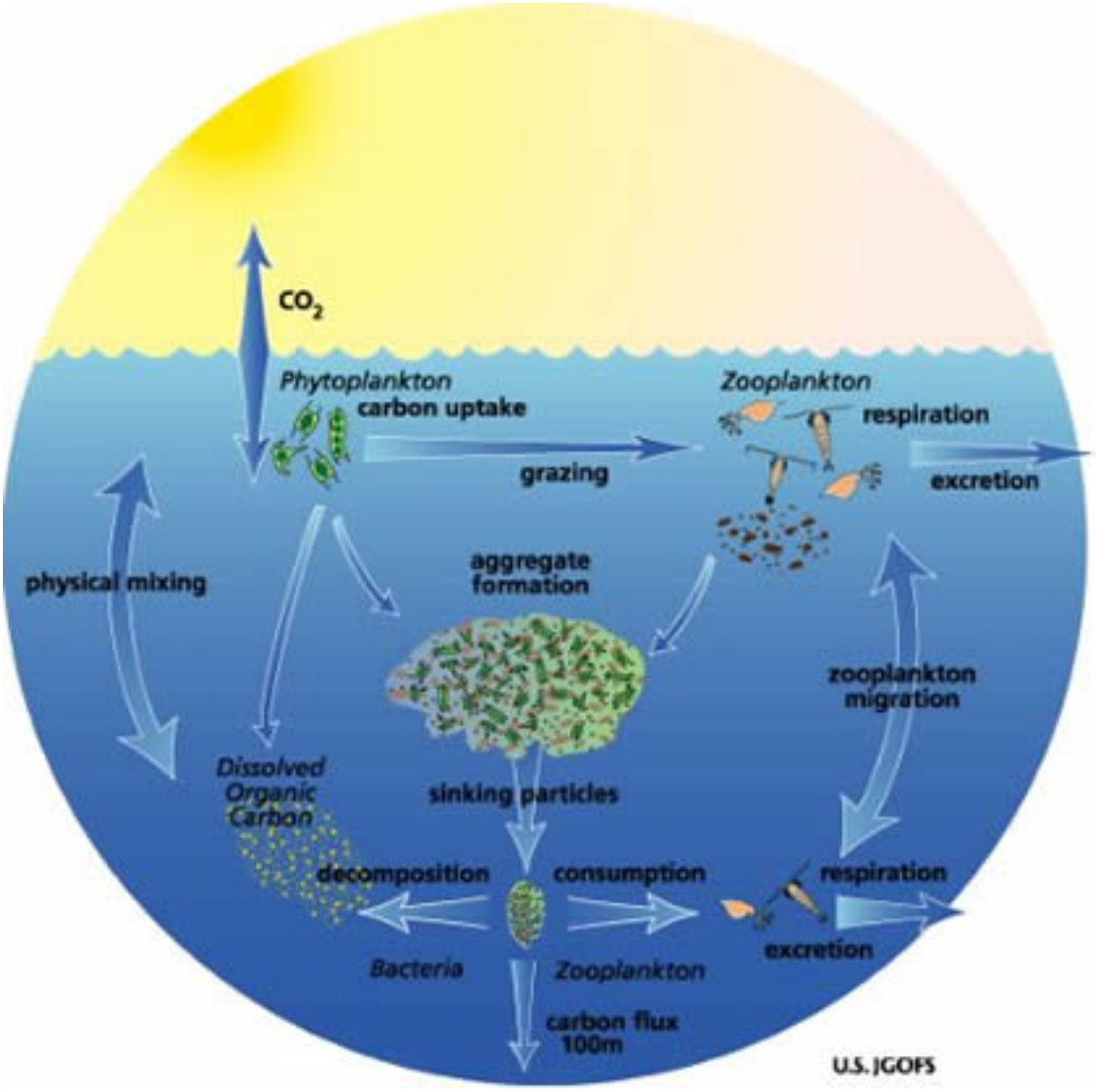

Figure 24. Schéma simplifié de la pompe biologique (http://www.literacynet.org)

Les facteurs majeurs influençant l'intensité de la productivité phytoplanctonique de surface et son export vers le sédiment aux latitudes qui nous intéressent sont la durée de la saison de croissance, la présence de banquise, la stabilité de la colonne d'eau et la disponibilité en nutriments et métaux traces (Arrigo et al., 2008) mais aussi le broutage zooplanctonique, la dégradation bactérienne et les infections virales (Smetacek et al., 2004). Ainsi, la biosphère marine antarctique est étroitement liée aux autres compartiments climatiques des hautes latitudes Sud (cryosphère, atmosphère, océan) qui régulent la longueur de la saison de croissance, et la quantité de nutriment, ainsi que la stratification des eaux.

2.2. Histoire climatique du Continent et de l'Océan Antarctique

2.2.1. Récente : la période instrumentale

L'instrumentation de l'Antarctique a débuté avec l'année Géophysique internationale de 1957 qui a vu l'installation de 48 stations opérationnelles sur le continent. Ces stations ont dès lors fourni des données plus ou moins régulières de vents, de champs de pression et de températures atmosphériques et océaniques. L'acquisition de données fiables et continues de banquise a débuté avec l'avènement des satellites, c'est-à-dire depuis les années 70, bien que des données historiques existent ponctuellement depuis le début du XX^{ème} siècle (de la Mare, 1997). Cependant, les données satellites ne sont vraiment reproductibles qu'à partir des années 80. On a donc un recul de 50 ans sur les conditions climatiques sur le Continent et l'Océan Antarctique et de 30 ans environ en ce qui concerne le couvert de banquise.

2.2.1.1. Tendances climatiques générales

Les tendances climatiques observées montrent :

- un renforcement du vortex circumpolaire et un déplacement vers le Sud ainsi qu'une intensification des westerlies depuis les années 60 (~ 15%) (Kushner et al., 2001 ; Marshall, 2002).

- un réchauffement de l'Océan Austral depuis les années 50, particulièrement accentué au niveau du Courant Antarctique Circumpolaire où le changement des températures océaniques est comparable à celui des températures atmosphériques (Gille, 2002).

- une légère augmentation de l'extension de la banquise sur les 25 dernières années (Rayner et al., 2003 ; Cavalieri et Parkinson, 2008). Cette tendance est inversée dans les mers de Bellingshausen et d'Amundsen (Rayner et al., 2003 ; Cavalieri et

Parkinson, 2008) (Figure 25). Les données antérieures à l'avènement des satellites pourraient montrer un déclin de la banquise dans certaines régions antarctiques depuis les années 50 mais elles sont trop disparates pour dresser une tendance antarctique générale (Rayner et al, 2003 ; IPCC, 2007) (Figure 25).

La tendance des températures de surface atmosphériques en Antarctique fait actuellement débat puisque certaines études montrent :

- un refroidissement global en Est Antarctique et un réchauffement prononcé en péninsule Antarctique qui serait particulièrement accentué en été (Kwok et Comiso, 2002; Thompson et Solomon, 2002 ; Turner et al., 2005).

- un réchauffement moyen sur le continent AA équivalent à celui enregistré au niveau de l'hémisphère Sud qui serait notamment accentué dans la partie Ouest de l'Antarctique (Steig et al., 2009) (Figure 25). Ce réchauffement serait particulièrement prononcé en hiver et au printemps (Steig et al., 2009).

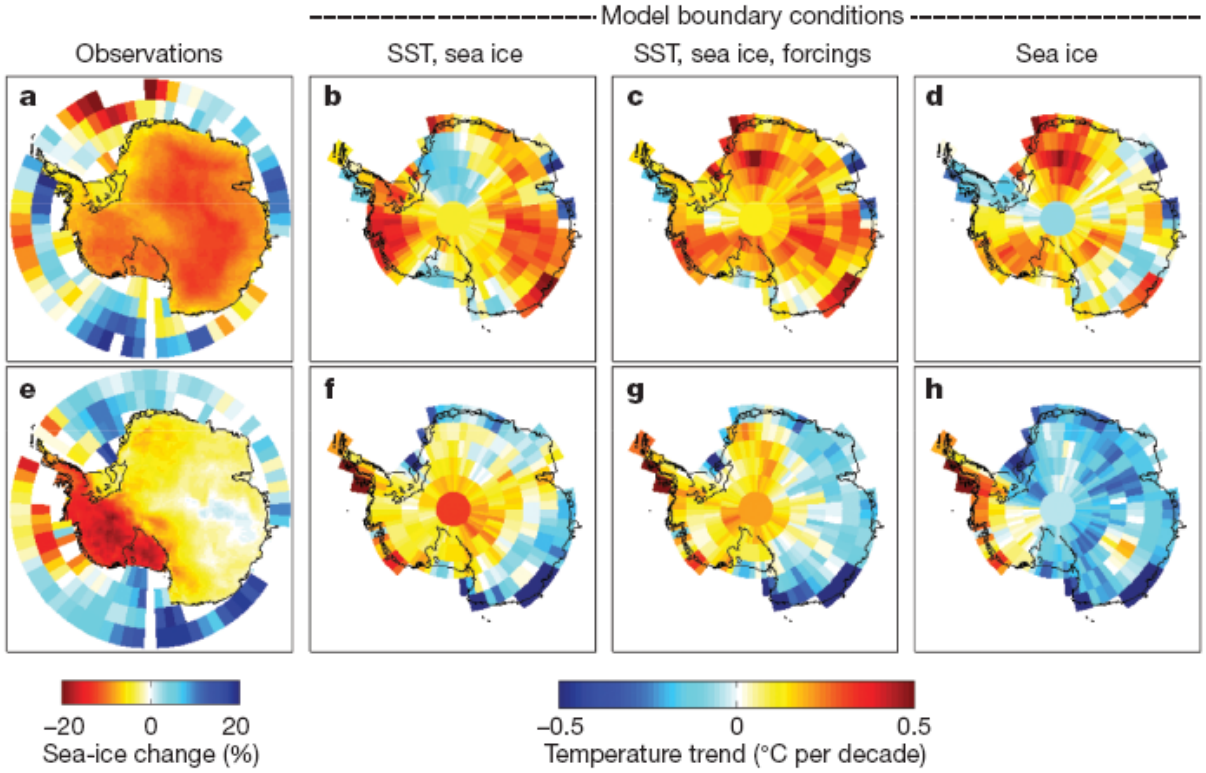

Figure 25. Comparaison des tendances des températures de surface annuelles atmosphériques (°C par décennie) reconstruites et modélisées pour les périodes 1957-1981 (a-d) et 1979-2003 (e-h). a, e, températures de surface atmosphériques reconstruites et variations du couvert de banquise observées (Rayner et al., 2003). b, f, simulations des températures de surface atmosphériques à partir du modèle de la NASA « Goddard Institute for Space Studies (GISS) ModelE atmosphere-only » qui est couplé à un modèle de circulation générale, avec des conditions aux limites de SST et de banquise. c, g, simulations avec les mêmes conditions aux limites plus des forçages atmosphériques (concentrations atmosphériques des espèces actives au niveau radiatif comme l'ozone). d, h, simulations avec l'effet de la banquise seule, d'après Steig et al. (2009).

Un réchauffement concernant exclusivement la Péninsule Antarctique serait attribué à l'isolement du reste de l'Antarctique par le renforcement des westerlies, du aux variations de concentrations en ozone stratosphérique et en gaz à effet de serre (IPCC, 2007). Steig et al. (2009) suggère que cet effet est contrebalancé par des intrusions d'air chaud et humide qui étendraient le réchauffement à toute la partie Ouest Antarctique. Les disparités du réchauffement climatique en Antarctique seraient ainsi fortement modulées par la circulation atmosphérique qui régulerait régionalement le transfert des anomalies climatiques (Steig et al., 2009).

2.2.1.2. Mode de variabilité climatique

Différents modes de variabilité climatique « sévissent » en Antarctique et résultent d'un intime couplage océan-atmosphère-banquise : le modèle Pacifique Sud Américain (PSA), le modèle Stationnaire « wave-3 », le Mode Annulaire Austral (SAM) et l'Oscillation Semi-Annuelle (SAO) (Yuan et Li, 2008) (Table 2, Figure 26). Ces différents modes climatiques se caractérisent par des perturbations à plusieurs échelles de temps (saisonnières, interannuelles, décennales) des champs de vents, de pressions, de températures et de banquise.

	Modèle Pacifique Sud Américain (PSA)	**Modèle Stationnaire "Wave-3" (wave-3)**	**Mode Annulaire Austral (SAM)**	**Oscillation Semi-Annuelle (SAO)**
Champs de surface impliqué	SLP	Banquise, SLP, vents	SLP, vents	Gradients méridiens des SAT et SLP
Caractéristiques	3 anomalies de pressions alternativement centrées sur le Pacifique Sud, les eaux polaires du Pacifique Sud-est et l'Amérique du Sud	Ondes-3 quasi-stationnaires à moyenne latitudes, fortes en hiver, dansant d'Est en Ouest sur un cycle annuel	Anomalie de pressions antiphasées en forme d'anneau entre les latitudes polaires et moyennes	Gradients de température méridien accentué au sud de 50°S au printemps et en automne
Causes dynamiques ou physiques	Train d'onde de Rossby	Distribution aux moyennes latitudes des terres et Océans	Interaction entre les cyclones et les flux atmosphériques moyens	Réchauffement solaire différentiel à moyenne et haute latitude
Tendance linéaire (variations par décennie)	0.175	-0.098	0.346	0.282

Table 2. Description des modes climatiques majeurs aux moyennes et hautes latitudes de l'hémisphère Sud, et de leur tendances générales qui sont significatives à p>0.01, modifié d'après Yuan et Li, 2008. PSA: Pacific South American pattern, SAM: South Annular Mode, SAO: Semi-Annual Oscillation, SLP: Sea Level Pressure, SAT: Surface Atmospheric Temperature.

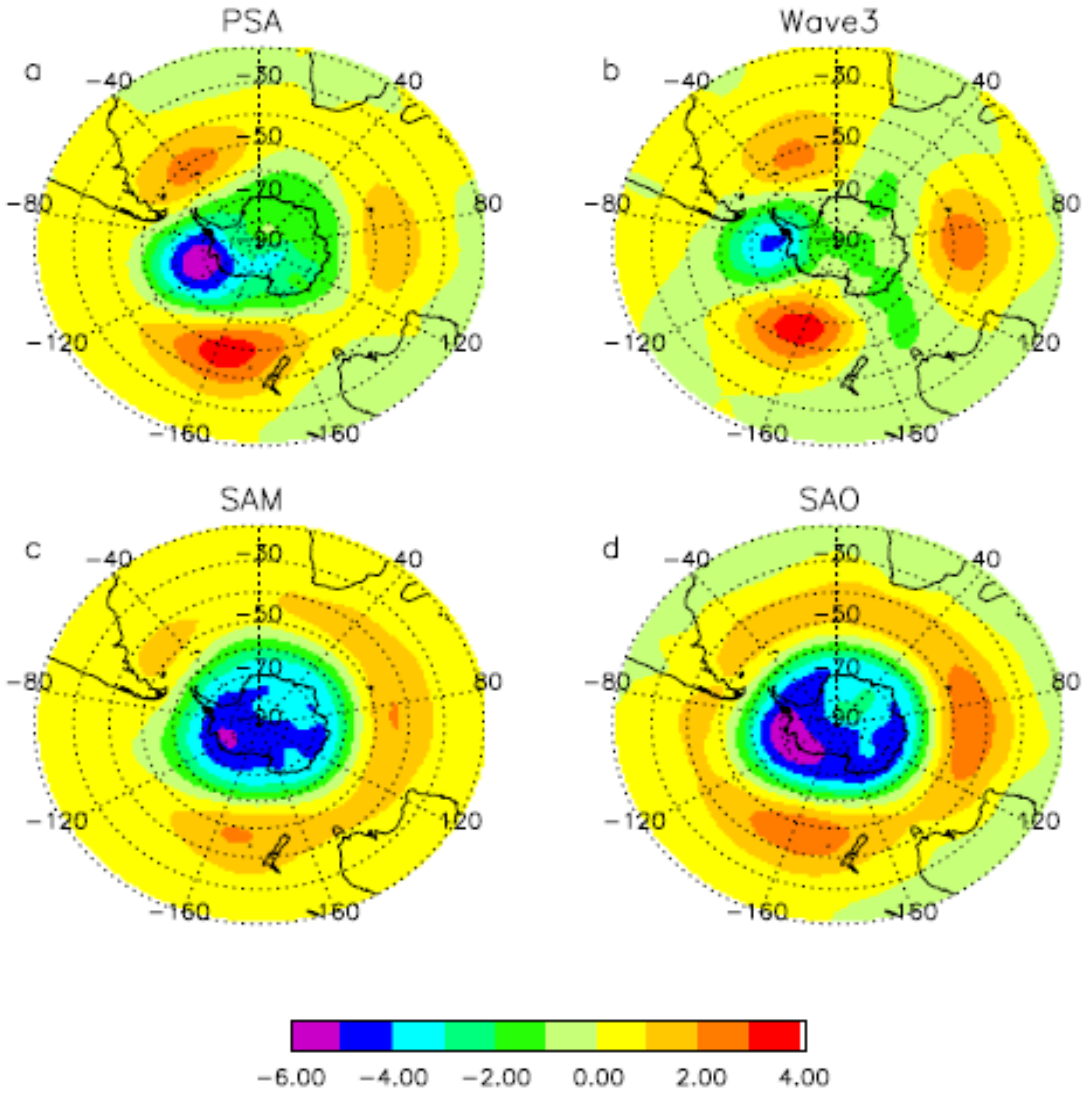

Figure 25. Coefficients de régressions linéaires de (a) PSA, (b) wave-3, (c) SAM, et (d) SAO sur la pression du niveau de la mer. Tous les indices climatiques ont été standardisés avant d'appliquer la régression linéaire. L'unité est 1 mb par unité de déviation standard de chaque indice. Source : Yuan et Li, 2008.

Surimposée à leur variabilité saisonnière, interannuelle, ces modes climatiques montrent des tendances générales sur les dernières décennies avec une augmentation des indices PSA, SAM et SAO et une diminution de l'indice wave-3 (Table 2). L'augmentation de l'indice SAM a été mis en relation avec la diminution de l'ozone stratosphérique (Sexton, 2001; Thompson et Solomon, 2002; Gillett et Thompson, 2003), l'augmentation des gaz à effet de serres (Hartmann et al., 2000; Marshall et al., 2004) et la variabilité de l'ENSO pendant l'été austral (L'Heureux et Thompson, 2006).

Ces modes climatiques, générés indépendamment les uns des autres (Table 2) interagissent entre eux et avec les modes climatiques des basses latitudes comme L'ENSO et rendent ainsi complexe la compréhension du climat Antarctique à ces échelles de temps. Par exemple, la conjugaison des modes PSA et Wave-3 influencent la répartition du couvert de

banquise et induirait un dipôle Antarctique (ADP). Celui s'exprime par des variations interannuelles de la limite d'extension de la banquise et du champ de SST de l'Océan Austral qui sont en antiphases entre la Mer de Amundsen-Bellingshausen (Secteur du Pacifique Centre-Est) et la Mer de Weddell (Secteur Atlantique) (Yuan et Martinson, 2001). PSA et wave-3 peuvent se conjuguer avec l'ENSO ce qui va amplifier ou atténuer les anomalies de banquise par une modification du flux de chaleur méridien dans les différents secteurs de l'Océan Austral (Yuan, 2004 ; Yuan et Li, 2008).

A plus longues échelles temporelles, la tendance positive du PSA conjuguée à l'augmentation de la fréquence et de l'intensité des phénomènes El Niño de l'ENSO serait responsable du déclin de la banquise en Mer de Amundsen-Bellingshausen (Secteur du Pacifique Centre-Est) (Kwok et Comiso, 2002). A l'inverse, la tendance négative du mode « wave-3 » contrebalancerais l'isolement induit par la tendance positive du SAM permettant ainsi un réchauffement étendu à l'Ouest Antarctique (Steig et al., 2009).

Les modifications ainsi engendrées aux hautes latitudes de manière indépendante ou par couplage avec les basses latitudes agiraient en retour sur le climat global par des perturbations de la THC (Oke et England, 2004 ; Meredith et al., 2007), et de la circulation atmosphérique des basses latitudes, notamment l'ENSO (Ivchenko et al., 2004; Blaker et al., 2006).

La prédiction du climat futur en Antarctique et de ses interactions avec les autres régions du globe est encore source d'erreur du fait de cette complexité des modes climatiques, en partie due à la très forte imbrication des compartiments cryosphère-océan-atmosphère (Steig et al., 2009). La compréhension de la composante climatique « banquise » nécessite encore des améliorations autant du point de vue du repérage par satellite (marges d'erreur encore importantes) que de sa paramétrisation dans les modèles (processus de rétroactions encore mal connus) (ICPP, 2007) (Figure 26). L'étude d'enregistrements plus anciens et plus longs tels que l'Holocène pourrait apporter des éléments de réponse pour mieux appréhender les couplages océan-atmosphère-glace et leur incidence sur le climat de l'hémisphère Sud.

2.2.2. Holocène : les archives paléoclimatiques

A l'échelle de l'Holocène, d'importantes disparités paléoclimatologiques et paléocéanographiques existent aussi bien au niveau régional que local. Par exemple, un glacier peut avancer pendant que son voisin se retire, une zone peut subir des courants de fond intenses alors qu'ils sont faibles dans la zone contiguë … Cette complexité est due aux rétroactions régionales ou locales des systèmes cryosphériques (glaciers, ice shelves et banquise), océaniques et atmosphériques qui peuvent accélérer ou retarder les changements climatiques globaux.

Cette apparente disparité régionale peut être artificiellement amplifiée par les problèmes de datation des enregistrements sédimentaires et donc des interprétations paléoclimatiques et paléocéanographiques (problème de matériel, résolution, proxies, calibration, âge réservoir).

Pour clarifier l'état des connaissances actuelles sur la période Holocène en Antarctique nous avons essayé de synthétiser les informations existantes selon les grands secteurs étudiés (Figure 27). Cette synthèse regroupe des enregistrements climatiques sédimentaires (marins ou lacustres) et de glace, dont les sites sont représentés sur la carte ci-après (Figure 28). Néanmoins, le climat Holocène de nombreuses zones côtières reste inexploré en Antarctique (Figure 28). Ainsi, la compréhension des changements océanographiques et climatiques autour du Continent Antarctique au cours de l'Holocène est aujourd'hui encore incomplète même si les études préexistantes permettent de tracer quelques grandes lignes.

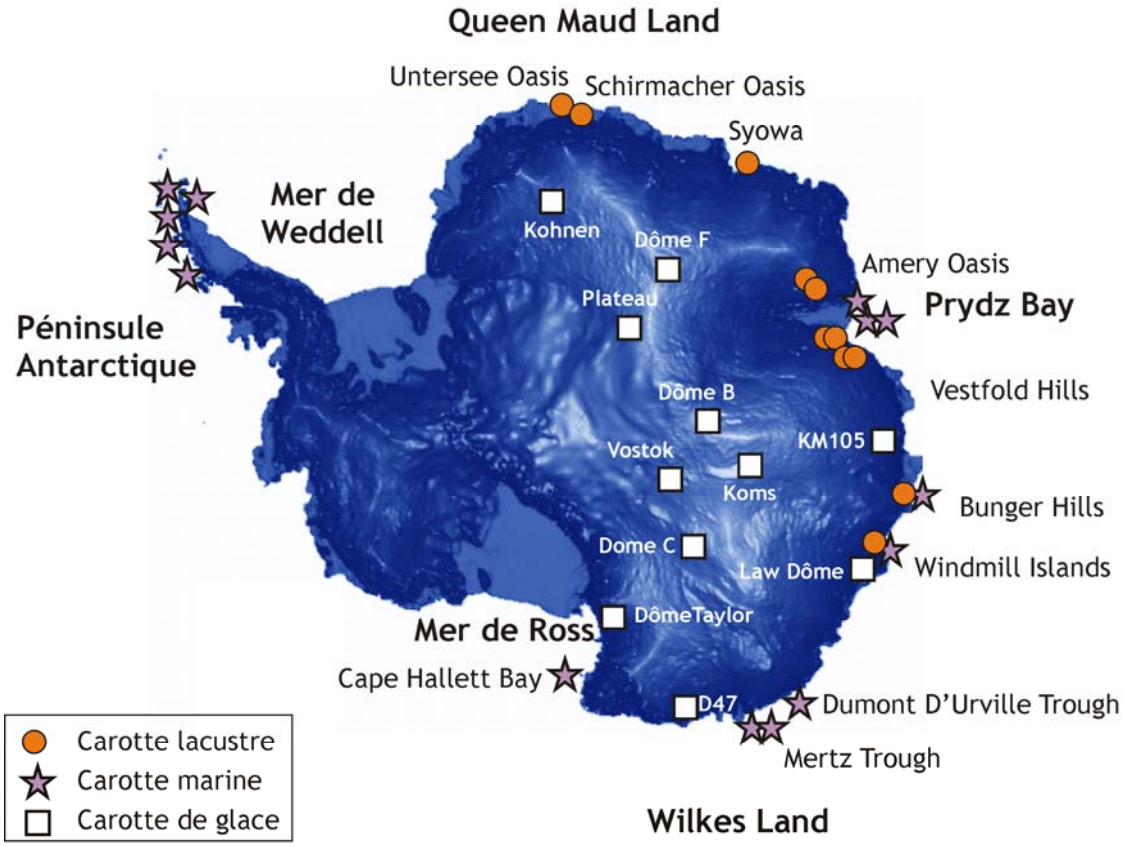

Figure 28. Carte topographique de l'Antarctique avec la location des sites utilisés dans la synthèse bibliographique de la Figure (27).

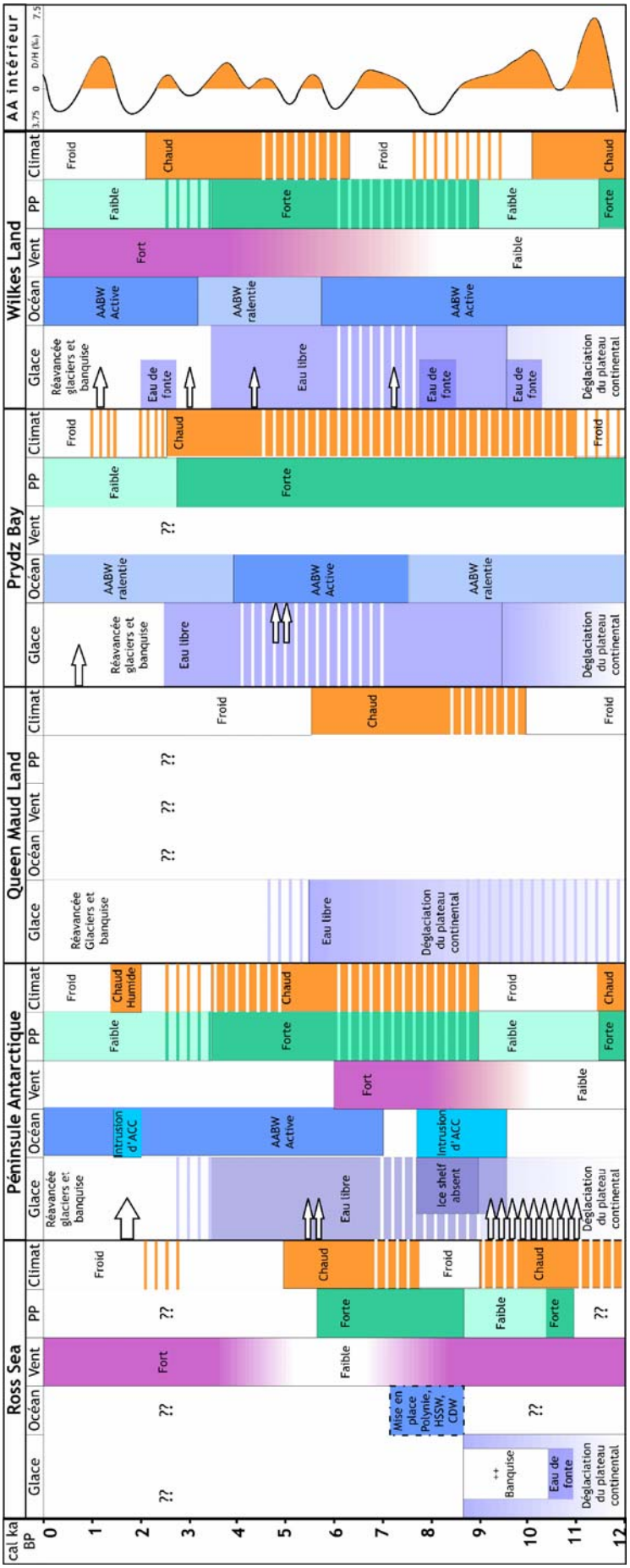

Figure 27. Synthèse des variations Holocène des compartiments : cryosphère (glacier, banquise), océan, atmosphère, biosphère (PP = production primaire) et du climat général, documentés dans les différents secteurs AA (Figure 28) d'après les études antérieures (Ross Sea : Denton et al., 1989 ; Stager et Mayewski, 1997 ; Domack et al., 1999 ; Masson et al., 2000 ; Finocchiaro et al., 2005; Péninsule Antarctique : Sarthein et al., 1994 ; Hjort et al., 1997 ; Brachfeld et al., 2002 ; Yoon et al., 2002 ; Leventer et al., 2002 ; Yoo et al., 2006 ; Smith et al., 2007 ; Queen Maud Land : Schawb, 1998 ; Prydz Bay : Roberts et McMinn, 1996 ; Harris, 2000 ; Taylor et Leventer, 2003 ; Verleyen et al., 2004 ; Wagner et al., 2004 ; Leventer et al., 2006 ; Wilkes Land : Ingólfsson et al.,1998; Harris et al., 2001; Kulbe et al., 2001; Verkulich et al., 2002; Presti et al., 2003; Van Ommen et al., 2004 ; Roberts et al., 2004; Leventer et al., 2006; Crosta et al., 2008) et comparés à une compilation de 11 carottes de glace d'Est AA (Masson et al., 2000). Les dates ^{14}C ka BP corrigées de l'âge réservoir ont été converties en âge calendaire grâce au logiciel Calib 5.0. Les avancées de glaciers sont représentées par les flèches blanches. Les stries blanches ou de couleurs au sein des rectangles représentent les périodes temporelles où les études ne s'accordent pas.

Les tendances climatiques à long terme s'inscrivent bien dans la tendance globale d'un refroidissement Holocène avec un début et un milieu d'Holocène plus chaud que le Tardi-Holocène (Figure 27). La déglaciation des plateaux continentaux internes débute entre 12 et 10 cal ka BP et se prolonge selon les régions jusqu'à 8-6 cal ka BP (Figure 27). La ré-avancée globale et relativement bien synchrone des systèmes glacier et banquise à 4-3 cal ka BP marque l'entrée dans le Néoglaciaire (Figure 27). D'une manière générale, le refroidissement Holocène est associé à un renforcement des vents et une diminution de la paleoproductivité (Figure 27), mais aussi à une augmentation de l'activité des courant de fond, même si cette dernière est encore pauvrement documentée (Figure 27).

Les délais interrégionaux, mis en avant par les données géologiques (Figure 27) pourraient être liés, comme cela a été démontré dans l'Hémisphère Nord (Kaufman et al., 2004 ; Renssen et al., 2005a), avec le rythme de la déglaciation au sein de chaque région.

Surimposée à cette tendance une variabilité millénaire apériodique apparaît nettement dans les températures reconstruites à partir des carottes de glace (Masson et al., 2000) (Figure 27). Cette variabilité est aussi enregistrée dans les séquences sédimentaires par des ré-avancée de glaciers (Figure 27). Cependant, les variations enregistrées dans la glace et dans les sédiments sont difficilement réconciliables. Ce manque de cohérence peut être attribué à un découplage entre le climat intérieur et la côte ou à des problèmes de datation, de résolution et d'effets locaux.

La faible résolution de la plupart des études ne permet pas non plus d'évaluer la rapidité de ces changements ainsi que leurs cyclicités. Néanmoins quelques carottes avec de forts taux de sédimentation ont mis en évidence des périodicités millénaires à centennales qui suggèrent des forçages solaires, océaniques et atmosphériques (Leventer et al., 1996 ; Leventer et al., 2002 ; Nielsen et al., 2004 ; Crosta et al., 2007). Enfin, peu d'études mettent en regard les changements climatiques millénaires et sub-millénaires au sein de chacun des sous-systèmes (cryosphère, atmosphère, océan, biosphère) pour évaluer les connections et rétroactions qui les unissent.

~ Partie 2 : Mise en œuvre ~

1. Séquences marines étudiées

1.1. Localisation géographique des carottes MD03-2601 et JPC24 et cadre environnemental

Notre étude porte sur deux carottes marines : MD03-2601 et JPC24, prélevées sur les marges continentales Est Antarctique, dans le secteur Indien de l'Océan Austral. Les carottes MD03-2601 et JPC24 ont été prélevées en Terre Adélie et en Baie de Prydz où la largeur du plateau continental s'étend sur 120 et 220 km, respectivement (Figure 29). Ces plateaux sont constitués de bancs relativement peu profonds (< 200 m de profondeur) et séparés par des bassins escarpés, reliquats de dépressions glaciaires (Harris et O'Brien, 1998), dont la profondeur est parfois supérieure à 1000 m (De Santis et al., 2003).

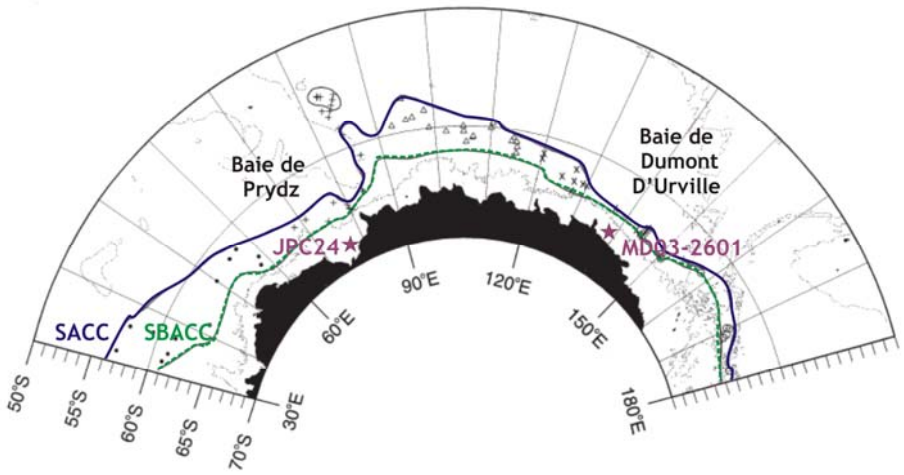

Figure 29. Localisation des carottes MD03-2601 et JPC24 et position du front sud de l'ACC (SACC) et de la frontière limite d'extension sud de l'ACC (SBACC) modifié d'après Orsi et al. (1999). Les lignes bathymétriques, représentant l'isobathe 2500 m, montrent ainsi le pied de pente continentale.

1.1.1. Carotte MD03-2601

La carotte MD03-2601 a été collectée au moyen du carottier Calypso lors de la campagne océanographique MD 130-*Images* X (CADO : Coring Adélie Diatom Oozes) qui s'est déroulée du 23/01 au 17/02/2003 entre la Tasmanie et la Terre Adélie. La carotte MD03-2601 a été prélevée à 66°33.07'S et 138°33.43'E et par 746 m de profondeur dans le bassin de Dumont D'Urville, à environ 55 kilomètres de la côte (Figure 30).

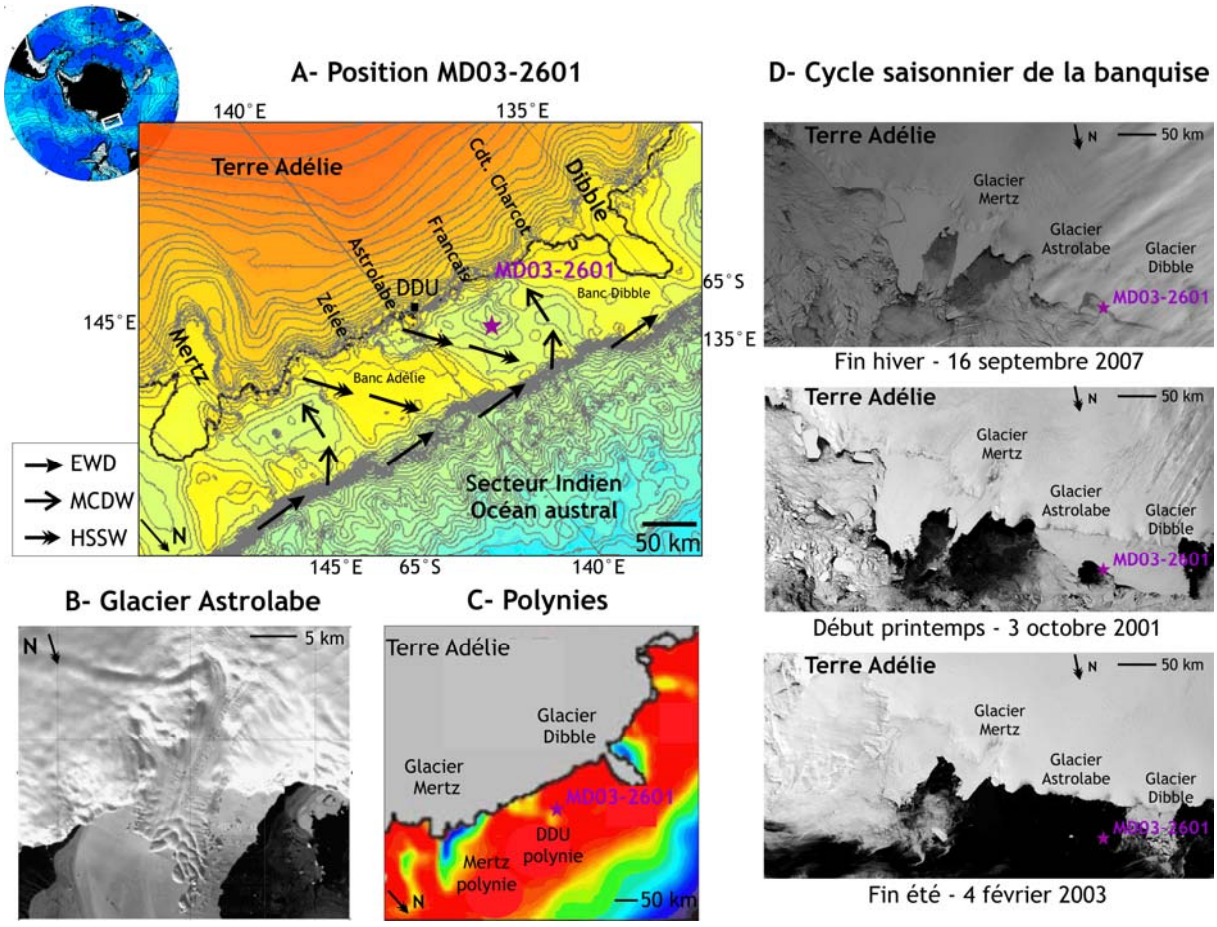

Figure 30. A. Localisation de la carotte MD03-2601 et de la station de Dumont D'Urville (DDU), bathymétrie, altimétrie de la zone, position des glaciers, détail des courants océaniques (EWD: East Wind Drift, MCDW: Modified Circumpolar Deep Water, HSSW: High Salinity Shelf Water) (Données ETOPO2 à partir de http://www.ngdc.noaa.gov/mgg/fliers/01mgg04.html; fond de carte, E. Marchès, 2007). B. Glacier de l'Astrolabe (Image MODIS d'après http://remy.omp.free.fr/FTP/image-satellite-poles/). C. Position des différentes polynies, pérennes entre 1997 et 2001 (Le code couleur représente le % de jour en hiver avec banquise, de 100 % vers 0% du rouge au violet) (Arrigo et van Dijken, 2003). D. Evolution saisonnière du couvert de banquise reconstituée à partir d'images satellites MODIS (http://nsidc.org/data/iceshelves_images/mertz.htlm.).

Le bassin de Dumont d'Urville (DDUT), orienté SE-NW, est composé d'une série de dépressions pouvant atteindre 1000 m de profondeur et séparées par des seuils d'environ 500 m de profondeur. Il est entouré par le banc d'Adélie à l'Est et par le banc de Dibble à l'Ouest. Le DDUT entaille le plateau continental depuis Dumont d'Urville jusqu'à la rupture de pente (Figure 30).

Actuellement, trois glaciers s'écoulent dans la mer de Dumont d'Urville, le Zélée, l'Astrolabe et le Français, situés à 200, 120 et 55 km du site de carottage, respectivement. L'Astrolabe semble à l'heure actuelle le plus « proéminant » (Figure 30). Ces glaciers drainent des bassins versants limités par rapport aux glaciers de Mertz et Dibble, de chaque côté de notre zone d'étude, qui ont une influence majeure sur les eaux adjacentes (Figure 30).

Les eaux côtières de la Terre Adélie sont exposées aux vents catabatiques parmi les plus violents du continent AA (Périard et Pettré, 1993). Ces vents violents participent à la pérennité et à l'étendue des cinq polynies récurrentes qui ont été répertoriées dans cette zone (Massom et al., 1998 ; Arrigo et Van Dijken, 2003 ; Tamura et al., 2008) (Figure 30), dont celle de DDU (66.11°S - 139.31°E) qui est néanmoins la polynie de moindre ampleur dans la région (Adolphs et Wendler, 1995, Arrigo et van Dijken, 2003) (Figure 28). Comme les vents catabatiques sont directement induits par la topographie, nous supposons que la polynie de DDU a été un phénomène persistent tout au long de l'Holocène, possiblement avec des variations d'extension et de persistance annuelle.

Les conditions océanographiques de la région de Wilkes/Mertz, dont fait partie notre zone d'étude, sont influencées par l'action conjuguée de plusieurs masses d'eau (Rintoul, 1998 ; Bindoff et al., 2000a, 2000b ; Williams et Bindoff, 2003) (Figure 30) :

- le Courant Côtier Antarctique ou Est Wind Drift (EWD) qui est un courant de surface entraîné vers l'Ouest par les vents d'Est.
- l'Eau Antarctique de surface (AASW) qui constitue la couche de surface des eaux estivales du plateau continental qui rejoint l'EWD vers l'Ouest (Whitworth et al., 1998).
- l'Eau Circumpolaire Profonde Modifiée (MCDW) qui fait résurgence au niveau de la divergence Antarctique et s'écoule vers le Sud sur le plateau continental.
- les eaux hivernales hautement et faiblement salées (HSSW et LSSW, respectivement) se mélangent avec la MCDW pour former l'Adélie Land Bottom Water (ALBW) qui s'écoule, vers l'Ouest sur le plateau continental et ensuite vers le Nord où elle va se joindre/participer à l'Eau Antarctique de fond (AABW).

Le plateau continental de Terre Adélie a été identifié comme une source importante de l'AABW. Ainsi, la dépression de Mertz pourrait fournir environ 25% de l'AABW (Rintoul, 1998).

Actuellement, le couvert de banquise est présent au dessus du site de carottage de 7 à 9 mois par an à partir de février/mars jusqu'à novembre/décembre (Schweitzer, 1995 ; Arrigo et van Dijken, 2003). L'extension spatiale (jusqu'à 64°S vers le nord) et temporelle (7-9 mois) du couvert de banquise est ainsi limitée en Terre Adélie par la proximité de l'EWD et l'intensité du couplage vents catabatiques/upwellings qui accélère la destruction printanière et retarde la reformation automnale du couvert de banquise (Orsi et al., 1995 ; Schweitzer, 1995 ; Arrigo et van Dijken, 2003).

Le plateau continental de Terre Adélie est riche en macro- et micro- nutriments. Ceux-ci proviennent de différentes sources:

- upwellings de la MCDW (Sambrotto et al., 2003; Coale et al., 2005)
- re-suspension des sédiments du plateau (Fitzwater et al., 2000; Sedwick et al., 2000)

- apports éoliens (Cassar et al., 2007)
- fonte des glaces continentales et de la glace de mer (Sedwick et Ditullio, 1997; Edwards et Sedwick, 2001; Vaillancourt et al., 2003; Lannuzel et al., 2007).

Généralement, les macronutriments ne sont pas considérés comme limitants dans cette zone (Strutton et al., 2000) tandis que les métaux traces tels que le fer peuvent être un facteur limitant de la productivité phytoplanctonique en fin de saison de croissance (Arrigo et al., 2003; Smith et Lancelot, 2004; Smetacek et Nicol, 2005).

En Terre Adélie, la productivité primaire (PP) est moyenne, autour de 25 à 60 gC/m²/an, en comparaison avec les valeurs proches de 150 gC/m²/an, observées en Mer de Ross (Ishii et al., 1998 ; Arrigo et van Dijken, 2003). Au sein des eaux côtières de Terre Adélie, la PP et les types d'assemblages phytoplanctoniques associés sont assez variés en fonction des conditions environnementales (Arrigo et van Dijken, 2003 ; Beans et al., 2008). La production phytoplanctonique consiste principalement en blooms de diatomées intenses au printemps et moins importants durant l'été (Wright et van den Enden, 2000 ; Beans et al., 2008). D'autres organismes phytoplanctoniques sont présents dans cette zone, tels que les Haptophytes, les Prasinophytes, les silicoflagellés et les coccolithophoridés. Ils représentent cependant une fraction plus faible de la biomasse phytoplanctonique en comparaison avec les diatomées (Wright et van den Enden, 2000; Beans et al., 2008).

1.1.2. Carotte JPC24

La carotte JPC24 (Jumbo Piston Core) a été collectée lors de la campagne océanographique NBP0101 (Nathaniel B. Palmer) qui s'est déroulée entre la Terre de Wilkes et le Golfe d'Edward VIII sur la Côte Est Antarctique. La carotte JPC24 a été prélevée à 68°41,637 S et 76°42,712 E par 816 m de profondeur dans la partie Est de la Baie de Prydz, à environ 50 kilomètres de la côte (Figure 31).

La Baie de Prydz, orientée Sud-Nord, est composée dans sa partie interne par la Dépression d'Amery, un large bassin pouvant atteindre 800 m de profondeur (Figure 31). Les entailles majeures de la dépression d'Amery forment le chenal de Prydz à l'Ouest et le chenal de Svenner à l'Est, la carotte JPC24 ayant été prélevée dans ce dernier (O'Brien et Harris, 1996) (Figure 31). La dépression d'Amery est bordée au Sud par l'Amery Ice Shelf, au Nord-Ouest par le banc de Fram, au Nord-Est par le banc de Four Ladies, et s'étend vers le Nord jusqu'au bord du plateau continental (Figure 31). Ces deux bancs sont relativement peu profonds (<200m à certains endroits), et forment une barrière partielle aux échanges de masses d'eaux avec l'océan profond (Smith et Tréguer, 1994) (Figure 31).

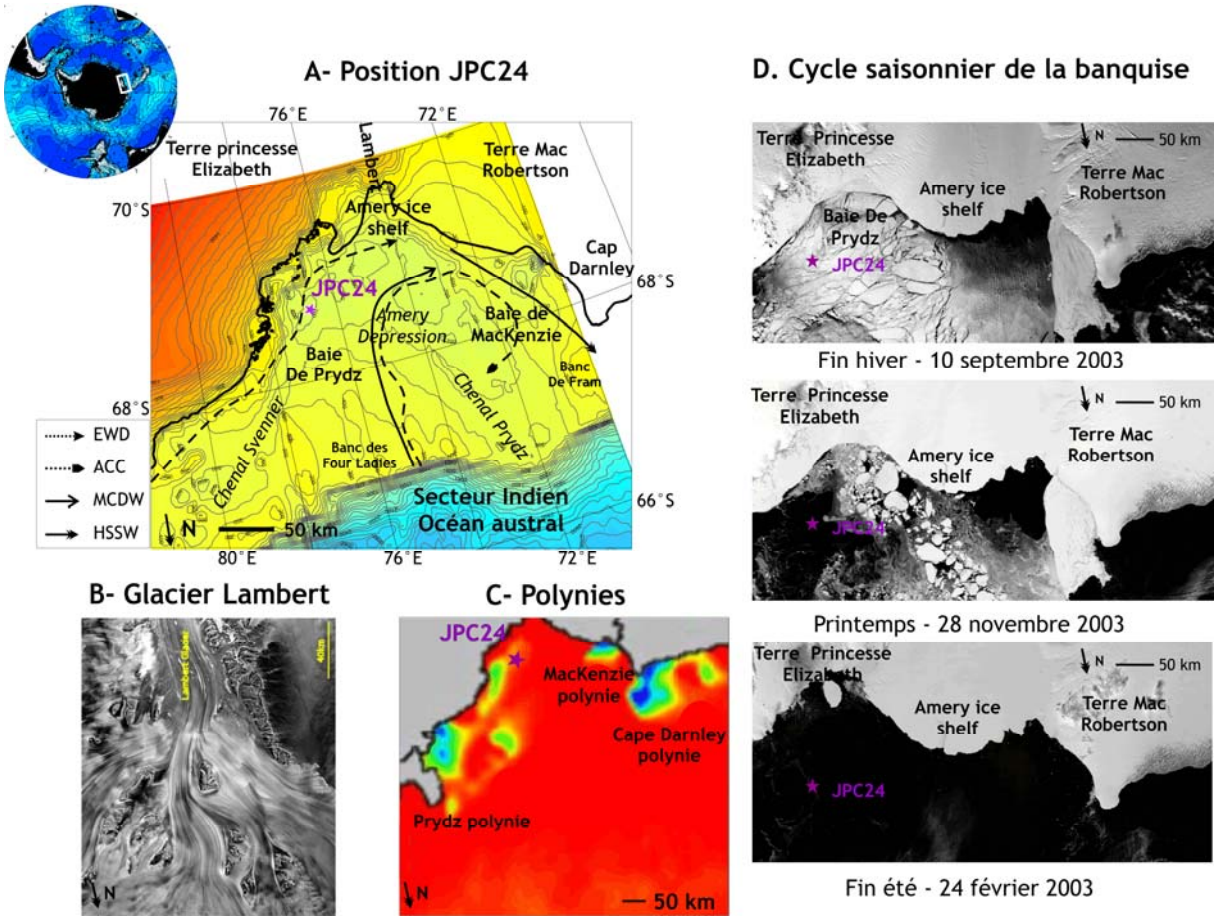

Figure 31. A. Localisation de la carotte JPC24, bathymétrie, altimétrie de la zone, position du glacier Lambert et de l'Amery ice shelf et détail des courants océaniques (WIS : West Ice Shelf, EWD : East Wind Drift, MCDW, Modified Circumpolar Deep Water, HSSW : High Salinity Shelf Water) (Données ETOPO2 à partir de http://www.ngdc.noaa.gov/mgg/fliers/01mgg04.html.; fond de carte, Marchès, 2007).B. Glacier Lambert (http://www.gdargaud.net/Antarctica/MapSatellite/LambertGlacier.jpg). C. Position des différentes polynies, pérennes entre 1997 et 2001 (Le code couleur représente le % de jour en hiver avec banquise, de 100 % vers 0% du rouge au violet) (Arrigo et van Dijken, 2003). D. Evolution saisonnière du couvert de banquise reconstituée à partir d'images satellites MODIS (http://nsidc.org/data/iceshelves_images/amery_aux_images.html.).

Le glacier Lambert, l'un des glaciers majeurs du continent Antarctique, s'écoule dans l'océan via l'Amery Ice Shelf, une gigantesque plateforme de glace qui recouvre les eaux côtières. La limite actuelle de cet « ice shelf » est située à environ 100 km du site de carottage de la carotte JPC24 (Figure 31).

Les eaux côtières de la Baie de Prydz sont aussi soumises à de forts vents catabatiques et de nombreux cyclones. C'est d'ailleurs ici qu'a été enregistré le record de vitesse de vents en Antarctique : 360 km/h (Xie et al., 2002).

Sept polynies récurrentes ont été répertoriées dans cette zone, les deux plus importantes étant situées dans les baies de MacKenzie et Prydz, non loin du site de carottage (Massom et al., 1998 ; Arrigo et Van Dijken, 2003 ; Tamura et al., 2008) (Figure 31).

Les conditions océanographiques de la Baie de Prydz sont influencées par l'action conjuguée des mêmes masses d'eaux que celles précédemment citées (EWD, AASW, MCDW, HSSW, ISW (~LSSW)). Cependant, l'ACC se rapproche davantage des côtes de la Baie Prydz que de celles de la Terre Adélie (Smith et al., 1984; Smith et Tréguer, 1994 ; Wong, 1994 ; Nunes Vaz et Lennon, 1996) (Figure 31). L'AASW résulte du mélange des masses d'eaux apportées par deux courants de surface qui pénètrent dans la baie. D'une part, une gyre cyclonique induite par les vents et la présence même de la baie. La gyre, centrée dans la partie ouest de la baie vers 73°E, aspire une branche de l'ACC qui amène ainsi des eaux « chaudes » à l'intérieur de la baie (Wong, 1994) (Figure 31). D'autre part, un courant de surface côtier provenant du « West Ice Shelf » pénètre à l'Est de la zone et draine des eaux relativement froides et peu salées ainsi que des icebergs (Smith et al., 1984) (Figure 31). L'ASSW se mélange avec les eaux froides et salées au voisinage de l'Amery Ice Shelf et sort de la Baie par le cap Darnley. La MCDW est aussi aspirée par cette gyre cyclonique et fait résurgence dans la baie aux alentours de 75°E (Yakubi et al., 2006) (Figure 31). La MCDW se mélange ensuite avec la HSSW et la ISW (Yakubi et al., 2006). La masse d'eau de fond qui résulte de ce mélange serait assez dense pour s'écouler en dehors du plateau continental et alimenter l'AABW. De nouvelles campagnes océanographiques sont nécessaires pour attester cette hypothèse (Smith et Tréguer, 1994 ; Nunes Vaz et Lennon, 1996 ; Orsi et al., 1999 ; Yakubi et al., 2006).

Actuellement, le couvert de glace de mer en Baie de Prydz est présent durant 9 à 10 mois par an (Smith et al., 1984; Schweitzer, 1995), et peut s'étendre jusqu'à 58°S de latitude (Worby et al., 1998). La baie présente une dichotomie avec : 1) la zone Ouest, qui chaque année est libre de glace durant la saison estivale, et dont la banquise s'évacue par la partie Nord-Ouest sous l'action des courants de surface ; 2) la zone Est, dont la banquise est plus pérenne car maintenue en place par les icebergs transportés vers le Sud par le EWD (Smith et al., 1984). Ainsi, des conditions d'océan ouvert prédominent en général en Février-Mars à l'Ouest alors qu'un couvert de glace de mer puisse persister durant plusieurs années à proximité des côtes Est dans les environnements peu profonds (Gloersen et al., 1992).

Les eaux de surface de la Baie de Prydz sont riches en macronutriments (Tréguer et al., 1988 ; Ishii et al., 1998 ; Gibson et Trull, 1999 ; Zhu et al., 2003). Peu d'études se sont attachées à caractériser la provenance exacte de ces nutriments ainsi que les stocks en métaux traces. Néanmoins, les sources sont potentiellement les mêmes qu'en Terre Adélie, à savoir : l'upwelling, la re-suspension de sédiments, les apports éoliens, et la fonte de la glace continentale et de la banquise. En outre, les apports à l'océan de surface par la fonte du glacier Lambert, qui draine un important bassin versant, et par l'Amery Ice Shelf, qui représente une importante zone de stockage pour les apports atmosphériques, doivent être des sources majeures de micronutriments pour les communautés phytoplanctoniques.

En Baie de Prydz, la productivité primaire (PP) est plus élevée qu'au large de la Terre Adélie, soit autour de 35 à 100 gC/m²/an (Ishii et al., 1998 ; Arrigo et van Dijken, 2003). La production phytoplanctonique en Baie de Prydz résulte principalement d'intenses blooms de diatomées au printemps ainsi que de blooms de moindre intensités en été (Zhu et al., 2003). D'autres organismes phytoplanctoniques sont présents dans cette zone, tels que les Haptophytes, les Prasinophytes, les silicoflagellés, mais ils représentent généralement une fraction plus faible de la biomasse phytoplanctonique en comparaison avec les diatomées (Zhu et al., 2003).

1.2. Description et chronologie des carottes MD03-2601 et JPC24

1.2.1. Carotte MD03-2601

La carotte MD03-2601, d'une longueur de 40,24 m, est constituée majoritairement de boues à diatomées laminées plus ou moins argileuses. Ces lamines présentent pour la plupart une même inclinaison, mise en évidence par l'imagerie RX, qui peut être due au carottage, à une pente naturelle du terrain ou encore à la conjonction de ces deux phénomènes (Annexe 1). La carotte semble très peu perturbée permettant ainsi des reconstructions paléocéanographiques fiables. Toutefois, dans les premiers mètres, les lamines ne sont pas discernables. Ceci peut être dû à des conditions d'oxygénation plus favorables à l'interface eau-sédiment ou au processus de carottage en lui-même (Figure 32).

La chronologie de la carotte MD03-2601 est basée sur 7 datations radiocarbones AMS, retenues parmi les 10 effectuées au Leibniz Laboratory (Kiel, Germany) (Table 3).

Profondeur (cm)	Matériel daté	Age ^{14}C brut (ans BP)	σ (ans)	Age calibré (ans cal BP)	σ (ans)
2	Acide humique	2350	70	1002	151
498	Acide humique	3235	30	1951	92
998	Acide humique	5175	60	4388	179
1440	Météorite	4550		4000	
1498	Acide humique	6135	35	5598	66
1998	Acide humique	6310	100	5782	216
2498	Acide humique	7450	40	7069	122
2998	Acide humique	8775	40	8344	55
3498	Acide humique	9570	50	9348	125
3661	Carbonate	9730	50	9491	77
3998	Acide humique	10855	45	10923	49

Table 3. Dates radiocarbones brutes et corrigées/calibrées de la carotte MD03-2601. Les zones grisées montrent les dates ^{14}C qui ont été écartées de la construction du modèle d'âge.

Pour plus de cohérence, le modèle d'âge a été construit avec les dates obtenues sur le même type de matériel, e.g. les acides humiques de la matière organique décarbonatée. En effet, il peut exister des différences d'âge entre les carbonates et la matière organique, cette dernière fournissant des âges environ 400 ans plus jeune que les âges carbonates dans notre région (Dunbar, communication personnelle, 2005 ; Crosta et al., 2007). Parmi les dates « acides humiques », celles obtenues à 998 et à 1498 cm sortaient franchement du modèle d'âge et ont donc été écartées (Crosta et al., 2007) (Figure 32). Une datation indépendante, à partir d'indices sédimentaires d'un évènement météoritique daté à 4 cal ka BP (Courty et al., 2007), affichait une date parfaitement en ligne avec les autres datations et a appuyé ce choix (Crosta et al., 2007) (Figure 32).

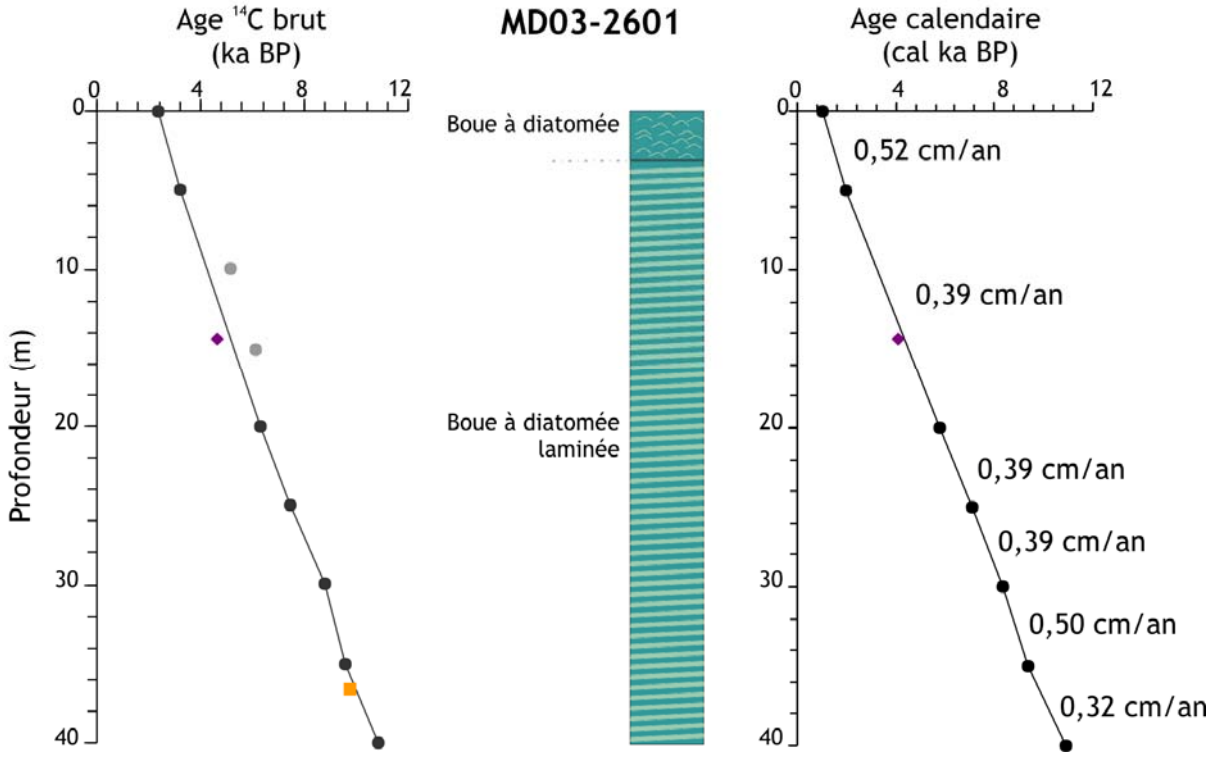

Figure 32. Modèle d'âge et log synthétique de la carotte MD03-2601. Les âges ^{14}C bruts et calendaires, répertoriés dans la table 3, sont figurés par des points noirs pour les acides humiques, par des points gris pour les âges acides humiques non utilisés, par des losanges violets pour l'évènement météoritique, et par un carré orange pour la date carbonate. Les déviations standards des datations sont de même dimension que les symboles utilisés. Les taux de sédimentation, calculés à partir du modèle d'âge, sont notés à droite de la figure.

Les dates ^{14}C brutes ont été corrigées d'un âge réservoir de 1300 ans, comme il est conseillé de procéder en Antarctique de l'Est (Ingólfsson et al., 1998). Les dates ainsi corrigées ont été calibrées avec le logiciel Calib 5.0 (Stuiver et al., 2005) et la calibration Marine04 (Hughen et al., 2004) pour les convertir en âges calendaires. La carotte marine MD03-2601 semble donc enregistrer la période Holocène comprise entre 1 et 11 cal ka BP avec un taux de sédimentation moyen de 0,4 cm/an (Figure 32).

1.2.2. Carotte JPC24

La carotte JPC24, d'une longueur de 17,35 m, est aussi constituée majoritairement de boues à diatomées laminées plus ou moins argileuses (au-dessus de 15,76 m), puis d'une partie caractérisée par du sable gris argileux, faciès caractéristique de la dernière période glaciaire, appelé diamicton (au-dessous de 15,80 m) (Figure 33). La limite entre ces deux faciès est peu épaisse, et se distingue par une dizaine de paires de lamines rouges entre 15,80 m et 15,58 m (Leventer et al., 2006) (Figure 33). Peu perturbée, cette carotte est aussi adaptée à une étude paléocéanographique haute résolution.

La chronologie de la carotte JPC24 est basée sur 7 datations radiocarbones AMS parmi les 8 disponibles, analysées au Lawrence Livermore National Laboratory Center for Accelerator Mass Spectrometry (Livermore, USA) (Table 4). Elles ont été obtenues sur les acides humiques de la matière organique décarbonatée, et sur les carbonates quand ils étaient présents dans le sédiment (coquilles et bivalves).

Profondeur (cm)	Matériel daté	Age ^{14}C brut (ans BP)	σ (ans)	Age calibré (ans cal BP)	σ (ans)
2.5	Acide humique	2020	50	693	83
746	Carbonate	8840	35	8417	82
840.5	Acide humique	10060	60	9942	529
891	Carbonate	9242	40	8955	120
924	Carbonate	9395	35	9146	138
1312	Carbonate	10325	35	10288	109
1350	Carbonate	10315	50	10285	131
1576	Extrapolation	10931	-	11069	139
1743.5	Acide humique	26960	680	Non calibré	-

Table 4. Dates radiocarbones brutes et corrigées/calibrées sur la carotte JPC24. La zone grisée montre la date ^{14}C qui a été écartée du modèle d'âge.

Une extrapolation linéaire entre les 5 dates ^{14}C, issues des carbonates, a permis de déterminer un âge pour la limite entre le diamicton et la boue à diatomée à 1576 cm (Table 4, Figure 33). En effet, la différence de sédimentation entre la dernière période glaciaire, lorsque le plateau continental était largement englacé à cause de l'avancée de l'inlandsis antarctique, et l'Holocène, soumis à un cycle saisonnier de la banquise, ne permet pas de relier la date à 1350 cm avec celle du diamicton à 1743,5 cm par un taux de sédimentation constant (Table 4; Figure 33).

Pour calculer l'âge réservoir à appliquer aux âges bruts, nous disposions d'une carotte voisine (KC24) qui a préservé l'interface eau/sédiment (Leventer, communication personnelle, 2006). L'âge du sommet de la carotte KC24 a été calculé à 1280 ans ^{14}C, et a donc été retenu comme âge réservoir de la zone. Cette valeur, en très bon accord avec

l'âge réservoir moyen préconisé pour les zones côtières antarctiques, a été utilisée pour corriger les âges bruts. Enfin, les âges corrigés ont été calibrés de la même façon que ceux de la carotte MD03-2601. La carotte marine JPC24 enregistre donc la période Holocène comprise entre 0,6 et 11,1 cal ka BP avec un taux de sédimentation moyen de 0,25 cm/an (Figure 33).

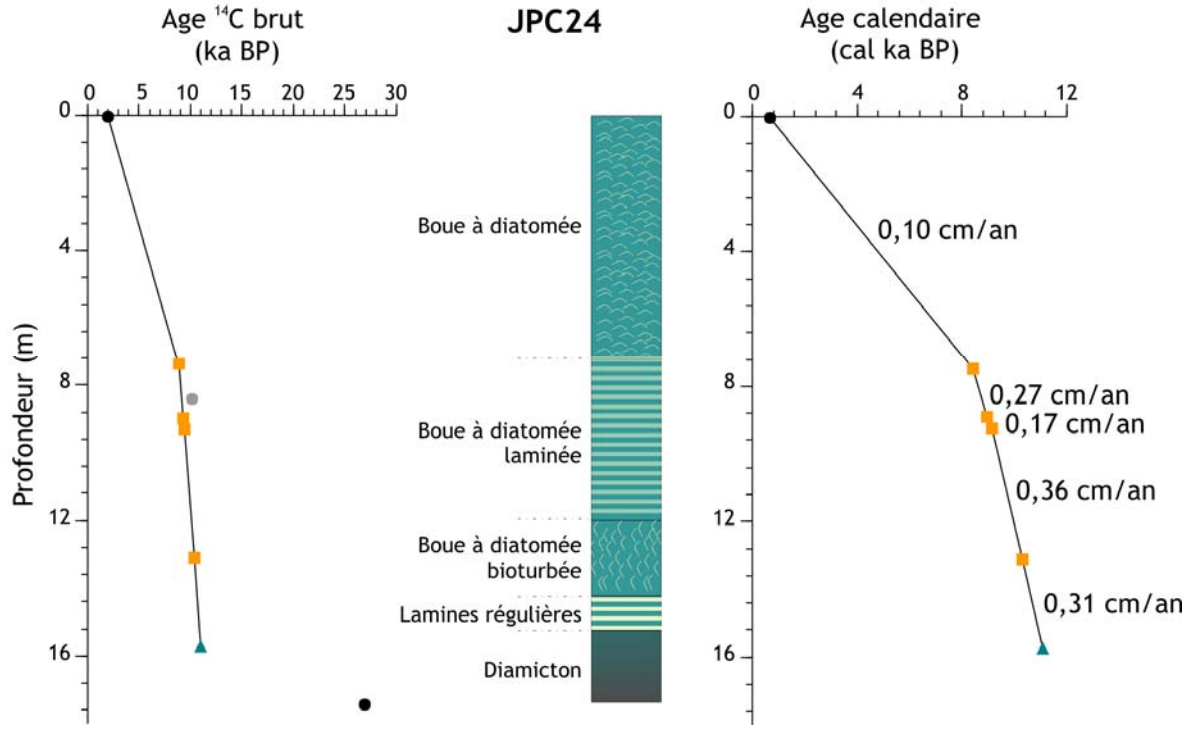

Figure 33. Modèle d'âge et log synthétique de la carotte JPC24, modifié d'après Barbara (2008). Les âges ^{14}C bruts et calendaires, répertoriés dans la table 4, sont figurés par des points noirs pour les âges acides humiques, par des points gris pour les âges acides humiques non utilisés, par des carrés orange pour les âges carbonates et par un triangle vert pour l'âge extrapolé. Les déviations standards des datations sont de même dimension que les symboles utilisés. Les taux de sédimentation, calculés à partir du modèle d'âge sont notés à droite de la figure.

Ainsi en dépit des erreurs associées aux datations (disparité des matériaux sources, estimation et évolution de l'âge réservoir au cours de l'Holocène), les deux enregistrements marins MD03-2601 et JPC24 couvriraient la même période de temps avec des taux de sédimentation du même ordre de grandeur. Les tendances Holocène de l'évolution des abondances relatives de la diatomée *Fragilariopsis curta*, une des espèces dominantes inféodées à la banquise, sont relativement synchrones dans les deux carottes et en accord avec d'autres reconstitutions du couvert de banquise Holocène (Hodell et al., 2001 ; Nielsen et al., 2004 ; Iizuka et al., 2008) (Figure 34). Ceci nous conforte dans la validité des modèles d'âge des deux carottes. La carotte JPC24 enregistre cependant la fin de la dernière période glaciaire qui manque dans la carotte MD03-2601.

Les carottes MD03-2601 et JPC24 permettent donc une étude comparative de la variabilité climatique Holocène en Terre Adélie et en Baie de Prydz avec une résolution décennale (cf. Chapitre 4).

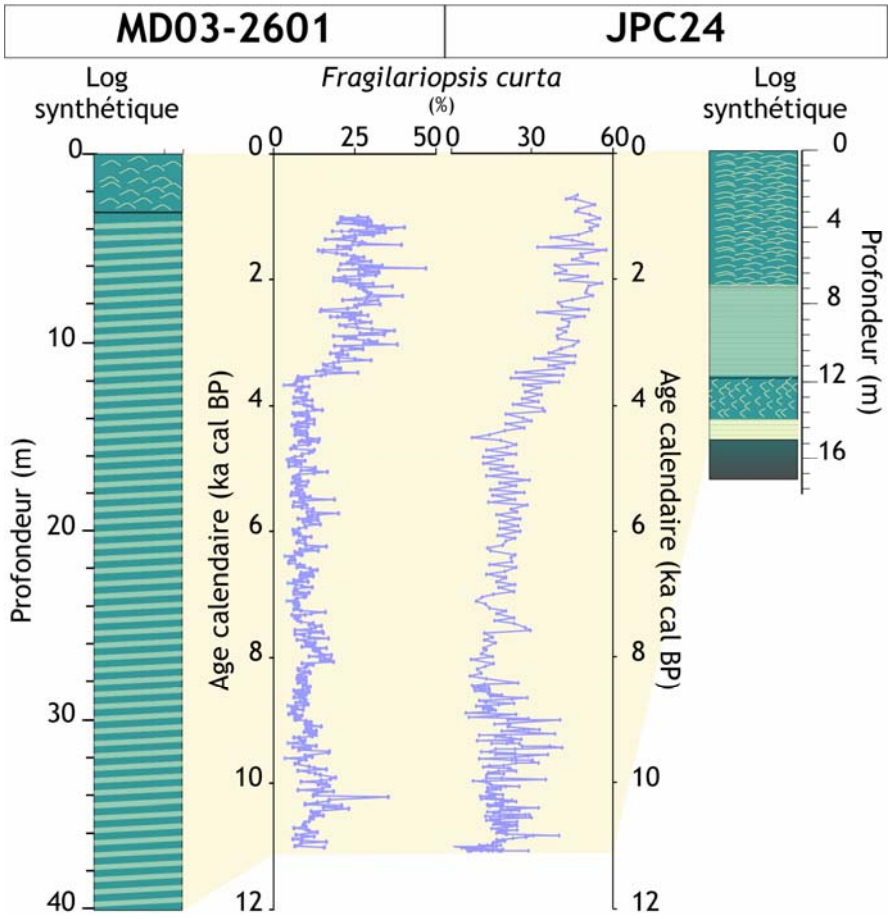

Figure 34. Log synthétique des carottes MD03-2601 et JPC24 en fonction de la profondeur et abondances relatives de l'espèce *Fragilariopsis curta* des carottes MD03-2601 et JPC24 en fonction de l'âge. La zone beige indique les séquences communes à ces deux enregistrements sédimentaires.

2. Outils utilisés et stratégies d'échantillonnage

La carotte MD03-2601 a fait l'objet d'une approche multi-proxies, visant à documenter précisément les conditions de sédimentation ainsi que l'ensemble des compartiments climatiques : cryosphère, atmosphère, océan et biosphère marine (cf. Chapitre 2 et 3).

Le travail effectué sur la carotte JPC24 s'insère dans un projet en collaboration avec l'Université de Colgate aux Etats-Unis. Dans ce cadre, notre contribution constituait à documenter les conditions de surface au moyen des outils micropaléontologique (e.g. les diatomées) et biomoléculaire (e.g. les HBis). Les proxies développés par les autres collaborateurs (taille des grains, susceptibilité magnétique, géochimie isotopique) ne sont pas encore disponibles et feront l'objet de publications ultérieures.

Ainsi, dans le cadre de cette thèse, les deux carottes marines MD03-2601 et JPC24 seront comparées sur la base de leurs proxies communs (e.g. diatomée et HBi) afin d'étudier la cohérence de la variabilité climatique Holocène des conditions de surface en Est Antarctique (cf. Chapitre 4).

En outre, en collaboration avec Hans Renssen de l'Université d'Amsterdam, nous avons obtenu des sorties de modèles des derniers 9000 ans, spécifiques au deux zones étudiées, qui seront utilisées dans les chapitres 2, 3 et 4 ainsi que dans l'article complémentaire n°3. Les caractéristiques, limites et applications du modèle ECBilt-CLIO-VECODE sont expliquées ci-après.

Au cours de cette thèse, j'ai été amenée à interpréter des données produites par d'autres collaborateurs et à produire des données utilisées par d'autres collaborateurs qui ne sont pas intégrées dans ce travail. Afin de ne pas perdre le lecteur, j'ai synthétisé le travail effectué par chacun des collaborateurs du projet dans les tables 5 et 6. Les principes et applications de chacun des proxies utilisés y sont aussi exposés ainsi que les détails des analyses effectuées (matériel, méthode, nombre d'échantillons).

Nous détaillerons donc dans un premier temps les outils communs aux deux carottes marines puis le panel de proxies supplémentaires utilisés sur la carotte MD03-2601.

Carotte marine	Proxies	Paramètres étudiés	Laboratoire	Matériel d'analyse	Précision	Nb Ech	Résolution cm	Résolution ans	Opérateur préparation	Opérateur analyse
MD03-2601	Diatomées	Conditions de surface	Bordeaux, France	Microscope	_	528	4 à 8	10 à 20	O.Ther	X.Crosta
	HBi	Banquise	Plymouth, UK	Chromatographe	5%	135	32	80	G.Massé	G.Massé
	Radionucléides	Sédimentation verticale et latérale	Bordeaux, France	Spectromètre Alpha	4,9 %	65	66	165	**D.Denis**	**D.Denis**
	Grains détritiques	Intensité des courants de fond	Bordeaux, France	Microscope digital	2 à 9 %	101	40	100	B.Martin	**D.Denis**
	$\delta^{15}N$	Utilisation relative des nutriments	Bordeaux, France	Spectromètre IRMS	0.25 ‰	607	4 à 8	10 à 20	J.Crespin	J.Crespin
	C_{org} et N_{org}	Sédimentation biogénique	Bordeaux, France	Analyseur élémentaire	0.03 et 0.01 %	607	5 à 8	10 à 20		
	Opale	Sédimentation biogénique	Bordeaux, France	Spectrophotomètre	1%	127	32	80	P-D.Fortin	P-D.Fortin
	Métaux	Sédimentation détritique, anoxie	Edimbourg, UK	Spectromètre RX	0.05 à 6 %	127	32	80	D.Carson	D.Carson
JPC24	Diatomées	Conditions de surface	Bordeaux, France	Microscope	_	218 131	5	20	**D.Denis**/O.Ther	**D.Denis**/L.Barbara
	HBi	Banquise	Bordeaux, France	Chromatographe GC-SD	5%	244	8	32	L.Barbara	L.Barbara

Table 5. Détail des analyses effectuées et utilisées pendant la thèse sur les carottes MD03-2601 et JPC24. « Ech » signifie échantillon.

Carotte marine	Raisons	Proxies	Méthode d'analyse	Matériel d'analyse	Laboratoire	Nombre Ech	Opérateur
MD03-2601	**Nombre d'Ech insuffisant**	Argiles	Bout-Roumazeilles et al., 1999	Diffractomètre	Lille, France	48/120	V.Bout-Roumazeilles
KC09	**Pas de datations**	Diatomées	Rathburn et al., 1997	Microscope	Bordeaux, France	45	**D.Denis**
		Radionucléides	Anderson and Fleer, 1982	Spectromètre Alpha	Bordeaux, France	4	**D.Denis**
		$\delta^{15}N$ et $\delta^{13}C$	Crosta et al., 2005	Spectromètre IRMS	Bordeaux, France	44	**D.Denis**
		C_{org} et N_{org}	Crosta et al., 2005	Analyseur élémentaire	Bordeaux, France	44	**D.Denis**
MD03-2603	**Pas Holocène**	Radionucléides	Anderson and Fleer, 1982	Spectromètre Alpha	Bordeaux, France	19	**D.Denis**
VC243	**Pas de datations**	Décarbonatation en vue des isotopes			Bordeaux, France	272	**D.Denis**

Table 6. Détail des analyses effectuées et non-exploitées dans cette thèse sur les carottes MD03-2601, KC09, MD03-2603 et VC243. « Ech » signifie échantillon.

2.1. Outils communs à la MD03-2601 et à la JPC24

2.1.1. Diatomées

Les diatomées, ou Bacillariophycées, sont des algues unicellulaires microscopiques appartenant à l'embranchement des Chromophytes. Les diatomées colonisent pratiquement tous les milieux aquatiques et sont à la base de chaînes alimentaires florissantes, tant dans les océans que dans les lacs ou les rivières. La diversité spécifique des assemblages de diatomées est très riche sur les plateaux continentaux antarctiques (Leventer, 1991, 1992 ; Armand et al., 1995) et particulièrement dans nos deux zones d'étude puisque l'on a rencontré environ 50-60 espèces avec, en moyenne, une trentaine d'espèces différentes dans chaque échantillon (Figure 35). De plus, les frustules de diatomées sont particulièrement bien préservés dans le sédiment, ce qui a permis une identification précise jusqu'à l'espèce. Dans ce cadre, l'outil micropaléontologique permet d'appréhender les conditions de surface (température de surface, couvert de banquise, longueur de la saison de croissance, stratification de la colonne d'eau, pool de nutriments) ainsi que les conditions d'exportation et de préservation à l'interface eau-sédiment. Les diatomées présentent une variété de préférences écologiques et de stratégies adaptatives relativement bien connues et spécifiques à chaque espèce (cf. Crosta et Koç, 2007) qui, une fois appliquées aux assemblages fossiles, permettent de reconstituer les paléo-environnements selon le principe de l'actualisme.

On distingue dans les eaux antarctiques côtières (Figure 35):

- Les espèces benthiques, néritiques, qui sont strictement inféodées à la banquise des zones très côtières. Elles peuvent se développer dans la partie supérieure de la glace où filtre encore une partie de l'énergie lumineuse incidente, indispensable à ces organismes photosynthétiques. Elles peuvent aussi se développer dans la partie inférieure de la glace quand la luminosité est suffisante. Elles appartiennent le plus souvent à l'ordre des Pennales, de type raphidé, et représentent un faible pourcentage des espèces préservées dans le sédiment de nos deux carottes. Parmi elles, les genres que l'ont retrouve le plus fréquemment dans nos échantillons sédimentaires sont : *Navicula*, *Cocconeis*, *Banquisa*, et *Diploneis* (Figure 35).

- Les espèces pélagiques associées à la banquise qui ensemencent les eaux adjacentes dès la fonte printanière de la banquise. Ces espèces sont donc caractéristiques d'eaux froides, dessalées, très stratifiées et riches en nutriments. Elles présentent le plus souvent des taux de croissance rapides et des besoins en nutriments assez élevés, d'où leur surnom de « bloomers ». Les espèces dominantes dans nos échantillons sédimentaires sont les *Fragilariospsis curta* et *F. cylindrus*, et les spores de *Chaetoceros Hyalochaete* sp. (Figure 35).

- Les espèces dites d'océan ouvert qui se développent dans des eaux plus chaudes, libres de glace, le plus souvent en été. Ces espèces sont caractéristiques d'une thermocline profonde mais d'eaux néanmoins bien stratifiées. Elles présentent le plus souvent des taux de croissance plus lents et des besoins en nutriments moins élevés. Les espèces dominantes dans nos échantillons sédimentaires sont : *F. kerguelensis*, *F. rhombica* et *Thalassiosira lentiginosa* (Figure 35).

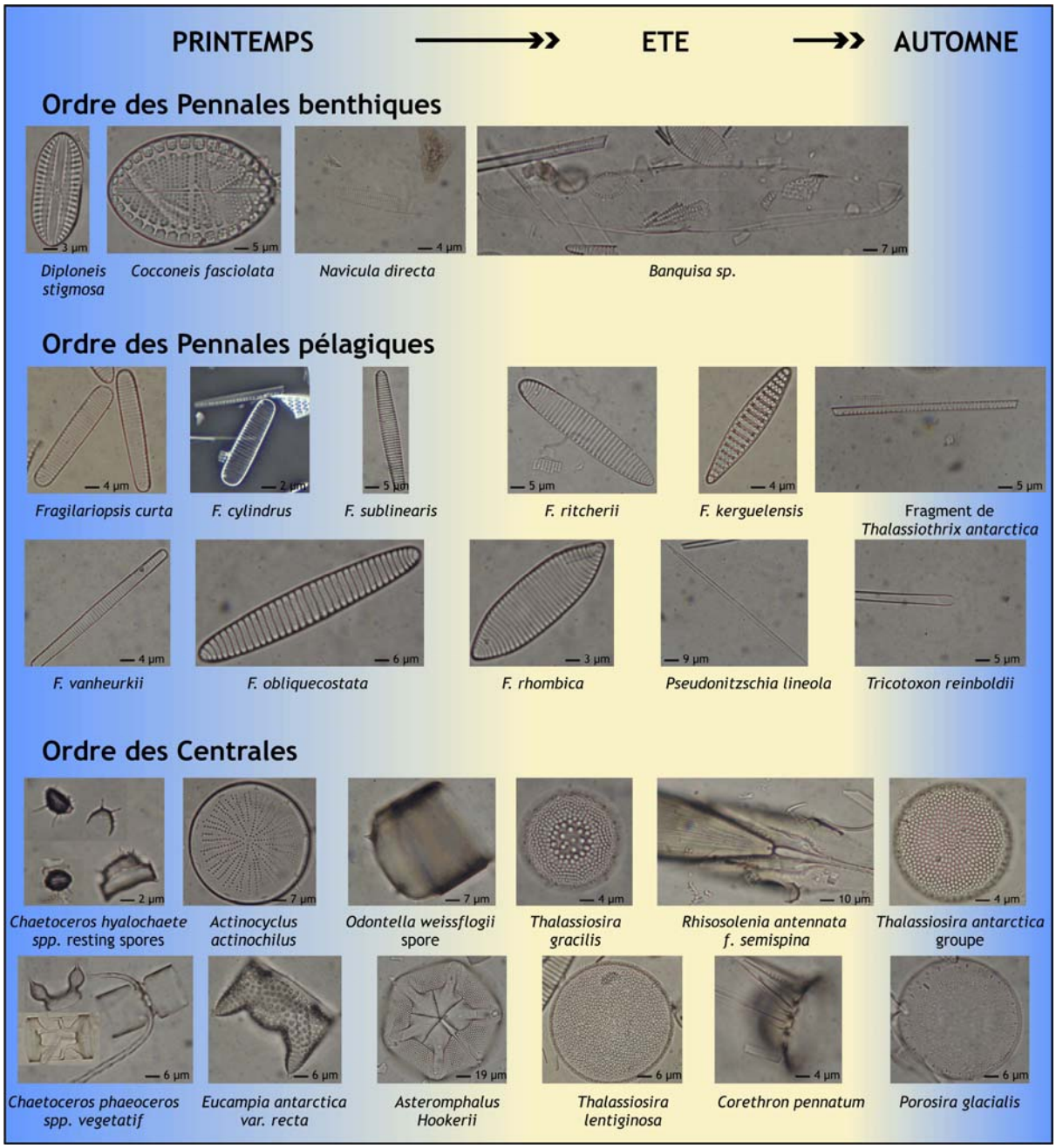

Figure 35. Principales espèces de diatomées des côtes antarctiques en fonction de leur classification et de leur préférence écologique saisonnière. Les photos ont toutes été prises à partir d'un microscope optique par X. Crosta, à l'exception de la photo de l'espèce *F. cylindrus* prise par E. Maddison sur microscope électronique à balayage.

- Les espèces caractéristiques de la saison automnale qui est marquée par le retour de la banquise et d'un régime de vent actif. Ces espèces sont donc caractéristiques d'eaux plus froides, plus salées et plus mélangées. On retrouve notamment les groupes : *T. antarctica* et *Porosira glacialis* ainsi que des espèces filamenteuses : *Thalassiothrix antarctica* et *Tricotoxon reinboldii* (Figure 35).

- Les espèces ubiquistes, dont les préférences écologiques sont encore mal connues. Elles peuvent se développer tout au long de la saison et leur développement est probablement davantage lié à la profondeur de mélange de la colonne d'eau et à l'abondance en nutriments, plutôt qu'à des conditions particulières de température et de couvert de banquise. On peut citer par exemple : *Corethron pennatum*, le groupe des *Rhizosolenia* sp. et des *Proboscia* sp. (Figure 35).

Les techniques utilisées pour l'analyse des diatomées, le traitement du sédiment, et la préparation des lames, sont celles décrites dans Rathburn et al. (1997) (Annexe 2). Le protocole permet la concentration et la dispersion des valves de diatomées par la dissolution des carbonates et l'oxydation de la matière organique. Les diatomées sont ensuite fixées entre lames et lamelles. Les méthodes d'identification et de comptage des diatomées se réfèrent à Schrader et Gersonde (1978) et Laws (1983), complétées par Crosta et Koç (2007). Chaque lame (3 par échantillon), observée par microscope Olympus BH-2 avec une magnification de 1250, a été traversée horizontalement jusqu'à atteindre le nombre de 300-350 valves de diatomées. Seules les valves au moins à demi intactes sont comptabilisées afin d'éviter de recenser le même spécimen deux fois. Pour les espèces allongées (i.e., *Trichotoxon* sp., *Thalassiothrix* sp., *Pseudonitzschia* sp.), seules les extrémités des valves ont été comptées puis divisées par deux, sachant que deux extrémités représentent une valve (Figure 35). Les diatomées ont été identifiées au niveau de l'espèce ou du groupe d'espèces, et l'abondance relative de chaque espèce a été déterminée comme la fraction de l'espèce sur l'assemblage total de diatomées de chaque échantillon.

2.1.2. Highly Branched isoprenoids

Les Highly Branched isoprenoids (HBi) sont des alcènes que l'on retrouve au sein des sédiments des régions Arctique et Antarctique. Ces composés lipidiques à chaîne carbonée de type C25 sont synthétisés par un nombre restreint de diatomées telles que *Haslea* sp., *Rhizosolenia* sp., *Pleurosigma* sp. et quelques *Navicula* sp. (Volkman et al., 1994; Massé et al., 2004; Sinninghe-Damsté et al., 2004) et vont sédimenter en même temps que la cellule pour se retrouver piégés dans les sédiments. Ils sont probablement produits dans les chloroplastes (Massé et al., 2004) mais, actuellement, leur rôle dans la cellule est méconnu.

Dans la nature, on peut rencontrer différents degrés d'insaturation des chaînes carbonées C25. Rowland et al. (2001) ont démontré que le nombre de doubles liaisons de la molécule co-varie avec la température. La forme di-insaturée C25:2 (Diène) n'est synthétisée que par des diatomées vivant en étroite relation avec la banquise (Johns et al., 1999) tandis que la forme tri-insaturée C25:3 (Triène) est produite par les diatomées phytoplanctoniques vivant dans des conditions d'océan ouvert (Belt et al., 2000) (Figure 36).

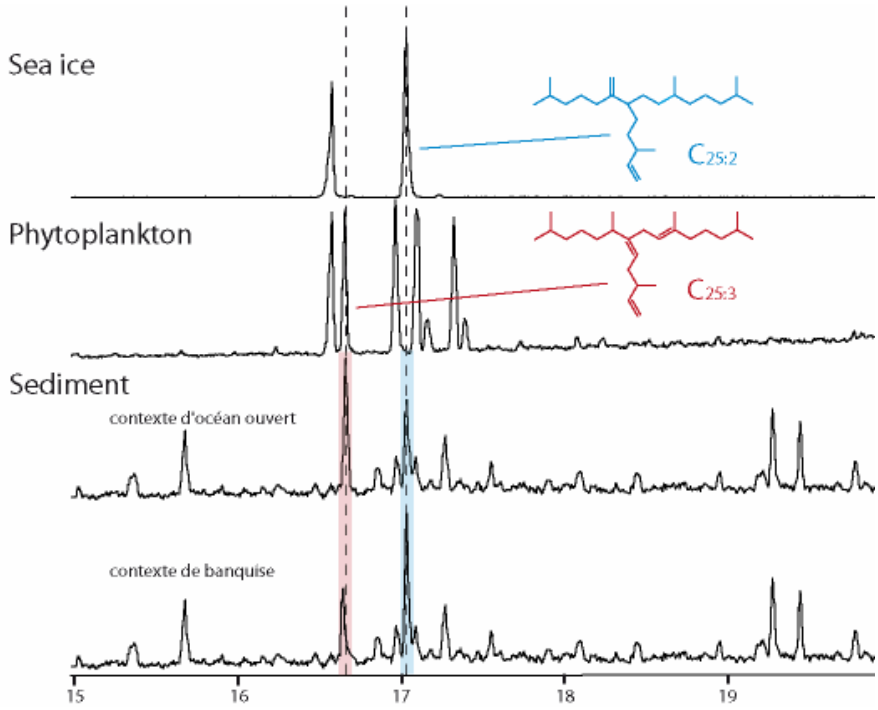

Figure 36. Chromatogrammes extraits de glace de mer, de phytoplancton, et de sédiment. Dans le sédiment, le pic bleu correspond au diène (C25:2), et le pic rouge correspond au triène (C25:3) (Barbara, 2008).

Le diène est présent dans les sédiments de surface des régions connues pour avoir une oscillation saisonnière de banquise et il est absent dans les sédiments des régions où le couvert de glace est permanent voire totalement absent (Rowland et Robson, 1990 ; Belt et al., 2000). A l'inverse, le triène est présent dans les sédiments des régions sans banquise ou à faible couvert de banquise saisonnier. Ces bio-marqueurs peuvent donc être utilisés comme un indicateur des fractions liées à la banquise et au phytoplancton et, par extension, à la présence/absence de la banquise et à sa saisonnalité (Belt et al., 2007) (Figure 36).

La méthode d'analyse utilisée pour mesurer les HBi est décrite dans Belt et al. (2007) et en Annexe 3. Ce procédé non-destructif permet d'extraire les HBi du sédiment, de les purifiés par chromatographie sur colonne, puis de les analyser par chromatographie en phase gazeuse. Les spectres ont ensuite été traités à partir du logiciel Hewlett-Packard *MS-Chemstation*.

2.1.3. Le modèle ECBilt-CLIO-VECODE version 3

Ce modèle tridimensionnel de complexité intermédiaire résulte du couplage entre les modules d'atmosphère, de végétation dynamique, de circulation générale des océans, et de banquise (Figure 37). La représentation de chacun des modules dans le modèle est expliquée de façon détaillée dans Renssen et al. (2005b).

ECBilt-CLIO-VECODE, renommé actuellement LOVECLIM (Driesschaert, 2005), est capable de simuler le climat avec certains détails tout en gardant une efficacité de calcul qui permet des simulations pluri-millénaires continues. Les simulations sont forcées par les variations annuelles d'ensoleillement (Berger, 1978) et lissées des concentrations en CO_2 et CH_4 (Raynaud et al.,2000) (Renssen et al., 2005a, 2005b). Les autres forçages tels que la constante solaire, les autres gaz à effet de serre et la configuration des calottes de glace ont été fixés à leurs niveaux de 1750 AD. L'évolution des calottes de glace au cours de l'Holocène n'est donc pas prise en compte dans ces expériences.

Cette version et la version antérieure du modèle ECBilt-CLIO ont déjà été utilisé de façon satisfaisante pour modéliser l'impact des décharges d'eaux douces sur le climat durant le dernier stade glaciaire (Knutti et al., 2004), le climat moderne et sa variabilité naturelle (Goosse et al., 2001, 2002, 2003; Goosse et Renssen, 2004), l'évènement 8.2 ka (Renssen et al., 2001, 2002) et la future évolution climatique (Goosse et Renssen, 2001; Schaeffer et al., 2002). De plus, la sensibilité du modèle est de l'ordre de 0.58°C/ ($W.m^{-2}$), ce qui est parmi les plus basses des modèles climatiques couplés (Cubasch et al., 2001).

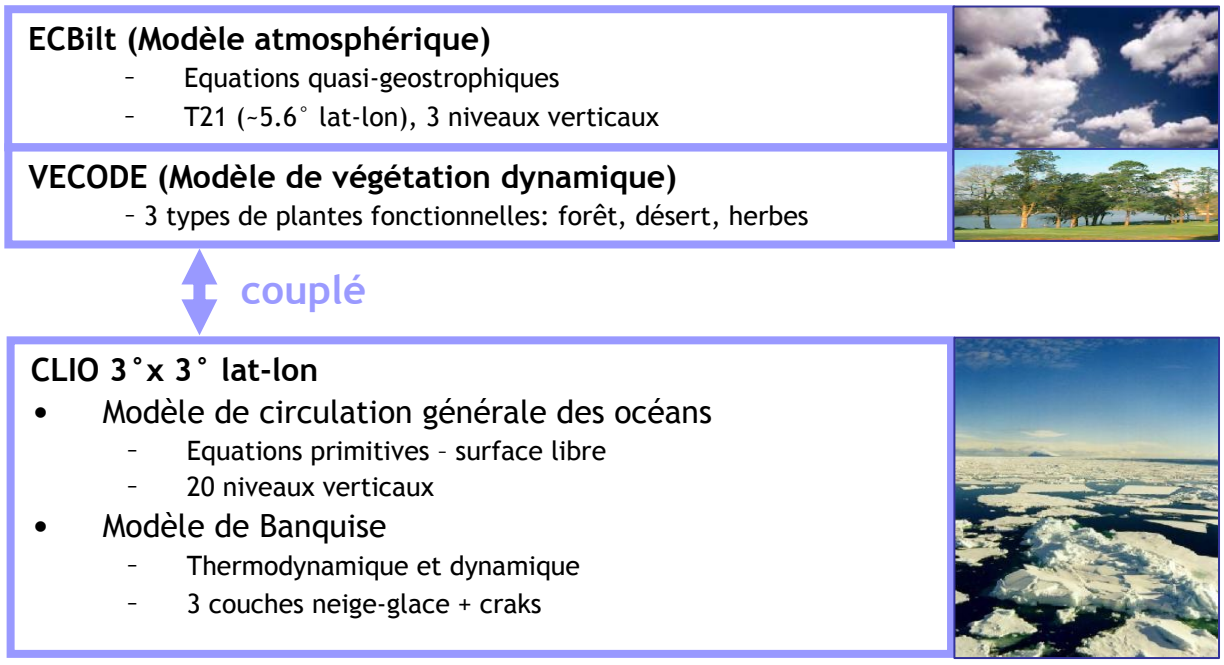

Figure 37. Description des modules du modèle ECBilt-Clio-VECODE, modifié d'après H. Renssen (personnel communication, 2008).

ECBilt-CLIO-VECODE apparaît donc bien adapté pour étudier les relations océan-atmosphère-banquise et leur évolution Holocène en fonction des variations orbitales. Notamment, la résolution mensuelle des sorties de modèle est particulièrement adaptée à l'étude d'environnement très contrasté saisonnièrement tel que la zone marginale des glaces. En collaboration avec Hans Renssen de l'Université d'Amsterdam, nous avons obtenus des simulations journalières sur les derniers 9 cal ka BP des températures atmosphériques, océaniques, de la surface couverte par la banquise et des précipitations en mer de Dumont D'Urville (130-150°E ; 64-70°S), et en Baie de Prydz (64-70°E ; 60-70°S). Nous avons aussi utilisées des données déjà publiées par Renssen et al. (2005b), à savoir la vitesse des vents entre 45 et 60°S et le gradient de températures (20-30°S moins 50-60°S) de l'Océan Austral en hiver et en été.

Cependant, ce modèle comporte quelques limitations qu'il est important de garder en mémoire pour la comparaison modèle-données. ECBilt-CLIO-VECODE :

- utilise une physique de l'atmosphère simplifiée, à une faible résolution spatiale
- ne simule pas la calotte de glace et les particularités locales (glaciers, langue de glace, polynie…)
- ne tient pas compte des forçages antérieures à 9 cal ka BP comme la déglaciation qui peut influencer les conditions aux limites à 9 cal ka BP et les premier milliers d'années via l'effet mémoire de l'océan (Renssen et al., 2005b).

2.2. Proxies analysés uniquement sur la carotte MD03-2601

2.2.1. Radionucléides

Dans le milieu marin, les différents éléments des familles radioactives naturelles de l'uranium et du thorium présentent deux types de comportement : les premiers (^{238}U, ^{235}U, ^{234}U) sont solubles dans l'eau de mer tandis que les deuxièmes (^{234}Th, ^{232}Th, ^{230}Th) sont très réactifs vis à vis des particules et sont extraits de la colonne d'eau par adsorption, co-précipitation, ou par des processus biologiques (Bacon et Anderson, 1982). Cette disparité de comportements chimiques entraîne des ruptures dans les chaines radioactives et, par conséquent, des déséquilibres radioactifs dans les différentes phases du milieu marin : eau de mer, particules en suspension, sédiment (Figure 38). Le rééquilibrage par recroissance ou décroissance au sein de la série radioactive fourni des chronomètres adaptés à l'étude des cinétiques de nombreux phénomènes biologiques, océanographiques et géologiques (Schmidt, 1991). Les études paléoceanographiques sont à la recherche d'enregistrements haute-résolution. Cependant, les forts taux de sédimentation résultent souvent d'importants apports latéraux, notamment dans les zones de courants de fond actifs (Francois et al., 2004), suppléant la sédimentation verticale hémipélagique. Des corrections s'imposent alors pour avoir accès aux flux verticaux.

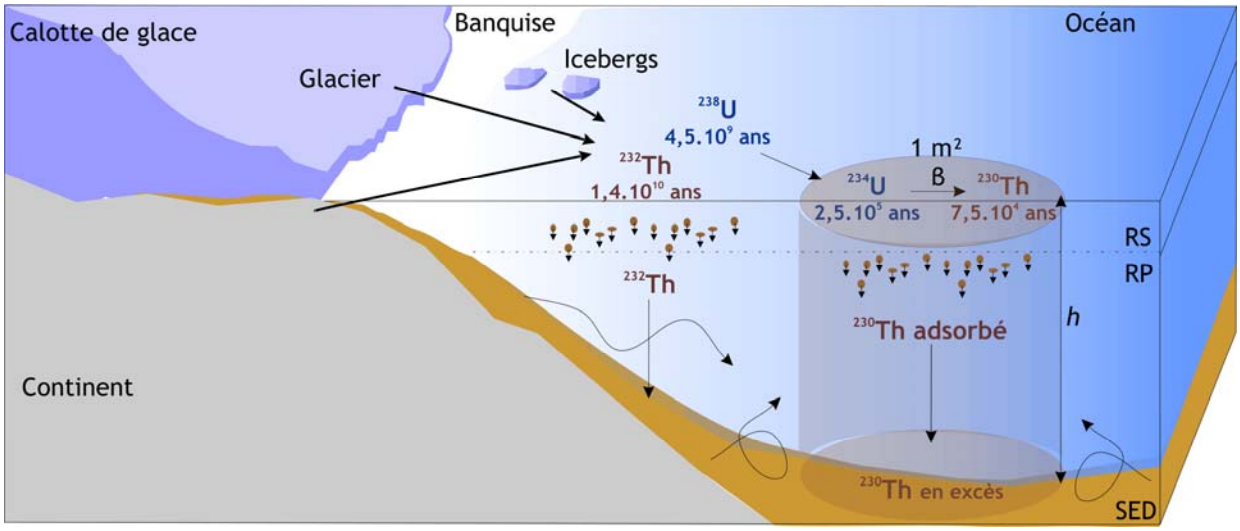

Figure 38. Schéma du cycle des éléments des familles de l'uranium et du thorium le long des côtes Antarctique. Les isotopes de l'uranium et du thorium sont marqués en bleu et en marron pour symboliser leur affinité pour la phase liquide et solide, respectivement. Le temps de demi-vie (e.g. la moitié du temps nécessaire à la désintégration des atomes) de chacun des isotopes représentés, est noté sous celui-ci. B et *h* représentent, respectivement, le taux de production constant du ^{230}Th à partir de la désintégration de son père ^{234}U et la hauteur de colonne d'eau. Les flèches ondulées symbolisent l'apport de radionucléides par voie latérale via la circulation océanique, et les processus de remise en suspension du sédiment.

Notamment, deux applications s'avèrent primordiales pour les études paléocéanographiques : la détermination du facteur de « focusing » et la normalisation des flux au ^{230}Th qui permettent respectivement de quantifier les flux latéraux et verticaux (Francois et al., 2004) (Figure 38).

"Focusing"

La méthode du ^{230}Th en excès estime la contribution des apports sédimentaires latéraux, dénommée facteur de «focusing» (Francois et al., 2004). Le taux de production du ^{230}Th dans l'eau de mer est une constante car elle résulte de la désintégration de ^{234}U dont la concentration dans l'océan est quasiment stationnaire grâce à son long temps de résidence et à son affinité pour la phase soluble (Chen et al., 1986). A l'inverse, l'affinité du ^{230}Th pour la phase particulaire induit un transfert et un dépôt rapide du thorium vers le fond des océans (Bacon et Anderson, 1982).

Ce comportement géochimique du ^{230}Th (e.g. taux de production constant; advection sur les particules), permet de calculer un flux théorique de Th « scavengé » (e.g. entrainer de la colonne d'eau vers le sédiment) qui sera fonction de la hauteur de la colonne d'eau et de la loi de désintégration du ^{234}U.

Le flux mesuré dans le sédiment ($^{230}Th_{xs}$) préalablement corrigé des contributions lithogéniques et authigéniques (voir détails dans chapitre 2) est ensuite comparé à ce flux théorique pour déterminer le facteur de focusing (ψ) (Figure 38):

$$\psi = \frac{\int_{z1}^{z2} [^{230}Th_{xs}]_0 \rho dz}{\beta h[t_2 - t_1]}$$

où $[^{230}Th_{xs}]_0$ est le ^{230}Th en excès dans le sédiment, corrigé de l'âge, en dpm.g^{-1}, ρ est la densité sèche du sédiment en g.cm^{-3}, dz est l'intervalle de profondeur en cm dans la carotte sédimentaire, ß est le taux de production du ^{230}Th à partir de l'^{234}U (ß = 2.63×10^{-5} dpm.cm^{-3}.ka^{-1}), h est à la hauteur de colonne d'eau, et t est l'âge en ka. ψ supérieur à 1 indique des apports latéraux.

Normalisation des flux

L'estimation des paléo-flux par le calcul classique des "mass accumulation rate" (e.g. multiplication des teneurs d'un élément donné par le taux de sédimentation et la densité du sédiment), dans des zones fortement affectées par des apports sédimentaires latéraux peut induire des biais d'interprétation par :

- une surestimation des flux verticaux
- des effets de dilution d'un élément sur un autre
- la propagation des erreurs chronologiques aux flux (10% d'erreur sur les flux pour 1 ka d'erreur sur l'âge pendant l'Holocène).

La normalisation des flux ^{230}Th permet de s'affranchir des apports latéraux et des effets de dilution, et diminue l'importance des erreurs chronologiques (1% pour une erreur de 1 ka sur l'Holocène) (Bacon, 1984; Suman et Bacon; 1989; Francois et al., 2004; Adkins et al., 2006). Cette méthode développée par Bacon (1984) est basée sur le principe que le flux de ^{230}Th « scavengé » qui atteint le sédiment est connu et égal au taux de production du ^{230}Th produit par la désintégration du ^{234}U dans la colonne d'eau sus-jacente (Francois et al., 2004).

Le flux vertical préservé ($^{PR}F_v$) dans le sédiment est obtenu par la normalisation du taux de production du ^{230}Th par le flux en excès mesuré dans le sédiment ($^{230}Th_{xs}$), selon la formule ci-dessous :

$$^{PR}F_v = \frac{\beta h[t_2 - t_1]}{[^{230}Th_{xs}]_0}$$

où ß est le taux de production du ^{230}Th à partir de l'^{234}U (ß = 2.63×10^{-5} dpm.cm^{-3}.ka^{-1}), h est à la hauteur de colonne d'eau, t est l'âge en ka et $[^{230}Th_{xs}]_0$ est le ^{230}Th en excès dans le sédiment, corrigé de l'âge, en dpm.g^{-1}.

Le flux vertical préservé pour chaque composante sédimentaire est déterminé par la formule suivante :

$$F_v = {}^{PR}Fv \times fi$$

où fi est la concentration ou le % de la composante sédimentaire dans chaque échantillon. Par exemple, dans le cadre de cette thèse, ont été normalisés les pourcentages des éléments biogéniques tels que le carbone, l'azote, l'opale et les concentrations en certains métaux comme l'aluminium et le fer.

L'utilisation des radioéléments peut être sujette à caution sur les marges peu profondes, munies d'un système hydrologique particulièrement actif, de formation d'eaux profondes et d'upwellings. En effet, il peut exister des phénomènes d'advection de ^{230}Th dans les zones de forts flux (« boundary scavenging » ; Spencer et al., 1981 ; Rutgers van der Loeff et Berger, 1993 ; Henderson et al., 1999), ou au contraire un export du thorium dû aux faibles temps de résidence des masses d'eaux (Moran et al., 2005 ; Chase et al., 2003). Des différences dans l'efficacité du « scavenging » du ^{230}Th on aussi été mises en évidence en fonction de la vitesse de sédimentation et du type de particules (Chase et Anderson, 2004).

Ces processus et leurs implications ont été pris en compte et discutés (cf. article complémentaire n°2) et ne remettent pas en cause l'utilisation des radionucléides dans le cadre de cette étude qui vise à documenter les variations du facteur de « focusing » et des flux verticaux au sein d'un même enregistrement sédimentaire. Le protocole d'expérimentation est décrit en annexe 4.

2.2.2. Analyse d'image des grains détritiques

Pour caractériser l'intensité des paléo-courants au cours de l'Holocène, nous cherchions à acquérir les variations de taille de grains détritiques au sein de la carotte MD03-2601 (McCave et Hall, 2006). Nos carottes marines présentent une texture très cotonneuses et une granularité très fine, dues à la très forte abondance des diatomées (30 à 65 % de silice biogène ; Crosta et al., 2005). Ainsi, les mesures classiques de granulométrie, réalisées au diffractomètre laser sur l'auto-analyseur Malvern, ne permettaient pas de caractériser les grains détritiques, même après traitement pour ôter l'opale.

L'induration de sédiments meubles, sans phénomène de dilatation ou de réduction de celui-ci, permet de conserver et d'observer les structures fines du sédiment et, notamment, de caractériser les tailles des grains détritiques. La caractérisation de la taille et du nombre de grains au microscope digital sur des lames de 10 cm avait permis de tester cette technique sur la carotte MD03-2601 (Denis, 2005 ; Denis et al., 2006). En effet, la matrice siliceuse amorphe de la carotte MD03-2601 permet une bonne différentiation des grains détritiques sous lumière polarisée. De plus, la confrontation des résultats avec les données des teneurs en métaux mesurées par XRF core-scanner, tel que

le titane et l'aluminium, avait validé les comptages de grains détritiques par analyse d'image (Denis, 2005 ; Denis et al., 2006). Nous avons donc utilisé la même technique, mais cette fois-ci, sur des lames de 2 cm^2 pour avoir une surface statistiquement représentative mais assez restreinte pour permettre une étude à haute résolution le long des 40 m de la carotte MD03-2601 (Figure 39, Table 5).

Les protocoles d'induration et d'analyse d'image sont détaillés en annexes 5 et 6. Cette méthode considère tous les grains détritiques supérieurs à 5 µm, valeur seuil à partir de laquelle l'outil microscope est performant pour discriminer les grains. Les paramètres retenus pour notre étude concernent la taille des grains (surface, longueur, diamètre…). Les lames ont d'abord été analysées de façon automatique sur des surfaces de 104 mm^2. Il est important de noter que les lames des échantillons à texture très cotonneuse ont fourni des contrastes moins nets et que la reconnaissance des grains pouvait s'en trouver altérée. Les surfaces prises en compte pour chaque grain étaient alors plus floues et surestimaient généralement la taille du grain.

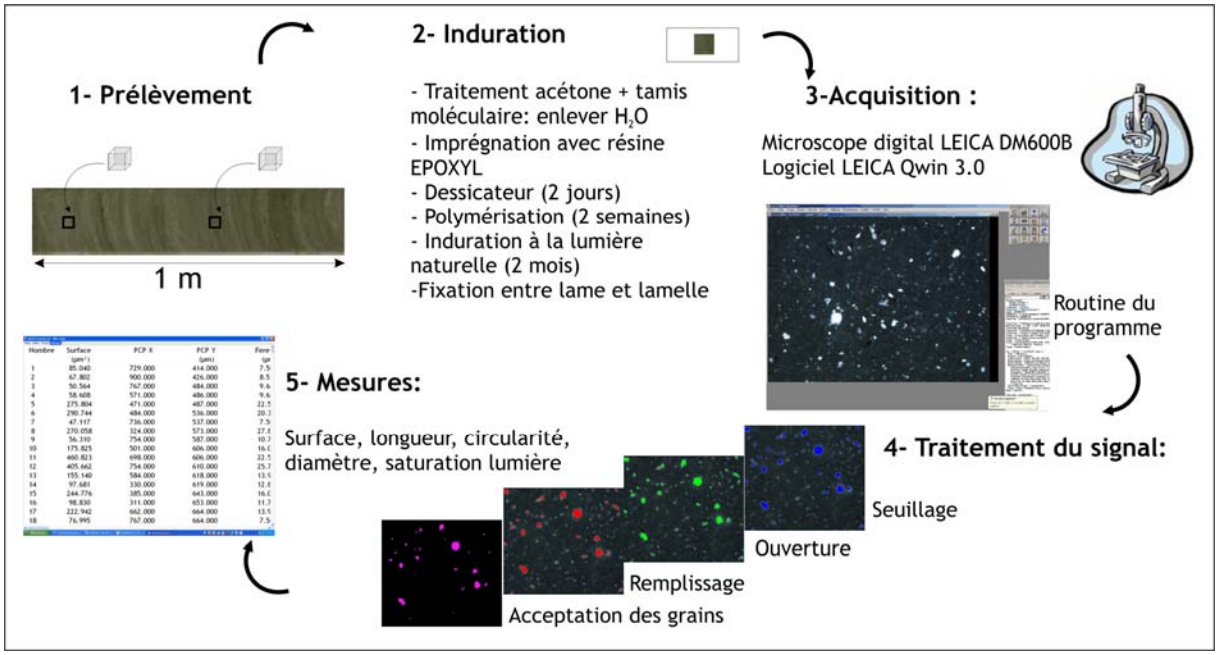

Figure 39. Schéma simplifié de la technique d'induration et du traitement des échantillons au microscope.

C'est pourquoi, nous avons aussi procédé à une acquisition manuelle des échantillons, assistée d'une tablette graphique WACOM sur des surfaces de 13.3 mm^2. Le nombre de grains considérés est alors réduit, mais les tailles de grains sont plus fiables et reproductibles d'une lame à l'autre quelle que soit la texture de l'échantillon. La comparaison de ces deux approches automatique et manuelle sur les échantillons à texture nette indique une bonne représentativité des acquisitions manuelles. L'erreur associée à la mesure, compte tenu du nombre de grain analysés, est de 2 à 9 % selon les échantillons, ce qui est largement inférieur à l'amplitude des variations de taille de grains observée sur la

carotte MD03-2601. Pour ces raisons, ce sont les résultats manuels qui ont été utilisés par la suite.

A partir de ces données morphologiques acquises par microscopie digitale, le but était de calculer dans nos échantillons les indices sédimentologiques couramment utilisés pour caractériser les courants de fond et le mode de dépôt, et usuellement obtenus par mesure au diffractomètre laser. Ces indices sont :

- le sortable silt qui est la valeur moyenne de la fraction grossière des silts, i.e. entre 10 et 63 µm, donnant une estimation de l'intensité des courants de fond sur le site de carottage (McCave et Hall, 2006). Cette moyenne a été calculée géométriquement selon la formule de Folk et Ward (1957):

$$\overline{SS} = \exp \frac{\ln P_{16} + \ln P_{50} + \ln P_{84}}{3}$$

Où $\overline{SS}$ est le « sortable silt », exprimé en µm, et P_{16}, P_{50} et P_{84} sont les tailles en µm qui correspondent aux classes de taille qui contiennent 16, 50 et 84 % du total des grains compris entre 10 et 63 µm.

- la déviation standard, appelée « sorting », qui informe sur la qualité de tri des grains déposés. Plus le courant est intense, plus les grains déposés sont bien triés. Le « sorting » a été calculé sur l'ensemble du spectre de taille de grains, c'est-à-dire sur la fraction supérieure à 5 µm, et sur la fraction 10-63 µm, selon la formule de Folk et Ward (1957):

$$\sigma = \exp\left(\frac{\ln P_{16} - \ln P_{84}}{4} + \frac{\ln P_5 - \ln P_{95}}{6{,}6}\right)$$

Où σ est le « sorting », et P_5, P_{16}, P_{84} et P_{95} sont les tailles en µm qui correspondent aux classes de taille qui contiennent 5, 16, 84 et 95 % de la population totale des grains et de la population de grains de la fraction 10-63 µm.

- le « skewness » qui caractérise la géométrie du spectre des tailles de grains qui peut être symétrique, tirée vers les fins ou tirée vers les grossiers. Ainsi, le skewness peut appuyer ou nuancer les interprétations d'intensité de courant, suggérées par l'évolution de la moyenne des tailles de grains. Cet indice a été calculé sur l'ensemble du spectre de taille de grains, c'est-à-dire supérieure à 5 µm, et sur l'ensemble du spectre de taille de grains de la fraction 10-63 µm, selon la formule de Folk et Ward (1957):

$$Sk = \left(\frac{\ln P_{16} + \ln P_{84} - 2(\ln P_{50})}{2(\ln P_{84} - \ln P_{16})} + \frac{\ln P_5 + \ln P_{95} - 2(\ln P_{50})}{2(\ln P_{25} - \ln P_5)}\right)$$

Où *Sk* est le « skewness » et P_5, P_{16}, P_{25}, P_{50}, P_{84} et P_{95} sont les tailles en µm qui correspondent aux classes de taille qui contiennent 5, 16, 25, 50, 84 et 95 % de la population totale des grains et de la population de grains de la fraction 10-63 µm.

L'étude de la morphologie des grains par analyse d'images est couramment utilisée, notamment dans les nanotechnologies. Cependant, l'utilisation de ces résultats pour documenter une intensité de courants n'avait encore jamais été testée. La caractérisation des tailles de grains par analyse d'images en 2D sur des lames de sédiments indurées implique plusieurs limitations par rapport aux analyses plus classiques (Sedigraph, Coulter Counter, Malvern laser sizer) :

- Le seuillage à 5 µm ne donne pas accès à la fraction granulométrique complète des grains. Ce problème est aussi rencontré avec les « Laser sizer », type Malvern (McCave et Hall, 2006). Cette limitation n'est pas cruciale dans notre cas puisque nous nous focaliserons sur la fraction 10-63 µm.

- Le nombre de grains considéré par échantillon est plus faible. Cependant, comme expliqué précédemment, l'erreur associée, inférieure à 10%, est inférieure à l'amplitude des changements mis en évidence sur la carotte MD03-2601. Les barres d'erreurs associées sont spécifiées sur les figures de résultats.

- Les résultats sont issus de mesures de surface et non de volume ce qui peut être gênant pour parler d'un courant qui lui est considéré en 3D. En effet, deux grains occupant la même surface peuvent avoir des volumes différents selon qu'ils sont plats ou sphériques. Ce problème est insignifiant dans notre cas puisque la majeure partie des grains détritiques sont des Quartz, qui sont plutôt ronds par définition. De plus, le changement d'unité entre des mesures de surface et de volume (facteur 100) pourrait induire une sous-estimation de la variabilité entre les échantillons. Nos résultats seraient en quelque sorte une estimation basse de la variabilité des courants de fond au cours de l'Holocène. Les tendances sont donc représentatives.

Ainsi, malgré ces limitations, la méthode de mesure des tailles de grains par microscopie digitale, à partir de lames minces de sédiments indurés, apparait appropriée pour documenter les variations des courants de fond pendant l'Holocène dans ce type de sédiment.

2.2.3. Isotopes stables de l'azote

L'azote est constitué de deux isotopes, le ^{14}N majoritaire (99.64 %) et le ^{15}N minoritaire (0.36 %). Pour synthétiser leur matière organique, les organismes phytoplanctoniques (e.g. diatomées) consomment préférentiellement le ^{14}N (isotope « léger »), ce qui a pour conséquence un appauvrissement du milieu ambiant en ^{14}N et corrélativement un enrichissement du milieu ambiant en ^{15}N (isotope « lourd ») d'où un alourdissement de la signature isotopique des nitrates dissous ($\delta^{15}NO_{3^-}$). Lorsque la consommation des nitrates augmente, les $^{14}NO_{3^-}$ sont de moins en moins disponibles (puisque déjà préférentiellement consommé) et se retrouvent progressivement remplacé par une absorption des $^{15}NO_{3^-}$

entraînant ainsi un alourdissement de la signature isotopique de la matière organique produite ($\delta^{15}N_{bulk}$) à partir de cette source enrichie. Dés lors, il est possible de corréler positivement les variations du $\delta^{15}N$ de la matière organique avec l'utilisation relative des nitrates dans la couche euphotique. Cette utilisation relative représente un équilibre entre les apports par les upwellings et les exports par la consommation phytoplanctonique.

Cependant, d'autres facteurs en amont ou en aval modifient la relation entre le $\delta^{15}N_{bulk}$ et l'utilisation relative des nitrates. Ainsi, il faut contraindre la valeur isotopique de la source, l'origine de la matière organique (marine *versus* continentale), les variations du fractionnement isotopique (différent suivant : les groupes phytoplanctoniques, le taux de croissance, et le rapport surface/volume) (Waser et al., 1998), les phénomènes de reminéralisation et la diagénèse (Altabet et Francois, 1994) pour interpréter les enregistrements fossiles du $\delta^{15}N_{bulk}$.

La composition isotopique est calculée par rapport à l'Air, qui représente le standard international de valeur 0‰ par définition, et peut être exprimée de la manière suivante :

$$\delta X\ (‰) = \left[\frac{\left(\frac{^{H}X}{^{L}X} \right)_{Ech}}{\left(\frac{^{H}X}{^{L}X} \right)_{Air}} - 1 \right] \times 1000$$

où X est l'élément, H est l'isotope lourd, L est l'isotope léger, Ech est l'échantillon et Air est le standard.

Le rapport isotopique de l'azote a été mesuré sur les échantillons bruts, et la moitié des échantillons a été analysée en duplicats. Le détail des analyses et du fonctionnement du spectromètre de masse couplé à un analyseur élémentaire utilisé pour les mesures est donné en annexe 7.

2.2.4. Géochimie élémentaire

La géochimie élémentaire nous a permis de déterminer les teneurs en carbone organique (C_{org}), en azote organique (N_{org}) et en silice biogène (BSi) au sein de la carotte MD03-2601. Ces concentrations en matériel biogène fournissent des indications sur la productivité enfouie et, par extension, sur la productivité de surface.

Cependant, ces proxies sont aussi perturbés par d'autres phénomènes : export, transport, préservation de la matière organique (corrosivité et oxygénation des eaux de fond) et dilution par des apports latéraux. L'étude des conditions de préservation à l'interface eau/sédiment a fait l'objet de l'article complémentaire n°2 (Carson et al., soumis). Chacune de ces composantes de la matière organique a été normalisée au ^{230}Th, comme

expliqué précédemment (section 2.2.1.), afin de prendre en compte les flux issus de la sédimentation verticale.

Les teneurs en C_{org} et N_{org} ont été mesurées simultanément avec les rapports isotopiques (détail annexe 7). La moitié des échantillons a été dupliquée.

Les teneurs en silice biogène ont été mesurées grâce à un protocole similaire à celui de Mortlock et Froelich (1989) qui est décrit dans l'annexe 8. Les mesures ont été réalisées en duplicats, et les teneurs en opale sont obtenues par l'équation suivante :

$$\%_{\text{massique}}\ SiO_2 = [SiO_2] \times \left[\frac{\left(\frac{0,5}{A}\right) \times V \times M(SiO_2) \times 0.0001}{m_{Ech}} \right]$$

où [Si02] est égale à [(absorbance$_{Ech}$ – b)/pente] de la courbe de calibration; A est le volume d'échantillon prélevé des tubes à centrifuger (aliquot = 0.25 ml), V est le volume de NaOH ajouté au sédiment dans les tubes (40 ml), M est la masse molaire de la silice biogène (60.1 g/mol), 0.0001 = 1.10^{-6} g/µg pour passer en %, et m_{Ech} est la masse d'échantillon pesée (mg).

L'analyse de la silice biogène est une manipulation coûteuse en temps (Annexe 8). Des tests ont été effectués pour essayer de mettre en place une méthode plus rapide et plus précise, au sein de l'équipe ECOBIOC du laboratoire EPOC, notamment avec l'aide précieuse d'Aurélia Mouret et Jonathan Deborde. Dans le cadre de cette thèse, nous n'avons pas achevé ces expérimentations. Cependant, le détail du protocole préliminaire est fourni en annexe 9.

2.2.5. Métaux

En collaboration avec Damien Carson et Raja Ganeshram de l'Université d'Edimbourg en Ecosse, nous avons obtenu les concentrations absolues en différents métaux (titane, aluminium, molybdène, fer) sur la carotte MD03-2601. Le détail du protocole d'analyse est fourni dans l'article complémentaire n°2 (Carson et al., soumis). Ces données quantitatives des teneurs en métaux ont été utilisées dans le cadre de cette thèse pour :

- contraindre les conditions redox à l'interface eau/sédiment à l'aide des teneurs en $^{238}U_{authigénique}$, obtenues par nos mesures des radionucléides, et des teneurs en $Mo_{authigénique}$, obtenues par leurs mesures à fluorescence X (XRF) (cf. Carson et al., soumis)

- reconstituer les flux terrigènes totaux et verticaux grâce à la normalisation au ^{230}Th (section 4.2.2.) (cf. Chapitre 2 et 3).

CHAPITRE 2

Interactions et rétroactions Glacier-Banquise-Océan

De récentes études ont mis en avant la sensibilité des glaciers, de la banquise et de la circulation thermohaline (THC) aux variations climatiques. En effet, le réchauffement climatique des 200 dernières années a été mis en parallèle avec un recul global des glaciers, de la banquise arctique et une diminution du transfert méridien d'eaux chaudes et salées par la Dérive Nord Atlantique en lien avec la vigueur de la THC qui est encore très discutée (IPCC, 2007). Ces changements apparaissent alarmants et pourraient indiquer un « dérèglement » profond de la machine climatique en lien avec les activités humaines (IPCC, 2007). La communauté scientifique a très peu de recul pour évaluer l'impact que ces changements pourraient engendrer sur le climat mondial et donc de grande difficulté à prédire le climat futur.

Les études paléoclimatologiques ont démontré que la dernière période glaciaire a subi d'importants bouleversements climatiques, initiés dans l'Hémisphère Nord, qui se sont répétés à intervalles réguliers et ont affecté l'ensemble du climat mondial (Broecker et Denton, 1989 ; Broecker et Hemming, 2001 ; Alley et al., 2001 ; Bond et al., 1993). Ces évènements, dits de Dansgaard-Oeschger et de Heinrich, s'expriment par des refroidissements rapides enregistrés dans l'ensemble de l'Hémisphère Nord, voire plus globalement. Ils découlent de forçages encore mal connus qui font intervenir la THC et la dynamique des calottes de glaces (Broecker, 2000 ; Hemming, 2004). La durée de ces

évènements, d'abord estimée en milliers d'années (Hemming, 2004) serait maintenant comptée en centaine d'années voir en décennies (McAyeal, 1993 ; Dowdeswell et Dowdeswell, 1989 ; Roche et al., 2004). Des évènements similaires de moindre amplitude auraient aussi été documentés en Hémisphère Nord pendant l'Holocène (Bond et al., 1997, 2001) mais restent très discutés. Un évènement fais toutefois l'unanimité dans c'est celui du 8.2 ka BP (Rholing and Pälike, 2005).

Cette variabilité rapide enregistrée pendant la dernière période glaciaire et l'Holocène, mettant en jeu les glaciers et l'océan, montre l'importance de ces deux sous-systèmes climatiques sur le climat global et de leur rapidité de réaction. Ainsi, l'Homme prend conscience que des évènements qui seraient catastrophiques pour son environnement et ses activités socio-économiques peuvent se produire à son échelle de vie. Ces évènements mettent en avant l'importance d'étudier l'activité des glaciers, et de la circulation océanique à haute résolution pour évaluer leur rapidité de réponse et les rétroactions climatiques qui en découlent.

Dans ce premier volet, notre intérêt était de documenter l'activité des glaciers et de l'océan au cours de l'Holocène de l'échelle plurimillénaire à séculaire pour évaluer leur mode de réponse aux changements climatiques qui surviennent en période interglaciaire. De plus, nous nous somme attachés à mettre en parallèle ces résultats avec l'évolution du couvert de banquise qui joue un grand rôle dans l'albédo, la formation d'eau profonde et la stratification des eaux et constitue un compartiment intermédiaire entre la cryosphère et l'océan. Le troisième intérêt était de réaliser ce type d'étude dans l'Océan Austral où les modélisateurs suspectent que les rétroactions climatiques conséquentes aux décharges d'eaux douces, aux changements de THC… sont totalement différentes, notamment en raison de l'éloignement du Continent Antarctique et donc de la large dispersion des anomalies climatiques (Stouffer et al., 2007). Les résultats de cette étude, réalisée sur les marges de Terre Adélie en Antarctique de l'Est, ont abouti à la réalisation d'une publication, actuellement sous-presse à *Quaternary Science Reviews*, qui fait l'objet de ce chapitre.

ARTICLE IN PRESS

Quaternary Science Reviews xxx (2009) 1–13

Contents lists available at ScienceDirect

Quaternary Science Reviews

journal homepage: www.elsevier.com/locate/quascirev

Holocene glacier and deep water dynamics, Adélie Land region, East Antarctica

Delphine Denis [a,*], Xavier Crosta [a], Sabine Schmidt [a], Damien S. Carson [b], Raja S. Ganeshram [b], Hans Renssen [c], Viviane Bout-Roumazeilles [d], Sebastien Zaragosi [a], Bernard Martin [a], Michel Cremer [a], Jacques Giraudeau [a]

[a] EPOC, UMR 5805 CNRS, Université Bordeaux 1, Avenue des Facultés, F-33405 Talence Cedex, France
[b] School of GeoSciences. The University of Edinburgh, Grant Institute, West Mains Road, Edinburgh EH9 3JW, UK
[c] Faculty of Earth and Life Sciences, Vrije Universiteit Amsterdam, De Boelelaan 1085, NL-1081 HV Amsterdam, The Netherlands
[d] FRE 2255 Sédimentologie & Géodynamique, Université des Sciences et Technologies de Lille 1, F-59655 Villeneuve d'Ascq, France

ARTICLE INFO

Article history:
Received 21 March 2008
Received in revised form
10 December 2008
Accepted 30 December 2008
Available online xxx

ABSTRACT

This study presents a high-resolution multi-proxy investigation of sediment core MD03-2601 and documents major glacier oscillations and deep water activity during the Holocene in the Adélie Land region, East Antarctica. A comparison with surface ocean conditions reveals synchronous changes of glaciers, sea ice and deep water formation at Milankovitch and sub-Milankovitch time scales. We report (1) a deglaciation of the Adélie Land continental shelf from 11 to 8.5 cal ka BP, which occurred in two phases of effective glacier grounding-line retreat at 10.6 and 9 cal ka BP, associated with active deep water formation; (2) a rapid glacier and sea ice readvance centred around 7.7 cal ka BP; and (3) five rapid expansions of the glacier–sea ice systems, during the Mid to Late Holocene, associated to a long-term increase of deep water formation. At Milankovich time scales, we show that the precessionnal component of insolation at high and low latitudes explains the major trend of the glacier–sea ice–ocean system throughout the Holocene, in the Adélie Land region. In addition, the orbitally-forced seasonality seems to control the coastal deep water formation via the sea ice–ocean coupling, which could lead to opposite patterns between north and south high latitudes during the Mid to Late Holocene. At sub-Milankovitch time scales, there are eight events of glacier–sea ice retreat and expansion that occurred during atmospheric cooling events over East Antarctica. Comparisons of our results with other peri-Antarctic records and model simulations from high southern latitudes may suggest that our interpretation on glacier–sea ice–ocean interactions and their Holocene evolutions reflect a more global Antarctic Holocene pattern.

1. Introduction

The East Antarctic Ice Sheet (EAIS) stores 79% of the global ice volume (Wagner and Melles, 2007), and thus directly influences both Antarctic and global climate, due to its influence on the albedo of the Southern Hemisphere, thermohaline circulation, and atmospheric circulation (Ingólfsson and Hjort, 1999). A better understanding of the impact of glacier systems and the associated climate feedbacks, particularly through the sea ice cycle and the magnitude of deep water formation (Joughin and Padman, 2003) is important for future climate predictions (DeConto et al., 2007). Glaciers appear to react rapidly to Holocene climatic changes as demonstrated by several glacier advances and retreats documented around Antarctica (Ingólfsson et al., 1998 and references therein) and around the world (Solomina et al., 2008, and references therein). However, these reconstructed glacier movements appear erratic in time and space around Antarctica and lack significant correlation with major changes during the Holocene (Wagner and Melles, 2007) as documented from ice cores (Masson et al., 2000; Masson-Delmotte et al., 2004), continental archives (Ingólfsson et al., 1998), marine sediment cores (Hodell et al., 2001; Nielsen et al., 2004) and model simulations (Renssen et al., 2005a). It is expected that ice sheets, bedrock topography, atmosphere, ocean circulation and sea ice factors determine the timing, the dynamic and the amplitude of glacier fluctuations. There is, however, no clear evidence of the implicated forcing factors and subsequent impacts of glacier movement on other climatic components such as

* Corresponding author. Tel.: +33 5 40 00 84 38; fax: +33 5 56 84 08 48.
E-mail addresses: d.denis@epoc.u-bordeaux1.fr (D. Denis), x.crosta@epoc.u-bordeaux1.fr (X. Crosta), s.schmidt@epoc.u-bordeaux1.fr (S. Schmidt), d.s.carson@sms.ed.ac.uk (D.S. Carson), r.ganeshram@ed.ac.uk (R.S. Ganeshram), hans.renssen@geo.falw.vu.nl (V. Renssen), viviane.bout@univ-lille1.fr (V. Bout-Roumazeilles), s.zaragosi@epoc.u-bordeaux1.fr (S. Zaragosi), b.martin@epoc.u-bordeaux1.fr (Bernard Martin), m.cremer@epoc.u-bordeaux1.fr (M. Cremer), j.giraudeau@epoc.u-bordeaux1.fr (J. Giraudeau).

0277-3791/$ – see front matter © 2009 Elsevier Ltd. All rights reserved.
doi:10.1016/j.quascirev.2008.12.024

Please cite this article in press as: Denis, D., et al., Holocene glacier and deep water dynamics, Adélie Land region, East Antarctica, Quaternary Science Reviews (2009), doi:10.1016/j.quascirev.2008.12.024

sea ice and deep water formation. Laminated sediments from Antarctic inner shelf basins, allow sub-seasonal to millennial reconstructions of the Holocene that may improve our understanding of climatic changes that occurred on decadal time scales. The Dumont d'Urville Trough in the Adélie Land region of the East Antarctica Margin (EAM) has received little attention despite evidence of very high sediment accumulation rates (Leventer et al., 2006). Here we present a study on marine sediment core MD03-2601, retrieved from the Dumont d'Urville Trough, located in the Adélie Land margin that contains 40 m of Holocene laminated diatom ooze. Previous data obtained from the same sedimentary archive have shown that in this region, the Holocene can be divided into two different climatic periods: a warm Hypsithermal, interrupted by a cool event, and a colder Neoglacial (Crosta et al., 2007). Based on a multi-proxy approach, this study aims to better understand the interaction of the different climatic sub-systems during the Holocene, with particular focus on episodes of glacier advance and retreat that occurred throughout these different climatic regimes. Holocene movements of glaciers are investigated in parallel to deep water production, and compared with surface ocean conditions (Crosta et al., 2008), modelled sea ice cover, air temperatures and precipitations (Renssen et al., 2005a, this study), and East Antarctic climate (Masson et al., 2000).

2. Adélie Land margin setting

The Dumont d'Urville Trough (DDUT) is located off Adélie Land on the EAM and is oriented SE–NW (Fig. 1A). It is composed of a succession of glacial depressions enclosed between the Dibble Bank to the west, and the Adélie Bank to the East. The Adélie Land region is dissected by several glaciers injecting freshwater and terrigenous particles in the coastal area. The majority of freshwater and terrigenous material comes from the Zélée, Astrolabe and Français glaciers, located 200, 120 and 55 km from the core site respectively (Fig. 1A). The DDUT shows evidences of streamlined elongated ridges, known as mega-scale glacial lineations (Shipp et al., 1999; McMullen et al., 2006) that testify to past ice streaming (Fig. 1B). Two different ice stream directions are apparent, one perpendicular to the costal line and in front of the Français glacier, and the other parallel to the coastal line, which probably originates from the Zélée glacier (Fig. 1B).

At present , the coastal area off Adélie Land is exposed to strong katabatic winds (Periard and Pettre, 1993) that support the DDU polynya throughout the winter season (Adolphs and Wendler, 1995; Arrigo and van Dijken, 2003) (Fig. 1A), located southward at 66.11°S, 139.31°E. Considered as ice factories, polynyas partly control the sea ice production. At the present time, sea ice covers the core site for 7–9 months of the year from February/March to November/December (Arrigo and van Dijken, 2003). As katabatic winds are directly induced by topography, we assume that the DDU polynya has been a persistent phenomenon throughout the Holocene period.

The DDUT is influenced by several water masses (Rintoul, 1998; Bindoff et al., 2000a,b; Williams and Bindoff, 2003): (1) the wind-driven East Wind Drift (EWD) also called Antarctic Coastal Current (ACC), which flows westward at the surface; (2) the Antarctic Surface water (AASW) constituting the near-surface layer on the continental shelf that joins up westward the EWD; (3) the Modified Circumpolar Deep Water (MCDW), which upwells at the Antarctic Divergence; and (4) the High Salinity Shelf Water (HSSW), formed by brine-rejection during winter sea ice formation and cooling of the MCDW, which flows northward as part of the Adélie Land Bottom Water (ALBW) (Fig. 1A). ALBW is characterised by cold, relatively fresh waters with high O_2 content that can rest for several years in the depressions of the continental shelf (Rintoul and Bullister, 1999). A CTD profile obtained on the MD03-2601 core site displays the same characteristic as the ALBW (θ: −1.465 °C, S: 34.511 at 721 m water depth). On Adélie Land, significant cross-shelf transport of ALBW is recorded at about 135°E (Beckmann and Pereira, 2003). Westward flow of ALBW indicates that bottom water formation occurs east of 135°E and may originate from Commonwealth Bay and Mertz Glacier Tongue, where large perennial and recurrent polynyas occur (Cavalieri and Martin, 1985; Massom et al., 1998; Rintoul, 1998; Williams and Bindoff, 2003; Arrigo and

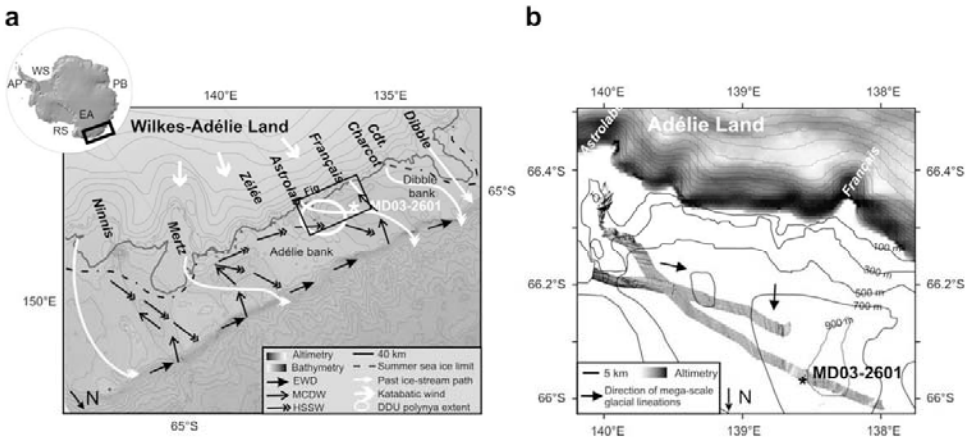

Fig. 1. Map showing the location of sediment core MD03-2601, altimetry and bathymetry in the study area, location of glaciers (in italic). (A) Limit of summer sea-ice cover (Schweitzer, 1995), location of past ice-streams (Massom et al., 1998; Escutia et al., 2003), detail of oceanographic currents and different water masses (Rintoul, 1998; Harris and Beaman, 2003; Williams and Bindoff, 2003), katabatic wind directions and average winter extent of the DDU polynya (Arrigo and van Dijken, 2003). Winter sea ice covers the whole oceanic area encompassed by the map. EWD, East Wind Drift; MCDW, Modified Circumpolar Deep Water; HSSW, High Salinity Shelf Water; MGT, Mertz Glacier Tongue. The inset narrows the location of the studied area regarding Antarctica, AP, Antarctic Peninsula; WS, Weddell Sea; PB, Prydz Bay; RS, Ross Sea; EA, East Antarctica plateau. (B) Shaded Bathymetric data are provided from the multibeam echosounder (TSM 5265) surveys of the area conducted onboard the R/V *Marion Dufresne II* (IPEV) during the CADO cruise. Note the location of mega-scale lineation, testifying to past ice streaming. Bathymetry data are based on ETOPO02 data set from http://www.ngdc.noaa.gov/mgg/fliers/01mgg04.html.

Please cite this article in press as: Denis, D., et al., Holocene glacier and deep water dynamics, Adélie Land region, East Antarctica, Quaternary Science Reviews (2009), doi:10.1016/j.quascirev.2008.12.024

van Dijken, 2003). The Marginal Ice Zone is believed to be macro- and micro-nutrient rich, and ice melting produces a stratified stable environment favourable for diatom blooms (Leventer, 1992).

3. Material and methods

Piston core MD03-2601 (66°03.07′S; 138°33.43′E; 746 m water depth) was recovered from the slope of one of the depressions composing the DDUT in 2003, during MD130 Images X cruise (CADO—Coring Adélie Diatom Oozes) on board R.V. *Marion Dufresne II* (Fig. 1A). The 40 m long sediment core is composed of diatom ooze alternating with structureless greenish ooze and millimetre to centimetre thick green-to-dark seasonal laminations (Denis et al., 2006). Sediment lithology is very fine from clay to silt fraction. The sediment texture is cottony due to the high abundance of diatom frustules. Bioturbation marks are very scarce throughout the core.

3.1. Age model

Ten radiocarbon dates were performed on MD03-2601 at the Leibniz Laboratory, Kiel, Germany. Nine ^{14}C were completed on the humic fraction of bulk organic matter and one ^{14}C was completed on calcite shells and fragments (Crosta et al., 2007). The radiocarbon dates used to construct the age model are the same dates used in Crosta et al. (2007, 2008), e.g. the humic acid dates, with the exception of both 998 and 1498 cm dates, which are incoherent with the meteoritic impact signal, recorded elsewhere at 4 cal ka BP (Courty et al., 2007). Nevertheless, the MD03-2601 age model constructed in this study is different from these previous studies (Fig. 2, Table 1). We calibrated raw ^{14}C dates to calendar ages using Calib 5.0 (Stuiver et al., 2005) and the marine calibration curve Marine04 (Hughen et al., 2004) with a reservoir age of 1300 years as advised for this region (Ingólfsson et al., 1998) (Table 1). Furthermore, we used a linear interpolation between control points, instead of linear regression (Crosta et al., 2007) to conserve changes of sedimentation rates that is necessary to calculate the $^{230}Th_{xs}$ (Fig. 2, see Section 3.2.1). It is worth noting that the date based on the calcite shells and fragments of the crinoid pieces presents an age only 400 years younger than surrounding humic dates. This difference highlights the maximum age error within humic acid dates of the age model. MD03-2601 therefore spans the last 11 cal ka BP, with an average sedimentation rate of 0.4 cm yr^{-1}. The first millennium was lost during coring (Fig. 2).

3.2. Rationale for proxy selection

Margin sites of high sediment accumulation are often zones of preferential deposition of redistributed sediment, especially when bottom water circulation is intense (Hall and McCave, 2000; Francois et al., 2004). We used two proxies ($^{230}Th_{excess}$, sortable silt) in order to better constrain the sediment redistribution and the bottom water circulation.

3.2.1. $^{230}Th_{excess}$

The ^{230}Th excess method estimates the contribution of the lateral sedimentary inputs, named the focusing factor (Francois et al., 2004, and references therein). The ^{230}Th geochemical behaviour permits to calculate an expected flux of scavenged ^{230}Th, which is function of the thickness of the water column and of the radioactive decay law. Indeed, the production rate of ^{230}Th in sea water is constant because it results from the disintegration of ^{234}U, which is nearly constant in the ocean because of its long residence time (Chen et al., 1986). Furthermore, and contrary to its radioactive parent, ^{230}Th presents a strong affinity with the particulate phase and is therefore rapidly scavenged and deposited on the sea floor

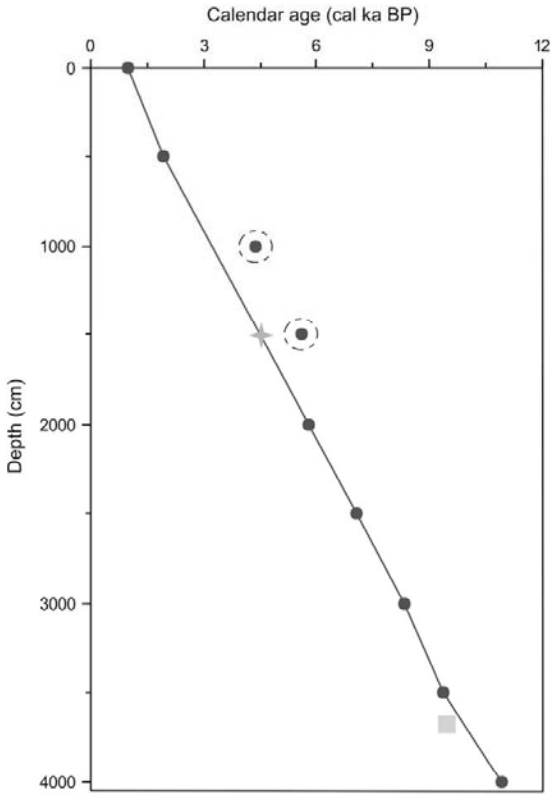

Fig. 2. MD03-2601 age model (black line). ^{14}C dates from humic acid are represented by black point. Two points appear out of the age model possibly because of old carbon input (dashed circles). The grey star represents the depth at which the 4000 yr BP meteoritic impact was evidenced (Courty et al., 2007). ^{14}C date from calcite shells and fragments is symbolised by a grey square. Dating uncertainties at 1σ level are within by the symbol points.

Table 1
Age model of core MD03-2601.

Depth	Material	Raw ages	Calibrated age for this study	SR	Calibrated age from Crosta et al. (2007)	Δ Age
cm bsf		^{14}C yr BP	cal yr BP	cm yr^{-1}	cal yr BP	yr
2	Humic	2350	1002	0.52	916	86
498	Humic	3235	1951	0.39	1871	80
998	**Humic**	**5175**	**4388**		**4314**	**74**
1440	**Meteorite**	**4000**	**4000**		–	–
1498	**Humic**	**6135**	**5598**		**5496**	**102**
1998	Humic	6310	5782	0.39	5703	79
2498	Humic	7450	7069	0.39	6984	85
2998	Humic	8775	8344	0.50	8369	−25
3498	Humic	9570	9348	0.32	9208	140
3661	**Carbonate**	**9730**	**9491**		**9384**	**107**
3998	Humic	10855	10923		10742	181

Raw dates were calibrated using CALIB 5.0 after removing a reservoir age of 1300 years (Ingólfsson et al., 1998). The rows in boldface show the dates that were discarded (see text). The sedimentation rates used for $^{230}Th_{xs}$ calculation are based on the calibrated ages used in the model. Δ ages between Crosta et al. (2007) that used Bard's polynome (Bard et al., 1998) and this study that used CALIB 5.0 (Stuiver et al., 2005) are reported. The maximum age difference between the two age models is less than 200 years.

Please cite this article in press as: Denis, D., et al., Holocene glacier and deep water dynamics, Adélie Land region, East Antarctica, Quaternary Science Reviews (2009), doi:10.1016/j.quascirev.2008.12.024

(Bacon and Anderson, 1982). The ^{230}Th measured in the sediment is corrected for lithogenic and authigenic contributions (See Veeh et al., 2000, for details) and for radioactive in-growth, in order to calculate the amount of ^{230}Th originated from scavenging in the water column, referred to as being "in excess" ($^{230}Th_{xs}$). These corrections are based on the estimation of detrital uranium ($^{238}U_{det}$), which permits constraint of lithogenic and authigenic contributions. To estimate the $^{238}U_{det}$, we used the ^{232}Th concentrations, which have uniquely a detrital origin (Brewer et al., 1980), by multiplying them with the ratio $(^{238}U/^{232}Th)_{det} = 0.58$, estimated for the Indian Southern Ocean (Dézileau et al., 2000). This ratio is within the range of ratios measured for other sectors of the Southern Ocean (Francois et al., 1993; Frank, 1996). Authigenic uranium was calculated as the difference between total and detrital uranium, correcting for in-situ growth of ^{230}Th.

Focusing factor (ψ) values are calculated by comparing downcore excess ^{230}Th ($[^{230}Th_{xs}]_0$) to the expected flux of ^{230}Th from the overlying water column (Francois et al., 2004):

$$\psi = \frac{\int_{z1}^{z2}[^{230}Th_{xs}]_0 \rho dz}{\beta h[t_2 - t_1]}$$

where $[^{230}Th_{xs}]_0$ is the age-corrected excess ^{230}Th in the sediment in dpm g^{-1}, ρ is the Dry Bulk Density (DBD) in g cm^{-3}, dz is the interval depth in cm, β is the rate of ^{230}Th production from ^{234}U ($\beta = 2.63 \times 10^{-5}$ dpm cm^{-3} ka^{-1}), h is the water depth, and t is the age in ka. ψ greater than 1 indicates focusing. This approach on active hydrodynamic shallow shelves close to sea ice system is not as straightforward as for open marine sites (Francois et al., 2004). Nevertheless, as shown later on, the comparison of $[^{230}Th_{xs}]_0$ with other indicators obtained from core MD03-2601, supports the use of ψ as a qualitative proxy of changes in lateral sedimentary input to the core site during the Holocene.

3.2.2. Sortable silt

The mean grain size of the non-cohesive 10–63 μm fraction, sortable silt ($\overline{SS}$) has been used as a palaeo-flow intensity proxy (McCave and Hall, 2006). Laboratory analyses with a Malvern grain size auto-analyser, performed on the raw sediment, measured the size of the diatoms rather than the terrigenous particles. The opal fraction reaches 35– 70% of the total sediment (Crosta et al., 2005) and entire or broken diatoms frustules strongly impact on the grain size value. Similar analyses on NaOH-treated material, though producing a better measure of the size of the terrigenous particles, still show contamination by broken diatoms and possibly loss of terrigenous particles. Therefore, we attempted to determine $\overline{SS}$ from lithic grain microscopic measurements directly on sediment indurated slides. Lithic grain counts, discernible under polarised light, have already been tested on permanent sediment slides and positively compared to titanium content (Denis et al., 2006). The lithic grain data obtained by this method does not allow access to the complete granulometric fraction because of the 5 μm microscopic threshold, but this problem is also encountered using a Coulter Counter or Malvern grain size auto-analyser (McCave and Hall, 2006). Two further limiting factors are apparent when comparing with the more classical methodologies. Firstly, the number of grains analysed is lower, the error bars associated with the calculation of $\overline{SS}$ due to the low numbers of grain counted are shown in Fig. 3. Secondly, the results arise from surface and not volume measurements that can induce two biases. First of all, flat grains occupy the same surface but a reduced volume in comparison to spherical grain, though the two types of grains have a different relationship with current velocity. Most of the grains preserved in core MD03-2601, and counted under the microscope, are quartz grains and thus are always rounded. We therefore believe that our measurements are relatively unbiased due to shape orientation. Additionally, given the unit change (factor ~100) between surface and volume measurements, surface results underestimate the importance of coarser grains versus finer grains on log-normal distribution. This bias induces a lesser differentiation of $\overline{SS}$ between samples. Thereby, the $\overline{SS}$ Holocene trends based on surface measurement should be even more obvious with volume measurement. Despite these limitations, we believe that the mean sortable silt values we produced are valid to identify variations in the bottom current flow over the core site throughout the Holocene. Finally, in the DDUT region, $\overline{SS}$ can be also be influenced by ice rafted transport (Hass, 2002). To consider this point, we have looked the distribution type in the total grain population and have calculated the sorting (σ) and the skewness (Sk) degrees that inform on the dispersion and the symmetry of the total grain population, respectively, and thus identify if there were significant contribution of IRD supply throughout the Holocene.

3.3. Laboratory procedures

The distribution of laminations along the entire core is based on X-ray imagery (Denis et al. (2006).

Aluminium (Al) contents were measured every 32 cm (~80 years resolution) by XRF analysis. Full XRF methodology is described in Fitton et al. (1998).

The activity of U series radioelement was determined at 60 depth horizons (Appendix A). Samples of 1–2 g dried sediment were spiked with yield monitors (^{232}U, ^{228}Th) before digestion in mixtures of HCl, HNO_3, $HClO_4$ and HF. DBD was measured by determining the dry weight of a known volume of wet sediment with a mean precision of 0.05 g cm^{-3} (Appendix A). The radioelements of interest were purified by ion exchange on anionic resins (Anderson and Fleer, 1982; Sicre et al., 2005). ^{238}U, ^{234}U, ^{232}Th and ^{230}Th activities were determined by α counting (mean 1 σ error: 4.9%, $n = 218$) as previously explained in Schmidt (2006).

Results of grain-size analysis have been obtained by digital analysis of lithic grains, from 101 permanent sediment slides with a mean 40 cm sampling step, corresponding to ~100 years resolution (Appendix B). Poly-propylene cubes (8 cm^3) were sampled from core section without disturbing the in situ repartition of the sediment. These sediment samples were thereafter hardened following the method described in Zaragosi et al. (2006). Image acquisition was performed manually using an imagery system composed of a Leica DM600B digital microscope and Leica Qwin 3.0 software on lithic grains larger than 5 μm. Analyses were based on 13.3 mm^2 area (e.g. 25 images). The final results were statistically treated to obtain the most relevant sedimentological parameters such as mean grain-size of the 10–63 μm fraction ($\overline{SS}$), sorting (σ), and skewness (Sk) with the geometric graphical method, modified after Folk and Ward (1957) (Blott and Pye, 2001). The surface grain areas in each sample are distributed, according to incremental logarithmic step, in 52 and 28 size classes, for the total particles population (e.g. >5 μm) and for the 10–63 μm fraction, respectively (given that the average number of counted grains in each sample is 770 and 540 for total and 10–63 μm fraction, respectively, Appendix B). The $\overline{SS}$ confidence intervals are between 0.5 and 2.3 μm, calculated according to Diógenes et al. (2005), which corresponds to a relative accuracy from 2% to 9% on $\overline{SS}$ (Fig. 3E).

Age model, laminae counts, aluminium content, radionucleides and grain size data are available electronically from the Pangaea Data Centre, Bremerhaven, Germany at http://doi.pangaea.de/10.1594/Pangaea.713060, -62, -63, -66 and -71, respectively.

Please cite this article in press as: Denis, D., et al., Holocene glacier and deep water dynamics, Adélie Land region, East Antarctica, Quaternary Science Reviews (2009), doi:10.1016/j.quascirev.2008.12.024

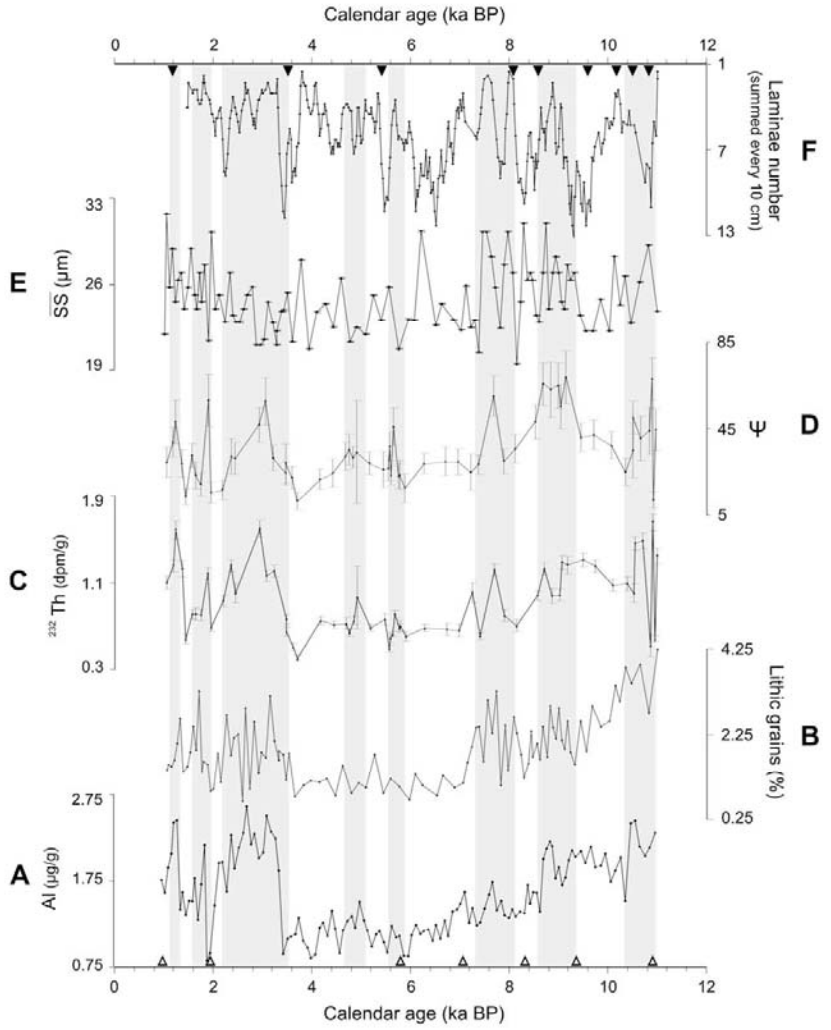

Fig. 3. MD03-2601 data versus time: (A) aluminium content, (B) percentage of the sediment surface held by lithic grains, (C) ^{232}Th, (D) focusing factor (φ) with error bars ($p < 0.05$), (E) sortable silt ($\overline{SS}$) with error bars ($p < 0.05$) that are within the symbol points, and (F) 4-point running average of the laminae number summed every 10 cm (note the reversed axis). Shaded areas highlight phases with high focusing and lithic inputs. The white triangles show the position of the ^{14}C dates used to construct the age model (Table 1 and Fig. 2) and the black triangles show the position of the samples chosen for illustrating Fig. 4.

4. Results

Detrital proxies (Al, lithic grain and ^{232}Th contents) show the same Holocene pattern with a general decreasing trend between 11 and 3.5 cal ka BP, interrupted by several rebounds at ~11–10.3, 9.4–8.6 and 8.1–7.3 cal ka BP, and subsequently followed by a three-phase rebound at 3.5–2.2 and 2–1.6 and 1.3–1.1 cal ka BP (Fig. 3A–C). Al and ^{232}Th contents show also a peak at around 5.1–4.8 cal ka BP (Fig. 3A–C).

The focusing factor (ψ) presents relatively high values from 10 to 70 over the last 11 cal ka BP (Fig. 3D). ψ shows similar variations to the detrital proxy records. The highest values of ψ ($\psi \geq 30$) are congruent to the abovementioned peaks in the detrital proxies with a supplementary peaks at 5.9–5.6 cal ka BP (Fig. 3D).

$\overline{SS}$ results show statistically significant variations between 19 µm and 33 µm (Fig. 3E). $\overline{SS}$ general trends display high values between 11 and 7.4 cal ka BP, followed by a low-stand plateau between 7.4 and 5 cal ka BP and then a continuous increase from 5 to 1 cal ka BP (Fig. 3E). More precisely, the first interval 11–7.4 cal ka BP shows two episodes with higher values of $\overline{SS}$ at ~10.8–10.1 and 9.3–7.4 cal ka BP. The sorting (σ) and the skewness (Sk) show low variations throughout the Holocene around 0.6 and 0, respectively, both on the total fraction (>5 µm) and on the 10–63 µm fraction, which indicates very well sorted and symmetrical grain population distributions (Blott and Pye, 2001) (Appendix B). The total grain size population (>5 µm) in our laboratory study shows a log-normal distribution (Fig. 4). The more subtle oscillations superimposed on the log-normal distribution plots are reflections of the limited number of grains considered in this study (Fig. 4, Appendix B). Holocene variations, recorded by $\overline{SS}$, coincide with significant shifts in the principal grain size mode of about 25, 21 and 35 µm (Fig. 4).

Please cite this article in press as: Denis, D., et al., Holocene glacier and deep water dynamics, Adélie Land region, East Antarctica, Quaternary Science Reviews (2009), doi:10.1016/j.quascirev.2008.12.024

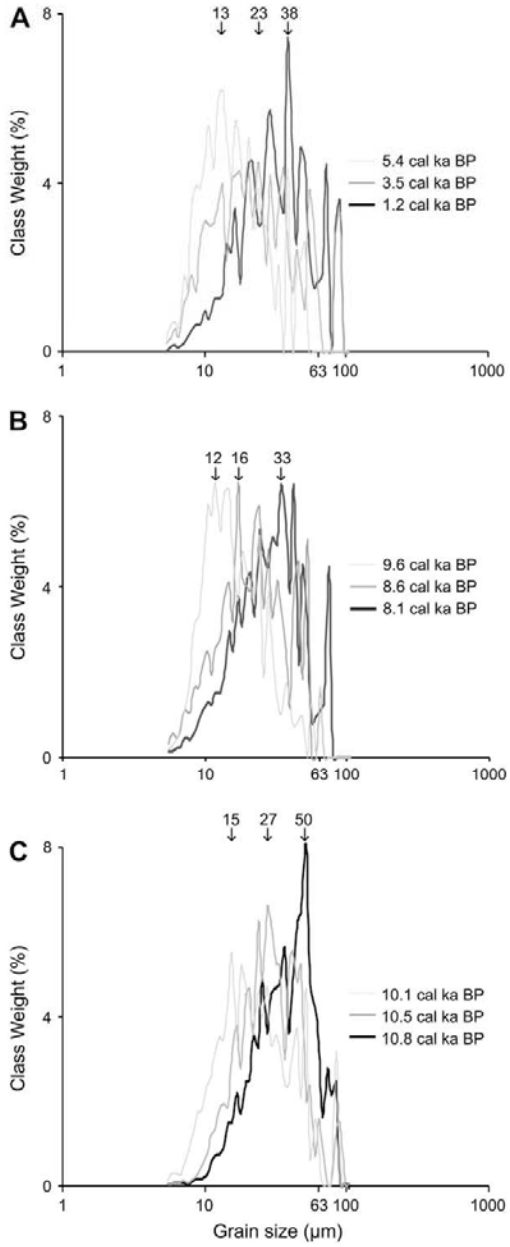

Fig. 4. Logarithmic frequency plots of surface area of the total grain fraction (>5 µm) for a selection of samples distributed throughout the core (black triangles in Fig. 3). Surface areas of each sample are distributed in 52 size classes between 5 and 190 µm, with a logarithmic incremental step. The age of each sample is noted on the right side and the principal mode of grain size is noted at the top of each case. Cases reported in plots A and B describe a decreasing trend of principal mode values whereas the case reported in plot C illustrates an increasing trend of principal mode value.

The number of laminae shows an opposite pattern to sortable silt with low laminae number congruent to larger and more abundant silt fraction (Fig. 3E,F). Low laminae numbers are recorded at around 11, 10.5–9.7, 9.1–8.3, 8.1–6.7 cal ka BP, and a decreasing trend is observed from 6.5–6 cal ka BP to 1 cal ka BP (Fig. 3F).

5. Discussion

5.1. Sedimentary processes

In order to decipher the sedimentary processes associated with changes in detrital content, focusing, and grain size (Figs. 3 and 5B,C), we compare our results with diatom assemblages that document the regional surface ocean conditions (Crosta et al., 2008). Here we use the *F. curta* /*F. kerguelensis* ratio (Fc/Fk ratio), which indicates the predominance of sea ice over ice- free conditions during the growing season (Leventer, 1991, 1998; Armand et al., 2005), reconstructing changes in the spring–summer sea ice cover. *Chaetoceros* resting spore (CRS) relative abundance is used as a proxy of increased surface water stratification (Leventer, 1991; Leventer et al., 1993), tracing the levels of glacier meltwater input (Leventer et al., 2002; Bianchi and Gersonde, 2004; Leventer et al., 2006) (Fig. 5C,D).

5.1.1. Lateral sediment supply

High lateral sedimentary input has affected the core site during the Holocene (Figs. 3D and 5A). Focusing by bottom currents is common on Antarctic continental shelves where bathymetric depressions act as sediment funnels (Camerlenghi et al., 2001; McMullen et al., 2006). The sea-floor bathymetry of the DDUT thus constitutes an area of favourable sediment accumulation. However, the presence of well-preserved seasonal diatom succession in laminations (Denis et al., 2006) demonstrates a local source of sediment focusing during periods of moderate lateral inputs. Superimposed to the baseline values, ψ shows long-term variations, marked by a decreasing trend between 11 and 3.5 cal ka BP and a three-phase rebound after 3.5 cal ka BP (Fig. 3A–C). Within this general pattern, eight periods with higher lateral sedimentary inputs are observed during the Holocene period at ~11–10.3, 9.4–8.6, 8.1–7.3, 5.9–5.6, 5.1–4.8, 3.5–2.2, 2–1.6 and 1.3–1.1 cal ka BP (Fig. 3D), referred to hereafter as events E1 to E8 (Fig. 5A). At both Milankovitch and sub-Milankovich time scales, except during E4, the lateral input pattern is congruent to terrigenous content changes, as shown by the agreement of the ψ record with the records of detrital proxies (Fig. 3A–D). On the Adélie Land continental shelf, southward and northward bottom transports can act simultaneously to supply terrigenous material to the inner deeper basin (Presti et al., 2003). E1 to E8 events correspond to an increase of cryophilic diatoms in comparison to open-ocean diatoms as evidenced by high Fc/Fk ratio values (Fig. 5A–C), which is not consistent with a supply from the outer shelf. Therefore, we suggest that the most predominant sediment supply at MD03-2601 during E1 to E8 and during the Holocene is from the coast via bottom water transport.

5.1.2. Bottom current

The well-sorted and symmetrical modal distribution of grain size and the small amount of grains superior to 63 µm demonstrate that the terrigenous particle transport and deposition is dependent on current-sorting rather than ice-rafted supply (Figs. 3E and 4). Variations of $\overline{SS}$ and principal mode values are thus attributed to significant changes of the bottom current competence during the Holocene. This is further confirmed by the negative correlation between the trends of sortable silt and laminae number records (Fig. 3E,F). The presence of biogenic laminae in marine cores is directly related to export productivity (Leventer et al., 2002) and to the level of bottom water oxygen (Anderson et al., 1990). The distribution of well-preserved laminae in MD03-2601 shows no similarities with productivity variations estimated from ^{230}Th normalised biogenic fluxes (Carson et al., submitted). Therefore, we suggest that the laminae distribution in MD03-2601 is the result of

Please cite this article in press as: Denis, D., et al., Holocene glacier and deep water dynamics, Adélie Land region, East Antarctica, Quaternary Science Reviews (2009), doi:10.1016/j.quascirev.2008.12.024

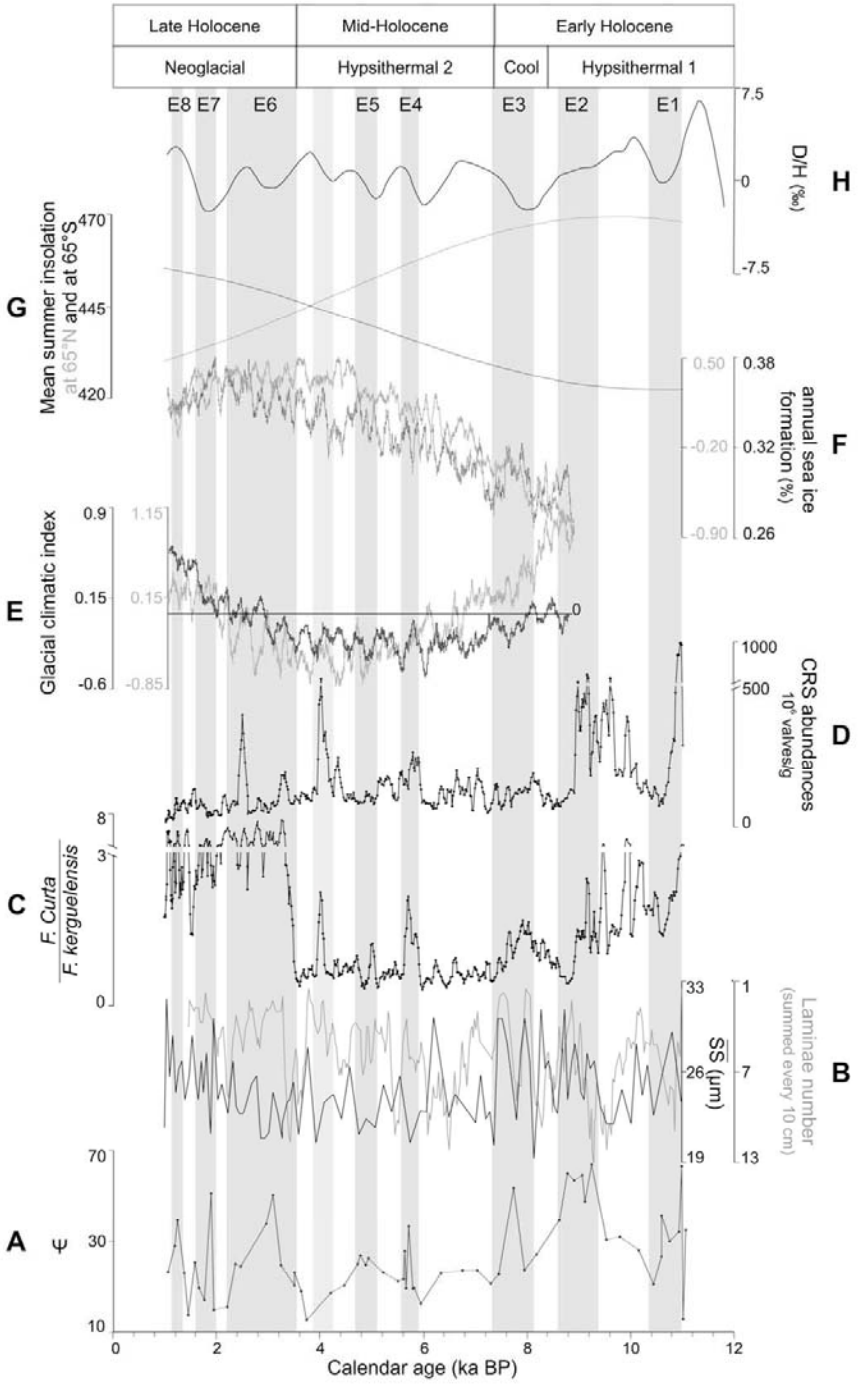

Fig. 5. MD03-2601 data compared to other climatic records versus time: (A) focusing factor (φ), (B) deep current proxies: $\overline{SS}$ (black line) and laminae number (4-point running average, grey line), (C) *F. curta* /*F. kerguelensis* ratio, (D) *Chaetoceros* resting spores (CRS) abundances, (E) glacier climatic index from modelled winter precipitation and summer temperature for our area (black line) and for the whole Antarctica (grey line, Renssen et al., 2005a), (F) annual sea ice formation in % to the surface area from modelled summer and winter sea ice cover for the study area (black line) and for the whole southern Ocean (grey line, Renssen et al., 2005a), (G) summer insolation at 65°N and 65°S (Berger and Loutre, 1991), and (H) empirical orthogonal function (EOF) analysis performed on D/H isotopic ratio from 11 East Antarctica ice core sites (Masson et al., 2000). At the top, climatic periods defined by Crosta et al. (2007) are reported. Dark shaded areas, reported from Fig. 3, highlight major changes in the glacier–sea ice–ocean system, called E1 to E8, while the light shaded area at 4 cal ka BP shows a sea ice expansion.

Please cite this article in press as: Denis, D., et al., Holocene glacier and deep water dynamics, Adélie Land region, East Antarctica, Quaternary Science Reviews (2009), doi:10.1016/j.quascirev.2008.12.024

changes in bottom water production, as observed in the Mertz region (Harris et al., 2001). In the Adélie Land region, changes in bottom current intensity is the result of variations in ALBW formation, initiated by HSSW formation during winter sea ice formation. We hereafter focus on the long-term pattern of the $\overline{SS}$ and laminae number records to infer ALBW Holocene dynamics (Fig. 5B). We believe the use of these proxies to interpret ALBW variations at shorter time scales is limited due to (1) calibration control on the proxies and (2) different resolution of the records.

5.1.3. Source and mode of sediment supply

During the Holocene, in particular at E1 to E8 events, variations of lateral terrigenous supply may result from sediment redistribution by bottom currents or from increased sediment load in coastal waters. There were no reworked diatoms and the overall diatom preservation is excellent (i.e. few dissolution) throughout the core (Crosta et al., 2005, 2007, 2008), which argues against sediment remobilisation or bedload transport. Additionally, variations in the focusing factor do not correspond with the changes of ALBW strength throughout the Holocene (Figs. 3 and 5). We therefore believe that both long-term variations of lateral input, in particular events E1 to E8, are the result of increased sediment load in coastal waters.

Glaciers in the Adélie Land region (e.g. Français, Astrolabe and Zélée) have clean upper and basal layers because off the weak aeolian flux during the Holocene (Delmonte et al., 2002; Edwards et al., 2006) and the solid bedrock (Monbeirg-Andrieu and Cailleux, 1962; Chamley, 1965; R.-P. Ménot, personal communication, 2008). Therefore, the release of particles by surface or basal melting is low when glacier activity is steady and important during glacier advance-retreat cycles (Gilbert et al., 2002; Oerlemans and Nick, 2006).

We therefore suggest the variations of detrital lateral inputs are related to glacier recession or expansion that release terrigenous particles into the surrounding waters during increased HSSW-ALBW terrigenous charge.

5.2. Palaeoclimatic interpretations

The goal of this study is to document the Holocene movements of Adélie Land glaciers and deep water formation and their links with the sea ice production at Milankovitch and sub-Milankovitch scale. We thus compare our results with records of surface ocean conditions (Crosta et al., 2008), model outputs of Holocene climate evolution for our study area, and High Southern Latitudes (Renssen et al., 2005a), mean summer insolation at 65°N and 65°S (Berger and Loutre, 1991), Antarctic continental climate (Masson et al., 2000), and other investigations of glacier fluctuations in East Antarctica (Ingólfsson et al., 1998; Roberts et al., 2004; Verkulich et al., 2002; Leventer et al., 2006; Fig. 6).

Winter precipitation, atmospheric summer temperature, winter and summer sea ice cover are extracted from the ECBilt-CLIO-VECODE coupled atmosphere–sea ice–ocean–vegetation model experiment, forced by annually varying orbital parameters and greenhouse gas (Renssen et al., 2005a), between 64–70°S and 130–150°E for this study and South of 60°S. It is worth noting that the model output for our study region and the rest of Antarctica (Renssen et al., 2005a) can be examined over the Milankovich time scale (Fig. 5E,F). The two most important parameters controlling ice mass-balance changes are winter precipitation and mean temperature during the ablation season (Andrews, 1975; Porter, 1975; Lie et al., 2003; Bakke et al., 2008). We have constructed a climatic index based on the normalised variations of the total winter precipitation (from April to October) minus the normalised variations of mean summer temperatures (between November and March) (Fig. 5E). Positive variations of this glacier climatic index indicate potential favourable periods for glacier advance in the study area and in Antarctica. The annual sea ice cover built up represents the difference between modelled winter and summer sea ice cover in the study area and for the whole Southern Ocean (Fig. 5F).

Deuterium/Hydrogen isotopic records from 11 East Antarctic ice cores have been analysed using an empirical orthogonal function and these results are used as an indicator of climatic trends on the East Antarctic plateau (Masson et al., 2000). Negative values signify colder conditions and positive values signify warmer conditions (Masson et al., 2000) (Fig. 5H).

5.2.1. Milankovitch variability

5.2.1.1. Early Holocene. The decreasing pattern of glacier discharge between 11 and 8.5 cal ka BP likely reflects the terminal glacier recession at the inner part of the Adélie Land continental shelf (Fig. 5A). Larger terrigenous inputs are expected at the onset of glacier recession. Terrigenous supply subsequently decreases during glacier grounding-line retreat and stabilisation. In addition, the decrease of the glacier climatic index confirms a suitable period of glacier retreat occurred between 9 (e.g. start of model experiment) and 7 cal ka BP over Adélie Land margin and around whole Antarctica (Fig. 5E). The additional effect of lower winter precipitations and warmer summer temperature is directly induced by the precessional component of the insolation at low and high southern latitudes (Renssen et al., 2005a; Fig. 5G). The Adélie Land glacier retreat coincides with the timing of the East Antarctic Ice Sheet (EAIS) deglaciation, documented from 13 to 8 cal ka BP (Fig. 6; Goodwin, 1993; Morgan et al., 1997; Ingólfsson et al., 1998; Taylor and McMinn, 2002; Leventer et al., 2006), which was forced by temperature warming and sea level rise (Masson et al., 2000; Masson-Delmotte et al., 2004; Leventer et al., 2006).

The decrease of the Fc/Fk ratio and CRS abundances between 11 and 9 cal ka BP (Fig. 5C,D) suggests the seasonal sea ice cover over the continental shelf was progressively ice free during the spring and summer seasons. Southward migration of the sea ice front associated with glacier grounding-line retreat also occurred between 11 and 9 cal ka BP in the Southern Ocean Atlantic Sector (Bianchi and Gersonde, 2004). During the Early Holocene, the sea ice cycle (e.g. initiation, extent, and duration) was influenced by the combination of global warm conditions (Masson et al., 2000; Masson-Delmotte et al., 2004) and EAIS decay.

High $\overline{SS}$ values and low laminae numbers between 11 and 7.4 cal ka BP argue for an active ALBW (Fig. 5B). The onset of a seasonal sea ice formation on the continental shelf was certainly responsible for the intense ALBW activity. Indeed, the southward migration of the sea ice front associated with glacier grounding-line retreat likely induced a relocation of deep water formation sites on the continental shelf. In the same way, the total retreat of sea ice in the spring–summer season enhanced winter sea ice production on the continental shelf, which increased HSSW, and thus ALBW, formation via sea ice brine rejection (Schmittner, 2003). Our results that suggest a vigorous seasonal sea ice cycle differ from model output during the 9–7 cal ka BP period (Fig. 5B,C,F). The receding glacial conditions affecting the Antarctic climate until 7 cal ka BP are, however, not evidenced by the model that did not "account for the effect of the long-term memory for events that occurred before 9 ka" (Renssen et al., 2005a).

5.2.1.2. Mid to Late Holocene. Between 7 and 3.5 cal ka BP, reduced glacier discharge reflects a stabilisation of the Adélie Land glacier that is in agreement with the flat trend of the glacier climatic index that shows slightly negative values (Fig. 5A–E). Increased snow accumulation rates have been reported since 7 cal ka BP on coastal East Antarctica at Taylor Dome and Law Dome (Steig et al., 2000;

Please cite this article in press as: Denis, D., et al., Holocene glacier and deep water dynamics, Adélie Land region, East Antarctica, Quaternary Science Reviews (2009), doi:10.1016/j.quascirev.2008.12.024

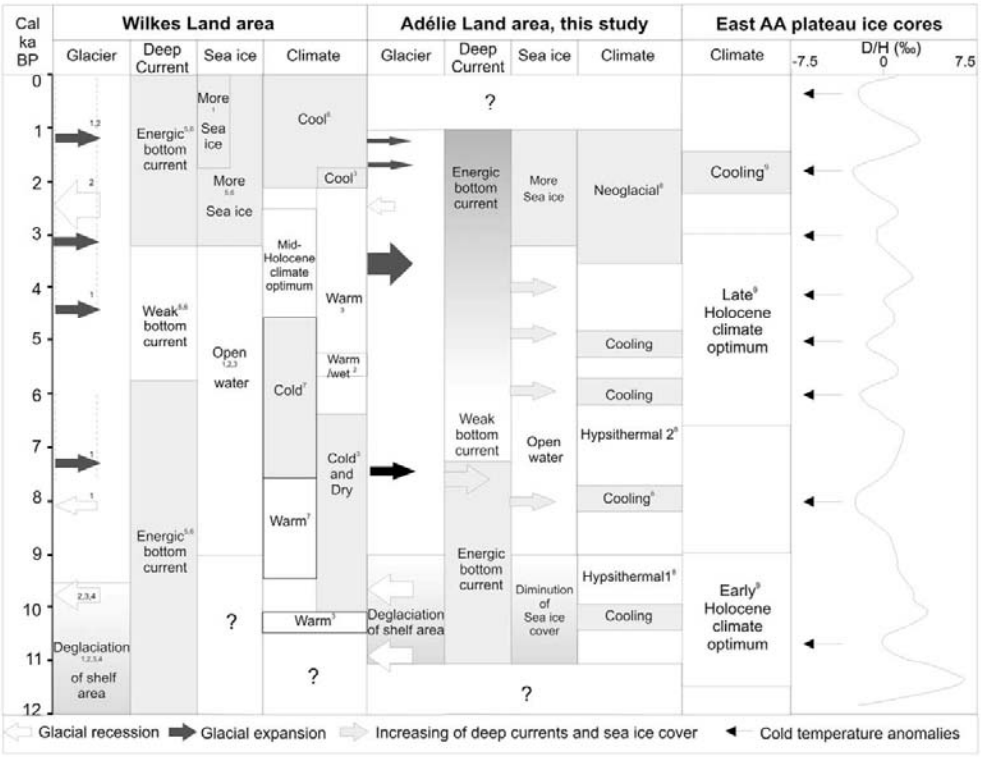

Fig. 6. Synthesis of the different glacier movements, deep current activity, sea ice conditions and climatic trends documented in the Adélie Land area by previous studies ([1]Ingólfsson et al.,1998; [2]Roberts et al., 2004; [3]Verkulich et al., 2002; [4]Leventer et al., 2006; [5]Harris et al., 2001; [6]Presti et al., 2003; [7]Kulbe et al., 2001; [8]Crosta et al., 2007) and by this study, in comparison to East Antarctica climate ([9]Masson et al., 2000). The ^{14}C ka BP dates reported in the publications were converted to calendar ages using Calib 5.0 for comparison with our age model.

van Ommen et al., 2004). These elevated snow accumulation rates have been attributed to enhanced latitudinal insolation gradients since 10 cal ka BP, favouring poleward atmospheric transport (Vimeux et al., 2001) and thus enhanced precipitations over Antarctica (Rind, 2000). Increased snow fall was likely compensated by greater ice melting due to warmer summer atmospheric temperatures (Renssen et al., 2005a), thus maintaining a stable glacier mass balance.

The Fc/Fk ratio and CRS abundances show low steady values (Fig. 5C,D), which infers an earlier sea ice waning and a longer ice-free season (Crosta et al., 2008). The reduced amount of easy-to-freeze runoffs, in comparison to deglacial conditions, may explain the lower Fc/Fk ratio values and CRS abundances and the reduced seasonal sea ice cycle though the Mid Holocene presents cooler conditions than during the Early Holocene (Masson et al., 2000; Masson-Delmotte et al., 2004).

Since 3.5 cal ka BP, glacier discharges has increased concomitantly with the glacier climatic index (Fig. 5A–E). The decrease in spring–summer surface temperature since 4–3.5 cal ka BP (Renssen et al., 2005a) has reduced the melting of winter snow and may have permitted the expansion of the glacier grounding-line during the Late Holocene. Studies on Law Dome and in the coastal margin of Adélie Land, show similar readvance of glaciers since 4 cal ka BP, forced by accumulation rate changes (Goodwin, 1998). The rapid increase of the spring–summer sea ice cover is also in line with this orbital forcing favourable to a latter sea ice waning and a shorter ice-free season (Fig. 5C; Renssen et al., 2005a; Crosta et al., 2008).

Both laminae number and sortable silt records indicate a progressive increase of the ALBW activity between 6.5–5 and 1 cal ka BP (Fig. 5B). The ALBW pattern is remarkably similar to modelled yearly sea ice formation since 7 cal ka BP (Fig. 5F), demonstrating the importance of the seasonal sea ice cycle on the deep water formation.

5.2.1.3. Larger implications. The long-term evolution of Adélie Land glaciers during the Holocene appears forced by precessional orbital changes, evident from the sea ice sub-system (Crosta et al., 2008). The strong synchronicity of these two climatic components argues for a similar sensitivity to the forcing factors such as seasonality and spring–summer temperature. This indicates a strong interconnection via positive feedbacks such as the albedo, which can affect the amplitude of their responses to climate changes. Adélie Land glaciers show a coherent pattern with model prediction for the whole of Antarctica (Fig. 5E), with most glaciers around Antarctica (Fig. 6; Ingólfsson et al., 1998; Leventer et al., 2006; Yoon et al., 2007) and around the world (Solomina et al., 2008 and references therein). Perhaps, some strong specificity of local climate and bedrock topography can induce time lag (Goodwin, 1998).

In-situ measurements indicated that the ALBW can supply 25% of the Antarctic Bottom Water (AABW) (Gordon and Tchernia, 1972; Rintoul, 1998), in agreement with model output (Baines and Condie, 1998; Goosse et al., 2001). If the close relationship between deep water formation and sea ice formation observed off Adélie Land is valid for the whole Antarctic Ocean (Fig. 5F; Renssen et al.,

Please cite this article in press as: Denis, D., et al., Holocene glacier and deep water dynamics, Adélie Land region, East Antarctica, Quaternary Science Reviews (2009), doi:10.1016/j.quascirev.2008.12.024

2005a), our results suggest a long-term increase of AABW formation between 6.5–5 and 1 cal ka BP. Although no other high-resolution Antarctic marine records of deep water formation exist, studies of sediment facies (Harris et al., 2001; Presti et al., 2003) and of grain size sorting (Yoon et al., 2007) similarly suggest enhanced bottom water formation during Early and Late Holocene in the Mertz area (Fig. 6) and the northern Antarctic Peninsula, respectively. Accordingly, $\delta^{13}C$ records measured on benthic foraminifera in several cores from the East Atlantic showed enhanced AABW flow since 7.5 cal ka BP, which was concomitant to a Mid-Holocene reduction of the North Atlantic Deep Water (NADW) ventilation (Sarnthein et al., 1994). Indeed, in the Northern Hemisphere, NADW contribution shows intensification between 10 and 6.5 cal ka BP, followed by a decreasing trend (Oppo et al., 2003). A slowing down of the northern end-member of the thermohaline circulation is also suggested since 7 cal ka BP, based on proxies related to surface and bottom waters (Duplessy et al., 2001; Rasmussen et al., 2002; Hall et al., 2004; Solignac et al., 2004), and during the Mid Holocene, based on model experiment (Ganopolski et al., 1998). To summarise, these results may suggest that: (1) a similar behaviour of deep water formation in both hemispheres occurs during the Early Holocene as a result of the onset of post-glacial seasonal sea ice cycle and, thus, re-initiation of deep water formation, and (2) an opposite behaviour of deep water formation since the Mid Holocene as a result of opposite precessional insolation trends that lead to increase seasonality in the Southern Hemisphere (Renssen et al., 2005a), and to decrease seasonality in the Northern Hemisphere (Renssen et al., 2005b; Naughton et al., 2007) (Fig. 5H).

5.2.2. Sub-Milankovitch variability

At the sub-orbital time scale, the glaciers, and sea ice climatic sub-systems demonstrate millennial oscillations that are well expressed during E1 to E8. These occurred within different climatic regimes: the warm Hypsithermal, the cool period and the colder Neoglacial (Fig. 5; Crosta et al., 2007). Interpretations are within the uncertainties of the age model.

5.2.2.1. Hypsithermal 1 (11–8.5 cal ka BP). During the deglaciation, we observe two events of high terrigenous input E1 and E2 dated at 11–10.3 cal ka BP and 9.4–8.6 cal ka BP (Fig. 5A). High CRS abundances occur at the beginning of E1 and before E2 until 9 cal ka BP (Fig. 5D). The focusing and CRS records would suggest there was increased surface water stratification during enhanced glacier meltwater input. High values of the Fc/Fk ratio also occurred until 9 cal ka BP, indicating persistent spring–summer sea ice cover during the warmer climate of the Early Holocene (Masson et al., 2000; Masson-Delmotte et al., 2004) (Fig. 5C). We suggest that glacier meltwaters decreased the surface salinity, which promoted sea ice freezing that persisted during diatom growing seasons. As negative feedback, sea ice formation isolated the atmosphere from the warmer ocean surface and increased the albedo, thus resulting in an additional cooling.

The CRS record also indicates that ice-melting pre-dated the effective glacier grounding-line recession off Adélie Land evidenced by E1 and E2 (Fig. 5A). Initiation of the ice melting (Fig. 5D) is in phase with warming phases recorded in East Antarctica (Fig. 5H) while E1 and E2 occurred 500 and 1000 years later respectively, during cooling phases (Masson et al., 2000) in relation to the great inertia of glacier mass-balances. The reaction time of ice sheet mass balance was calculated to be around 500 years at the ice cap margin (Goodwin, 1996, 1998). Massive freshwater discharges may have initiated or contributed to the two cooling events recorded over East Antarctica during the Early Holocene (Masson et al., 2000), in agreement with modelled climatic impacts of Antarctic freshwater runoffs (Mikolajewicz, 1998; Richardson et al., 2005; Stouffer et al., 2007).

5.2.2.2. Cool event (8.5–7 cal ka BP). During E3 (8.1–7.3 cal ka BP), the peak in focusing and terrigenous content is associated with low values of CRS abundances (Fig. 5A–D). These results suggest that the high terrigenous input is not related to glacier recession. Conversely, E3 is synchronous to increased sea ice cover as shown by higher values of the Fc/Fk ratio between 8.6 and 7.3 cal ka BP (Fig. 5C–H). E3 is also concomitant to one of the strongest Holocene atmospheric cooling over the East Antarctica plateau (Masson et al., 2000; Fig. 5H). This cooling may have triggered a glacier advance and sea ice expansion during the deglaciation. Glacier and sea ice advance during E3 are in phase with sea ice expansion recorded between 8 and 7 cal ka BP in the Atlantic sector of the Southern Ocean (van Beek et al., 2002; Bianchi and Gersonde, 2004; Nielsen et al., 2004), and follow the multi-centennial cold event at 8.2 cal ka BP observed around the globe (Mayewski et al., 2004; Rohling and Pälike, 2005). The end of E3 is marked by a relatively abrupt decrease in terrigenous content, focusing factor and sortable silt values, which is probably related to the return of warmer conditions at the onset of the Hypsithermal 2. This shift post-dates the abrupt Early to Mid-Holocene climatic transition (EMHT), recorded between 8.3 and 7.8 cal ka BP (Stager and Mayewski, 1997; Stager et al., 2003). This cool event and the following EMTH recorded here at high southern latitudes follow the climatic changes at low and high northern latitudes, supporting the idea of a coherent Holocene global pattern (Mayewski et al., 2004).

5.2.2.3. Hypsithermal 2 (7–3.5 cal ka BP). During the Hypsithermal 2, the 'steady' state of Adélie Land glaciers is interrupted by E4 and E5 at 5.9–5.6 cal ka BP and 5.1–4.8 cal ka BP (Fig. 5A). E4 is associated with higher values of the Fc/Fk ratio (Fig. 5C) and to a short peak in CRS abundances (Fig. 5D). Conversely, the terrigenous proxies show no increase during E4 (Fig. 3). On the other hand, E5 is associated to low values of the Fc/Fk ratio and CRS abundances but to greater values of Al content and ^{232}Th (Figs. 3 and 5). Both events are lagging small atmospheric cooling periods by 200–100 years (Figs. 2 and 5H; Masson et al., 2000). It is therefore believed that the cooling events triggered short-lived glacier re-advances and sea-ice waxing, which resulted in the small influx of terrigenous particles.

A third cooling event is evidenced in the diatom records at around 4 cal ka BP but is not reflected in the ψ, and the terrigenous proxies (Figs. 3 and 5A–D). This event may be triggered by the small atmospheric cooling centred at 4.2 cal ka BP (Fig. 5H; Masson et al., 2000). Our data indicate that this small cooling impacted the sea ice cover but had little effect on the glacier system of Adélie Land.

5.2.2.4. Neoglacial (3.5–1 cal ka BP). Three events of high focusing, E6 at 3.5–2.2 cal ka BP, E7 at 2–1.6 cal ka BP and E8 at 1.3–1.1 cal ka BP, are found during the Neoglacial period (Fig. 5A). These three events are associated with high terrigenous input (Fig. 3) implying important glacier discharges. These events are also concomitant to the highest Holocene values of the Fc/Fk ratio (Fig. 5C) but to non-significant changes of CRS abundances except for a short-lived peak at 2.4 cal ka BP (Fig. 5D). Given these data, we propose that E6, E7 and E8, events of terrigenous discharge, represent episodes of glacier and sea ice expansion rather than retreat because they are associated with spring–summer sea ice assemblages rather than with glacier meltwater assemblages. E6 was triggered by a small temperature fall as recorded over East Antarctica (Fig. 5H; Masson et al., 2000). It is possible that the amplitude of E6 is due to the increase of the glacier climatic index since 3.8 cal ka BP (Fig. 5E) that amplified the response of the glacier system, and to the concomitant sea ice expansion that

Please cite this article in press as: Denis, D., et al., Holocene glacier and deep water dynamics, Adélie Land region, East Antarctica, Quaternary Science Reviews (2009), doi:10.1016/j.quascirev.2008.12.024

provided a positive feedback. A similar expansion of Wilkes Land glaciers has been reported at ~3.3 ^{14}C ka BP (ca 3.5 cal ka BP) for the Mertz and the Ninnis glaciers (Fig. 6; McMullen et al., 2006). After a stabilisation, or even a small retreat of the glacier system between 3 cal ka BP and 2 cal ka BP that coincides with the ice margin retreat identified in Windmill island (101°E) between 2.8 and 1.9 ^{14}C ka BP (ca 2.9 cal ka BP and 1.85 cal ka BP) (Roberts et al., 2004), we observe two small glacier expansions. E7 lasted around 400 years and is triggered by an important temperature fall whereas E8 lasted 200 years and is congruent to a temperature rise (Fig. 5H; Masson et al., 2000). Additional work is necessary to understand the apparent paradox between warm atmospheric conditions, glacier advance and sea ice expansion during E8.

6. Conclusions

Major Holocene changes in lateral terrigenous inputs in the Adélie Land margin were triggered by the retreat and/or advance of the nearby glaciers. High-resolution analyses of grain size, diatom assemblages together with the quantification of well-preserved laminae in MD03-2601 provide complementary information about deep water formation and sea ice cover changes in the Adélie Land region. All records show long-term and millennial variability of the glacier–sea ice–oceanic systems into three distinct features:

- An Early Holocene period (11–8.5 cal ka BP) when glacier and sea ice retreat have favoured increased bottom water formation. At millennial time scale, two events of effective glacier recessions at 10.5 cal ka BP and 8.9 cal ka BP occurred after warming phases. Intense meltwater outflow associated with glacier recessions stratified the surface waters and enhanced the persistence of spring–summer sea ice. Increased sea ice cover provided a negative feedback on East Antarctic atmospheric temperatures by increasing albedo.
- One event of glacier advance at 7.7 cal ka BP occurred during a cooling phase (8.5–7 cal ka BP), documented in East Antarctica (Masson et al., 2000), in the Atlantic Sector of Southern Ocean (Bianchi and Gersonde, 2004) and around the world (Mayewski et al., 2004). Sea ice expansion during the cool event provided a positive feedback on East Antarctic atmospheric temperatures.
- A Mid- to Late Holocene (7–1 cal ka BP), when we observe an orbital-forced transition from a relatively 'steady' state of the glacier and sea ice systems to their major expansion after 3.5 cal ka BP. Increasing sea ice seasonality, by complete spring–summer retreat and active winter production, concomitantly enhanced deep water formation in DDUT due to greater brine rejection. At the millennial time scale, five glacier–sea ice advances triggered by atmospheric cooling on East Antarctica plateau occurred during the Mid- to Late Holocene.

The interconnections evident between glacier, sea ice and ocean climatic components point out the important impact of sea ice as a link between glacier and deep water dynamics, and its complex role because of its strong sensitivity to seasonality. Future work should improve the reconstruction of centennial-to-millennial oscillations of glaciers and sea ice in the Adélie Land region during the Holocene and the understanding of these components on the ALBW signal at this time scale.

Acknowledgements

We thank Elodie Marchès and Samuel Toucanne for their help in the understanding of sedimentological processes. We are grateful to both of the anonymous reviewers for their constructive suggestions. We personally thank people from Images X (CADO) cruise and from NSF-funded NBP0101 cruise for data and suggestions concerning the Dumont d'Urville Trough. Financial support for this study was provided by TARDHOL project through the national PNEDC Program (INSU-CNRS) with the logistic support of the French IPEV (Institut Paul Emile Victor), the International Marine Past Global Change Study (IMAGES) and the ACI JC ARTTE. This is an EPOC contribution No. 1721.

Appendix A. Supplemental material

Supplementary information for this manuscript can be downloaded at doi: 10.1016/j.quascirev.2008.12.024.

References

Adolphs, U., Wendler, A., 1995. A pilot-study on the interactions between katabatic winds and polynyas at the Adélie coast, eastern Antarctica. Antarctic Sciences 7, 307–314.
Anderson, R.F., Fleer, A.P., 1982. Determination of natural actinides and plutonium in marine particulate matter. Analytical Chemistry 54, 1142–1147.
Anderson, R.Y., Linsley, B.K., Gardner, J.V., 1990. Expression of seasonal and ENSO forcing in climatic variability at lower than ENSO frequencies: evidence from Pleistocene marine varves off California. Palaeogeography, Palaeoclimatology, Palaeoecology 78, 287–300.
Andrews, J.T., 1975. Glacial Systems. An Approach to Glaciers and their Environments. Duxbury Press, North Scituate.
Armand, L.K., Crosta, X., Romero, O., Pichon, J.J., 2005. The biogeography of major diatom taxa in Southern Ocean sediments: 1. Sea ice related species. Palaeogeography, Palaeoclimatology, Palaeoecology 223, 93–126.
Arrigo, K.R., van Dijken, G.L., 2003. Phytoplankton dynamics within 37 Antarctic coastal polynya systems. Journal of Geophysical Research 108 (C8), 3271. doi:10.1029/2002JC001739. 2003.
Bacon, M.P., Anderson, R.F., 1982. Distribution of thorium isotopes between dissolved and particulate forms in the deep sea. Journal of Geophysical Research 87, 2045–2056.
Baines, P.G., Condie, S., 1998. Observations and modelling of Antarctic downslope flows: a review. In: Jacobs, S.S., Weiss, R. (Eds.), Ocean, Ice and Atmosphere: Interactions at the Antarctic Continental Margin. Antarctic Research Series, vol. 75. American Geophysical Union, pp. 29–49.
Bakke, J., Lie, O., Dahl, S.O., Nesje, A., Bjune, A.E., 2008. Strength and spatial patterns of the Holocene wintertime westerlies in the NE Atlantic region. Global and Planetary Change 60, 28–41.
Bard, E., Arnold, M., et al., 1998. Radiocarbon calibration by means of mass spectrometric Th-230/U-234 and C-14 ages of corals: an updated database including samples from Barbados, Mururoa and Tahiti. Radiocarbon 40 (3), 1085–1092.
Beckmann, A., Pereira, A.F., 2003. Lateral tidal mixing in the Antarctic marginal seas. Ocean Dynamics 53, 21–26.
Berger, A., Loutre, M.F., 1991. Insolation values for the climate of the last 10 million years. Quaternary Science Reviews 10 (4), 297–317.
Bianchi, C., Gersonde, R., 2004. Climate evolution at the last deglaciation: the role of the Southern Ocean. Earth and Planetary Science Letters 228, 407–424.
Bindoff, N.L., Rintoul, S.R., Massom, R., 2000a. Bottom water formation and polynyas in Adélie Land, Antarctica. Papers and Proceedings of the Royal Society of Tasmania 133 (3), 51–57.
Bindoff, N.L., Rosenberg, M.A., Warner, M.J., 2000b. On the circulation and water masses over the Antarctic continental slope and rise between 80 and 150°E. Deep-Sea Research II 47, 2299–2326.
Blott, S.J., Pye, K., 2001. GRADISTAT: a grain size distribution and statistics package for the analysis of unconsolidated sediments. Earth Surface Processes and Landforms 26, 1237–1248.
Brewer, P.G., Nozaki, Y., Spencer, D., Fleer, A.P., 1980. Sediment trap experiments in the deep North Atlantic: isotopic and elemental fluxes. Journal of Marine Research 38, 703–728.
Camerlenghi, A., Domack, E., Rebesco, M., Gilbert, R., Ishman, S., Leventer, A., Brachfeld, S., Drake, A., 2001. Glacial morphology and post-glacial contourites in northern Prince Gustav Channel (NW Weddell Sea, Antarctica). Marine Geophysical Researches 22, 417–443.
Carson, D.S., Denis, D., Ganeshram, R.S., Crosta, X., Schmidt, S., submitted for publication. Reconstructing paleoproductivity throughout the Holocene: A case study from Adélie Land, East Antarctica. Geochimica et Cosmochimica Acta
Cavalieri, D.J., Martin, S., 1985. A passive microwave study of polynyas along the Antarctic Wilkes Land Coast. edited by S.S. Jacobs in Oceanology of the Antarctic Continental Shelf, Antarctic Research. Series 43, 177–201.
Chamley, H., 1965. Observations sur quelques sédiments marins prélevés près des côtes de Terre Adélie. Rec. Trav. Stat. Mar. Endoumé 36 (52), 215–228.
Chen, J.H., Wasserburg, G.J., von Damm, K.L., Edmond, J.M., 1986. The U-Th-Pb systematics in hot springs on the East Pacific Rise at 21°N and Guaymas Basin. Geochimica Cosmochimica Acta 50, 2467–2479.

Please cite this article in press as: Denis, D., et al., Holocene glacier and deep water dynamics, Adélie Land region, East Antarctica, Quaternary Science Reviews (2009), doi:10.1016/j.quascirev.2008.12.024

Courty, M.A., Cortese, G., Crisci, A., Crosta, X., Dewever, P., Fedoroff, M., Guichard, F., Mermoux, M., Michel, E., Smith, D., Thiemens, M., 2007. Impact fingerprints of the 4 kyr BP dust event based on archaeological, soil, lake and marine archives. General Assembly of the European Geosciences Union, Vienna, Austria. 16–20 April 2007.

Crosta, X., Crespin, J., Billy, I., Ther, O., 2005. Major factors controlling Holocene $\delta 13C_{org}$ changes in a seasonal sea ice environment, Adélie Land, East Antarctica. Global Biogeochemical Cycles 19, GB4029. DOI: 4010.1029/2004GB002426

Crosta, X., Debret, M., Denis, D., Courty, M.A., Ther, O., 2007. Holocene long- and short-term climate changes off Adélie Land, East Antarctica, Geochemistry. Geophysics, and Geosystems 8, Q11009. doi:10.1029/2007GC001718.

Crosta, X., Denis, D., Ther, O., 2008. Sea ice seasonality during the Holocene, Adélie Land, East Antarctica. Marine Micropaleontology 66, 222–232.

DeConto, R., Pollard, D., Harwood, D., 2007. Sea ice feedback and Cenozoic evolution of Antarctic climate and ice sheets. Paleoceanography 22, PA3214. 3210.1029/2006PA001350.

Delmonte, B., Petit, J.R., Maggi, V., 2002. LGM-Holocene changes and Holocene millennial-scale oscillations of dust particles in the EPICA Dome C ice core, East Antarctica. Annals of Glaciology 35, 306–312.

Denis, D., Crosta, X., Zaragosi, S., Martin, B., Mas, V., 2006. Seasonal and sub-seasonal climate changes recorded in laminated diatom ooze sediments, Adélie Land, East Antarctica. The Holocene 16, 1143–1153.

Dézileau, L., Bareille, G., Reiss, J.L., Lemoine, F., 2000. Evidence for strong sedment redistribution by bottom currents along the southeast Indian Ridge. Deep-Sea research I 47, 1899–1936.

Diógenes, A.N., Hoff, E.A., Fernandes, C.P., 2005. Grain size measurement by image analysis: An application in the ceramic and in the metallic industries. Proceedings of COBEM 2005, 18th International Congress of Mechanical Engineering, November 6–11, 2005, Ouro Preto, MG.

Duplessy, J.C., Ivanova, E., Murdmaa, I., Paterne, M., Labeyrie, L., 2001. Holocene paleoceanography of the northern Barents Sea and variations of the northward heat transport by the Atlantic Ocean. Boreas 30, 1–16.

Edwards, R., Sedwick, P., Morgan, V., Boutron, C., 2006. Iron in ice cores from Law Dome: A record of atmospheric iron deposition for maritime East Antarctica during the Holocene and Last Glacial Maximum. Geochemistry, Geophysics, and Geosystems 7 (12), Q12Q01. doi:10.1029/2006GC001307.

Escutia, C., Warnke, D., Acton, G.D., Barcena, A., Burckle, L., Canals, M., Frazee, C.S., 2003. Sediment distribution and sedimentary processes across the Antarctic Wilkes Land margin during the Quaternary. Deep-Sea Research II 50, 1481–1508.

Fitton, J.G., Saunders, A.D., Larsen, L.M., Hardarson, B.S., Norry, M.J., 1998. Volcanic rocks from the southeast Greenland margin at 63°N: Composition, petrogenesis, and mantle sources. Proceedings of the Ocean Drilling Program. Scientific Results 152, 331–350.

Folk, R.L., Ward, W.C., 1957. Brazos River bar: a study in the significance of grain size parameters. Journal of Sedimentary Petrology 27, 3–26.

Francois, R., Bacon, M.P., Altabet, M.A., 1993. Glacial/interglacial changes in sediment rain rate in the SW Indian sector of subantarctic waters as recorded by 230Th, 231Pa, U, and 15N. Paleoceanography 8, 611–629.

Francois, R., Frank, M., van de Loeff, M.M.R., Bacon, M.P., 2004. 230 Th normalization: An essential tool for interpreting sedimentary fluxes during the late Quaternary. Paleoceanography 19, PA1018, doi:10.1029/PA000939.

Frank, M., 1996. Reconstruction of late Quaternary environmental conditions applying the natural radionuclides 230Th, 10Be, 231Pa and 238U: A study of deep-sea sediments from the eastern Atlantic sector of the Antarctic Circumpolar Current system. Reports on Polar Research 186, 136.

Ganopolski, A., Kubatzki, C., Claussen, M., Brovkin, V., Petoukhov, V., 1998. The influence of vegetation–atmosphere–ocean interaction on climate during the mid-holocene. Science 280, 1916–1919.

Gilbert, R., Nielsen, N., Moller, H., Desloges, J.R., Rasch, M., 2002. Glacimarine sedimentation in Kangerdluk (Disko Fjord), West Greenland, in response to a surging glacier. Marine Geology 191, 1–18.

Goodwin, I.D., 1993. Holocene deglaciation, sea-level change, and the emergence of the Windmill Islands, Budd Coast, Antarctica. Quaternary Research 40, 70–80.

Goodwin, 1996. A mid to late Holocene readvance of the Law Dome ice margin, Budd Coast, East Antarctica. Antarctic Science 8, 395–406.

Goodwin, 1998. Did changes in Antarctic ice volume influence Late Holocene sea-level lowering? Quaternary Science Reviews 17, 319–332.

Goosse, H., Campin, J.-M., Tartinville, B., 2001. The sources of Antarctic bottom water in a global ice-ocean model. Ocean Modelling 3, 51–65.

Gordon, A.L., Tchernia, P., 1972. Waters of the continental margin off Adélie coast, Antarctica. In: Hayes, D.E. (Ed.), Antarctic Oceanology: II. The Australian–New Zealand Sector. Antarctic Research Series, vol. 19, pp. 59–70.

Hall, I.R., McCave, I.N., 2000. Palaeocurrent reconstruction, sediment and thorium focussing on the Iberian margin over the last 140 ka. Earth and Planetary Science Letters 178, 151–164.

Hall, I.R., Bianchi, G.G., Evans, J.R., 2004. Centennial to millennial scale Holocene climate-deep water linkage in the North Atlantic. Quaternary Science Reviews 23 (14-15), 1529–1536.

Harris, P.T., Beaman, R.J., 2003. Processes controlling the formation of the Mertz Drift, George Vth continental shelf, East Antarctica: evidence from 3.5 kHz sub-bottom profiling and sediment cores. Deep Sea Research Part II: Topical Studies in Oceanography 50, 1463–1480.

Harris, P.T., Brancolini, G., Armand, L., Busetti, M., Beaman, R.J., Giorgetti, G., Presti, M., Trincardi, F., 2001. Continental shelf drift deposit indicates non-steady state Antarctic bottom water production in the Holocene. Marine Geology 179, 1–8.

Hass, H.C., 2002. A method to reduce the influence of ice-rafted debris on a grain-size record from the northern Fram Strait, Arctic Ocean. Polar Research 21, 299–306.

Hodell, D.A., Kanfoush, S.L., Shemesh, A., Crosta, X., Charles, C.D., Guilderson, T.P., 2001. Abrupt cooling of Antarctic surface waters and sea ice expansion in the South Atlantic sector of the Southern Ocean at 5000 cal yr B.P. Quaternary Research 56, 191–198.

Hughen, K.A., Baillie, M.G.L., Bard, E., Bayliss, A., Beck, J.W., Bertrand, C.J.H., Blackwell, P.G., Buck, C.E., Burr, G.S., Cutler, K.B., Damon, P.E., Edwards, R.L., Fairbanks, R.G., Friedrich, M., Guilderson, T.P., Kromer, B., McCormac, F.G., Manning, S.W., Bronk Ramsey, C., Reimer, P.J., Reimer, R.W., Remmele, S., Southon, J.R., Stuiver, M., Talamo, S., Taylor, F.W., van der Plicht, J., Weyhenmeyer, C.E., 2004. Marine04 Marine radiocarbon age calibration, 26–0 ka BP. Radiocarbon 46, 1059–1086.

Ingólfsson, O., Hjort, C., 1999. The Antarctic contribution to Holocene global sea level rise. Polar Research 18, 323–330.

Ingólfsson, O., Hjort, C., Berkman, P.A., Björck, S., Colhoun, E., Goodwin, I.D., Hall, B., Hirakawa, K., Melles, M., Möller, P., Prentice, M.L., 1998. Antarctic glacial history since the last glacial maximum: an overview of the record on land. Antarctic Science 10, 326–344.

Joughin, I., Padman, L., 2003. Melting and freezing beneath Filchner-Ronne Ice Shelf, Antarctica. Geophysical Research Letters 30, 1477. doi: 1410.1029/2003GL016941.

Kulbe, T., Melles, M., Verkulich, S.R., Pushina, Z.V., 2001. East Antarctic climate and environmental variability over the last 9400 years inferred from marine sediments of the Bunger Oasis. Arctic. Antarctic and Alpine Research 33, 223–230.

Leventer, A., 1991. Sediment trap diatom assemblages from the northern Antarctic Peninsula region. Deep Sea Research Part I: Oceanographic Research Papers 38, 1127–1143.

Leventer, A., 1992. Modern distribution of diatoms in sediments from the George V Coast, Antarctica. Marine Micropaleontology 19, 315–332.

Leventer, A., 1998. The fate of Antarctic "sea-ice diatoms" and their use as paleoenvironmental indicators. In: Lizotte, M., Arrigo, K. (Eds.), Antarctic Sea Ice Biological Processes, Interactions and Variability. American Geophysical Union Antarctic Research Series, vol. 73, pp. 121–137.

Leventer, A., Dunbar, R.B., DeMaster, D.J., 1993. Diatom evidence for Late Holocene climatic events in Granite Harbor, Antarctica. Paleoceanography 8, 373–386.

Leventer, A., Domack, E., Barkoukis, A., McAndrews, B., Murray, J., 2002. Laminations from the Palmer Deep: A diatom-based interpretation. Paleoceanography 17 (2) 3-1 to 3–15.

Leventer, A., Domack, E., Dunbar, R., Pike, J., Stickley, C., Maddison, E., Brachfeld, S., Manley, P., McClennen, C., 2006. Marine sediment record from the East Antarctic margin reveals dynamics of ice sheet recession. Geological Society of America Today 16 (12), 4, doi:10.1130/GSAT01612A.1.

Lie, Ø., Olaf Dahl, S., Nesje, A., 2003. A theoretical approach to glacier equilibrium-line altitudes using meteorological data and glacier mass-balance records from southern Norway. Holocene 13, 365–372.

Massom, R.A., Harris, P.T., Michael, K.J., Potter, M.J., 1998. The distribution and formative processes of latent-heat polynyas in East Antarctica. Annals of Glaciology 27, 420–426.

Masson, V., Vimeux, F., Jouzel, J., Morgan, V., Delmotte, M., Ciais, P., Hammer, C., Johnsen, S., Lipenkov, Y., Mosley-Thompson, V.E., Petit, J.-R., Steig, E.J., Stievenard, M.R.V., 2000. Holocene climatic variability in Antarctica: what can be inferred from 11 ice core isotopic records? Quaternary Research 54, 348–358.

Masson-Delmotte, V., Stenni, B., Jouzel, J., 2004. Common millennial-scale variability of Antarctic and Southern Ocean temperatures during the past 5000 years reconstructed from the EPICA Dome C ice core. The Holocene 14 (2), 145–151.

Mayewski, P.A., Rohling, E.J., Curt Stager, J., Karlen, W., Maasch, K.A., David Meeker, L., Meyerson, E.A., Gasse, F., van Kreveld, S., Holmgren, K., Lee-Thorp, J., Rosqvist, G., Rack, F., Staubwasser, M., Schneider, R.R., Steig, E.J., 2004. Holocene climate variability. Quaternary Research 62, 243–255.

McCave, I.N., Hall, I.R., 2006. Size sorting in marine muds: Processes, pifalls, and prospects for paleoflow-speed proxies. Geochemistry, Geophysics, Geosystems 7, Q10N05. doi:10.1029/2006GC001284.

McMullen, K., Domack, E., Leventer, A., Olson, C., Dunbar, R., Brachfeld, S., 2006. Glacial morphology and sediment formation in the Mertz Trough, East Antarctica. Palaeogeography, Palaeoclimatology, Palaeoecology 231, 169–180.

Mikolajewicz, U., 1998. Effect of meltwater input from the Antarctic ice sheet on the thermohaline circulation. Annals of Glaciology 27, 311–315.

Monbeirg-Andrieu, M., Cailleux, A., 1962. Grains éolisés dans les grès erratiques de Terre Adélie. C.R. Soc. Géol. Fr. 5, 151.

Morgan, V.I., Wookey, C.W., Li, J., Ommen, T.D.V., Skinner, W., Fitzpatrick, M.F., 1997. Site information and initial results from deep ice drilling on Law Dome. Journal of Glaciology 43, 3–10.

Naughton, F., Bourillet, J.F., Goñi, M.F.S., Turon, J.L., Jouanneau, J.M., 2007. Long-term and millennial-scale climate variability in northwestern France during the last 8850 years. Holocene 17, 939–953.

Nielsen, S.H.H., Koç, N., Crosta, X., 2004. Holocene climate in the Atlantic sector of the Southern Ocean: Controlled by insolation or oceanic circulation? Geology 32, 317–320.

Oerlemans, J., Nick, F.M., 2006. Modelling the advance-retreat cycle of a tidewater glacier with simple sediment dynamics. Global and Planetary Change 50, 148–160.

Oppo, D.W., McManus, J.F., Cullen, J.L., 2003. Deepwater variability in the Holocene Epoch. Nature 422, 277–278.

Please cite this article in press as: Denis, D., et al., Holocene glacier and deep water dynamics, Adélie Land region, East Antarctica, Quaternary Science Reviews (2009), doi:10.1016/j.quascirev.2008.12.024

Periard, C., Pettre, P., 1993. Some aspects of the climatology of Dumont d'Urville, Adelie Land, Antarctica. International Journal of Climatology 13 (3), 313–327.
Porter, S.C., 1975. Equilibrium-line altitudes of late Quaternary glaciers in the Southern Alps, New Zealand. Quaternary Research 5, 27–47.
Presti, M., De Santis, L., Busetti, M., Harris, P.T., 2003. Late Pleistocene and Holocene sedimentation on the George V Continental Shelf, East Antarctica. Deep Sea Research Part II: Topical Studies in Oceanography 50, 1441–1461.
Rasmussen, T.L., Backstrom, D., Heinemeier, J., Klitgaard-Kristensen, D., Knutz, P.C., Kuijpers, A., Lassen, S., Thomsen, E., Troelstra, S.R., Van Weering, T.C.E., 2002. The Faroe–Shetland Gateway: Late Quaternary water mass exchange between the Nordic seas and the northeastern Atlantic. Marine Geology 188, 165–192.
Renssen, H., Goosse, H., Fichefet, T., Massom-Delmotte, V.A., Koç, N., 2005a. Holocene climate evolution in the high-latitude Southern Hemisphere simulated by a coupled atmosphere-sea-ice-ocean-vegetation model. The Holocene 15, 951–964.
Renssen, H., Goosse, H., Fichefet, T., Brovkin, V., Driesschaert, E., Wolk, F., 2005b. Simulating the Holocene climate evolution at northern high latitudes using a coupled atmosphere-sea ice-ocean-vegetation model. Climate Dynamics 24, 23–43.
Richardson, G., Wadley, M.R., Heywood, K.J., Stevens, D.P., Banks, H.T., 2005. Short-term climate response to a freshwater pulse in the Southern Ocean. Geophysical Research Letters 32, 1–4.
Rind, D., 2000. Relating paleoclimate data and past temperature gradients: Some suggestive rules. Quaternary Science Reviews 19, 381–390.
Rintoul, S.R., 1998. On the origins and influence of Adélie Land bottom water. In: Jacobs, S.S., Weiss, R.F. (Eds.), Ocean, Ice and Atmosphere: Interactions at the Antarctic Continental Margin. Antarctic Research Series, vol. 75, pp. 151–171.
Rintoul, S.R., Bullister, J.L., 1999. A late winter hydrographic section from Tasmania to Antarctica. Deep Sea Research Part I. Oceanographic Research Papers 46, 1417–1454.
Roberts, D., McMinn, A., Cremer, H., Gore, D.B., Melles, M., 2004. The Holocene evolution and palaeosalinity history of Beall Lake, Windmill Islands (East Antarctica) using an expanded diatom-based weighted averaging model. Palaeogeography, Palaeoclimatology, Palaeoecology 208, 121–140.
Rohling, E.J., Pälike, H., 2005. Centennial-scale climate cooling with a sudden cold event around 8200 years ago. Nature 434, 975–979.
Sarnthein, M., Winn, K., Jung, S.J.A., Duplessy, J.-C., Labeyrie, L., Herlenkeuser, H., Ganssen, G., 1994. Changes in east Atlantic deepwater circulation over the last 30,000 years: Eight time slice reconstructions. Paleoceanography 9 (2), 209–267.
Schmidt, S., 2006. Impact of Mediterranean Outflow Water on particle dynamics in intermediate waters of the North-East Atlantic, as revealed by 234Th and 228Th. Marine Chemistry 100, 289–298.
Schmittner, A., 2003. Southern Ocean sea ice and radiocarbon ages of glacial bottom waters. Earth and Planetary Science Letters 213, 53–62.
Schweitzer, P.N., 1995. Monthly Averaged Polar Sea Ice Concentration. U.S. Geological Survey Digital Data Series, Virginia.
Shipp, S., Anderson, J., Domack, E., 1999. Late Pleistocene–Holocene retreat of the West Antarctic ice-sheet system in the Ross Sea: Part 1—Geophysical results. Bulletin of the Geological Society of America 111, 1486–1516.
Sicre, M.A., Labeyrie, L., Ezat, U., Duprat, J., Turon, J.L., Schmidt, S., Michel, E., Mazaud, A., 2005. Mid-latitude Southern Indian Ocean response to Northern Hemisphere Heinrich events. Earth and Planetary Science Letters 240, 724–731.
Solignac, S., de Vernal, A., Hillaire-Marcel, C., 2004. Holocene sea-surface conditions in the North Atlantic—contrasted trends and regimes in the western and eastern sectors (Labrador Sea vs. Iceland Basin). Quaternary Science Reviews 23, 319–334.
Solomina, O., Haeberli, W., Kull, C., Wiles, G., 2008. Historical and Holocene glacier-climate variations: General concepts and overview. Global and Planetary Change 60, 1–9.
Stager, J.C., Mayewski, P.A., 1997. Abrupt Early to Mid-Holocene climatic transition registered at the equator and the poles. Science 276, 1834–1836.
Stager, J.C., Cumming, B.F., Meeker, L.D., 2003. A 10,000-year high-resolution diatom record from Pilkington Bay, Lake Victoria, East Africa. Quaternary Research 59, 172–181.
Steig, E.J., Morse, D.L., Waddington, E.D., Stuiver, M., Grootes, P.M., Mayewski, P.A., Twickler, M.S., Whitlows, S.I., 2000. Wisonsinan and Holocence climate history from an ice core at Taylor Dome, western Ross embayment, Antarctica. Geografiska Annaler, Series A: Physical Geography 82, 213–232.
Stouffer, R.J., Seidov, D., Haupt, B.J., 2007. Climate response to external sources of freshwater: North Atlantic versus the Southern Ocean. Journal of Climate 20, 436–448.
Stuiver, M., Reimer, P.J., Reimer, R.W., 2005. CALIB 5.0. [WWW program and documentation].
Taylor, F., McMinn, A., 2002. Late Quaternary diatom assemblages from Prydz Bay, Eastern Antarctica. Quaternary Research 57, 151–161.
van Beek, P., Reyss, J.L., Paterne, M., Gersonde, R., van der Loeff, M.R., Kuhn, G., 2002. 226Ra in barite: Absolute dating of Holocene Southern Ocean sediments and reconstruction of sea-surface reservoir ages. Geology 30, 731–734.
van Ommen, T.D., Morgan, V.I., Curran, M.A.J., 2004. Deglacial and Holocene changes in accumulation at Law Dome. Annals of Glaciology 39, 359–365.
Veeh, H.H., McCorkle, D.C., Heggie, D.T., 2000. Glacial/interglacial variations of sedimentation on the West Australian continental margin: constraints from excess 230Th. Marine Geology 166, 11–30.
Verkulich, S.R., Melles, M., Hubberten, H.-W., Pushina, Z.V., 2002. Holocene environmental changes and evolution of Figurnoye Lake in the southern Bunger Hills, East Antarctica. Journal of Paleolimnology 28, 253–267.
Vimeux, F., Masson, V., Jouzel, J., Petit, J.R., Steig, E.J., Stievenard, M., Vaikmae, R., White, J.W.C., 2001. Holocene hydrological cycle changes in the Southern Hemisphere documented in East Antarctic deuterium excess records. Climate Dynamics 17, 503–513.
Wagner, B.,Melles, M., 2007. The heterogeneity of Holocene climatic and environmental history along the East Antarctic coastal regions. In: Cooper, A.K., Raymond, C.R. et al. (Eds.), Antarctica: a Keystone in a Changing World—Online Proceedings of the 10th ISAES, USGS Open-file Report 2007-1047, Extended Abstract 161, 4 pp.
Williams, G.D., Bindoff, N.L., 2003. Wintertime oceanography of the Adélie Depression. Deep-Sea Research II 50, 1373–1392.
Yoon, H.I., Khim, B.K., Yoo, K.C., Bak, Y.S., Lee, J.I., 2007. Late glacial to Holocene climatic and oceanographic record of sediment facies from the South Scotia Sea off the northern Antarctic Peninsula. Deep Sea Research Part II: Topical Studies in Oceanography 54, 2367–2387.
Zaragosi, S., Bourillet, J.-F., Eynaud, F., Toucanne, S., Denhard, B., Van Toer, A., Lanfumey, V., 2006. The impact of the last European deglaciation on the deep-sea turbidite systems of the Celtic-Armorican margin (Bay of Biscay). Geo-Marine Letters 26, 317–329.

Please cite this article in press as: Denis, D., et al., Holocene glacier and deep water dynamics, Adélie Land region, East Antarctica, Quaternary Science Reviews (2009), doi:10.1016/j.quascirev.2008.12.024

Appendix

Depth (cm)	Age (y)	DBD g/cm^{-3}	^{238}U dpm/g	1 σ error	$^{238}U_a$ dpm/g	1 σ error	^{232}Th dpm/g	1 σ error	^{230}Th dpm/g	1 σ error	$(^{230}Th_{xs})_0$ dpm/g	1 σ error	ψ	1 σ error
35	1065	0.17	2.05	0.10	1.41	0.11	1.10	0.06	1.29	0.07	0.64	0.15	29	7
99	1188	0.20	2.87	0.09	2.14	0.09	1.26	0.06	1.47	0.07	0.72	0.13	39	7
130	1247	0.23	2.08	0.10	1.16	0.11	1.58	0.08	1.72	0.09	0.80	0.17	48	10
198	1377	0.16	2.19	0.09	1.48	0.10	1.23	0.07	1.38	0.08	0.66	0.15	29	7
230	1438	0.13	1.81	0.07	1.47	0.08	0.58	0.04	0.74	0.05	0.38	0.11	13	4
298	1568	0.21	2.22	0.07	1.74	0.07	0.81	0.04	1.07	0.05	0.58	0.10	33	6
340	1649	0.18	1.60	0.07	1.13	0.08	0.81	0.06	0.95	0.06	0.47	0.13	23	6
398	1760	0.14	2.16	0.10	1.69	0.11	0.80	0.05	0.97	0.06	0.48	0.14	19	6
470	1897	0.27	2.78	0.13	2.09	0.14	1.19	0.06	1.51	0.07	0.80	0.17	58	12
498	1951	0.14	2.38	0.10	1.98	0.10	0.69	0.04	0.84	0.04	0.40	0.13	15	5
594	2196	0.15	2.23	0.11	1.69	0.11	0.93	0.05	1.09	0.06	0.52	0.14	16	4
660	2365	0.28	2.36	0.11	1.63	0.12	1.26	0.05	1.32	0.06	0.56	0.15	32	8
697	2459	0.19	2.88	0.12	2.30	0.13	1.00	0.09	1.43	0.11	0.81	0.19	31	7
890	2952	0.28	2.42	0.08	1.49	0.09	1.60	0.08	1.78	0.08	0.84	0.15	47	8
940	3080	0.39	2.48	0.11	1.80	0.11	1.16	0.05	1.45	0.06	0.74	0.14	58	11
1002	3238	0.23	3.12	0.10	2.42	0.10	1.21	0.05	1.45	0.06	0.68	0.13	31	6
1098	3483	0.20	1.98	0.10	1.53	0.10	0.77	0.04	1.06	0.05	0.58	0.13	24	5
1100	3489	0.25	2.25	0.14	1.88	0.15	0.65	0.04	0.99	0.05	0.56	0.18	29	9
1147	3609	0.29	1.45	0.06	1.15	0.06	0.51	0.03	0.70	0.04	0.37	0.09	22	5
1190	3718	0.18	1.88	0.09	1.65	0.09	0.40	0.03	0.60	0.03	0.31	0.11	11	4
1370	4178	0.23	1.81	0.07	1.37	0.07	0.75	0.04	0.95	0.05	0.47	0.10	21	5
1476	4449	0.22	2.24	0.12	1.82	0.12	0.71	0.04	1.01	0.04	0.54	0.15	24	7
1572	4694	0.24	2.18	0.09	1.76	0.10	0.72	0.05	1.13	0.07	0.66	0.14	32	7
1600	4766	0.28	1.78	0.09	1.41	0.09	0.64	0.04	1.04	0.05	0.63	0.13	35	7
1634	4852	0.26	1.75	0.06	1.31	0.07	0.76	0.04	1.09	0.05	0.61	0.10	32	5
1660	4919	0.28	2.44	0.09	1.88	0.19	0.97	0.29	1.24	0.31	0.61	0.44	34	24
1770	5200	0.28	1.86	0.07	1.47	0.07	0.69	0.03	0.97	0.04	0.52	0.10	29	5
1880	5481	0.28	1.88	0.11	1.44	0.11	0.76	0.06	0.96	0.06	0.46	0.15	26	8
1919	5580	0.27	1.91	0.08	1.63	0.08	0.49	0.03	0.84	0.05	0.48	0.11	26	6
1929	5606	0.26	1.72	0.08	1.37	0.09	0.59	0.04	1.09	0.06	0.70	0.13	37	7
1940	5634	0.26	1.87	0.07	1.51	0.07	0.63	0.02	0.87	0.03	0.44	0.09	23	4
1962	5690	0.29	2.22	0.12	1.75	0.13	0.81	0.04	1.31	0.05	0.78	0.15	46	9
1995	5774	0.25	2.12	0.08	1.73	0.09	0.68	0.04	0.92	0.05	0.45	0.11	23	6
2005	5800	0.26	2.24	0.10	1.83	0.10	0.70	0.05	0.93	0.05	0.44	0.13	23	7
2050	5916	0.19	2.25	0.14	1.90	0.15	0.61	0.04	0.90	0.05	0.46	0.18	17	7
2200	6302	0.22	2.26	0.08	1.86	0.08	0.69	0.03	1.14	0.05	0.67	0.11	29	5
2368	6734	0.25	1.94	0.08	1.55	0.09	0.67	0.06	1.05	0.07	0.59	0.13	30	7
2470	6997	0.23	2.15	0.07	1.77	0.08	0.66	0.06	1.12	0.08	0.65	0.13	29	6
2572	7258	0.26	2.16	0.08	1.57	0.10	1.01	0.09	1.14	0.10	0.47	0.16	25	9
2632	7411	0.24	2.52	0.07	2.17	0.07	0.61	0.03	1.06	0.04	0.58	0.09	28	5
2750	7712	0.31	2.45	0.11	1.74	0.11	1.22	0.06	1.75	0.07	0.97	0.15	60	10
2832	7921	0.20	2.17	0.09	1.70	0.10	0.80	0.06	1.28	0.07	0.73	0.14	30	6
2925	8158	0.24	1.96	0.09	1.55	0.09	0.71	0.06	1.21	0.08	0.72	0.14	36	7
3114	8577	0.27	1.98	0.08	1.41	0.08	0.98	0.05	1.33	0.06	0.69	0.12	48	8
3190	8730	0.27	2.46	0.11	1.75	0.11	1.23	0.05	1.75	0.07	0.96	0.15	66	10
3266	8882	0.34	2.00	0.09	1.43	0.10	0.98	0.07	1.36	0.09	0.72	0.15	63	13
3342	9035	0.27	2.99	0.11	2.41	0.12	0.99	0.06	1.65	0.08	0.93	0.15	65	11
3366	9083	0.27	2.71	0.11	1.96	0.11	1.29	0.06	1.66	0.08	0.80	0.15	56	10
3424	9199	0.29	2.75	0.10	2.01	0.11	1.27	0.08	1.79	0.10	0.94	0.17	69	12
3546	9499	0.29	2.60	0.10	1.84	0.11	1.31	0.06	1.74	0.07	0.88	0.14	41	7
3626	9751	0.33	2.33	0.08	1.60	0.09	1.25	0.06	1.60	0.07	0.78	0.13	42	7
3742	10117	0.29	2.46	0.09	1.83	0.10	1.08	0.05	1.53	0.07	0.79	0.14	37	6
3834	10406	0.23	2.83	0.12	2.19	0.13	1.09	0.07	1.45	0.08	0.65	0.17	25	6
3878	10545	0.31	2.31	0.19	1.72	0.20	1.01	0.08	1.39	0.10	0.68	0.25	35	13
3880	10551	0.38	2.18	0.07	1.33	0.08	1.46	0.06	1.73	0.07	0.82	0.12	50	8
3930	10709	0.30	2.51	0.16	1.65	0.17	1.49	0.07	1.78	0.08	0.82	0.21	40	11
3984	10879	0.28	3.25	0.15	2.95	0.16	0.52	0.10	1.49	0.14	0.96	0.24	44	11
4000	10929	0.39	2.47	0.09	1.51	0.10	1.66	0.08	2.10	0.09	1.08	0.15	69	10
4015	10977	0.19	2.23	0.10	1.89	0.10	0.58	0.03	0.89	0.04	0.38	0.12	12	4
4025	11008	0.43	2.62	0.09	1.84	0.10	1.35	0.07	1.56	0.08	0.64	0.14	44	10

Appendix 1. Geochemical data for MD03-2601.

		Total grain size fraction (> 5 µm)						10-63 µm grain size fraction					
Depth cmbsf	**Age** cal yr BP	**GN**	**Mean** µm	**σ** µm	**Sk**	**CI** µm	**RA** %	**GN**	**SS** µm	**σ** µm	**Sk**	**CI** µm	**RA** %
14	1025	364	21.6	0.63	-0.08	0.07	0.31	289	21.94	0.64	-0.04	0.08	0.4
38	1071	423	34.5	0.55	-0.02	0.05	0.16	322	31.85	0.62	-0.09	0.07	0.2
64	1119	328	25.7	0.58	0.10	0.07	0.26	286	25.82	0.59	0.13	0.07	0.3
94	1176	471	31.8	0.55	-0.03	0.05	0.16	370	29.01	0.62	-0.10	0.07	0.2
125	1237	457	24.8	0.65	-0.08	0.06	0.25	419	24.65	0.66	-0.11	0.07	0.3
158	1300	952	25.7	0.59	-0.04	0.04	0.15	727	26.43	0.60	0.01	0.05	0.2
195	1369	163	26.9	0.65	-0.10	0.11	0.39	149	27.06	0.66	-0.09	0.11	0.4
226	1431	654	23.3	0.55	-0.04	0.04	0.19	446	24.08	0.59	0.00	0.06	0.2
267	1507	302	26.4	0.61	0.04	0.07	0.27	279	25.82	0.61	0.07	0.08	0.3
290	1553	843	29.9	0.53	-0.08	0.04	0.13	603	29.01	0.58	-0.09	0.05	0.2
331	1630	502	24.7	0.58	-0.01	0.05	0.22	391	25.23	0.60	-0.01	0.06	0.2
354	1675	1346	23.5	0.58	0.06	0.03	0.14	1030	24.08	0.61	0.02	0.04	0.2
383	1729	267	27.2	0.55	0.11	0.07	0.26	207	27.06	0.60	0.06	0.09	0.3
410	1783	796	22.8	0.54	0.03	0.04	0.17	494	24.65	0.56	0.07	0.05	0.2
443	1844	288	27.2	0.62	-0.11	0.08	0.28	232	27.69	0.63	-0.02	0.08	0.3
474	1905	392	20.6	0.65	-0.19	0.07	0.33	284	21.43	0.67	-0.14	0.08	0.4
511	1982	99	29.5	0.63	-0.35	0.13	0.44	76	30.40	0.65	-0.36	0.16	0.5
538	2053	703	23.7	0.60	-0.05	0.05	0.20	509	24.08	0.66	-0.03	0.06	0.3
571	2135	166	33.7	0.51	0.25	0.08	0.24	135	25.23	0.67	-0.05	0.12	0.5
613	2245	1548	22.2	0.59	-0.03	0.03	0.14	1131	22.98	0.61	0.08	0.04	0.2
651	2339	343	26.3	0.65	-0.09	0.07	0.27	302	27.06	0.65	-0.12	0.08	0.3
674	2401	987	24.1	0.55	0.07	0.04	0.15	679	23.53	0.63	-0.04	0.05	0.2
702	2469	648	22.6	0.65	-0.10	0.05	0.23	546	22.98	0.67	-0.14	0.06	0.3
733	2551	330	23.3	0.49	0.10	0.06	0.24	201	22.98	0.59	0.01	0.09	0.4
766	2633	811	24.3	0.64	0.01	0.05	0.19	691	24.08	0.66	0.00	0.05	0.2
793	2704	303	25.4	0.62	-0.11	0.07	0.29	250	25.23	0.64	-0.09	0.08	0.3
831	2799	913	24.60	0.64	-0.15	0.04	0.18	810	25.90	0.66	-0.21	0.05	0.2
862	2881	868	20.10	0.62	-0.02	0.04	0.22	509	21.08	0.66	0.09	0.06	0.3
895	2962	489	19.83	0.63	-0.05	0.06	0.30	400	21.08	0.64	-0.04	0.07	0.3
926	3044	1171	20.03	0.59	0.07	0.04	0.18	632	21.52	0.63	0.17	0.05	0.2
959	3126	728	26.03	0.52	0.21	0.04	0.15	657	24.61	0.64	-0.09	0.05	0.2
994	3218	1175	22.94	0.59	0.06	0.04	0.15	758	22.90	0.63	0.14	0.05	0.2
1026	3300	1231	19.84	0.58	0.07	0.03	0.17	622	21.08	0.64	0.14	0.05	0.3
1029	3305	427	20.80	0.68	-0.08	0.07	0.32	365	22.20	0.70	-0.02	0.08	0.3
1062	3391	1050	25.92	0.47	0.21	0.03	0.11	612	23.88	0.60	0.12	0.05	0.2
1082	3440	223	22.57	0.57	0.01	0.08	0.35	157	23.99	0.60	0.06	0.10	0.4
1113	3522	956	26.62	0.49	0.12	0.03	0.12	580	25.43	0.57	0.09	0.05	0.2
1151	3616	200	21.43	0.61	0.09	0.09	0.41	179	21.31	0.66	-0.03	0.10	0.5
1222	3798	248	27.09	0.58	-0.07	0.08	0.28	203	28.09	0.60	-0.03	0.09	0.3
1279	3943	377	20.19	0.58	0.07	0.06	0.30	322	20.72	0.59	0.13	0.07	0.3
1346	4114	261	24.42	0.55	0.05	0.07	0.29	211	23.84	0.61	0.03	0.09	0.4
1410	4278	313	23.29	0.61	-0.26	0.07	0.30	258	24.50	0.63	-0.29	0.08	0.3
1474	4441	218	23.42	0.54	0.17	0.08	0.32	186	22.55	0.62	0.07	0.09	0.4
1534	4594	334	27.31	0.61	-0.15	0.07	0.25	280	26.60	0.64	-0.14	0.08	0.3
1602	4768	266	20.53	0.57	-0.02	0.07	0.35	215	21.31	0.64	-0.23	0.09	0.4
1662	4921	286	33.60	0.46	0.29	0.06	0.17	274	22.55	0.66	-0.09	0.08	0.4
1726	5085	281	37.82	0.38	0.28	0.05	0.12	244	21.92	0.62	-0.12	0.08	0.4
1791	5251	477	27.95	0.54	-0.12	0.05	0.18	407	25.19	0.61	-0.19	0.06	0.2
1853	5412	591	22.54	0.59	0.18	0.05	0.22	327	23.15	0.62	0.32	0.07	0.3
1914	5565	365	25.01	0.56	-0.17	0.06	0.24	269	25.89	0.60	-0.20	0.08	0.3
1990	5759	840	20.56	0.62	0.22	0.04	0.21	425	20.72	0.66	0.35	0.07	0.3

Appendix 2. Grain size data from sediment core MD03-2601. GN: Grain number analysed, σ: sorting, Sk: skewness, CI: confidence interval at 95% level, and RA: relative accuracy.

		Total grain size fraction (> 5 µm)						10-63 µm grain size fraction					
Depth cmbsf	**Age** cal yr BP	**GN**	**Mean** µm	**σ** µm	**Sk**	**CI** µm	**RA** %	**GN**	**SS** µm	**σ** µm	**Sk**	**CI** µm	**RA** %
2067	5957	258	21.32	0.54	-0.25	0.07	0.33	141	23.18	0.64	-0.28	0.11	0.5
2114	6081	879	23.33	0.58	0.09	0.04	0.17	480	23.15	0.61	0.12	0.06	0.2
2166	6212	292	33.12	0.52	-0.23	0.06	0.19	192	30.45	0.59	-0.21	0.09	0.3
2285	6521	610	22.10	0.58	0.12	0.05	0.22	290	22.72	0.66	0.23	0.08	0.4
2326	6624	429	24.29	0.56	-0.13	0.06	0.23	280	24.50	0.64	-0.16	0.08	0.3
2418	6861	331	20.40	0.59	-0.10	0.07	0.33	240	23.18	0.62	-0.05	0.08	0.4
2486	7036	1027	20.68	0.56	0.25	0.04	0.17	389	22.30	0.61	0.35	0.06	0.3
2522	7128	1223	24.27	0.51	0.06	0.03	0.12	489	25.94	0.58	0.09	0.05	0.2
2559	7222	609	22.30	0.56	-0.03	0.05	0.21	505	22.55	0.61	-0.08	0.06	0.2
2589	7301	1778	22.92	0.58	0.14	0.03	0.12	931	23.15	0.62	0.10	0.04	0.2
2621	7383	1524	19.4	0.55	0.11	0.03	0.15	883	20.46	0.60	0.15	0.04	0.2
2649	7454	440	35.4	0.54	-0.08	0.05	0.15	337	30.40	0.62	-0.16	0.07	0.2
2683	7538	766	30.8	0.60	-0.08	0.04	0.14	691	30.40	0.63	-0.19	0.05	0.2
2718	7630	743	28.9	0.56	-0.10	0.04	0.15	535	28.35	0.63	-0.19	0.06	0.2
2753	7719	1347	24.5	0.57	-0.02	0.03	0.13	912	25.82	0.61	-0.02	0.04	0.2
2789	7811	526	21.1	0.57	-0.08	0.05	0.24	311	22.46	0.62	-0.09	0.07	0.3
2823	7895	812	29.1	0.60	-0.01	0.04	0.15	718	27.69	0.63	-0.02	0.05	0.2
2852	7972	445	30.4	0.57	-0.09	0.06	0.18	299	30.40	0.61	-0.01	0.07	0.2
2888	8064	883	27.8	0.58	-0.08	0.04	0.14	647	27.06	0.64	-0.11	0.05	0.2
2920	8145	1381	18.5	0.60	0.04	0.03	0.18	868	19.53	0.63	0.07	0.04	0.2
2953	8227	794	25.3	0.59	0.05	0.04	0.17	658	24.65	0.60	0.10	0.05	0.2
2980	8298	404	34.7	0.51	-0.21	0.05	0.15	265	31.11	0.58	-0.11	0.07	0.2
3008	8364	594	25.9	0.56	-0.05	0.05	0.18	424	26.43	0.59	0.03	0.06	0.2
3036	8420	1151	25.7	0.51	-0.14	0.03	0.12	627	27.06	0.58	-0.09	0.05	0.2
3065	8477	621	26.9	0.63	-0.05	0.05	0.19	545	26.43	0.66	-0.13	0.06	0.2
3100	8549	1047	22.3	0.56	-0.01	0.04	0.16	623	23.53	0.59	0.08	0.05	0.2
3132	8611	810	22.3	0.58	-0.02	0.04	0.19	565	22.98	0.61	0.08	0.05	0.2
3164	8677	924	26.0	0.57	-0.11	0.04	0.15	630	27.06	0.60	-0.06	0.05	0.2
3201	8750	459	32.3	0.63	-0.09	0.06	0.19	431	31.11	0.64	-0.09	0.06	0.2
3231	8812	1318	23.3	0.56	0.03	0.03	0.14	937	24.08	0.60	0.00	0.04	0.2
3262	8874	803	28.2	0.56	-0.07	0.04	0.14	615	27.06	0.62	-0.10	0.05	0.2
3293	8936	746	30.4	0.54	-0.06	0.04	0.13	509	28.35	0.59	-0.13	0.05	0.2
3325	8999	1060	26.6	0.60	-0.05	0.04	0.14	926	27.06	0.61	-0.08	0.04	0.2
3356	9063	913	23.9	0.58	-0.09	0.04	0.17	604	24.65	0.62	-0.12	0.05	0.2
3384	9117	973	22.4	0.54	-0.04	0.04	0.16	554	24.08	0.59	-0.02	0.05	0.2
3412	9173	797	27.9	0.59	-0.08	0.04	0.16	602	27.69	0.63	-0.02	0.05	0.2
3444	9238	722	26.0	0.61	-0.06	0.05	0.18	652	26.43	0.62	-0.12	0.05	0.2
3483	9318	507	30.2	0.53	0.03	0.05	0.16	408	27.06	0.60	-0.06	0.06	0.2
3524	9427	1315	23.1	0.52	0.08	0.03	0.13	884	23.53	0.57	0.10	0.04	0.2
3564	9556	1319	21.57	0.61	0.22	0.03	0.16	802	22.22	0.64	0.21	0.05	0.2
3605	9682	1078	24.33	0.55	0.04	0.03	0.14	935	22.22	0.60	-0.03	0.04	0.2
3656	9843	1494	26.93	0.49	0.23	0.03	0.10	931	24.83	0.62	0.10	0.04	0.2
3713	10022	931	21.58	0.60	0.01	0.04	0.19	824	22.22	0.62	-0.06	0.04	0.2
3748	10132	1562	28.57	0.55	0.08	0.03	0.10	1103	28.37	0.60	0.11	0.04	0.1
3781	10239	1814	24.00	0.58	0.15	0.03	0.12	1185	24.37	0.61	0.24	0.04	0.1
3817	10350	2075	26.70	0.54	0.10	0.02	0.09	1340	26.78	0.59	0.15	0.03	0.1
3854	10466	1035	23.14	0.62	-0.03	0.04	0.17	950	22.85	0.63	-0.05	0.04	0.2
3906	10630	2159	27.52	0.49	0.24	0.02	0.08	1411	26.27	0.61	0.08	0.03	0.1
3962	10806	573	31.18	0.62	-0.13	0.05	0.17	530	29.31	0.64	-0.27	0.06	0.2
4021	10995	2670	23.59	0.59	0.12	0.02	0.10	1683	23.92	0.63	0.19	0.03	0.1
Average		770	25.34	0.57	0.00	0.05	0.20	537	24.99	0.62	-0.02	0.06	0.25
Minimum value		99	18.49	0.38	-0.35	0.02	0.08	76	19.53	0.56	-0.36	0.03	0.12
Maximum value		2670	37.82	0.68	0.29	0.13	0.44	1683	31.85	0.70	0.35	0.16	0.51

Appendix 2. Continued. GN: Grain number analysed, σ: sorting, Sk: skewness, CI: confidence interval at 95% level, and RA: relative accuracy.

CHAPITRE 3

Interactions et rétroactions Climat-Biosphère marine

L'étude sur les interactions et rétroactions des compartiments climatiques cryosphère, banquise et océan au sein de la marge antarctique de Terre Adélie qui a fait l'objet du chapitre précédent, a mis en évidence une variabilité à long et à court terme au cours de l'Holocène. Nous avons montré, via une comparaison avec des données de modélisation numérique, que la variabilité à long terme est directement induite par les changements orbitaux de l'ensoleillement local qui régissent l'évolution holocène des températures atmosphérique et océanique ainsi que des précipitations, induisant une expansion des glaciers au Tardi-Holocène associé à une augmentation de la formation annuelle de banquise et à une augmentation de la formation d'eaux de fond antarctique. Les changements holocènes observés en Terre Adélie semblent généralisables à l'Antarctique et mettent en avant le rôle important de la banquise dans la formation d'eaux de fond. Nous avons aussi montré qu'à l'échelle millénaire, les glaciers côtiers et la banquise réagissent mutuellement aux changements de régimes climatiques du centre de l'Antarctique dans un délai de 1000 à 100 ans suivant les évènements. A cette échelle, l'étude de la réponse de la circulation océanique requiert d'avantage d'investigations.

Les tendances à long et à court terme exprimées par les glaciers, la banquise et l'océan au cours de l'Holocène nous ont interrogées quant à leur impact sur les eaux adjacentes et la biosphère marine qu'elles abritent. L'évolution de la productivité des eaux est une

question majeure de la communauté scientifique par son rôle primordiale dans le cycle du carbone via la pompe biologique. En effet, la productivité marine contribue actuellement à la moitié de la consommation en CO_2 atmosphérique du système terrestre (Ban et al., 1999). Quels effets vont produire ces changements des systèmes glacier, banquise et océan sur la stratification, le renouvellement en nutriments et la longueur de la saison de croissance ? Et quelles vont en être les conséquences sur la productivité marine et son enfouissement et ainsi sur l'efficacité de la pompe biologique à extraire du CO_2 de la machine climatique ? La réponse à ces questions peut fournir des clés aux scientifiques pour mieux contraindre l'évolution future de la productivité des eaux côtières antarctiques en réponse à une réduction du couvert de banquise et à une augmentation des vents et des upwellings prédites pour le climat à venir (Russel et al., 2006 ; Lefebvre et Gossse, 2008a).

Ainsi, le deuxième volet de ce travail s'est attaché à quantifier la productivité marine et son enfouissement à long et à court terme pendant l'Holocène et à mettre en relation ces variations avec les paramètres environnementaux (banquise, upwelling, saison de croissance) pour dégager les facteurs de contrôle régissant l'efficacité de la pompe biologique à ces différentes échelles de temps. Les résultats de cette étude ont été exposés dans un article qui est en révision dans la revue *Paleoceanography* et qui fait l'objet de ce chapitre.

Holocene productivity changes off Adélie Land (East Antarctica)

Delphine Denis,[1] Xavier Crosta,[1] Sabine Schmidt,[1] Damien S. Carson,[3] Raja S. Ganeshram,[3] Hans Renssen,[4] Julien Crespin,[2] Olivier Ther,[1] Isabelle Billy,[1] and Jacques Giraudeau[1].

[1] EPOC, UMR-CNRS 5805, Université Bordeaux 1, av. des facultés, Talence, 33405 cedex, France.
[2] CEREGE, UMR-CNRS 6635, Aix en provence, Europôle de l'Arbois, 13545 Aix-en-Provence Cedex 4, France.
[3] School of GeoSciences. The University of Edinburgh, Grant Institute, West Mains Road EDINBURGH EH9 3JW, UK.
[4] Faculty of Earth and Life Sciences, Vrije Universiteit Amsterdam, De Boelelaan 1085, NL-1081 HV, The Netherlands.

Abstract

This study presents the first high-resolution multi-proxy investigation of primary productivity (PP) during the Holocene from the Antarctic continental margins. Micropaleontological and geochemical data from the sediment core MD03-2601, associated to sea ice model outputs, give unprecedented insights into the biological pump of the Antarctic coastal area off Adélie Land in response to climatic changes. Pluri-millennial and millennial changes of PP are observed in the study area in response to changes in nutrient availability, stratification and growing season duration, which are linked to sea ice, upwelling, wind and glacier dynamics. The precessional cycle seems to be responsible in the PP long-term variations while forcing factors involved at the millennial timescale remain more enigmatic. Our results emphasize enhanced biological pump during warmer and windier Holocene phases because of a longer growing season and greater nutrient input. Antarctic coastal and continental shelf zones may therefore represent a more intense carbon sink in the future.

Index terms: Paleoclimatology and Paleoceanography (0473), Abrupt and rapid climate change (1605), Sedimentary geochemistry (1051), Arctic and Antarctic oceanography, Sea ice (0750).

Key words: Holocene, Antarctica, Sea ice, Nutrient, Paleoproductivity, ^{230}Th normalized flux, diatoms.

1. Introduction

Coastal and continental shelf zones (CCSZ) are among the most productive ecological provinces of the Southern Ocean which account for ca. 76 % and 3.5 % of the total primary productivity (PP) of the Marginal Ice Zone (MIZ) and Southern Ocean, respectively (Smith and Gordon, 1997; Arrigo et al., 2008). Enhanced PP levels in ice-edge zones are commonly related to a combination of nutrient enrichment, seasonal stratification of the surface ocean by ice melting, and growing season duration (Smith and Nelson, 1985; Leventer, 1992; Arrigo and van Dijken, 2003; Arrigo et al., 2008). Enhanced seasonality in CCSZ, which favours a high export/production ratio, subsequently induces higher accumulation and burial of organic matter in the underlying sediment (Berger and Wefer, 1990; Buesseler, 1998). Therefore, the Antarctic sea ice zones are significantly involved in the global carbon biological pump (i.e. the amount of carbon removed from the atmosphere and permanently buried in the sediment) and related atmospheric pCO2 modulations (Longhurst and Harrison, 1989; Nelson et al., 1995).

Currently, the response of PP and resultant global carbon cycle in sea ice zones to global warming remains unclear and controversial (Arrigo et al., 1999; Collier et al., 2000; Arrigo and Thomas, 2004; Tortell et al., 2008; Arrigo et al., 2008). However, model studies predict that the ongoing climate change will induce enhanced Southern Ocean upwelling of nutrient rich waters (Toggweiler et al., 2006; Russell et al., 2006), reduced iron availability (Kattenberg et al., 1996; Sarmiento et al., 1998), and retreat of sea ice extent (Goosse and Renssen, 2001; Lefebvre and Goosse, 2008a). These parameters are important in controlling PP levels via the modulation of the nutrient supply, stratification and growing season duration.

Given the debate surrounding the impact of climate change on PP in the CCSZ, we have investigated the response of PP to glacier, oceanic, atmospheric, and sea-ice changes in a Holocene sediment archive from the CCSZ off Adélie Land, East Antarctica. Records of opal and organic carbon vertical fluxes, which are robust tracers of the biological pump efficiency in the CCSZ (Carson et al., submitted), are compared to new records of ^{230}Th-normalized iron and organic nitrogen fluxes, nitrogen stable isotopic ratio, diatom assemblages and sea ice cover model transient simulations for the Holocene period. This new data set allows us 1) to constrain Holocene variations of buried paleoproductivity, 2) to identify the main controlling factors of past PP variations, 3) to better understand the impact of past climatic conditions (sea ice, upwelling, wind, temperature, glacier) on PP controlling factors in order to 4) construct a comprehensive picture of the biological pump changes throughout the last 11 kyrs. Interpretations drawn for the Holocene period can be used to infer future PP in warming climate.

2. Environmental and biological settings

The Dumont d'Urville Trough (DDUT), which comprises many glacial depressions, is located off Adélie Land on the East Antarctica Margin (Figure 1). These depressions act as sediment traps, which focus the phytoplankton detritus produced in the area, increasing their preservation potential.

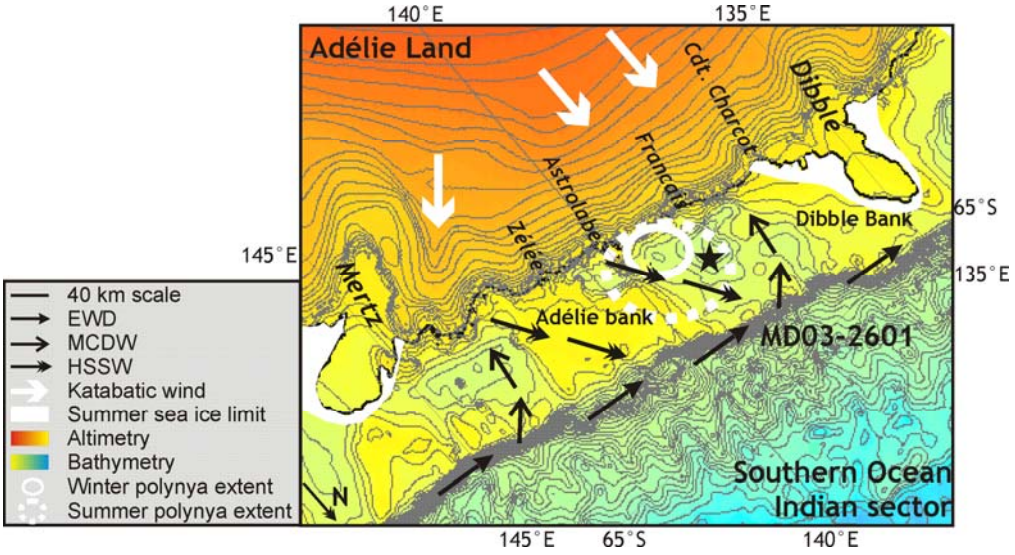

Figure 1. Map of the study area (modified after Denis et al., in-press), showing the location of sediment core MD03-2601, altimetry and bathymetry, location of glaciers (in italic), limit of summer sea-ice cover (Schweitzer, 1995), detail of oceanographic currents and different water masses (Rintoul, 1998; Harris and Beaman, 2003; Williams and Bindoff, 2003), katabatic wind directions (Massom et al., 1998) and the average winter and summer extent of the DDUT polynya (Arrigo and van Dijken, 2003). Winter sea ice covers the whole oceanic area encompassed by the map. EWD: East Wind Drift, MCDW: Modified Circumpolar Deep Water, HSSW: High Salinity Shelf Water. Bathymetry data are based on ETOPO2 data set from http://www.ngdc.noaa.gov/mgg/fliers/01mgg04.html.

The DDUT region is influenced by several water masses and currents (Rintoul, 1998, Bindoff et al., 2000a, 2000b; Williams and Bindoff, 2003): (1) the wind-driven East Wind Drift (EWD), also called Antarctic Coastal Current, which flows westward at the surface; (2) the Antarctic Surface water (AASW) constituting the summer near-surface water mass on the continental shelf; (3) the Modified Circumpolar Deep Water (MCDW) which upwells at the Antarctic Divergence; (4) the High Salinity Shelf Water (HSSW), formed by brine-rejection during winter sea ice formation and cooling of the MCDW (Figure 1), which flows northward as part of the Adélie Land Bottom Water (ALBW).

The CCSZ is supplied with macro- and micro-nutrients from several sources such as upwelling of MCDW (Coale et al., 2005), re-suspension of shelf sediments (Sedwick et al., 2000), aeolian input (Cassar et al., 2007), and melting of glacial ice and sea ice (Edwards and Sedwick, 2001; Lannuzel et al., 2007). In the CCSZ, macro-nutrients are generally not exhausted at the end of the growing season (Strutton et al., 2000) whereas trace metals

such as iron (Fe) can become a limiting factor for annual PP (Arrigo et al., 2003; Smetacek and Nicol, 2005).

The coastal area off Adélie Land is presently exposed to strong katabatic winds (Périard and Pettré, 1993) that support the Dumont D'Urville polynya, located southward at 66.11°S-139.31°E, throughout the winter season (Adolphs and Wendler, 1995, Arrigo and van Dijken, 2003) (Figure 1). The DDUT area is totally ice-free or under the influence of the Dumont D'Urville post-polynya (e.g. the winter polynya that extends into the spring-summer season) from late spring to late summer (Schweitzer, 1995; Arrigo and van Dijken, 2003). The ice-free conditions last between 3 and 5 months (e.g. between November-December to February-March), and hence give a good estimation of the length of the phytoplanktonic growing season in the DDUT area (Figure 1).

Primary productivity in surface waters of the DDUT is around 4.6 molC/m²/yr, which is on the lower side of the range of PP estimates in CCSZ, between 1 and 13 molC/m²/yr (Nelson et al., 1996; Arrigo and van Dijken, 2003; Beucher et al., 2004; Beans et al., 2008). The only data set available on PP preserved in the CCSZ sediment shows values around 0.02 molC/m²/yr (values not ^{230}Th-normalized) in the Ross Sea (Nelson et al., 1996), which is among the most productive CCSZ areas (Arrigo and van Dijken, 2003). PP is initiated in spring when light availability and stratification are favoured by sea ice waning, whereas decreasing PP at the end of the summer-autumn season likely results from trace metal limitation and grazing pressure (Smetacek et al., 2004). The algal community is mainly controlled by surface water stratification, which depends on temperature, wind stress, sea ice and glacial runoff (Wright and van den Enden, 2000). Diatoms blooms are favoured by injection of freshwater that produces a stratified stable environment (Leventer, 1992) and are dominant in the Adélie Land region at present time (Wright and van den Enden, 2000).

3. Material and Methods

3.1. Core description

Piston core MD03-2601 (66°03.07'S; 138°33.43'E; 746 m water depth) was recovered from the slope of one of the depressions comprising the DDUT (Figure 1) in 2003 during the CADO cruise (MD130 – Images - Coring Adélie Diatom Oozes) on board the R.V. Marion Dufresne II. The age model used here, detailed in Denis et al. (in-press), is based on 7 radiocarbon dates (depths shown on the figure 2) completed on the humic fraction of bulk organic matter, corrected with a 1300 years age reservoir (Ingólfsson et al., 1998), calibrated using Calib 5.0 software (Stuiver et al., 2005) and the marine calibration Marine04 (Hughen et al., 2004). The 40 m-long sediment core covers the 1-11 cal ka BP period with a mean accumulation rate of 0.4 cm per year and shows sub-millimetric to centrimetric seasonal laminations (Denis et al., 2006; Denis et al., in-press).

3.2. Geochemical data

Down-core iron (Fe) measurements were performed every 32 cm (~ 80 years resolution) by X-Ray Fluorescence (XRF) analysis, optimised for major elements. Complete XRF methodology is described in Fitton et al. (1998). Standard deviations of Fe measures are 0.03. Iron content has been ^{230}Th-normalized thanks to high-resolution ^{230}Th measurements (n=60, Denis et al., in-press) following Francois et al. (2004) calculation, yielding to a 170 year resolution (see method details in Carson et al., submitted). ^{230}Th-normalized Fe fluxes present a mean σ error of 24 % ($p > 0.05$) by addition of the errors associated to the ^{14}C age, thorium and uranium extraction and treatment, DBD calculation and Fe determination (see error bars on Figure 2E). The ^{230}Th-normalization permits to circumvent problems of lateral focusing and sediment component changes, and therefore allows accurate reconstructions of the vertical flux (Francois et al., 2004).

Nitrogen isotopic measurements ($\delta^{15}N_{bulk}$) and organic nitrogen content (N_{org}) on bulk organic matter were undertaken every 4 cm to 8 cm (~10-20 years resolution) on a Carlo Erba 2500 elemental analyzer in line with a VG Isoprime, following the method described by Crosta et al. (2005a). The mean standard deviation is 0.25 ‰ for the $\delta^{15}N_{bulk}$ and 0.01 % for the N_{org}. Organic nitrogen content (%) has been ^{230}Th-normalized as explained for Fe in order to reconstruct the preserved vertical flux of nitrogen at a 170 years resolution (mean σ error = 24 % for $p > 0.05$, see error bars on Figure 2A).

Micropaleontological data

Diatom census counts, followed Schrader and Gersonde (1978) and Laws (1983) were performed every 4-8 cm at the same depth than C_{org} and N_{org} samples, presenting a ~10-20 years resolution. More details about slide preparation and diatom identification are found in Crosta et al. (2004). Around 350 diatom valves were counted in each sample and the relative abundance of each was determined as the fraction of diatom species against total diatom abundance in the sample.

The relative abundances of some diatom species have been summed according to their relative similar ecological preferences. *Fragilariopsis kerguelensis* and *F. rhombica*, which have been both previously published in Crosta et al., (2005a, 2008) are summed with *F. ritcherii*, *F. separanda*, *Pseudonitzschia* spp., *Thalassiosira tumida*, *Thalassiothrix* spp. and *Thrichotoxon reinboldii* in the summer diatom group. Studies of diatom distribution in surface sediments and in laminated fossil sediments have shown that these species grow during the summer season with ice free conditions (Armand et al., 2005; Crosta et al., 2005b; Maddison et al., 2005, 2006; Stickley et al., 2005; Denis et al., 2006; Timmermans et al., 2008).

Chaetoceros Phaeoceros spp. (dominated by *C. dichaeta*), *Corethron pennatum*, *Rhizosolenia* spp. and *Proboscia* spp. have been summed in the setae diatom group. Several studies have identified these species during spring (Denis et al., 2006, Maddison et al., 2006) and/or summer and fall seasons (Leventer et al., 2002), in neritic and/or more oceanic waters (Armand et al., 2005; Crosta et al., 2005b), in well-stratified (Leventer et al., 2002) and/or mixed water column (Beans et al., 2008), and in oligotrophic (Stickley et al., 2005) and/or nutrient-rich surface waters (Beans et al., 2008). Nonetheless, in Adélie Land region, Beans et al. (2008) associated clearly the species of the setae diatom group with nutrient-rich and mixed surface waters.

Finally, we use the *Chaetoceros Hyalochaete* spp. resting spore (CRS) relative abundances, which the 9-1 cal ka BP part of the MD03-2601 record have been previously published in Crosta et al. (2005a, 2008). Resting spore formation of *Chaetoceros Hyalochaete* spp. are mainly associated to surface waters depleted in nutrient after intense spring blooms, which have been promoted in well-stratified nutrient-rich water column (Leventer, 1991, 1992; Crosta et al., 1997; Leventer et al., 2002).

Model simulations

Variations of annual sea ice cover was extracted between 130-150°E and 64-70°S from a 9000-yr-long transient experiment simulated with the ECBilt-CLIO-VECODE coupled atmosphere-sea ice-ocean-vegetation model (Renssen et al., 2005). This experiment was forced by millennial-scale forcings, i.e. variations in orbital parameters and atmospheric greenhouse gas levels. Using the simulated sea ice cover, the number of months per year with ice-free conditions was determined according to Arrigo and van Dijken (2003), i.e. considering a mean sea ice cover of less than 50%. At the end of the experiment (e.g. 200 yr BP), yearly ice-free duration are slightly lower than those reported by Arrigo and van Dijken, (2003) on the 1997-2002 period (3 instead of 4 months per year). This under-estimation of ice-free duration in the model is possibly due to the non-representation of the DDU polynya and post-polynya, which favour earlier ice-free conditions. It is worth noting that the model outputs can be examined over the Milankovitch timescale and not at the sub-Milankovitch one, as external forcings important at the latter timescale (such as variations in solar irradiance and volcanic aerosol content of the atmosphere) were not considered in the experiment of Renssen et al. (2005).

4. Results

Our results are presented and described concomitantly to ^{230}Th-normalized BSi and C_{org} fluxes, which have been previously presented in Carson et al. (submitted).

The 3-order polynomial functions applied to ^{230}Th-normalized fluxes of N_{org}, C_{org} and BSi show similar trends during the Holocene with relatively low values between 11 and 9 cal ka

BP, a long-term increase between 9 and 3 cal ka BP and a slight decrease after 3 cal ka BP (Figure 2A). Between 9 and 3 cal ka BP, the ^{230}Th-normalized fluxes of N_{org}, C_{org} and BSi show a 1.5-fold increase from 0.004 to 0.006 molN/m²/yr, 0.03 to 0.05 molC/m²/yr and 0.2 to 0.3 molSiO_2/m²/yr (Figure 2A). Based on the general trend, highest C_{org} and N_{org} fluxes occurred between 5 and 1 cal ka BP while highest flux of BSi occurred between 6 and 2 ka BP (Figure 2A). The Holocene general trend is punctuated by several increases of the ^{230}Th-normalized fluxes of N_{org}, C_{org} and BSi at around 10.6-10.2, 8.7-8, 7.6-7, 6.2-5.3, 4.6-3.5, and 2.4-1.4 cal ka BP and noted hereafter P1 to P6, respectively (Figure 2A). We note that the amplitude and the duration of the PE follow the Holocene pattern with an increase from PE1 to PE5 and a decrease since PE5. The amplitude increased by 1.5 to 2.5-fold while the duration increased from 500 to 1000-1200 years between the early and the late Holocene, respectively (Figure 2A). ^{230}Th-normalized biogenic fluxes are significantly correlated together (Table 1).

The summer diatom group accounts for 13 to 40 % of the diatom assemblages. It is the more abundant diatom group between 9 and 3.5 cal ka BP, representing more than one third of the diatom assemblage during this period (Figure 2B). The summer diatom group shows a long-term increase between 9 and 3.5 cal ka BP, subsequently followed by a pronounced decrease (Figure 2B). Millennial events of increasing occurrence at around 10.6-10.2, 8.7-8, 7.6-7, 6.2-5.3, 5.1-4.9, 4.6-3.5, 2.4-2 and 1.5-1 cal ka BP are superimposed to the Holocene trend (Figure 2B). The summer diatom group record is significantly correlated with ^{230}Th-normalized BSi flux (Table 1). The summer diatom group record also shows positive correlations with ^{230}Th-normalized C_{org} and N_{org} fluxes though the test of significance is just below the threshold (Table 1).

CRS relative abundances show a long-term decrease from 60 to 10 % between 11 and 1 cal ka BP (Crosta et al., 2008) (Figure 2C). This general trend is interrupted by several drops at around 10.6-10.2, 8.7-8.3, 7.6-7, 6.4-6, 5.6-5.3, 4.7-4.4, 4-2.6, 2.4-2 and 1.4-1 cal ka BP (Figure 2C). CRS relative abundances are significantly anti-correlated along the Holocene with relative abundances of the summer diatom group and ^{230}Th-normalized N_{org} flux. CRS abundances also display negative correlations with ^{230}Th-normalized fluxes of BSi and C_{org} though the test of significance is just below the threshold (Table 1).

The setae diatom group reaches 1 to 8 % of the diatom abundances along the Holocene with relatively low percentages around 2% in the first part of the Holocene and a steady increase since 5 cal ka BP to reach around 6% at the core top (Figure 2D). This general trend is punctuated by several peaks of higher relative abundances at around 8.7-8, 7.6-7, 6.2-5.3, 4.1-3.9, 3.4-2.6, 2.4-1.6 and 1.5-1 cal ka BP (Figure 2D). The setae diatom group record shows strong negative correlations with CRS relative abundances and ^{230}Th-normalized N_{org} flux and negative but non-significant correlations with ^{230}Th-normalized fluxes of BSi and C_{org} (Table 1).

The ^{230}Th-normalized flux of iron varies between 130 and 580 µg/m²/yr along the Holocene. This record displays a relatively similar evolution than the setae diatom group record with a linear trend between 11 and 5 cal ka BP and a steady increase between 5 and 1 cal ka BP (Figure 2E) though these two records display a non-significant negative correlation (Table 1). Surimposed to this general trend, the ^{230}Th-normalized Fe flux exhibits several increases at around 10.6-10.2, 8.9-8.2, 7.6-7, 6.2-5.3, 4.5-3.5, and 2.4-1.4 cal ka BP (Figure 2E).

Values of the nitrogen stable isotope ratio of the bulk sediment ($\delta^{15}N_{bulk}$) vary from 1.5 to 3 ‰. When inversed on its Y axis, the $\delta^{15}N_{bulk}$ record shows a similar trend than the setae diatom group record and the ^{230}Th-normalized Fe flux record with heavier values between 11 and 5 cal ka BP and a steady trend since 5 cal ka BP toward lighter values (Figure 2F). Episodic decreases (lighter values) at around 10.6-10.2, 9.9-9.4, 8.7-8, 7.6-7, 6.5-6, 3-2.6 and 1.6-1 cal ka BP are superimposed on the general trend (Figure 2F). The $\delta^{15}N_{bulk}$ signal displays significant negative correlations with the setae diatom group and the ^{230}Th-normalized Fe flux and a negative but non-significant correlation with the ^{230}Th-normalized N_{org} flux (Table 1). Conversely, the $\delta^{15}N_{bulk}$ record is significantly correlated to records of the summer diatom group and the CRS relative abundances (Table 1).

Modelled ice-free duration in months per year shows a long-term increase from 9 to 1.7 cal ka BP, followed by a slight decrease until 0.2 cal ka BP (Figure 2H). Model output indicates that the ice-free season was shorter during the Early Holocene (January to February) than during the Late Holocene (January to March at 1.7 cal ka BP).

Figure 2. Micropaleontological, geochemical and isotopic records in core MD03-2601 versus time compared to records of Antarctic climate. Marine, ice core and model records are presented on independent timescales. A) ^{230}Th-normalized fluxes of N_{org} (black line), BSi (dark grey line) and C_{org} (light grey line) from Carson et al. (submitted) (error bars represent the confident interval at p>0.05) and their pluri-millennial trends, emphasized by a 3-order polynomial function, B) relative abundances of the summer diatom group (10-point running average), C) relative abundances of *Chaetoceros Hyalochaete* spp. resting spores (CRS) (10-point-running average, note the reversed Y axis) (Crosta et al., 2008), D) relative abundances of the setae diatom group (10-point running average), E) ^{230}Th-normalized iron flux (error bars represent the confident interval at p>0.05), F) nitrogen stable isotope ratio in bulk sediments ($\delta^{15}N_{bulk}$) (10-point-running average, note the reversed Y axis), G) non-sea-salt Ca^{2+} content in Siple Dome ice core (Mayewski et al., 2006, 2009, personal communication, 2008) (10-point-running average), H) orbital precessional index (Berger and Loutre, 1991), I) duration of the ice-free season modelled for the study area (130°-140°E, south of 64°S) (200-point-running average), J) empirical orthogonal function (EOF) of Deuterium isotopic ratio records in 11 ice cores from East Antarctica (Masson et al., 2000), K) periods of glacier/sea ice advance and retreat reported from Denis et al. (in-press) and L) world wide Rapid Climatic Changes (RCC) presented in Mayewski et al. (2004) stacked from 50 Holocene paleoclimatic records. At the top, triangles represent the positions of the ^{14}C dates used in the age model (Denis et al., in-press) and, at the bottom, the climatic periods of the Holocene are defined from Crosta et al., 2005a. Grey shaded areas highlight millennial increases of paleoproductivity called PE1 to PE6, which are reported at the top.

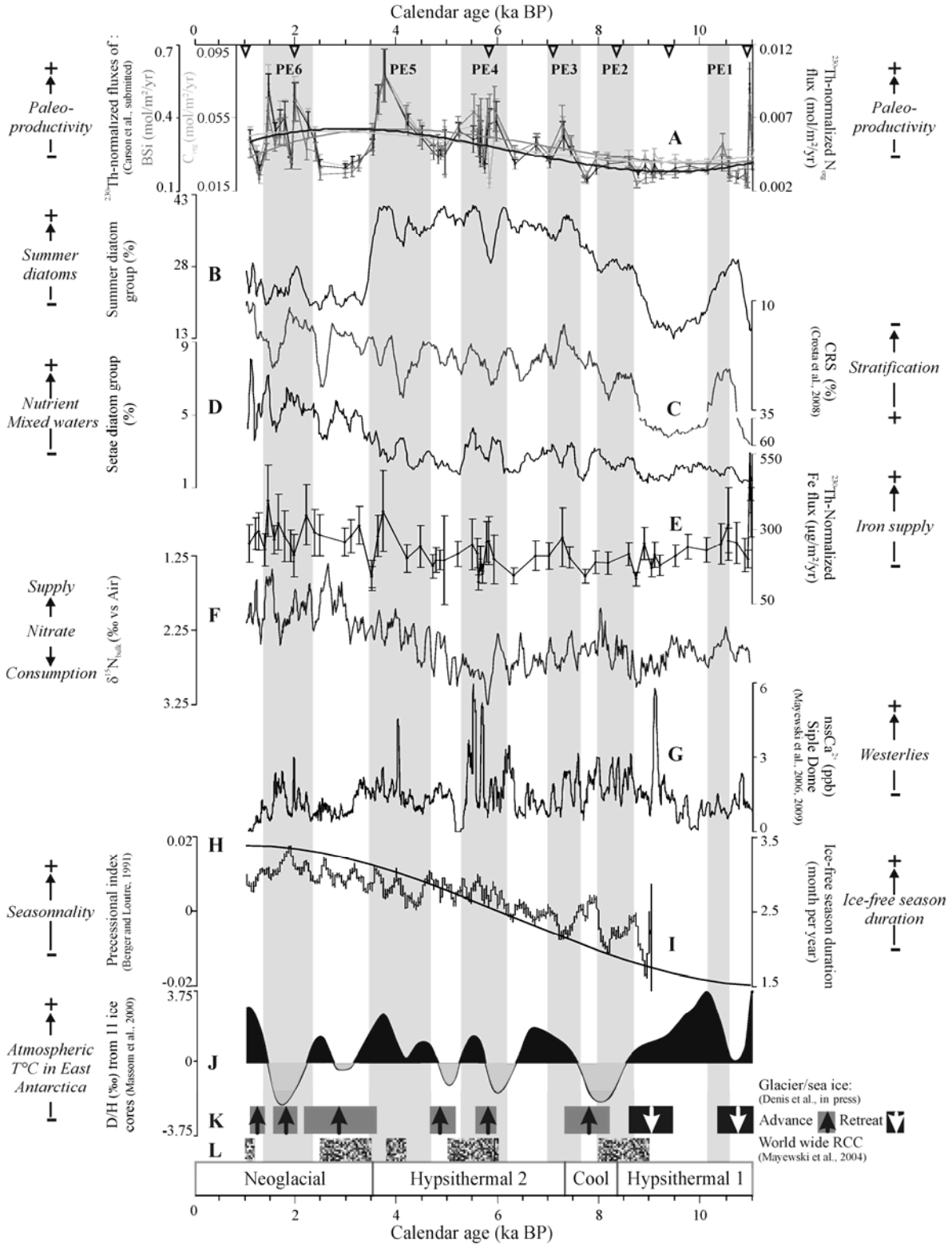
Calendar age (ka BP)
PE6
PE5
PE4
PE3
PE2
PE1
A
B
C
D
E
F
G
H
I
J
K
L
Paleo-productivity
Summer diatoms
Nutrient Mixed waters
Supply Nitrate Consumption
Seasonality
Atmospheric T°C in East Antarctica
Stratification
Iron supply
Westerlies
Ice-free season duration
Glacier/sea ice: (Denis et al., in press)
Advance
Retreat
World wide RCC (Mayewski et al., 2004)
Neoglacial
Hypsithermal 2
Cool
Hypsithermal 1

	^{230}Th-BSi	^{230}Th-C_{org}	^{230}Th-N_{org}	Fe	Summer gp	CRS	Setae gp	$\delta^{15}N_{bulk}$	n	σ (0.001)	σ (0.1)
^{230}Th-BSi		**1.5E-15**	**4.4E-18**	2.1E-01	**7.5E-06**	9.0E-03	8.0E-03	8.4E-01	60	**1.7E-05**	**1.8E-03**
^{230}Th-C_{org}	**0.707**		**2.1E-20**	2.6E-02	8.0E-03	5.0E-03	4.0E-03	1.3E-01	60	**1.7E-05**	**1.8E-03**
^{230}Th-N_{org}	**0.768**	**0.820**		5.7E-03	4.1E-03	**1.2E-03**	**8.0E-04**	1.8E-01	60	**1.7E-05**	**1.8E-03**
Fe	0.111	0.197	0.245		1.8E-02	2.2E-01	1.5E-01	**1.0E-03**	60	**1.7E-05**	**1.8E-03**
Summer gp	**0.397**	0.236	0.254	-0.210		**3.6E-10**	5.0E-02	**1.1E-12**	528	**1.9E-06**	**2.0E-04**
CRS	-0.229	-0.246	**-0.287**	-0.109	**-0.183**		**2.7E-80**	**5.4E-34**	528	**1.9E-06**	**2.0E-04**
Setae gp	-0.232	-0.258	**-0.297**	-0.127	-0.050	**-0.552**		**3.7E-59**	528	**1.9E-06**	**2.0E-04**
$\delta^{15}N_{bulk}$	0.018	-0.135	-0.119	**-0.303**	**0.207**	**0.354**	**-0.472**		528	**1.9E-06**	**2.0E-04**

Table 1. Table of Kendall's Tau correlation coefficients. Correlation coefficients are reported in the bottom triangle and significance values (p-values) are reported in the top triangle (dark and light grey rectangles represent p>0.001 and p> 0.1, respectively). The test is significant if its associated probability (p-value) is smaller than the level of confidence σ. Here, we used the Šidàk-Bonferonni correction, which takes into account the number of samples considered (n), to determine the σ required following the equation: $\sigma_{required} = 1- (1-\sigma)^{1/n}$, where σ is the p-value chosen and n is the number of samples considered (Abdi, 2007). Number of samples and σ required to have significant correlation at p>0.001 and p>0.1 are reported on the right side. The Kendall's Tau correlation coefficient calculations have been calculated using the free software PAST 1.75 (Hammer et al., 2007). This test has been performed on ^{230}Th-normalized fluxes of BSi, C_{org}, N_{org} and Fe, on diatom relative abundances and on $\delta^{15}N_{bulk}$ values. Diatom relative abundances and $\delta^{15}N_{bulk}$ are particularly sensitive to seasonal variability. We therefore smoothed their high-resolution records to reduce the seasonal noise possibly captured in the stepwise sampling of the laminated MD03-2601 core. Given the laminated structure of the core, it appears hazardous to calculate correlation coefficients between records having different resolutions. We therefore calculated the Kendall's Tau correlation coefficient between two records at the highest common resolution.

5. Discussion

5.1. Holocene Paleoproductivity

Records of ^{230}Th-normalized fluxes of BSi, C_{org} and N_{org} present similar patterns during the Holocene (Figure 2A) as attested by the significant positive correlation coefficients between the three records (Table 1). ^{230}Th-normalized fluxes of BSi, C_{org} and N_{org} in core MD03-2601 display significant changes in Holocene paleoproductivity. Carson et al. (submitted) compared ^{230}Th-normalized BSi and C_{org} fluxes in core MD03-2601 to modern estimations of opal and organic carbon fluxes. This study demonstrated that these fluxes did not result from differential preservation at the sea-sediment interface, therefore, representing an accurate reconstruction of past buried productivity.

Paleoproductivity, and resultant organic matter sequestration in the DDUT area, during the Holocene show changes at two timescales. At pluri-millennial timescale, the Hypsithermal 1 period, which was affected by the end of the deglaciation, is characterized by globally low paleoproductivity, whereas the Hypsithermal 2 period is marked by a long-term increase of organic matter burial. During the Neoglacial period, the organic matter sequestration in the DDUT remained high though decreasing toward modern time. The Neoglacial pluri-millennial trend should however be taken with caution because it here

covers only the 3.5-1 ka BP period and presents a strong millennial signature. Nonetheless, the Holocene can be coarsely divided with lower and higher biological pump efficiency before and after 5 cal ka BP, respectively (Figure 2A).

At the millennial timescale, 6 major events of higher organic burial have occurred at around 10.6-10.2, 8.7-8, 7.6-7, 6.2-5.3, 4.6-3.5, and 2.4-1.4 cal ka BP (Figure 2A). These productive events, referred as PE1 to PE6, are defined within the age model uncertainties. The amplitude and duration of PE increased along the Holocene until 3 cal ka BP and decreased since 3 cal ka BP, in agreement with the pluri-millennial pattern (Figure 2A).

5. 2. Paleoproductivity and diatom assemblages

In Adélie Land, diatoms are the dominant phytoplankton group in surfaces waters (Wright and van den Enden, 2000; Beans et al., 2008). At the Holocene scale, diatoms have dominated the hemipelagic sedimentation as demonstrated by the good concordance between total diatom abundances and paleoproductivity proxies between 9 and 2.4 cal ka BP (Carson et al., submitted).

The summer diatom group shows congruent variations with the three paleoproductivity records both at pluri-millennial and millennial timescales though relative abundances of the summer diatom group slightly predate PE1 and are subdued during PE6 (Figure 2A-B, Table 1). The summer diatom assemblage in the CCSZ presents generally low growth rates, high degrees of silicification and high cellular content (Martin-Jézéquel et al., 2000; Menden-Deuer and Lessard, 2000; Kemp et al., 2006; Assmy et al., 2006; Armand et al., 2008). High degree of silicification reduces dissolution and grazing pressure while promoting rapid export of BSi and organic matter to the sea floor (Smetacek et al., 2004). The capacity of these diatom species to stock large amount of organic matter and efficiently export it to the sea floor explains the concomitant Holocene changes between the relative abundances of the summer diatom group and the paleoproductivity proxies observed here.

In contrast, "bloomer" species such as *Chaetoceros* spp. are thought to participate little to the preserved paleoproductivity signals. Indeed, relative abundances of *Chaetoceros Hyalochaete* spp. resting spores display opposite trends to the paleoproductivity proxies with significant negative correlation with the N_{org} flux record and almost significative negative correlations with BSi and C_{org} flux records (Figure 2A-C, Table 1). CRS can achieve high relative abundances in surface water and be efficiently buried in sediment thanks to high sinking rates (Leventer, 1991) as observed during the Early Holocene (Figure 2C). However, the residual burial in term of BSi and organic material is low (Figure 2A-C) mainly because of their small size and low biogenic content (Armand et al., 2008).

Our diatom results in core MD03-2601 demonstrate that periods of strong organic matter burial in the CCSZ do not result from rapid and intense blooms, but are generally due to the slow summer production of large and highly silicified diatoms. However, the amplitude of burial fluxes during PE6 are higher than the corresponding signal in the relative abundances of the summer diatom group (Figure 2A-B) and in total diatom absolute abundances (Carson et al., submitted). This may indicate that the summer diatom community was not the only vector of the biogenic vertical fluxes to the sea floor during these periods. Several processes, possibly acting together with diatoms, may explain PE6. First, high abundances of species of the setae diatom group can achieve great abundances in surface waters of the CCSZ (Leventer et al., 2002; Beans et al., 2008). However, these species are generally scarce in the sediment due to their low export efficiency. Diatom species that possess setae and large spines are more easily dissolved because of their great buoyancy and high surface/volume ratio (Beucher et al., 2004; Ragueneau et al., 2006). In core MD03-2601, the summed relative abundances of these species peak during PE2, PE3, PE4, PE5 and especially PE6 (Figure 2D) indicating that they may participate to biogenic silica and organic matter export when abundant. Second, high occurrence of other Antarctic siliceous phytoplankton groups such as parmales and sponge spicules may participate to BSi export though they may little participate to C_{org} and N_{org} burial. Other siliceous organisms present low abundances in core MD03-2601, generally not in phase with PE. Third, other sources such as bacteria, broken diatoms and other phytoplankton, and faecal pellets can export BSi, C_{org} and N_{org} (Krell et al., 2005). These fractions are difficult to assess down-core.

The efficiency of the biological pump, which has increased between 9 and 5 cal ka BP to reach highest Holocene levels between 5-1 cal ka BP for Corg and Norg and 6-2 cal ka BP for BSi at the pluri-millennial timescale and during PE at millennial timescale, was clearly associated with greater export of large and heavily-silicified diatoms thriving during ice-free summer season, except during PE6. Warmer temperatures and less icy environmental conditions promoting the summer species were prevailing during the 9-3.5 ka BP period (Crosta et al., 2005a, 2008). It is therefore possible that the recent and future warming inducing longer sea-ice free season at high southern latitudes will be favourable to higher paleoproductivity and consequently more active biological pump. There is however a need to better understand what are the environmental factors controlling modern and past productivity.

5.3. Factors controlling paleoproductivity

We now compared our results with a set of proxies that document the nutrient pool, the stratification and the duration of the growing season in order to identify the role of these controlling factors on past biological pump efficiency.

5.3.1. Nutrient and trace metal availability

Variations in macronutrient and micronutrient pools and utilization are here investigated thanks to the records of the setae diatom group, the ^{230}Th-normalized Fe flux and the $\delta^{15}N_{bulk}$, respectively. According to Beans et al. (2008) conducted in the Adélie Land region, the setae diatom group is associated to nutrient-rich and mixed surface waters. This is here supported at the Holocene scale by the significant anti-correlation between relative abundances of the setae group and of CRS. *Chaetoceros* resting spores are known to form in well-stratified surface waters that prevent nutrient refill (Leventer, 1991, 1992; Crosta et al., 1997; Leventer et al., 2002) (Table 1). The ^{230}Th-normalized Fe flux here reconstructs Holocene changes of iron stocks in surface waters, and thus, more largely, of micronutrient availability. The $\delta^{15}N_{bulk}$ is considered as a proxy for relative nutrient utilization in nitrate replete environments whereby enriched $\delta^{15}N_{bulk}$ values indicate higher nitrate relative utilization (Altabet and Francois, 1994). The nitrate relative utilization here represent a balance between nitrate supply via the MCDW upwelling and consumption by the phytoplankton.

Records of the setae diatom group and ^{230}Th normalized Fe flux show significant inverse relationship with the $\delta^{15}N_{bulk}$ record, thus indicating less nitrate relative utilization under replete conditions (Table 1). Conversely, the $\delta^{15}N_{bulk}$ record shows significant and positive correlations with the summer diatom group and the CRS relative abundances (Table 1).

At the pluri-millennial timescale, both the macronutrient pool and the iron pool display lower levels prior to 5 cal ka BP and higher levels after 5 cal ka BP. Low nutrient levels older than 5 cal ka BP are congruent to high nitrate relative utilization and lower paleoproductivity while high nutrient levels younger than 5 cal ka BP are concomitant to decreasing nitrate relative utilization and higher paleoproductivity (Figure 2A-D-E-F).
At the millennial timescale, macronutrient and trace metal availabilities in Adélie Land surface waters increased concomitantly during PE2, PE3, PE4 and PE6. In same time, nitrate relative utilization decreased (Figure 2A-D-E-F). During PE1, the iron pool increased and the nutrient relative utilization decreased, and the setae diatom group showed no significant changes. During PE5, both the macronutrient and iron pools increased but were not accompanied by significant change in the $\delta^{15}N_{bulk}$ (Figure 2A-B-E-F-G).

The $\delta^{15}N_{bulk}$ signal follows the pattern of nutrient and micronutrient proxies, except during PE1, and is opposite to the paleoproductivity records. Statistically, the $\delta^{15}N_{bulk}$ signal presents a stronger correlation with the setae diatom group (Table 1), which is a proxy for the upwellling of MCDW. In core MD03-2601, the $\delta^{15}N_{bulk}$ signal appears, therefore, mainly controlled by changes in the nitrogen supply rather than in the nitrogen uptake by phytoplankton. The $\delta^{15}N_{bulk}$ signal along the setae group and the Fe flux records are coherent to depict an increase in macro- and micronutrient supply during periods of highest paleoproductivity, observed after 6-5 cal ka BP and during PE. Higher nutrient

supply sustained phytoplankton production by delaying the appearance of limiting conditions. Several studies in coastal Antarctic environments demonstrate that nutrients, and particularly iron, stimulate surface water productivity by accelerating the growth rate of small diatom species (Smetacek et al., 2004; Leventer et al., 2006; Timmermans et al., 2008). In contrast in core MD03-2601, nutrient-rich periods congruent to higher paleoproductivity are associated with large diatom species having low growth rate. Thereby, other factors are certainly involved to explain the relationships between paleoproductivity, diatom assemblages and nutrient supply in the DDUT region during the Holocene.

5.3.2. Water column stratification

Water column stratification is another key environmental factor for the biological pump efficiency because it determines phytoplankton community and, here, diatom speciation. Different diatom species present different organic and silica contents along with different sinking rates, which in turn dictates the quality of the organic matter exported (e.g. new or recycled production, broken or intact phytoplanktonic cells) (Arrigo et al., 1999, 2008; Kemp et al., 2000, 2006; Wright and van den Enden, 2000). In DDUT, we observe a decrease of the water column stratification over the course of the Holocene, demonstrated by the decrease of the CRS (Crosta et al., 2008) and the increase of the diatom setae group (Figure 2D). The inferred trend in surface water stratification is opposite to the long-term increase of Holocene paleoproductivity, at least until 3-4 cal ka BP (Figure 2A-C-D). Since then, productivity started to decrease slightly while stratification continued to diminish at the same pacing. Similarly, at the millennial timescale, drops in CRS abundances are concomitant to peaks in the setae diatom group abundances (Figure 2C-D). Thereby, in Adélie Land, the periods of higher paleoproductivity at both pluri-millennial and millennial timescales are associated to nutrient-rich and mixed surface waters.

The two majors processes that control both stratification and nutrient supply in CCSZ are spring sea ice melting and upwelling of MCDW (Edwards and Sedwick, 2001; Sambrotto et al., 2003; Lannuzel et al., 2007), with opposite impacts on the water column stratification. Sea ice and ice melting release fresh, cold and nutrient-rich waters at the origin of a strong pycnocline that reduces the exchange with underlying waters. In contrast, upwelling of MDCW, which mixes and renews the CCSZ water masses, is promoted by winds (Toggweiler et al., 2006). The prevalence of mixed and nutrient-rich conditions during periods of higher paleoproductivity (e.g. Late Holocene and PE) could indicate a strengthening of the upwelling/wind regime that recurrently destroyed the upper water column stratification induced by sea ice melting. More precisely, spring conditions, e.g. well-stratified water column with a well established pycnocline, were rapidly disappearing because of stronger winds, thus promoting the onset of summer conditions, e.g. deeper and less stable water column with a more permeable pycnocline, earlier in the season and extended later in the autumn. The early destruction (just after sea ice waning) of the

upper water column stratification would reduce the development of small, high growth rate diatom species that are most competitive in well-stratified water column conditions (Leventer, 1991, 1992; Maddison et al., 2005, 2006; Stickley et al., 2005; Beans et al., 2008).

5.3.3. Growing season duration

The length of the growing season or ice-free season strongly impacts diatom speciation and therefore productivity and export/burial. In the CCSZ, the growing season duration is mainly controlled by the annual sea ice cycle, e.g. the timing of sea ice waning and waxing, which depend on several parameters such as temperature, wind, oceanic circulation, glacier.

Our results (Figure 2B) suggested that the ice-free season increased along the Holocene since 3.5 cal ka BP and then decreased as previously shown in Crosta et al. (2008). These changes in sea ice duration are accompanied to a later sea ice melting in spring and later sea ice freezing autumn during the Neoglacial than the Hypsithermal period (Crosta et al., 2008; Pike et al., submitted). Modelled ice-free season duration in DDUT increased from 9 cal ka BP to 1.7 cal ka BP and subsequently diminished (Figure 2I). The ice-free season is progressively extended on the autumn season with January to February ice-free conditions on the Early Holocene to January to March ice free conditions on the Late Holocene (at 1.7 cal ka BP) (Figure 2I). At the Southern Ocean scale, the model reports similar increase of the ice-free season duration until 5 cal ka BP, as a result of later sea ice melting in spring and later sea ice freezing in autumn (Renssen et al., 2005). After 5 cal ka BP, the model output for the Southern Ocean shows a shortening of the ice-free season by a later sea ice melting in spring and an earlier sea ice freezing in autumn (Renssen et al., 2005).

Therefore up to 5 cal ka BP, diatom records and model outputs support each other and demonstrate an increase of the ice-free season duration toward the autumn. After 5 cal ka BP, some discrepancies appear between the different model outputs and the geological data, which are certainly link to local specificity such as the impact of glacier re-advance on sea ice that have occurred at 3.5 cal ka BP (Denis et al., in-press) (Figure 2K). Thereby, we believe that in DDUT, longer ice-free conditions are maintained up to 3.5 cal ka BP.

The long-term variations in duration and timing of the ice-free season resulted from an increase of oceanic and atmospheric temperatures and wind strength combined to changes in the seasonality of local insolation at the precessional timescale (Renssen et al., 2005) (Figure 2H). These orbitally-forced Holocene changes work in the same direction to provoke early waning and later waxing of sea ice up to 3.5-5 cal ka BP though the modelled winter sea ice cover increases during the Holocene (Renssen et al., 2005; Denis et al., in press). The apparent paradox between winter and summer sea ice cover results from the

increasing seasonality caused by the Holocene evolution of the precessional index (Figure 2H).

The increased duration of ice-free conditions until 3.5 ka BP (Figure 2B) induced a progressive longer phytoplanktonic growing season favourable to the production of summer diatoms that have lower growth rates (Martin-Jézéquel et al., 2000; Kemp et al., 2006; Armand et al., 2008; Assmy et al., 2006). A longer growing season is also suitable to the build up of more robust diatoms frustules by incorporation of more nutrients (Martin-Jézéquel et al., 2000), supported by concomitant higher nutrient supply. Larger and heavier-silicified diatoms sink more rapidly and are more resistant to grazing pressure, which both contribute to an efficient drawdown of organic matter (Figure 2A-B). Reduction of the ice-free season, and resulting phytoplankton growing season, since 3.5 cal ka BP led to less summer diatom production and decreasing of the paleoproductivity though it can be partly counterbalanced by auspicious nutrient conditions (Figure 2A-B-D-E-F). At pluri-millennial timescales, the length of the phytoplanktonic growing season, which is closely linked to sea ice dynamics, appears, thus, a key factor in determining the specific composition of the diatom assemblage and the intensity of the PP.

At millennial timescale, PE1, PE3 and PE5 occurred during warmer Holocene phases in East Antarctica, which could be favourable to extended ice-free season (Figure 2J; Masson et al., 2000). In contrast, PE4 spanned over a warm and a cold phase, which is associated to glacier and sea ice advance (Figure 2J-K; Masson et al., 2000; Denis et al., in-press). PE2 and PE6 occurred during cold phases and glacier/sea ice advances (Figure 2J-K; Masson et al., 2000; Denis et al., in-press). At face value, no general pattern between climate/sea ice dynamic and millennial scale PE is discernable in the DDUT region. All PE show an increase in the summer diatom group abundances (Figure 2B), which argue for a longer summer season during millennial events. A longer growing season during cold phases may be related to the mechanical break-up of the sea ice by more intense winds (Figure 2F).

Lower paleoproductivity are reported during periods of massive freshwater input at ~11 and ~9.5 cal ka BP and of major glacier/sea ice re-advances at ~7.7 and ~3 cal ka BP (Figure 2K; Denis et al., in-press). Therefore, the local behaviour of glacier can strongly modulate the growing season duration through its impact on the sea ice cycle, on the surface water stratification and resulting upwelling.

5.4. Paleoclimatic implications

Climate-forced changes in nutrient supply, stratification and growing season duration determined the type and amount of surface water PP at both pluri-millennial and millennial timescales. Periods of enhanced wind and upwelling associated to longer ice-free season led to nutrient-rich mixed surface waters that supported high surface and exported/buried PP as a result of the development of larger and heavier silicified diatoms.

In contrast, periods of reduced wind and upwelling activity associated to shorter ice-free season led to nutrient depleted and well-stratified surface waters that supported low surface PP and subsequently limited organic matter burial.

We highlight here the positive effects of stronger winds and enhanced seasonal sea ice cycle on the Si, C and N biological pump in the CCSZ off Adélie Land. A pluri-millennial increase of the upwelling/wind intensity during the Holocene is consistent with several geological and model studies that reported/suggested a long-term increase of the wind intensity over the Holocene in East Antarctica (Steig et al., 2000; van Ommen et al., 2004) and high southern latitudes (Vimeux et al., 2001; Renssen et al., 2005). Accordingly, long-term changes in ice-free season duration, recorded in Adélie Land area, may represent a Holocene Antarctic-wide feature because Holocene patterns in winds, ocean and atmosphere temperatures are similar around AA (Renssen et al., 2005). Therefore, pluri-millennial changes in the CCSZ would be dictated by the Milankovitch precessionnal cycle with feedback from the regional cryosphere.

Much less is known about forcing factors of the Antarctic PP at the millennial scale. Our results demonstrate that wind intensity and sea ice dynamic are the main controlling factors with strong feedback from the regional glaciers. Indeed, though homogenous wind variations over the Southern Ocean and CCSZ are expected (Figure 2G, Mayewski et al., 2006, 2009), local ice cap morphology and glacier dynamic (Ingólfsson et al., 1998; Denis et al., in-press) strongly modulate local winds, sea ice cycle and water column structure. As a result, millennial productivity variations may be decoupled from climate changes (Figure 2A-J). It is also worth exploring whether high latitude climate modes, such as the Antarctic Dipole, characterized by an out-of-phase relationship between sea ice and surface temperature anomalies in the South Pacific and South Atlantic (Yuan, 2004) prevailed during the Holocene at the millennial scale and could affected organic matter sequestration. Finally, we note that PE2, PE4, PE5 and the major glacier re-advance at 3.5 cal ka BP recorded in core MD03-2601 coincide with the worldwide rapid climatic changes (RCC) reported in the 50-paleorecord study of Mayewski et al. (2004) (Figure 2L). Therefore, millennial climatic variations recorded in Adélie Land and possibly in Antarctic CCSZ could be part of a more general Holocene pattern

Predictions of future climate suggest enhanced Southern Ocean winds, enhanced upwelling of nutrient-rich waters (Toggweiler et al., 2006; Russell et al., 2006), retreat of sea ice extent and longer ice free-season (Goosse and Renssen, 2001; Lefebvre and Goosse, 2008a). In that perspective, our results would emphasize an increase of the carbon biological pump in the CCSZ, which would implicate a slight negative feedback on climate warming as suggested by Arrigo and Thomas (2004), Tortell et al. (2008) and Arrigo et al. (2008). In addition, the decrease in dust-bearing iron to Antarctica and surrounding waters (Kattenberg et al., 1996; Sarmiento et al., 1998), which represent a minor source to

coastal Antarctic waters, will have a limited impact on the phytoplankton productivity of the CCSZ (Edwards and Sedwick, 2001; Lannuzel et al., 2007).

5. Conclusion

This study provides the first ^{230}Th-normalized high-resolution Holocene record of primary productivity (PP) from the Antarctic Continental Shelf (CCSZ), therefore giving unprecedented insights on the biological pump of the CCSZ in response to climatic changes at both pluri-millennial and millennial timescales. A long-term increase of PP since 9 cal ka BP to reach highest values between 5-1 cal ka BP for C_{org} and N_{org} and 6-2 for BSi and six events of higher paleoproductivity at 10.6-10.2, 8.7-8, 7.6-7, 6.2-5.3, 4.6-3.5, and 2.4-1.4 cal ka BP are evidenced along the Holocene. More efficient biological pump at these two timescales was mainly promoted by higher PP and the development of large and heavily-silicified summer diatoms, which are associated to higher nutrient supply, reduced stratification and longer ice-free season. These environmental conditions were mainly controlled at these timescales by the wind regime and the sea ice cycle as well as the dynamic of adjacent glaciers. Our results, emphasizing enhanced PP during warmer and windier Holocene periods, suggest stronger CO_2 biological pump in the future though the relationships between the biological pump and the environmental conditions in the CCSZ were not straightforward throughout the Holocene. In this vein, additional studies are necessary to constrained the influence of seeding, aggregate formation, bacterial and grazing pressure in relation to the sea ice cycle.

Acknowledgements

We personally thank people from Images X (CADO) cruise and from NSF-funded NBP0101 cruise for data and suggestions concerning the Dumont d'Urville Trough. Financial support for this study was provided by TARDHOL and JC ARTTE projects through the national LEFE-EVE and ACI programs (INSU-CNRS), with the logistic support of the French IPEV (Institut Paul Emile Victor) and the International Marine Past Global Change Study (IMAGES). This is an EPOC contribution N°x.

CHAPITRE 4

Connections Haute-Basse latitudes via le couplage Océan-Banquise-Atmosphère

Dans les deux précédents volets, nous nous sommes attachés à caractériser le fonctionnement de la machine climatique des hautes latitudes sud dans son ensemble, c'est à dire au sein de ces différents compartiments climatiques : cryosphère, océan, atmosphère et biosphère, au travers des variations climatiques à long et à court terme exprimées au sein de la zone marginale des glaces de Terre Adélie, en Antarctique de l'Est. Cette approche multi-proxies et multi-échelles, nous a permis d'identifier des tendances à long terme en lien avec les variations saisonnières d'ensoleillement local et des tendances à court terme dont les forçages restent plus mystérieux. A ces deux échelles de temps, plurimillénaire et millénaire, nous avons caractérisé le temps et le mode de réponse des différents sous-systèmes climatiques et leurs interconnections. Nous avons aussi démontré que les tendances à long terme observées d'après la carotte marine de Terre Adélie avaient vraisemblablement un écho équivalent autour de l'Antarctique grâce à la confrontation des résultats avec des sorties de modèle numérique reconstituant la variabilité climatique long terme Holocène au sud de 60°S.

Dans ce troisième volet, nous avons voulu tester la représentativité en Antarctique des variations plurimillénaires et regarder si cette cohérence s'exprime aussi à l'échelle millénaire. Pour cela nous avons comparé les données obtenues en Terre Adélie avec les données d'un autre enregistrement marin prélevé en Baie de Prydz, c'est-à-dire à plus de 2000 km à l'Ouest de notre zone. Pour cette étude comparative, nous nous sommes focalisés sur les compartiments climatiques « banquise » et « atmosphère » et leurs interconnections. La banquise est à l'interface entre les compartiments climatiques « océan » et « atmosphère » et agit sur la machine climatique à travers de nombreux processus : l'albédo, la formation d'eaux profondes, les échanges de gaz et chaleur entre l'océan et l'atmosphère, la productivité marine et la position des ceintures climatiques. C'est ce dernier point qui a motivé notre étude dont les buts sont multiples :

1) caractériser la relation banquise-atmosphère dans l'environnement périantarctique de l'échelle plurimillénaire à millénaire, en comparant les deux enregistrements haute-résolution de Terre Adélie et de la Baie de Prydz,

2) comparer la variabilité climatique enregistrée aux hautes latitudes avec un transect latitudinal et longitudinal d'enregistrements paléoclimatiques holocènes des moyennes aux hautes latitudes pour caractériser le couplage océan-atmosphère en Hémisphère Sud à ces deux échelles de temps,

3) identifier les facteurs forçants de la variabilité aux hautes latitudes à ces deux échelles de temps,

4) comparer les forçages des hautes et basses latitudes et leur incidence sur le couplage océan-atmosphère aux moyennes latitudes Sud.

Les résultats de ce travail sont présentés dans ce chapitre sous format d'un article scientifique, préparé en vue d'une soumission dans le journal *Earth and Planetary Science Letters*. Nous sommes conscients que les hypothèses développées dans le cadre de ce chapitre requièrent encore réflexions et discussions avant d'être soumis dans une forme définitive à *EPSL*.

Antarctic sea ice and wind variability during the Holocene: Insight on low-high latitude coupling.

Delphine Denis[a,*] Xavier Crosta[a], Loic Barbara[a], Guillaume Massé[b], Hans Renssen[c], Amy Leventer[d], Olivier Ther[a], and Jacques Giraudeau[a].

[a] EPOC, UMR-CNRS 5805, Université Bordeaux 1, av. des facultés, Talence, 33405 cedex, France.
[b] LOCEAN, Université Pierre et Marie Curie, Paris VI, Jussieu, Paris, 1, France.
[c] Faculty of Earth and Life Sciences, Vrije Universiteit Amsterdam, De Boelelaan 1085, NL-1081 HV, The Netherlands.
[d] Department of Geology, Colgate University, 13 Oak Drive Hamilton, NY 13346, USA.

Abstract

This study presents a Holocene high-resolution investigation of sea ice and wind stress based on micropaleontological and biomarker data in two cores from the coastal East Antarctic area (Adélie Land at ~140°E and eastern Prydz Bay at ~77°E). This high latitude view is discussed with regard to low- and middle latitude records to decipher the forcing factors acting at both pluri-millennial and millennial timescales on the ocean-atmosphere coupling. At pluri-millennial timescales, ocean, sea ice and atmosphere climatic components present opposite patterns according to the different latitudinal bands of the southern Hemisphere in relation to the local insolation and to the latitudinal insolation gradient, enhanced by ice and sea ice expansions since 5 cal ka BP. Chiefly, disctintive climatic patterns north and south of 45°S are controlled by precession and obliquity respectively, which governed the heat exchange fluxes from low to high latitudes. At millennial timescales, sea ice dynamic and atmospheric perturbations appear out-of-phase between the Adélie Land region and the Prydz Bay area older than 4.5 ka BP and in-phase since 4.5 cal ka BP, certainly in relation with the onset of Neoglacial conditions over Antarctica and of modern El Niño-Southern Oscillation conditions in the tropics.

Keywords: Holocene, ocean-sea ice-atmosphere coupling, Antarctica, ADP, ENSO.

1. Introduction

On glacial/interglacial timescales (Stuut et al., 2004; Lamy et al., 2004; Stuut and Lamy, 2004) as well as during the Holocene period (Lamy et al., 2002), the position and the strength of the westerlies and oceanic currents have been linked to past sea ice extent variations. At decadal timescales, variations in Antarctic sea ice cover have been correlated to tropical El Niño Southern Oscillation (ENSO) events through its impact on the position of the sub-tropical jet and subsequently the heat flux from the mean meridional circulation (Yuan, 2004). In return, Antarctic sea ice is supposed to influence the position of the low latitude climatic belts such as the InterTropical Convergence Zone (Chiang and Bitz, 2005). These examples well-illustrate the mutual and reciprocal relationships, linking the ocean, the Antarctic sea ice and the atmosphere, which complicate the identification of the forcing factors and the understanding of the internal response at different timescales.

Models and paleo-series highlight the role of obliquity and precession to explain the different climate stories, which took place in the different hemispheric latitudinal bands at pluri-millennial scales (Lorenz et al., 2006; Davis et al., 2009) and of complex climatic modes at decadal to millennial timescales, which forcing factors remains enigmatic (Clement et al., 2000; Naugthon et al., in-press; Yuan, 2004; Yuan and Li, 2008).

In this study, we use high resolution reconstructions of Holocene sea ice cover and wind stress from two marine cores off East and West Indian Southern Ocean sectors in complement to Holocene paleo-data set documenting, the ocean, the sea ice, and the atmosphere climatic sub-systems from high to low southern latitudes. The confrontation of these large datasets allows us to 1) characterize the synchronicity of the sea ice and wind Holocene patterns in Adélie Land and Prydz Bay regions at both pluri-millennial and millennial timescales, 2) to better understand the different latitudinal responses of the ocean, sea ice, and atmosphere climatic components, 3) to identify the forcing factors involved in each latitudinal bands at both pluri-millennial to millennial timescales, and 4) to apprehend the response of the East and West Indian Southern Ocean sectors to ENSO millennial variability.

2. Environmental settings

The Dumont d'Urville Trough (DDUT) and the Prydz Bay regions are located in the East and West SO Indian sector along the East Antarctic coast, respectively (Figure 1). Both areas are influenced by glaciers and ice shelves that release fresh water and terrigenous particles in the surrounding waters. Lambert glacier and Amery ice shelf that composed the cryospheric system of Prydz Bay, are larger than those in DDUT and figure among the most important in Antarctica (Figure 1).

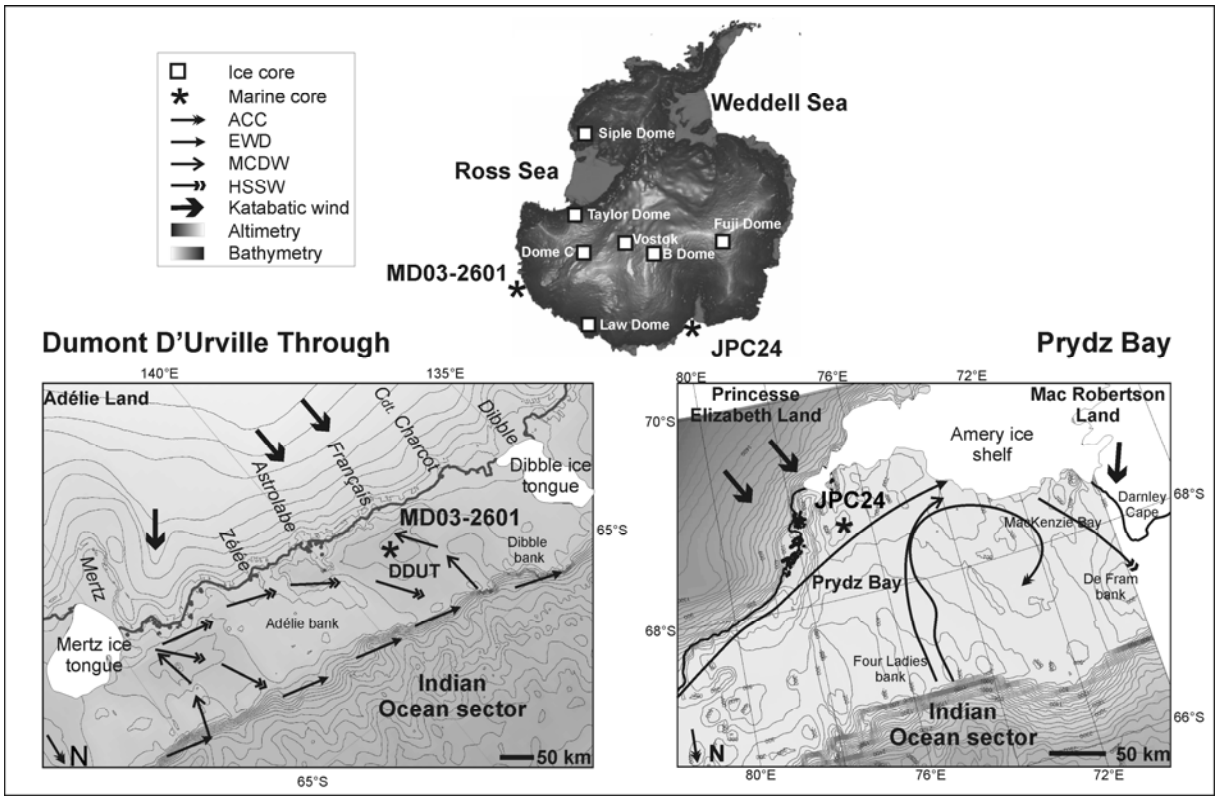

Figure 1: Topographic map of Antarctica showing the location of the different ice cores mentioned in the text and, maps showing the location of MD03-2601 and JPC24 marine cores along with altimetry and bathymetry, location of glaciers (in italic), ice shelf and ice tongues, detail of oceanographic currents and different water masses (Smith and Tréguer, 1994; Wong, 1994; Nunes Vaz and Lennon, 1996; Rintoul, 1998; Harris and Beaman, 2003; Williams and Bindoff, 2003), katabatic wind directions (Massom et al., 1998). Winter sea ice covers the whole oceanic area encompassed by the map. ACC: Antarctic Circumpolar Current, EWD: East Wind Drift, MCDW: Modified Circumpolar Deep Water, HSSW: High Salinity Shelf Water. Altimetry and bathymetry data are based on ETOPO2 data set from http://www.ngdc.noaa.gov/mgg/fliers/01mgg04.html.

The coastal areas off DDUT and Prydz Bay are presently exposed to the strongest Antarctic katabatic winds (Périard and Pettré, 1993; Xie et al., 2002) that create several recurrent polynya (Adolphs and Wendler, 1995, Massom et al., 1998; Arrigo and van Dijken, 2003; Tamura et al., 2008) (Figure 1). The Prydz Bay is also known to catch synoptic depressions that maintain a gyre system in the bay (Wong, 1994). The ice-free conditions last 3-5 and 2-3 months per year in DDUT and Prydz Bay, respectively, hence giving a good estimation of the length of the phytoplankton growing season (Schweitzer, 1995; Worby et al., 1998; Arrigo and van Dijken, 2003). The more enclosed morphology and the larger cryospheric system of the Prydz Bay regions are certainly responsible for the longer persistence of annual sea ice cover.

Both regions are influenced by similar water masses and currents (Smith et al., 1984; Smith and Tréguer, 1994; Wong, 1994; Nunes Vaz and Lennon, 1996; Rintoul, 1998, Bindoff et al., 2000a, 2000b; Williams and Bindoff, 2003) (Figure 1): (1) the wind-driven East Wind Drift (EWD), also called Antarctic Coastal Current, which flows westward at the surface transporting westward the Antarctic Surface water (AASW) that constitutes the near-

surface layer on the continental shelf; (2) the Modified Circumpolar Deep Water (MCDW) that upwells at the Antarctic Divergence; (3) the High Salinity Shelf Water (HSSW), formed by brine-rejection during winter sea ice formation and cooling of the MCDW, which flows northward as part of the Antarctic Bottom Water (AABW). The major oceanographic distinction between the two areas is the intrusion of an ACC (Antarctic Circumpolar Current) branch attracted in Prydz Bay area by the cyclonic gyre, while the ACC flows more offshore in the DDUT region (Wong, 1994).

3. Material and Methods

Piston cores MD03-2601 (66°03.07'S; 138°33.43'E; 746 m water depth) and JPC24 (68°41.637'S; 76°42.712'E; 816 m water depth) were recovered from the slope of one of the depressions composing the DDUT Trough and the Prydz Bay during the CADO and the NBP0101 cruises, respectively (Figure 1) (Crosta et al., 2005a; Leventer et al., 2006).

3.1. Age models

The age models of cores JPC24 and MD03-2601 are based on five and seven radiocarbon dates completed on carbonate material and on the humic fraction of bulk organic matter, respectively (Figure 2). For core JPC24, a modern reservoir age of 1280 years was determined by dating the core-top of the twin Karsten core, which has preserved the water/sediment interface (Leventer et al., 2006; Leventer, personal communication, 2006). This reservoir age was subsequently applied to correct the ^{14}C raw dates of core JPC24. For core MD03-2601, without this information, we applied the general age reservoir of 1300 years advised for East Antarctic shelves (Ingólfsson et al., 1998). It is worth noting that reservoir ages are very consistent between the two areas. The corrected ^{14}C dates of JPC24 and MD03-2601 cores were then calibrated to calendar ages using Calib 5.0 (Stuiver et al., 2005) and the marine calibration Marine04 (Hughen et al., 2004). Further details on the age-models of JPC24 and MD03-2601 are provided in Leventer et al. (2006) and Denis et al. (in-press), respectively. The laminated 17 m-long and 40 m-long sediment cores cover the 0.6-11 and 1-11 cal ka BP periods with mean accumulation rates of 0.25 cm/yr and 0.4 cm/yr for cores JPC24 and MD03-2601, respectively (Figure 2).

3.2. Proxies

3.2.1. Biomarkers

Biomarker analyses present a ~70 years resolution in both MD03-2601 and JPC24 marine cores. Detailed methods of extraction and analyses of the Highly Branched isoprenoids (HBi) are found in Belt et al., 2007. Briefly, after chemical and physical extraction, HBi was purified using open column chromatography before being analysed by gas

chromatography–mass spectrometry (GC–MS). All biomarkers were identified on the basis of their characteristic GC–MS retention times and mass spectra. Relative abundances of the bi-unsaturated C25:2 (HBi Diene) and the tri-unsaturated C25:3 (HBi Triene) were calculated on the basis of the magnitudes of their GC–MS responses compared with those of the internal standard, with these ratios corrected according to the mass of sediment analysed. Analytical reproducibility was checked using a standard sediment with known abundances of biomarkers for every 8–16 sediment sample extractions (analytical error <5%, n = 10).

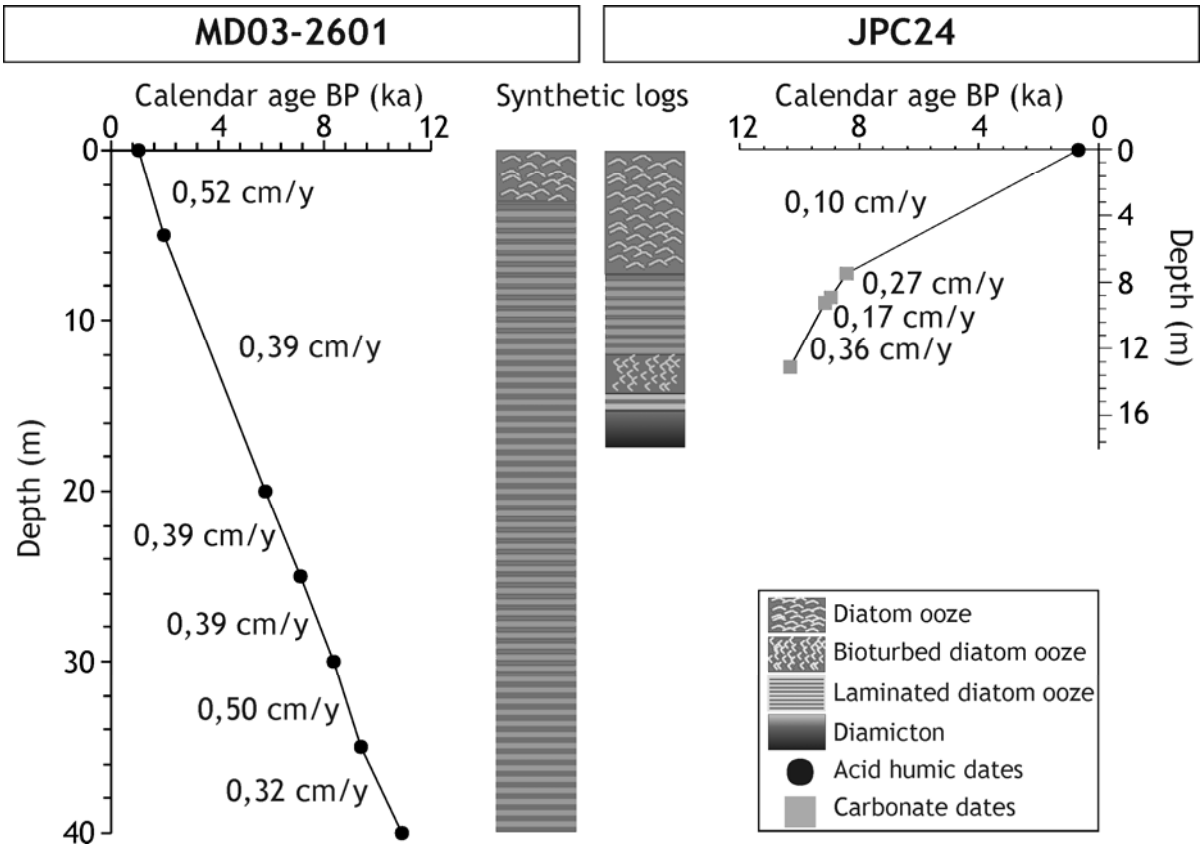

Figure 2: Age models, linear sedimentation rates and synthetic logs of MD03-2601 and JPC24 marine cores.

HBi diene is synthesized by sea ice diatoms, mainly by the raphide pennate group of the bottom ice community that grows during spring. In contrast, HBi Triene z is produced by open ocean diatoms such as Rhizosolenoids (*Proboscia* spp., *Rhizosolenia* spp.)(Johns et al., 1999; Belt et al., 2000). The biomarker ratio (diene/triene z), which was demonstrated to successfully reconstruct sea ice presence/absence and seasonality in modern sediments of DDUT (Massé et al., in preparation), is here used in complement to diatom assemblages, both in Adélie Land and Prydz Bay areas. It is worth noting that a neighbour HBi ratio (diene/monoene) was successfully used to reconstruct past sea ice duration in the Northern Hemisphere (Massé et al., 2007; Vare et al., 2009).

3.2.2. Diatoms

Diatom census counts, following Crosta and Koç (2007) counting convention, present a ~10-20 years resolution in core MD03-2601 and a ~50-60 years resolution in core JPC24. More details about slide preparation and diatom identification are found in Crosta et al. (2004). Around 350 diatom valves were counted in each sample and the relative abundance of each was determined as the fraction of diatom species against total diatom abundance in the sample. Diatom species have been regrouped according to their ecological preferences.

Fragilariopsis curta, *F. cylindrus*, *F. sublinearis*, *F. obliquecostata*, *F. vanheurkii* and *Porosira glacialis* thrive within sea ice environments during spring and/or autumn seasons (Leventer et al., 1993; Taylor and McMinn et al., 2002; Stickley et al., 2005; Armand et al., 2005; Maddison et al., 2005, 2006; Denis et al., 2006; Crosta et al., 2008; Pike et al, accepted). They constitute the sea ice diatom group (Si-DG) in the present study, expressed as the sum of their relative abundances. *Fragilariopsis curta* relative abundances from core MD03-2601 and *P. glacialis* relative abundances from cores MD03-2601 and JPC24 have been previously published in Crosta et al. (2005a, 2007, 2008) and Pike et al. (accepted), respectively.

Chaetoceros Phaeoceros spp. (dominated by *C. dichaeta*), *Corethron pennatum*, *Rhizosolenia* spp. and *Proboscia* spp., which present protuberances and/or setae, are often found together in waters and, subsequently, sediment samples of Antarctic coastal environments (Maddison, 2005; Maddison et al., 2005, 2006; Stickley et al., 2005; Crosta et al., 2005b; Beans et al., 2008, Denis et al., in revision). They have been grouped in the setae diatom group (S-DG), which the MD03-2601 record has been already presented in Denis et al. (in revision). This group has been associated in Adélie Land region with nutrient-rich and mixed surface waters (Beans et al., 2008; Denis et al., in revision) promoted by enhanced upwelling and/or windy conditions (Denis et al., in revision).

4. Results

4.1. Pluri-millennial scale

The HBi ratio in core JPC24 ranges from 0.0 at 9 cal ka BP to 1.6 at 2.8 cal ka BP, with a significant increase along the course of the Holocene. The increasing trend is accentuated since 4.5 cal ka BP (Figure 3A). The Sea ice Diatom Group (Si-DG) record in JPC24 presents variations ranging from 24 % at 7.8 cal ka BP to 72 % at 1.7 cal ka BP (Figure 3B). Relative abundances of the Si-DG increased over the Holocene, and especially since 4.5 cak ka BP. The HBi and Si-DG records in core JPC24 are significantly correlated along the Holocene (Table 1, Figure 4A). The Setae Diatom Group (S-DG) in core JPC24 shows variations ranging from 1.2 % at 5.6 cal ka BP to 10.5 % at 9 cal ka BP with a significant decreasing

trend during the Early Holocene and a slightly increasing trend over the Mid- and Late Holocene (Figure 3C). As a result, there exists a negative, significant correlation between the S-DG and HBi ratio records and a negative, non-significant correlation between the S-DG and the Si-DG in JPC24 when the whole Holocene is considered (Table 1).

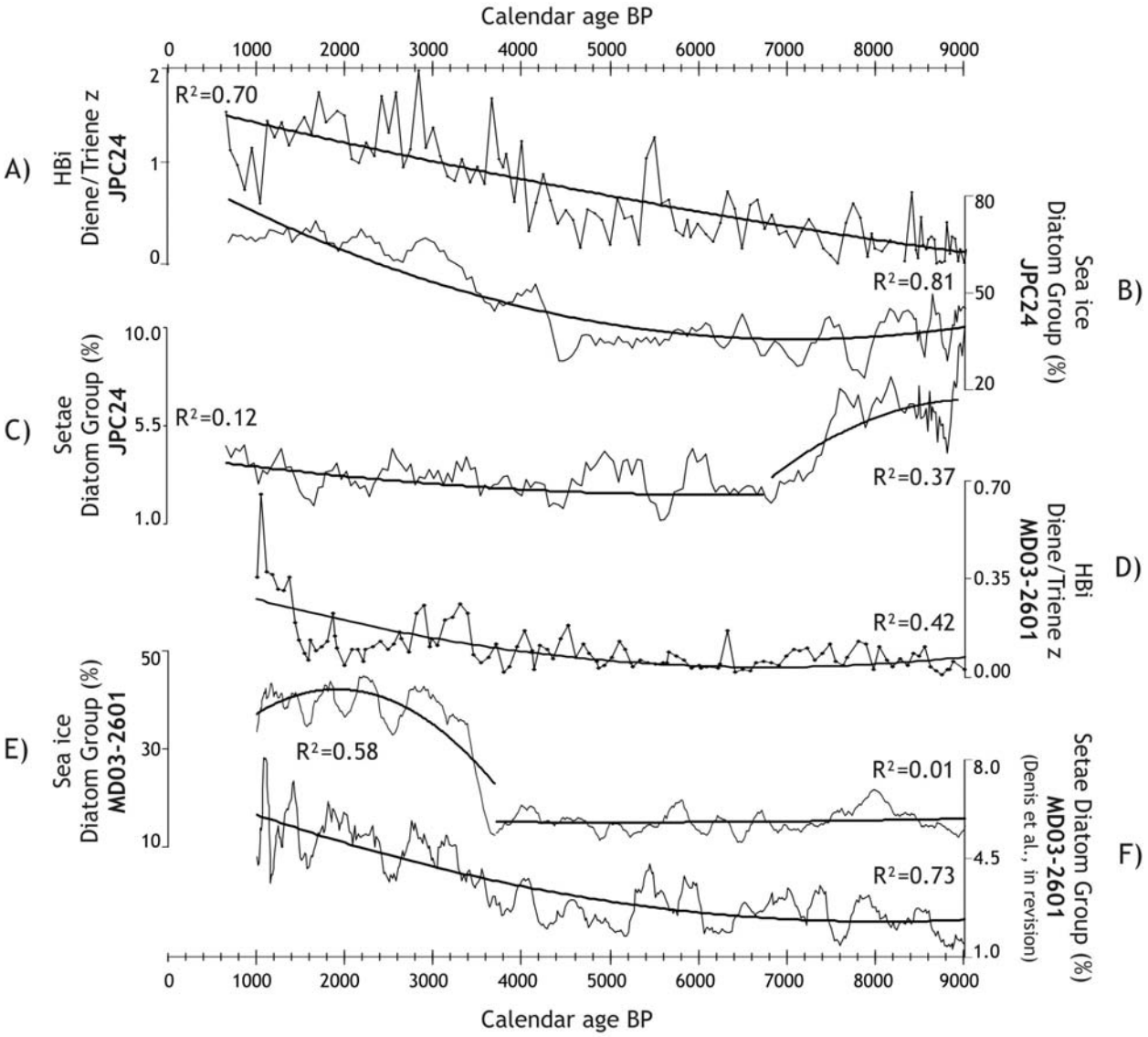

Figure 3: JPC24 and MD03-2601 marine records *versus* time: A) HBi ratio in core JPC24, B) relative abundances of the Si-DG in core JPC24 (5-point running mean), C) relative abundances of the S-DG in core JPC24 (5-point running mean), D) HBi ratio in core MD03-2601, E) relative abundances of the Si-DG in core MD03-2601 (10-point running mean), F) relative abundances of the S-DG in core MD032601 (10-point running mean) from Denis et al. (in revision). Thick lines represent a 2-order polynomial function to extract the pluri-millennial Holocene patterns. When large amplitude shifts exist (C and E), we applied two separate polynomial regressions to prevent the large low that would have been created at the transition (7500 cal yr BP in C and 3700 cal yr BP in E) by a single 2-order polynomial function. Corresponding correlation coefficients are indicated above the curves.

However, deeper inspection on an X-Y plot demonstrates that the S-DG displays significant positive correlations with both the Si-DG (Figure 4C) and HBi (not shown) records when the records are split at 7 cal ka BP where the large amplitude shift in S-DG relative abundances

is observed. Slopes of the linear regressions are however completely different older (0.13) and younger (0.015) than 7 cal ka BP (Figure 4C).

		JPC24 records			MD03-2601 records		
		HBi ratio	Si-DG	S-DG	HBi ratio	Si-DG	S-DG
JPC24 records	HBi ratio		**3,E-10**	**2,E-10**	**3,E-12**	**3,E-12**	**6,E-20**
	Si-DG	**0,39**		7,E-01	**3,E-08**	**1,E-18**	**7,E-13**
	S-DG	**-0,40**	-0,02		4,E-01	2,E-01	**4,E-06**
MD03-2601 records	HBi ratio	**0,44**	**0,35**	-0,05		**4,E-16**	**2,E-13**
	Si-DG	**0,44**	**0,45**	-0,07	**0,51**		**3,E-66**
	S-DG	**0,58**	**0,37**	**-0,24**	**0,46**	**0,55**	

Table 1. Table of Kendall's Tau correlation coefficients between marine records in and within cores JPC 24 and MD03-2601. Correlation coefficients are reported in the lower triangle and significance values (p-values) are reported in the upper triangle. The test is significant (bold values) if its associated probability (p-value) is smaller than the level of confidence σ. Here, we used the Šidàk-Bonferonni correction, which takes into account the number of samples considered (n), to determine the σ required following the equation: $\sigma_{required} = 1- (1-\sigma)\ 1/n$, where σ is the p-value chosen and n is the number of samples considered (Abdi, 2007). According to the number of samples considered here (from n= 115 to n= 440), the $\sigma_{required}$ varies between 9.10^{-6} and 2.10^{-6} to have significant correlation at p>0.001 (bold values). The Kendall's Tau correlation coefficients have been calculated using the free software PAST 1.75 (Hammer et al., 2007). This test has been performed on HBi ratio, and on relative diatom abundances of Si-DG and S-DG on the two marine cores and between them. These data are particularly sensitive to seasonal variability. We therefore smoothed the high-resolution records to reduce the seasonal noise possibly captured in the stepwise sampling of the laminated JPC24 and MD03-2601 cores. The Kendall's Tau correlation coefficients have been, thus, calculated on a 3-point running mean for the HBi ratio records, and on the 5-point and 10-point running mean for the diatom records from JPC24 and MD03-2601 cores, respectively. Given the laminated structure of the core, it appears hazardous to calculate correlation coefficients between records having different resolutions. We therefore calculated the Kendall's Tau correlation coefficients between two records at the highest common resolution.

In core MD03-2601, HBi ratio values vary from 0.0 at 8.8 cal ka BP to 0.5 at 1.1 cal ka BP (Figure 3D). A slight pluri-millennial decrease until 6-7 cal ka BP followed by a slight increase since then and accentuated since 4.5 cal ka BP is observable. Greater sea ice cover is discernable at 3.5-2.8 cal ka PP and after 1.5 cal ka BP (Figure 3D). The Si-DG record in MD03-2601 shows variations from 11% at 6.5 cal ka BP to 44% at 2.3 cal ka BP. The overall Holocene pattern is toward an increasing trend marked by a large amplitude shift at 3.5 cal ka BP (Figure 3E). However, cutting the Si-DG record in two at this transition evidences a slight decreasing trend until 3.5 cal ka BP followed by an increasing trend since then. The HBi and Si-DG records present a strong, significant Kendall's Tau correlation coefficient (Table 1). Nonetheless, further look on X-Y plot shows that values younger than 1.5 cal ka BP are out of their Holocene relationships (Figure 4B). The S-DG shows a significant Holocene long-term increase from 1.3% at 8.8 cal ka BP to 8.1% at 1.1 cal ka BP.

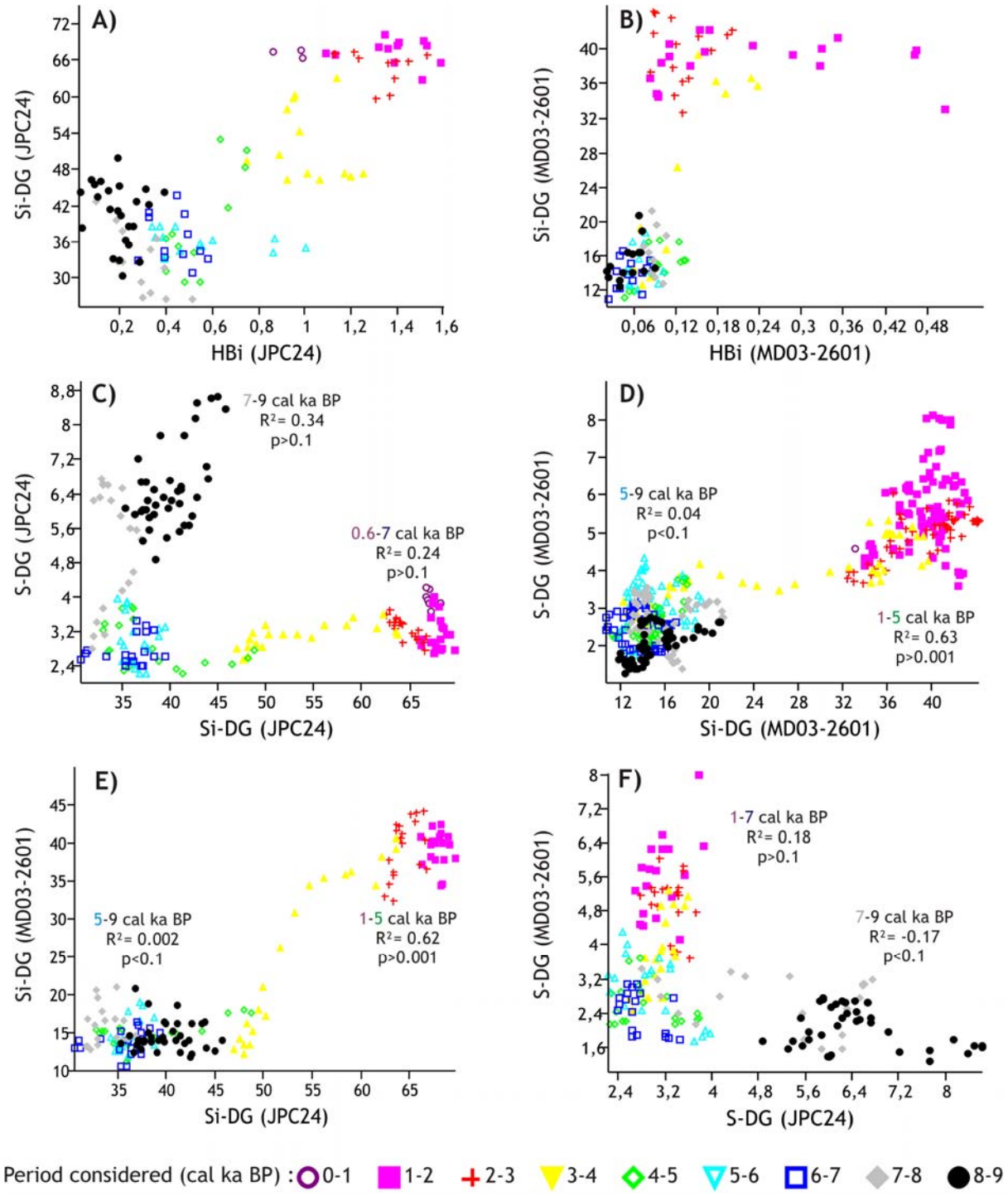

Figure 4: X-Y plots of JPC24 and MD03-2601 data : A) HBi ratio (3-point running mean) *versus* Si-DG (5-point running mean) in core JPC24, B) HBi ratio (3-point running mean) *versus* Si-DG in core MD03-2601 (10-point running mean), C) Si-DG (5-point running mean) *versus* S-DG (5-point running mean) in core JPC24, D) Si-DG (10-point running mean) *versus* S-DG (10-point running mean) in core MD03-2601. E) Si-DG (5-point running mean) in core JPC24 *versus* Si-DG (10-point running mean) in core MD03-2601, F) S-DG (5-point running mean) in core JPC24 *versus* S-DG (10-point running mean) in core MD03-2601. At the bottom, the colour code highlights the different periods considered. Additional Kendall's Tau correlation coefficients have been calculated for separate Holocene periods on C, D, E and F because of the presence of large amplitude shifts (Figure 3C, E). Considered periods, correlation coefficients and their significance are shown on the right side of the X-Y plots. All the X-Y plots and the additional Kendall's Tau correlation coefficients have been performed with the free software PAST 1.75 (Hammer et al., 2007).

Similar to other records, the increase in S-DG relative abundances is accentuated since 4.5 cal ka BP (Figure 3F). At the Holocene scale, the S-DG record is significantly correlated with the HBi ratio and Si-DG records in core MD03-2601 (Table 1). Deeper inspection on X-Y plot shows that this relationship is more positive and significant during the Mid- and Late Holocene than during the Early Holocene (Figure 4D).

Relative abundances of the Si-DG are twice as high in core JPC24 as in core MD03-2601 (Figure 3B-E). Similarly, the HBI ratio is also 2-3 higher in core JPC24 than in core MD03-2601. The Holocene pluri-millennial trends are however relatively similar with a marked increase since 4.5 cal ka BP even though the large amplitude shift in Si-DG abundances in core MD03-2601 is absent from core JPC24 (Figure 3A-B-D-E). At the Holocene scale, sea ice records in core JPC24 show positive, significant correlation coefficients with sea ice records in core MD03-2601 (Table 1). However, an X-Y plot demonstrates that the similarities between JPC24 and MD03-2601 sea ice records are significant only after 5 cal ka BP (Figure 4E).

Conversely, relative abundances of the S-DG records in the two cores show similar amplitude variations and similar increasing trends since 7 cal ka BP, which are accentuated since 4.5 cal ka BP (Figure 3C-F). In contrast, on the 9-7 cal ka BP period, the two S-DG records show opposite patterns with high S-DG values in core JPC24 and low S-DG values in core MD03-2601 (Figure 3C-F). As a result, the X-Y plot between S-DG relative abundances in the two cores presents different slopes and significance older and younger than 7 cal ka BP (Figure 4F).

4.2. Millennial scale

Superimposed to the pluri-millennial patterns evidenced in HBi ratio, Si-DG and S-DG records in cores JPC24 and MD03-2601, a millennial variability is observable (Figure 3). Millennial variability in the HBI records is often represented by single points because of the lower resolution of the records. We therefore focused on the diatom records that were investigated at higher resolution. Short-term changes in the diatom records were evidenced by subtracting the respective pluri-millennial trends, highlighted by the 2-order polynomial regressions shown in Figure 3. The events described below and their comparisons are defined within the age control accuracy.

At the millennial scale, the Si-DG and S-DG records in core JPC24 show a marked variability with 12 events each. Events represent increases in diatom relative abundances. They spanned from 200 to 700 years (Figure 5A-B). The 12 “sea ice” events are centred on 9, 8.7, 8.3, 7.5, 6.9, 6.5, 6.1, 4.1, 3.1, 2.3, 1.7, and 1.3 cal ka BP whereas the “setae” events are centred on 9, 8.2, 7.7, 6, 5, 4.2, 3.8, 3.4, 2.6, 2, 1.3, and 0.9 cal ka BP (Figure 5A-B). Six of the “sea ice” and “setae” events occurred concomitantly. Most of congruent events are concentrated during the Early Holocene (Figure 5A-B).

The millennial variability in core MD03-2601 is represented by 11 Si-DG events and 15 S-DG events. Here again, events span from 200 to 700 years (Figure 5C-D). The 11 "sea ice" events, called Si-11 to Si-1, are centred on 8, 6.7, 6.2, 5.8, 5.1, 4.6, 4, 3, 2.3, 1.8, and 1.3 cal ka BP (Figure 5C). These events are hereafter taken as reference events to which the other events are compared. The 15 "setae" events are centred on 8.5, 7.9, 7.4, 6.9, 6.5, 5.9, 5.4, 4.6, 4, 3.2, 2.8, 2.3, 1.8, 1.4, and 1.1 cal ka BP (Figure 5D). The "sea ice" and "setae" events in core MD03-2601 are out-of-phase until event Si-6 at 4.6 cal ka BP and subsequently in-phase younger than 4.6 cal ka BP. The positive relationship between sea ice and setae events younger than 4.6 cal ka BP is ensured by a strong, significant Kendall's Tau correlation coefficient on the 1-5 cal ka BP period (Figure 4D).

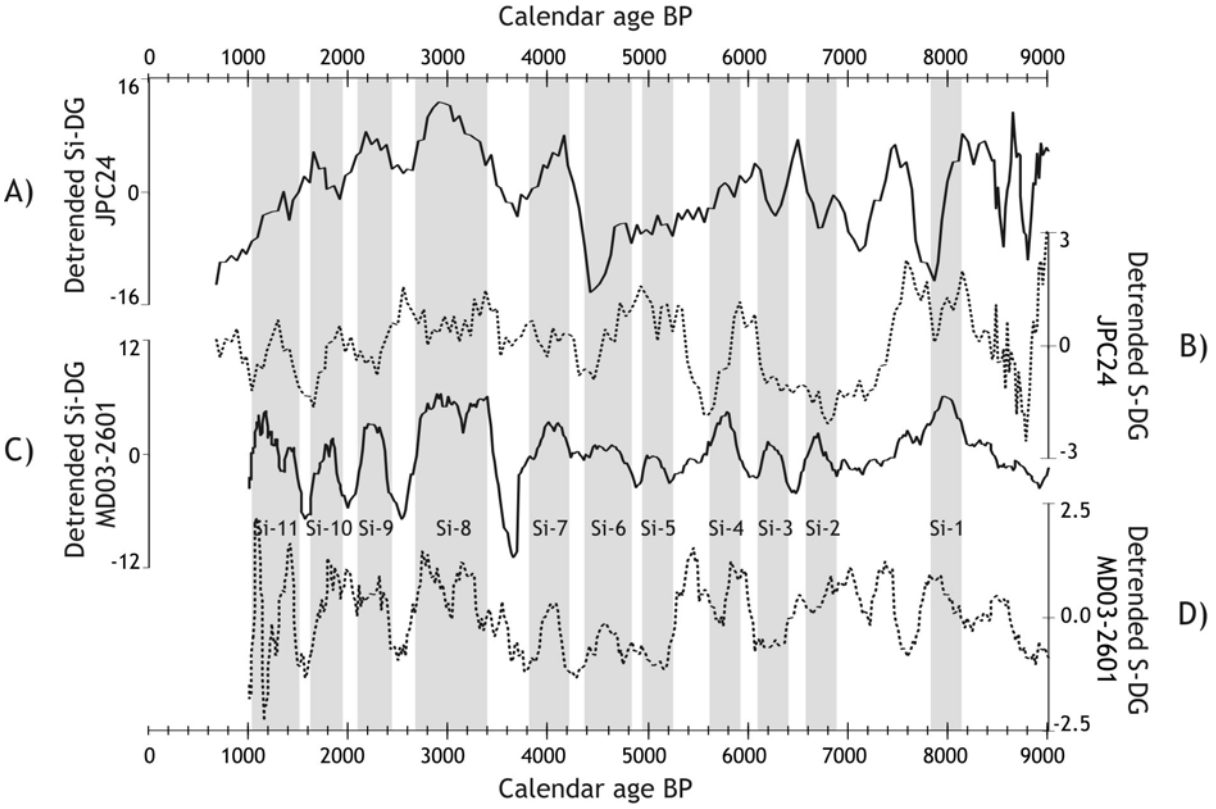

Figure 5: Detrended records of sea ice and setae DG *versus* time: A) detrended record of the relative abundances of the Si-DG in core JPC24 (5-point running mean), B) detrended record of the relative abundances of the S-DG in core JPC24 (5-point running mean), C) detrended record of the Si-DG in core MD03-2601 (10-point running mean) and D) detrended record of the S-DG in core MD03-2601 (10-point running mean). Detrended records are obtained by subtracting the corresponding trend of the 2-order polynomial functions shown in figure 3. Shaded areas figure the millennial increases of sea ice cover in MD03-2601, defined as Sea ice event 1 (Si-1) to Sea ice event 11 (Si-11).

The comparison of the millennial variability between the two marine cores shows no reliable relationship between "setae" events and highlights an out-of-phase relationship between the JPC24 and MD03-2601 "sea ice" events older than 4.5 cal ka BP and an in-phase relationship younger than 4.5 cal ka BP (Figure 5A-C). The in-phase relationship between sea ice events in the two marine cores younger than 4.5 cal ka BP is ensured by a

strong, significant Kendall's Tau correlation coefficient on the 1-5 cal ka BP period (Figure 4E).

5. Discussion

5.1. Holocene changes in the CCSZ at the pluri-millennial scale

5.1.1. Sea ice cover

HBi are suspected to represent spring sea ice cover (Massé et al., 2007) whereas the diatom species included in the Si-DG characterize both spring and autumn sea ice cover. Therefore, the results presented here show an increase of the annual sea ice cover in Prydz Bay and DDUT. Both HBi and Si-DG records show a gradual increase in Prydz Bay since 9 cal ka BP, however accentuated since 4.5 cal ka BP (Figure 3A, B). Similarly, HBi and Si-DG records in DDUT show a gradual increase since 9 cal ka BP, accentuate since 3.5 cal ka BP (Figure 3D, E). The Si-DG record however indicates a larger, more abrupt shift at 3.5 cal ka BP than the HBi record. This discrepancy may be imputed to a threshold response of the Si-DG proxy (governed here by *F. curta*) whereby modern environmental conditions at MD03-2601 core site lie at the upper ecological boundary of *F. curta* (Armand et al., 2005). A small warming such as the one estimated for the Mid-Holocene Climate Optimum (Crosta et al., 2008) would have trespass the ecological boundary favourable for *F. curta*. Diatoms synthesizing HBi do not suffer the same threshold response. Less sea ice before 4.5 cal ka BP, both in concentration and yearly presence, would have only reduce the bottom ice community at the core location and therefore C25:2 synthesis, export and burial while increasing phytoplankton diatoms and therefore C25:3 synthesis, export and burial. Conversely, modern environmental conditions at JPC24 core site lie within the optimal *F. curta* ecological range, so were environmental conditions during the Mid-Holocene Climate Optimum. A large amplitude shift in Si-DG relative abundances is therefore not expected there and a better coherence between HBi and Si-DG records is evident in core JPC24. Additionally, it is possible that local morpho-bathymetric and cryospheric features have amplified/modulated the threshold responses of the Si-DG in the two areas. Indeed, the enclosed shelf configuration, the presence of the Prydz Bay gyre and the positive ice feedbacks induced by the large Amery cryopsheric possibly explains the less abrupt and earlier cooling observed at JPC24 core site.

Despite the large amplitude shift in Si-DG in core MD03-2601, all sea ice records from the two cores appear well-correlated (Table 1), especially since 5 cal ka BP just before sea ice cover started to increase more intensively (Figure 4E), demonstrating a similar long-term evolution over the Holocene of the sea ice cover in both regions. However, both Si-DG relative abundances and HBi values are higher in core JPC24 than in core MD03-2601 indicating a greater sea ice cover in the Prydz Bay region than in the DDUT region

throughout the Holocene (Figure 3A-B-D-E). Inferred icier conditions in eastern Prydz Bay than in DDUT over the last 9 cal ka BP agree well with modern data that show larger extent, greater duration and concentration of the sea ice cover in Prydz Bay than in DDUT (Schweitzer, 1995; Worby et al., 1998; Arrigo and van Dijken, 2003).

The long-term increase in annual sea ice cover inferred here from the HBi and Si-DG records agrees well with marine and lake records around Antarctica that similarly document sea ice retreat during the Early Holocene and sea ice expansion during the Late Holocene since 5-3 cal ka BP, depending on the regions and environments investigated (Barcena et al., 1998; Ingólfsson et al., 1998; Domack et al., 1999; Leventer et al., 2002; Brachfeld et al., 2002; Presti et al., 2003; Roberts et al., 2004). These geological data are comforted by model predictions that showed progressive increase of the spring, autumn and annual sea ice cover for the whole Southern Ocean south of 60°S since 5-4 cal ka BP (Renssen et al., 2005b). Therefore, we believe that increasing sea ice cover over the Holocene is a common feature of the global coastal Antarctic, though local morpho-bathymetric and cryospheric features may modulate the amplitude and timing of the sea ice response.

5.1.2. Wind/upwelling activity

In the DDUT, diatom species or species groups included in the S-DG are found in nutrient-rich and mixed surface waters promoted by enhanced upwelling and/or windy conditions during the spring/summer season (Beans et al., 2008; Denis et al., in revision). In contrast, in the Prydz Bay region, the same species were associated to warmer surface waters from open ocean provenance during the local deglaciation ~10500 years ago (Stickley et al., 2005). No investigation of modern distribution and ecology in the Prydz Bay region confirms what was inferred for the deglaciation context. The S-DG in core JPC24 presents decreasing relative abundances over the 9-7 cal ka BP and increasing relative abundance since 7 cal ka BP, accentuated since 4.5 cal ka BP (Figure 3C). This record may indicate greater intrusion of warmer surface waters during late deglaciation between 9-7 cal ka BP in agreement with a more southern position of the southern ACC as reported during the same period in Antarctic Peninsula (Leventer et al., 2002; Smith et al., 2007). It is worth noting that the modern southern ACC boundary is much closer to the Prydz Bay region, where the gyre can pump warm surface waters into the bay, compared to the DDUT region (Orsi et al., 1995). In this context, the S-DG in core MD03-2601 is not expected to show high relative abundances during late deglaciation. It conversely presents increasing relative abundance throughout the Holocene, accentuated since 4.5 cal ka BP (Figure 3F) as a response of more intense spring/summer wind mixing.

At the Holocene scale, the two S-DG records present a negative, significant correlation. However, this negative correlation results from their different patterns in the late deglaciation - Early Holocene (Figure 4F). Disregarding the 9-7 cal ka BP period, the two S-

DG records are well correlated (Figure 4F). Based on the modern ecology of the diatom species of the S-DG in DDUT (Beans et al., 2008), we thus believe that the S-DG record in core JPC24 similarly tracks spring/summer wind mixing activity in the Prydz Bay region out of the late deglaciation context. The two S-DG records therefore suggest, in both regions, enhanced mixing of surface conditions during the spring-summer season since 7 cal ka BP in relation to increasing intensity of spring/summer wind stress and resulting Southern Ocean upwelling (Denis et al., in revision). This general trend is particularly accentuated since 4.5 cal ka BP in the two marine records, though the increase is more evident in core MD03-2601. The two geographic regions present today similar activity of katabatic winds, MCDW upwelling and synoptic depressions. We suggest that the smaller amplitude increase in core JPC24 resulted from local morpho-bathymetric and cryospheric features in western Prydz Bay. More precisely, important seasonal glacial runoffs from the local large ice shelves possibly modulated increasing wind stress intensity, as observed in DDUT.

We do not know other high latitude records tracking wind stress and upwelling in the Coastal and Continental Shelf Zone (CCSZ) during the Holocene. We therefore compared our records with ice core records that track large scale atmospheric circulation features. The long-term increase of wind stress since 7 cal ka BP, inferred from our S-DG records, matches well with chemical data of East Antarctic ice cores. Taylor Dome, Law Dome and Dome C records (Stager and Mayewski, 1997; Steig et al., 2000; Van Ommen et al., 2004, Wolff et al., 2006) similarly suggest a strengthening of the atmospheric circulation along the Holocene. Additionally, model outputs demonstrated increasing intensity of summer Southern Hemisphere Westerlies between 45-60°S during the 9-4 cal ka BP period and strong westerlies since 4 cal ka BP (Renssen et al., 2005b). Our results coupled to ice core results and model outputs thus demonstrate a global reinforcement of the Southern Hemisphere spring/summer atmospheric systems during the Holocene.

In conclusion, both annual sea ice cover and spring-summer upwelling/wind stress in the East Antarctic Margin show a similar increasing pattern since 7 cal ka BP, which is accentuated since 4.5 cal ka BP. These Holocene trends seemingly reflect more global Holocene climate evolution at high southern latitudes.

5.2. Holocene changes in the CCSZ at the millennial scale

Superimposed to the pluri-millennial trends, records of sea ice and wind/upwelling activity show a well-marked millennial variability in both JPC24 and MD03-2601 cores with 11 to 15 well-defined events according to the records (Figure 5). Interpretations on phase relationships between millennial events in the two cores are within the age model accuracies.

Between 9 and 4.5 cal ka BP, in each sediment record, events of higher sea ice cover are generally decoupled from events of more intense summer upwelling/wind activity (Figure

5). Furthermore, “sea ice” and “upwelling/wind” events are generally not in line between Prydz Bay and DDUT (Figure 5). In contrast, after 4.5 cal ka BP, “sea ice” DDUT events became in-phase with “upwelling/wind” DDUT events and with “sea ice” Prydz Bay events (Figure 5). This alignment of the “sea ice” and “upwelling/wind” events within DDUT and of the “sea ice” events between DDUT and Prydz Bay occurred concomitantly to the accentuation of the long-term increase at 4.5 cal ka BP of both sea ice concentration and upwelling/wind regime in the two regions.

DDUT and Prydz Bay results argue for a reorganisation of the sea ice, oceanic and atmospheric fields at millennial timescale in East Antarctica since 4.5 cal ka BP. This reorganisation may simply result from the onset of the colder, icier Neoglacial period that could have trespass locally-induced responses and thus forced the cryospheric system to oscillate congruently in the two regions. The atmospheric and oceanic systems would have subsequently responded to the cryospheric forcing. Such reorganisation may also result from changes in the millennial expression of the Antarctic climatic modes such as the Pacific South America mode (PSA), the wave-3 mode, the Antarctic Oscillation (AO), and the Southern Annular Mode (SAM) (Yuan and Li, 2008). Combinations of PSA, wave-3 and ENSO climatic modes are know to provoke an Antarctic Dipole (ADP), which affects pressure, sea ice cover, wind strength and SST fields around Antarctica (Yuan and Martinson, 2001; Yuan, 2004). Chiefly, the ADP leads to contrasted patterns between Pacific and Atlantic sectors of the Southern Ocean (Kwok and Comiso, 2002; Yuan, 2004; Yuan and Li, 2008) (Figure 6). Though ADP-induced large scale anomalies are well identified small scale anomalies in coastal areas are less obvious because of local feedbacks (Yuan, 2004). However, similar anomaly fields of sea ice occur between DDUT and Prydz Bay while different anomaly fields of zonal winds exist today (Kwok and Comiso, 2002) (Figure 6). More precisely, more sea ice and less intense winds are expected the year after an intense ENSO event (Kwok and Comison, 2002). These modes are known to oscillate with a sub-decadal period around mean states that last several decades (Stammerjohn et al.,2008). These climatic modes induce sea ice, oceanic, and atmospheric anomalies, which are regionally contrasted around Antarctica (Yuan and Li, 2008).

A millennial expression of such climatic modes would block the anomalies in a positive or negative state for a much longer time period, which can explain the sea ice and wind/upwelling events observed in both Antarctic regions. ENSO-like events were observed at the millennial timescale in the Equatorial Pacific (Beaufort et al., 2000). For this reason, we refer here to Antarctic Dipole-like events that have a millennial expression based on the existence of modern climatic modes. In this vein, our results indicate that DDUT and Prydz Bay were in regions of different anomaly fields older than 4.5 cal ka BP and regions of similar anomaly fields younger than 4.5 cal ka BP. It is however difficult to assess whether they were then part of the same cell that may have enlarged or migrated at 4.5 cal ka BP to eventually encompass the two regions or in two regions of similar anomaly fields.

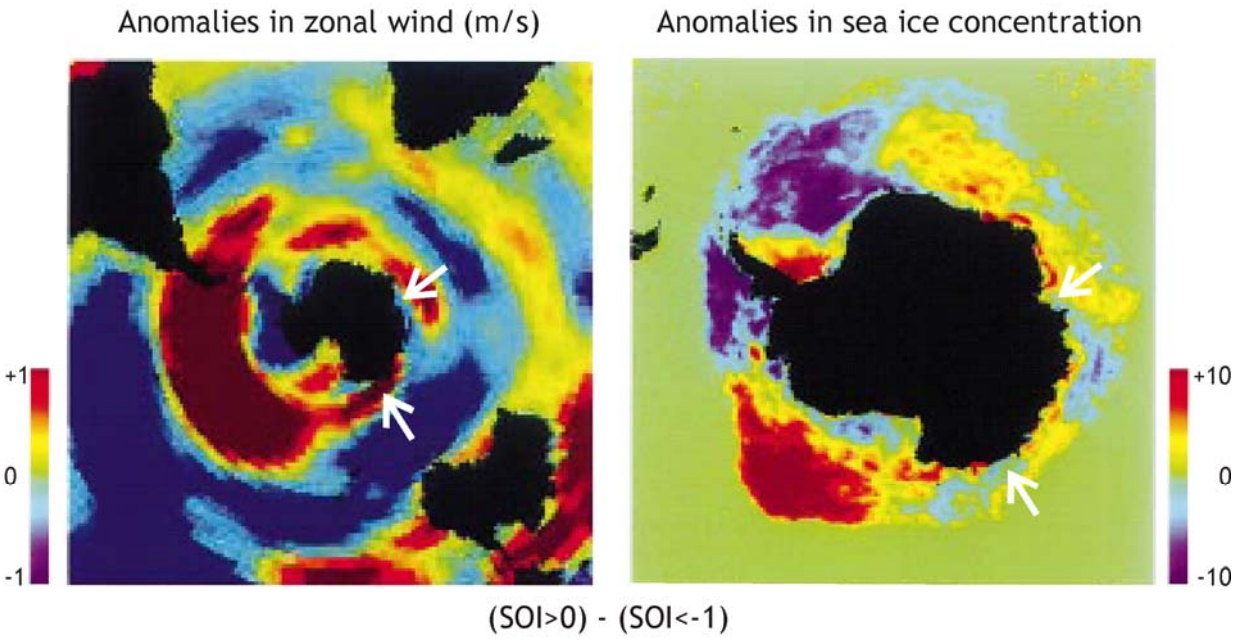

Figure 6. Composite anomaly maps of zonal winds and sea ice edge/concentration (1982–98) during three phases of Southern Oscillation Index (SOI >0, 0> SOI >-1, SOI <-1) and the difference between the two extremes (SOI >0 and SOI <-1). The anomalies are scaled to emphasize the spatial pattern. The SOI is defined as the difference between the standardized Tahiti sea level pressure (SLP) and the standardized Darwin SLP measurements. Large negative excursions of the SOI are associated with intense El Niño–Southern Oscillation (ENSO) episodes. Therefore, the maps show anomalies of zonal winds and sea ice concentration during La Niña events. El Niño episodes provoke the opposite anomalies. The white arrows show the location of Prydz Bay and DDUT areas, modified after Kwok and Comiso, 2002.

No other marine records have sufficient resolution to investigate millennial sea ice and wind/upwelling variability over the Holocene. We found no significant relationships with chemical data in ice cores (Ilsuka et al., 2008; Stager and Mayewski, 1997; Steig et al., 2000; Mayewski et al., 2006, 2009) possibly because ice core records bear too large climatic signals that embedded various climatic modes or that the source zones of the sea salts or aeolian dusts derive from northern climatic belts with different millennial forcings. Because of these limitations, it is difficult to replace our own results in a larger perspective.

5.3. Connections between high and low southern latitudes

We now compare our results at high Southern High latitude with a latitudinal/longitudinal transect of ice, marine and continental paleo-records throughout the Southern Hemisphere (locations shown in Figure 7) to determine what are the interactions between high latitude sea ice and wind changes and low-mid latitude climate change during the Holocene in order to better understand the ocean-atmosphere-sea ice coupling at the pluri-millennial and millennial timescales.

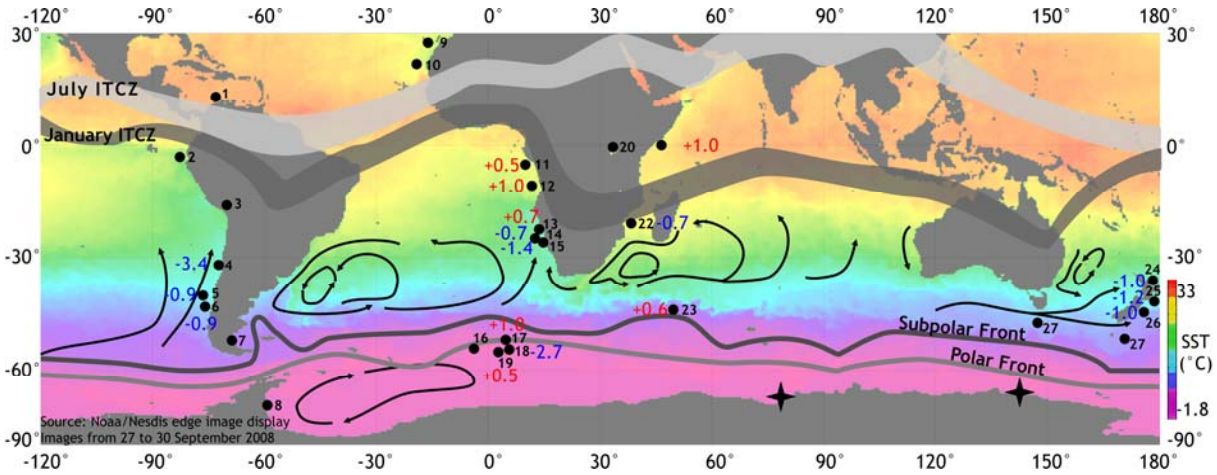

Figure 7: Map of the Southern Hemisphere with modern position of summer and winter ITCZ, main oceanic currents south of 20°S, and Subpolar and Polar oceanic fronts. Stars indicate the location of studied records while points show the location of records mentioned in the text and corresponding SST changes over the last 9 ka BP (Blue and red notes indicates cooling and warming trends, respectively) (1: Haug et al., 2001; 2: Moy et al., 2002; 3: Cross et al., 2000; 4: Kim et al., 2002a; 5: Kaiser et al., 2007; 6: Lamy et al., 2001, 2002; 7: Mayr et al., 2007; 8: Smith et al., 2007; 9: Holz et al., 2007; 10: Zhao et al., 1995; DeMenocal et al., 2000; Adkins et al., 2006; 11-12: Schneider et al., 1995; 13: Kim et al., 2003; 14: Farmer et al., 2005; 15: Kim et al., 2002b; 16: Van Beek et al., 2002; 17: Nielsen et al., 2004; 18: Hodell et al., 2001; 19: Bianchi and Gersonde, 2004; 20: Stager and Mayewski, 1997; 21-22: Bard et al., 1997; 23: Salvignac, 1998; 24: Samson et al., 2005; 25-26: Pahnke et al., 2005; and 27: Findlay and Giraudeau, 2002). Map of modern SST is provided by NOAA imagery averages on 27 to 30 September 2008.

5.3.1. Pluri-millennial timescales

5.3.1.1. South of 55°S

At high southern latitudes, increase in sea ice concentration (Figure 8A-B-E) is accompanied by ice sheet expansion (Ingólfsson et al., 1998; Denis et al., in-press). Land-based ice and sea ice progressive expansion was mainly driven by seasonal variations in local insolation (Renssen et al., 2005b). The decreasing winter insolation at high southern latitudes is associated to a reduction of the winter latitudinal temperature gradient (LTG), which led to less winter heat transfer from low to high latitudes after 5 cal ka BP (Renssen et al., 2005b) (Figure 8H). Therefore both winter local insolation and latitudinal insolation gradient (LIG) (Figure 8G) conducted to colder winter conditions promoting enhanced ice and sea ice building over the Holocene.

Holocene spring/summer wind stress increase over DDUT and Prydz Bay areas since 7 cal ka BP (Figure 8C-D) seems to be a general feature in East Antarctica (Stager and Mayewski, 1997; Steig et al., 2000; Van Ommen et al., 2004, Wolff et al., 2006). The increase of the summer LTG (Figure 8H, Renssen et al., 2005b) between the tropics and polar areas have enhanced the summer poleward atmospheric transport and strengthened the extra-tropical wind intensity during the Holocene (Vimeux et al., 2001; Davis et al., 2009). Furthermore, Antarctic ice sheet and sea ice expansion since 4.5 cal ka BP have certainly reinforced the

summer LTG. The opposite behaviour of the winter and summer LTG during the Holocene in the Southern Hemisphere is partly controlled by the winter and summer LIG in response to precession and obliquity indexes, respectively (Davis et al., 2009, and references herein) (Figure 8G). Thereby, sea ice and ice expansion could be mainly influenced by precession changes while summer wind stress would be controlled by obliquity changes.

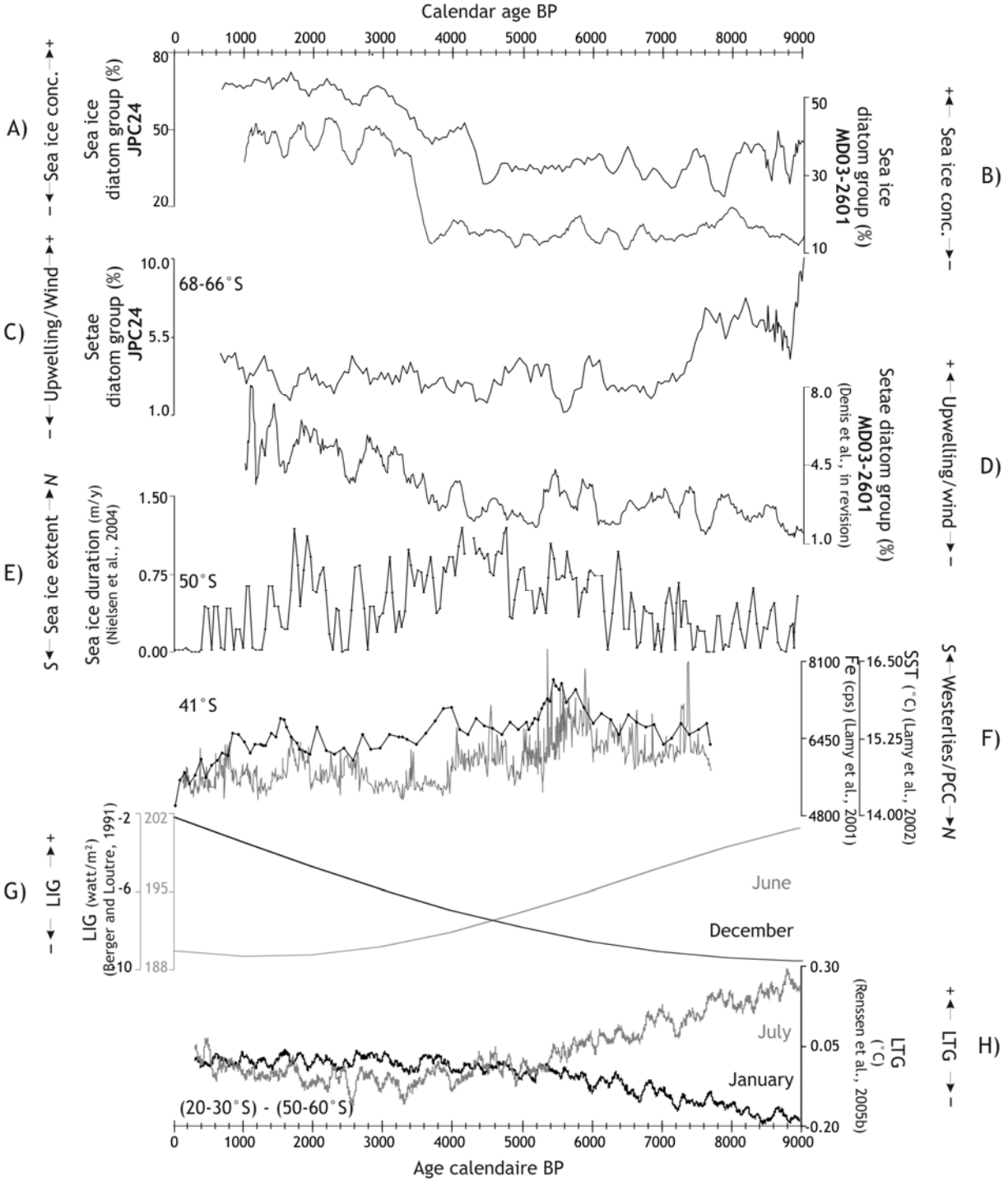

Figure 7: Compilation of paleodata and model outputs *versus* time: A) Sea ice DG in core JPC24 (5-point running mean), B) Sea ice DG in core MD03-2601 (10-point running mean), C) Setae DG in core JPC24 (5-point running mean), D) Setae DG in core MD03-2601 (10-point running mean) (Denis et al., in revision), E) Sea ice duration in the South East Atlantic from core TTN057-17-PC1 (Nielsen et al., 2004), F) iron content and SST in South West Pacific from core GeoB3313-1 (Lamy et al., 2001, 2002), G) Latitudinal insolation gradient (LIG) between 30°S and 60°S for winter and summer after insolation values of Berger and Loutre (1991), and H) models outputs of winter and summer anomalies of the latitudinal temperature gradients (LTG) between 20-30 and 50-60°S (Renssen et al., 2005b).

5.3.1.2. Between 55 and 45°S

In the Polar Frontal Zone of the East Atlantic Southern Ocean sector (~ 50°S), several diatoms records argue for an increase of the sea ice cover duration and cooling during the Early to Mid-Holocene (Hodell et al., 2001; van Beek et al., 2002; Nielsen et al., 2004; Bianchi and Gersonde, 2004; Cortese et al., 2007) (Figure 8E). In East Pacific and Indian sectors of the Southern Ocean, a northward migration of the Antarctic Polar Front and the ACC is recorded after 8-7 cal ka BP (Findlay and Giraudeau, 2002; Leventer et al., 2002; Smith et al., 2007, this study) (Figure 8C). Thereby, the Southern Ocean between 55-45°S experimented a northward migration of the oceanic fronts and a northward progression of sea ice limit during the Early to Mid-Holocene, while peri-Antarctic sequences congruently recorded the Climatic Optimum.

After 5-3 cal ka BP, four of the five records from the eastern Atlantic sector of the Southern Ocean show a decreasing trend in sea ice persistence and a warming of sea surface temperatures (SST) (Hodell et al., 2001; van Beek et al., 2002; Nielsen et al., 2004; Bianchi and Gersonde, 2004; Cortese et al., 2007) (Figure 7, 8E). Accordingly, records from the western Indian sector of the Southern Ocean displayed SST warming over the Holocene course (Salvignac, 1998) (Figure 7). Thereby, sea ice decline and SST warming recorded after 3-5 cal ka BP indicate a southward migration of the sea ice margin during Late Holocene which is at odds with concomitant increase in sea ice concentration in coastal areas around Antarctica (Barcena et al., 1998; Ingólfsson et al., 1998; Domack et al., 1999; Leventer et al., 2002; Brachfeld et al., 2002; Presti et al., 2003; Roberts et al., 2004; Crosta et al., 2008) (Figure 8A-B-E).

Therefore, Holocene patterns of sea ice duration at southern mid-latitudes and at high southern latitudes are opposite. A similar discrepancy was observed between Holocene atmospheric temperatures North and South of 47°N in Europe, which has been attributed to the decreasing obliquity that modulated the latent and heat fluxes between low and high northern latitudes (Davis et al., 2009). Similarly for the Southern Hemisphere, the heat flux increase between low and high latitudes since 5 cal ka BP (Figure 8H), in response to decreasing obliquity and positive feedback of the growing Antarctic cryospheric system, favoured an earlier sea ice retreat in the latitudinal band between 55 and 45°S, accompanied by the reinforcement of wind strength over the Southern Ocean as

suggested by model outputs (Renssen et al., 2005b). Thereby, opposite patterns between high and middle latitude bands could be due to a predominance of the obliquity and precessional signal at mid latitudes (~40-55°S) and high latitude (~60-65°S), respectively. Unfortunately, the reduced available dataset does not permit to assess whether this Holocene trend is restricted to the eastern Atlantic and western Indian sectors of the Southern Ocean or whether it is a common circumpolar feature.

5.3.1.3. Between 45 and 20°S

Paleodata from the 45-20°S latitudinal band report a consistent SST cooling and a northward shift and strengthening of the westerlies in South America (Kim et al., 2002a; Lamy et al., 2002; Jenny et al., 2002; Villa-Martínez et al., 2003; Kaiser et al., 2007), South Africa (Bard et al., 1997; Kim et al., 2002b; Holmgren et al., 2003, Stuut and Lamy, 2004; Farmer et al., 2005), and South Australia and New-Zealand (Schulmeister, 1999; McGlone, 2002; Samson et al., 2005; Pahnke et al., 2005), particularly enhanced after 5-3 cal ka BP (Figure 7 and 8F). Thereby, north of ~ 45°S, oceanic and atmospheric long-term changes are concomitant and affect the whole longitudinal transect (Figure 7).

The strengthening of the LTG reinforced by increasing in sea ice extent since 7 cal ka BP in the 45-55°S latitudinal band and since 5-3 cal ka BP south of 55°S induced 1) a northward shift of the westerlies and oceanic fronts, 2) a strengthening of the westerlies and 3) an enhancement of subpolar water intrusions in each oceanic basin. The persistent SST cooling throughout the Holocene at 45-20°S, despite the southward retreat of the sea ice limit since 5-3 cal ka BP was possibly maintained by enhanced subpolar water intrusions thanks to the stronger westerlies (Oke and England, 2004) forced by the growing Antarctic cryospheric system. These interpretations are supported by recent modelling studies that clearly show greater meridional transport between 50 and 30°S, and lower meridional transport between 70 and 50°S, when westerlies moved northward (Delworth and Zeng, 2008; Sijp and England, 2008), as a result of a better alignment between westerlies and ACC that modified the Ekman pumping north and south of 50°S.

Thereby, orbital insolation is the main forcing of the LTG during the Holocene though feedbacks from the Antarctic cryosphere are important, especially since 5-3 cal ka BP. Coupling between low and high southern latitudes conducted to strong reorganisation of the oceanic, atmospheric and sea ice fields, which are responsible of the different climate evolution in the three latitudinal bands investigated here.

5.3.2. Millennial timescales

We have shown that sea ice and wind/upwelling millennial events experimented out-of-phase relationships in Prydz Bay area throughout the Holocene (Figure 9A-B). In contrast in the DDUT region, sea ice and wind/upwelling millennial events were out-of-phase until 4.5

cal ka BP and congruent since 4.5 cal ka BP (Figure 9C-D). In addition, sea ice millennial events in Prydz Bay and DDUT regions were out-of-phase until 4.5 cal ka BP and in-phase since 4.5 cal ka BP (Figure 9A-C). Our data therefore suggest a reorganisation of the atmospheric, oceanic, and sea ice fields since 4.5 cal ka BP at the millennial timescales in DDUT and Prydz Bay regions.

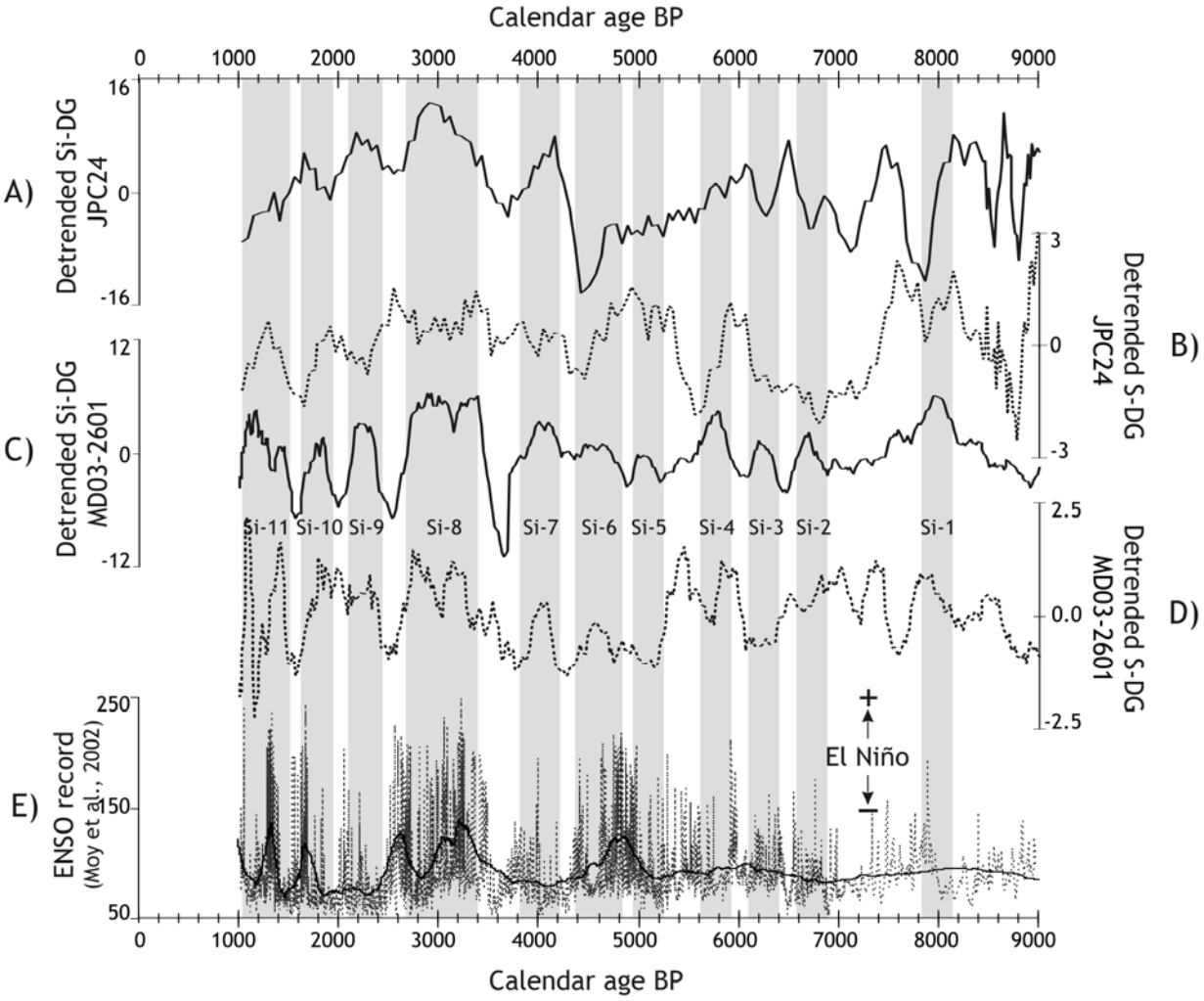

Figure 9: Compilation of paleodata *versus* time: A) detrended record of the relative abundances of the Si-DG in core JPC24 (5-point running mean – ~250 yr-running mean), B) detrended record of the relative abundances of the S-DG in core JPC24 (5-point running mean), C) detrended record of the Si-DG in core MD03-2601 (10-point running mean – ~200 yr-running mean), D) detrended record of the S-DG in core MD03-2601 (10-point running mean), E) red colour intensity recording El Niño events (Moy et al., 2002) (thick line represents a 200 yr-running mean). Detrended records and shaded areas, which figure the millennial increases of sea ice cover in MD03-2601, defined as Sea ice event 1 (Si-1) to Sea ice event 11 (Si-11), are reported from the Figure 5.

We have proposed that these climatic reorganisations could be enhanced by the increase of sea ice concentration and ice sheet expansion in these two areas and generally over and around Antarctica (Ingólfsson et al., 1998; Denis et al., in-press; this study). Orbitally-forced onset of the Antarctic Neoglacial period since 5-3 cal ka BP (Renssen et al., 2005b; Crosta et al., 2008), at the origin of glacial readvances (Ingólfsson et al., 1998; Denis et

al., in-press), could have conducted to modified the wind strengths and heat flux exchanges with low latitudes by increasing the LTG. Furthermore, glacial readvances have been irregular around Antarctica according to the regions (Ingólfsson et al., 1998 and reference herein), which could have led to differential ice feedbacks in coastal areas since 4.5 cal ka BP.

We however believe that the observed patterns in the millennial oscillations result from the reorganisation of the millennial expression of the Antarctic climate modes. As Holocene records of Antarctic climatic modes such as SAM, PSA and wave-3, are not available we here compared our data with a high-resolution record of Holocene ENSO variability from the Cariaco Basin (Moy et al., 2002) (Figure 9E).

Sea ice events recorded in DDUT (Si 1 to Si 11) occurred concomitantly to periods of intense El Niño episodes (Figure 9C-E) in agreement with the modern relationship between positive ENSO and greater sea ice cover in DDUT. Conversely, sea ice events recorded in western Prydz Bay were out-of-phase with ENSO events until 5 cal ka BP and became congruent with intense ENSO since 5 cal ka BP (Figure 9A-E). Wind/upwelling events appear anti-phased with ENSO episodes in DDUT while wind/upwelling events appear positively correlated with ENSO episodes in Prydz Bay, especially since 5 cal ka BP (Figure 9B-D-E) in agreement with the modern anomaly fields (Figure 6). Spectral analyses of Ba and BSi content in Late Holocene sediments from DDUT calculated productivity cycles of ~3-4 years, which were attributed to ENSO-induced changes in sea ice cover (Costa et al., 2007). This study has two reachings. First, it shows a relationship between ENSO and sea ice cover in the DDUT region where the impact of ENSO is weaker due to the remote position of the Indian sector relative to the ENSO source region and to the interaction with other climatic modes. Second, it shows that the relationship between ENSO and sea ice cover in DDUT probably continued alike until 1200 cal yr BP.

Our study goes a step further both temporally and spatially. Here, we show 1) a millennial influence of the ENSO (probably through interactions with Antarctic climatic modes; Yuan, 2004) throughout the Holocene along the eastern Indian sectors of the Southern Ocean and after 4.5 cal ka BP in the western Indian sector, and 2) a stronger influence of ENSO in DDUT than in Prydz Bay older than 4.5 cal ka BP, which became alike after 4.5 cal ka BP. This suggests that less intense and less numerous ENSO events during the Early Holocene could not propagate as far as the remote Prydz Bay while reaching DDUT. More intense ENSO events after 4.5 cal ka BP impacted the western Indian sector alike than DDUT. We can not assess whether DDUT and Prydz bay regions, that were in different anomaly fields cells older than 4.5 cal ka BP, were subsequently in a same, large anomaly cell that would have progressed from DDUT to Prydz Bay as a response to more intense ENSO events, or in two separate cells as observable today.

6. Conclusion

This study provides insights into the oceanic-sea ice-atmosphere coupling at both pluri-millennial and millennial timescales in the Southern Hemisphere during the Holocene via an integrated comparison of high-, mid-, and low-latitudes climate changes. At the pluri-millennial timescales, we evidenced opposite patterns of high- and mid-latitude Antarctic sea ice concentration mainly controlled by precession and obliquity indexes, respectively. Orbitally-forced latitudinal temperature gradient in addition to glacial ice and sea ice expansion since 4.5 cal ka BP induced a northward movement of Westerlies and higher export of subpolar water intrusions, which affected the three oceanic basins since this time.

At the millennial timescales, predominance of El Niño event occurs within a millennial variability that had repercussions in ocean-sea ice-atmosphere changes at high latitudes in Prydz Bay and Adélie Land. El Niño events are associated to higher sea ice concentration in Adélie Land throughout the Holocene and since 4.5 cal ka BP in Prydz Bay. We propose that the ENSO millennial events resulted in a millennial expression of the Antarctic dipole, which became in-phase between Adélie Land and Prydz Bay since 4.5 cal ka BP, e.g. since the onset of the modern frequencies of the ENSO and of Neoglacial conditions over Antarctica.

This study gives flavour about the temporal and spatial climate variability in the Southern Ocean and its forcings during the Holocene. To support this preliminary, large scale study about the response of the Southern Hemisphere to long- and short-term ocean-sea ice-atmosphere coupling, it appears crucial to investigate other Southern Ocean and Antarctic regions at comparable high resolution.

Acknowledgements

We warmly thank Frank Lamy to provide his data, and Bruno Malaizé for constructive discussions. We personally thank people from Images X (CADO) cruise and from NSF-funded NBP0101 cruise for data and suggestions concerning the Dumont d'Urville Trough. Financial support for this study was provided by TARDHOL project through the national LEFE-EVE program (INSU-CNRS) with the logistic support of the French IPEV (Institut Paul Emile Victor), the International Marine Past Global Change Study (IMAGES). This is an EPOC contribution N°x.

Conclusion générale & Perspectives

Le but de ce travail de thèse était de documenter la machine climatique le long de la chaine de connections et rétroactions qui lient de manière très complexe ses différents compartiments. Ce travail s'inscrit plus particulièrement dans l'étude climatique de l'environnement singulier de la zone marginale des glaces en Antarctique de l'Est. Notre approche consistait (1) à documenter finement la variabilité climatique, de l'échelle plurimillénaire à séculaire au sein de toutes les composantes climatiques (cryosphère, atmosphère, océan, biosphère), à partir de l'enregistrement sédimentaire haute-résolution de Terre Adélie; puis (2) à utiliser les connaissances acquises au moyen de cette étude multi-proxy pour élargir notre champ d'investigation à une autre zone d'Antarctique de l'Est, en se focalisant sur un aspect particulièrement intéressant de la machine climatique : le couplage océan-atmosphère.

Principaux résultats

En réponse à ces deux objectifs, notre étude a pu mettre en évidence deux échelles temporelles de variabilité climatique : l'échelle long-terme, c'est-à-dire plurimillénaire et l'échelle court-terme, c'est-à-dire millénaire. L'ensemble des compartiments climatiques des marges Est antarctiques est affecté par ces deux modes de variabilité climatique.

A long terme, la variabilité climatique semble majoritairement dictée par les variations de l'indice de précession, associés à des rétroactions internes qui modulent le « timing » et l'amplitude des changements climatiques. A l'échelle de l'Holocène, aux hautes latitudes

Sud, c'est notamment le cycle de précession via les variations d'ensoleillement local associées, qui semble avoir un impact majeur sur :

- **Les glaciers côtiers et l'extension du couvert de banquise**. Ces derniers répondent de manière synchrone et non linéaire aux changements de températures et de précipitations induits par les paramètres orbitaux. Cette réponse commune du compartiment cryosphérique se traduit par une expansion graduelle des glaciers et du couvert de banquise, certainement accentuée à partir de 3,5 cal ka BP par des processus internes à la machine climatique. En effet, lors de l'avancée massive des glaciers et de la banquise à 5-3.5 cal ka BP, l'augmentation de l'albédo local renforce très probablement l'extension de ces systèmes cryosphériques par une rétroaction positive. Les rétroactions mises en jeu à une échelle régionale, voire globale, sont plus dures à déconvoluer. Cependant l'extension des systèmes glaciaires à travers le monde au Néoglaciaire a certainement joué un rôle complémentaire dans la chute des températures des moyennes et hautes latitudes à cette période, notamment dans l'Hémisphère Sud, où les paramètres orbitaux sont moins favorables à la croissance des systèmes cryosphériques. De plus, nous avons mis en avant le rôle prépondérant joué par le couvert de banquise sur la position des ceintures climatiques de l'Hémisphère Sud et ainsi sur le couplage océan-atmosphère qui régule la répartition et l'intensité des échanges de chaleur au niveau spatio-temporel.

- **La dynamique saisonnière de la banquise avec une augmentation graduelle de sa formation annuelle** (e.g. formation intense en hiver, retrait total en été qui induit une reformation intense en hiver). Cette dernière a été proposée comme instigateur de l'augmentation graduelle de **formation d'eaux de fond** originaires du plateau continental Est Antarctique au cours de l'Holocène. A l'échelle d'un cycle de précession, cette relation étroite entre banquise et circulation thermohaline pourrait être ainsi antiphasée entre l'Hémisphère Nord et l'Hémisphère Sud. Cet antiphasage serait expliqué par l'action de ce paramètre orbital sur la saisonnalité de chaque hémisphère et ainsi sur la dynamique saisonnière de la banquise.

- **La productivité de la biosphère marine**. Celle-ci semble être contrôlée à cette échelle temporelle en premier lieu par la longueur de la saison de croissance et en deuxième lieu par la dynamique convective de la circulation océanique qui apporte les nutriments indispensables à la croissance phytoplanctonique. Ces deux paramètres sont forcés par les paramètres orbitaux qui régulent le « timing » du développement printanier et du retrait automnal de la banquise contrôlant ainsi la durée de croissance phytoplanctonique et la position et l'intensité des vents qui modulent l'intensité des upwellings.

A court terme, la variabilité climatique s'exprime aussi à travers tous les compartiments. Les réponses de chaque compartiment ainsi que leurs connections réciproques, expliqués précédemment, semblent agir et se coordonner pareillement à l'échelle millénaire.

L'identification des facteurs forçants reste cependant plus énigmatique. On a mis en évidence le synchronisme entre les avancées de glaces, de banquise, et les variations de paléoproductivité avec les changements de régimes climatiques enregistrés à l'intérieur du continent Antarctique par les carottes de glace. On a aussi relié les changements au sein des compartiments banquise, atmosphère, océan enregistrés aux hautes latitudes Sud avec des changements aux moyennes et aux basses latitudes Sud, et notamment avec la variabilité millénaire de l' « ENSO-like ».

Les facteurs forçants de cette variabilité millénaire, semblant affecter le climat terrestre de manière globale, restent encore très débattus (Mayewski et al., 2004). L'impact des changements externes (activité solaire) et internes (volcanisme, océan, banquise, atmosphère, végétation et feux) à la machine climatique restent difficile à déchiffrer et à quantifier. Ici, nous avons pu mettre en exergue le rôle prépondérant de la banquise au sein du système climatique en montrant ses interactions avec tous les autres compartiments climatiques. A ces deux échelles de temps, l'identification et la quantification des forçages de la machine climatique ainsi que des rétroactions associées restent un des défis majeurs de la communauté scientifique pour affiner la prédiction des climats futurs.

Ce travail a aussi mis en évidence à travers la comparaison des deux enregistrements de la Baie de Prydz et de la Terre Adélie que les singularités locales souvent citées en Antarctique comme la cause de beaucoup d'asynchronismes en Antarctique ne semblent pas si importantes malgré les configurations vraiment différentes des deux baies, leur éloignement géographique et la taille de leur systèmes cryosphériques respectifs. Ainsi, la plupart des asynchronismes répertoriés en Antarctique sont probablement amplifiés par le manque de résolution des enregistrements et certainement aussi, dans une moindre mesure, par les problèmes inhérents aux méthodes de datation en Antarctique. En effet, la quasi absence de matériel carbonaté à ces latitudes contraint les paléocéanographes à dater le sédiment au moyen de la matière organique sur laquelle réside des incertitudes en raison de la contamination possible par du carbone remanié. De plus, les marges antarctiques sont un domaine actif dans la formation d'eaux profondes qui varie spatialement et temporellement même à l'échelle de l'Holocène comme nous l'avons démontré en Terre Adélie. Ainsi, des variations régionales dans l'âge réservoir et temporelles le long d'un même enregistrement sédimentaire rajoutent encore des incertitudes. Celles-ci sont d'autant plus accentuées sur des enregistrements qui présentent de faibles taux de sédimentation ou des périodes de hiatus sédimentaires comme c'est souvent le cas au débouché des glaciers. Les enregistrements à haute-résolution comme ceux utilisés dans cette étude ont pu être comparés avec des enregistrements de glace souvent mieux datés que les sédiments marins, autorisant la mise en place d'un cadre stratigraphique robuste pour ces séries marines.

Perspectives et apports de cette étude

A l'issu de ce travail, il apparait important de multiplier l'étude d'**enregistrements marins circum-antarctiques** autant sur le plateau continental Antarctique qu'aux limites Nord de l'Océan Austral afin de vérifier la cohérence spatio-temporelle de la variabilité climatique Holocène aux échelles plurimillénaires à millénaires. De même, les études aux échelles saisonnières à séculaires réalisées sur les laminations des carottes marines épicontinentales sont une voie intéressante (Denis et al., 2006, article complémentaire) pour mieux comprendre les effets des modes climatiques tels que l'ENSO et le Dipôle Antarctique sur la variabilité spatio-temporelle en Antarctique et ainsi mieux appréhender ces effet à des échelles plus longues comme suggéré ici aux échelles plurimillénaires à millénaires. Ces travaux permettraient de mieux caractériser et quantifier l'influence globale du Continent et de l'Océan Antarctique, notamment leur rôle dans la variabilité climatique rapide pour palier aux incertitudes des modèles prédictifs dans ces régions.

Dans ce cadre, il est primordial de porter une attention toute particulière à la qualité des modèles d'âge construit à partir des enregistrements marins. Par exemple, le développement de méthodes **complémentaires de datation** comme les datations ^{14}C sur la matière intrinsèque des diatomées limiterait les problèmes de contamination par du matériel remanié. Les datations au Radium 226, quant à elles, fourniraient des dates indépendantes de la contamination et des âges réservoirs (Van Beek et al., 2002). Il nous apparaît important de mener ces différentes méthodes de front pour s'affranchir de leurs problèmes respectifs et dégager des modèles d'âge les plus pertinents possibles. Ces méthodes couteuses sont cependant indispensables à une interprétation juste des mécanismes climatiques. L'amélioration du cadre stratigraphique de l'enregistrement sédimentaire de Terre Adélie est déjà en cours via ces deux méthodes. Les mesures préliminaires de ^{226}Ra tendraient à confirmer le cadre stratigraphique de la carotte MD03-2601. A terme, un meilleur cadre chronologique permettra de mieux contraindre les corrélations effectuées avec les autres enregistrements climatiques au cours de cette thèse (glace, marin et continent) et ainsi de statuer sur les phasages et anti-phasages observés spatio-temporellement aux échelles plurimillénaires à millénaires.

Enfin, le travail effectué avec les **radionucléides** a permis de mieux comprendre les processus de sédimentation et ainsi de reconstituer de manière fiable les transports sédimentaires latéraux et verticaux ainsi que quantifier les apports biogéniques et terrigènes. L'outil radio-isotope nous parait un proxy indispensable pour les études paléocéanographiques et nous préconisons son emploi sur les marges continentales. Malgré les nombreuses limitations de cette technique dans cette partie de l'océan, elle semble particulièrement utile dans cet environnement où interviennent d'importants phénomènes de redistribution sédimentaire. De plus, la comparaison avec d'autres proxies permet de contourner les limitations d'utilisation comme démontré dans le chapitre 2 et dans Carson et al. (soumis) (Article complémentaire n°2).

Références Bibliographiques

A

Abdi, H., 2007. Bonferroni and Sidak corrections for multiple comparisons. in N.J. Salkind (ed.). Encyclopedia of Measurement and Statistics. Thousand Oaks, CA: Sage. http://www.utdallas.edu/~herve/Abdi-Bonferroni2007-pretty.pdf.

Adkins, J., deMenocal, P., Eshel, G., 2006. The "African humid period" and the record of marine upwelling from excess ^{230}Th in Ocean Drilling Program Hole 658C. Paleoceanography 21, PA4203, doi: 10.1029/2005PA001200.

Adolphs, U., Wendler, G., 1995. A pilot study on the interactions between katabatic winds and polynyas at the Adelie Coast, eastern Antarctica. Antarctic Science 7, 307-314.

Alley, R.B., 2000. Ice-core evidence of abrupt climate changes. Proceedings of the National Academy of Sciences of the United States of America 97, 1331-1334.

Alley, R.B., Ágústsdóttir, A.M., 2005. The 8k event: Cause and consequences of a major Holocene abrupt climate change. Quaternary Science Reviews 24, 1123-1149.

Alley, R.B., Anandakrishnan, S., Jung, P., 2001. Stochastic resonance in the North Atlantic. Paleoceanography 16, 190-198.

Altabet, M.A., François, R., 1994. Sedimentary nitrogen isotopic ratio as a recorder for surface ocean nitrate utilization. Global Biogeochemical Cycles 8(1), 103-116.

Altabet, M.A., Francois, R., Murray, D.W., Prell, W.L., 1995. Climate-related variations in denitrification in the Arabian Sea from sediment ^{15}N/^{14}N ratios. Nature 373, 506-509.

Andersen, C., Koç, N., Jennings, A., Andrews, J.T., 2004. Non-uniform response of the major surface currents in the Nordic Seas to insolation forcing: Implications for the Holocene climate variability. Paleoceanography 19, PA2003, doi:10.1029/2002PA000873.

Anderson, J.B., 1999. Antarctic Marine Geology. Thesis. Cambridge University Press 289 pp.

Anderson, J.B., Shipp, S.S., Lowe, A.L., Wellner, J.S., Mosola, A.B., 2002. The Antarctic Ice Sheet during the Last Glacial Maximum and its subsequent retreat history: a review. Quaternary Science Reviews 21, 49-70.

Anderson, R.F., Fleer, A.P., 1982. Determination of natural actinides and plutonium in marine particulate matter. Analytical Chemistry 54, 1142-1147.

Anderson, R.Y., Linsley, B.K., Gardner, J.V., 1990. Expression of seasonal and ENSO forcing in climatic variability at lower than ENSO frequencies: evidence from Pleistocene marine varves off California. Palaeogeography, Palaeoclimatology, Palaeoecology 78, 287-300.

Andrews, J.T., 1975. Glacial systems. An approach to glaciers and their environments. North Scituate: Duxbury Press, 191 pp.

Armand, L.K., Cornet-Barthaux, V., Mosseri, J., Quéguiner, B., 2008. Late summer diatom biomass and community structure on and around the naturally iron-fertilised Kerguelen Plateau in the Southern Ocean. Deep-Sea Research Part II 55, 653-676.

Armand, L.K., Crosta, X., Romero, O., Pichon, J.J., 2005. The biogeography of major diatom taxa in Southern Ocean sediments: 1. Sea ice related species. Palaeogeography, Palaeoclimatology, Palaeoecology 223, 93-126.

Arrigo, K.R., Robinson, D.H., Worthen, D.L., Dunbar, R.B., DiTullio, G.R., Woert, M.V., Lizotte, M.P., 1999. Phytoplankton community structure and the drawdown of nutrients and CO_2 in the Southern Ocean. Science 283, 365-367.

Arrigo, K.R., Thomas, D.N., 2004. Large scale importance of sea ice biology in the Southern Ocean. Antarctic Science 16, 471-486.

Arrigo, K.R., van Dijken, G.L., 2003. Phytoplankton dynamics within 37 Antarctic coastal polynya systems. Journal of Geophysical Research 108(C8), 3271, doi:10.1029/2002JC001739.

Arrigo, K.R., van Dijken, G.L., Bushinsky, S., 2008. Primary production in the Southern Ocean, 1997–2006. Journal of Geophysical Research 113, C08004, doi: 08010.01029 /02007JC004551.

Arrigo, K.R., Worthen, D.L., Robinson, D.H., 2003. A coupled ocean-ecosystem model of the Ross Sea: 2. Iron regulation of phytoplankton taxonomic variability and primary production. Journal of Geophysical Research 24.21-24.17.

Assmy, P., Henjes, J., Smetacek, V.a., Montresor, M., 2006. Auxospore formation by the silica-sinking, oceanic diatom Fragilariopsis kerguelensis (Bacillariophyceae). Journal of Phycology 42, 1002-1006.

B

Bacon, M.P., 1984. Glacial to interglacial changes in carbonate and clay sedimentation in the Atlantic Ocean estimated from ^{230}Th measurements. Isotope geoscience 2, 97-111.

Bacon, M.P., Anderson, R.F., 1982. Distribution of thorium isotopes between dissolved and particulate forms in the deep sea. Journal of Geophysical Research 87, 2045–2056.

Baines, P.G., Condie, S., 1998. Observations and modelling of Antarctic downslope flows: a review. Ocean, Ice and Atmosphere: Interactions at the Antarctic Continental Margin, American Geophysical Union, S.S. Jacobs & R. Weiss editors. Antarctic Research Series 75, 29-49.

Bakke, J., Lie, O., Dahl, S.O., Nesje, A., Bjune, A.E., 2008. Strength and spatial patterns of the Holocene wintertime westerlies in the NE Atlantic region. Global and Planetary Change 60, 28-41.

Ban, S., Burns, G., Castel, J., Chaudron, Y., Christou, R., Escribano, R., Umani, S.F., Gasparini, S., Ruiz, F.G., Hoffmeyer, M., Lanora, A., Kang, H.K., Laabir, M., Lacoste, A., Miralto, A., Ning, X., Poulet, S., Smetacek, V., 1999. Diatoms and the ocean carbon cycle. Protist 150, 25-32.

Barbara, L., 2008. La déglaciation en Baie de Prydz, Antarctique de l'Est, diatomées et biomarqueurs. Rapport de Stage de Master 2, Université Bordeaux 1, 35 pp.

Barber, D.C., Dyke, A., Hillaire-Marcel, C., Jennings, A.E., Andrews, J.T., Kerwin, M.W., Bilodeau, G., McNeely, R., Southon, J., Morehead, M.D., Gagnon, J.-M., 1999. Forcing of the cold event of 8,200 years ago by catastrophic drainage of Laurentide lakes. Nature 400, 344 - 348.

Bárcena, M. A., Gersonde, R., Ledesma, S., Fabrès, J., Calafat, A.M., Canals, M., Javier Sierro, F., Flores, J.A., 1998. Record of holocene glacial oscillations in Bransfield basin as revealed by siliceous microfossil assemblages. Antarctic Science 10, 269-285.

Bard, E., Rostek, F., Sonzogni, C., 1997. Interhemispheric synchrony of the last deglaciation inferred from alkenone palaeothermometry. Nature 385, 707-710.

Beans, C., Hecq, J.H., Koubbi, P., Vallet, C., Wright, S., Goffart, A., 2008. A study of the diatom-dominated microplankton summer assemblages in coastal waters from Terre Adélie to the Mertz Glacier, East Antarctica (139°E-145°E). Polar Biology 31, 1101-1117.

Beckmann, A., Pereira, A.F., 2003. Lateral tidal mixing in the Antarctic marginal seas. Ocean Dynamics 53, 21-26.

Beer, J., Mende, W., Stellmacher, R., 2000. The role of the sun in climate forcing. Quaternary Science Reviews 19, 403-415.

Belt, S.T., Allard, W.G., Masse, G., Robert, J.M., Rowland, S.J., 2000. Highly branched isoprenoids (HBIs): Identification of the most common and abundant sedimentary isomers. Geochimica et Cosmochimica Acta 64, 3839-3851.

Belt, S.T., Masse, G., Rowland, S.J., Poulin, M., Michel, C., LeBlanc, B., 2007. A novel chemical fossil of palaeo sea ice: IP25. Organic Geochemistry 38, 16-27.

Berger, A., 1978. Long-term variations of caloric insolation resulting from the Earth's orbtal elements. Quaternary Research 9, 139-167.

Berger, A., Loutre, M.F., 1991. Insolation values for the climate of the last 10 million years. Quaternary Science Reviews 10, 297-317.

Berger, W.H., Wefer, G., 1990. Export production: seasonality and intermittency, and paleoceanographic implications. Palaeogeography, Palaeoclimatology, Palaeoecology 89, 245-254.

Beucher, C., Tréguer, P., Hapette, A.M., Corvaisier, R., Metzl, N., Pichon, J., 2004. Intense summer Si recycling in the surface Southern Ocean. Geophysical Research Letters 31, L09305, doi: 10.1029/2003GL018998.

Bianchi, C., Gersonde, R., 2004. Climate evolution at the last deglaciation: the role of the Southern Ocean. Earth and Planetary Science Letters 228, 407-424.

Bianchi, G.G., McCave, I.N., 1999. Holocene periodicity in North Atlantic climate and deep-ocean flow south of Iceland. Nature 397, 515-517.

Bindoff, N.L., Rintoul, S.R., Massom, R., 2000a. Bottom water formation and polynyas in Adélie Land, Antarctica. Papers and Proceedings of the Royal Society of Tasmania 133(3), 51-57.

Bindoff, N.L., Rosenberg, M.A., Warner, M.J., 2000b. On the circulation and water masses over the Antarctic continental slope and rise between 80 and 150°E. Deep-Sea Research Part II 47, 2299-2326.

Biondi, F., Gershunov, A., Cayan, D.R., 2001. North Pacific Decadal Climate Variability since 1661. Journal of Climate 14, 5-10.

Bjørck, S., Kromer, B., Johnsen, S., Bennike, O., Hammarlund, D., Lemdahl, G., Possnert, G., Rasmussen, T.L., Wohlfarth, B., Hammer, C.U., Spurk, M., 1996. Synchronized terrestrial-atmospheric deglacial records around the North Atlantic. Science 274, 1155-1160.

Bjørck, S., Muscheler, R., Kromer, B., Andresen, C.S., Heinemeier, J., Johnsen, S.J., Conley, D., Koc, N., Spurk, M., Veski, S., 2001. High-resolution analyses of an early Holocene climate event may imply decreased solar forcing as an important climate trigger. Geology 29, 1107-1110.

Blain, S., Quéguiner, B., Armand, L., Belviso, S., Bombled, B., Bopp, L., Bowie, A., Brunet, C., Brussaard, C., Carlotti, F., Christaki, U., Corbière, A., Durand, I., Ebersbach, F., Fuda, J.L., Garcia, N., Gerringa, L., Griffiths, B., Guigue, C., Guillerm, C., Jacquet, S., Jeandel, C., Laan, P., Lefèbvre, D., Lo Monaco, C., Malits, A., Mosseri, J., Obernosterer, I., Park, Y.H., Picheral, M., Pondaven, P., Remenyi, T., Sandroni, V., Sarthou, G., Savoye, N., Scouarnec, L., Souhaut, M., Thuiller, D., Timmermans, K., Trull, T., Uitz, J., Van Beek, P., Veldhuis, M., Vincent, D., Viollier, E., Vong, L., Wagener, T., 2007. Effect of natural iron fertilization on carbon sequestration in the Southern Ocean. Nature 446, 1070-1074.

Blaker, A.T., Sinha, B., Ivchenko, V.O., Wells, N.C., Zalesny, V.B., 2006. Identifying the roles of the ocean and atmosphere in creating a rapid equatorial response to a Southern Ocean anomaly. Geophysical Research Letters 33, L06720, doi: 10.1029/2005GL025474.

Blott, S. J., Pye, K., 2001.GRADISTAT: a grain size distribution and statistics package for the analysis of unconsolidated sediments. Earth Surface Processes and Landforms 26, 1237-1248.

Blunier, T., Chappellaz, J., Schwander, J., Stauffer, B., Raynaud, D., 1995. Variations in atmospheric methane concentration during the Holocene epoch. Nature 374, 46-49.

Bond, G., Broecker, W., Johnsen, S., McMannus, J., Labeyrie, L., Jouzel, J., Bonani, G., 1993. Correlations between climate records from the North Atlantic sediments and Greenland ice. Nature 365, 143-147.

Bond, G., Kromer, B., Beer, J., Muscheler, R., Evans, M.N., Showers, W., Hoffman, S., Lotti-Bond, R., Hajdas, I., Bonani, G., 2001. Persistent solar influence on North Atlantic climate during the Holocene. Science 294, 2130-2136.

Bond, G., Showers, W., Cheseby, M., Lotti, R., Almasi, P., deMenocal, P., Priore, P., Cullen, H., Hadjas, I., Bonani, G., 1997. A pervasive millenial-scale cycle in the North Atlantic Holocene and Glacial climates. Science 278, 1257-1266.

Boulay, S., 2003. Enregistrements sédimentaires des variations de la mousson sud-asiatique au cours des deux derniers millions d'années. Thèse. Université de Paris XI Orsay, France, 265 pp.

Bout-Roumazeilles, V., Cortijo, E., Labeyrie, L., Debrabant, P., 1999. Clay mineral evidence of nepheloid layer contributions to the Heinrich layers in the northwest Atlantic. Palaeogeography, Palaeoclimatology, Palaeoecology 146, 211-228.

Boyd, P.W., Watson, A.J., Law, C.S., Abraham, E.R., Trull, T., Murdoch, R., Bakker, D.C.E., Bowie, A.R., Buesseler, K.O., Chang, H., Charette, M., Croot, P., Downing, K., Frew, R., Gall, M., Hadfield, M., Hall, J., Harvey, M., Jameson, G., LaRoche, J., Liddicoat, M., Ling, R., Maldonado, M.T., McKay, R.M., Nodder, S., Pickmere, S., Pridmore, R., Rintoul, S., Safi, K., Sutton, P., Strzepzk, R., Tanneberger, K., Turner, S., Waite, A., Zeldis, J., 2000. A mesoscale phytoplankton bloom in the polar Southern Ocean stimulated by iron fertilization. Nature 407, 695-702.

Brachfeld, S.A., Banerjee, S.K., Guyodo, Y., Acton, G.D., 2002. A 13200 year history of century to millenial-scale paleoenvironmental change magnetically recorded in the Palmer Deep, western Antarctic Peninsula. Earth and Planetary Science Letters 194, 311-326.

Brewer, P.G., Nozaki, Y., Spencer, D., Fleer, A.P., 1980. Sediment trap experiments in the deep North Atlantic: isotopic and elemental fluxes. Journal of Marine Research 38, 703–728.

Broecker, W.S., 2000. Abrupt climate change: Causal constraints provided by the paleoclimate record. Earth Science Reviews 51, 137-154.

Broecker, W.S., Denton, G.H., 1989. The role of ocean-atmosphere reorganizations in glacial cycles. Geochimica et Cosmochimica Acta 53, 2465-2501.

Broecker, W.S., Hemming, S., 2001. Climate swings come into focus. Science 294, 2308-2309.

Bromwich, D.H., Kurtz, D.D., 1984. Katabatic wind forcing of the Terra Nova Bay polynya. Journal of Geophysical Research 89, 3561-3572.

Budd, W.F., 1975. Antarctic sea-ice variations from satellite sensing in relation to climate. Journal of Glaciology 15, 417-527.

Buesseler, K.O., 1998. The decoupling of production and particulate export in the surface ocean. Global Biogeochemical Cycles 12, 297-310.

Bye, J., May, J., Simmonds, I., 2006. Control of the Antarctic ice sheet by ocean-ice interaction. Global and Planetary Change 50, 99-111.

C

Camerlenghi, A., Domack, E., Rebesco, M., Gilbert, R., Ishman, S., Leventer, A., Brachfeld, S., Drake, A., 2001. Glacial morphology and post-glacial contourites in northern Prince Gustav Channel (NW Weddell Sea, Antarctica). Marine Geophysical Researches 22, 417–443.

Carson, D. S., Denis, D., Ganeshram, R. S., Crosta, X., Schmidt, S. (submitted). Reconstructing Paleoproductivity throughout the Holocene: A Case Study from Adélie Land, East Antarctica. Submitted to Geochemistry, Geophysics, and Geosystems.

Cassar, N., Bender, M.L., Barnett, B.A., Fan, S., Moxim, W.J., Levy Ii, H., Tilbrook, B., 2007. The southern ocean biological response to aeolian iron deposition. Science 317, 1067-1070.

Cavalieri, D.J., Martin, S., 1985. A passive microwave study of polynyas along the Antarctic Wilkes Land Coast. edited by S. S. Jacobs in Oceanology of the Antarctic Continental Shelf, Antarctic Research Series 43, 177-201.

Cavalieri, D.J., Parkinson, C.L., 2008. Antarctic sea ice variability and trends, 1979–2006. Journal of Geophysical Research 113, C07004, doi: 10.1029/2007JC004564.

Chamley, H., 1965. Observations sur quelques sédiments marins prélevés près des côtes de Terre Adélie. Recueil des Travaux de la Station Maritime d'Endoumé 36, 215-228.

Chappellaz, J., Blunier, T., Raynaud, D., Barnola, J.M., Schwander, J., Stauffer, B., 1993. Synchronous changes in atmospheric CH_4 and Greenland climate between 40 and 8 kyr BP. Nature 366, 443-445.

Chase, Z., Anderson, R., Fleisher, M., Kumar, P., 2003. Accumulation of biogenic and lithogenic material in the Pacific sector of the Southern Ocean during the past 40,000 years. Deep-Sea Research Part II 50(3-4), 799-832.

Chase, Z., Anderson, R.F., 2004. Comment on "On the importance of opal, carbonate, and lithogenic clays in scavenging and fractionating ^{230}Th, ^{231}Pa and ^{10}Be in the ocean" by S. Luo and T.-L. Ku. Earth and Planetary Science Letters 220, 213-222.

Chen, J.H., Wasserburg, G.J., von Damm, K.L., Edmond, J.M., 1986. The U-Th-Pb systematics in hot springs on the East Pacific Rise at 21°N and Guaymas Basin. Geochimica Cosmochimica Acta 50, 2467-2479.

Chiang, J.C.H., Bitz, C.M., 2005. The influence of high latitude ice on the position of the marine Intertropical Convergence Zone. Climate Dynamics 25, 477– 496.

Claquin, P., Martin-Jézéquel, V., Kromkamp, J.C., Veldhuis, M.J.W., Kraay, G.W., 2002. Uncoupling of silicon compared with carbon and nitrogen metabolisms and the role of the cell cycle in continuous cultures of Thalassiosira pseudonana (Bacillariophyceae) under light, nitrogen, and phosphorus control. Journal of Phycology 38, 922-930.

Clark, P.U., Pisias, N.G., Stocker, T.F., Weaver, A.J., 2002. The role of the thermohaline circulation in abrupt climate change. Nature 415, 863-869.

Clement, A.C., Seager, R., Cane, M.A., 1999. Orbital controls on the El Niño/Southern Oscillation and the tropical climate. Paleoceanography 14, 441-456.

Clement, A.C., Seager, R., Cane, M.A., 2000. Suppression of El Niño during the mid-Holocene by changes in the Earth's orbit. Paleoceanography 15, 731-737.

Coale, K.H., Gordon, R.M., Wang, X., 2005. The distribution and behaviour of dissolved and particulate iron and zinc in the Ross Sea and Antarctic circumpolar current along 170°W. Deep-Sea Research Part I 52, 295-318.

Cobb, K.M., Charles, C.D., Cheng, H., Edwards, R.L., 2003. El Niño/Southern Oscillation and tropical Pacific climate during the last millennium. Nature 424, 271-276.

Collier, R., Dymond, J., Honjo, S., Manganini, S., Francois, R., Dunbar, R., 2000. The vertical flux of biogenic and lithogenic material in the Ross Sea: moored sediment trap observations 1996-1998. Deep Sea Research Part II 47, 3491-3520.

Comiso, J.C., Gordon, A.L., 1996. Cosmonaut polynya in the Southern Ocean: structure and variability. Journal of Geophysical Research 101(C8), 18,297-18,313.

Courty, M.A., Cortese, G., Crisci, A., Crosta, X., Dewever, P., Fedoroff, M., Guichard, F., Mermoux, M., Michel, E., Smith, D., Thiemens, M., 2007. Impact fingerprints of the 4 kyr BP dust event based on archaeological, soil, lake and marine archives. General Assembly of the European Geosciences Union, Vienna, Austria, 16-20 April 2007.

Crespin, J., 2004. La période Holocène (Terre Adélie, Antarctique de l'Est): Age réservoir et paléoproductivité. Rapport de Stage de Master 2, Université Bordeaux 1, 27 pp.

Cross, S.L., Baker, P.A., Seltzer, G.O., Fritz, S.C., Dunbar, R.B., 2000. A new estimate of the Holocene lowstand level of Lake Titicaca, central Andes, and implications for tropical palaeohydrology. The Holocene 10, 21-32.

Crosta, X., Crespin, J., Billy, I., Ther, O., 2005. Major factors controlling Holocene $\delta^{13}C_{org}$ changes in a seasonal sea ice environment, Adélie Land, East Antarctica. Global Biogeochemical Cycles 19, GB4029, doi: 4010.1029/2004GB002426.

Crosta, X., Debret, M., Courty, M.-A., Denis, D., Ther, O., 2007. Holocene long- and short-term climate changes off Adélie Land, East Antarctica. Geochemistry, Geophysics, Geosystems 8, Q11009, doi: 11010.11129/12007GC001718.

Crosta, X., Denis, D., Ther, O., 2008. Sea ice seasonality during the Holocene, Adélie Land, East Antarctica. Marine Micropaleontology 66, 222-232.

Crosta, X., Koç, N., 2007. Diatoms: From micropaleontology to isotope geochemistry. In: Hillaire-Marcel, C. and de Vernal, A. (eds.) Developments in Marine Geology 1, 327-369.

Crosta, X., Pichon, J.J., Burckle, L.H., 1998. Application of modern analog technique to marine Antarctic diatoms: Reconstruction of the maximum sea ice extent at the last glacial maximum. Paleoceanography 13(3), 284-297.

Crosta, X., Pichon, J.J., Labracherie, M., 1997. Distribution of Chaetoceros resting spores in modern peri-Antarctic sediments. Marine Micropaleontology 29, 238-299.

Crosta, X., Sturm, A., Armand, L., Pichon, J.J., 2004. Late Quaternary sea ice history in the Indian sector of the Southern Ocean as recorded by diatom assemblages. Marine Micropaleontology 50, 209-223.

Crow, A.J., Tucker, W.B., 1990. Sea ice in polar regions. In "Polar Oceanography, Part A: Physical Science." (W.O. Smith, Ed.), Academic Press, Inc., San Diego, USA, 47-77.

Crucifix, M., Loutre, M.F., Tulkens, P., Fichefet, T., Berger, A., 2002. Climate evolution during the Holocene: A study with an Earth system model of intermediate complexity. Climate Dynamics 19, 43-60.

Cubasch, U., Meehl, G.A., Boer, G.J., Stouffer, R.J., Dix, M., Noda, A., Senior, C.A., Raper, S., Yap, K.S., 2001. Projections of future climate change. In Houghton, J.T., Ding, Y., Griggs, D.J., Noguer, M., van der Linden, P.J., Dai, X., Maskell, K. and Johnson, C.A., editors, Climate change 2001: the scientific basis. Contribution of working group I to the third assessment report of the Intergovernmental Panel on Climate Change Cambridge and New York: Cambridge University Press, 525-582.

Cubasch, U., Voss, R., Hegerl, G.C., Waszkewitz, J., Crowley, T.J., 1997. Simulation of the influence of solar radiation variations on the global climate with an ocean-atmosphere general circulation model. Climate Dynamics 13, 757-767.

D

Damon, P.E., Sonett, C.P., 1991. Solar and Terrestrial. Components of the Atmospheric 14C Variation Spectrum. In: Sonett, C.P., Giampapa, M.S., Matthews, M.S. (eds.), The Sun in Time, University of Arizona. Press, Tucson, 360-388.

Danial-Fortin, P., 2004. Variations des teneurs en silice biogène au cours de l'Holocène (Terre Adélie, Antarctique de l'Est). Rapport de Stage de Master 2, Université Bordeaux I, 11 pp.

Davis, A.M.J., McNider, R.T., 1997. The development of antarctic katabatic winds and implications for the coastal ocean. Journal of the Atmospheric Sciences 54, 1248-1261.

Davis, B.A.S., Brewer, S., Stevenson, A.C., Guiot, J., Allen, J., Almqvist-Jacobson, H., Ammann, B., Andreev, A.A., Argant, J., Atanassova, J., Balwierz, Z., Barnosky, C.D., Bartley, D.D., De Beaulieu, J.L., Beckett, S.C., Behre, K.E., Bennett, K.D., Berglund, B.E.B., Beug, H.J., Bezusko, L., Binka, K., Birks, H.H., Birks, H.J.B., Björck, S., Bliakhartchouk, T., Bogdel, I., Bonatti, E., Bottema, S., Bozilova, E.D.B., Bradshaw, R., Brown, A.P., Brugiapaglia, E., Carrion, J., Chernavskaya, M., Clerc, J., Clet, M., Coûteaux, M., Craig, A.J., Cserny, T., Cwynar, L.C., Dambach, K., De Valk, E.J., Digerfeldt, G., Diot, M.F., Eastwood, W., Elina, G., Filimonova, L., Filipovitch, L., Gaillard-Lemdhal, M.J., Gauthier, A., Göransson, H., Guenet, P., Gunova, V., Hall, V.A.H., Harmata, K., Hicks, S., Huckerby, E., Huntley, B., Huttunen, A., Hyvärinen, H., Ilves, E., Jacobson, G.L., Jahns, S., Jankovská, V., Jóhansen, J., Kabailiene, M., Kelly, M.G., Khomutova, V.I., Königsson, L.K., Kremenetski, C., Kremenetskii, K.V., Krisai, I., Krisai, R., Kvavadze, E., Lamb, H., Lazarova, M.A., Litt, T., Lotter, A.F., Lowe, J.J., Magyari, E., Makohonienko, M., Mamakowa, K., Mangerud, J., Mariscal, B., Markgraf, V., McKeever, Mitchell, F.J.G., Munuera, M., Nicol-Pichard, S., Noryskiewicz, B., Odgaard, B.V., Panova, N.K., Pantaleon-Cano, J., Paus, A.A., Pavel, T., Peglar, S.M., Penalba, M.C., Pennington, W., Perez-Obiol, R., 2003. The temperature of Europe during the Holocene reconstructed from pollen data. Quaternary Science Reviews 22, 1701-1716.

Davis, B.A.S., Brewer, S., 2009. Orbital forcing and role of the latitudinal insolation/temperature gradient. Climate Dynamics 32,143–165.

de la Mare, W.K., 1997. Abrupt mid-twentieth-century decline in Antarctic sea ice extent from whalling records. Nature 389, 57-60.

De Santis, L., Brancolini, G., Donda, F., 2003. Seismo-stratigraphic analysis of the Wilkes Land continental margin (East Antarctica): Influence of glacially driven processes on the Cenozoic deposition. Deep-Sea Research Part II 50, 1563-1594.

de Vernal, A., Hillaire-Marcel, C., Darby, D.A., 2005. Variability of sea ice cover in the Chukchi Sea (western Arctic Ocean) during the Holocene. Paleoceanography 20, PA4018, doi: 10.1029/2005PA001157.

Debret, M., Bout-Roumazeilles, V., Grousset, F., Desmet, M., McManus, J.F., Massei, N., Sebag, D., Petit, J.-R., Copard, Y., Trentesaux, A., 2007. The origin of the 1500-year climate cycles in Holocene North-Atlantic records. Climate of the Past Discussions 3, 679–692.

Debret, M., Sebag, D., Crosta, X., Massei, N., Petit, J.-R., Chapron, E., Bout-Roumazeilles, V., in revision. Spectral imprint of Holocene climate variability in the Atlantic and circum-Antarctic area: A worldwide pattern? Quaternary Science Reviews.

DeConto, R., Pollard, D., Harwood, D., 2007. Sea ice feedback and Cenozoic evolution of Antarctic climate and ice sheets. Paleoceanography 22, PA3214, doi: 3210.1029 /2006PA001350.

Delmonte, B., Petit, J., Krinner, G., Maggi, V., Jouzel, J., Udisti, R., 2005. Ice core evidence for secular variability and 200-year dipolar oscillations in atmospheric circulation over East Antarctica during the Holocene. Climate Dynamics 24, 641-654.

Delmonte, B., Petit, J.R., Maggi, V., 2002. LGM-Holocene changes and Holocene millennial-scale oscillations of dust particles in the EPICA Dome C ice core, East Antarctica. Annals of Glaciology 35, 306-312.

deMenocal, P., Ortiz, J., Guilderson, T., Sarnthein, M., 2000. Coherent high- and low-latitude climate variability during the Holocene warm period. Science 288, 2198-2202.

Denis, D., 2005. Quel signal est enregistré dans les laminations de la carotte sédimentaire MD03-2601? (Terre Adélie, Antarctique de l'Est). Rapport de Master 2, Université Bordeaux 1 30 pp.

Denis, D., Crosta, X., Schmidt, S., Carson, D.S., Ganeshram, R.S., Renssen, H., Bout-Roumazeilles, V., Zaragosi, S., Martin, B., in-press. Holocene glacier and deep water dynamics, Adélie Land, East Antarctica. Quaternary Science Reviews.

Denis, D., Crosta, X., Schmidt, S., Carson, D.S., Ganeshram, R.S., Renssen, H., Crespin, J., Ther, O., Billy, I., Giraudeau, J., in revision. Holocene productivity changes off Adélie Land (East Antarctica). In revision to Paleoceanography.

Denis, D., Crosta, X., Zaragosi, S., Martin, B., Mas, V., 2006. Seasonal and sub-seasonal climate changes recorded in laminated diatom ooze sediments, Adélie Land, East Antarctica. The Holocene 16, 1143-1153.

Denton, G.H., Bockheim, J.G., Wilson, S.C., Stuiver, M., 1989. Late Wisconsin and early Holocene glacial history, inner Ross Embayment, Antarctica. Quaternary Research 31, 151-182.

Denton, G.H., Karlén, W., 1973. Holocene climatic variations—Their pattern and possible cause. Quaternary Research 3, 155-174.

Dergachev, V.A., Raspopov, O.M., Damblon, F., Jungner, H., Zaitseva, G.I., 2007. Natural Climate Variability during the Holocene. Radiocarbon 49, 837-854.

Dézileau, L., Bareille, G., Reiss, J.L., Lemoine, F., 2000. Evidence for strong sediment redistribution by bottom currents along the southeast Indian Ridge. Deep-Sea Research Part I 47, 1899-1936.

Diógenes, A. N., Hoff, E. A., Fernandes, C. P., 2005. Grain size measurement by image analysis: An application in the ceramic and in the metallic industries. Proceedings of COBEM 2005, 18th International Congress of Mechanical Engineering, Ouro Preto, MG, November 6-11.

Dodson, J.R., Ono, Y., 1997. Timing of late quaternary vegetation response in the 30-50° latitude bands in south-eastern Australia and north-eastern Asia. Quaternary International 37, 89-104.

Domack, E.W., Mayewski, P., 1999. Bi-polar ocean linkages: Evidence from Late-Holocene Anatarctic marine and Greenland ice-core records. The Holocene 9, 247-251.

Dowdeswell, J.A., Dowdeswell, E.K., 1989. Debris in icebergs and rates of glacio-marine sedimentation: observations from Spitsbergen and a simple model. Journal of Geology 97, 221-231.

Driesschaert, E., 2005. Climate change over the next millennia using LOVECLIM, a new Earth system model including the polar ice sheets. Ph.D. Thesis, Univ. Catholique de Louvain, Louvain-la-Neuve, Belgium, 214 pp.

Drijfhout, S.S., Maier-Reimer, E., Mikolajewicz, U., 1996. Tracing the conveyor belt in the Hamburg large-scale geostrophic ocean general circulation model. Journal of Geophysical Research 101, 22563-22575.

Duplessy, J.C., Ivanova, E., Murdmaa, I., Paterne, M., Labeyrie, L., 2001. Holocene paleoceanography of the northern Barents Sea and variations of the northward heat transport by the Atlantic Ocean. Boreas 30, 1-16.

E

Edwards, R., Sedwick, P., 2001. Iron in east Antarctic snow: Implications for atmospheric iron deposition and algal production in Antarctic waters. Geophysical Research Letters 28, 3907-3910.

Edwards, R., Sedwick, P., Morgan, V, Boutron, C., 2006. Iron in ice cores from Law Dome: A record of atmospheric iron deposition for maritime East Antarctica during the Holocene and Last Glacial Maximum. Geochemistry, Geophysics, and Geosystems 7, Q12Q01, doi: 10.1029/2006GC001307.

Emiliani, C., 1955. Pleistocene temperatures. Journal of Geology 63, 538-578.

Enomoto, H., Ohmura, A., 1990. The influences of atmospheric half-yearly cycle on the sea ice extent in the Antarctic. Journal of Geophysical Research 95(C6), 9497-9511.

EPICA Community Members, 2004. Eight glacial cycles from an Antarctic ice core. Nature 429, 623-628.

Escutia, C., Warnke, D., Acton, G.D., Barcena, A., Burckle, L., Canals, M., C.S., F., 2003. Sediment distribution and sedimentary processes across the Antarctic Wilkes Land margin during the Quaternary. Deep-Sea Research Part II 50, 1481-1508.

F

Farmer, E.C., deMenocal, P.B., Marchitto, T.M., 2005. Holocene and deglacial ocean temperature variability in the Benguela upwelling region: Implications for low-latitude atmospheric circulation. Paleoceanography 20, 1-16.

Findlay, C.S., Giraudeau, J., 2002. Extent calcareous nannoplankton in the Australian Sector of the Southern Ocean (austral summers 1994 and 1995). Marine Micropaleontology 40, 417-439.

Finkel, R.C., Nishizumi, K., 1997. Beryllium 10 concentrations in the Greenland Ice Sheet Project 2 ice core from 3–40 ka. Geophysical Research Letters 102, 26,699-26,706.

Finocchiaro, F., Langone, L., Colizza, E., Fontolan, G., Giglio, F., Tuzzi, E., 2005. Record of the early Holocene warming in a laminated sediment core from Cape Hallett Bay (Northern Victora Land, Antarctica). Global and Planetary Change 45, 193-206.

Fitch, D.T., Moore, J.K., 2007. Wind speed influence on phytoplankton bloom dynamics in the Southern Ocean Marginal Ice Zone. Journal of Geophysical Research 112, C08006, doi: 10.1029/2006JC004061.

Fitton, J.G., Saunders, A.D., Larsen, L.M., Hardarson, B.S., Norry, M.J., 1998. Volcanic rocks from the southeast Greenland margin at 63°N: Composition, petrogenesis, and mantle sources. Proceedings of the Ocean Drilling Program Scientific results 152, 331-350.

Fitzwater, S.E., Johnson, K.S., Gordon, R.M., Coale, K.H., Smith, W.O., 2000. Trace metal concentrations in the Ross Sea and their relationship with nutrients and phytoplankton growth. Deep-Sea Research Part II 47, 3159-3179.

Fleitmann, D., Burns, S.J., Mudelsee, M., Neff, U., Kramers, J., Mangini, A., Matter, A., 2003. Holocene forcing of the Indian monsoon recorded in a stalagmite from Southern Oman. Science 300, 1737-1739.

Fleitmann, D., Mudelsee, M., Burns, S.J., Bradley, R.S., Kramers, J., Matter, A., 2008. Evidence for a widespread climatic anomaly at around 9.2 ka before present. Paleoceanography 23, PA1102, doi: 10.1029/2007PA001519.

Folk, R. L., Ward, W. C., 1957. Brazos River bar: a study in the significance of grain size parameters. Journal of Sedimentary Petrology 27, 3-26.

Francois, R., Bacon, M.P., Altabet, M.A., 1993. Glacial/interglacial changes in sediment rain rate in the SW Indian sector of subantarctic waters as recorded by ^{230}Th, ^{231}Pa, U, and ^{15}N. Paleoceanography 8, 611-629.

Francois, R., Frank, M., Loeff, M.M.R.v.d., Bacon, M.P., 2004. ^{230}Th normalization: An essential tool for interpreting sedimentary fluxes during the late Quaternary. Paleoceanography 19, PA1018, doi: 10.1029/PA000939.

Frank, M., 1996. Reconstruction of late Quaternary environmental conditions applying the natural radionuclides ^{230}Th, ^{10}Be, ^{231}Pa and ^{238}U: A study of deep-sea sediments from the eastern Atlantic sector of the Antarctic Circumpolar Current system. Reports on Polar Research 186, 136 pp.

G

Gammaitoni, L., Hanggi, P., Jung, P., Marchesoni, F., 1998. Stochastic resonance. Reviews of Modern Physics 70, 223–287.

Ganopolski, A., Kubatzki, C., Claussen, M., Brovkin, V., Petoukhov, V., 1998. The Influence of Vegetation-Atmosphere-Ocean Interaction on Climate during the Mid-Holocene. Science 280, 1916-1919.

Gibson, J.A.E., Trull, T.W., 1999. Annual cycle of fCO_2 under sea-ice and in open water in Prydz Bay, East Antarctica. Marine Chemistry 66, 187-200.

Gilbert, R., Nielsen, N., Moller, H., Desloges, J.R., Rasch, M., 2002. Glacimarine sedimentation in Kangerdluk (Disko Fjord), West Greenland, in response to a surging glacier. Marine Geology 191, 1-18.

Gille, S.T., 2002. Warming of the Southern Ocean Since the 1950s. Science 295, 1275 - 1277.

Gillett, N.P., Thompson, D., 2003. Simulation of recent Southern Hemisphere climate change. Science 302, 273–275.

Gloersen, P., Campbell, W.J., Cavalieri, D.J., Comiso, J.C., Parkinson, C.L., Zwally, H.J., 1992. Arctic and Antarctic Sea Ice, 1978-1987: Satellite Passive-microwave Observations and Analysis. NASA Scientific and Technical Information Program, NASA SP-511. Washington.

Goodwin, I.D., 1993. Holocene deglaciation, sea-level change, and the emergence of the Windmill Islands, Budd Coast, Antarctica. Quaternary Research 40, 70-80.

Goodwin, I.D., 1996. A mid to late Holocene readvance of the Law Dome ice margin, Budd Coast, East Antarctica. Antarctic Science 8, 395-406.

Goodwin, I.D., 1998. Did changes in Antarctic ice volume influence Late Holocene sea-level lowering? Quaternary Science Reviews 17, 319-332.

Goosse, H., Campin, J.-M., Tartinville, B., 2001. The sources of Antarctic bottom water in a global ice-ocean model. Ocean Modelling 3, 51-65.

Goosse, H., Masson-Delmotte, V., Renssen, H., Delmotte, M., Fichefet, T., Morgan, V., van Ommen, T., Khim, B.K., Stenni, B., 2004. A late medieval warm period in the Southern Ocean as a delayed response to external forcing? Geophysical Research Letters 31, L06203, doi: 10.1029/2003GL019140.

Goosse, H., Renssen, H., 2001. A two-phase response of the Southern Ocean to an increase in greenhouse gas concentrations. Geophysical Research Letters 28, 3469-3472.

Goosse, H., Renssen, H., 2004. Exciting natural modes of variability by solar and volcanic forcing: idealized and realistic experiments. Climate Dynamics 23, 153-163.

Goosse, H., Selten, F.M., Haarsma, R.J., Opsteegh, J.D., 2001. Decadal variability in high northern latitudes as simulated by an intermediate-complexity climate model. Annals of Glaciology 33, 525-532.

Goosse, H., Selten, F.M., Haarsma, R.J., Opsteegh, J.D., 2002. A mechanism of decadal variability of the sea-ice volume of the Northern Hemisphere. Climate Dynamics 19, 61-83.

Goosse, H., Selten, F.M., Haarsma, R.J., Opsteegh, J.D., 2003. Large sea-ice volume anomalies simulated in a coupled climate model. Climate Dynamics 20, 523-536.

Gordon, A.L., Huber, A.H., 1995. Warm Weddell Deep Water west of Maud Rise. Journal of Geophysical Research 100(C7), 13,747-13,753.

Gordon, A.L., Tchernia, P., 1972. Waters of the continental margin off Adélie coast, Antarctica. In: D.E. Hayes, Eds, Antarctic Oceanology: II. The Australian–New Zealand Sector, Antarctic Research Series 19, 59–70.

Gordon, A.L., Visbeck, M., Huber, B., 2001. Export of Weddell Sea Deep and Bottom Water. Journal of Geophysical Research 106, 9005-9017.

Grove, J.M., 2004. Little Ice Ages Ancient and Modern. (2nd edition), Routledge, London 2 volumes.

Gupta, A.K., Das, M., Anderson, D.M., 2005. Solar influence on the Indian summer monsoon during the Holocene. Geophysical Research Letters 32 (17), 1-4.

H

Hall, I.R., Bianchi, G.G., Evans, J.R., 2004. Centennial to millennial scale Holocene climate-deep water linkage in the North Atlantic. Quaternary Science Reviews 23(14-15), 1529-1536.

Hall, I.R., McCave, I.N., 2000. Palaeocurrent reconstruction, sediment and thorium focussing on the Iberian margin over the last 140 ka. Earth and Planetary Science Letters 178, 151-164.

Hambrey, M.J., Glasser, N.F., 2005. Glaciers. In "Encyclopedia of Geology", Elsevier, Oxford, 663-678.

Hammer, Ø., Harper, D.A.T., Ryan, P.D., 2007. PAST - PAlaeontological STatistics, ver. 1.75. Available at http://folk.uio.no/ohammer/past, 81 pp.

Harris, P.T., 2000. Ripple cross-laminated sediments on the East Antarctic Shelf: evidence for episodic bottom water production during the Holocene? Marine Geology 170, 317-330.

Harris, P.T., Beaman, R.J., 2003. Processes controlling the formation of the Mertz Drift, George Vth continental shelf, East Antarctica: evidence from 3.5 kHz sub-bottom profiling and sediment cores. Deep Sea Research Part II 50, 1463-1480.

Harris, P.T., Brancolini, G., Armand, L., Buseti, M., Beaman, R.J., Giorgetti, G., Presti, M., Trincardi, F., 2001. Continental shelf drift deposit indicates non-steady state Antarctic bottom water production in the Holocene. Marine Geology 179, 1-8.

Harris, P.T., O'Brien, P.E., 1998. Bottom currents, sedimentation and ice-sheet retreat facies successions on the Mac Robertson shelf, East Antarctica. Marine Geology 151, 47-72.

Hartmann, D.L., Wallace, J.M., Limpasuvan, V., Thompson, D., Holton, J.R., 2000. Can ozone depletion and global warming interact to produce rapid climate change? Proceedings of the National academy of Sciences of the United States of America 97, 1412–1417.

Hass, H.C., 2002. A method to reduce the influence of ice-rafted debris on a grain-size record from the northern Fram Strait, Arctic Ocean. Polar Research 21, 299-306.

Haug, G.H., Hughen, K.A., Sigman, D.M., Peterson, L.C., Röhl, U., 2001. Southward migration of the Intertropical Convergence Zone through the Holocene. Science 293, 1304-1308.

Hays, J.D., Imbrie, J., Shackleton, N.J., 1976. Variation in the Earth's orbit: pacemaker of the ice ages. Science 194, 1121–1132.

He, Y., Theakstone, W.H., Zhang, Z., Zhang, D., Yao, T., Chen, T., Shen, Y., Pang, H., 2004. Asynchronous Holocene climatic change across China. Quaternary Research 61, 52-63.

Heil, P., Allison, I., 1999. The pattern and variability of Antarctic sea-ice drift in the Indian Ocean and western Pacific sectors. Journal of Geophysical Research 104, 15,789-15,802.

Hemming, S.R., 2004. Heinrich events: Massive late Pleistocene detritus layers of the North Atlantic and their global climate imprint. Reviews of Geophysics 42, 1001-1043.

Henderson, G.M., Heinze, C., Anderson, R.F., Winguth, A.M.E., 1999. Global distribution of the ^{230}Th flux to ocean sediments constrained by GCM modelling. Deep Sea Research Part I 46, 1861-1893.

Hense, I., Bathmann, U.V., Timmermann, R., 2000. Plankton dynamics in frontal systems of the Southern Ocean. Journal of Marine Systems 27, 235-252.

Heusser, C.J., Stephen Streeter, S., 1980. A temperature and precipitation record of the past 16,000 years in Southern Chile. Science 210, 1345-1347.

Hillaire-Marcel, C., De Vernal, A., Polyak, L., Darby, D., 2004. Size-dependent isotopic composition of planktic foraminifers from Chukchi Sea vs. NW Atlantic sediments - Implications for the Holocene paleoceanography of the western Arctic. Quaternary Science Reviews 23, 245-260.

Hjørt, C., Ingólfsson, O., Moller, P., Lirio, J.M., 1997. Holocene glacial history and sea-level changes on James Ross Island, Antarctic Peninsula. Journal of Quaternary Science 12, 259-273.

Hodell, D.A., Curtis, J.H., Jones, G.A., Higuera-Gundy, A., Brenner, M., Binford, M.W., Dorsey, K.T., 1991. Reconstruction of Caribbean climate change over the past 10,500 years. Nature 352, 790-793.

Hodell, D.A., Kanfoush, S.L., Shemesh, A., Crosta, X., Charles, C.D., Guilderson, T.P., 2001. Abrupt Cooling of Antarctic Surface Waters and Sea Ice Expansion in the South Atlantic Sector of the Southern Ocean at 5000 cal yr B.P. Quaternary Research 56, 191-198.

Hoelzmann, P., Jolly, D., Harrison, S.P., Laarif, F., Bonnefille, R., Pachur, H.J., 1998. Mid-Holocene land-surface conditions in northern Africa and the Arabian peninsula: A data set for the analysis of biogeophysical feedbacks in the climate system. Global Biogeochemical Cycles 12, 35-51.

Holmgren, K., Lee-Thorp, J.A., Cooper, G.R.J., Lundblad, K., Partridge, T.C., Scott, L., Sithaldeen, R., Talma, A.S., Tyson, P.D., 2003. Persistent millennial-scale climatic variability over the past 25,000 years in Southern Africa. Quaternary Science Reviews 22, 2311-2326.

Holz, C., Stuut, J.-B.W., Henrich, R., Meggers, H., 2007. Variability in terrigenous sedimentation processes off northwest Africa and its relation to climate changes: Inferences from grain-size distributions of a Holocene marine sediment record. Sedimentary Geology 202, 499-508.

Hormes, A., Müller, B.U., Schlüchter, C., 2001. The Alps with little ice: evidence for eight Holocene phases of reduced glacier extent in the Central Swiss Alps. The Holocene 11, 255-265.

Hughen, K.A., Baillie, M.G.L., Bard, E., Bayliss, A., Beck, J.W., Bertrand, C.J.H., Blackwell, P.G., Buck, C.E., Burr, G.S., Cutler, K.B., Damon, P.E., Edwards, R.L., Fairbanks, R.G., Friedrich, M., Guilderson, T.P., Kromer, B., McCormac, F.G., Manning, S.W., Bronk Ramsey, C., Reimer, P.J., Reimer, R.W., Remmele, S., Southon, J.R., Stuiver, M., Talamo, S., Taylor, F.W., van der Plicht, J., Weyhenmeyer, C.E., 2004. Marine04 Marine radiocarbon age calibration, 26 - 0 ka BP. Radiocarbon 46, 1059-1086.

Hurrell, J.W., Van Loon, H., 1997. Decadal variations in climate associated with the North Atlantic oscillation. Climatic Change 36, 301-326.

I

Iizuka, Y., Horikawa, S., Sakurai, T., Johnson, S., Dahl-Jensen, D., Steffensen, J.P., Hondoh, T., 2008. A relationship between ion balance and the chemical compounds of salt inclusions found in the Greenland Ice Core Project and Dome Fuji ice cores. Journal of Geophysical Research 113, D07303, doi: 10.1029/2007JD009018.

Imbrie, J., Hays, J.D., Martinson, D.G., McIntyre, A., Mix, A.C., Morley, J.J., Pisias, N.G., Prell, W.L., Shackleton, N.J., 1984. The orbital theory of Pleistocene climate: support from a revised chronology of the Marine del-18O record. In: Berger A, Imbrie J, Hays JD, Kukla G, Saltzman B (eds) Milankovitch and Climate, Part 1. Reidel Publishing Co., Dordrecht, 269–305.

Indermühle, A., Stocker, T.F., Joos, F., Fisher, H., Smith, H.J., Wahlen, M., Deck, B., Mastroianni, D., Tschumi, J., Blunier, T., Meyer, R., Stauffer, B., 1999. Holocene

carbon-cycle dynamics based on CO_2 trapped in ice at Taylor dome, Antarctica. Nature 398, 121-126.

Ingølfsson, O., Hjort, C., 1999. The Antarctic contribution to Holocene global sea level rise. Polar Research 18, 323-330.

Ingølfsson, O., Hjort, C., Berkman, P.A., Björck, S., Colhoun, E., Goodwin, I.D., Hall, B., Hirakawa, K., Melles, M., Möller, P., Prentice, M.L., 1998. Antarctic glacial history since the last glacial maximum: an overview of the record on land. Antarctic Science 10, 326-344.

IPCC, 2001. Climate Change 2001: The scientific Basis. Contribution of Working Group I to the Third Assessment Report of the Intergovernmental Panel on Climate Change. Cambridge University Press Cambridge and New York, 881 pp.

IPCC, 2007. Climate Change 2007: The Physical Science Basis. Contribution of Working Group I to the Fourth Assessment Report of the Intergovernmental Panel on Climate Change. Accessed online at http://ipcc-wg1.ucar.edu/.

Iriondo, M.H., 1999. Last Glacial Maximum and Hypsithermal in the Southern Hemisphere. Quaternary International 62, 11-19.

Ishii, M., Inoue, H.Y., Matsueda, H., Tanoue, E., 1998. Close coupling between seasonal biological production and dynamics of dissolved inorganic carbon in the Indian Ocean sector and the western Pacific Ocean sector of the Antarctic Ocean. Deep Sea Research Part I 45, 1187-1209.

Ivchenko, V.O., Zalesny, V.B., Drinkwater, M.R., 2004. Can the equatorial ocean quickly respond to Antarctic sea ice/salinity anomalies? Geophysical Research Letters 31(15), doi: 10.1029/2004GL020472.

J

Jenny, B., Valero-Garcès, B.L., Villa-Martiñez, R., Urrutia, R., Geyh, M., Veit, H., 2002. Early to mid-Holocene aridity in central Chile and the southern Westerlies: The Laguna Aculeo record (34°S). Quaternary Research 58, 160-170.

Johns, L., Wraige, E.J., Belt, S.T., Lewis, C.A., Massé, G., Robert, J.-M., Rowland, S.J., 1999. Identification of C25 Highly branched isoprenoid (HBI) dienes in Antarctic sediments, sea-ice diatoms and laboratory cultures of diatoms. Organic Geochemistry 30, 1471-1475.

Johnsen, S.J., Dahl-Jensen, D., Gundestrup, N., Steffensen, J.P., Clausen, H.B., Miller, H., Masson-Delmotte, V., Sveinbjörnsdottir, A.E., White, J., 2001. Oxygen isotope and palaeotemperature records from six Greenland ice-core stations: Camp Century, Dye-3, GRIP, GISP2, Renland and NorthGRIP. Journal of Quaternary Science 16, 299-307.

Joughin, I., Padman, L., 2003. Melting and freezing beneath Filchner-Ronne Ice Shelf, Antarctica. Geophysical Research Letters 30, doi: 1410.1029/2003GL016941.

Jouzel, J., Masson-Delmotte, V., Cattani, O., Dreyfus, G., Falourd, S., Hoffmann, G., Minster, B., Nouet, J., Barnola, J.M., Chappellaz, J., Fischer, H., Gallet, J.C., Johnsen, S., Leuenberger, M., Loulergue, L., Luethi, D., Oerter, H., Parrenin, F., Raisbeck, G., Raynaud, D., Schilt, A., Schwander, J., Selmo, E., Souchez, R., Spahni, R., Stauffer, B., Steffensen, J.P., Stenni, B., Stocker, T.F., Tison, J.L., Werner, M., Wolff., E.W., 2007.

Orbital and Millennial Antarctic Climate Variability over the Past 800,000 Years. Science 317, 793-797.

K

Kaiser, J., Lamy, F., Arz, H.W., Hebbeln, D., 2007. Dynamics of the millennial-scale sea surface temperature and Patagonian Ice Sheet fluctuations in southern Chile during the last 70 kyr (ODP Site 1233). Quaternary International 161, 77-89.

Kattenberg, A., Giorgi, F., Grassl, H., Meehl, G.A., Mitchell, J.F.B., Stouffer, R.J., Tokioka, T., Weaver, A.J., Wigley, T.M.L., 1996. Climate Models - Projections of Future Climate. In: Houghton, J.T., L.G.M. Filho, B.A. Callandar, N. Harris, A. Kattenberg, and K. Maskell (eds). 1996. Climate Change 1995: The Science of Climate Change. Contribution of Working Group 1 to the Second Assessment Report of the Intergovernmental Panel on Climate Change. Cambridge University Press, New York, 572 pp. 285-357.

Kaufman, D.S., Ager, T.A., Anderson, N.J., Anderson, P.M., Andrews, J.T., Bartlein, P.J., Brubaker, L.B., Coats, L.L., Cwynar, L.C., Duvall, M.L., Dyke, A.S., Edwards, M.E., Eisner, W.R., Gajewski, K., Geirsdóttir, A., Hu, F.S., Jennings, A.E., Kaplan, M.R., Kerwin, M.W., Lozhkin, A.V., MacDonald, G.M., Miller, G.H., Mock, C.J., Oswald, W.W., Otto-Bliesner, B.L., Porinchu, D.F., Ru?hland, K., Smol, J.P., Steig, E.J., Wolfe, B.B., 2004. Holocene thermal maximum in the western Arctic (0-180°W). Quaternary Science Reviews 23, 529-560.

Keeling, R.F., Stephens, B.B., 2001. Antarctic sea ice and the control of Pleistocene climate instability. Paleoceanography 16(1), 112-131.

Keigwin, L.D., 1996. The Little Ice Age and Medieval Warm Period in the Sargasso Sea. Science 274, 1504-1508.

Keigwin, L.D., Boyle, E.A., 2000. Detecting Holocene changes in thermohaline circulation. Proceedings of the National Academy of Sciences of the United States of America 97, 1343-1346.

Kemp, A.E.S., Pearce, R.B., Grigorov, I., Rance, J., Lange, C.B., Quilty, P., Salter, I., 2006. Production of giant marine diatoms and their export at oceanic frontal zones: Implications for Si and C flux from stratified oceans. Global Biogeochemical Cycles 20, GB4S04, doi: 10.1029/2006GB002698.

Kennett, J.P., 1977. Cenozoic evolution of Antarctic glaciation, the circum-Antarctic Ocean, and their impact on global paleoceanography. Journal of Geophysical Research 82, 3843-3860.

Kim, J.H., Rimbu, N., Lorenz, S.J., Lohmann, G., Nam, S.-I., Schouten, S., Ruhlemann, C., Schneider, R.R., 2004. North Pacific and North Atlantic sea-surface temperature variability during the Holocene. Quaternary Science Reviews 23, 2141-2154.

Kim, J.H., Schneider, R.R., Hebbeln, D., Müller, P.J., Wefer, G., 2002a. Last deglacial sea-surface temperature evolution in the Southeast Pacific compared to climate changes on the South American continent. Quaternary Science Reviews 21, 2085-2097.

Kim, J.H., Schneider, R.R., Mulitza, S., Müller, P.J., 2003. Reconstruction of SE trade-wind intensity based on sea-surface temperature gradients in the Southeast Atlantic over the last 25 kyr. Geophysical Research Letters 30, doi: 10.1029/2003GL017557.

Kim, J.H., Schneider, R.R., Müller, P.J., Wefer, G., 2002b. Interhemispheric comparison of deglacial sea-surface temperature patterns in Atlantic eastern boundary currents. Earth and Planetary Science Letters 194, 383-393.

Knies, J., Brookes, S., Schubert, C.J., 2007. Re-assessing the nitrogen signal in continental margin sediments: New insights from the high northern latitudes. Earth and Planetary Science Letters 253, 471-484.

Knutti, R., Flückiger, J., Stocker, T.F., Timmermann, A., 2004. Strong hemispheric coupling of glacial climate through freshwater discharge and ocean circulation. Nature 430, 851-856.

Korb, R.E., Whitehouse, M., 2004. Contrasting primary production regimes around South Georgia, Southern Ocean: Large blooms versus high nutrient, low chlorophyll waters. Deep-Sea Research Part I 51, 721-738.

Krell, A., Schnack-Schiel, S.B., Thomas, D.N., Kattner, G., Zipan, W., Dieckmann, G.S., 2005. Phytoplankton dynamics in relation to hydrography, nutrients and zooplankton at the onset of sea ice formation in the eastern Weddell Sea (Antarctica). Polar Biology 28, 700-713.

Kulbe, T., Melles, M., Verkulich, S.R., Pushina, Z.V., 2001. East Antarctic climate and environmental variability over the last 9400 years inferred from marine sediments of the Bunger Oasis. Artic, Antartic, and Alpine Research 33(2), 223-230.

Kushner, P.J., Held, I.M., Delworth, T.L., 2001. Southern Hemisphere atmospheric circulation response to global warming. Journal of Climate 14, 2238-2249.

Kwok, R., Comiso, J.C., 2002. Southern Ocean climate and sea ice anomalies associated with the Southern Oscillation. Journal of Climate 15, 487-501.

L

L'Heureux, M.L., Thompson, D.W.J., 2006. Observed relationships between the El Niño–Southern Oscillation and the extratropical zonal mean circulation. Journal of Climate 19, 276–287.

Lambeck, K., Chappell, J., 2001. Sea level change through the last glacial cycle. Science 292, 679-686.

Lamy, F., Hebbeln, D., Röhl, U., Wefer, G., 2001. Holocene rainfall variability in Southern Chile: A marine record of latitudinal shifts of the Southern Westerlies. Earth and Planetary Science Letters 185, 369-382.

Lamy, F., Kaiser, J., Ninnemann, U., Hebbeln, D., Arz, H.W., Stoner, J., 2004. Antarctic timing of surface water changes off Chile and Patagonian ice sheet response. Science 304, 1959-1962.

Lamy, F., Rühlemann, C., Hebbeln, D., Wefer, G., 2002. High- and low-latitude climate control on the position of the southern Peru-Chile Current during the Holocene. Paleoceanography 17, 16-11.

Lannuzel, D., Schoemann, V., de Jong, J., Tison, J.-L., Chou, L., 2007. Distribution and biogeochemical behaviour of iron in the East Antarctic sea ice. Marine Chemistry 106, 18-32.

Laut, P., 2003. Solar activity and terrestrial climate: An analysis of some purported correlations. Journal of Atmospheric and Solar-Terrestrial Physics 65, 801-812.

Laws, R.A., 1983. Preparing strewn slides for quantitative microscopical analysis: A test using calibrated microspheres. Micropaleontology 24, 60-65.

Lea, D.W., Pak, D.K., Peterson, L.C., Hughen, K.A., 2003. Synchroneity of tropical and high-latitude Atlantic temperatures over the last glacial termination. Science 301, 1361-1364.

Lee-Thorp, J.A., Holmgren, K., Lauritzen, S.E., Linge, H., Moberg, A., Partridge, T.C., Stevenson, C., Tyson, P.D., 2001. Rapid climate shifts in the southern African interior throughout the mid to late Holocene. Geophysical Research Letters 28, 4507-4510.

Lefebvre, W., Goosse, H., 2008a. Analysis of the projected regional sea-ice changes in the Southern Ocean during the twenty-first century. Climate Dynamics 30, 59-76.

Lefebvre, W., Goosse, H., 2008b. An analysis of the atmospheric processes driving the large-scale winter sea ice variability in the Southern Ocean. Journal of Geophysical Research 113, C03S90, doi: 10.1029/2007JC004269.

Leventer, A., 1991. Sediment trap diatom assemblages from the northern Antarctic Peninsula region. Deep Sea Research Part I 38, 1127-1143.

Leventer, A., 1992. Modern distribution of diatoms in sediments from the George V Coast, Antarctica. Marine Micropaleontology 19, 315-332.

Leventer, A., 1998. The fate of Antarctic "sea-ice diatoms" and their use as paleoenvironmental indicators. In Lizotte, M., and Arrigo, K. (eds.), Antarctic sea ice biological processes, interactions and variability: American Geophysical Union, Antarctic Research Series 73, 121-137.

Leventer, A., Domack, E., Barkoukis, A., McAndrews, B., Murray, J., 2002. Laminations from the Palmer Deep: A diatom-based interpretation. Paleoceanography 17(2), 3-1 to 3-15.

Leventer, A., Domack, E., Dunbar, R., Pike, J., Stickley, C., Maddison, E., Brachfeld, S., Manley, P., McClennen., C., 2006. East Antarctic Margin Marine Sediment Record of Deglaciation. Geological Society of America Today 16, doi: 10.1130/GSAT01612A.01611.

Leventer, A., Domack, E.W., Ishman, S.E., Brachfeld, S., McClennen, C.E., Manley, P., 1996. Productivity cycles of 200-300 years in the Antarctic Peninsula region: Understanding linkages among the sun, atmosphere, oceans, sea ice, and biota. Geological Society of America Bulletin 108(12), 1626-1644.

Leventer, A., Dunbar, R.B., DeMaster, D.J., 1993. Diatom evidence for the Late Holocene climatic events in Granite Harbor, Antarctica. Paleoceanography 8, 373-386.

Lie, Ø., Olaf Dahl, S., Nesje, A., 2003. A theoretical approach to glacier equilibrium-line altitudes using meteorological data and glacier mass-balance records from southern Norway. The Holocene 13, 365-372.

Lisiecki, L.E., Raymo, M.E., 2005. A Pliocene-Pleistocene stack of 57 globally distributed benthic $\delta^{18}O$ records. Paleoceanography 20, 1-17.

Longhurst, A.R., Glen Harrison, W., 1989. The biological pump: Profiles of plankton production and consumption in the upper ocean. Progress in Oceanography 22, 47-123.

Lorenz, S.J., Kim, J.H., Rimbu, N., Schneider, R.R., Lohmann, G., 2006. Orbitally driven insolation forcing on Holocene climate trends: Evidence from alkenone data and climate modeling. Paleoceanography 21, PA1002, doi: 10.1029/2005PA001152.

Lumpkin, R., Speer, K., 2007. Global ocean meridional overturning. Journal of Physical Oceanography 37, 2550-2562.

M

MacDonald, G.M., Velichkob, A.A., Kremenetskib, C.V., Borisovab, O.K., Golevab, A.A., Andreevb, A.A., Cwynarc, L.C., Ridingc, R.T., Formand, S.L., Edwardse, T.W.D., Aravenae, R., Hammarlundf, D., Szeiczg, J.M., Gattaulinh, V.N., 2000. Holocene treeline history and climate change across northern Eurasia. Quaternary Research 53, 302-311.

Maddison, E.J., 2005. Seasonally laminated Late Quaternary Antarctic sediments. PhD. Thesis, Cardiff University, UK, 218 pp.

Maddison, E.J., Pike, J., Leventer, A., Domack, E., 2005. Deglacial seasonal and sub-seasonal diatom record from Palmer Deep, Antarctica. Journal of Quaternary Science 20(5), 435-446.

Maddison, E.J., Pike, J., Leventer, A., Dunbar, R., Brachfeld, S., Domack, E.W., Manley, P., McClennen, C., 2006. Post-glacial seasonal diatom record of the Mertz Glacier Polynya, East Antarctica. Marine Micropaleontology 60, 66-88.

Mann, M.E., Jones, P.D., 2003. Global surface temperatures over the past two millennia. Geophysical Research Letters 30(15), doi:10.1029/2003GL017814.

Marchal, O., Cacho, I., Stocker, T.F., Grimalt, J.O., Calvo, E., Martrat, B., Shackleton, N., Vautravers, M., Cortijo, E., van Kreveld, S., Andersson, C., Koc, N., Chapman, M., Sbaffi, L., Duplessy, J.-C., Sarnthein, M., Turon, J.-L., Duprat, J., Jansen, E., 2002. Apparent long-term cooling of the sea surface in the northeast Atlantic and Mediterranean during the Holocene. Quaternary Science Reviews 21, 455-483.

Marchitto, T.M., deMenocal, P.B., 2003. Late Holocene variability of upper North Atlantic Deep Water temperature and salinity. Geochemistry, Geophysics and Geosystems 4, doi: 1110.1029/2003GC000598.

Marshall, G.J., 2002. Analysis of recent circulation and thermal advection change on the northern Antarctic Peninsula. International Journal of Climatology 22, 1557–1567.

Marshall, G.J., Stott, P.A., Turner, J., Connolley, W.M., King, J.C., Lachlan-Cope, T.A., 2004 Causes of exceptional atmospheric circulation changes in the Southern Hemisphere. Geophysical Research Letters 31, doi: 10.1029/2004GL019952.

Martin, J., 1990. Glacial-interglacial CO2 change: the iron hypothesis. Paleoceanography 5, 1-13.

Martin-Jézéquel, V., Hildebrand, M., Brzezinski, M.A., 2000. Silicon metabolism in diatoms: Implications for growth. Journal of Phycology 36, 821-840.

Massé, G., Belt, S.T., Allard, W.G., Lewis, C.A., Wakeham, S.G., Rowland, S.J., 2004. Occurrence of novel monocyclic alkenes from diatoms in marine particulate matter and sediments. Organic Geochemistry 35, 813-822.

Massé, G., Rowland, S.J., Sicre, M.-A., Jacob, J., Jansen, E., Belt, S.T., 2007. Abrupt climate changes for Iceland during the last millennium: Evidence from high resolution sea ice reconstructions. Earth and Planetary Science Letters 269, 564-568.

Massom, R., Harris, P.T., Michael, K.J., Potter, M.J., 1998. The distribution and formative processes of latent-heat polynyas in East Antarctica. Annals of Glaciology 27, 420-426.

Masson, V., Vimeux, F., Jouzel, J., Morgan, V., Delmotte, M., Ciais, P., Hammer, C., Johnsen, S., Lipenkov, V.Y., Mosley-Thompson, E., Petit, J.R., Steig, E.J., Stievenard, M., Vaikmae, R., 2000. Holocene climate variability in Antarctica based on 11 ice-core isotopic records. Quaternary Research 54, 348-358.

Masson-Delmotte, V., Landais, A., Combourieu-Nebout, N., von Grafenstein, U., Jouzel, J., Caillon, N., Chappellaz, J., Dahl-Jensen, D., Johnsen, S.J., Stenni, B., 2005. Rapid climate variability during warm and cold periods in polar regions and Europe. Comptes Rendus Geosciences 337, 935-946.

Masson-Delmotte, V., Stenni, B., Jouzel, J., 2004. Common millenial-scale variability of Antarctic and Southern Ocean temperatures during the past 5000 years reconsructed from the EPICA Dome C ice core. The Holocene 14(2), 145-151.

Mayewski, P.A., Maasch, K.A., 2006. Recent warming inconsistent with natural association between temperature and atmospheric circulation over the last 2000 years. Climate of the Past Discussions 2, 327-355.

Mayewski, P.A., Meeker, L.D., Twickler, M.S., Whitlow, S., Qinzhao, Y., Berry Lyons, W., Prentice, M., 1997. Major features and forcing of high-latitude Northern Hemisphere atmospheric circulation using a 110 000-year-long glaciochemical series. Journal of Geophysical Research 102, 26345-26366.

Mayewski, P.A., Meredith, M.P., Summerhayes, C.P., Turner, J., Worby, A., Barrett, P.J., Casassa, G., Bertler, N.A.N., Bracegirdle, T., Garabato, A.C.N., Bromwich, D., Campbell, H., Hamilton, G.S., Lyons, W.B., Maasch, K.A., Aoki, S., Xiao, C., Ommen, T.v., 2009. State of the Antarctic and Southern Ocean climate system. Review of Geophysics 47, RG1003, doi: 1010.1029/2007RG000231.

Mayewski, P.A., Rohling, E.E., Curt Stager, J., Karlen, W., Maasch, K.A., David Meeker, L., Meyerson, E.A., Gasse, F., van Kreveld, S., Holmgren, K., Lee-Thorp, J., Rosqvist, G., Rack, F., Staubwasser, M., Schneider, R.R., Steig, E.J., 2004. Holocene climate variability. Quaternary Research 62, 243-255.

Mayewski, P.A., Twickler, M.S., Whitlow, S.I., Meeker, L.D., Yang, Q., Thomas, J., Kreutz, K., Grootes, P.M., Morse, D.L., Steig, E.J., Waddington, E.D., Saltzman, E.S., Whung, P.Y., Taylor, K.C., 1996. Climate change during the last deglaciation in Antarctica. Science 272, 1636-1638.

Mayr, C., Wille, M., Haberzettl, T., Fey, M., Janssen, S., Lucke, A., Ohlendorf, C., Oliva, G., Schabitz, F., Schleser, G.H., Zolitschka, B., 2007. Holocene variability of the Southern Hemisphere westerlies in Argentinean Patagonia (52°S). Quaternary Science Reviews 26, 579-584.

McAyeal, D.R., 1993. Binge/purge oscillations of the laurentide ice sheet as a cause of the North Atlantic's Heinrich events. Paleoceanography 8 (6), 775–784.

McCave, I.N., Hall, I.R., 2006. Size sorting in marine muds: Processes, pifalls, and prospects for paleoflow-speed proxies. Geochemistry, Geophysics and Geosystems 7, Q10N05, doi: 10.1029/2006GC001284.

McGlone, M.S., 2002. The late Quaternary peat, vegetation and climate history of the southern Oceanic Islands of New Zealand. Quaternary Science Reviews 21, 683-707.

McKnight, T., Hess, D., 2000. Katabatic Winds. Physical Geography: A Landscape Appreciation 131-132.

McManus, J., Oppo, D., Cullen, J., Healey, S., 2003. Marine Isotope Stage 11 (MIS 11): Analog for Holocene and future climate? Geophysical monograph 137, 69-85.

McManus, J.F., Francois, R., Gherardl, J.M., Kelgwin, L., Drown-Leger, S., 2004. Collapse and rapid resumption of Atlantic meridional circulation linked to deglacial climate changes. Nature 428, 834-837.

McMullen, K., Domack, E., Leventer, A., Olson, C., Dunbar, R., Brachfeld, S., 2006. Glacial morphology and sediment formation in the Mertz Trough, East Antarctica. Palaeogeography, Palaeoclimatology, Palaeoecology 231, 169-180.

Meeker, L.D., Mayewski, P.A., 2002. A 1400 year long record of atmospheric circulation over the North Atlantic and Asia. The Holocene 12, 257-266.

Menden-Deuer, S., Lessard, E.J., 2000. Carbon to volume relationships for dinoflagellates, diatoms and other protist plankton. Limnology and Oceanography 45(3), 569-579.

Meredith, M.P., Murphy, E.J., Hawker, E.J., King, J.C., Wallace, M.I., 2008. On the interannual variability of ocean temperatures around South Georgia, Southern Ocean: forcing by El Niño/Southern Oscillation and the Southern Annular Mode. Deep Sea Research Part II 55 (18-19), 2007-2022.

Mikolajewicz, U., 1998. Effect of meltwater input from the Antarctic ice sheet on the thermohaline circulation. Annals of Glaciology 27, 311-315.

Milankovitch, M., 1941. Kanon der erdbestrahlung und seine anwendung auf das eiszeitenproblem. Royal Serb. Acad., Belgrade, Spec. Publ. 133, 1-633.

Mitchell, B.G., Holm-Hansen, O., 1991. Observations and modeling of the Antarctic phytoplankton crop in relation to mixing depth. Deep Sea Research Part II 38 (8-9), 981-1007.

Moberg, A., Sonechkin, D.M., Holmgren, K., Datsenko, M.H., Karlèn, W., 2005. Highly variable Northern Hemisphere temperatures reconstructed from low- and high-resolution proxy data. Nature 433, 613-617.

Monbeirg-Andrieu, M. and Cailleux, A., 1962. Grains éolisés dans les grès erratiques de Terre Adélie. Comptes Rendus sommaires des Séances de la Société géologique de France 5, 151 pp.

Monnin, E., Steig, E.J., Siegenthaler, U., Kawamura, K., Schwander, J., Stauffer, B., Stocker, T.F., Morse, D.L., Barnola, J.-M., Bellier, B., Raynaud, D., Fischer, H., 2004. Evidence for substantial accumulation rate variability in Antarctica during the Holocene, through synchronization of CO_2 in the Taylor Dome, Dome C and DML ice cores. Earth and Planetary Science Letters 224, 45-54.

Moore, J.K., Abbott, M.R., Richman, J.G., Nelson, D.M., 2000. The Southern Ocean at the Last Glacial maximum: A strong sink for atmospheric CO_2. Global Biogeochemical Cycles 14(1), 455-475.

Moran, S.B., Shen, C.C., Edwards, R.L., Edmonds, H.N., Scholten, J.C., Smith, J.N., Ku, T.L., 2005. ^{231}Pa and ^{230}Th in surface sediments of the Arctic Ocean: Implications for ^{231}Pa/^{230}Th fractionation, boundary scavenging, and advective export. Earth and Planetary Science Letters 234, 235-248.

Morgan, V.I., Wookey, C.W., Li, J., Ommen, T.D.V., Skinner, W., Fitzpatrick, M.F., 1997. Site information and initial results from deep ice drilling on Law Dome. Journal of Glaciology 43, 3–10.

Mortlock, R.A., Froelich, P.N., 1989. A simple method for the rapid determination of biogenic opal in pelagic marine sediments. Deep Sea Research Part I 36(9), 1415-1426.

Moy, C.M., Seltzer, G.O., Rodbell, D.T., Anderson, D.M., 2002. Variability of El Niño/Southern Oscillation activity at millennial timescales during the Holocene epoch. Nature 420, 162-165.

Mullan, A.B., Hickman, J.S. (1990). Chapter 2: Meteorology. In "Antarctic Sector of the Pacific". (G.P. Glasby, Ed.), Elsevier, Amsterdam, 21-54.

Müller, P.J., Schneider, R., 1993. An automated leaching method for the determination of opal in sediments and particulate matter. Deep Sea Research Part I 40, 425-444.

Muscheler, R., Beer, J., Wagner, G., Finkel, R.C., 2000. Changes in deep-water formation during the Younger Dryas event inferred from ^{10}Be and ^{14}C records. Nature 408, 567-570.

Muscheler, R., Beer, J., Wagner, G., Laj, C., Kissel, C., Raisbeck, G.M., Yiou, F., Kubik, P.W., 2004. Changes in the carbon cycle during the last deglaciation as indicated by the comparison of ^{10}Be and ^{14}C records. Earth and Planetary Science Letters 219, 325-340.

Muscheler, R., Joos, F., Beer, J., Muller, S.A., Vonmoos, M., Snowball, I., 2007. Solar activity during the last 1000 yr inferred from radionuclide records. Quaternary Science Reviews 26, 82-97.

N

Naughton, F., Bourillet, J.F., Sanchez Goñi, M.F., Turon, J.L., Jouanneau, J.M., 2007. Long-term and millennial-scale climate variability in northwestern France during the last 8850 years. The Holocene 17, 939-953.

Naughton, F., Sanchez Goñi, M.F., Kageyama, M., Bard, E., Duprat, J., Cortijo, E., Desprat, S., Malaizé, B., Joly, C., Rostek, F., Turon, J.L., (in revision). Wet to dry climatic trend in north western Iberia within Heinrich events. In revision to Earth and Planetary Science Letters.

Nelson, D.M., Brzezinski, M.A., Sigmon, D.E., Franck, V.M., 2001. A seasonal progression of Si limitation in the Pacific sector of the Southern Ocean. Deep Sea Research Part II 48, 3973-3995.

Nelson, D.M., DeMaster, D.J., Dunbar, R.B., Smith Jr., W.O., 1996. Cycling of organic carbon and biogenic silica in the Southern Ocean: estimates of water-column and sedimentary fluxes on the Ross Sea continental shelf. Journal of Geophysical Research 101(C8), 18,519-18,532.

Nelson, D.M., Tréguer, P., brzezinski, M.A., Leynaert, A., Quéguiner, B., 1995. Production and dissolution of biogenic silica in the ocean: Revised global estimates, comparison with regional data and relationship to biogenic sedimentation. Global Biogeochemical Cycle 9(3), 359-372.

Nicol, S., Pauly, T., Bindoff, N.L., Strutton, P.G., 2000. "BROKE" a biological/oceanographic survey off the coast of East Antarctica (80-150°E) carried out in January-March 1996. Deep Sea Research Part II 47, 2281-2297.

Nielsen, S.H.H., Koç, N., Crosta, X., 2004. Holocene climate in the Atlantic sector of the Southern Ocean: Controlled by insolation or oceanic circulation? Geology 32, 317-320.

Noren, A.J., Biennan, P.R., Steig, E.J., Lini, A., Southon, J., 2002. Millennial-scale storminess variability in the northeastern United States during the Holocene epoch. Nature 419, 821-824.

Nunes Vaz, R., Lennon, G., 1996. Physical oceanography of the Prydz bay region of Antarctic waters. Deep-Sea Research Part I 43 (5), 603-641.

O

O'Brien, P.E., Harris, P.T., 1996. Patterns of glacial erosion and deposition in Prydz Bay and the past behaviour of the Lambert Glacier. Papers and Proceedings - Royal Society of Tasmania 130, 79-85.

Oerlemans, J., Nick, F.M., 2006. Modelling the advance-retreat cycle of a tidewater glacier with simple sediment dynamics. Global and Planetary Change 50, 148-160.

Oke, P.R., England, M.H., 2004. Oceanic response to changes in the latitude of the Southern Hemisphere subpolar westerly winds. Journal of Climate 17, 1040–1054.

Oppo, D. W., McManus, J. F., Cullen, J. L., 2003. Deepwater variability in the Holocene Epoch. Nature 422, 277-278.

Orsi, A.H., Johnson, G.C., Bullister, J.L., 1999. Circulation, mixing, and production of Antarctic Bottom Water. Progress in Oceanography 43, 55-109.

Orsi, A.H., Whitworth, T., Nowlin, W.D., 1995. On the meridional extent and fronts of the Antarctic Circumpolar Current. Deep Sea Research Part I 42, 641-673.

Osborn, T.J., 1997. Thermohaline oscillations in the LSG OGCM: Propagating anomalies and sensitivity to parameterizations. Journal of Physical Oceanography 27, 2233-2255.

P

Pahnke, K., Zahn, R., 2005. Southern Hemisphere water mass conversion linked with North Atlantic climate variability. Science 307, 1741-1746.

Parish, T.R., 1988. Surface winds over the Antarctic continent: a review. Reviews of Geophysics 26, 169-180.

Parkinson, C.L., 2002. Trends in the length of the Southern Ocean sea-ice season, 1979-99. Annals of Glaciology 34, 435-440.

Peacock, S., Lane, E., Restrepo, J.M., 2006. A possible sequence of events for the generalized glacial-interglacial cycle. Global Biogeochemical Cycles 20, GB2010, doi: 10.1029/ 2005GB002448.

Periard, C., Pettre, P., 1993. Some aspects of the climatology of Dumont d'Urville, Adélie Land, Antarctica. International Journal of Climatology 13, 313-327.

Peters, K.E., Sweeney, R.E., Kaplan, I.R., 1978. Correlation of carbon and nitrogen stable isotopes in sedimentary organic matter. Limnology and Oceanology 23, 598–604.

Petit, J.R., Raynaud, D., Barkov, N.I., Barnola, J.M., Basile, I., Benders, M., Chappellaz, J., Davis, M., delaygue, G., Delmotte, M., kotlyakov, V.M., Legrand, M., Lipenkov, V.Y., lorius, C., Pepin, L., Ritz, C., Saltzman, E., Stievenard, M., 1999. Climate and atmospheric history of the past 420.000 years from the Vostok ice core, Antarctica. Nature 399, 429-436.

Pétus, C., Valencia, C.G., Thomas, Y.F., Cesaracio, M., 2007. Etude de la variabilité saisonnière et interannuelle de la résurgence de la guajira (Colombie) par analyse de données satellitaires AMI-WIND, SEAWINDS et AVHRR. Revue Télédétection 7, 143-156.

Pierce, D.W., Barnett, T.P., Mikolajewicz, U., 1995. Competing roles of heat and freshwater flux in forcing thermohaline oscillations. Journal of Physical Oceanography 25(9), 2046-2064.

Pike, J., Crosta, X., Maddison, E.J., Stickley, C.E., Denis, D., Barbara, L., Renssen, H., Leventer, A., (Accepted). Observations on the relationship between the Antarctic coastal diatoms *Thalassiosira antarctica* Comber and *Porosira glacialis* (Grunow) Jørgensen and sea ice concentrations during the Late Quaternary. Accepted in Marine Micropalaeontology.

Pike, J., Kemp, A.E.S., 1997. Early Holocene decadal-scale ocean variability recorded in Gulf of California laminated sediments. Paleoceanography 12(2), 227-238.

Polyakov, I., Martin, S., 2000. Interaction of the Okhotsk Sea diurnal tides with the Kashevarov Bank polynya. Journal of Geophysical Research 105, 3281-3294.

Poore, R.Z., Dowsett, H.J., Verardo, S., Quinn, T.M., 2003. Millennial- to century-scale variability in Gulf of Mexico Holocene climate records. Paleoceanography 18(2), doi: 10.1029/2002PA000868.

Porter, S.C., 1975. Equilibrium-line altitudes of late Quaternary glaciers in the Southern Alps, New Zealand. Quaternary Research 5, 27-47.

Presti, M., De Santis, L., Busetti, M., Harris, P.T., 2003. Late Pleistocene and Holocene sedimentation on the George V Continental Shelf, East Antarctica. Deep Sea Research Part II 50, 1441-1461.

R

Ragueneau, O., Schultes, S., Bidle, K., Claquin, P., Moriceau, B., 2006. Si and C interactions in the world ocean: Importance of ecological processes and implications for the role of diatoms in the biological pump. Global Biogeochemical Cycles 20, GB4S02, doi: 10.1029/2006GB002688.

Rahmstorf, S., 2002. Ocean circulation and climate during the past 120,000 years. Nature 419, 207-214.

Rahmstorf, S., Schellnhuber, H.J., 2006. Der Klimawandel – Diagnose, Prognose, Therapie. SBN 3-406-50866-9, C.H. Beck, München.

Rasmussen, T.L., Backstrom, D., Heinemeier, J., Klitgaard-Kristensen, D., Knutz, P.C., Kuijpers, A., Lassen, S., Thomsen, E., Troelstra, S.R., Van Weering, T.C.E., 2002. The Faroe-Shetland Gateway: Late Quaternary water mass exchange between the Nordic seas and the north-eastern Atlantic. Marine Geology 188, 165-192.

Raspopov, O.M., Shumilov, O.I., Kasatkina, E.A., 1998. Cosmic Rays as Main Factor of Influence of Solar Variability on Climatic and Atmosperic Parameters. Biofizika 43, 907-908.

Rathburn, A.E., Pichon, J.J., Ayress, M.A., De Deckker, P., 1997. Microfossil and stable-isotope evidence for changes in Late Holocene palaeoproductivity and palaeoceanographic conditions in the Prydz Bay region of Antarctica. Palaeogeography, Palaeoclimatology, Palaeoecology 131, 485-510.

Rayner, N.A., Parker, D.E., Horton, E.B., Folland, C.K., Alexander, L.V., Rowell, D.P., Kent, E.C., Kaplan, A., 2003. Global analyses of sea surface temperature, sea ice, and night marine air temperature since the late nineteenth century. Journal of Geophysical Research 108(D14), doi:10.1029/2002JD002670.

Renssen, H., Goosse, H., Fichefet, T., 2002. Modeling the effect of freshwater pulses on the early Holocene climate: The influence of high-frequency climate variability. Paleoceanography 17, doi: 10.1029/2001PA000649.

Renssen, H., Goosse, H., Fichefet, T., Brovkin, V., Driesschaert, E., Wolk, F., 2005a. Simulating the Holocene climate evolution at northern high latitudes using a coupled atmosphere-sea ice-ocean-vegetation model. Climate Dynamics 24, 23-43.

Renssen, H., Goosse, H., Fichefet, T., Campin, J.-M., 2001. The 8.2 kyr BP event simulated by a global atmosphere/sea-ice/ocean model. Geophysical Research Letters 28, 1567-1570.

Renssen, H., Goosse, H., Fichefet, T., Massom-Delmotte, V.a., Koç, N., 2005b. Holocene climate evolution in the high-latitude Southern Hemisphere simulated by a coupled atmosphere-sea-ice-ocean-vegetation model. The Holocene 15, 951-964.

Richardson, G., Wadley, M.R., Heywood, K.J., Stevens, D.P., Banks, H.T., 2005. Short-term climate response to a freshwater pulse in the Southern Ocean. Geophysical Research Letters 32, 1-4.

Rignot, E.A., Jacobs, S.S., 2002. Rapid Bottom Melting Widespread near Antarctic Ice Sheet Grounding Lines. Science 296, 2020-2023.

Rimbu, N., Lohmann, G., Lorenze, S.J., Kim, J.H., Schneider, R.R., 2004. Holocene climate variability as derived from alkenone sea surface temperature and coupled ocean-atmosphere model experiments. Climate Dynamics 23, 215-227.

Rind, D., 2000. Relating paleoclimate data and past temperature gradients: Some suggestive rules. Quaternary Science Reviews 19, 381-390.

Rind, D., 2002. The sun's role in climate variations. Science 296, 673-677.

Rintoul, S.R., 1998. On the origins and influence of Adélie Land bottom water. Ocean, Ice and Atmosphere: Interactions at the Antarctic Continental Margin in: S.S. Jacobs and R.F. Weiss (eds.), Antarctic Research Series 75, 151–171.

Rintoul, S.R., Bullister, J.L., 1999. A late winter hydrographic section from Tasmania to Antarctica. Deep Sea Research Part I 46, 1417-1454.

Rintoul, S.R., Hughes, C.W., Olbers, D., 2001. The Antarctic Circumpolar Current. In “Ocean Circulation and Climate: Observing and Modelling the Global Ocean”, Academy Press: G. Siedler, J. Church, and J. Gould (eds.), 271-302.

Risebrobakken, B., Jansen, E., Andersson, C., Mjelde, E., Hevroy, K., 2003. A high-resolution study of Holocene paleoclimatic and paleoceanographic changes in the Nordic seas. Paleoceanography 18(1), doi: 10.1029/2002PA000764.

Roberts, D., McMinn, A., 1996. Relationships between surface sediment diatom assemblages and water chemistry gradients in saline lakes of the Vestfold Hills, Antarctica. Antarctic Science 8, 331-341.

Roberts, D., McMinn, A., Cremer, H., Gore, D.B., Melles, M., 2004. The Holocene evolution and palaeosalinity history of Beall Lake, Windmill Islands (East Antarctica) using an expanded diatom-based weighted averaging model. Palaeogeography, Palaeoclimatology, Palaeoecology 208, 121-140.

Roche, D., Paillard, D., Cortijo, E., 2004. Constraints on the duration and freshwater release of Heinrich event 4 through isotope modelling. Nature 432, 379-382.

Rodbell, D.T., Seltzer, G.O., Anderson, D.M., Abbott, M.B., Enfield, D.B., Newman, J.H., 1999. A ~15.000-year record of El Nino-driven alluviation in south-western Ecuador. Science 283, 516-520.

Rohling, E.J., Pälike, H., 2005. Centennial-scale climate cooling with a sudden cold event around 8200 years ago. Nature 434, 975–979.

Rosqvist, G.C., Schuber, P., 2003. Millennial-scale climate changes on South Georgia, Southern Ocean. Quaternary Research 59, 470-475.

Rowland, S.J., Belt, S.T., Wraige, E.J., Masse, G., Roussakis, C., Robert, J.M., 2001. Effects of temperature on polyunsaturation in cytostatic lipids of Haslea ostrearia. Phytochemistry 56, 597-602.

Rowland, S.J., Robson, J.N., 1990. The widespread occurrence of highly branched acyclic C20, C25 and C30 hydrocarbons in recent sediments and biota - a review. Marine Environmental Research 30, 191-216.

Ruddiman, W.F., 2001. Earth's Climate: Past and Future. Publisher: W.H. Freeman & Company 465 pp.

Russell, J.L., Dixon, K.W., Gnanadesikan, A., Stouffer, R.J., Toggweiler, J.R., 2006. The Southern hemisphere westerlies in a warming world: Propping open the door to the deep ocean. Journal of Climate 19, 6382-6390.

Rutgers van der Loeff, M.M., Berger, G.W., 1993. Scavenging of ^{230}Th and ^{231}Pa near the Antarctic Polar Front in the South Atlantic. Deep Sea Research Part I 40, 339-357.

S

Salvignac, M.E., 1998. Variabilité hydrologique et climatique dans l'Océan Austral (secteur indien) au cours du Quaternaire terminal. Essai de corrélations inter-hémisphériques. Thèse Université de Bordeaux 1, France, 308 pp.

Sambrotto, R.N., Matsuda, A., Vaillancourt, R., Brown, M., Langdon, C., Jacobs, S.S., Measures, C., 2003. Summer plankton production and nutrient consumption patterns in the Mertz Glacier Region of East Antarctica. Deep Sea Research Part II 50, 1393-1414.

Samson, C.R., Sikes, E.L., Howard, W.R., 2005. Deglacial paleoceanographic history of the Bay of Plenty, New Zealand. Paleoceanography 20, PA4017, doi: 10.1029/2004PA001088.

Sarmiento, J.L., Hughes, T.M.C., Stouffer, R.J., Manabe, S., 1998. Simulated response of the ocean carbon cycle to anthropogenic climate warming. Nature 393, 245-249.

Sarnthein, M., 1994. Changes in east Atlantic deepwater circulation over the last 30 000 years: eight time slice reconstructions. Paleoceanography 9, 209-267.

Schaeffer, M., F.M., S., Opsteegh, J.D., Goosse, H., 2002. Intrinsic limits to predictability of abrupt regional climate change in IPCC SRES scenarios. Geophysical Research Letters 29, doi: 10.1029/2002GL015254.

Schmidt, S., 1991. Cycle des radionucléides naturels dans l'océan: exemples d'application à l'étude des flux de matières en méditerranée occidentale et dans l'Atlantique Nord. Thèse Université Paris VI, France, 157 pp.

Schmidt, S., 2006. Impact of Mediterranean Outflow Water on particle dynamics in intermediate waters of the North-East Atlantic, as revealed by ^{234}Th and ^{228}Th. Marine chemistry 100, 289-298.

Schmittner, A., 2003. Southern Ocean sea ice and radiocarbon ages of glacial bottom waters. Earth and Planetary Science Letters 213, 53-62.

Schneider, R.R., Müller, P.J., Ruhland, G., 1995. Late Quaternary surface circulation in the east equatorial South Atlantic: evidence from alkenone sea surface temperatures. Paleoceanography 10, 197-219.

Schrader, H.J., Gersonde, R. (1978). Diatoms and Silicoflagellates. "Micropaleontological Counting Methods and Techniques - An exercise on an Eight Meters Section of the Lower Pliocene of Capo Rossello" in Zachariasses et al., (eds.), Silicy, Utrecht Micropaleontology Bulletin, 129-176.

Schroder-Ritzrau, A., Mangini, A., Lomitschka, M., 2003. Deep-sea corals evidence periodic reduced ventilation in the North Atlantic during the LGM/Holocene transition. Earth and Planetary Science Letters 216, 399-410.

Schulmeister, J., 1999. Australasian evidence for mid-Holocene climate change implies precessional control of Walker Circulation in the Pacific. Quaternary International 57-58, 81–91.

Schwab, M.J., 1998. Reconstruction of Late Quaternary climatic and environmental history of the Schirmacher Oasis and the Wohlthat Massif (East Antarctica). Reports on Polar Research 293, 1–128.

Schwabe, H., Solar observations during 1843. Astronomische Nachrichten 21, 283–286.

Schweitzer, P.N., 1995. Monthly averaged polar sea ice concentration. U.S. Geological Survey Digital Data Series, Virginia.

Sedwick, P.N., DiTullio, G.R., 1997. Regulation of algal blooms in Antarctic shelf waters by the release of iron from melting sea ice. Geophysical Research Letters 24(20), 2515-2518.

Sedwick, P.N., DiTullio, G.R., Mackey, D.J., 2000. Iron and manganese in the Ross Sea, Antarctica: Seasonal iron limitation in Antarctic shelf waters. Journal of Geophysical Research C: Oceans 105, 11321-11336.

Selvaraj, K., Chen, C.T.A., Lou, J.Y., 2007. Holocene East Asian monsoon variability: Links to solar and tropical Pacific forcing. Geophysical Research Letters 34, L01703, doi: 10.1029/2006GL028155.

Sexton, D.M.H., 2001. The effect of stratospheric ozone depletion on the phase of the Antarctic Oscillation Geophysical Research Letters 28, 3697–3700.

Shin, S.I., Liu, Z., Otto-Bliesner, B.L., Kutzbach, J.E., Vavrus, S., 2003. Southern Ocean sea-ice control of the glacial North Atlantic thermohaline circulation. Geophysical Research Letters 30 (2), doi: 10.1029/2002GL015513.

Shindell, D.T., Schmidt, G.A., Mann, M.E., Rind, D., Waple, A., 2001. Solar forcing of regional climate change during the Maunder Minimum. Science 294, 2149-2152.

Shiotani, M., Kuroi, K., Hirota, I., 1990. Eastward travelling waves in the Southern Hemisphere stratosphere during the spring of 1983. Quarterly Journal of the Royal Meteorological Society 116, 913-927.

Shipp, S., Anderson, J., Domack, E., 1999. Late Pleistocene-Holocene retreat of the West Antarctic Ice-Sheet system in the Ross Sea: Part 1 - Geophysical results. Bulletin of the Geological Society of America 111, 1486-1516.

Sicre, M.A., Labeyrie, L., Ezat, U., Duprat, J., Turon, J.L., Schmidt, S., Michel, E., Mazaud, A., 2005. Mid-latitude Southern Indian Ocean response to Northern Hemisphere Heinrich events. Earth and Planetary Science Letters 240, 724-731.

Silvestri, G.E., Vera, C.S., 2003. Antarctic oscillation signal on precipitation anomalies over south-eastern South America. Geophysical Research Letters 30(21), doi: 10.1029/2003GL018277.

Simmonds, I., Budd, W.F., 1991. Sensitivity of the Southern Hemisphere circulation to leads in the Antarctic pack ice. Quarterly Journal of the Royal Meteorological Society 117, 1003-1024.

Sinninghe Damste, J.S., Rijpstra, W.I.C., Schouten, S., Fuerst, J.A., Jetten, M.S.M., Strous, M., 2004. The occurrence of hopanoids in planctomycetes: Implications for the sedimentary biomarker record. Organic Geochemistry 35, 561-566.

Smetacek, V., Assmy, P., Henjes, J., 2004. The role of grazing in structuring Southern Ocean pelagic ecosystems and biogeochemical cycles. Antarctic Science 16, 541-558.

Smetacek, V., Nicol, S., 2005. Polar ocean ecosystems in a changing world. Nature 437, 362-368.

Smith Jr, W.O., Gordon, L.I., 1997. Hyperproductivity of the Ross Sea (Antarctica) polynya during austral spring. Geophysical Research Letters 24, 233-236.

Smith Jr, W.O., Lancelot, C., 2004. Bottom-up versus top-down control in phytoplankton of the Southern Ocean. Antarctic Science 16, 531-539.

Smith Jr, W.O., Nelson, D.M., 1985. Phytoplankton biomass near a receding ice-edge in the Ross Sea. Antarctic nutrient cycles and food webs 70-77.

Smith, J.A., Bentley, M.J., Hodgson, D.A., Roberts, S.J., Leng, M.J., Lloyd, J.M., Barrett, M.S., Bryant, C., Sugden, D.E., 2007. Oceanic and atmospheric forcing of early Holocene ice shelf retreat, George VI Ice Shelf, Antarctica Peninsula. Quaternary Science Reviews 26, 500-516.

Smith, N., Tréguer, P., 1994. Physical and chemical oceanography in the vicinity of Prydz bay, Antarctica. "Southern Ocean Ecology: The BIOMASS Perspective" in N. Smith and P. Tréguer, (eds.), Cambridge University Press.

Smith, N.R., Zhaoquian, D., Kerry, K.R., Wright, S., 1984. Water masses and circulation in the Prydz Bay, Antarctica. Deep Sea Research I 31(9), 1121-1147.

Solanki, S.K., Usoskin, I.G., Kromer, B., Schüssler, M., Beer, J., 2004. Unusual activity of the Sun during recent decades compared to the previous 11,000 years. Nature 431, 1084-1087.

Solignac, S., de Vernal, A., Hillaire-Marcel, C., 2004. Holocene sea-surface conditions in the North Atlantic--contrasted trends and regimes in the western and eastern sectors (Labrador Sea vs. Iceland Basin). Quaternary Science Reviews 23, 319-334.

Solomina, O., Haeberli, W., Kull, C., Wiles, G., 2008. Historical and Holocene glacier-climate variations: General concepts and overview. Global and Planetary Change 60, 1-9.

Sonett, C.P., Suess, H.E., 1984. Correlation of bristlecone pine ring widths with atmospheric ^{14}C variations: A climate-Sun relation. Nature 307, 141-143.

Spencer, D.W., Bacon, M.P., Brewer, P.G., 1981. Models of the distribution of ^{210}Pb in a section across the North Equatorial Atlantic Ocean. Journal of Marine Research 39, 119–138.

Stager, J.C., Cumming, B.F., Meeker, L.D., 2003. A 10,000-year high-resolution diatom record from Pilkington Bay, Lake Victoria, East Africa. Quaternary Research 59, 172-181.

Stager, J.C., Mayewski, P.A., 1997. Abrupt Early to mid-Holocene climatic transition registered at the Equator and the Poles. Science 276, 1834-1836.

Stammerjohn, S.E., Drinkwater, M.R., Smith, R.C., Liu, X., 2003. Ice-atmosphere interactions during sea-ice advance and retreat in the western Antarctic Peninsula region. Journal of Geophysical Research 108(C10), doi: 10.1029/2002JC001543.

Steig, E.J., Morse, D.L., Waddington, E.D., Stuiver, M., Grootes, P.M., Mayewski, P.A., Twickler, M.S., Whitlows, S.I., 2000. Wisonsinan and Holocence climate history from an ice core at Taylor Dome, western Ross embayment, Antarctica. Geografiska Annaler, Series A: Physical Geography 82, 213-232.

Steig, E.J., Schneider, D.P., Rutherford, S.D., Mann, M.E., Comiso, J.C., Shindell, D.T., 2009. Warming of the Antarctic ice-sheet surface since the 1957 International Geophysical Year. Nature 457, 459-463.

Stickley, C.E., Pike, J., Leventer, A., Dunbar, R., Domack, E.W., Brachfeld, S., Manley, P., McClennen, C., 2005. Deglacial ocean and climate seasonality in laminated diatom sediments, Mac.Robertson Shelf, Antarctica. Palaeogeography, Palaeoclimatology, Palaeoecology 227, 290-310.

Stott, L., Cannariato, K., Thunell, R., Haug, G.H., Koutavas, A., Lund, S., 2004. Decline of surface temperature and salinity in the western tropical Pacific Ocean in the Holocene epoch. Nature 430, 56-59.

Stouffer, R.J., Seidov, D., Haupt, B.J., 2007. Climate response to external sources of freshwater: North Atlantic versus the Southern Ocean. Journal of Climate 20, 436-448.

Strutton, P.G., Brian Griffiths, F., Waters, R.L., Wright, S.W., Bindoff, N.L., 2000. Primary productivity off the coast of East Antarctica (80-150°E): January to March 1996. Deep Sea Research Part II 47, 2327-2362.

Stuiver, M., Braziunas, T.F., 1993. Sun, ocean, climate and atmospheric $^{14}CO_2$, an evaluation of causal and spectral relationships. The Holocene 3, 289-305.

Stuiver, M., Reimer, P.J., Braziunas, T.F., 1998. High-precision radiocarbon age calibration for terrestrial and marine samples. Radiocarbon 40(3), 1127-1151.

Stuiver, M., Reimer, P.J., Reimer, R.W., 2005. CALIB 5.0. [WWW program and documentation].

Stuut, J.B., Crosta, X., Borg, K.v.d., Schneider, R., 2004. Relationship between Antarctic sea ice and southwest African climate during the last Quaternary. Geology 32(10), 909-912.

Stuut, J.B., Lamy, F., 2004. Climate variability at the southern boundaries of the Namib (southwestern Africa) and Atacama (northern Chile) coastal deserts during the last 120.000 yr. Quaternary Research 62, 301-309.

Suman, D.O., Bacon, M.P., 1989. Variations in Holocene sedimentation in the North American Basin determined from ^{230}Th measurements. Deep Sea Research Part I 36(6), 869-878.

Sweeney, C., Hansell, D.A., Carlson, C.A., Codispoti, L.A., Gordon, L.I., Marra, J., Millero, F.J., Smith, W.O., Takahashi, T., 2000. Biogeochemical regimes, net community production

and carbon export in the Ross Sea, Antarctica. Deep Sea Research Part II 47, 3369-3394.

T

Takeda, S., 1998. Influence of iron availability on nutrient consumption ratio of diatoms in oceanic waters. Nature 393, 774-777.

Tamura, T., Ohshima, K.I., Nihashi, S., 2008. Mapping of sea ice production for Antarctic coastal polynyas. Geophysical Research Letters 35, L07606, doi: 10.1029/2007GL032903..

Taylor, F., Leventer, A., 2003. Late Quaternary palaeoenvironments in Prydz Bay, East Antarctica: Interpretations from marine diatoms. Antarctic Science 15, 512-521.

Taylor, F., McMinn, A., 2002. Late Quaternary diatom assemblages from Prydz Bay, Eastern Antarctica. Quaternary Research 57, 151-161.

Tchernia, P., 1978. Océan Austral. « Océanographie Régionale, Description Physique des Océans et des Mers » dans Ecole Nationale Supérieure de Techniques Avancées, 45-85.

Thompson, D.W.J., Solomon, S., 2002. Interpretation of recent Southern Hemisphere climate change. Science 296, 895-899.

Thompson, D.W.J., Wallace, J.M., 1998. The Arctic oscillation signature in the wintertime geopotential height and temperature fields. Geophysical Research Letters 25, 1297-1300.

Thompson, D.W.J., Wallace, J.M., 2000. Annular modes in the extratropical circulation. Part II: Trends. Journal of Climate 13, 1018-1036.

Thompson, L.G., Mosley-Thompson, E., Davis, M.E., Henderson, K.A., Brecher, H.H., Zagorodnov, V.S., Mashiotta, T.A., Lin, P.N., Mikhalenko, V.N., Hardy, D.R., Beer, J., 2002. Kilimanjaro ice core records: Evidence of holocene climate change in tropical Africa. Science 298, 589-593.

Thompson, L.G., Mosley-Thompson, E., Davis, M.E., Lin, P.N., Henderson, K.A., Cole-Dai, J., Bolzan, J.F., Liu, K.B., 1995. Late glacial stage and holocene tropical ice core records from Huascarán, Peru. Science 269, 46-50.

Timmermans, K.R., Veldhuis, M.J.W., Laan, P., Brussaard, C.P.D., 2008. Probing natural iron fertilization near the Kerguelen (Southern Ocean) using natural phytoplankton assemblages and diatom cultures. Deep-Sea Research Part II 55, 693-705.

Toggweiler, J.R., Russell, J.L., Carson, S.R., 2006. Midlatitude westerlies, atmospheric CO_2, and climate change during the ice ages. Paleoceanography 21, PA2005, doi: 10.1029/2005PA001154.

Tortell, P.D., Payne, C.D., Li, Y., Trimborn, S., Rost, B., Smith, W.O., Riesselman, C., Dunbar, R.B., Sedwick, P., DiTullio, G.R., 2008. CO_2 sensitivity of Southern Ocean phytoplankton. Geophysical Research Letters 35, L04605, doi: 10.1029/2007GL032583.

Tréguer, P., Gueneley, S., Kamatani, A., 1988. Biogenic silica and particulate organic matter from the Indian sector of the Southern Ocean. Marine Chemistry 23, 167-180.

Tréguer, P., Jacques, G., 1992. Dynamics of nutrients and phytoplaknton, and fluxes of carbon, nitrogen and silicon in the Antarctic Ocean. Polar Biology 12, 149-162.

Turner, J., Colwell, S.R., Marshall, G.J., Lachlan-Cope, T.A., Carleton, A.M., Jones, P.D., Lagun, V., Reid, P.A., Iagovkina, S., 2005. Antarctic climate change during the last 50 years. International Journal of climatology 25, 279–294.

V

Vaillancourt, R.D., Sambrotto, R.N., Green, S., Matsuda, A., 2003. Phytoplankton biomass and photosynthetic competency in the summertime Mertz Glacier Region of East Antarctica. Deep Sea Research Part II 50, 1415-1440.

van Beek, P., Reyss, J.L., Paterne, M., Gersonde, R., Loeff, M.R.v.d., Khun, G., 2002. ^{226}Ra in barite: Absolute dating of Holocene Southern Ocean sediments and reconstruction of sea-surface reservoir ages. Geology 30(8), 731-734.

van Geel, B., Raspopov, O.M., Renssen, H., Plicht, J.v.d., Dergachev, V.A., Meijer, H.A.J., 1999. The role of solar forcing upon climate change. Quaternary Science Reviews 18, 331-338.

van Geel, B., Renssen, H., 1998. Abrupt climate change around 2,650 BP in North-West Europe: evidence for climatic teleconnections and a tentative explanation. "Water, environment and society in times of climatic change" in A.S. Issar, and N. Brown, (eds.), Kluwer, Dordrecht, 21-41.

van Ommen, T.D., Morgan, V.I., Curran, M.A.J., 2004. Deglacial and Holocene changes in accumulation at Law Dome. Annals of Glaciology 39, 359-365.

Vare, L.L., Massé, G., Gregory, T.R., Smart, C.W., Belt, S.T., 2009. Sea ice variations in the central Canadian Arctic Archipelago during the Holocene. Quaternary Science Reviews doi:10.1016/j.quascirev.2009.01.013.

Veeh, H.H., McCorkle, D.C., Heggie, D.T., 2000. Glacial/interglacial variations of sedimentation on the West Australian continental margin: constraints from excess ^{230}Th. Marine Geology 166, 11-30.

Verkulich, S.R., Melles, M., Hubberten, H.-W., Pushina, Z.V., 2002. Holocene environmental changes and evolution of Figurnoye Lake in the southern Bunger Hills, East Antarctica. Journal of Paleolimnology 28, 253-267.

Verleyen, E., Hodgson, D.A., Sabbe, K., Vyverman, W., 2004. Late quaternary deglaciation and climate history of the Larsemann Hills (East Antarctica). Journal of Quaternary Science 19, 361-375.

Villa-Martínez, R., Villagrán, C., Jenny, B., 2003. The last 7500 cal yr B.P. of westerly rainfall in Central Chile inferred from a high-resolution pollen record from Laguna Aculeo (34°S). Quaternary Research 60, 284-293.

Vimeux, F., Masson, V., Jouzel, J., Petit, J.R., Steig, E.J., Stievenard, M., Vaikmae, R., White, J.W.C., 2001. Holocene hydrological cycle changes in the Southern Hemisphere documented in East Antarctic deuterium excess records. Climate Dynamics 17, 503-513.

Volkman, J.K., Barrett, S.M., Dunstan, G.A., 1994. C25 and C30 highly branched isoprenoid alkenes in laboratory cultures of two marine diatoms. Organic Geochemistry 21, 407-414.

Vonmoos, M., Beer, J., Muscheler, R., 2006. Large variations in Holocene solar activity: Constraints from ^{10}Be in the Greenland Ice Core Project ice core. Journal of Geophysical Research 111, A10105, doi: 10.1029/2005JA011500.

W

Wagner, B., Cremer, H., Hultzsch, N., Gore, D.B., Melles, M., 2004. Late Pleistocene and Holocene history of Lake Terrasovoje, Amery Oasis, East Antarctica, and its climatic and environmental implications. Journal of Paleolimnology 32, 321-339.

Wagner, B., Melles, M., 2007. The heterogeneity of Holocene climatic and environmental history along the East Antarctic coastal regions. in Antarctica: a Keystone in a Changing World - Online Proceedings of the 10th ISAES, edited by A.K. Cooper and C.R. Raymond et al., USGS Open-file Report 2007-1047, Extended Abstract 161, 4 pp.

Wang, Y., Cheng, H., Edwards, R.L., He, Y., Kong, X., An, Z., Wu, J., Kelly, M.J., Dykoski, C.A., Li, X., 2005. The holocene Asian monsoon: Links to solar changes and North Atlantic climate. Science 308, 854-857.

Wanner, H., Beer, J., Bütikofer, J., Crowley, T.J., Cubasch, U., Flückiger, J., Goosse, H., Grosjean, M., Joos, F., Kaplan, J.O., Küttel, M., Müller, S.A., Prentice, I.C., Solomina, O., Stocker, T.F., Tarasov, P., Wagner, M., Widmann, M., 2008. Mid- to Late Holocene climate change: an overview. Quaternary Science Reviews 27, 1791-1828.

Waser, N.A.D., Harrison, P.J., Nielsen, B., Calvert, S.E., Turpin, D.H., 1998. Nitrogen isotope fractionation during the uptake and assimilation of nitrate, nitrite, ammonium, and urea by a marine diatom. Limnology and Oceanography 43, 215-224.

Weber, S.L., Crowley, T.J., der Schrier, G., 2004. Solar irradiance forcing of centennial climate variability during the Holocene. Climate Dynamics 22, 539-553.

Weber, S.L., Oerlemans, J., 2003. Holocene glacier variability: Three case studies using an intermediate-complexity climate model. The Holocene 13, 353-363.

White, W.B., Peterson, R.G., 1996. An Antarctic circumpolar wave in surface pressure, wind, temperature and sea-ice extent. Nature 380, 699-702.

Whitworth III, T., Orsi, A.H., Kim, S.J., Nowlin Jr., W.D., Locarnini, R.A., 1998. "Water masses and mixing near the Antarctic Slope Front" - Interactions at the Antarctic Continental Margins in S. S. Jacobs & R. F. Weiss (eds.), Washington, DC: American Geophysical Union, Antarctic Research Series 74, 1–27.

Williams, G.D., Bindoff, N.L., 2003. Wintertime oceanography of the Adélie Depression. Deep Sea Research Part II 50, 1373-1392.

Williams, P.W., King, D.N.T., Zhao, J.-X., Collerson, K.D., 2004. Speleothem master chronologies: combined Holocene 18O and 13C records from the North Island of New Zealand and their palaeoenvironmental interpretation. The Holocene 14, 194-208.

Wong., A.P.S., 1994. Structure and Dynamics of Prydz Bay, Antarctica, as Inferred from a Summer Hydrographic Data Set. Thesis of the University of Tasmania - Institute of Antarctic and Southern Ocean Studies, Hobart.

Worby, A.P., Massom, R.A., Allison, I., Lytle, V.I., Heil, P., 1998. East Antarctic sea ice: A review of its structure, properties ans drift. Antarctic Research Series 74, 41-67.

Wright, S.W., van den Enden, R.L., 2000. Phytoplankton community structure and stocks in the East Antarctic marginal ice zone (BROKE survey, January-March 1996) determined by CHEMTAX analysis of HPLC pigment signatures. Deep Sea Research Part II 47, 2363-2400.

Wright, T.O., 1983. Geological investigations of portions of northern Victoria Land. Antarctic Journal of the United States 18, 8-9.

X

Xia, Q., Zhao, J.X., Collerson, K.D., 2001. Early-Mid Holocene climatic variations in Tasmania, Australia: Multi-proxy records in a stalagmite from Lynds Cave. Earth and Planetary Science Letters 194, 177-187.

Xie, S., Mei, S., Liu, K., Wei, L., 2002. Cyclone formation and development in the Antarctic Prydz Bay. Acta Oceanologica Sinica 21, 45-54.

Y

Yabuki, T., Suga, T., Hanawa, K., Matsuoka, K., Kiwada, H., Watanabe, T., 2006. Possible source of the antarctic bottom water in the Prydz Bay Region. Journal of Oceanography 62, 649-655.

Yan, Y., Mayewski, P.A., Kang, S., Meyerson, E., 2005. An ice-core proxy for Antarctic circumpolar zonal wind intensity. Annals of Glaciology 41, 121-130.

Yoo, K.C., Yoon, H.I., Park, B.K., Kim, Y., 2006. Advance of the outlet glaciers during regional warming as inferred from Late Holocene massive diamicton in the King George Island fjords, the South Shetland Islands, West Antarctica. Quaternary Research 65, 57-69.

Yoon, H.I., Khim, B.K., Yoo, K.C., Bak, Y.S., Lee, J.I., 2007. Late glacial to Holocene climatic and oceanographic record of sediment facies from the South Scotia Sea off the northern Antarctic Peninsula. Deep Sea Research Part II 54, 2367-2387.

Yoon, H.I., Park, B.K., Kim, Y., Kang, C.Y., 2002. Glaciomarine sedimentation and its paleoclimatic implications on the Antarctic Peninsula shelf over the last 15000 years. Palaeogeography, Palaeoclimatology, Palaeoecology 185, 235-254.

Yu, Y., Cai, X., Qie, X., 2007. Influence of topography and large-scale forcing on the occurrence of katabatic flow jumps in Antarctica: Idealized simulations. Advances in Atmospheric Sciences 24, 819-832.

Yuan, X., 2004. ENSO-related impacts on Antarctic sea ice: A synthesis of phenomenon and mechanisms. Antarctic Science 16(4), 415-425.

Yuan, X., Li, C., 2008. Climate modes in southern high latitudes and their impacts on Antarctic sea ice. Journal of Geophysical Research 113, C06S91, doi: 10.1029/2006JC004067.

Yuan, X., Martinson, D.G., 2001. The Antarctic Dipole and its predictability. Geophysical research Letters 28(18), 3609-3612.

Z

Zaragosi, S., Bourillet, J.-F., Eynaud, F., Toucanne, S., Denhard, B., Van Toer, A., Lanfumey, V., 2006. The impact of the last European deglaciation on the deep-sea turbidite systems of the Celtic-Armorican margin (Bay of Biscay). Geo-Marine Letters 26, 317-329.

Zhao, M., Beveridge, N.A.S., Shackleton, N.J., Sarnthein, M., Eglinton, G., 1995. Molecular stratigraphy of cores off northwest Africa: sea surface temperature history over the last 80 ka. Paleoceanography 10, 661-675.

Zhu, G.H., Ning, X.R., Cai, Y.M., Liu, Z.L., 2003. Phytoplankton in Prydz Bay and its adjacent sea area of Antarctica during the austral summer (1998/1999). Acta Botanica Sinica 45, 390-398.

Zielinski, G.A., Mayewski, P.A., Meeker, L.D., Whitlow, S.I., Twickler, M.S., 1996. A 110,000 year record of explosive volcanism from GISP2 (Greenland) ice core. Quaternary Research 45, 109-118.

Zwally, H.J., Comiso, J.C., Gordon, A.L., 1985. Antarctic offshore leads and polynyas and oceanographic effects. "Oceanology of the Antarctic Continental Shelf", Antarctic Research Series 43, 203-226.

Annexe 1 : SCOPIX de la carotte MD03-2601 (Joël Saint-Paul)

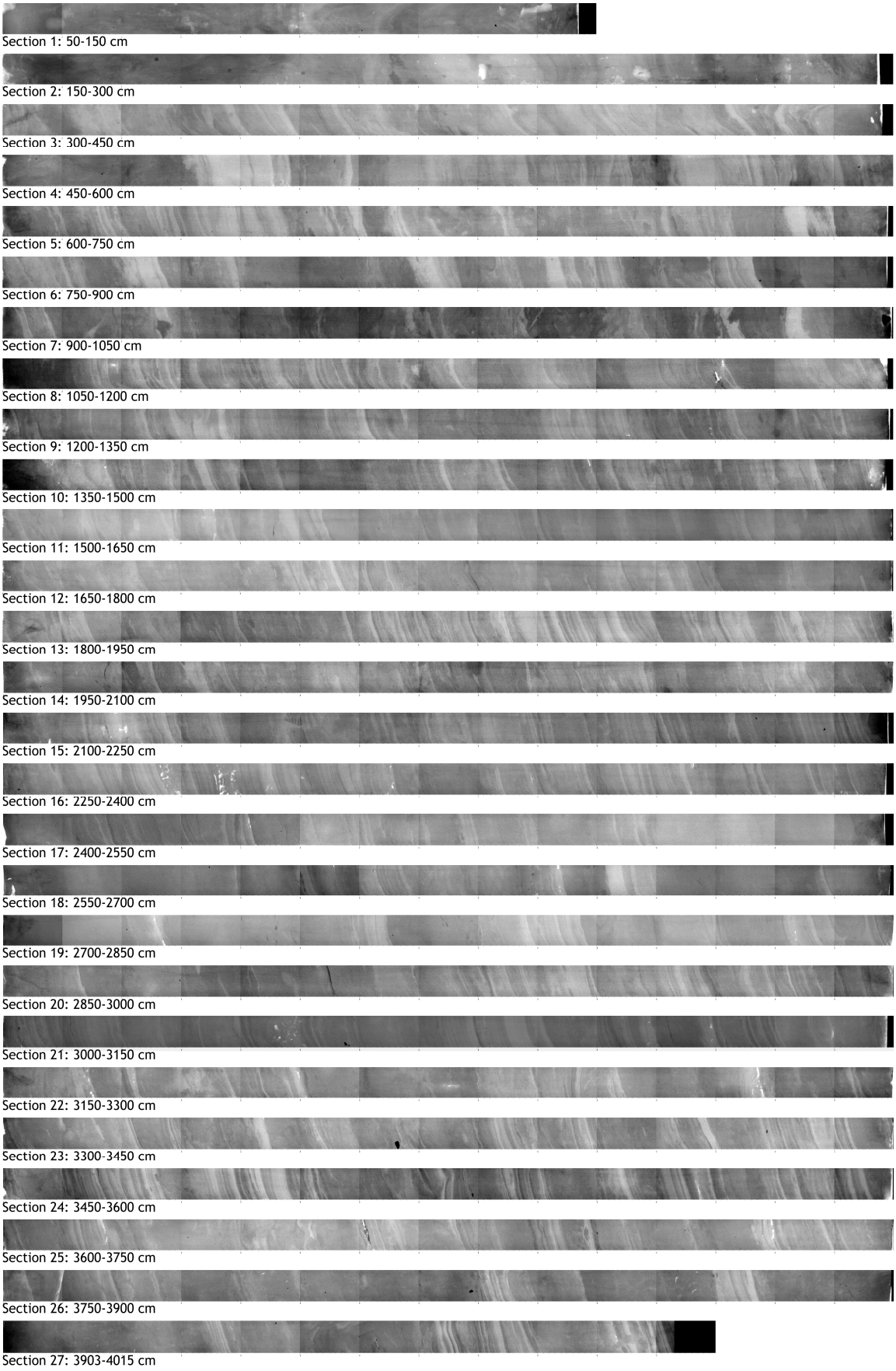

Annexe 2 : Extraction et montage sous lame des diatomées Antarctiques (Barbara, 2008)

1- Faire sécher le sédiment à l'étuve (60°C environ).
2- Mettre le sédiment sec dans un bêcher, et le recouvrir d'H_2O_2 (afin de détruire la matière organique et de favoriser la séparation des valves de diatomées).
3- Faire chauffer au bain-marie (thermostat 7) jusqu'à absence d'effervescence.
4- Laver à l'eau distillée par centrifugation (7mn à 1200tr/mn) jusqu'à pH neutre.
5- Sécher à l'étuve (60°C environ).
6- Ajouter HCl 10% jusqu'à absence de réaction (afin de détruire les carbonates). On peut augmenter la concentration de HCl si la réaction persiste avec une concentration de 10%.
7- Laver à l'eau distillée par centrifugation (7mn à 1200tr/mn) jusqu'à pH neutre.
8- Diluer dans 50ml, ou 100ml, d'eau distillée suivant la quantité de sédiment restant (et de diatomées supposées).
9- Homogénéiser la solution obtenue sans créer de gyre (sinon on obtient une stratification des diatomées en fonction de leur poids), et pipeter au centre de la solution avec une pipette de 150 µl.
10- Déposer 1 ou plusieurs gouttes de la solution, suivant la concentration de celle-ci, sur une lamelle préalablement disposée dans une boite de pétri et recouverte d'une fine couche d'eau + une goutte de lessive liquide (de marque Calgon en France).
- La lamelle doit être collée au fond de la boite. Pour cela, déposer une goutte d'eau distillée au fond de la boite et poser délicatement la lamelle dessus.
- La couche d'eau et la lessive liquide permettent une meilleure dispersion des valves de diatomées.
11- Afin de favoriser la dispersion des valves de diatomées, remplir la boite de pétri d'eau distillée en un mouvement tournant.

Remarque:
- Chaque échantillon doit être l'objet de 3 répliquas (au cas où un problème survienne dans une des boites de pétri.
- Les étapes 9 à 11 doivent être faites à la suite pour un échantillon (3 boites) avant de passer à l'échantillon suivant. Ceci afin qu'il n'y ait pas de sédimentation préférentielle des diatomées les plus lourdes.

12- Afin de favoriser l'évacuation de l'eau distillée, déposer un bout de laine de faible diamètre dans la boite de pétri sans qu'il touche la lamelle. Il ne faut pas que le débit soit trop fort pour ne pas créer de courant déplaçant les diatomées. Pour cela, compter une nuit de décantation.
13- Une fois sèche, monter entre lames et lamelles avec du NAPHRAX (ou HYRAX). Pour cela, déposer 3 lames par échantillons sur une plaque chauffante (250°C environ). Mettre 2 ou 3 gouttes de liquide de montage sur les lames, et les porter à ébullition. Ensuite, déposer les lamelles sur les lames jusqu'à que le liquide soit bien réparti. Sortir les lames et les déposer sur une surface froide pour permettre la coagulation du liquide de montage.

Annexe 3 : Protocole d'extraction pour l'analyse des « Highly Branched Isoprenoid » (HBi) d'un sédiment (Barbara, 2008)

Extraction :

1- Faire sécher le sédiment dans le lyophilisateur
2- Peser le sédiment dans une fiole de 7ml – approximativement 2g
3- Ajouter 10µl du standard à 10µg/ml (C25 alkane - 7 hexyl nonadecane)
4- Ajouter 2ml de DCM et 1ml de méthanol, agiter la fiole
5- Placer la fiole pendant 10min aux ultrasons
6- Centrifuger les échantillons pendant 1min à 2500 tours/min
7- Transférer le liquide extrait dans une nouvelle fiole de 7ml
8- Répéter l'opération de l'ajout de DCM et méthanol 2 fois
9- Laisser évaporer les solvants en utilisant un Dry block avec de l'azote

Purification :

1- Dans les échantillons extrait, ajouter 2ml de méthanol et secouer jusqu'à qu'il ne reste plus d'extrait sur les parois, et que tout soit dissous
2- Ajouter 2ml d'hexane et agiter vigoureusement
3- Ajouter 1ml d'eau et agiter encore vigoureusement (l'ordre d'ajout des solvants et de l'eau est très important). Deux phases se forment de différentes polarités : la phase du dessus contient l'hexane et les HBi, la phase du dessous contient le méthanol et l'eau.
4- Préparer des colonnes de silice dans des pipettes en utilisant un petit bout de coton et de la silice
5- Nettoyer les colonnes de silice en faisant passer 2ml d'hexane
6- Ajouter l'hexane extrait dans les colonnes (la phase du dessus)
7- Ajouter un autre ml d'hexane dans l'extrait, secouer, et le faire passer dans la colonne
8- Répéter cette opération 2 fois
9- Laisser passer tout l'extrait dans la colonne
10- Eluer la colonne avec 2 contenues de colonne d'hexane (l'extrait doit être clair)
11- Laisser évaporer l'hexane en utilisant un Dry block avec de l'azote
12- Transférer l'extrait final dans des fioles de 2 ml pour chromatographie en phase gazeuse (GC) en utilisant environ 100µl d'hexane

Annexe 4 : Protocole chimique d'extraction et de purification de l'uranium et du thorium

1- Peser 1 ml du mélange de traceurs (^{232}U, ^{228}Th) dans un bécher en téflon et y verser ~ 1-2 g de sédiment.
2- Attaque par HNO_3 (8N) pour dissoudre les carbonates.
3- A sec, ajouter du $HCLO_4$ et mettre sur plaque chauffante à 200°C pour dissoudre la matière organique.
4- Attaque par HF, à chaud pour détruire la matière silicatée.
5- Reprise du culot par HCl (1.5N).
6- Précipitation des hydroxydes avec NH_3, on atteint pH = 7.
7- Rinçage par 2 cycles de centrifugation (5 mn à 3000 tr/mn) puis rinçage à l'eau distillée.
8- Reprise de la solution par HCl concentré puis passage sur résine anionique (conditionnée en HCl (8N)).
9- U et Fe sont fixés. Récupérer le thorium dans un bécher et mener à sec. Rinçage HCl (8N).
10- Elimination d'une partie du Fe par le passage de 20 ml d'HNO_3 (8N) sur la colonne.
11- Elution de U et Fe par HCl (0.1N) (eau distillée plus une goutte d'HCL (8N)).
12- A sec, reprendre par HCl (8N).
13- Extraction du Fe avec l'éther diisopropylique, conditionné en HCl (8N).
14- Mener à sec la phase aqueuse contenant U, puis rincer à l'eau distillée.
15- A sec, reprendre le résidu d'U ou de Th avec HNO_3 (pH=3) plus du TTA puis agiter (15 min).
16- Déposer la phase organique dans laquelle U ou Th est passé, à chaud, sur une plaque d'aluminium.
17- Carboniser au bec Bunsen, il ne reste que U ou Th.
18- Echantillon prés à être compter au spectromètre alpha (1 à 2 jours pour l'Uranium et idem pour le thorium).

Spectromètre Alpha Canberra du laboratoire EPOC
(Photo S. Schmidt)

Annexe 5 : Protocole de la technique d'induration sur lames minces de sédiments meubles (Bernard Martin et Sébastien Zaragosi)

Echantillonnage :
Prélèvement sur le demi-tronçon ou plaquettes de carotte avec des cubes en polypropylène (résistant à l'acétone) perforés de 8cc sans altérer la disposition du sédiment.

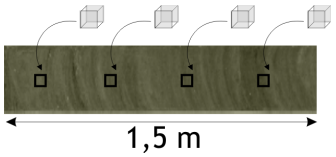

Déshydratation par acétone :
1- Immersion de l'échantillon dans une solution d'acétone pur pendant 1 jour.
2- Par le biais d'un tamis moléculaire, injection d'acétone en continu à l'aide d'une pompe péristaltique afin d'éliminer toute trace d'eau.
3- Test au distillat de pétrole pour vérifier la disparation d'H_2O.

Imprégnation :
1- Dégazage de la solution d'imprégnation (Résine Epoxyl (Crystic 17449), catalyseur (Butanox M50), acétone, pigment (fluorescent pour permettre l'analyse en lumière fluorescente)) dans une boite pendant 48h minimum en ammenant la pression de 1028 mbar à 147 mbar.
2- Immersion de l'échantillon dans cette résine.
3- Placement de la boite dans un dessiccateur où l'on fait aussi le vide de 1028 mbar à 200 mbar pendant 48h.
4- Placer l'échantillon sous hôte à température ambiante pour la polymérisation pendant 1 mois.
5- Placer l'échantillon à la lumière du jour, pour que les UV achèvent la polymérisation et le durcissement de l'échantillon pendant 2 à 3 semaines.

Préparation des lames :
1- Avec une scie diamantée, première découpe verticale au milieu du bloc.
2- Polissage manuel du talon avec un tout lapidaire et du carbone de silicium.
3- Fixage sur lame de verre avec la même résine d'imprégnation.
4- Réduction du talon à 100 µm d'épaisseur avec une micro-scie.
5- Réduction manuelle à 30 µm d'épaisseur avec un tout lapidaire.

Déshydratation au tamis moléculaire

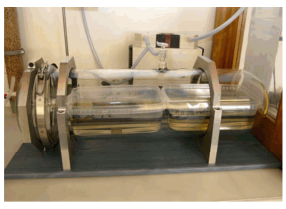

Imprégnation sous vide contrôlé

Polymérisation

Polissage

(Photos S. Zaragosi)

Annexe 6 : Analyse des lames indurées au microscope digital

Réglages de la station de microscopie LEICA DM600B et du logiciel LEICA QWIN 3.0 utilisés pour l'analyse des grains lithiques en lumière polarisée :

Paramètres du microscope :

1- Mettre les molettes polarisées sur 90°
2- Grossissement : x 10
3- Intensité : 15
4- Ouverture : 33
5- Champ : 33

Paramètres du logiciel :

1- Résolution : 1280 x 1280
2- Exposition : 206,4 ms
3- Gain : 1.5
4- Saturation couleur : 1.5

(Photo S. Zaragosi)

Routine du programme d'analyse d'image modifiée d'après celle réalisée par Virginie Mas :

```
Routine Header:
    Number of fields: 1
    Standard Frames
Calibration (System)
PauseText ("Nom du dossier")
Input (NOMFIC$)
NOMFIC$= « C:\users\delphine\ «+NOMFIC$+».txt »
OPENFILES$= NOMFIC$
Open File (OPENFILE$, channel#CHAN)

PauseText ("Définissez la taille de la fenêtre de mesure (bleue) »)
Measure frame (x 294, y 294, Width 692, Height 666)
Pause Message Group:
PauseText ("Définissez le balayage à appliquer")
PauseText ("Pensez à cliquer sur le bouton "Définir Pas"")
Stage (Scan pattern, 14 x 14 fields, size 742 x 714)
For (FIELD = 1 to FIELDS, step 1)
    Wait (2000 msec)
    Acquire (into Colour0)
    Colour detect (HIS: 21-555, 0-240, 219-255, from Colour0 into Binary0)
    Binary Amend (Open from Binary0 to Binary1, cycles 2, operator Octagon, edge erode on)
    Binary Identify (FillHoles from Binary1 to Binary2)
    Measure feature (plane Binary2, 8 ferets, minimum area: 50, grey image: Colour0)
        Selected parameters: Area, X FCP, Y FCP, Feret0, Feret90, VertProj, HorizProj, Lengh, Breadth,
        OrthoFeret, Orientation, OrthOrient, Perimeter, ConvxPerim, Roundness, Y Max(F90), X Max(F0), Y
        Min(F90), X Min(F0), Feret22.5, Feret45, Feret67.5, Feret112.5, Feret135, Feret157.5, XCentroid,
        DerivOrient, AspectRatio, EquivDiam, CurveLengh, CurveWidth, ConvexArea, FullRatio, Forks, Joins,
        Tops, Ends, Int. Red, Mean Red, Red Var, Int. Green, Mean Green, Green Var, Int. Blue, Mean Blue,
        Blue Var, X Stage Pos, Y Stage Pos, Z Stage Pos
    Colour Code Features
    File Feature Results (channel #1)
    Stage (Step, Wait until stopped = 55 msecs)

Next (FIELD)
Close File (channel #1)
END
```

Annexe 7 : Principe de fonctionnement des analyses sur spectromètre de masse et analyseur élémentaire (Crespin, 2004)

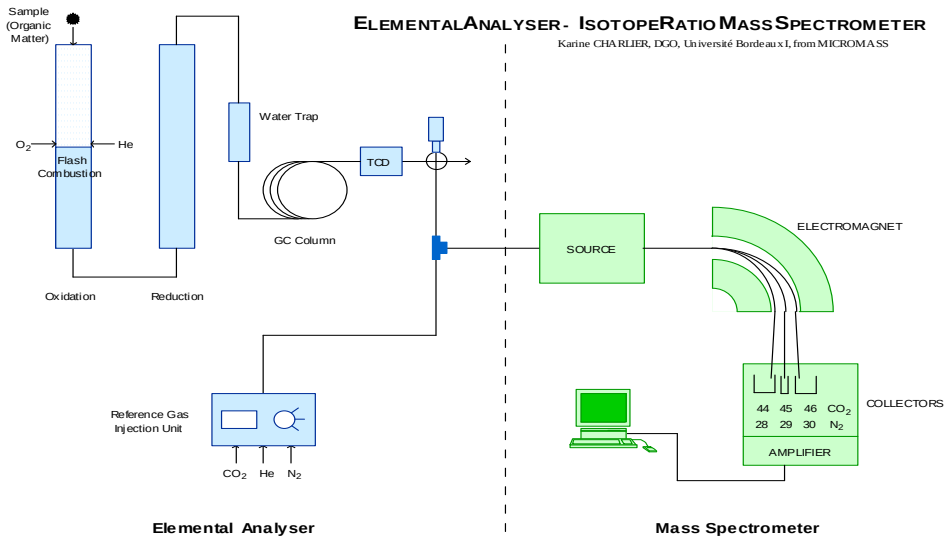

Figure 1 : Principe de fonctionnement de l'analyseur élémentaire et du spectromètre de masse (d'après K. Charlier).

Pour chaque échantillon séché, environ 20 mg de sédiment sont scellés dans des capsules en étain puis placés dans le carrousel de l'analyseur élémentaire. Les capsules vont tour à tour tomber dans la colonne d'oxydation où un flux d'oxygène va permettre la combustion du sédiment (à 1040°C). Les gaz ainsi libérés vont êtres transportés par un flux d'hélium à travers tout le système. À la sortie de la colonne d'oxydation, seuls les gaz NO_2 et CO_2 sont présents. Ils pénètrent alors dans la colonne de réduction constituée de cuivre pur et sont transformés en N_2 et CO_2. Les gaz traversent ensuite un piège à eau qui retient l'eau libérée lors de la combustion des échantillons, puis la colonne de chromatographie qui sépare les gaz CO_2 et N_2 et enfin le TCD (Détecteur à Conductivité Thermique qui permet la détermination des pourcentages d'azote et de carbone). Les gaz N_2 et CO_2 pénètrent ensuite dans le spectromètre de masse au niveau de la source (Figure 1). Les molécules vont être ionisées puis accélérées par un voltage de 400 µA. Les ions sont ensuite regroupés en faisceau et dirigés vers une zone magnétique intense engendrée par une bobine aimantée. Cette dernière va dévier sélectivement les ions selon leur poids moléculaire. Ils traversent alors un tube analyseur et frappent différentes boîtes de Faraday (3 collecteurs au total) en fonction de leur poids moléculaire. Le nombre d'impacts dans les différents collecteurs va être ensuite traduit en termes de $\delta^{15}N$ et de $\delta^{13}C$ mais aussi en termes de teneurs en azote et carbone organique total, par l'ordinateur couplé au spectromètre de masse. Les valeurs isotopiques sont constamment calibrées au moyen de standards de laboratoire ayant des valeurs connues comme l'Acétanilide, la Glycine et la Caséine. Ce sont ces standards qui sont calibrés par rapport au gaz de référence et qui permettent de corriger les valeurs brutes obtenues pour les échantillons. Toutes les valeurs sont données en notation δ et ont pour référence le PDB (Pee Dee Belemnite) pour le $\delta^{13}C$ et l'air pour le $\delta^{15}N$. L'erreur standard sur la mesure est de 0.1‰ pour le $\delta^{13}C$, de 0.25‰ pour le $\delta^{15}N$, de 0.03 % pour le C_{org} et de 0.01% pour le N_{org}.

Annexe 8 : Détermination de la teneur en silice biogène de sédiments marins (Modifié d'après Danial-Fortin, 2004)

Protocole expérimental:

1- Peser entre 8 et 15 mg d'échantillons secs si les teneurs attendues sont >20-25%. Placer ensuite le matériel dans des tubes à centrifugation (Séries de 8 échantillons).

2- Pipeter 40 ml de la solution d'hydroxyde de Sodium (NaOH) à O.5 mol/L à l'aide de la dispensette et les ajouter à chacun des tubes.

3- Agiter les tubes, et les mettre au bain-marie préalablement chauffé à 65°C. Agitation des tubes toutes les 30 minutes.

4- Au temps de dissolution voulu, retirer les tubes du bain-marie et les centrifuger pendant 3 minutes.

5- Prélever 250 µl de la solution surnageante de chaque tube à l'aide d'une micropipette et les placer dans des fioles de 12 ml préalablement rempli avec 4.750 ml d'eau distillée (volume total = 5 ml).

6- Ajouter 0.5 ml de chaque solution standard dans des fioles de 12 ml préalablement numérotées et remplies avec 4.5 ml d'eau distillée (volume total = 5 ml).

7- Le « blanc » sera fait avec 5 ml d'eau distillée dans une fiole de 12ml.

8- En notant l'heure exacte, ajouter 2 ml de la solution de Molybdate dans chacune des fioles contenant le blanc, les échantillons et les standards avec un intervalle de temps constant entre chaque ajout (exemple : 15 secondes).

9- Laisser reposer entre 10 et 30 mn, puis ajouter 3 ml de la solution réductrice dans chacune des fioles contenant le blanc, les échantillons et les standards avec le même intervalle de temps que précédemment entre chaque ajout.

10- Fermer les fioles et attendre 1h que la réaction ait lieu, et donc que le complexe silicomolybdate bleu se forme avant de lire les résultats au spectrophotomètre à 812 nm.

Détermination du temps de dissolution :

La durée de dissolution dépend du matériel sédimentaire (Mortlock et Froelich, 1989). Il est nécessaire de déterminer cette durée avant les analyses en routine. Pour ce faire, il est nécessaire d'échantillonner et de mesurer la teneur en silice biogène (BSi) pour chaque heure pendant 5 heures.

On obtient une courbe de référence dont la 1° partie est représentative de la dissolution de la BSi tandis que la 2° partie est représentative de la dissolution de la silice lithogénique. L'intersection de l'asymptote avec l'axe Y des ordonnées représente la mesure de BSi et indique la durée à appliquer pour dissoudre la totalité de la BSi sans « attaquer » la silice lithogénique.

Méthode de lecture

La mesure au spectrophotomètre s'effectue après 1h de réaction.

- Prélever 3.5 ml de chacune des fioles grâce à une micropipette et les placer dans les cuves spectrophotométriques préalablement numérotées.

- Mesurer l'absorbance en commençant par le blanc (« pour faire le zéro ») puis continuer avec les standards et les échantillons.

Les erreurs sur la mesure sont faibles, de l'ordre de 1%.

Annexe 9 : Tests sur les mesures de silice biogène en continue

Le principe de cette méthode, développée par Müller et Schneider (1993) est de dissoudre la BSi en continue et de mesurer simultanément l'augmentation des teneurs en BSi par spectrophotométrie. On obtient donc une courbe de dissolution de la silice biogène pour chaque échantillon à partir de laquelle, on peut mesurer la teneur en BSi. Cette méthode présente plusieurs avantages :

- La précision sur la mesure est meilleur (0.4% contre 1%) car la courbe de dissolution est propre à chaque échantillon et une nouvelle gamme d'étalonnage est passée avant chaque échantillon.
- Le temps requis est plus faible, car on pourrait passer en routine au moins une dizaine d'échantillons par jours contre 8 pour l'autre méthode avec une vaisselle beaucoup moins contraignante. De plus, pendant le passage de chaque échantillon, on dispose de 40 min libre avant l'échantillon suivant.

Schéma de fonctionnement :

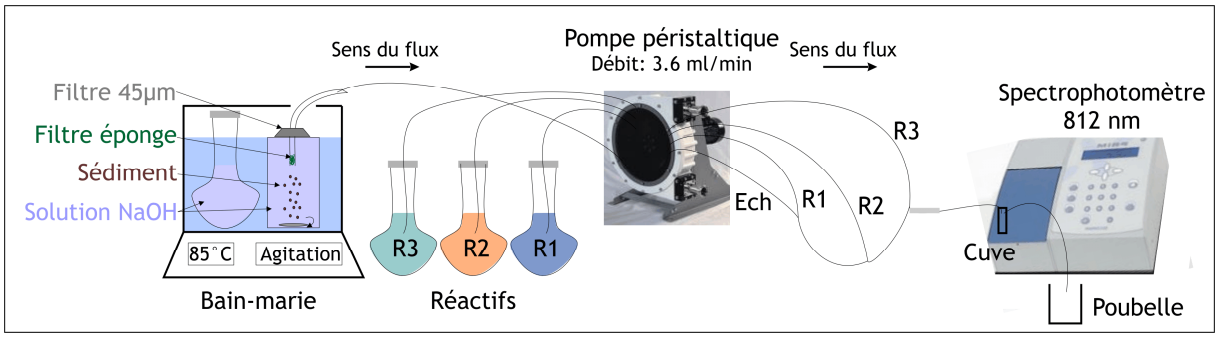

Protocole expérimental :

1- Passage de la gamme d'étalonnage (6 points : 0, 150, 250, 350, 500 et 750 µmol/L).

2- Dissolution de l'échantillon 1 avec une solution de NaOH (0,5 M) dans un mini bain-marie à 85°C. La dissolution totale de BSi prend environs 40 min par échantillon.

3- Filtration de la silice dissoute par deux systèmes de filtre, un grossier, puis un fin de diamètre 0.45 µm.

4- Aspiration continue de la BSi dissoute et des trois réactifs (les mêmes que ceux utilisés dans l'autre méthode) au moyen d'une pompe péristaltique.

5- Rencontre de l'échantillon 1 avec la solution de Molybdate (R1).

6- Rencontre du mélange « échantillon 1- R1 » avec la solution d'Acide oxalique (R2).

7- Rencontre du mélange « échantillon 1-R1-R2 » avec la solution d'Acide Ascorbique (R3). Le temps de réaction de l'échantillon avec les trois réactifs est de 1 min.

8- Passage de cette solution « échantillon 1-R1-R2-R3 » dans la cuve du spectrophotomètre, réglé à 812 nm.

9- Rinçage à l'eau de toute la tuyauterie durant 4 min.

10- Passage dune gamme d'étalonnage réduite (3 points : 0, 350, 750 µmol/L).

11- Dissolution de l'échantillon 2….

Matériel requis :
- Bain-marie muni d'un couvercle, pouvant monter à 85°C et dont la température est ajustable rapidement + thermomètre.
- Filtre 0,45 µm.
- Tuyaux en téflon de diamètre : 0.64, 0.89 et 2.29 µm.
- Connectiques de tuyaux.
- Produits chimiques : réactifs + soude + standard certifié.
- Pompe péristaltique à 4 entrées ou 6 si on installe un système de reflux.
- Cuve de spectromètre et spectromètre.

Dosages adaptés aux connectiques et au débit :
L'astuce pour respecter les temps de réactions nécessaires après l'ajout de chaque réactif R1, R2 et R3 (voir annexe 8), est un compromis entre la dilution des réactifs, le débit de la pompe péristaltiques, le diamètre des connectiques et la longueur des tuyaux.
Pour un débit de 3.6 ml/min,

Les connectiques utilisées sont :
- 0.64 µm du trajet bain-marie à R1
- 0.89 µm du trajet R1 à R3
- 2.29 µm du trajet R3 à la cuve du spectrophotomètre

Les dosages requis sont :
- R1 : Dosage initial : Acide sulfurique (4,5 M) + solution de Molybdate (12.666 g/100 ml d'H_2O) ; Dilution adéquate (/2): 60 ml dans 120 ml.
- R2 : Dosage initial : Acide oxalique (10 g/100 ml); Dilution adéquate (/10): 12 ml dans 120 ml.
- R3 : Dosage initial : Acide ascorbique (2.8 g/100 ml); Dilution adéquate (/14): 4,28 ml dans 60 ml.

La longueur des tuyaux, nécessaire entre R1 et R2 et après R3, était en cours de test (voir Figure 1).

Problèmes rencontrés :
- La stabilité et la précision des mesures dépendent fortement de la stabilité de la température de dissolution qui doit être maintenue de manière constante à 85°C, d'où la nécessité d'un bain-marie couvert.
- Des bulles peuvent survenir au sein du réseau de tuyaux si les branchements ne sont pas étanches. Acheter des connectiques adéquates.
- Amas de sédiments dans le filtre qui se dissolve d'un coup et qui entraîne un phénomène d' »overshooting », c'est à dire une bosse dans la courbe de dissolution, enregistrée au spectrophotomètre. Deux pistes sont à creuser pour résoudre ce problème majeure : 1) installer un système de reflux qui divise le flux sortant du bain-marie en deux, dont une moitié est réinjecté dans le flacon de dissolution et l'autre moitié est analysée, ou 2) faire un calcul de régression du volume sur la courbe de dissolution de BSi.

The Holocene 16,8 (2006) pp. 1137–1147

Seasonal and subseasonal climate changes recorded in laminated diatom ooze sediments, Adélie Land, East Antarctica

D. Denis,[1]* X. Crosta,[1] S. Zaragosi,[1] O. Romero,[2] B. Martin[1] and V. Mas [1–3]

([1]UMR-CNRS 5805 EPOC, université Bordeaux 1, av. des Facultés, 33405 Talence cedex, France; [2]Department of Geosciences and RCOM, University of Bremen, PO Box 330440, 28334 Bremen, Germany; [3]IFREMER, Géosciences Marines, Laboratoire Environnements Sédimentaires, BP70, 29280 Plouzané Cedex, France)

Received 16 January 2006; revised manuscript accepted 6 June 2006

A HOLOCENE RESEARCH PAPER

Abstract: A 40 m long sediment core covering the 1000–9600 years BP period was retrieved from the Dumont d'Urville Trough off Adélie Land, East Antarctica, during the MD 130-*Images* X-CADO cruise. This sedimentary sequence allows the documentation of changes in climate seasonality during the Holocene. Here we show preliminary results of diatom communities, lithic grain distribution and titanium content measured on two 30 cm long sequences of thin sections. The two sequences originate from two different climate regimes, the colder Neoglacial and the warmer Hypsithermal. Proxies were measured at microscale resolution on 25 laminations for the Neoglacial and 14 laminations for the Hypsithermal. The two sequences reveal alternating light-green and dark-green laminae. Light laminae result from low terrigenous input and high sea-ice edge diatom fluxes and are interpreted to represent the spring season. Dark laminae result from high terrigenous input mixed with a diversified open ocean diatom flora and are interpreted to represent the summer–autumn season. The two sequences therefore resolve annual couplets composed of one light plus one dark lamina. Variations in the relative thickness of laminations and annual couplets, associated with diatom assemblage changes, are observed in each sequence and between the two sequences giving information on interannual to millennial changes in environmental conditions.

Key words: Adélie Land, Holocene, laminated sediments, diatom ooze, seasonality, sea ice, East Antarctica.

Introduction

Based on ice core records (Masson *et al.*, 2000; NGICP members, 2004), the Holocene period was believed rather stable in comparison with the last glacial period. However recent palaeo-oceanographic investigations have revealed rapid and large amplitude variations in the North Atlantic (de Menocal *et al.*, 2000; Bond *et al.*, 2001) and in the Southern Ocean (Hodell *et al.*, 2001; Nielsen *et al.*, 2004). Sites of high sediment accumulation are therefore necessary to document these variations and to understand their frequency and origin. In that perspective, Antarctic inner shelf basins that present laminated sediments allow annual to subseasonal reconstructions of Holocene oceanographic and climatic conditions, which may help to understand better both the interactions between Antarctic atmospheric–oceanic–cryospheric–sea-ice processes, deep ocean circulation and teleconnections between high and low latitudes. Most of the studies aimed at deciphering the signal recorded in laminations originate from the Antarctic Peninsula (eg, Pike *et al.*, 2001; Leventer *et al.*, 2002; Bahk *et al.*, 2003; Maddison *et al.*, 2005) and the Mac Robertson Shelf (Stickley *et al.*, 2005). Nonetheless, evidence for strong Antarctic regional heterogeneities in recent climate changes (Jones *et al.*, 1993; King *et al.*, 2003) call for additional sedimentary records in order to provide a more comprehensive view of past climate dynamics at high southern latitudes. The Adélie Land region in the East Antarctica Margin (EAM) has received little attention so far, despite evidences for very high sediment accumulation (Leventer *et al.*, 2006). Core MD03-2601 from the Dumont d'Urville Trough is a 40 m long sequence of laminated diatom ooze that covers the Holocene. Investigation of diatom communities, lithic grain distribution and titanium content at microscale resolution on two 30 cm long laminated sequences aimed to document (1) the nature of

*Author for correspondence (e-mail: d.denis@epoc.u-bordeaux1.fr)

10.1177/0959683606069414

the signal preserved in the laminations and (2) whether laminations may be used here to track climate change at the interannual timescale.

Oceanographic setting

The SE–NW oriented Dumont d'Urville Trough off Adélie Land is located on the EAM (Figure 1). It is composed of a succession of glacial depressions enclosed between the Dibble Bank to the west and Adélie Bank to the East. Core MD03-2601 (66°03.07′S; 138°33.43′E; 746 m water depth) was recovered from the slope of a small depression located ~60 km off the Adélie Land coast. This region is influenced by three water masses (Bindoff *et al.*, 2001): the Antarctic Coastal Current (ACC), which flows westward at the surface (Figure 1); the Modified Circumpolar Deep Water (MCDW), which upwells at the Antarctic Divergence; and the High Salinity Shelf Water (HSSW) formed by brine-rejection during winter sea ice formation and cooling of the MCDW, which flows northward as part of the Antarctic Bottom Water (AABW) (Harris, 2000). The Adélie Land region is dissected by several small glaciers (Figure 1) injecting fresh water and terrigenous particles in the coastal area although these small glaciers have much less influence than the larger Mertz Glacier located few degrees to the East (Escutia *et al.*, 2003). Sea ice is present ~9 months per year over the core site (Schweitzer, 1995) with more open marine conditions between January and March. Sea ice advances rapidly from April to June to reach its maximum extension between July and September, then retreats slowly during spring melting to attain its minimum extent during February. The Marginal Ice Zone is believed to be macro- and micronutrient rich, and ice melting produces a stratified stable environment favourable for diatom blooms (Leventer, 1992).

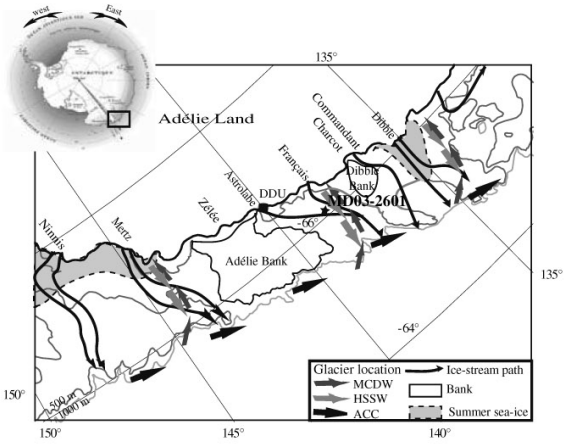

Figure 1 Location of core MD03-2601, limit of summer sea ice cover (Schweitzer, 1995), location of glaciers and ice-streams (Massom *et al.*, 1998; Escutia *et al.*, 2003), detail of oceanographic currents and different water masses (Harris and Beaman, 2003). DDU, Dumont d'Urville Base; ACC, Antarctic Coastal Current; MCDW, Modified Circumpolar Deep Water; HSSW, High Salinity Shelf Water. Winter sea ice covers the whole oceanic area encompassed by the map

Material and methods

Material and core stratigraphy

Core MD03-2601 was collected using the MDII Calypso piston corer during the MD130-*Images* X-CADO cruise in 2003. This 40.24 m long sequence of diatom ooze alternates between laminated and massive facies, and does not show any obvious visual disturbance. Stratigraphic control is based on five AMS ^{14}C dates on humic acid (Crosta *et al.*, 2005) that were subsequently corrected by a marine reservoir age of 1300 years (Ingólfsson *et al.*, 1998). The core covers the period from 9600 to 1000 yr BP. Diatom census counts and δ^{15}N and δ^{13}C investigations (Crosta *et al.*, 2005) have shown that the Holocene period off Adélie Land can be divided into two different climatic phases: a colder Neoglacial (after 4000 yr BP), and a warm Hypsithermal (4000–9600 yr BP), which contains a cooling event (6350–8000 yr BP).

Laboratory procedures

Laboratory procedures involve preparations for macroscale investigations on half-core sections and for microscale analyses on thin sections.

Titanium content (Ti) expressed in counts per second (cps) was measured on half-core sections at 2 cm spacing along the entire core and at 2 mm spacing on the studied sections, on the Bremen University CORTEX XRF core-scanner following Jansen *et al.* (1998) method. Daily calibration of the XRF core-scanner precluded drift over time, thus ensuring low standard deviations of the data. Titanium is believed to be of terrigenous origin as this element does not participate in biological and diagenetic cycles, in contrast to iron and aluminium (Taylor and McLennan, 1985; Yarincik and Murray, 2000). Aluminium, which is actively uptaken and accumulated by diatoms, cannot be applied here to normalize Ti values (Van Bennekom *et al.*, 1989; Moran and Moore, 1992).

Positive x-ray pictures of half-core sections were done using the SCOPIX image-processing tool (Migeon *et al.*, 1999). Variations in grey levels indicate changes in the sediment density and thus composition. The light and dark laminations observed here correspond to sediment layers of low and high density, respectively.

Based on x-ray pictures, we determined the distribution and thickness of laminations along the entire core (Figure 2). We used a slightly modified technique from Francus *et al.* (2002), which involves drawing a suite of ellipses representative of each lamina and calculation of the distribution and thickness of laminae based on the ellipses in Scion Image®. This technique was applied to laminae only because sublaminae are difficult to distinguish on x-ray pictures. This approach helped us to sample two ~30 cm long sections of continuously laminated sediment. Section 5 (619–648.5 cm) originates from the Neoglacial while section 13 (1880.8–1910.7 cm) comes from the Hypsithermal.

Each lamina observed on x-ray pictures from sections 5 and 13 was sampled for diatom census counts and bulk isotopic ratios. Permanent slides were mounted following the procedure of Rathburn *et al.* (1997). This sampling strategy that takes the sediment over the entire thickness of the half-core sections cannot give access to diatom successions at the lamination scale because laminae are here inclined in both the horizontal and vertical plains. Such diatom census counts are, however, essential to interpret diatom assemblages at microscale on the thin sections.

Three thin sections (TS) were made for each period (TS 1, 2, 3 for core section 5 and TS 4, 5, 6 for core section 13) using the impregnating method detailed in Zaragosi *et al.* (2006).

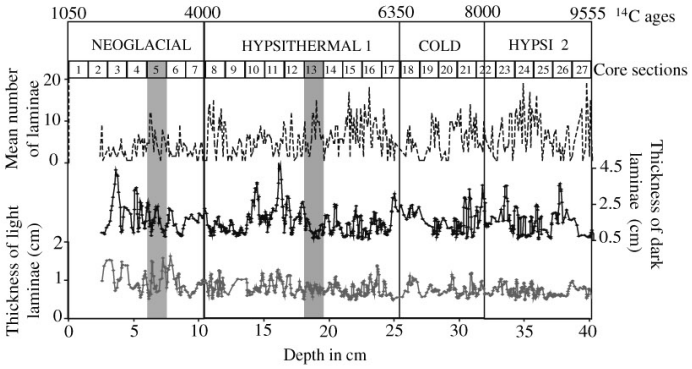

Figure 2 Mean number of laminations per 10 cm intervals (dashed line) and thickness of dark (black line) and light (grey line) laminations versus depth. Laminae thicknesses are smoothed with a 50 cm running average. Core sections, climatic periods and ^{14}C dates are reported at the top. The location of the studied sections 5 and 13 is represented by shaded zones

The goal of this technique is to embed a large sediment volume into a permanent medium without disturbing the sediment structure. The resulting thin sections (TS) are used here to document variations in the biogenic and lithogenic content.

Optical observations were conducted on the TS using an Olympus BH2 light microscope at magnification of 250 × and 500 × to determine diatom community changes with a focus on the relative importance of dominant species. Diatom census counts along the entire core (Crosta *et al.*, 2005) and within each lamina over the studied sections give us complementary insight on diatom assemblages and dominant species at decacal to subdecadal scales, which ascertains diatom identification on the TS.

Detrital material was similarly studied on the TS to determine (1) the mineral type via polarized light and (2) the distribution and number of lithics particles as grain number per square millimetre using an imagery system composed of a LEICA DM600B Digital microscope and Leica QWin 3.0 software. We conducted image analysis on 2.5–3.5 cm^2 TS areas, later referred to as Photomosaic (PM) (see Figure 4). Because of the homogeneous amorphous matrix of the diatom ooze sediment and of the impregnating Epoxy resin, the sediment matrix appeared darker than the clastic grains in the analysed polarized light. The picture processing method, detailed in Francus (1998), counts all the grains present in the area and estimates several characteristics as surface, width and length of the lithic grain. Two slides (TS2 and TS3) with very cottony texture did not allow coherent image acquisition and were not used in the calculations.

Results

General observations

Because of the sediment composition, laminations are almost invisible to the naked eye on half-core sections. They are, however, visualized on x-ray images as light and dark layers and on TS as light and brown layers. We will hereafter refer to light and dark laminae, which together form a couplet.

Mean thicknesses of light and dark laminations are 0.7 cm ($n = 937$, $\sigma = 0.4$) and 1.12 cm ($n = 1018$, $\sigma = 1.22$), respectively (Figure 2). Light and dark lamination thickness and lamination number reveals no obvious trend with depth but rather cyclic variations, whereas thickness of light laminations shows a slight decrease with depth.

Generally, x-ray images and TS show gradational colour contact between a light lamina and the overlying dark lamina and sharp colour contact from a dark to the overlying light lamina. Microscopic observations on TS reveal that light laminations are mainly composed of biogenic debris whereas dark laminations are composed of a mixture of biogenic and detrital debris, the latter being mainly clay and silt. Petrographic observations indicate that the clastic grains are mainly quartz. Only observable on TS, thin light laminae, called sublaminae, are found in dark laminations.

Section 5: Neoglacial period

Twenty-five laminations and four sublaminations are distinguished on TS 1, 2 and 3 that represent a ~30 cm long sequence of undisturbed sediment within section 5 (see Figure 4a for TS location). These laminations include 12 lights, 11 darks and 2 transitional laminae with average thicknesses of 1.1 cm ($\sigma = 0.8$), 0.8 cm ($\sigma = 0.8$) and 0.4 cm ($\sigma = 0.03$), respectively. The mean thickness of a couplet reaches 2.1 cm ($n = 10$, $\sigma = 1.4$).

Diatom assemblages

Diatom census counts performed between 608 cm and 670 cm ($n = 50$) show few dominant species among a highly diverse diatom community (~50 species), thus confirming results from lower resolution diatom counts (Crosta *et al.*, 2005). In section 5, *Fragilariopsis curta* and *Chaetoceros* resting spores (CRS), mainly *Hyalochaete Chaetoceros neglectus*, represent the dominant species with 26% and 19%, respectively. They are accompanied by a set of subordinate species or species groups such as other cryophilic *Fragilariopsis* species (12%), *F. rhombica* (10%), *F. kerguelensis* (8%), large centric species thriving in cold waters (8%), *Thalassiosira antarctica* (6%), *Phaeoceros* vegetative cells (5%), *Corethron pennatum* + rhizosolenoid species (4%) and needle-like species mainly represented by *Thalassiothrix antarctica* (2%) (Figure 3a).

Qualitative examinations of diatom assemblages on the TS demonstrate the same dominant species as mentioned above. These investigations, however, show the fine distribution of the diatom species that was invisible in the stepwise sampling. As a general statement, diatom distribution follows the colour changes of the laminations with a gradational evolution in the assemblages from light to dark laminae and an abrupt change from dark to light laminae. A close investigation depicts the following five main diatom assemblages, labelled A-B for the ones occurring in the light laminae and D-E-F for the ones encountered in dark laminae (Figure 3a and see Figure 5).

Assemblage type A is characterized by a co-dominance of *F. curta* plus other cryophilic *Fragilariopsis* species and CRS

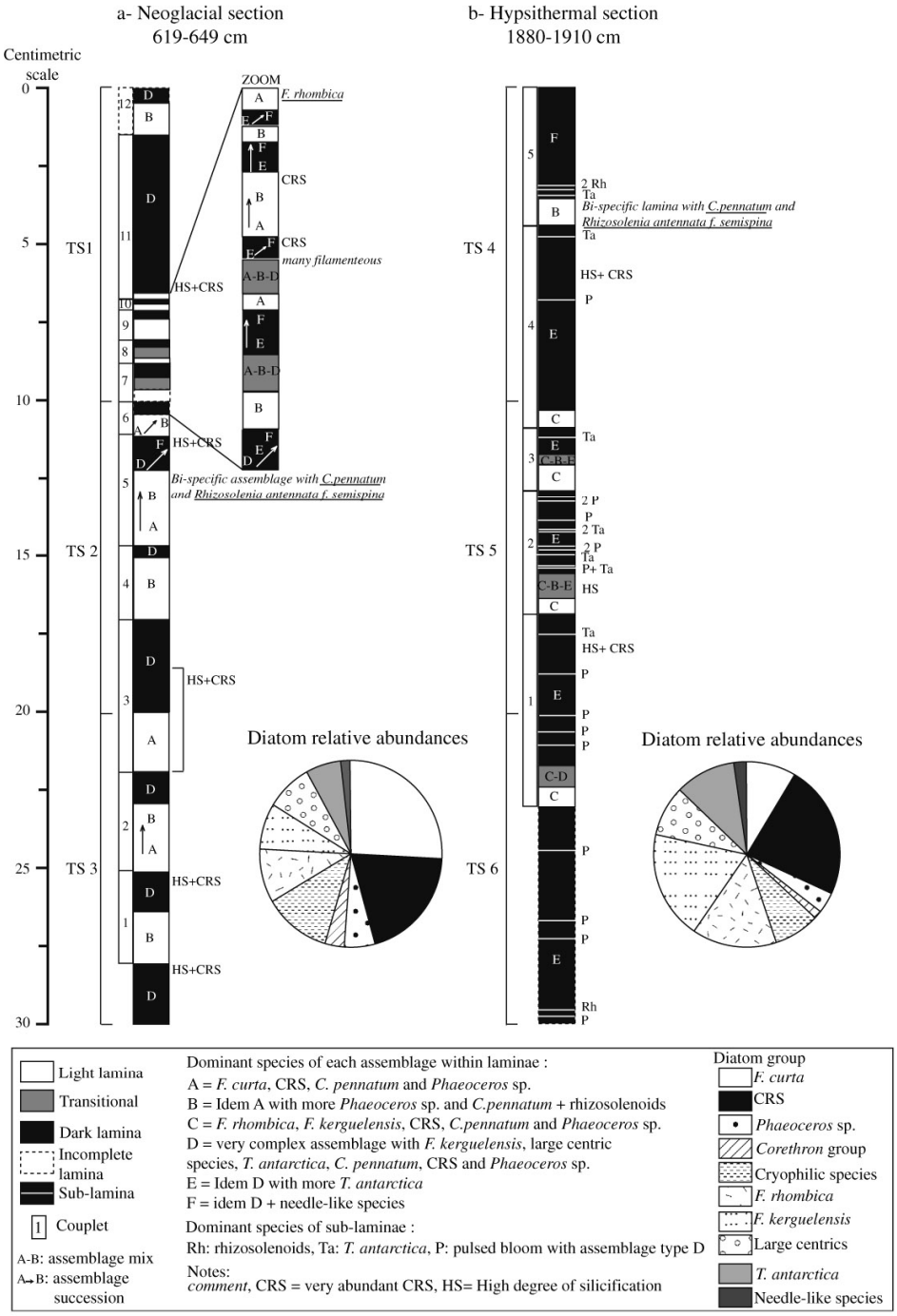

Figure 3 Schematic log of lamination and sublamination distribution in section 5 (a) and in section 13 (b). Location of the centimetric scale thin sections, and number of annual couplets are reported on the left side. Pie-charts illustrate the relative abundance of the various diatom groups from centimetric-scale diatom census counts in section 5 (a) and 13 (b)

plus vegetative *Phaeoceros* sp. and *C. pennatum*. *Chaetoceros* RS relative abundance increases progressively toward the top of the laminae while cryophilic *Fragilariopsis* species dominance decreases (Figure 3a). Assemblage type B is similar to assemblage type A with greater abundances of *C. pennatum*, rhizosolenoids and vegetative *Phaeoceros* sp. Assemblage type B becomes nearly bispecific in *C. pennatum* and rhizosolenoids in one occasion at the top of light lamination number five (Figure 3a). We counted 11 light laminae in the three TS of section 5, from which three laminae are characterized by assemblage type A, five laminae by assemblage type B and four laminae by a slow transition from assemblage type A to assemblage type B. The third and the ninth light laminae contained more CRS.

Assemblage type D shows a mixed flora composed of *F. kerguelensis*, CRS, *T. antarctica*, large centric species,

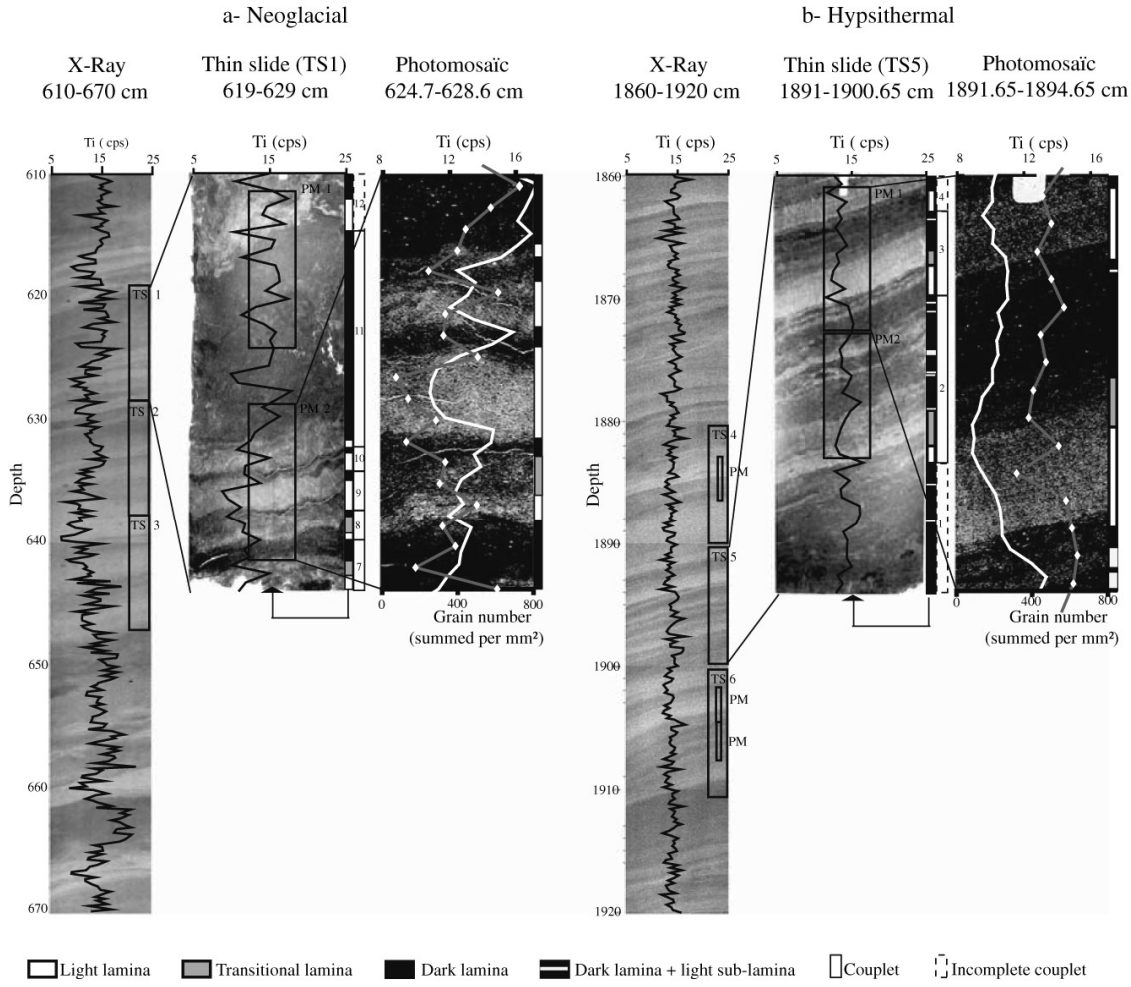

Figure 4 Location of the investigated sections on positive x-ray radiographs, thin sections and photomosaics for section 5 (a) and section 13 (b). Three thin sections (TS) were taken from each section. Two photomosaics (PM) were analysed in TS1 from section 5 while five photomosaics were analysed in the three TS from section 13. In each section, Ti content is visualized by the black curve. In the photomosaics, Ti content is represented by the grey curve with white points whereas the grain number per millimetre is illustrated by the white curve. Types of laminae and couplet succession are shown on the right of TS following the nomenclature depicted in Figure 3

Phaeoceros sp. and *C. pennatum*. Assemblage type E is similar to assemblage type D but with greater presence of *T. antarctica.* Assemblage type F also resembles assemblage type D but with a greater dominance of needle-like species (Figure 3a). We counted 11 dark laminations, from which seven are composed of the assemblage type D. The other dark laminations display a succession of assemblage types. Four laminations show a slow evolution from assemblage type E to assemblage type F, one lamination from assemblage type D to assemblage type F, and one lamination from assemblage type D to assemblage type E to assemblage type F (Figure 3a). Diatoms at the top of the dark laminations generally show a higher degree of silicification (see Figure 5). Complex dark laminations are encountered in couplets number five to ten in which light laminations also demonstrate a more complex structure. Transitional laminations between the light and the overlying dark lamination and showing a mixture of assemblage types A, B and D characteristics are also present here.

Detrital content

Titanium content is correlated to density changes visualized by x-ray photography with lower Ti content in light laminations than in dark laminations with mean values of 11.6 and 13.7 cps respectively (Figure 4a). Titanium content is similarly correlated to TS colour changes even though some variability is encountered within each lamina. We used the Wilcoxon-Mann-Whitney (WMW) test to determine whether the Ti content is significantly different in light and dark laminations. Briefly, the WMW is a non-parametric variance analysis test adapted for small data sets ($n_{light} = 45$, $n_{dark} = 47$, here) (Saporta, 1990). This test determines whether Ti values are randomly distributed or organized according to different populations (light and dark laminations). At the 1% confidence level, the WMW test yields a $H_{Ti\ content}$ value of 4.32 that is superior to the rejection threshold of 2.58. This demonstrates that different Ti content indeed prevails in light and dark laminations and that intracouplet differences are greater than homochromic intercouplet differences.

Determination of grain distribution and characteristics was only possible on TS 1 within two study zones: PM 1 and 2 (Figure 4a). The digital approach recognizes grains with diameter greater than 5 μm. In this population, silts are dominant with an unimodal histogram frequency centred at ~ 10 μm of diameter. In agreement with the Ti content data,

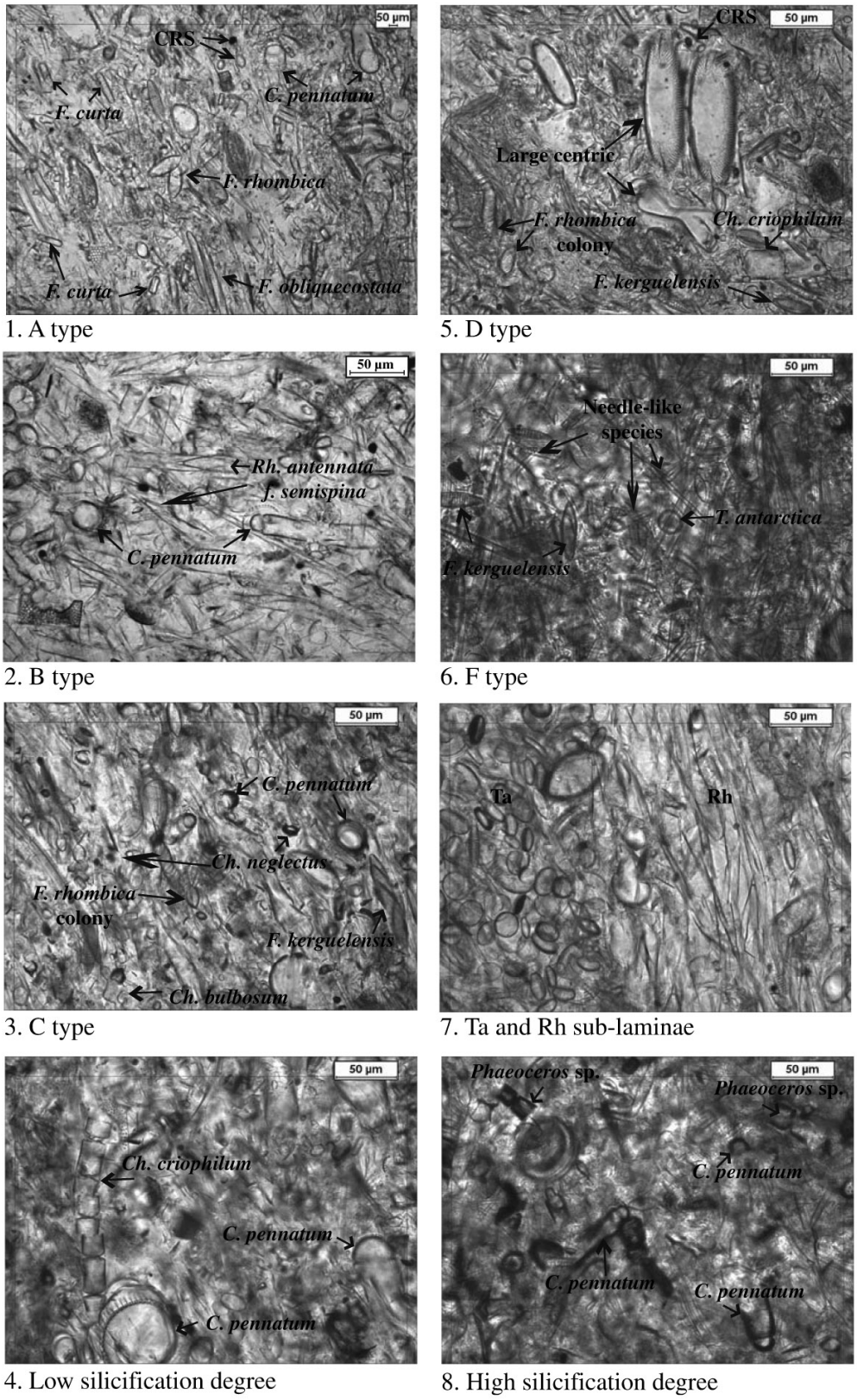

Figure 5 Various diatom assemblage types. Photographs 1–3 and 5–6 show, respectively, typical light/biogenic laminae and dark/terrigenous laminae assemblages. Photograph 7 illustrates two types of sublaminae. Photographs 4 and 8 compare two different degrees of silicification on two diatom species

the number of lithic grains (GN) is generally lower in light ($n_{laminae} = 4$) than in dark laminae ($n_{laminae} = 5$) with mean values of 303 and 548 grains/mm^2, respectively (Figure 4a). We ascertained the significance of different grain populations in light versus dark laminations through the WMW statistic test. At the 1% confidence level, the WMW test yields a H_{GN} value of 2.84 superior to the rejection threshold of 2.58 ($n_{light} = 23$, $n_{dark} = 43$). Different GN thus prevails in light and dark laminations, indicating that intracouplet differences are greater than intercouplet differences between laminae of the same colour.

Section 13: Hypsithermal period

Fourteen laminations and 26 sublaminations were observed in section 13 (TS 4, 5, 6) (see Figure 4b for TS location). The laminations divide up into five lights, six darks and three transitional laminae with respective thicknesses of 0.7 cm (σ = 0.1 cm), 3.6 cm ($\sigma = 1.8$ cm) and 0.6 cm ($\sigma = 0.2$ cm), yielding an average thickness of 4.6 cm ($\sigma = 1.6$) for the couplets. Thickness of sublaminae varies between 0.1 and 2.1 mm (n = 26, mean = 1 mm, $\sigma = 0.6$ mm).

Diatom assemblages

Diatom census counts performed between 1858 cm and 1919 cm ($n = 62$) evidence the same diatom species as in section 5 but with an important shift in dominance. *Chaetoceros* resting spores (22%), *F. kerguelensis* (19%), *F. rhombica* (15%) and *T. antarctica* (11%) are more abundant and are accompanied by a suite of subordinate species such as large centric diatoms (9%), *F. curta* (9%), other cryophilic *Fragilariopsis* diatoms (8%), *Phaeoceros* vegetative cells (4%), needle-like species (2%) and *C. pennatum* and rhizosolenoids (1%) (Figure 3b).

Qualitative examinations of diatom assemblages on the TS demonstrate the same dominant species as mentioned above with a gradational evolution of the assemblages from light to dark laminae and an abrupt change from dark to light laminae. Three main assemblages are documented: assemblages type C in the light laminae and assemblages type E and F in the dark laminae (Figure 5).

Assemblage type C is mainly composed of *F. rhombica* associated with cryophilic *Fragilariopsis* sp., *F. kerguelensis* and CRS. The relative occurrence of CRS increases from bottom to top of the laminae. Out of five light laminations analysed on the TS taken from section 13, four are composed of assemblage type C. The last lamination is represented by the bi-specific assemblage type B defined before (Figure 3b).

Dark laminations are characterized by the above-described assemblage types E and F. Of six dark laminations, five are characterized by assemblage type E while the last lamination is composed of assemblage type F. We noted the presence of three transitional laminae, showing a mixture of assemblage types C, B and D in the lower part of the TS sequence (Figure 3b). We also noted that dark laminations numbers 1 and 4 present greater relative abundances of CRS and higher frustule silicification (Figure 5).

Twenty-six sublaminae appear as thin light laminae within dark laminations with upper and lower sharp contacts. Diatom examinations evidence three diatom assemblage types. Two are near monospecific assemblages, composed of *T. antarctica* ($n = 8$) or rhizosolenoids ($n = 3$) and referred to Ta and Rh, respectively (Figure 5). The last one, named P for pulsed event, is similar to assemblage type D ($n = 15$) (Figure 3b). The Rh sublaminae appear at the bottom of dark laminations while the Ta sublaminae generally occur at the top of dark laminations. P sublaminae are scattered throughout dark laminations. Ta, Rh and P display mean thicknesses of 371 μm ($\sigma = 289$ μm), 860 μm ($\sigma = 470$ μm) and 1300 μm ($\sigma = 460$ μm), respectively. These sublaminae cannot be interpreted as light laminations because of their specific diatom assemblages and reduced thickness. They conversely represent abrupt events during deposition of the dark laminations.

Detrital content

Ti relative concentrations are lower in light laminae than in dark laminae both at the x-ray and TS scale, with mean values of 13 and 14 cps, respectively (Figure 4b). Digital analysis of grains larger than 5 μm indicates dominance of the silt fraction with a unimodal histogram frequency centred at ~10 μm diameter. The number of grains (GN) calculated on 5 PM (Figure 4b) follows the same pattern as Ti content with mean values of 152 grains/mm^2 in light laminations and 264 grains/mm^2 in dark laminations. At the 1% confidence level, the WMW test yields a $H_{Ti\ content}$ value of 1.72, greater than the rejection threshold of 1.64, and a H_{GN} value of 5.61, also superior to the rejection threshold of 2.58 ($n_{light} = 25$, $n_{dark} = 111$ for Ti content; $n_{light} = 58$, $n_{dark} = 94$ for GN). This demonstrates that different detrital populations prevail in light and dark laminations of the sequence studied here and that the intracouplet differences in Ti content and GN are greater than intercouplet differences of the same colour type lamination.

Discussion

The presence of well-preserved frustules of needle-like species and of the easily dissolved species *C. pennatum* (Beucher *et al.*, 2004) indicates that buried diatom communities are barely influenced by differential preservation and, thus, accurately record surface environment changes. We hereafter use data on detrital content as well as the ecological preferences of dominant species to determine the significance of lamination types and to link their succession to environmental conditions.

Seasonal and subseasonal signals

Light/biogenic laminae

Light laminae are characterized by low density, low Ti content and low GN. They are therefore mainly composed of biogenic material, ie, diatoms. Light laminae are characterized by assemblage types A and C in which cryophilic *Fragilariopsis* species (mainly *F. curta* in section 5 and *F. rhombica* in section 13) and CRS are the co-dominant species groups, with subordinate presence of *C. pennatum* and vegetative *Phaeoceros* sp.

Fragilariopsis curta and CRS show a preference for stable, stratified waters and sea ice proximity (Leventer, 1991; McMinn and Hodgson, 1993; Crosta *et al.*, 1997) that seeds the surrounding surface water as it melts. This seems also true for *F. rhombica*, with the difference that this species thrives in waters slightly warmer than *F. curta* (Armand *et al.*, 2005). These conditions are encountered in spring and, when associated with sufficient light and nutrients levels, promote intense diatom blooms. Blooms may eventually deplete the nutrient pool thus leading to CRS formation (Leventer, 1991). We therefore interpret the light/biogenic laminae to represent the spring season. Spring laminae evidence here, however, depart from previous studies in other cores from the EAM (Stickley *et al.*, 2005) and the Antarctic Peninsula (Leventer *et al.*, 2002; Bahk *et al.*, 2003; Maddison *et al.*, 2005) in which the spring season is characterized by greater abundances of CRS (60%). Low CRS occurrence is confirmed by diatom census counts all core long (Crosta *et al.*, 2005) and may result from more oceanic conditions prevailing at the core location.

Indeed, presence of *Phaeoceros* vegetative cells suggests an oceanic influence (Maddison, 2005) and *Ch. neglectus* has not been reported to be seeded from sea ice (Garrison *et al*., 1987; Riaux-Gobin *et al*., 2003).

Assemblage type A may be followed by the predominance of migrant species such as *C. pennatum* and rhizosolenoids that characterize the diatom assemblage type B. These species thrive normally in open water with little sea ice during the growing season (Fryxell and Hasle, 1971) and display positive buoyancy (Crawford, 1995; Leventer *et al*., 2002; Bahk *et al*., 2003). Out of Antarctica, these species groups were shown to be part of the shade flora that reaches very high biomass at the pycnocline (Kemp *et al*., 1999). Their record in the sediment was interpreted as an event of rapid sedimentation when the pycnocline weakened (Kemp *et al*., 2000). Increasing occurrence of *C. pennatum* and rhizosolenoids throughout the light laminae suggest here a strengthening of the pycnocline during the spring season, thus conducting to increasing biomass accumulation and export after cell senescence. This assemblage therefore may be an indicator of warmer, more oligotrophic, open-water intrusion (Stickley *et al*., 2005) or reduced wind stress.

The diatom succession from cryophilic *Fragilariopsis* species to CRS and finally to migrant species observed here indicates a transition from a cold-stratified environment with extensive sea ice cover at the beginning of the spring season to more open water as temperatures rise, with increasing seasonal insolation coupled to a decrease of the nutrient pool. Sea ice persistence implies low terrigenous input from the continent, which is additionally diluted by the intense diatom fluxes to the sea floor.

Dark/terrigenous laminae

Dark laminae are characterized by higher density, higher Ti content and higher GN. They are composed of a mixture of biogenic and terrigenous material. Dark laminae are characterized by more diverse diatom assemblages dominated by *F. kerguelensis*, *T. antarctica* and large centric species. These species preferentially thrive in open ocean water and do not support sea ice presence during the growing season (Armand *et al*., 2005; Crosta *et al*., 2005). They also exhibit lower nutrient requirements and lower growth rates than bloom-related species (Leventer and Dunbar, 1987; Zielinski and Gersonde, 1997). We interpret these assemblages as representative of summer production in open water when sea ice has retreated and nutrient levels are low, in agreement with previous studies conducted in the EAM (Leventer *et al*., 2002; Bahk *et al*., 2003; Maddison, 2005; Stickley *et al*., 2005).

Corethron pennatum and *Phaeoceros* vegetative cells are less abundant than in light laminae but display larger size and a higher degree of silicification, indicating a slow biomass build-up during the summer months. At the end of the summer season, the presence of needle-like species may become predominant, forming the assemblage type F. Here again, they may indicate the return of atmospheric perturbations during autumn that disrupt the pycnocline thus exporting downward the shade flora slowly growing at the nutricline (Bahk *et al*., 2003).

Both Neoglacial and Hypsithermal sections display greater GN and Ti content in dark laminations than in light laminations, suggesting higher terrigenous input during dark laminae deposition. In our study area, lithogenic input may have several sources including aeolian dust, focusing by deep currents (Presti *et al*., 2003), glacial runoff and subglacial melting (Rignot and Jacobs, 2002). The aeolian source, even with melting dirty sea ice, cannot account for the terrigenous fraction based on its timing. Indeed one would expect greater deposition during spring when sea ice decay releases dust particles. Strong winnowing that transports diatom frustules along with the detrital particles is not coherent with the seasonal and subseasonal signature of diatom assemblages. We therefore suggest that glacial and subglacial inputs are the dominant detrital sources to our core site and occur mainly during the summer/autumn season before the return of sea ice. Material input is primarily controlled by the extent and persistence of sea ice cover with secondary influence of atmospheric conditions. This inferred seasonal cycle in the detrital supply may be affected by the diluting effect of rapid and intense biogenic settling events.

The described sedimentary record preserves the imprint of seasonal and subseasonal biological and sedimentological dynamics, with biogenic laminae representing spring fluxes and more terrigenous laminae corresponding to summer/autumn fluxes. The gradational contact between light and overlying dark laminations is due to slow changes in the biological and sedimentological inputs, while the sharp contact between dark and overlying light laminations is due to the winter hiatus as annual sea ice re-forms. These findings support the interpretation of an annual light–dark couplet.

Sublaminae

Terrigenous laminae may be interrupted by sublaminae that represent events of rapid biogenic export during summer that dilute the terrigenous fraction. The rhizosolenoids sublaminae are encountered at the bottom of the dark laminations, therefore occurring at the beginning of summer season. They demonstrate nutrient limitation above a well-defined pycnocline that enhances their development to the detriment of other species. Nutrient limitation may be linked to a pulsed input of oligotrophic warmer water as evidenced in the Mac Robertson Shelf (Stickley *et al.*, 2005). The abruptness of the Rh events probably records punctual pycnocline breakdown. P sublaminae, present throughout dark laminations, may indicate short bloom events in response to renewal of the nutrient pool via pulsed resurgence of deep waters. Ta sublaminae, generally found at the end of the summer/autumn season, certainly indicate an environmental stress such as decrease in light level and increase in salinity when sea ice returns (Leventer *et al*., 2002; Maddison *et al*., 2005; Stickley *et al*., 2005). Closer to the Adélie Coast, similar sublaminae of nearly monospecific *Porosira glacialis* RS are found to interrupt dark summer laminations (Maddison, 2005). Although both species are thought to have similar growth requirements (Stickley *et al*., 2005) and forecast the autumn/winter transition, we show here that *P. glacialis* may thrive at colder temperatures and higher sea ice cover than *T. antarctica*, in agreement with their occurrence in surface sediments (Armand *et al*., 2005). Diatom census counts evidence anti-correlated occurrences of these two species in core MD03-2601 during the Holocene (data not shown) and ascertain the dominance of *T. antarctica* over *P. glacialis* in the TS.

The three above-described sublaminae types record spring/summer transition (Rh), punctual intense summer blooms (P) and autumn/winter transition (Ta). The distribution of the sublaminae may provide information on atmospheric and oceanic shifts and on sea ice seasonality at the annual scale.

A model of lamina deposition

We developed a schematic model to explain the climatic and oceanic conditions leading to the deposition of the laminations (Figure 6). At the beginning of spring, sea ice starts to melt but a large extent still limits continental input to the water column.

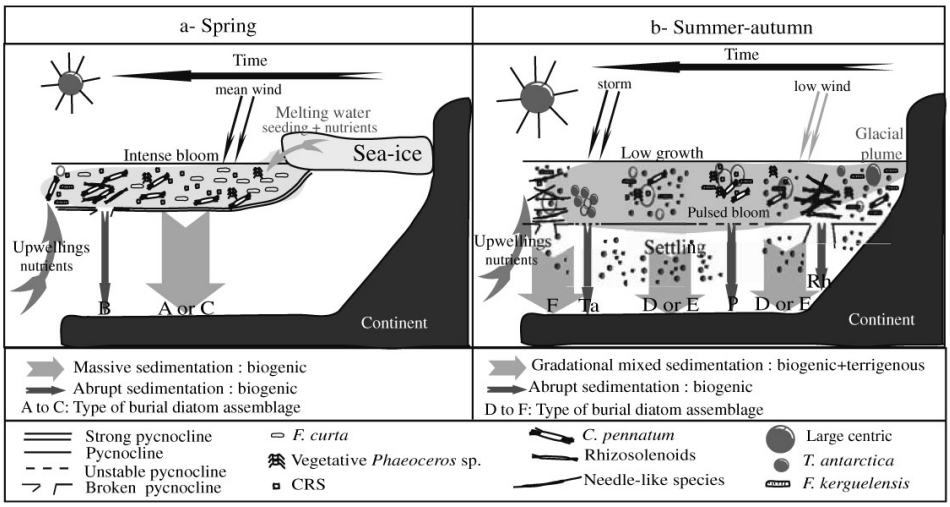

Figure 6 Conceptual model for the deposition of the different laminations and sublaminae recorded in core MD03-2601 for the spring season (a) and the summer–autumn season (b)

Sea ice melting creates strong water column stratification while supplying diatoms and macro- and micronutrients to the surface waters. The beginning of spring is also a time of decrease in the wind regime, of increase in light levels and of high nutrient content in response to the winter overturning. These factors create a favourable environment supporting an intense bloom of cryophilic pennate diatoms and *Chaetoceros* species. As spring advances, the reduction of sea ice influence and the intense nutrient uptake eventually cause CRS formation. Meanwhile, *C. pennatum* and rhizosolenoids slowly build up high biomass at the well-defined pycnocline. They eventually settle after cell senescence or after episodic pycnocline breakdown. In the Antarctic Peninsula, similar laminations have been interpreted to represent autumn mass sedimentation of diatoms that have grown during the period of summer stratification. Summer stratification is promoted by reduced wind activity and the local 'island effect' (Amos, 1987; Huntley *et al.*, 1987). In our study area, more oceanic and more chaotic atmospheric conditions (King and Turner, 1997) conducting to less stable surface water layer, explain episodic export events early in the season. High spring primary production in the form of successive diatom blooms and low detrital supply produces thick biogenic spring laminae.

As summer approaches, light increases and sea ice disappears, driving a transitional diatom assemblage characterized by the appearance of the open water species *F. kerguelensis* and of centric species, mixed with cold water species. At the beginning of summer, punctual pycnocline disruption leads to pulsed exports of rhizosolenoids, imprinted by thin sublaminae. Dilution of sea ice meltwater reduces water column stratification and increases the depth of the pycnocline. The summer light levels are maximum and nutrient content is maintained via MCDW upwelling. These conditions lead to the development of mixed diatom communities primarily dominated by *F. kerguelensis*, while centric species that present a slower growth rate may become co-dominant as the summer develops. A slower but longer diatom growth during summer than during spring is inferred from the higher silicification degree of *C. pennatum*, vegetative *Phaeoceros* sp. and *Fragilariopsis* specimens. The biogenic sedimentation is, however, lower than during spring which, coupled with increased glacial runoff, enables the concomitant settling of terrigenous particles from overflow glacial plumes (Leventer *et al.*, 2002; Finocchiaro *et al.*, 2005). Events of high productivity during summer dilute the terrigenous supply and are recorded as P sublaminae. During autumn, light level decreases, storm activity increases and sea ice returns, thus stimulating the formation of *T. antarctica* that may even lead to Ta sublaminae when the export is rapid.

Interannual variability

While TSs represent snapshots of only a few years that may be lost in the centennial to millennial climate variability, it is attractive to compare the two sequences in term of diatom assemblages. The difference in terrigenous content between the two sections is not conclusive. Section 5 from the Neoglacial period shows expanded spring laminations, dominated by *F. curta*, and reduced summer laminations (Figure 3a). Section 13 from the Hypsithermal period shows reduced spring laminations, dominated by *F. rhombica*, and expanded summer laminations (Figure 3b). These findings demonstrate cooler conditions during the period covered by TS 1–3 than during the period covered by TS 4–6, with late sea ice break up and early sea ice return during the Neoglacial.

Superimposed on the climatic trends, a strong variability in lamination thickness and diatom composition is encountered within each sequence of TS. In section 5, spring laminations of years 1–5 appear much thicker than spring laminations of years 6–11 (Figure 3a) indicating greater diatom productivity in relation to more stable and favourable environmental conditions. This is further confirmed by the reccurence of transitional laminae at the spring/summer transition in years 7–10, which possibly depicts enhanced wind activity during this period. The occurrence of assemblage type B at the beginning of the spring season instead of assemblage type A (Figure 3a) may result from more important injection of oligotrophic warmer water (Stickley *et al.*, 2005) may be resulting in earlier sea ice waning. In section 13, diatom assemblages and succession are more complex during years 1–3 than during years 4–5. Annual sedimentation rate is also reduced, especially because of thinner summer laminations, and many sublaminae are present during years 1–3 (Figure 3b). These findings again argue for less stable conditions during this period that reduced the overall diatom productivity. Lower productivity may also be related to lower nutrient input, as shown by events of greater CRS occurrence and higher silicification degree, may be in relation

to iron limitation (Hutchins and Bruland, 1998), or to earlier return of sea ice in late summer as shown by the Ta sublaminae (Figure 3b).

While TSs represent snapshots of a few years in 'cold' and 'warm' periods, they argue for strong environmental changes in nutrient supply and sea ice cover with a period of 3–5 years. At these latitudes, sea ice seasonal waning and waxing is strongly dependent upon the Antarctic Circumpolar Trough position (Enomoto and Ohmura, 1990). It is therefore attractive to link the observed changes in environmental conditions to the Antarctic Dipole that present a similar 4–5 years cyclicity (Yuan, 2004). Investigation of longer sequences of sediment fabric may help to confirm or refute this hypothesis.

Conclusions

Preliminary investigation of core MD06-2301 from the Adélie Trough illustrates the presence of laminated sedimentary layers that record seasonal and subseasonal diatom productivity and lithic input. Light laminae are mainly biogenic layers with co-dominance of cryophilic *Fragilariopsis* species and CRS. Light laminae correspond to the spring season. Dark laminations show a mixture between terrigenous particles and complex diatom assemblages dominated by *F. kerguelensis* and large centric species. Dark laminae represent the summer/autumn season. Variations in lamination thickness and in diatom assemblage types reveal a strong interannual variability that results from the interplay of sea ice, glacial runoff and oceanic currents in response to interactions between the atmosphere, ocean and cryosphere. These local to regional changes are possibly connected to the global sea ice cycle around Antarctica via the Antarctic Dipole. Further investigations of longer sections will provide a unique tool to document local to global Antarctic climate variability and cyclicity during the Holocene period at the seasonal resolution.

Acknowledgements

We thank Eleanor Maddison, Jacques Giraudeau and William Fletcher for constructive discussions. We also thank Jenny Pike, Amy Leventer and Lloyd Burckle whose helpful reviews greatly improved the manuscript. We personally thank people from Images X (CADO) cruise and from NSF-funded NBP0101 cruise for data and suggestions concerning the D'Urville Trough. Financial support for this study was provided by TARDHOL project through the national PNEDC Program (INSU-CNRS), and the Institut Paul Emile Victor (IPEV). This is an EPOC contribution No. 1597.

References

Amos, A.F. 1987: RACER: physical oceanography of the western Bransfield Strait. *Antarctic Journal of the United States* 22, 137–40.

Armand, L.K., Crosta, X., Romera, O. and **Pichon, J.J.** 2005: The biogeography of major diatom taxa in Southern Ocean sediments: 1. Sea ice related species. *Palaeogeography, Palaeoclimatology, Palaeoecology* 223, 93–126.

Bahk, J.J., Yoon, H.I., Kim, Y., Kang, C.Y. and **Bae, S.H.** 2003: Microfabric analysis of laminated diatom ooze (Holocene) from the eastern Bransfield Strait, Antarctica Peninsula. *Geosciences Journal* 7, 135–42.

Beucher, C., Tréguer, P., Corvaisier, R., Hapette, A.M. and **Elskens, M.** 2004: Production and dissolution of biosilica, and changing microphytoplankton dominance in the Bay of Brest (France). *Marine Ecology Progress Series* 267, 57–69.

Bindoff, N.L., Williams, G.D. and **Allison, I.** 2001: Sea ice growth and water mass modification in the Mertz Glacier Polynya during winter. *Annals of Glaciology* 33, 399–406.

Bond, G., Cromer, B., Beer, J., Muscheler, R., Evans, M.N., Showers, W., Hoffman, S., Lotti-Bond, R., Hajdas, I. and **Bonani G.** 2001: Persistent solar influence on North Atlantic climate during the Holocene. *Science* 294, 2130–36.

Crawford, R.M. 1995: The role of sex in the sedimentation of a marine diatom bloom. *Limnology and Oceanography* 40, 200–204.

Crosta, X., Pichon, J.J. and **Labracherie, M.** 1997: Distribution of *Chaetoceros* resting spores in modern peri-Antarctic sediments. *Marine Micropaleontology* 29, 238–99.

Crosta, X., Crespin, J., Billy, I. and **Ther, O.** 2005: Major factors controlling Holocene $\delta^{13}C_{org}$ changes in a seasonal sea ice environment, Adélie Land, East Antarctica. *Global Biogeochemical Cycles* 19, GB4029, DOI: 10.1029/2004GB002426.

de Menocal, P., Ortiz, J., Guilderson, T. and **Sarnthein, M.** 2000: Coherent high- and low-latitude climate variability during the Holocene warm period. *Science* 288, 2198–202.

Enomoto, H. and **Ohmura, A.** 1990: The influences of atmospheric half-yearly cycle on the sea ice extent in the antarctic. *Journal of Geophysical Research* 95, 9497–511.

Escutia, C., Warnke, D., Acton, G.D., Barcena, A., Burckle, L., Canals, M. and **Frazee, C.S.** 2003: Sediment distribution and sedimentary processes across the Antarctic Wilkes Land margin during the Quaternary. *Deep-Sea Research II* 50, 1481–508.

Finocchiaro, F., Langone, L., Colizza, E., Fontolan, G., Giglio, F. and **Tuzzi, E.** 2005: Record of the early Holocene warming in a laminated sediment core from Hallett Bay (Northern Victoria Land, Antarctica). *Global and Planetary Change* 45, 193–206.

Francus, P. 1998: An image-analysis technique to measure grain-size variation in thin sections of soft clastic sediments. *Sedimentary Geology* 121, 289–98.

Francus, P., Keimig, F. and **Besonen, M.** 2002: An algorithm to aid varve counting and measurement from thin-sections. *Journal of Paleolimnology* 28, 283–86.

Fryxell, G.A. and **Hasle, G.R.** 1971: *Corethron criophilum* castracane: its distribution and structure. *Antarctic Research Series* 17, 335–46.

Garrison, D.L., Buck, K.R. and **Fryxell, G.A.** 1987: Algal assemblages in Antarctic pack ice and in ice-edge plankton. *Journal of Phycology* 23, 564–72.

Harris, P.T. 2000: Ripple cross-laminated sediments on the East Antarctic Shelf: evidence for episodic bottom water production during the Holocene? *Marine Geology* 170, 317–30.

Harris, P.T. and **Beaman, R.J.** 2003: Processes controlling the formation of the Mertz Drift, George Vth continental shelf, East Antarctica: evidence from 3.5kHz sub-bottom profiling and sediment cores. *Deep-Sea Research II* 50, 1463–80.

Hodell, D.A., Shemesh, A., Crosta, X., Kanfoush, S., Charles, C. and **Guilderson, T.** 2001: Abrupt cooling of Antarctic surface waters and sea ice expansion in the South Atlantic sector of the Southern Ocean at 5000 cal yr BP. *Quaternary Research* 56, 191–98.

Huntley, M.E., Niiler, P., Holm-Hansen, O. and **Karl, D.M.** 1987. RACER: an inter-disciplinary field study. *Antarctic Journal of the United States* 22, 135–37.

Hutchins, D.A. and **Bruland, K.W.** 1998: Iron-limited diatom growth and Si:N uptake ratios in a coastal upwelling regime. *Nature* 393, 561–64.

Ingólfsson, O., Hjort, C., Berkman, P.A., Björck, S., Colhoun, E., Goodwin, I.D., Hall, B., Hirakawa, K., Melles, M., Möller, P. and **Prentice, M.L.** 1998: Antarctic glacial history since the last glacial maximum: an overview of the record on land. *Antarctic Science* 10, 326–44.

Jansen, J.H.F., Van der Gaast, S.J., Koster, B. and **Vaars, A.J.** 1998: CORTEX, a shipboard XRF-scanner for element analyses in split sediment cores. *Marine Geology* 151, 143–53.

Jones, P.D., Marsh, R., Wigley, T.M.L. and **Peel, D.A.** 1993: Decadal timescale links between Antarctic Peninsula ice core oxygen-18 and temperature. *The Holocene* 3, 14–26.

Kemp, A.E.S., Pearce, R.B., Koizumi, I., Pike, J. and **Rance, S.J.** 1999: The role of mat forming diatoms in formation of the Mediterranean Sapropels. *Nature* 398, 57–61.

Kemp, A.E.S., Pike, J., Pearce, R.B. and **Lange, C.B.** 2000: The 'fall dump': a new perspective on the role of a shade flora in the annual cycle of diatom production and export flux. *Deep-Sea Research II* 47, 2129–54.

King, J.C. and **Turner, J.** 1997**:** *Antarctic meteorology and climatology.* Cambridge Atmospheric and Space Science Series. Cambridge University Press, 409 pp.

King, J.C., Turner, J., Marshall, G.L., Connolley, W.M. and **Lachlan-Cope, T.A.** 2003: Antarctic Peninsula climate variability and its causes as revealed by analysis of instrumental records. *Antarctic Peninsula Climate Variability* 79, 12-1–12-4.

Leventer, A. 1991: Sediment trap diatom assemblages from the northern Antarctic Peninsula region. *Deep-Sea Research* 38, 1127–43.

—— 1992: Modern distribution of diatoms in sediments from the George V coast, Antarctica. *Marine Micropaleontology* 19, 315–32.

Leventer, A. and **Dunbar, R.B.** 1987: Diatom flux in McMurdo Sound, Antarctica. *Marine Micropaleontology* 12, 49–64.

Leventer, A., Domack, E., Barkoukis, A., McAndrews, B. and **Murray, J.** 2002: Laminations from the Palmer Deep: a diatom-based interpretation. *Paleoceanography* 17, 1–15.

Leventer, A., Domack, E., Dunbar, R., Pike, J., Stickley, C., Maddison, E., Brachfeld, S., Manley, P. and **McClennen, C.** 2006: East Antarctic margin marine sediment record of deglaciation. *GSA Today* in press.

Maddison, E.J. 2005: Seasonally laminated Late Quaternary Antarctic sediments. Ph.D. thesis, Cardiff University, 218 pp.

Maddison, E.J., Pike, J., Leventer, A. and **Domack, E.W.** 2005: Deglacial seasonal and sub-seasonal diatom record from Palmer Deep, Antarctica. *Journal of Quaternary Science* 20, 435–46.

Massom, R.A., Harris, P.T., Michael, K.J. and **Potter, M.J.** 1998: The distribution and formative processes of latent-heat polynyas in East Antarctica. *Annals of Glaciology* 27, 420–26.

Masson, V., Vimeux, F., Jouzel, J., Morgan, V., Delmotte, M., Ciais, P., Hammer, C., Johnsen, S., Lipenkov, Y., Mosley-Thompson, V.E., Petit, J.-R., Steig, E.J., Stievenard, M. and **Vaikmae, R.** 2000: Holocene climatic variability in Antarctica: what can be inferred from 11 ice core isotopic records? *Quaternary Research* 54, 348–58.

McMinn, A. and **Hodgson, D.** 1993: Seasonal phytoplankton succession in Ellis Fjord, eastern Antarctica. *Journal of Planktonic Research* 15, 925–38.

Migeon, S., Weber, O., Faugeres, J.-C. and **Saint-Paul, J.** 1999: SCOPIX: A new X-ray imaging system for core analysis. *Geo-Marine Letters* 18, 251–55.

Moran, S.B. and **Moore, R.M.** 1992: Kinetics of the removal of dissolved aluminium by diatoms in seawater: a comparison with thorium. *Geochimica et Cosmochimica Acta* 56, 3365–74.

NGICP members 2004: High-resolution record of Northern Hemisphere climate extending into the last interglacial period. *Nature* 431, 147–51.

Nielsen, S.H.H., Koç, N. and **Crosta, X.** 2004: Holocene climate in the Atlantic sector of the Southern Ocean: controlled by insolation or oceanic circulation? *Geology* 32, 317–20.

Pike, J., Moreton, S.G. and **Allen, C.A.** 2001: Data report: microfabric analysis of postglacial sediments from Palmer Deep, Western Antarctic Peninsula. In Barker, P.F., Camerlenghi, A., Acton, G.D. and Ramsay, A.T.S., editors, Proceedings of the ODP. *Science Research* 178, 1–17. Retreived 9 April 2005 from http://www.odp.tamu.edu/publications/178_SR/VOLUME/CHAPTERS/SR178_18.PDF

Presti, M., De Santis, L., Busetti, M. and **Harris, P.T.** 2003: Late Peistocene and Holocene sedimentation on the George V Continental Shelf, East Antarctica. *Deep-Sea Research* II 50, 1441–61.

Rathburn, A.E., Pichon, J.-J., Ayress, M.A. and **De Deckker, P.** 1997. Microfossil and stable-isotope evidence for changes in the late Holocene paleoproductivity and paleoceanographic conditions in the Prydz Bay region of Antarctica. *Palaeogeography, Palaeoclimatology, Palaeoecology* 131, 485–510.

Riaux-Gobin, C., Poulin, M., Prodon, R. and **Treguer, P.** 2003: Land-fast ice microalgal and phytoplanktonic communities (Adélie land, Antarctica) in relation to environmental factors during ice break-up. *Antarctic Science* 15, 353–64.

Rignot, E. and **Jacobs, S.S.** 2002: Rapid bottom melting widespread near Antarctic ice sheet grounding lines. *Science* 296, 2020–23.

Saporta, G. 1990: *Probabilités analyse des données et statistique.* Editions technip.

Schweitzer, P.N. 1995: *Monthly averaged polar sea ice concentration*. U.S. Geological Survey Digital Data Series.

Stickley, C.E., Pike, J., Leventer, A., Dunbar, R.B., Domack, E.W., Brachfeld S.A., Manley, P. and **McClennan, C.** 2005: Deglacial ocean and climate seasonality in laminated diatom sediments, Mac Robertson Shelf, East Antarctica Margin. *Palaeogeography, Palaeoclimatology, Palaeoecology* 227, 290–310.

Taylor, S.R. and **Mclennan, S.M.** 1985: *The continental crust: its composition and evolution*. Blackwell Science, 312 pp.

Van Bennekom, A.J., Jansen, J.H.F., Van der Gaast, S.J., Van Iperen, J.M. and **Pieters, J.** 1989: Aluminium-rich opal: an intermediate in the preservation of biogenic silica in the Zaire (Congo) deep-sea fan. *Deep-Sea Research* 36, 173–90.

Yarincik, K.M. and **Murray, R.W.** 2000: Climatically sensitive eolian and hemipelagic deposition in the Cariaco Basin, Venezuela, over the past 578,000 years: results from Al/Ti and K/Al. *Paleoceanography* 15, 210–28.

Yuan, X. 2004: ENSO-related impacts on Antarctic sea ice: a synthesis of phenomenon and mechanisms. *Antarctic Science* 16, 415–25.

Zaragosi, S., Bourillet, J-F., Eynaud, F., Toucanne, S., Denhard, B., Van Toer, A. and **Lanfumey, V.** 2006: The impact of the last European deglaciation on the deep-sea turbidite systems of the Celtic-Armorican margin (Bay of Biscay). *Geomarine Letters* in press.

Zielinski, U. and **Gersonde, R.** 1997: Diatom distribution in Southern Ocean surface sediments (Atlantic sector): implications for paleoenvironmental reconstructions. *Palaeoceanography, Palaeoclimatology, Palaeoecology* 129, 213–50.

Reconstructing Paleoproductivity throughout the Holocene: A Case Study from Adélie Land, East Antarctica

Carson, D. S.[1], Denis, D.[2], Ganeshram, R. S.[1], Crosta, X.[2], and Schmidt, S.[2]

[1] School of GeoSciences, The University of Edinburgh, West Mains Road, Edinburgh, EH9 3JW, UK
[2] Université Bordeaux 1, EPOC, UMR 5805 CNRS, av. des Facultés, Talence F-33405 cedex, France

Submitted to Geochimica et Cosmochimica Acta

Abstract

Marine sediment cores with high accumulation rates are attractive to ocean and climate scientists as they present an opportunity to study changes in paleoproductivity, ocean circulation, sea ice extent and seasonality at very high resolution. Piston core MD03-2601, retrieved from a depression in the Dumont D'Urville Trough in East Antarctica presents a 40 m long Holocene core with an average sedimentation rate of 0,4cm.yr^{-1}. However this core was severely influenced by sediment focusing (ψ). Therefore, to be able to accurately quantify mass fluxes in this region, careful correction using ^{230}Th normalisation was carried out. Using the corrected preserved fluxes, carbon, opal and excess Ba (Ba_{XS}) flux reconstructions were carried out to test the validity of using such proxies on a core heavily affected by ψ. In addition, Mo_{auth} and U_{auth} were used to monitor the redox conditions in the sediment to identify where the Ba_{XS} record may have been compromised as preservation of the Ba_{XS} signal in reducing sediments is highly variable and can decouple from the actual carbon flux this tracer is supposed to record. The results show increased levels of productivity and export production during the mid-Holocene warm period based on the carbon and opal fluxes, with sedimentary conditions becoming periodically reducing during these high flux periods, although the increasing paleo-oxygenation of deep waters during this period probably helped to prevent full anoxia ensuing. The episodic reducing conditions, however, precluded the use of the Ba_{XS} proxy as a quantitative tracer of carbon flux, although it did appear to trace some of the changes in carbon flux over the Holocene. In addition, we observe decoupling of the carbon and opal proxies, with increased opal:carbon ratios during the mid-Holocene warm period occurring as the larger diatoms such as *F. kerguelensis* dominated during this warmer period of reduced sea ice extent. This study therefore highlights how sediment cores heavily affected by ψ can be useful for tracing changes in paleoproductivity at high resolution.

1. Introduction

Reconstructing past productivity regimes in the Southern Ocean is of great importance in order to understand how it influenced or responded to changes in climate, for example during the different climatic periods of the Holocene [Hodell, et al., 2001; Nielsen, et al., 2004] or on glacial to interglacial timescales [Anderson, et al., 2002; Sigman and Boyle, 2000]. A wide variety of elemental and isotopic tracers have been developed and used on the many sediment cores taken in the Southern Ocean to detect changes in various ocean processes including; productivity, nutrient utilisation, sea ice extent, vertical mixing and macronutrient and micronutrient availability [Anderson et al., 1998; Bentaleb et al., 1996; Crosta et al., 2005a; Crosta et al., 1998; Crosta and Shemesh 2002; Crosta et al., 2004; De La Rocha et al., 1998; Elderfield and Rickaby, 2000; Ellwood and Hunter, 2000; Francois and Altabet, 1992; Francois et al., 1997; Kumar et al., 1995; Nurnberg et al., 1997; Robinson et al., 2005; Rosenthal et al., 2000; Wolff et al., 2006].

Core MD03-2601 taken from the Dumont d'Urville trough, East Antarctica, is a 40 m long sequence of laminated diatom ooze that covers the Holocene period and has an exceptionally high sedimentation rate. The goal of this study was to study a suite of paleoproxies on this core in an attempt to accurately constrain paleoproductivity during the different climatic periods of the Holocene. The Holocene period in this region is divided into four general climatic phases: an early Holocene warm period (8.5-11 cal ka BP), an early Holocene cool event (7-8.5 cal ka B.P.), a mid-Holocene warm period (3.5-7 cal ka B.P.), and a late Holocene Neoglacial (1.0-3.5 cal ka B.P), (Crosta et al., 2007).

Cores with a high sedimentation rates are attractive to paleoceanographers as they provide the chance to study sediment records at very high resolution, thus providing the chance to better constrain the interactions between Antarctic atmosphere, oceans, sea ice and glaciers, deep ocean circulation and teleconnections between high and low latitudes. Unfortunately, such cores are more often than not affected by processes such as sediment focusing that may significantly interfere with reconstructing vertical accumulation rates and subsequent estimations of carbon and opal export. This is a case study to assess the validity of elemental based export flux reconstructions in core MD03-2601.

2. Proxies

The following proxies for productivity and redox sensitive elements were used for the multi-proxy assessment of this core.

The carbon content of sediment cores has been widely used as a paleoproductivity proxy in the global ocean [Chase et al., 2003; Crosta et al., 2005b; Crosta et al., 2002; Ganeshram et al., 1995]. This proxy works on the assumption that the preserved carbon in the

sediment can be used in conjunction with the mass accumulation rate (MAR) to calculate the export of carbon to the deep ocean, although great care must be taken when determining the mass accumulation rates [Francois et al., 2004]. The carbon proxy should be used carefully as it is use as a paleoproductivity tracer assumes a consistent level of preservation over time, with variable preservation limiting the qualitative value of such reconstructions.

The opal content of sediment cores has also been a popular tool for paleoproductivity reconstructions in the global ocean [Chase et al., 2003; Bareille et al., 1998; Ganeshram and Pedersen, 1998]. This proxy works on the same calculation principle as carbon, and is a useful additional tool for studying regions dominated by diatoms to assess the export of silicate from the surface ocean. Once again, care should be taken with this tracer of paleoproductivity as the reconstruction assumes a consistent level of preservation over time though some attempts have been made to correct for differential preservation [Dézileau et al., 2000].

Barite formation in the marine water column and its flux to the seafloor appear linked to surface productivity and carbon export [Bishop 1988; Dehairs et al., 1992; Dehairs et al., 2000; McManus et al., 1998]. Thus the reconstruction of carbon export based on barium content of sediments may provide quantitative information about past changes in primary production [Francois *et al.*, 1997; Ganeshram and Pedersen, 1998; Ganeshram *et al.*, 1995]. A host of previous studies utilising sediment traps monitoring fluxes of carbon and excess Ba (barium of biogenic origin – Ba_{XS}) have produced preliminary algorithms linking the flux of biogenic barium to carbon export production [Dymond *et al.*, 1992; Francois *et al.*, 1995; McManus *et al.*, 2002; Nurnberg *et al.*, 1997]. Although relationships between Ba flux and organic carbon flux are poorly constrained in near shore areas [Dehairs et al., 2000; Fagel et al., 1999; Francois et al., 1995], a recent sediment trap study in the Western Antarctic Peninsula [Carson et al., in-prep] has identified that Ba_{XS} and carbon flux show relationships that are consistent with the previously published preliminary algorithms [Dymond and Collier, 1996; Francois et al., 1995]. This study therefore uses sedimentary Ba_{XS} as a tracer for changes in carbon flux to the sea floor.

Both Authigenic molybdenum (Mo_{auth}) and authigenic uranium (U_{auth}) enrichments are associated with the delivery of carbon to the seafloor and dissolved oxygen content at the sediment water interface [McManus, et al., 2006; Morford et, al., 1999; Morford, et al., 2005]. When low sedimentary dissolved oxygen leads to reducing conditions, soluble U (VI) is reduced into insoluble U(IV), resulting in U_{auth} precipitation [McManus, et al., 2006]. Similarly, Mo_{auth} in reducing sediments is precipitated in the presence of sulphur [Calvert and Pedersen, 1993] where soluble Mo is converted to a more particle reactive thiomolybdate [Erickson and Helz, 2000; Zheng et al., 2000] which are scavenged from sulphur containing organic material, or reacts in association with Fe-S phases [Erickson and Helz 2000; Helz, et al., 1996]. In highly reducing and carbon rich sediments, the degree of

Mo_{auth} enrichment compared to carbon delivery to the seafloor has been observed to be much higher than that of U_{auth} [McManus et al., 2006], thought to be as a result of increased sulphur cycling and removal of Mo from pore waters with no change in reduction of U(VI). These redox sensitive elements are therefore used in to trace any changes in redox conditions in core MD03-2601.

3. Materials and Methods

Piston Core MD03-2601 was retrieved from the Dumont D'Urville Trough, Adélie Land East Antarctica during the Images X cruise in February 2003. The core was retrieved aboard the *Marion Dufresne II* at 66°03.07'S, 138°33.43'E at a water depth of 746 m (Figure 1). The Dumont d'Urville Trough is composed of a number of small depressions reaching a maximum depth of 1000 m [De Santis et al., 2003] that each act as "funnels" for sinking organic material produced in the area, which improves preservation of phytoplankton cells, that are here mainly composed of diatoms [Wright and van den Enden, 2000]. Core MD03-2601 is composed of diatom ooze that alternated between structureless green ooze and green to dark green laminations of millimetre to centimetre thickness [Denis et al., 2006].

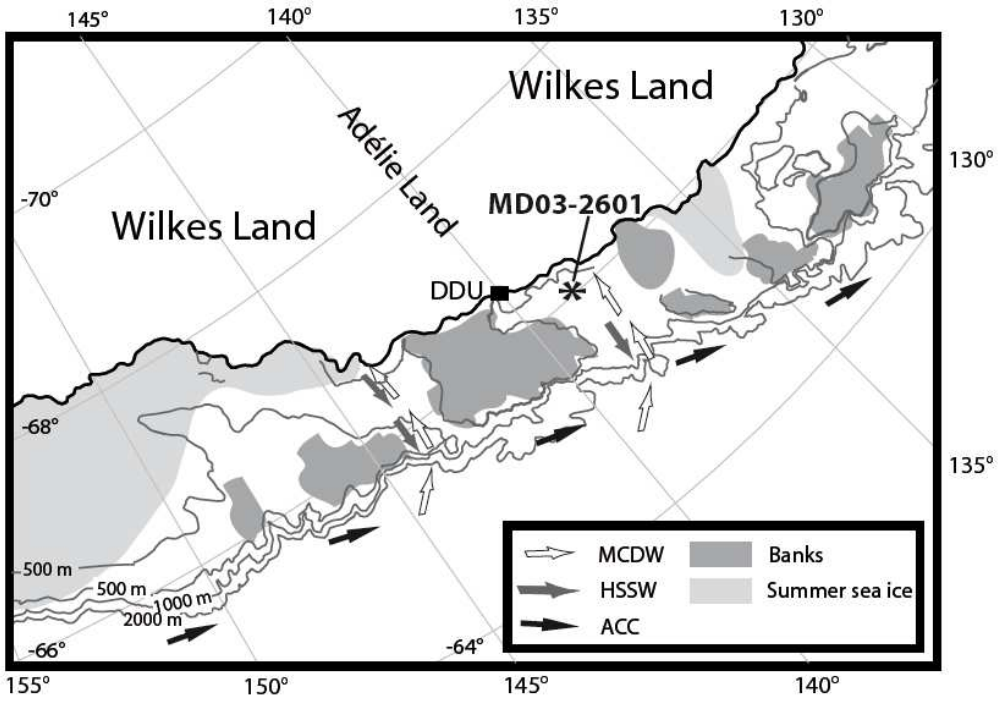

Figure 1. Location of core MD03-2601, altimetry and bathymetry of the study area (ETOPO02 data set from http://www.ngdc.noaa.gov/mgg/fliers/01mgg04.html), limit of summer sea-ice cover (Schweitzer, 1995), location of glaciers (in italic) and past ice-streams (Massom et al., 1998; Escutia et al., 2003), detail of oceanographic currents and different water masses (Rintoul, 1998; Harris and Beaman, 2003; Williams and Bindoff, 2003). Winter sea ice covers the whole oceanic area encompassed by the map. ACC: Antarctic Coastal Current, MCDW: Modified Circumpolar Deep Water, HSSW: High Salinity Shelf Water.

3.1. Age Model

We use the same age model described in Denis et al., (in-press), that used the Calib 5.0 software, the marine calibration Marine04 and a reservoir age of 1300 years as advised for this region. Core MD03-2601 records the last 11-1 cal ka BP period with an average sedimentation rate of 0.4 cm.yr^{-1}.

3.2. Diatom Census Counts

Diatoms were identified were identified every 4 to 8 cm providing a 10 to 20 year resolution [Crosta et al., 2007]. Diatom counts followed Schrader and Gersonde [1978] and Laws [1983]. More details about slide preparation, diatom identification and are found in Crosta et al., [2004]. Around 350 diatom valves were counted in each sample and the relative abundance of each was determined as the fraction of diatom species against total diatom abundance in the sample, here the *Fragilariopsis kerguelensis* are extracted from the total diatom counts.

3.3. Organic Carbon and Biogenic Opal Measurements

Organic carbon measurements were conducted every 4 cm to 8 cm. The method is described in [Crosta et al., 2005a]. Organic carbon content was measured using a Carlo Erba 2500 elemental analyser. Results were checked for internal consistency using calibrated laboratory standards such as Acetanilide, Glycine and Casein. The mean standard deviation of the carbon content is ±0.03%.

Biogenic opal measurements were conducted every 32 cm. Biogenic opal measurements follow a protocol slightly modified from [Mortlock and Froelich, 1989] in which biogenic opal was dissolved in a 0.5 M NaOH solution. Absorbance of the samples was measured each hour for 5 hours to build a dissolution curve [Muller and Schneider, 1993] and then calibrated using five standards of increasing silica concentration and a blank. More details can be found in Crosta et al. [2005a].

3.4. Elemental Analysis

Elemental analyses were determined using the methods described in [Fitton, et al., 1998] at 32 cm resolution for aluminium (Al), molybdenum (Mo) and barium (Ba). Standard deviations are 0.05 % for Al, 5.8 % for Mo, and 5 ppm for Ba. Although it should be noted that major element precision is governed more by reproducibility in making the glass disc than by counting statistics.

Excess barium, or Ba_{XS} (also known as biogenic barium) was calculated using the following formula [Francois, et al., 1995]:

$$Ba_{XS} = Ba_{total} - (Ba/Al_{terrigenous} \times Al_{total})$$

where Ba_{total} is the total barium content of sediment, $Ba/Al_{terrigenous}$ is 0.0067 for the Southern Ocean [Nurnberg, et al., 1997] and Al_{total} is the total aluminium content of sediment.

Authigenic Mo (Mo_{auth}) was calculated using the following formula [Morford and Emerson 1999]:

$$Mo_{auth} = Mo_{total} - (Mo/Al_{terrigenous} \times Al_{total})$$

3.5. Sediment fluxes normalisation

Regions of high sedimentation are often areas that are affected by lateral input of sediment, termed "sediment focusing", and this effect is often intensified by deep water currents [Francois et. al, 2004]. In order to reconstructed unbiased biogenic fluxes deposited, we use high-resolution measurements of ^{230}Th [n= 60; Denis et al., submitted] to normalize the opal, carbon and barium percentage contents, following the method developed by Bacon [1984]. This method is based on the "assumption that the flux of scavenged ^{230}Th reaching the seafloor is know and equal to the rate of ^{230}Th production from the decay of ^{234}U in the overlying water column" [Francois et al., 2004]. Thereby, the normalization of biogenic contents by instantaneous ratio of water column scavenged ^{230}Th flux allows an estimation of the mass flux deposition, unbiased by lateral sediment contribution and variations of one component on another, and less impacted by chronological errors [Bacon, 1984; Suman and Bacon; 1989; Francois et al., 2004; Adkins et al., 2006]. Thereby, the ^{230}Th normalised fluxes resituate the "preserved" vertical fluxes ($^{PR}F_v$) i.e. the material that remained after diagenetic alteration, following:

$$^{PR}F_v = FW / (^{230}Th_{XS})_0$$

where FW is the rate of $^{230}Th_{XS}$ production in the water column, and therefore its flux to the seafloor, and $(^{230}Th_{XS})_0$ is the measure of $^{230}Th_{XS}$ in the sediment sample.

The preserved vertical rain rate for each sedimentary component was determined using:

$$F_v = {}^{PR}Fv \times fi$$

where fi is the measured weight fraction of the constituent of interest in the sediment (here : opal, organic carbon and biogenic barium).

The application of this approach on active hydrodynamic shallow shelves close to a sea ice system like our study zone can implicate some precaution for using the ^{230}Th normalization. The boundary scavenging effect, defined by Spencer et al. [1981], leads to an advection of the ^{230}Th radioelement from low flux zone to high flux zone, inducing an overestimating of radioisotopes inventoried in the sediments underlying high productive areas. Such mechanism can occur in our area from low productive zones as northward to Polar Frontal Zone as well as southward to Marginal Ice Zone, which can scavenge ^{230}Th via MCDW [Rutgers van der Loeff and Berger, 1993] and/or HSSW [Henderson et al., 1999]. Nevertheless, in regions of deep bottom water formation, the renewal of deep waters is more rapid than the residence time of ^{230}Th (e.g. 40 years), as demonstrated in our area [Rintoul, 1998; Rintoul et al., 1999; Tanhua et al, 2004], leading to loss of ^{230}Th by northward advection. Therefore, an excess of ^{230}Th supply by boundary scavenging can be compensate by a loss of ^{230}Th by high waters renewal, as previously illustrated in the Pacific sector [Chase et al., 2003].

Differential efficiency scavenging of Th has been highlighted in function to rain rate and particles type in several studies [Chase and Anderson, 2004 and references herein]. Nevertheless, on the core MD03-2601, the fluxes based on ^{14}C dates not show variations exceeding a factor 3 and the lithogenic/biogenic ratio differs only by a maximum factor of 1.5 (data not shown). These variations cannot explain the ^{230}Th changes observed here because one order of magnitude fluxes changes is necessary to affect the scavenging of ^{230}Th [Francois et al., 1990; Yu, 1994], and any relationships between ^{230}Th content and different sediment components (opal, C_{org}, N_{org} and lithogenic content) are displayed ($r^2 < 0.2$) (data not shown). The position of core MD03-2601 in a shallow environment implicate great detrital and authigenic contributions (respectively, 20 to 55 % and 1 to 23 % of the total ^{230}Th) in comparison to the scavenged part of ^{230}Th. Therefore the absolute values of Ψ and of normalized flux reconstructions should be treated with some caution (see error bar on Figure 2).

In conclusion, we believe that the ^{230}Th normalization can be confidently used to document the relative changes of biogenic fluxes over the core site during the Holocene.

4. Results

Sediment focusing factors (Ψ), classical mass accumulation rates (MAR), ^{230}Th excess normalised fluxes and diatom abundances are presented in Figure 2. The MAR range from 50 to 175 mg/cm^2/yr and follow the variations of sediment focusing, whereas the ^{230}Th normalised MAR show an opposite pattern with much lower values of 2 to 9 mg/cm^2/yr. Total diatom abundances follow the same pattern as ^{230}Th normalised vertical flux, with values ranging from 112 – 2041 x 10^6 valves per gram of sediment.

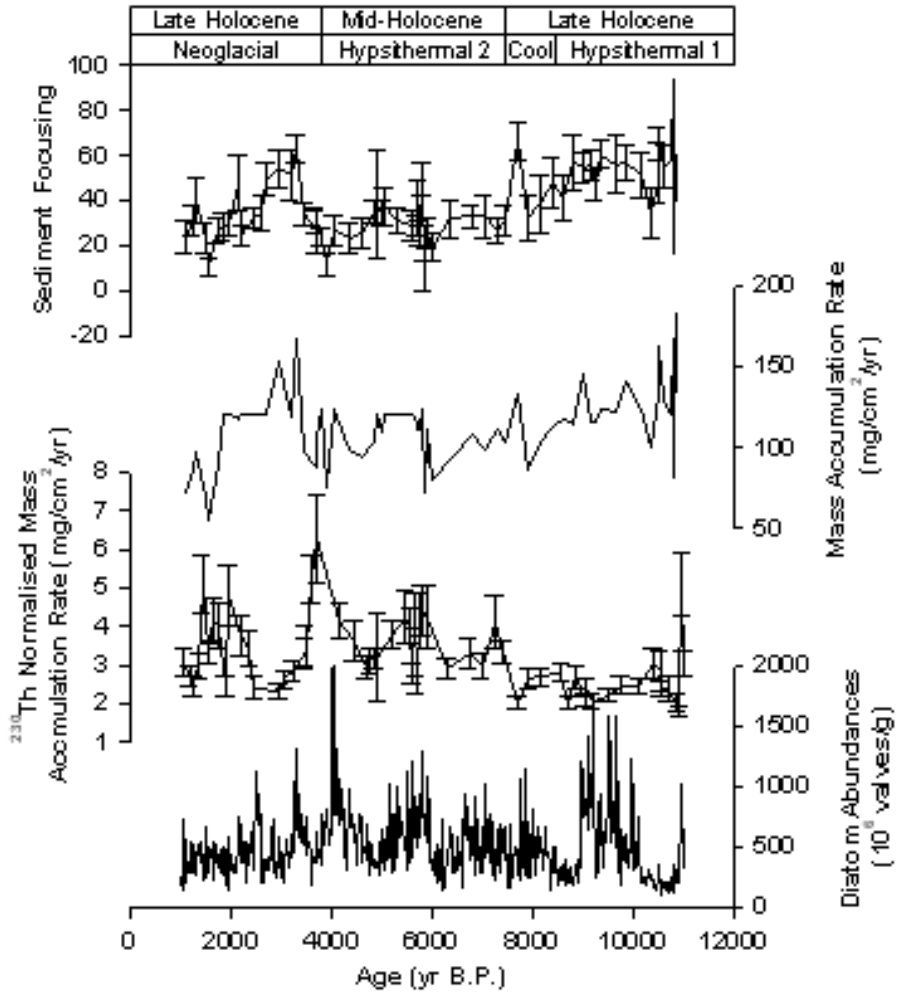

Figure 2. Down-Core profiles of (a) Sediment Focusing (b) Mass accumulation rate, (c) ^{230}Th normalised mass accumulation rate and (d) Diatom abundances. Boxes at the top of the figure represent the different climatic periods of the Holocene (Denis et al., in-press).

Carbon and opal data are presented in Figure 3. Carbon and opal percentages are plotted alongside ^{230}Th normalised vertical flux reconstructions. Carbon and opal percentages show slightly different patterns throughout the Holocene that disappear when they are converted in fluxes by the ^{230}Th normalisation. Vertical flux reconstructions of carbon and opal show relatively low values during the early Holocene warm period (11 – 9 cal ka BP), ranging from 0.03 – 0.06 mg/cm2/yr and 0.9 – 2.0 mg/cm2/yr for carbon and opal, respectively. During the cool event (8.5 – 7 cal ka BP), the fluxes of carbon and opal show an increasing trend reaching 0.04 mg/cm2/yr and 1.4 mg/m^2.yr for carbon and opal, respectively. The mid-Holocene warm period (7 – 3.5 cal ka BP) generally show much higher vertical fluxes of carbon and opal ranging from 0.03 – 0.07 mg/cm2/yr and 1.0 – 2.6 mg/cm2/yr, respectively, with two distinct peaks. The late Holocene Neoglacial (3.5 – 1 cal ka BP) are characterised by reduced fluxes as low as 0.03 mg/cm2/yr for carbon and 1.0 mg/cm2/yr BP for opal. There were, however, two flux peaks during the Neoglacial centred at 1.5 and 2.3 cal ka BP, reaching 0.09 mg/cm2/yr for carbon and 3.2 mg/cm^2/yr for opal.

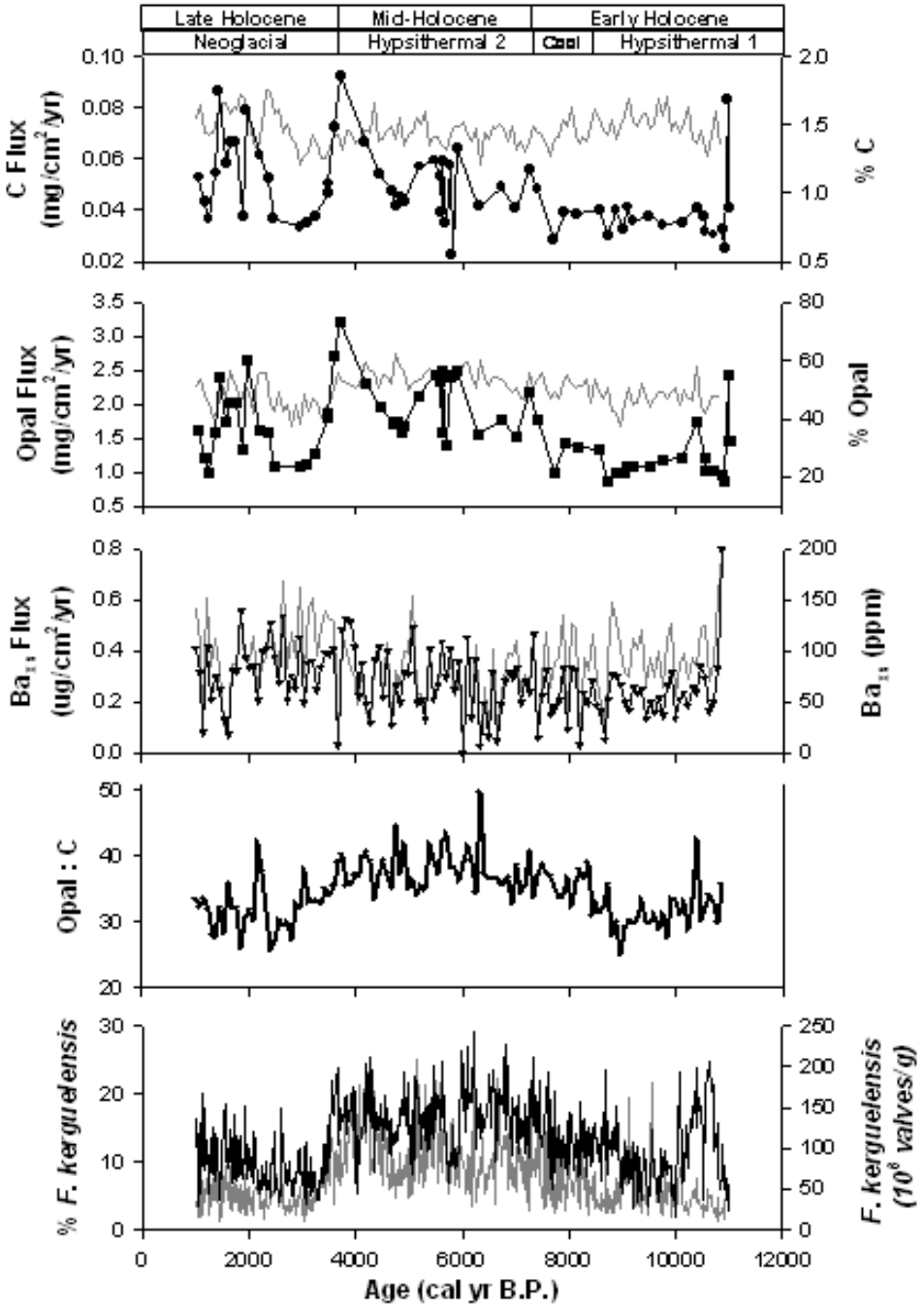

Figure 3. Down-Core profiles of (a) ^{230}Th normalised carbon flux and % C content of sediment, (b) ^{230}Th normalised opal flux and % opal content of the sediment, (c) ^{230}Th normalised Ba_{XS} flux and Ba_{XS} concentration of sediment, (d) opal:C ratios and (e) % *F. kerguelensis* of the total diatom community and *F. kerguelensis* abundances.

Ba_{XS} data are also presented in Figure 3 with Ba_{XS} plotted alongside ^{230}Th normalised vertical flux reconstructions of Ba_{XS}. Normalised Ba_{XS} fluxes range from 0.002 – 0.8 µg/cm^2/yr and display different patterns to the carbon and opal reconstructions. In addition to high amplitude variation throughout the core, significant Ba_{XS} flux minima occur at 8.7 during the early Holocene warm period (11-8.5 cal ka BP), 8.2, 8.0 and 7.4 cal ka BP during the cool event (8.5 – 7 cal ka BP), at 6.7, 6.6, 6.5, 6.4, 6.3, 6.2, 6.0, 5.8, 5.3,

4.8, 4.7, 4.6, 4.3 and 3.7 cal ka BP during the mid-Holocene warm period (7 – 3.5 cal ka BP), and at 2.2, 1.6 and 1.2 cal ka BP during the late Holocene Neoglacial (3.5-1 cal ka BP).

Opal:Carbon ratios in Figure 3 show maximum values during the mid-Holocene warm period, and generally lower values during the early Holocene warm period and late Holocene Neoglacial. The overall pattern of opal:carbon is similar to the abundances and % of *F. kerguelensis*, also presented in Figure 3.

Figure 4 presents the ^{230}Th normalised vertical flux reconstructions of Ba_{XS}, Mo_{auth}, U_{auth} and the C_{org}:Ba_{XS} ratio of sediment. The Mo_{auth} and U_{auth} show large variation throughout the Holocene, with each plot displaying a decreasing trend during the mid-Holocene warm period. The C_{org}:Ba_{XS} plot displays a fairly consistent flat pattern, apart from distinct peak values occurring in concert with the lows in Ba_{XS} vertical flux reconstructions.

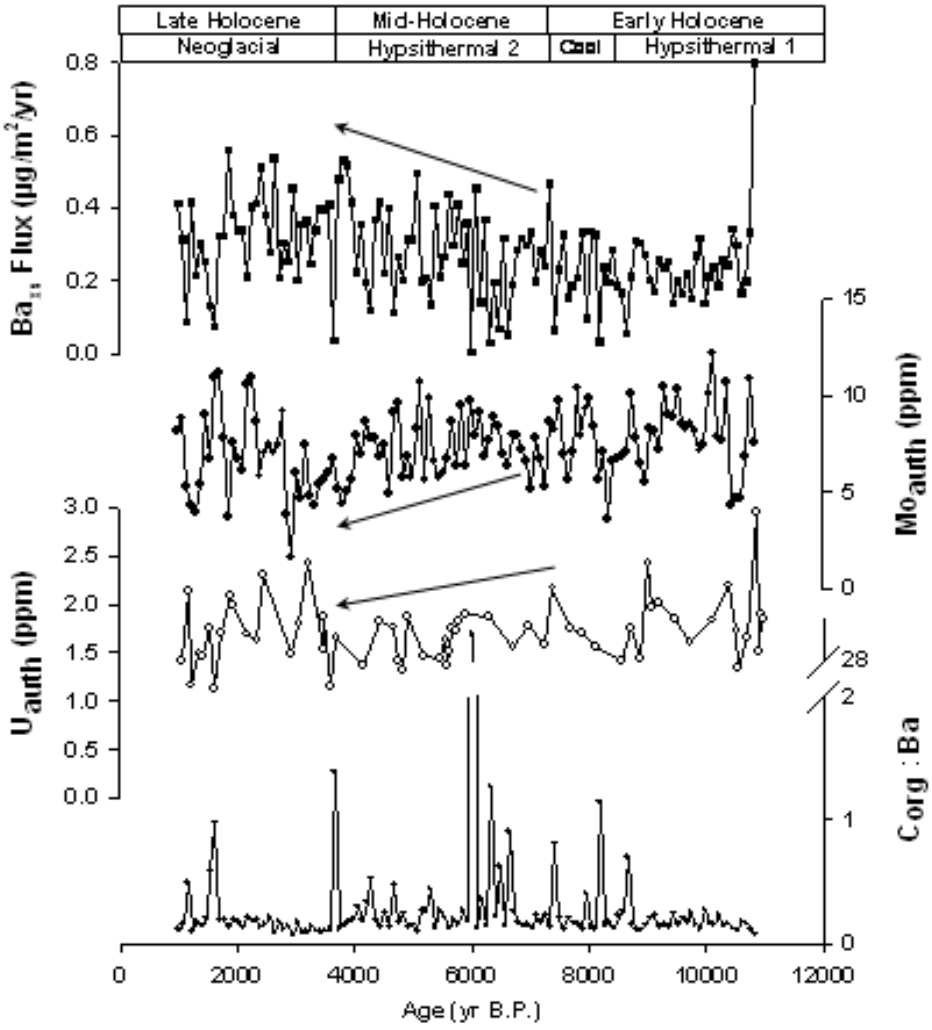

Figure 4. Down-Core profiles of (a) ^{230}Th normalised Ba_{XS} fluxes, (b) Mo_{auth}, (c) U_{auth}, and (d) C_{org}:Ba ratio of sediment. Lines show increasing Ba_{XS} fluxes and decreasing U_{auth} and Mo_{auth} during the mid-Holocene warm period.

5. Discussion

5.1. Biogenic Flux Reconstructions

Core MD03-2601 has an exceptionally high sedimentation rate (average of 0.4 $cm.yr^{-1}$), implying that it would be an excellent candidate for studying changes in Holocene paleoproductivity at high resolution. However, closer inspection using the ^{230}Th tracer [Denis et al., submitted] reveals that the extent of focusing far outweighs the vertical sedimentary fluxes at the core site (Figure 2), a common occurrence in margin systems. This required normalisation by ^{230}Th in order to reconstruct the vertical fluxes. The reconstructions of vertical carbon and opal fluxes (Figure 3) show good agreement with down-core abundances of diatoms, the major phytoplankton group in this region (Figure 2).

These records therefore appear to be good indicators of paleoproductivity in the Dumont D'Urville Trough during the Holocene. In despite of the uncertainty associated to our quantitative estimations of the vertical biogenic fluxes buried, they agree well with modern studies (Table 1). This method of normalisation guarantees the reconstruction of preserved material in the core, but not the total export flux [Francois et al., 2004]. Indeed, modern studies on the continental shelf of Antarctica show that less than 0.2% and 6% of organic carbon and opal, respectively, produced by phytoplankton is permanently buried in the sea bed [Nelson et al., 1996]. The ratios between our buried fluxes of organic carbon and opal with surface production estimated in our area by remote sensing [Arrigo et al., 2003] and water sampling [Beucher et al., 2004] are consistent with the other overall preservation efficiency data (OPE) observed in the coastal and continental shelf zones (CCSZ). The OPE of organic carbon and biogenic silica are relatively high (~0.8% and ~5.5% respectively) but the Si/C ratio in buried sediment (~7 and ~30 as mass and molar ratios, respectively) agrees well with previous studies in the area [Nelson et al., 1996].

The reconstructed Ba_{XS} fluxes do show similar patterns to the opal and carbon profile, but exhibit more variation than the carbon and opal record, and frequent occurrences of Ba_{XS} minima concentrated during the early Holocene cool period and mid-Holocene warm period. The decoupling of the carbon and opal proxies from the Ba_{XS} proxy is thought to be caused by changes to redox conditions in the sediment, that were traced using the redox sensitive elements Mo_{auth} and U_{auth}, with enrichment of these elements linked to organic carbon delivery to the seafloor and reducing conditions in the sediment [McManus et al., 2006].

		Organic carbon (Flux in molC/m²/yr)			Opal (Flux in molSi/m²/yr)		
Location	**Study**	**Production**	**^{230}Th-normalised accumulation**	**Overall Preservation Efficiency**	**Production**	**^{230}Th-normalised accumulation**	**Overall Preservation Efficiency**
Indian Sector - PFZ	Pondaven et al., 2000	-	-	-	2.43	0.075	3.1
Indian Sector - POOZ	Pondaven et al., 2000	-	-	-	3.34	0.21	6.3
Indian Sector - SIZ	Pondaven et al., 2000	-	-	-	1.62	-	-
Pacific Sector - PFZ	Nelson et al., 2002	6.9	0.0012	0.017391304	0.35	0.016	4.57
Pacific Sector - POOZ	Nelson et al., 2002	8.5	0.0017	0.020	0.95	0.048	5.05
Pacific Sector - SIZ	Nelson et al., 2002	8.7	0.0062	0.071	2.4	0.16	6.67
Ross Sea - CCSZ	Nelson et al., 1996	11.87	0.02*	0.18	2.02	0.12*	5.75
DDU - CCSZ **	Beucher et al., 2004 + this study	-	-	-	5.184	**0.275**	**5.30**
DDU - CCSZ	Arrigo and Van Dijken, 2003 + this study	4.64+/-1.15	**0.039**	**0.84**	-	-	-

Table 1. Estimate fluxes of organic carbon and biogenic silica in different sector of the Southern Ocean from the production in the water column to the burial in sea bed. PFZ= Polar Frontal Zone, POOZ= Permanently Open Ocean Zone, SIZ= Seasonal Sea ice zone, CCSZ= Coastal and Continental Shelf Zone, DDU= Dumont D'Urville. *: accumulation rates not normalized by ^{230}Th. ** Annual extrapolation realized here is based on summer measurments. Shaded area corresponds to estimations based on this study.

5.2. Preservation *versus* Export/Production Changes

Mo_{auth} and U_{auth} profiles in core MD03-2601 display high variation during the Holocene, but both exhibit a general decreasing trend, especially during the mid-Holocene warm period (Figure 4). Mo_{auth} and U_{auth} in core MD03-2601 are affected by both changes to the delivery of carbon to the seafloor and changes to the intensity of deep water currents. Increased export of carbon is evident during the mid-Holocene warm period (Figure 3), as is increasing deep water formation reconstructed from sortable silt [Denis et al., submitted], showing an abrupt weakening of deep water formation and bottom water oxygenation at ~7.5 cal ka BP, followed by a steady increase up until 1 cal ka BP. Focusing on the 7.5-4.0 cal ka BP period, the redox proxy data from this study are in agreement with the reconstructed paleo-oxygenation of bottom waters. The long term millennial trends of both Mo_{auth} and U_{auth} show a decreasing trend during this period (Figure 4). Therefore, at the Holocene scale, the variations of paleoproductivity evidenced here by ^{230}Th normalised biogenic fluxes reflect certainly changes of water column processes (i.e. production/remineralisation/export) than differential preservation at the sediment/water interface.

However, on shorter centennial time-scales there are episodic enrichments of both Mo_{auth} and U_{auth} that were likely caused by higher delivery of organic material to the seafloor, resulting in reducing conditions irrespective of active deep water ventilation. When organic sediment loads to the seafloor drive conditions towards anoxia, the enrichment of Mo_{auth} relative to carbon can increase by up to 5 times compared to oxic conditions thought to be as a result of more intense sulphur cycling, where little or no change is observed in U_{auth} [McManus et al., 2006]. This is consistent with many of the sharp peaks in Mo_{auth} in core MD03-2601, especially during the mid-Holocene warm period, not occurring in concert with peaks in U_{auth}. It should be noted that the sortable silt proxy from Denis et al [submitted] and U_{auth} were measured at lower resolution than the Mo_{auth}, so the Mo_{ath} may capture higher resolution changes in sediment redox chemistry but does not allow direct comparison with SS and U_{auth}.

5.3. Ba_{XS} Proxy Sensitivity

Reducing conditions severely compromise the preservation of barite in marine sediments [McManus et al., 1998; Schenau et al., 2001] and such conditions appear to have affected the Ba_{XS} proxy in this core. This precludes the assumption made with the Ba_{XS} proxy that preservation in the sediment record is predictable or consistent. Preservation in oxic sediments is usually very good as pore waters are generally considered to be saturated with dissolved Ba, resulting in low barite dissolution [Dymond et al., 1992]. However in reducing sediments, sulphate reduction during the oxidation of organic matter will reduce sulphate concentrations in sediments to a value that promotes remobilisation of Ba through dissolution of barite ($BaSO_4$), resulting in increased dissolved Ba concentrations in sediment

pore waters [McManus et al., 1998; Schenau et al., 2001]. This can also lead to re-precipitation of barite below the sulphate reduction layer, which may skew both sections (sulphate reducing and oxic sediment below) for latter day reconstruction.

Although the Mo_{auth} and U_{auth} data are consistent with periods of reducing conditions during the Holocene, thus precluding a quantitative reconstruction of paleoproductivity using the Ba_{XS} proxy, there is still some qualitative value in the data. During the early Holocene cool event and mid-Holocene warm period there is a general increasing trend in the reconstructed flux of Ba_{XS}, when the redox sensitive proxies Mo_{auth} and U_{auth} show a general decreasing trend. This observation is consistent with an increase in deep water currents and ALBW formation [Denis et al., submitted], and suggests that preservation of barium improved in the presence of better oxygenation of sediments. In Figure 4, the C_{org}:Ba ratio shows distinct peaks when the Ba_{XS} fluxes display minima and the Mo_{auth} display maxima. These peaks in C_{org}:Ba agree are consistent with reduced preservation of Ba during periods of sub-oxic diagenesis and sulphate reduction and lend support to the interpretation of the redox sensitive proxies. Any interpretation based on Ba_{XS}, however, should therefore be treated with caution due to the lack of constraint on the variable preservation of Ba_{XS} in sediments as a result of sedimentary oxygen deficiencies.

5.4. Opal:C_{org} decoupling ?

The opal:carbon ratio in Figure 3 highlights how opal and carbon decouple from one another as export proxies during the Holocene in the Dumont D'Urville Trough. The concave shape of the down-core profile shows that the opal:carbon ratio significantly increased during the early Holocene cool event, reached peak values during the mid-Holocene warm period, and then declined towards the onset of the late-Holocene Neoglacial. Opal:carbon ratios in diatoms can be affected by diatom species [Abelmann, et al., 2006; Smetacek, et al., 2004], growth rates [Assmy et al., 2006; Assmy et al., 2007], and iron availability [Armand, et al., 2008; Hutchins and Bruland 1998; Mosseri et. al., 2008; Takeda, 1998]. The high productivity and particle flux suggest that iron was not limited, and iron sources are not thought to have limited productivity during the Holocene [Vaillancourt et al., 2003], at least early on in the growing season, with sources including aeolian transport, melting ice, coastal sediments and transport of Upper Circumpolar Deep Water (UCDW) across the shelf [Sambrotto et al., 2003]. Larger diatom species such as *F. kerguelensis* (Figure 3) display an almost identical pattern to the down-core variations in opal:carbon ratios. This shift in diatoms is a result of the climate driven shortening of sea ice coverage in early spring and lengthening of the phytoplankton growing season [Crosta et al., 2005] leading to *F. kerguelensis* out-competing the sea ice associated *Fragilariopsis curta* as the dominant diatom species. The *F. kerguelensis* profile is similar to other large diatom species but *F. kerguelensis* is presented here as it is the dominant larger diatom species during the mid-Holocene warm period [Crosta et al., 2007]. *Fragilariopsis kerguelensis* is considered a slow growing species [Assmy, et al., 2006; Assmy, et al., 2007]

and its robust structure compared to the more fragile, pennate or needle-like diatom species gives it a higher opal:carbon ratio [Armand et al., 2008]. Field studies in the Southern Ocean confirmed the highest opal:carbon ratio in diatom blooms heavily dominated by *F. kerguelensis* [Queguiner et al., 1997]. In addition changes in diatom community composition, the slower but longer period of diatom growth resulted in higher silicification of other *Fragilariopsis* species and *Corethron pennatum* [Denis et al., 2006], possibly exacerbating the effect on the opal:carbon ratios at the species level.

Although we can not rule out differential preservation in this core based on the inferred differences in redox conditions, it is not suspected that the opal or carbon content of core MD03-2601 was significantly affected by variable preservation along the Holocene. Strong changes in degradation would have affected the opal:carbon ratios, with opal preferentially degrading over carbon [DeMaster et al., 1996] as opal is well preserved in diatom dominated environments of rapid export. However, the opal:carbon ratio appears to be principally affected by changes to diatom species (see above) and shows no variation consistent with the redox (Mo_{auth} and U_{auth}) or deep water ventilation proxies [Denis et al., submitted]. Similarly, the carbon:nitrogen ratio is around 7-8 all core long (data not shown). Heavier degradation of organic material would have increased the carbon:nitrogen ratio when preferential degradation of organic nitrogen during diagenesis occurred [Ganeshram et al., 1999; Hedges et al., 1986; Rosenfeld, 1981].

6. Conclusions

This study of core MD03-2601 was a useful case to identify how useful paleoproductivity proxies are for reconstructing export flux in regions of high sediment focusing.

Normalisation of the traditional mass accumulation rate calculations with ^{230}Th provides more the estimation of the preserved vertical fluxes. In despite of error bars associated to the ^{230}Th normalisation method, the reconstructed biogenic fluxes are in agreement with modern studies.

After ruling out changes in preservation affecting the carbon and opal flux reconstructions, we believe that the variations of preserved fluxes are representative of produced/exported biogenic flux variations in the Dumont D'Urville trough. Our data show higher fluxes of carbon and opal during the mid-Holocene warm period, and during the late Holocene Neoglacial period.

Although the down core Ba_{XS} profile traces some of the changes in carbon flux, this paleoproductivity proxy fails as a quantitative indicator of carbon export due to changes in the redox conditions of the sediment that were inferred using the redox sensitive elemental proxies Mo and U.

The increase in opal:carbon ratios during the mid-Holocene optimum is linked to changes in the diatom assemblages towards larger diatom species, such as *F. kerguelensis,* that export less carbon per unit silica. These species dominated due to the extended open water conditions during this climatic period.

References

Anderson, R. F., Z. Chase, M. Q. Fleisher, and J. Sachs (2002), The Southern Ocean's biological pump during the Last Glacial Maximum, *Deep-Sea Research Part Ii-Topical Studies in Oceanography,* doi:10.1016/S0967-0645(02)00018-8.

Anderson, R. F., N. Kumar, R. A. Mortlock, P. N. Froelich, P. Kubik, B. Dittrich-Hannen, and M. Suter (1998), Late-Quaternary changes in productivity of the Southern Ocean, *Journal of Marine Systems, 17*, 497-514.

Armand, L. K., V. Cornet-Barthaux, J. Mosseri, and B. Queguiner. (2008), Late summer diatom biomass and community structure on and around the naturally iron-fertilised Kerguelen Plateau in the Southern Ocean. *Deep-Sea Research II*, *55*, 653-676.

Bacon, M. P., and R. F. Anderson (1982), Distribution of thorium isotopes between dissolved and particulate forms in the deep sea, *Journal of Geophysical Research 87,* 2045–2056.

Bareille, G., M. Labracherie, P. Bertrand, L. Labeyrie, G. Lavaux, and M. Dignan (1998), Glacial-interglacial changes in the accumulation rates of major biogenic components in Southern Indian Ocean sediments, *Journal of Marine Systems, 17*, 527-539.

Bentaleb, I., M. Fontugne, C. Descolas-Gros, C. Girardin, A. Mariotti, C. Pierre, C. Brunet, and A. Poisson (1996), Organic carbon isotopic composition of phytoplankton and sea-surface pCO2 reconstructions in the Southern Indian Ocean during the last 50,000 yr, *Organic Geochemistry, 24*, 399-410.

Beucher, C., P. Tréguer, A.M. Hapette, R. Corvaisier, N. Metzl, JJ. Pichon (2004), Intense summer Si recycling in the surface Southern Ocean, Geophysical Research Letters, 31, L09305, doi: 10.1029/2003GL018998.

Bishop, J. K. (1988) The barite-opal-organic carbon association in oceanic particulate matter. *Nature, 332*, 341-343.

Calvert, S. E., and T. F. Pedersen (1993), Geochemistry of recent oxic and anoxic marine sediments: implications for the geological record, *Marine Geology, 113,* 67-88.

Carson, D. S., R. S. Ganeshram, R. Ellam and V. Olive (in-prep) Particulate barium transformations and fluxes in the coastal Antarctic sea ice environment. *For submission to Deep Sea Research*.

Chase, Z., R. F. Anderson, M. Q. Fleisher, and P. W. Kubik (2003), Accumulation of biogenic and lithogenic material in the Pacific sector of the Southern Ocean during the past 40,000 years, *Deep-Sea Research Part Ii-Topical Studies in Oceanography, 50*, 799-832.

Crosta, X., J. J. Pichon, and L. H. Burckle (1998), Application of modern analog technique to marine Antarctic diatoms: Reconstruction of maximum sea-ice extent at the last glacial maximum, *Paleoceanography, 13*, 284-297.

Crosta, X., and A. Shemesh (2002), Reconciling down core anticorrelation of diatom carbon and nitrogen isotopic ratios from the Southern Ocean, Paleoceanography, 17(1), doi: 10.1029/2000PA000565.

Crosta, X., A. Shemesh, M. Salvignac, H. Gildor, and R. Yam (2002), Late quaternary variations of elemental ratios (C/Si and N/Si) in diatom-bound organic matter from the Southern Ocean, *Deep-Sea Research Part Ii-Topical Studies in Oceanography, 49*, 1939-1952.

Crosta, X., A. Sturm, L. Armand, and J. J. Pichon (2004), Late Quaternary sea ice history in the Indian sector of the Southern Ocean as recorded by diatom assemblages, *Marine Micropaleontology, 50*, 209-223.

Crosta, X., J. Crespin, I. Billy, and O. Ther (2005a), Major factors controlling Holocene d13Corg changes in a seasonal sea-ice environment, Adelie Land, East Antarctica, *Global Biogeochemical Cycles, 19*, doi:10.1029/2004GB002426.

Crosta, X, A. Shemesh, J. Etourneau, R. Yam, I. Billy, and J. J. Pichon. (2005b), Nutrient cycling in the Indian sector of the Southern Ocean over the last 50,000 years, *Global Biogeochemical Cycles, 19*, doi:10.1029/2004GB002344.

Crosta, X., M. Debret, D. Denis, M. A. Courty, and O Ther (2007), Holocene long- and short-term climate changes off Adélie Land, East Antarctica. *Geochemistry, Geophysics, Geosystems, 8*(11), Q11009, doi: 10.1029/2007GC001718.

Crosta, X., D. Denis, and O. Ther (2008), Sea ice seasonality during the Holocene, Adelie Land, East Antarctica. *Marine Micropaleontology, 66*, 222-232.

De La Rocha, C. L., M. A. Brzezinski, M. J. Deniro, and A. Shemesh (1998), Silicon-isotope composition of diatoms as an indicator of past oceanic change, *Nature, 395*, 680-683.

De Santis, L., G. Brancolini, and F. Donda (2003), Seismo-stratigraphic analysis of the Wilkes Land continental margin (East Antarctica): Influence of glacially driven processes on the Cenozoic deposition, *Deep Sea Research Part II: Topical Studies in Oceanography, 50*, 1563-1594.

Dehairs, F., W. Baeyens, and L. Goeyens (1992), Accumulation of suspended barite at mesopelagic depths and export production in the Southern Ocean. *Science, 258*, 1332-1335.

Dehairs, F., N. Fagel, A. N. Anita, R. Peinert, M. Elskens, L. Goeyens (2000), Export production in the Bay of Biscay as estimated from barium - barite in settling material: a comparison with new production, *Deep-Sea Research Part I-Oceanographic Research Papers, 47*, 583-601.

DeMaster, D. J., O. Ragueneau, C. A. Nittrouer (1996), Preservation efficiencies and accumulation rates for biogenic silica and organic C, N, and P in high-latitude sediments: The Ross Sea, *Journal of Geophysical Research-Oceans, 101*, 18502-18518.

Denis, D., X. Crosta, S. Schmidt, D. S. Carson, R. S. Ganeshram, H. Renssen, V. Bout-Roumazeilles, S. Zaragosi, M, Bernard, M. Cremer, J. Giraudeau (submitted), Glacier and deep current dynamics and their imprints on Holocene sedimentary record, Adelie Land, East Antarctica Margin, *Submitted to Quaternary Science Reviews.*.

Denis, D., X. Crosta, S. Zaragosi, O. Romero, B. Martin, and V. Mas (2006), Seasonal and subseasonal climate changes recorded in laminated diatom ooze sediments, Adelie Land, East Antarctica, *The Holocene, 16*, 1137-1147.

Dézileau, L., G. Bareille, J. L. Reyss, and F. Lemoine (2000), Evidence for strong sediment redistribution by bottom currents along the southeast Indian Ridge, *Deep-Sea Research I, 47*, 1899-1936.

Dymond, J., E. Suess, and M. Lyle (1992), Barium in deep-sea sediment: A geochemical proxy for paleoproductivity, *Paleoceanography, 7*, 163-181.

Dymond, J., and R. Collier (1996), Particulate barium fluxes and their relationships to biological productivity, *Deep-Sea Research Part Ii-Topical Studies in Oceanography, 43*, 1283-&.

Elderfield, H., and R. E. M. Rickaby (2000), Oceanic Cd/P ratio and nutrient utilization in the glacial Southern Ocean, *Nature, 405*, 305-310.

Ellwood, M. J., and K. A. Hunter (2000), Variations in the Zn/Si record over the last interglacial glacial transition, *Paleoceanography, 15*, 506-514.

Erickson, B. E. and G. R. Helz (2000), Molybdenum (VI) speciation in sulfidic waters: stability and lability of thiomolybdates. *Geochimica et Cosmochimica Acta*, 64, 1149-1158.

Fagel, N., L. Andre, and F. Dehairs (1999), Advective excess Ba transport as shown from sediment and trap geochemical signatures, *Geochimica Et Cosmochimica Acta, 63*, 2353-2367.

Fagel, N., F. Dehairs, R. Peinert, A. Anita, and L. Andre (2004), Reconstructing export production at the NE Atlantic Margin: potential and limits of the Ba proxy, *Marine Geology, 204*, 11-25.

Fitton, J. G., A. D. Saunders, L. M. Larsen, B. S. Hardarson, and M. J. Norry (1998), Volcanic rocks from the Southeast Greenland Margin at 63oN: Composition, petrogenesis, and mantle sources, *Proceedings of the Ocean Drilling Programme, Scientific Results, 152*, 331-350.

Francois, R., and M. A. Altabet (1992), Glacial to interglacial changes in surface nitrate utilisation in the Indian sector of the Southern Ocean as recorded by sediment d15N, *Paleoceanography, 7*, 589-606.

Francois, R., M. A. Altabet, E. Yu, D. M. Sigman, M. P. Bacon, M. Frank, G. Bohrmann, G. Bareille, and L. D. Labeyrie (1997), Contribution of Southern Ocean surface-water stratification to low atmospheric CO2 concentrations during the last glacial period, *Nature, 389*, 929-935.

Francois, R., M. Frank, M. M. Rutgers van der Loeff and M. P. Bacon (2004), Th-230 normalization: An essential tool for interpreting sedimentary fluxes during the late Quaternary, *Paleoceanography, 19*, PA1018, doi:1010.1029/2003PA000939.

Francois, R., S. Honjo, S. J. Manganini, and G. E. Ravizza (1995), Biogenic Barium Fluxes to the Deep-Sea - Implications for Paleoproductivity Reconstruction, *Global Biogeochemical Cycles, 9*, 289-303.

Ganeshram, R. S., T. F. Pedersen, S. E. Calvert, and J. W. Murray (1995), Large Changes in Oceanic Nutrient Inventories from Glacial to Interglacial Periods, *Nature, 376*, 755-758.

Ganeshram, R. S., and T. F. Pedersen (1998), Glacial-interglacial variability in upwelling and bioproductivity off NW Mexico: Implications for quaternary paleoclimate, *Paleoceanography, 13*, 634-645.

Hutchins, D. A. and K. W. Bruland (1998), Iron-limited diatom growth and Si:N uptake ratios in a coastal upwelling regime. *Nature*, *393*, 561-564.

Helz, G. R., C. V. Miller, J. M. Charnock, J. F. W. Mosselmans, R. A. D. Pattrick, C. D. Garner, and D. J. Vaughan. (1996), Mechanisms of molybdenum removal from the sea and its concentration in black shales: EXAFS evidence. *Geochimica et Cosmochimica Acta*, *60*, 3631-3642.

Hodell, D. A., S. L. Kanfoush, A. Shemesh, X. Crosta, C. D. Charles, and T. P. Guilderson (2001), Abrupt cooling of Antarctic surface waters and sea ice expansion in the South Atlantic sector of the Southern Ocean at 5000 cal yr BP, *Quaternary Research, 56*, 191-198.

Hughen, K. A., et al. (2004), Marine04 Marine radiocarbon age calibration, 26-0 ka BP, Radiocarbon, 46, 1059-1086.

Kumar, N., R. F. Anderson, R. A. Mortlock, P. N. Froelich, P. Kubik, B. Dittrich-Hannen, and M. Suter (1995), Increased Biological Productivity and Export Production in the Glacial Southern-Ocean, *Nature, 378*, 675-680.

Laws, R. A. (1983), Preparing strewn slides for quantitative microscopical analysis: A test using calibrated microspheres, Micropaleontology, 24, 60-65.

McManus, J., W. M. Berelson, G. P. Klinkhammer, K. S. Johnson, K. H. Coale, R. F. Anderson, N. Kumar, D. J. Burdige, D. E. Hammond, H. J. Brumsack, D. C. McCorkle, and A. Rushdi (1998), Geochemistry of barium in marine sediments: Implications for its use as a paleoproxy, *Geochimica Et Cosmochimica Acta, 62*, 3453-3473.

McManus, J., J. Dymond, R. B. Dunbar, and R. W. Collier (2002) Particulate barium fluxes in the Ross Sea. *Marine Geology*, *184*, 1-15.

McManus, J., W. M. Berelson, S. Severmann, R. L. Poulson, D. E. Hammond, G. P. Klinkhammer, and C. Holm (2006), Molybdenum and uranium geochemistry in continental margin sediments: Paleoproxy potential. *Geochimica et Cosmochimica Acta*, *70*(18), 4643-4662.

Menden-Deuer, S. and E.J. Lessard (2000), Carbon to volume relationships for dinoflagellates, diatoms and other protist plankton, *Limnology and Oceanography, 45*(3), 569-579.

Morford, J. L. and S. Emerson, (1999), The geochemistry of redox sensitive trace metals in sediments. *Geochimica et Cosmochimica Acta, 63*, 1735-1750.

Morford, J. L., S. R. Emerson, E. J. Breckel, and S. H. Kim (2005) Diagenesis of oxyanions (V, U, Re and Mo) in pore waters and sediments from a continental margin. *Geochimica et Cosmochimica Acta, 69*, 5021-5032.

Mortlock, R. A., and P. N. Froelich (1989), A Simple Method for the Rapid-Determination of Biogenic Opal in Pelagic Marine-Sediments, *Deep-Sea Research Part a-Oceanographic Research Papers, 36*, 1415-1426.

Mosseri, J., B. Queguiner, L. Armand, and V. Cornet-Barthaux (2008) Impact of iron on silicon utilization by diatoms in the Southern Ocean: A case study of Si/N cycle decoupling in a naturally iron-enriched area. *Deep-Sea Research II, 55*, 801-819.

Muller, P. J., and R. Schneider (1993), An Automated Leaching Method for the Determination of Opal in Sediments and Particulate Matter, *Deep-Sea Research Part I-Oceanographic Research Papers, 40*, 425-444.

Nielsen, S. H. H., N. Koc, and X. Crosta (2004), Holocene climate in the Atlantic Sector of the Southern Ocean: controlled by insolation or oceanic circulation?, *Geology, 32*, 317-320.

Nurnberg, C. C., G. Bohrmann, M. Schluter, and M. Frank (1997), Barium accumulation in the Atlantic sector of the Southern Ocean: Results from 190,000-year records, *Paleoceanography, 12*, 594-603.

Queguiner, B., P. Treguer, I. Peeken, and R. Scharek (1997) Biogeochemical dynamics and the silicon cycle in the Atlantic sector of the Southern Ocean during austral spring 1992. *Deep-Sea Research II, 44*, 69-89.

Robinson, R. S., D. M. Sigman, P. J. DiFiore, M. M. Rhode, T. A. Mashiotta, and D. W. Lea (2005), Diatom-bound N-15/N-14: New support for enhanced nutrient consumption in the ice age subantarctic, *Paleoceanography, 20*, doi:10.1029/2004PA001114

Rosenthal, Y., D. Maimon, and A. Shemesh (2000), Southern Ocean contributions to glacial-interglacial changes of atmospheric pCO_2: An assessment of carbon isotope records in diatoms, *Paleoceanography, 15*, 65-75.

Sambrotto, R. N., A. Matsuda, R. Vaillancourt, M. Brown, C. Langdon, S. S. Jacobs, and C. Measures (2003), Summer plankton production and nutrient consumption patterns in the Mertz Glacier Region of East Antarctica. *Deep-Sea Research II, 50*, 1393-1414.

Schenau, S. J., M. A. Prins, G. J. De Lange, and C. Monnin (2001), Barium accumulation in the Arabian Sea: Controls on barite preservation in marine sediments, *Geochimica et Cosmochimica Acta, 65*, 1545-1556.

Sigman, D. M., and E. A. Boyle (2000), Glacial/interglacial variations in atmospheric carbon dioxide, *Nature, 407*, 859-869.

Suman, D. and M. P. Bacon (1989) Variations in Holocene sedimentation in the North American Basin determines from 230Th measurements. *Deep Sea Research. Part A, 36*, 869-878.

Takeda, S. (1998) Influence of iron availability on nutrient consumption ratio of diatoms in oceanic waters. *Nature*, *393*, 774-777.

Vaillancourt, R. D., R. N. Sambrotto, S. Green, and A. Matsuda (2003), Phytoplankton biomass and photosynthetic competency in the summertime Mertz Glacier Region of East Antarctica. *Deep-Sea Research II*, *50*, 1415-1440.

Wolff, E. W., H. Fischer, F. Fundel, U. Ruth, B. Twarloh, G. C. Littot, R. Mulvaney, R. Röthlisberger, M. de Angelis, C. F. Boutron, M. Hansson, U. Jonsell, M. A. Hutterli, F. Lambert, P. Kaufmann, B. Stauffer, T. F. Stocker, J. P. Steffensen, M. Bigler, M. L. Siggaard-Andersen, R. Udisti, S. Becagli, E. Castellano, M. Severi, D. Wagenbach, C. Barbante, P. Gabrielli and V. Gaspari (2006), Southern Ocean sea-ice extent, productivity and iron flux over the past eight glacial cycles, *Nature*, *440*, 491-496.

Wright, S. W., and R. L. van den Enden (2000), Phytoplankton community structure and stocks in the East Antarctic marginal ice zone (BROKE survey, January-March 996) determined by CHEMTAX analysis of HPLC pigment signatures, *Deep Sea Research Part II: Topical Studies in Oceanography, 47*, 2363-2400.

Observations on the relationship between the Antarctic coastal diatoms *Thalassiosira antarctica* Comber and *Porosira glacialis* (Grunow) Jørgensen and sea ice concentrations during the Late Quaternary

Jennifer Pike[a], Xavier Crosta[b], Eleanor J. Maddison[c], Catherine E. Stickley[d], Delphine Denis[b], Loïc Barbara[b] and Hans Renssen[e]

[a] School of Earth and Ocean Sciences, Cardiff University, Main Building, Park Place, Cardiff, CF10 3YE, U.K. pikej@cardif.ac.uk

[b] UMR-CNRS 5805 EPOC, Université Bordeaux 1, Avenue des Facultés, 33405 Talence Cedex, France x.crosta@epoc.u-bordeaux1.fr, d.denis@epoc.u-bordeaux1.fr

[c] Department of Earth and Environmental Sciences, The Open University, Walton Hall, Milton Keynes, MK7 6AA, U.K. e.j.maddison@open.ac.uk

[d] Department of Geology, University of Tromsø, Tromsø N-9037, Norway catherine.stickley@npolar.no

[e] Department of Paleoclimatology and Geomorphology, Vrije University, Amsterdam, The Netherlands hans.renssen@falw.vu.nl

1. Introduction

Most of the ecological and palaeoecological information available for sea ice-related marine diatoms *Thalassiosira antarctica* and *Porosira glacialis* suggests that these two species have similar sea surface temperature (SST), sea surface salinity (SSS) and sea ice proximity preferences and similar seasonal occurrences (summarised in Sections 1.1 and 1.2). For example, in Ross Sea surface waters that emerge from beneath the ice shelf, *T. antarctica* cells are associated with a diatom assemblage that also includes *P. glacialis* and *P. pseudodenticulata* (Cunningham and Leventer, 1998). Along the Mac.Robertson Shelf in Iceberg Alley (Figure 1) seasonally laminated sediments abundant *P. glacialis* resting spores (RS) are found within *T. antarctica* RS-dominated sub-laminae that were deposited during autumn (Stickley et al., 2005). On the other hand, in Dumont d'Urville Trough, Adélie Land (Figure 1), sub-laminae dominated by *T. antarctica* RS are found in mid-Holocene (relatively warm, Hypsithermal) laminated sediments (Core MD03-2601, Denis et al., 2006), whereas sub-laminae dominated by *P. glacialis* RS are found in late Holocene (cool, Neoglacial) sediments (Core MD03-2597, Maddison, 2006). Further, deglacial/early Holocene laminated sediment from Mertz Ninnis Trough, George V Coast (Figure 1), also

contain sub-laminae dominated by *P. glacialis* RS (Maddison et al., 2006). The *T. antarctica* RS and *P. glacialis* RS sub-laminae from both sites, and from both time intervals, occur at the top of late summer/autumn terrigenous-rich diatom laminae, which supports the contention that these two diatoms have broadly similar ecological preferences (Stickley et al., 2005). However, as pointed out by Denis et al. (2006), the more coastal position of the Mertz Ninnis Trough and MD03-2597 core sites (and associated *P. glacialis* RS sub-laminae) compared to the core site MD03-2601 (and associated *T. antarctica* RS sub-laminae) suggests that *P. glacialis* prefers cooler temperatures with higher sea ice concentrations than *T. antarctica*. In this study we review the available ecological information for these two diatom species. We then consolidate the perceived relationship between the two taxa as sedimentary indicators of autumnal conditions using laminated sediment sequences and published ecological information. Finally, we investigate down-core Holocene diatom assemblage records from two sites in coastal East Antarctica in order to establish whether the relationship developed from laminated sediment records and ecological information can be used as a more quantitative proxy for changing environmental conditions during the Late Quaternary.

1.1. Ecology of *Thalassiosira antarctica* Comber 1896

Thalassiosira antarctica is an Antarctic diatom species rarely found within sea ice (Fryxell and Kendrick, 1988; Hasle and Heimdal, 1968; Leventer and Dunbar, 1987; Zielinski and Gersonde, 1997), however, it is commonly described as a sea ice-associated diatom linked with low sea surface temperature (SST) and low sea surface salinity (SSS) (Villareal and Fryxell, 1983). Blooms of *T. antarctica* are often recorded in waters associated with newly forming sea ice, such as the formation of platelet ice next to the Ross Sea ice shelf (Cunningham and Leventer, 1998) and both frazil ice and platelet ice in the Weddell Sea (Gleitz et al., 1998; Smetacek et al., 1992). In the Weddell Sea, it has also been recorded under turbulent conditions (Gleitz et al., 1998) and from low salinity, nitrate-deplete, high pH crackpools associated with summer melting ice (Gleitz et al., 1996). *T. antarctica* commonly occurs in waters with SSTs between -2 to 2ºC (Zielinski and Gersonde, 1997) Although it is rare to find *T. antarctica* in sea ice samples due to its requirement for open water to bloom (Bárcena et al., 1998) and its sensitivity to low light intensities (Doucette and Fryxell, 1985; Fryxell et al., 1987), it has been observed in some spring sea ice samples which suggests over-wintering in sea ice or re-suspension from the sediments (Villareal and Fryxell, 1983).

Thalassiosira antarctica appears to be a summer and autumn bloom species. It has been observed as a common component of the early summer phytoplankton around the Antarctic Peninsula (Sommer, 1991) and was recorded in summer sediment traps in the Ross Sea (Leventer pers. comm. in Taylor and McMinn, 2002). It has been described as a major component of phytoplankton blooms in non-stratified or weakly stratified Antarctic surface waters (Cremer et al., 2003) (strong water column stratification is usually associated with

spring sea ice melt). *T. antarctica* has also been associated with autumn bloom conditions in the Ross Sea with production of resting spores related to the seasonally-late development of solid ice cover (Cunningham and Leventer, 1998).
However, contrary to these observations of natural populations, laboratory culture experiments revealed that *T. antarctica* can grow well in reduced light conditions in temperatures as low as -4°C (Aletsee and Jahnke, 1992; Bartsch, 1989), and that vegetative *T. antarctica* cells can survive in sea ice (Aletsee and Jahnke, 1992) and for prolonged periods of darkness (up to 214 days) without forming resting spores (Peters and Thomas, 1996a). It is believed that the formation of physiologically resting cells (identical in appearance to the vegetative cells) is induced by nutrient stress (Peters and Thomas, 1996b), or by low light intensities beneath the summer diatom bloom and/or associated nutrient depletion (Taylor and McMinn, 2001). However, culture experiments carried out at -1.5°C failed to induce resting spore formation by nitrogen depletion (Villareal and Fryxell, 1983). Significant lipid accumulation occurs in the resting spores as they form (Doucette and Fryxell, 1985) and this lipid synthesis has been attributed to a synergistic interaction between reduced light levels, reduced SST and increased SSS in other Antarctic sea-ice related phytoplankton species (Palmisano and Sullivan, 1982; Smith and Morris, 1980). In conclusion, the exact trigger for resting spore formation in *T. antarctica* is not well understood.

Observations of *T. antarctica* from the sediment record are almost exclusively the resting spore stage (Fryxell et al., 1981) (Figure 2). *T. antarctica* resting spores are heavily silicified and this has been suggested as a mechanism to facilitate rapid sinking out of freezing surface waters (Doucette and Fryxell, 1985). The heavily silicified resting spores are more readily transported, hence, often become concentrated in Antarctic near-coastal sediments (Gersonde and Wefer, 1987; Hemer and Harris, 2003). From spatially extensive surface sediment records, *T. antarctica* resting spores are most abundant beneath regions where February SSTs of 0 to 0.5°C and where sea ice is present for at least 6 months per year with winter sea ice concentrations >70% and unconsolidated summer sea ice concentrations between 15-40% (Armand et al., 2005). Early Holocene sediments from Prydz Bay are characterised by abundant *T. antarctica* resting spores (average of 31% of the assemblage) and this has been related to seasonally warmer, more open marine conditions (Taylor and Leventer, 2003; Taylor and McMinn, 2002). In the Bransfield Strait, western Antarctic Peninsula, maximum abundance of *T. antarctica* resting spores in Holocene sediments is related to cold climate episodes (Bárcena et al., 1998), persistent influence of cold Weddell Sea water (Gersonde and Wefer, 1987; Leventer, 1991; Zielinski and Gersonde, 1997) and proximity to ice edge (Heroy et al., 2008). In deglacial and Holocene seasonally laminated Antarctic coastal sediments, *T. antarctica* resting spores commonly dominate the last recorded flux of the season, indicating their prior prevalence in mid- to late-summer blooms (as vegetative cells) and a relationship with falling temperatures (ice formation) and falling light levels (Maddison et al., 2005; Stickley et al., 2005).

Figure 2

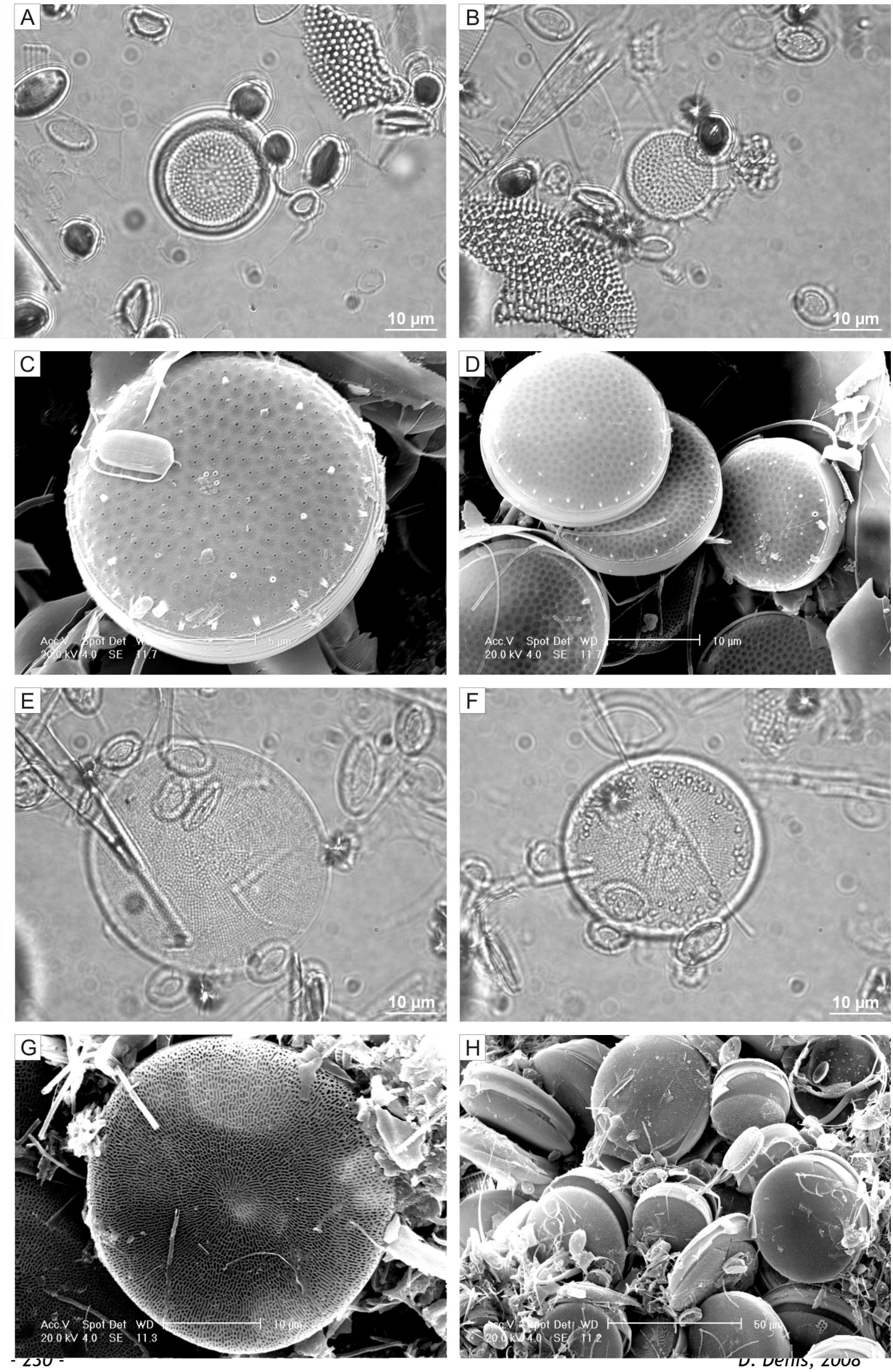
A
10 µm
B
10 µm
C
5 µm
D
Acc.V Spot Det WD
20.0 kV 4.0 SE 11.7
10 µm
E
10 µm
F
10 µm
G
Acc.V Spot Det WD
20.0 kV 4.0 SE 11.3
10 µm
H
50 µm

Figure 2: Light microscope (LM) and scanning electron microscope (SEM) images of *Thalassiosira antarctica* and *Porosira glacialis* resting spores. SEM micrographs taken of Au-Pd coated, lamina parallel sediment fracture surfaces. A-B. LM micrographs of *T. antarctica* resting spores (NBP01-01 JPC10, 19.536 cm). C-D. Secondary electron SEM micrographs of *T. antarctica* resting spores (MD03-2597, 5307.5 cm, scale bars G = 5 microns, H = 10 microns). E-F. LM micrographs of *P. glacialis* resting spores (NBP01-01 JPC10, 19.536 cm). G-H. Secondary electron SEM micrographs of *P. glacialis* resting spores (NBP01-01 JPC10, 19.463 cm; scale bars C = 10 microns, D = 50 microns).

1.2. Ecology of *Porosira glacialis* (Grunow) Jörgensen 1905

Generally, less is known about the ecological preferences of *Porosira glacialis* than for *Thalasiosira antarctica*. *Porosira glacialis* is a bipolar diatom species associated with cold coastal waters adjacent to sea ice (Hasle, 1973; Taylor et al., 1997; Zielinski and Gersonde, 1997).Of the two species of Antarctic *Porosira*, *P. pseudodenticulata* is commonly observed in pack ice and fast ice samples whereas *P. glacialis* is rarely recorded in sea ice (Armand, 1997; Scott et al., 1994; Watanabe, 1988). It has been suggested that *P. glacialis* predominantly grows in the open ocean beyond the sea ice edge (Zielinski and Gersonde, 1997), but *P. glacialis* has also been observed with slush and wave-exposed shore ice, although not living within the ice (Krebs et al., 1987). *P. glacialis* grows in summer waters with SSTs ranging from -2 to 1.5ºC (slightly cooler maximum temperature than *T. antarctica*) (Zielinski and Gersonde, 1997), and reaches maximum abundances with February SSTs of 0 to 0.5ºC (Armand et al., 2005). Similar to *T. antarctica*, in culture experiments, *P. pseudodenticulata* survived prolonged periods of darkness (up to 272 days) by forming physiologically resting cells, not by forming resting spores (Peters and Thomas, 1996a). Resting spore formation was not induced at -1.5ºC (Villareal and Fryxell, 1983), and the exact mechanism that promotes resting spore formation is not known.

P. glacialis is recorded in sediments predominantly as resting spores (Figure 2), and located within the maximum winter sea ice extent (Armand, 1997). From a spatially extensive sediment surface data set, *P. glacialis* is most abundant beneath regions that experience at least 7.5 months per year sea ice cover (slightly longer than *T. antarctica*), with <30% summer sea ice concentration and highly compacted winter sea ice (65-85% concentration) (Armand et al., 2005). In deglacial, seasonally laminated sediments from Iceberg Alley, Mac.Roberston Shelf, *P. glacialis* is abundant in the *Thalassiosira antarctica* sub-laminae that record the final flux event of the year, thus suggesting a similarity in their growth requirements (Stickley et al., 2005). In Holocene laminated sediments from the Mertz-Ninnis Trough, George V Coast, *P. glacialis* sub-laminae are interpreted as representing late summer/autumn deposition as sea ice concentration in the Mertz Glacier polynya increased (Maddison et al., 2006).

2. Materials and Methods

2.1. Materials

This study uses a suite of Late Quaternary sediment cores recovered from the East Antarctic margin. Cores from Mertz Ninnis Trough (NBP0101 JPC10/KC10A), Iceberg Alley (NBP0101 JPC43B) and Svenner Channel (NBP0101 JPC24) were recovered during RVIB *Nathaniel B. Palmer* cruise NBP0101 during 2001 (Table 1, Figure 1). Cores from the Dumont d'Urville Trough (MD03-2597/MD03-2601) were recovered during the MD130-Images X-CADO cruise of RV *Marion Dufresne II* in 2003 (Table 1, Figure 1). All cores are, in part, seasonally laminated with the remaining stratigraphy being either intermittently laminated or homogenous siliceous-mud ooze (Crosta et al., 2005; Leventer et al., 2006; Maddison, 2006; Maddison et al., 2006). Intervals selected for lamina-scale analyses and down-core diatom assemblage analysis in this study are illustrated in Figure 1 and listed in Table 1.

The early Holocene and Neoglacial (Figure 1) laminated sediment sequences from Mertz Ninnis Trough were deposited approximately 30 km from the coast, beneath the site of a persistent winter polynya (Maddison et al., 2006). The two cores from Dumont d'Urville Trough were recovered from biogenic drift deposits that accumulated in small depressions, approximately 30 km and 60 km offshore, within the trough (Crosta et al., 2005). The Dumont d'Urville Trough region is an open coastline with a typical regime of advance and retreat of seasonal sea ice, with the episodic presence of a polynya (Arrigo and Van Dijken, 2003). Today, the sites are covered by sea ice for 8-9 months of the year (Schweitzer, 1995). During the deposition of the deglacial laminated sediments in Iceberg Alley the long, across-shelf trough that comprises the basin was surrounded by a calving bay re-entrant (Leventer et al., 2006). This meant that even though the site is approximately 70 km offshore today, it would have been subject to a seasonal sea ice retreat and advance regime typical of more coastal sites. Svenner Channel is a coast-parallel trough on the eastern margin of Prydz Bay. The core site is approximately 60 km from the coast and is subject to a typical seasonal sea ice advance and retreat regime that results in a yearly sea ice presence of 10 months.

2.2. Lamina analyses: BSEI and LM sediment fabric analysis and quantitative diatom assemblage analysis

Laminated sediments (Figure 1) were embedded in resin and polished thin sections were produced for microscope analysis following the methods outlined in Maddison et al. (2006, NBP0101 JPC10/KC10A, MD03-2597), Denis et al. (2006, MD03-2601) and Stickley et al. (2005, NBP0101 JPC43B). Laminated sequences (polished thin sections) were logged for sediment fabric and diatom assemblages at the 100 micron-scale using either scanning

electron microscopy backscattered electron imagery (BSEI, Pearce et al., 1998; Pike and Kemp, 1996) or optical light microscopy (LM, Denis et al., 2006) (Table 2).

Figure 1

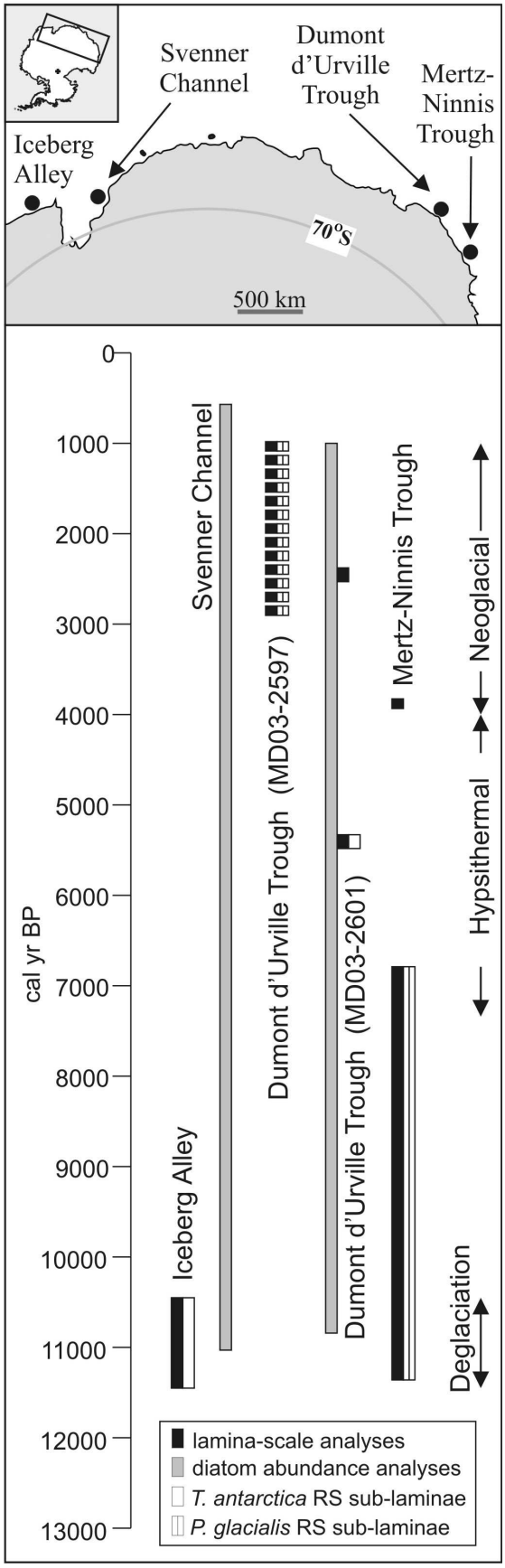

Figure 1: Locations of the East Antarctic margin sediment cores used in this investigation. The intervals sampled from each of the cores are shown by the black (BSEI and LM sediment fabric analyses) and grey (Holocene down-core quantitative diatom abundance analyses). The presence of *Thalassiosira antarctica* RS sub-laminae is indicated by white and *Porosira glacialis* RS sub-laminae by a vertical line.

Cruise	Location	Core	Latitude	Longitude	Water depth (m)	Distance from coast (km)	Core length (m)	Interval(s) analysed (m)	Age (cal yr BP)
NBP01-01	Mertz-Ninnis Trough	JPC10 KC10A	66°34.334′S	143°05.168′E	850	~30	21.35 2.5	Thin sections: 17.36-20.60 2.05-2.38	 6756-11384 3820-3892
MD130-Images X-CADO	Dumont d'Urville Trough	MD03-2597	66°24.74′S	140°25.26′E	1025	~30	57.34	Thin sections: 13 x 15-cm-intervals between 18.75-56.83	925-2814
MD130-Images X-CADO	Dumont d'Urville Trough	MD03-2601	66°03.07′S	138°33.43′E	746	~60	40.24	Diatom abundance: 0-40.25 Thin sections: 6.19-6.485 & 18.808-19.107	 1000-10843 ~2550 ~5635
NBP01-01	Iceberg Alley	JPC43B	66°55.943′S	64°07.376′E	465	~75	23.96	Thin sections: 19.30-23.96	 10500-11500
NBP01-01	Svenner Channel	JPC24	68°41.660′S	76°42.557′E	848	~60	15.35	Diatom abundance: 0-17.00	 655-11082

Table 1: East Antarctica margin sediment core information, including details of location, length, distance from coast, core intervals analysed and age of intervals analysed. Age models from Denis et al. (2006), Maddison (2006), Maddison et al. (2006), and Leventer et al (2006).

For core sites NBP0101 JPC10/KC10A and MD03-2597 additional quantitative diatom assemblage analyses were carried on specific lamination types following the method outlined in Maddison et al. (2006). These additional analyses facilitated quantitative comparison of the relative abundance of *T. antarctica* RS and *P. glacialis* RS in the laminations, as opposed to the more qualitative techniques involved in thin section analysis using BSEI and LM. Data are presented as absolute abundance (valves per gramme), relative abundance and *Hyalochaete Chaetoceros* resting spore-free (CRS-free) relative abundance (Table 3). CRS-free abundance is commonly used in Antarctic diatom assemblage analysis when CRS overwhelmingly dominate every assemblage (Allen et al., 2005; Leventer et al., 1996). The CRS-free abundance allows the ecological information within the minor species assemblage to be critically examined.

2.3. Down-core quantitative diatom assemblage analysis

Down-core quantitative diatom assemblage analysis was carried out on MD03-2601 (Dumont d'Urville Trough) and NBP0101 JPC24 (Svenner Channel) following the methods outlined in Crosta et al. (2007). These records allow the relationship between *T. antarctica* RS and *P. glacialis* RS, deduced from lamination-scale analyses of mainly deglacial sediments, to be investigated over the duration of the Holocene. *Porosira glacialis* RS and *Porosira pseudodenticulata* RS are grouped together, however, *P. glacialis* RS strongly dominates the group. The two forms of *T. antarctica* RS are grouped (T1 and T2, Buffen et al., 2007), however, the cool *T. antarctica* RS form (T1) overwhelmingly dominates in both Dumont d'Urville Trough and Svenner Channel sediments.

2.4. Modelled Holocene surface temperatures and sea ice concentrations

The diatom abundance and sediment fabric data and interpretations will be compared with the results of a 9000-yr Holocene climate simulation using the ECBilt-CLIO-VECODE coupled atmosphere-sea ice-ocean-vegetation model forced with annually varying orbital parameters and atmospheric greenhouse gas (carbon dioxide and methane) concentrations (Brovkin et al., 2002; Goosse and Fichefet, 1999; Opsteegh et al., 1998; Renssen et al., 2005). As well as comparing with the published East Antarctic modelled summer temperature record of Renssen et al. (2005), we will also compare our results to a sub-set of the whole model output for the Adélie Land sector that encompasses the Dumont d'Urville Trough core sites (south of 60°S, 140°E-150°E). Two 1000-year time periods from the Adélie Land mean monthly surface temperature and sea ice concentrations were selected to provide a measure of typical mean monthly conditions; the interval 4999-4000 yr BP was selected as typical of the Hypsithermal and 1999-1000 yr BP selected as representative of the Neoglacial. These two time periods were compared to investigate statistically significant differences in modelled monthly parameters between the Hypsithermal and Neoglacial. Significant differences in the means were found using a

standard z-test (with 2-tailed critical values) for assessing differences in the means between large sample sets (Table 4).

3. Results

3.1. Laminated sediments – BSEI, LM and quantitative diatom assemblage analysis

Data for the lamina-scale diatom assemblage analyses, using BSEI, LM and quantitative abundance, come from both published sources and from new analyses. BSEI lamina characterisations for sediments from the Mertz-Ninnis Trough (NBP0101 JPC10/KC10A) are summarised from Maddison (2006) and Maddison et al. (2006). Similar data for the Dumont d'Urville Trough (MD03-2597) are summarised from Maddison (2006) and LM lamina data (MD03-2601) are summarised from Denis et al. (2006). Lamina-scale diatom assemblage data for sediments from Iceberg Alley (NBP0101 JPC43B) are a combination of both published (Stickley et al., 2005, interval 21.84-23.96 m) and previously unpublished data (Stickley and Pike: interval 19.30-21.84 m). Tables 2 and 3 provide a summary of these data containing only the lamina or sub-lamina data relevant to this study.

3.1.1. *Thalassiosira antarctica* RS sub-laminae

Analysis of lamina occurrence data from the spectacularly laminated deglacial sediments of the East Antarctic margin reveals that when sub-laminae characterised by *T. antarctica* RS or *P. glacialis* RS occur, usually: (1) either one or the other species is dominant; and (2) they are found in a similar position within the seasonal succession of diatom assemblages and lamina types, i.e. at the end of the season of diatom production and subsequent flux to the sediment, late summer or autumn (Denis et al., 2006; Maddison, 2006; Stickley et al., 2005). In deglacial Iceberg Alley sediment, 43 of 68 *T. antarctica* RS sub-laminae occur in this position above a summer lamina (Table 2) and, consequently, directly below the following spring diatom ooze lamina from which they are separated by a sharp contact delineating the winter hiatus. Further, when a summer lamination is not present, 25 of 68 occurrences of *T. antarctica* RS sub-laminae follow a transitional lamination (Table 2), defined as having some characteristics of both spring diatom ooze laminae and summer terrigenous-rich laminae (Stickley et al., 2005). These transitional laminae nearly always grade upwards from a spring diatom ooze lamina and usually grade into a summer terrigenous-rich lamina, however, sometimes these transitional laminae are abruptly overlain by the following spring diatom ooze laminae. Usually, it is at the top of these latter transitional laminae that *T. antarctica* RS sub-laminae occur. When *T. antarctica* RS sub-laminae occur within the annual sediment increment, the mean annual sediment thickness is 2% greater than if sub-laminae do not occur.

Location	*P. glacialis* or *T. Antarctica*	Sediment Increment Type	Mean thickness (σ) (mm)	n	Min thickness (mm)	Max thickness (mm)
Mertz-Ninnis Trough (NBP0101 JPC10) Early Holocene	*P. glacialis*	Annual thickness	17.5 (16.9)	116	1.8	103.2
		Annual thickness if *P. glacialis* RS sub-laminae are present	20.6 (14.6)	22	3	53.3
		P. glacialis RS sub-lamina thickness	1.4 (1.1)	22	0.5	5.5
Dumont d'Urville Trough (MD03-2597) Neoglacial	*P. glacialis*	Annual thickness	18.1 (9.6)	119	1.1	46.7
		Annual thickness if *P. glacialis* RS sub-laminae are present	20.25 (9.1)	26	7.9	40.6
		P. glacialis RS sub-lamina thickness [1]	2.2 (1.4)	35	0.5	5.9
Dumont d'Urville Trough (MD03-2601) Neoglacial	—	Annual thickness	21 (14)	10		
Dumont d'Urville Trough (MD03-2601) Hypsithermal	*T. antarctica*	Annual thickness	46 (16)	6		
		T. antarctica RS sub-lamina thickness	0.371 (0.289)	8		
Iceberg Alley (NBP0101 JPC43B) Deglacial	*T. antarctica*	Annual thickness	21.59 (17.69)	223	1.04	99.05
		Annual thickness if *T. antarctica* RS sub-laminae are present	21.98 (16.16)	67	1.86	81.32
		T. antarctica RS sub-lamina thickness [2]	1.16 (1.70)	68	0.03	10.47
		Summer thickness	5.35 (5.45)	159	0.28	33.49
		Summer thickness if *T. antarctica* RS sub-laminae are present	5.74 (6.86)	46	0.33	33.49
		T. antarctica RS sub-lamina thickness if associated with top of summer lamina [3]	1.33 (2.04)	43	0.03	10.47
		Transitional lamina thickness	9.52 (9.28)	110	0.73	49.76
		Transitional lamina thickness if followed by *T. antarctica* RS sub-lamina	8.29 (4.49)	25	1.26	18.42
		T. antarctica RS sub-lamina thickness if associated with top of transitional lamina [4]	0.88 (0.81)	25	0.25	3.28

Table 2: Summary of lamina and sub-lamina thickness measurements from BSEI and LM of East Antarctic laminated sediment sequences. [1] 26 years have *P. glacialis* RS sub-laminae; 5 years have multiple sub-laminae, [2] 67 years have *T. antarctica* RS sub-laminae; 1 year has 2 sub-laminae, [3] 46 years have *T. antarctica* RS sub-laminae; in 43/46 years the sub-lamina is at the top of the summer lamina; in 3/46 years, the sub-lamina is within the summer laminae, [4] Four transitional laminae, overlain by *T. antarctica* RS sub-laminae, are followed by summer laminae associated with *T. antarctica* RS sub-laminae.

Location	Sub-lamina type	*P. glacialis* RS or *T. antarctica* RS abundance in lamina or sub-lamina types	Mean Abundance (σ) (10^6 valves/g)	n	Min (10^6 valves/g)	Max (10^6 valves/g)	Relative abundance (%)All/CRS-free
Mertz-Ninnis Trough (NBP0101 JPC10)	*P. glacialis* RS	*P. glacialis* RS abundance in summer mixed diatom lamina	6.9 (2.7)	5	3.9	9.5	0.38 / 2.29
		T. antarctica RS abundance in summer mixed diatom lamina	0 (0)	5	0	0	0 / 0.42
		P. glacialis RS abundance in *P. glacialis* RS sub-lamina	7.2 (3.9)	4	3.2	10.6	0.24 / 11.35
		T. antarctica RS abundance in *P. glacialis* RS sub-lamina	0 (0)	4	0	0	0 / 0
Dumont d'Urville Trough (MD03-2597)	*P. glacialis* RS	*P. glacialis* RS abundance in summer mixed diatom lamina	20.3 (9.9)	5	10.9	34.8	2.91 / 5.1
		T. antarctica RS abundance in summer mixed diatom lamina	2.4 (3.6)	5	0	8.6	0.39 / 0.81
		P. glacialis RS abundance in *P. glacialis* RS sub-lamina	53.9 (27.2)	3	33.5	84.8	7.08 / 15.48
		T. antarctica RS abundance in *P. glacialis* RS sub-lamina	6.7 (6.7)	3	0	13.4	0.89 / 3.16

Table 3: Quantitative abundance of *Porosira glacialis* and *Thalassiosira antarctica* from selected East Antarctic sediment laminae and sub-laminae.

Further, if a summer lamination is followed by a *T. antarctica* RS sub-lamina, the summer lamina is, on average, 7% thicker than one that is not associated with a sub-lamina (Table 2). Qualitative analysis of *T. antarctica* RS sub-laminae from Iceberg Alley also reveals that *P. glacialis* RS are more abundant in the sub-laminae than in the summer, terrigenous-rich laminae.

LM analysis of lamina sequences from the Holocene sediments of the less coastal MD03-2601 core from Dumont d'Urville Trough shows the presence of sub-laminae of *T. antarctica* RS associated with late summer/autumn in Hypsithermal-age sediments and the absence of the sub-laminae in Neoglacial-age sediments (Table 2, Denis et al., 2006). During the Hypsithermal period, annual sediment thickness was 46 mm compared with 21 mm during the Neoglacial, and mean thickness of *T. antarctica* RS sub-laminae during the Hypsithermal was 0.371 mm (Table 2, Denis et al., 2006). In contrast to the other, more coastal core site from Dumont d'Urville Trough (MD03-2597) these sections from MD03-2601 do not contain any *P. glacialis* RS sub-laminae during the Neoglacial.

3.1.2. *Porosira glacialis* RS sub-laminae

Nineteen out of twenty two occurrences of *P. glacialis* RS sub-laminae in deglacial Mertz-Ninnis Trough sediment appear in a late summer/autumn position in the seasonal lamina succession (Table 2). Quantitative diatom abundance analysis of Mertz-Ninnis Trough laminations reveals that although, in absolute terms, *P. glacialis* RS have a similar abundance in summer mixed diatom laminae as they do in *P. glacialis* RS sub-laminae (Table 3, Maddison et al., 2006), *P. glacialis* RS comprise 11.35% of the CRS-free assemblage in *P. glacialis* RS sub-laminae and only 2.29% in the summer mixed assemblage laminae (Table 3, Maddison et al., 2006). At this site, *T. antarctica* RS are absent from both the summer mixed diatom laminae and the *P. glacialis* RS sub-laminae (Table 3, Maddison et al., 2006). When a *P. glacialis* sub-lamina occurs within the annual sediment increment, the mean annual sediment thickness is 18% greater than if a sub-lamina does not occur (Table 2). BSEI analysis of a 0.28 m-long (17 year) sequence of early Neoglacial-age laminations from this site (NBP0101 KC10A; Table 1 and Figure 1) does not reveal any *T. antarctica* RS or *P. glacialis* RS sub-laminae (Maddison, 2006).

In Neoglacial laminated sediments from the more coastal Dumont d'Urville Trough core (MD03-2597), in 23 out of 26 years when *P. glacialis* RS sub-laminae occur, the sub-laminae appear in a late summer/autumn position (Table 2, Maddison, 2006), separated with a sharp contact from the overlying spring lamination. Quantitative diatom abundance analysis reveals that, in absolute terms, *P. glacialis* RS are more than 2.5 times as abundant in *P. glacialis* RS sub-laminae than they are in terrigenous-rich, summer mixed assemblage laminae. Further, *T. antarctica* RS are more than 2.5 times as abundant in *P. glacialis* RS sub-laminae than in terrigenous-rich, summer mixed assemblage laminae (Table 3, Maddison, 2006). When *P. glacialis* RS sub-laminae occur within the annual

sediment increment, the mean annual sediment thickness is 12% greater than if sub-laminae do not occur (Table 2).

3.2. Holocene records from Dumont d'Urville Trough and Svenner Channel

Holocene relative abundance of *T. antarctica* RS and *P. glacialis* RS from Dumont d'Urville Trough (MD03-2601) and Svenner Channel (NBP0101 JPC24) (Figure 1) are shown in Figure 3. In general, at both sites, relative abundances of *T. antarctica* RS are higher than *P. glacialis* RS. In the Dumont d'Urville Trough, the relative abundance of *T. antarctica* RS steadily rises to a peak at ~8.9 cal kyr BP (Figure 3B). Abundance then generally stays above 10% until ~3.4 cal kyr BP when it falls below 10% until ~2 cal kyr BP. Abundance then becomes very low (<5%) between 2 cal kyr BP until ~1.1 cal kyr BP, after which it recovers to about 10% at the top of the core. Relative abundance of *P. glacialis* RS displays an approximately inverse pattern. Abundance remains above 2% from ~10.8 cal kyr BP until ~8.7 cal kyr BP (Figure 3C), with a slight dip in abundance around 9.8 cal kyr BP. At 8.7 cal kyr BP, abundance falls abruptly below 2% until ~3.4 cal kyr BP, when it abruptly rises to above 2% until ~2.8 cal kyr BP when it falls below, and stays below, 2% until ~2 cal kyr BP. After 2.0 cal kyr BP, abundance rises to above 2% and then steadily falls towards the top of the core (~1 cal kyr BP).

In Svenner Channel, *T. antarctica* RS relative abundance rises from 11.2 cal kyr BP to a peak of >20% around 9.8 cal kyr BP (Figure 3E). Abundance dips below 20% around 9 cal kyr BP, rises to above 20% at ~8.7 cal kyr BP and then increases steadily to a peak at ~4.4 cal kyr BP. Relative abundance begins to decline and falls below 20% at ~3.4 cal kyr BP; it remains below 20% until the top of the core (~0.67 cal kyr BP). The relative abundance of *P. glacialis* RS remains below ~2% from 11.2 cal kyr BP until ~8.7 cal kyr BP when it begins to steadily rise (Figure 3F). At ~4.3 cal kyr BP, abundance rises above 2% and stays high until ~1 cal kyr BP when it falls below 2 % at the top of the core.

The relationship between *T. antarctica* RS and *P. glacialis* RS can be further investigated by looking at the ratio between the two diatoms, and also the statistical correlation between the two species curves. The ratio between *P. glacialis* RS and *T. antarctica* RS in Dumont d'Urville Trough is approaching 0.5 from the base of the core (~10.8 cal kyr BP) until ~10 cal kyr BP where it abruptly falls to very low values (Figure 3D). The ratio remains very low until ~3.4 cal kyr BP when it abruptly rises to >0.1 up to the top of the core (~1 cal kyr BP). Between ~2.8 cal kyr BP and ~2 cal kyr BP, the ratio falls, however, generally remains above 0.1. In Svenner Channel, the ratio between *P. glacialis* RS and *T. antarctica* RS remains generally <0.1 from ~11.2 cal kyr BP until ~4.3 cal kyr BP when it begins to rise (Figure 3G). The ratio reaches peak values (~0.5) at ~2.8 cal kyr BP and generally remains above 0.2 up to the top of the core (~0.7 cal kyr BP).

Figure 3

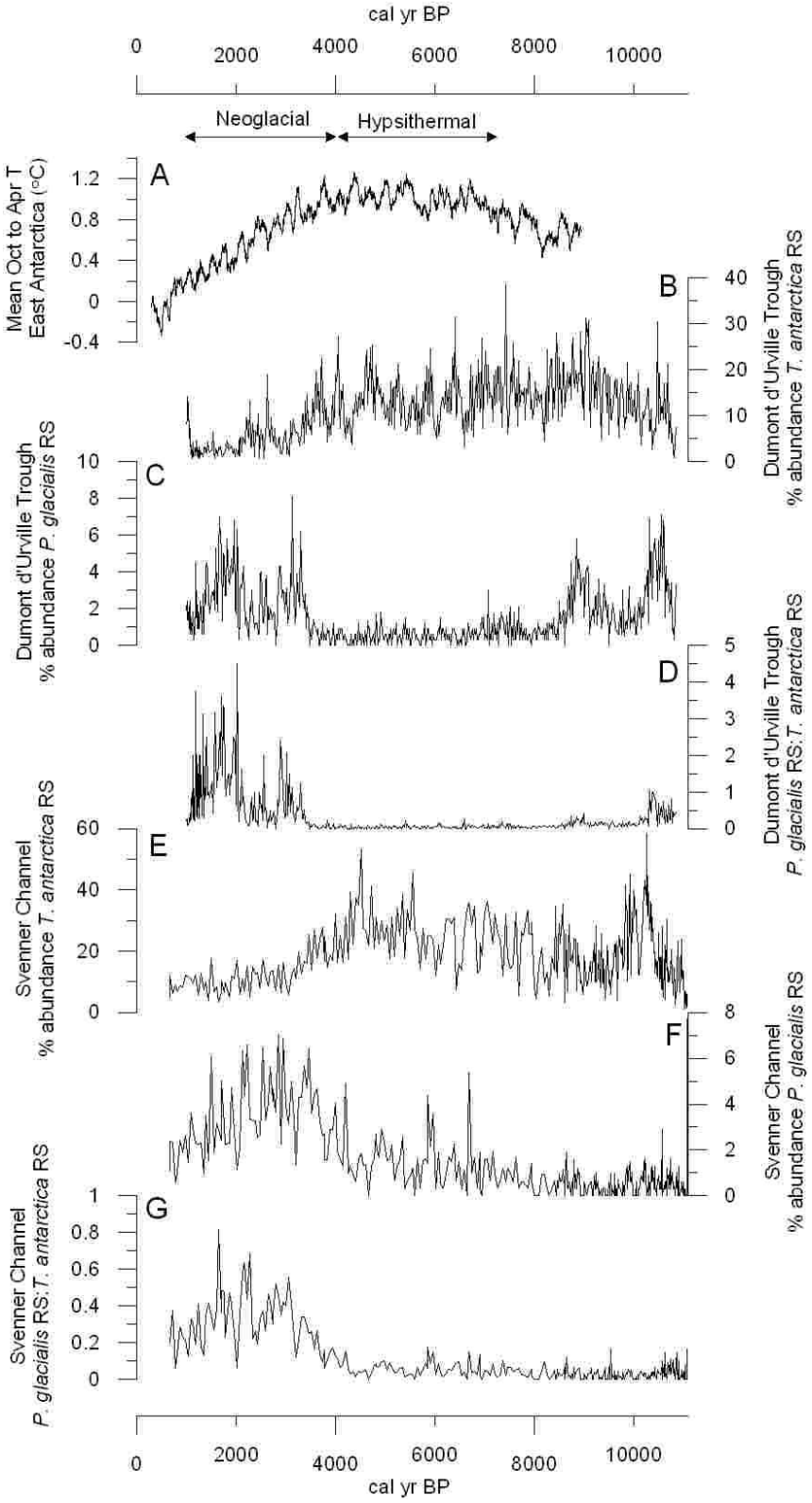

Figure 3: Holocene *Thalassiosira antarctica* and *Porosira glacialis* resting spore abundance from Dumont d'Urville Trough (MD03-2601) and Svenner Channel (NBP01-01 JPC24). **A.** Modelled mean summer (October to April) surface temperature (relative to the pre-industrial mean (1000-250 yr BP)) from Renssen et al. (2005). **B-D.** Dumont d'Urville Trough records. **B.** Relative abundance of *T. antarctica* RS. **C.** Relative abundance of *P. glacialis* RS. **D.** Ratio of *P. glacialis* RS:*T. antarctica* RS. **E-G.** Svenner Channel records. **E.** Relative abundance of *T. antarctica* RS. **F.** Relative abundance of *P. glacialis* RS. **G.** Ratio of *P. glacialis* RS:*T. antarctica* RS.

The Pearson correlation coefficient (r) between the relative abundance of *T. antarctica* RS and *P. glacialis* RS is -0.19 for the Dumont d'Urville record (n=528). This correlation coefficient appears weak, but a test of significance of r demonstrates that threshold for significant values of r for sample sizes of n=528, at the 99% significance level, is 0.14 (Lowry, 2008). There is no significant correlation between the relative abundances of *T. antarctica* RS and *P. glacialis* RS in the Svenner Channel record is negative, but not significant (r=-0.0004; n=348). However, the significant negative correlation between *T. antarctica* RS and *P. glacialis* RS for Dumont d'Urville Trough supports the qualitative observations of an inverse relationship between the two taxa.

The diatom relative abundance curves are also compared with the modelled mean October to April (i.e. austral summer) surface temperature record for the Holocene of East Antarctica (Renssen et al., 2005) (Figure 3A). The modelled surface temperature record reveals temperatures warming from ~0.4°C warmer than pre-industrial levels at 9.0 kyr BP, to temperatures ~1.0°C warmer than pre-industrial levels at ~4.3 kyr BP. Modelled temperatures then decline steadily until the end of the record, approximately 300 yr BP. The Pearson correlation between the relative abundance of *T. antarctica* RS and modelled mean summer temperature in Dumont d'Urville Trough and Svenner Channel is 0.44 and 0.64, respectively. The Pearson correlation between the relative abundance of *P. glacialis* RS and modelled mean summer temperature in Dumont d'Urville Trough and Svenner Channel is -0.48 and -0.11, respectively. The Pearson correlation between the modelled mean summer temperature and the ratio *P. glacialis* RS:*T. antarctica* RS is -0.55 for Dumont d'Urville Trough and -0.40 for Svenner Channel. All but one of these correlation coefficient values are above the threshold values of the Pearson's test of significance (r=-0.11 falls below the threshold). This highlights a positive correlation between the relative abundance of *T. antarctica* RS and modelled mean summer temperature; a negative correlation between relative abundance of *P. glacialis* RS and modelled mean summer temperature; and a more robust negative correlation between the ratio *P. glacialis* RS:*T. antarctica* RS and modelled mean summer temperature.

4. Interpretation and Discussion

4.1. Mechanism for formation of *T. antarctica* and *P. glacialis* resting spore sub-laminae

When sub-laminae characterised by *T. antarctica* RS or *P. glacialis* RS occur in the laminated sediments from the East Antarctic margin, three features are consistent: (1) one or the other species is dominant; (2) the sub-laminae predominantly occur in the same position within the seasonal sedimentary sequence – late summer to autumn; and (3) overall annual sediment thickness is greater when sub-laminae are present (in deglacial Iceberg Alley sediments, the sub-laminae are also associated with summer laminations that are thicker than average indicating increased summer production and flux to the

sediments). Hence (2) and (3) can be interpreted together as indicating that the sub-laminae are associated with years of higher diatom flux to the sediment. The occurrence of *T. antarctica* RS and *P. glacialis* RS sub-laminae (and thicker summer laminations) could indicate either a longer duration summer season of diatom productivity, promoting greater overall flux to the sediment, or enhanced summer conditions that favour higher *T. antarctica* and *P. glacialis* vegetative production, hence production and flux of the resting spores to the sediment in autumn.

Thalassiosira antarctica RS and *P. glacialis* RS sub-lamina production is likely to begin with a slow break up of sea ice over a sustained period in spring, i.e. slow increase of temperatures over a in spring leading to relatively high sea ice concentration when light levels increase sufficiently to promote phytoplankton growth. *Porosira glacialis* and *T. antarctica* have both been found associated with spring sea ice-rich regions (Krebs et al., 1987; Villareal and Fryxell, 1983). Relatively high spring sea ice concentrations would lead to summer production favouring sea ice-associated diatoms such as *T. antarctica* and *P. glacialis* (standing stocks enhanced by 'icy' spring) and both species are known to be abundant in Antarctic summer waters (Cremer et al., 2003; Sommer, 1991; Zielinski and Gersonde, 1997). Finally, sea ice formation in the autumn, accompanied by lowering SSTs, increased salinity and lowering light levels (Cunningham and Leventer, 1998; Doucette and Fryxell, 1985; Fryxell et al., 1987), would induce resting spore formation from a vegetative population that was sufficiently large to produce a sub-lamina in the sediments (Denis et al., 2006; Maddison et al., 2006; Stickley et al., 2005). Years without sub-laminae suggest more rapid melting and break-up of sea ice in spring favouring more marginal ice zone/open water species and reduced growth of *T. antarctica* and *P. glacialis* in the subsequent summer. Lower summer vegetative populations of *T. antarctica* and *P. glacialis* would not lead to the production of sufficient numbers of resting spores to produce a sub-lamina in autumn.

Key to confirming this sea ice-based model of sub-lamina formation are the two cores from Dumont d'Urville Trough which are geographically close to each other and would have experienced similar changes in external forcing (i.e. by insolation and greenhouse gases). At MD03-2601, during the Hypsithermal, *T. antarctica* RS sub-laminae were preserved (core MD03-2597 did not recover Hypsithermal-age sediments). In the Neoglacial, no sub-laminae of either species were preserved at site MD03-2601, although higher relative abundances of *P. glacialis* RS are observed (Figure 3C), whereas *P. glacialis* RS sub-laminae were preserved at MD03-2597 (Table 2). In the modern day, site MD03-2597 is covered by less than 65% sea ice concentration for, on average, 111 days of the year, whereas site MD-2601 is subject to less than 65% sea ice concentration for only 94 days of the year (difference between means is significant at >95%; mean values extracted from satellite-derived daily sea ice concentrations for 26 years between 1979 and 2006, National Snow and Ice Data Centre, http://nsidc.org/data/nsidc-0079.html). Site MD03-2597 becomes 'ice-free' (consistently less than 65% sea ice concentration), on average, 19 days earlier in

the spring than site MD03-2061 because the ice-edge not only retreats parallel with the coastline, but also retreats in a westward direction along the coast towards the Dumont d'Urville Trough as the Mertz Glacier Polynya opens to the ocean in summer. So, not only are there less ice-free days at MD03-2601, the sea ice retreats later. Hence, we would interpret the Neoglacial diatom sub-lamina occurrence pattern as indicating increasingly higher winter and spring sea ice concentrations in the Dumont d'Urville Trough region thus favouring the increased dominance of *P. glacialis* (relative to the Hypsithermal period), *P. glacialis* RS sub-lamina formation at site MD03-2597 and cessation of *T. antarctica* RS sub-lamina formation at MD-2601. Perhaps the environment became either too icy (given modern seasonal sea ice differences detailed above) or, more likely, had too short an ice-free summer season at site MD03-2601 during the Neoglacial for even *P. glacialis* to be able to form large enough populations to promote significant flux of resting spores to the sea floor and subsequent sub-laminae formation.

4.2. Environmental controls on the *P. glacialis* RS : *T. antarctica* RS ratio in Holocene sediments

From the lamination data, *T. antarctica* RS and *P. glacialis* RS sub-laminae are both interpreted as representing years with relatively high spring sea ice concentrations, however, what threshold under these conditions would govern changes in the relative abundance of the two species seen throughout the Holocene (Figure 3), given that they appear to have similar ecologies? Here we combine our sea ice-based mechanism of sub-lamina formation with published ecological preferences and modelled Holocene surface temperature and sea ice concentrations from the Adélie Land sector (Table 4, Figure 4) to present a model of the environmental conditions that alter the relative abundance of *T. antarctica* RS and *P. glacialis* RS in the sediments.

P. glacialis appears to prefer somewhat higher winter and spring sea ice concentrations than *T. antarctica*. Maximum abundances of *P. glacialis* RS in the sediment are found beneath regions subject to >7.5 months per year sea ice cover (*T. antarctica* prefers >6 months), <30% summer sea ice concentration (*T. antarctica* similar) and highly compacted winter sea ice (up to 85% concentration; *T. antarctica* prefers slightly less, but still >70%) (Armand et al., 2005). These ecological observations are supported by our Holocene records and comparisons with the modelled summer surface temperatures from East Antarctica (Renssen et al., 2005). Increased abundance of *T. antarctica* RS in the sediments from Dumont d'Urville Trough and Svenner Channel is positively correlated with modelled summer surface temperatures whereas increased abundance of *P. glacialis* RS is negatively correlated with modelled summer surface temperatures (Figure 3).

	Jan	Feb	Mar	Apr	May	Jun	Jul	Aug	Sep	Oct	Nov	Dec
Mean Hypsithermal SST (°C)	0.79	1.58	0.56	-0.94	-1.55	-1.62	-1.61	-1.61	-1.63	-1.65	-1.53	-0.63
Mean Neoglacial SST (°C)	0.68	1.59	0.63	-0.9	-1.54	-1.61	-1.61	-1.61	-1.63	-1.65	-1.58	-0.78
z value	2.79	-0.16	-2.11	-1.97	-2.05	-1.84	-0.18	0.55	0.22	-2.16	7.82	7.07
Significance level of difference between the mean SST	99%	none	95%	95%	95%	90%	none	none	none	95%	>99%	>99%
Mean Hypsithermal sea ice concentration (%)	0.29	0.25	0.33	0.53	0.8	0.88	0.88	0.87	0.83	0.76	0.58	0.41
Mean Neoglacial sea ice concentration (%)	0.28	0.24	0.3	0.5	0.79	0.88	0.89	0.88	0.85	0.77	0.59	0.41
z value	2.15	3.2	4.61	4.86	2.52	-0.53	-3.42	-3.72	-3.8	-2.76	-1.38	0.87
Significance of difference between the mean sea ice concentrations	95%	>99%	>99%	>99%	>98.5%	none	>99%	>99%	>99%	99%	none	none

Table 4: Summary of Adélie Land sector modelled Holocene surface temperature and sea ice concentrations for typical Hypsithermal (4000-4999 yr BP) and typical Neoglacial (1000-1999 yr BP) periods (extracted from Renssen et al., 2005). Surface temperatures and sea ice concentrations are given as anomalies from the pre-industrial mean (1000-250 yr BP).

The modelled sea ice concentration and surface temperature records for the Adélie Land sector suggest that the cool Neoglacial period had higher winter and early spring sea ice concentrations than the mid Holocene Hypsithermal (Table 4, Figure 4), with significantly lower late spring and early summer temperatures. In autumn, the Neoglacial had lower sea ice concentrations than the Hypsithermal with slightly higher temperatures. This model output supports the interpretation from ecological and seasonal sedimentological data that *P. glacialis* prefers slightly cooler and 'icier' winter and spring conditions than *T. antarctica*, which is why its abundance was enhanced during the Neoglacial off both Adélie Land and Princess Elizabeth Land. A subsequent long summer/autumn season, as suggested by the model data, would favour the build-up of larger populations of *P. glacialis* and concomitantly reduced populations of *T. antarctica*. Our interpretations are in agreement with those of Crosta et al. (2008) who state that seasonal sea ice distribution during the Holocene of East Antarctica is more complicated than a simple pattern of less sea ice during the warmer Hypsithermal, and more during the cooler Neoglacial.

Figure 4

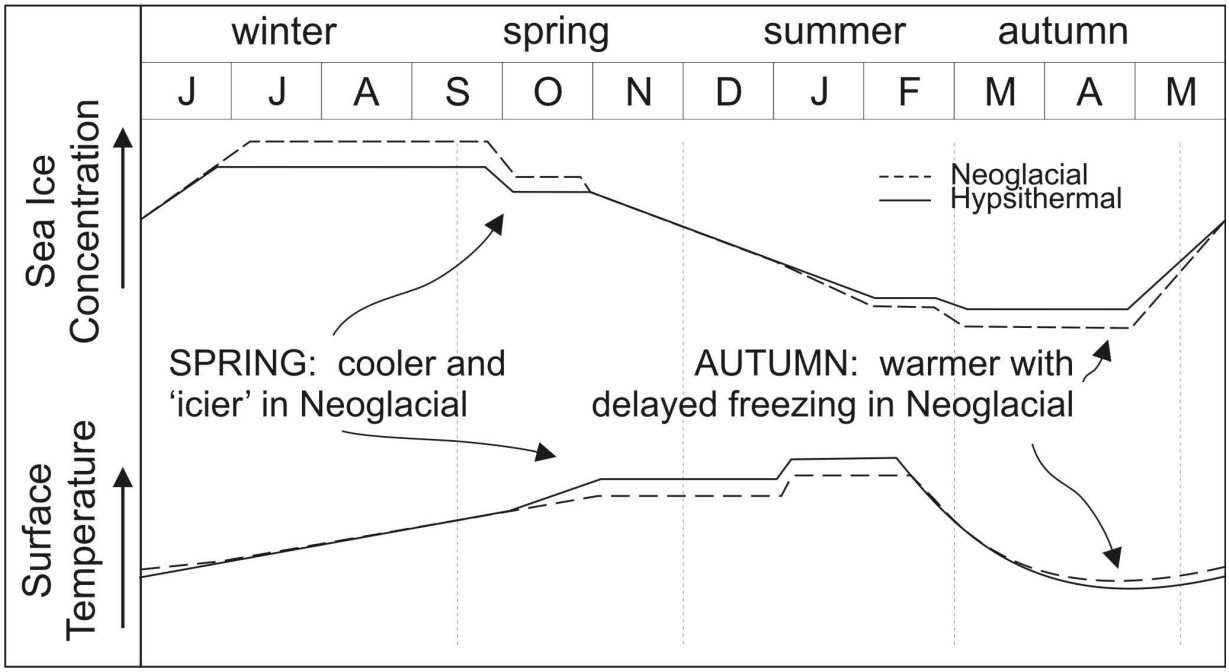

Figure 4: Schematic diagram illustrating differences modelled sea ice concentrations and surface temperatures between Hypsithermal and Neoglacial. Differences significant at the 99% confidence interval are shown with horizontal lines and differences at the 95% confidence interval are shown with horizontal curves. Where the Hypsithermal and Neoglacial lines overlap there is no statistically significant difference between the two records.

4.3. *P. glacialis* RS : *T. antarctica* RS – a new sediment proxy for winter and spring sea ice concentrations

The results from Dumont d'Urville Trough (MD03-2601) and Svenner Channel sediments presented here indicate that 0.1 appears to be a significant threshold value for the ratio *P. glacialis* RS:*T. antarctica* RS. An increase above 0.1 accompanies an important environmental change to increased winter sea ice concentration, cooler spring seasons with increased sea ice, and slightly warmer autumn seasons with less sea ice. In the Holocene sediments of coastal East Antarctica, the ratio changes from <0.1 to >0.1 between 4.3-3.4 cal kyr BP (i.e the transition from warmer Hypsithermal conditions to cooler, Neoglacial conditions, Crosta et al., 2007; Masson et al., 2000). However, it is possible to use the ecological information in an attempt to be more quantitative than this. Using the ecological preferences of *P. glacialis* and *T. antarctica* and it's distribution in modern core top samples (Armand et al., 2005), an increase in the sediment ratio above 0.1 (i.e. enhanced *P. glacialis* RS and/or relatively reduced *T. anatarctica* RS abundance) appears to indicate a change from ~7.5 months of annual sea ice cover (favouring *T. antarctica* production), to much greater than 7.5 months of annual sea ice cover (enhancing *P. glacialis* production), and an increase from ~70% winter sea ice concentration (favouring subsequent *T. antarctica* production) to highly compacted winter sea ice above 80% concentration (enhancing *P. glacialis* production). Although these may not seem like large changes, they appear to be key manifestations of the changes between warmer and cooler Holocene climate states as reflected in the diatom fossil record, and are in line with the changes suggested by previous diatom evidence for the Hypsithermal-Neoglacial transition (Crosta et al., 2008).

Attempts to apply the *P. glacialis* RS:*T. antarctica* RS proxy to west Antarctic Peninsula diatom records from Palmer Deep (Taylor and Sjunneskog, 2002) and Bransfield Strait (Heroy et al., 2008) have met with limited success because the relative warmth of the WAP compared to the East Antarctica margin limits the abundance of *P. glacialis* RS in the sediments to be almost always less than 10% of *T. antarctica* RS. However, a preliminary analysis of Holocene diatom abundance records from the cooler NW Weddell Sea has proved promising in that stratigraphic intervals when *P. glacialis* RS:*T. antarctica* RS was >0.1, interpreted as representing cool, sea ice-rich winter and spring conditions, are also intervals of high abundance of other sea ice-related diatoms such as *Fragilariopsis curta*, *F. cylindrus* and *Thalassiosira tumida* (Anna Hey, personal communication, 2008). This demonstrates the potential wider applicability of the *P. glacialis* RS:*T. antarctica* RS ratio around the Antarctic coast.

5. Conclusions

This synthesis of information on the abundance of *Thalassiosira antarctica* and *Porosira glacialis* has shown that these two diatoms have similar ecological preferences. The combination of modern phytoplankton analyses, laboratory experiments and late Quaternary laminated sediment records reveals that high fluxes of *T. antarctica* RS and *P. glacialis* RS to the sediment are associated with prior high winter and spring sea ice concentrations that promote the build-up of large vegetative cell populations. This is followed by late autumn, abrupt sea ice advance, accompanied by decreasing temperatures and irradiance and increased salinities that promote resting spore formation from high summer/autumn standing stocks. The investigation of two core records from the Dumont d'Urville Trough and one from Svenner Channel showed that despite their similar ecological preferences, there were interesting differences in the Holocene occurrence of the two taxa. Relative abundance of *T. antarctica* RS peaked during the warm mid-Holocene Hypsithermal period and declined into the cooler Neoglacial, whereas relative abundance of *P. glacialis* RS peaked during the late Holocene, cool Neoglacial period. Increased *P. glacialis* RS abundance appeared to be linked with higher winter and spring sea ice concentrations than *T. antarctica* RS. These conclusions are corroborated by a comparison with modelled Holocene sea ice concentrations and surface temperatures for the Adélie Land sector. The model output reveals higher winter and early spring sea ice concentrations, and lower spring and early summer temperatures during the Neoglacial relative to the Hypsithermal (which would promote increased populations of *P. glacilis*). Investigation of the ratio of relative abundance of the two diatoms, *P. glacialis* RS:*T. antarctica* RS, revealed that a threshold of 0.1 was important. The ratio abruptly increased from <0.1 to >0.1 at the Hypsithermal to Neoglacial transition. An increase in the ratio *P. glacialis* RS:*T. antarctica* RS to greater than 0.1 appears to indicate a change from ~7.5 months of annual sea ice cover to much greater than 7.5 months of cover, and an increase of winter sea ice concentrations from 70% to >80%. An attempt to apply the *P. glacialis* RS:*T. antarctica* RS ratio to other core sites from West Antarctica, in particular the NW Weddell Sea, shows that the relationship between these two diatom species may be able to reveal information about past winter and spring sea ice concentrations around the Antarctic margin.

Acknowledgements

This research was funded by Natural Environment Research Council (NERC) research grant NER/A/S/2001/01106 (JP), NERC postgraduate research studentship NER/A/2002/10350 (EJM at the School of Earth and Ocean Sciences, Cardiff University). XC was funded by the project TARDHOL through the national EVE-LEFE program (INSU-CNRS). This manuscript was developed during JP's stay at EPOC, funded by the Invited Professor Scheme of Bordeaux I University. The climate modelling work was supported by the Netherlands Organization for Scientific Research (HR). JP would like to thank Captain Joe Borkowski,

the Edison Chouest Offshore crew, the Raytheon Polar Services Company staff and scientific party aboard the RVIB *Nathaniel B. Palmer* during cruise NBP01-01, and the staff at the Antarctic Research Facility (Florida State University) for assistance with sampling. We (JP, CES, EJM, XC) particularly acknowledge discussion and encouragement over many stages of this research by Amy Leventer. XC personally thanks members of the Images X (CADO) cruise and from cruise NBP01-01 for providing data and suggestions. Logistical support for Images X (CADO) cruise was provided by IPEV-TAAF. JP would also like to thank Charlotte Sjunneskog for sharing west Antarctic Peninsula diatom data sets, and Ian Thomas for assistance in handling the NSIDC satellite daily sea ice concentration data set.

References

Aletsee, L. and Jahnke, J., 1992. Growth and productivity of the psychrophilic marine diatoms *Thalassiosira antarctica* Comber and *Nitzschia frigida* Grunow in batch cultures at temperatures below the freezing point of sea water. Polar Biology, 11: 643-647.

Allen, C.S., Pike, J., Pudsey, C.J. and Leventer, A., 2005. Submillennial variations in ocean conditions during deglaciation based on diatom assemblages from the southwest Atlantic. Paleoceanography, 20: PA2012, doi:10.1029/2004PA001055, pp 1-16.

Armand, L.K., 1997. The use of diatom transfer functions in estimating sea-surface temperature and sea-ice in cores from the southeast Indian Ocean. PhD Thesis, Australian National University, Canberra, Australia.

Armand, L.K., Crosta, X., Romero, O. and Pichon, J.-J., 2005. The biogeography of major diatom taxa in Southern Ocean sediments: 1. Sea ice related species. Palaeogeography, Palaeoclimatology, Palaeoecology, 223: 93-126.

Arrigo, K.R. and Van Dijken, G.L., 2003. Phytoplankton dynamics within 37 Antarctic coastal polynya systems. Journal of Geophysical Research - Oceans, 108(C8): 10.1029/2002JC001739.

Bárcena, M.A. et al., 1998. Record of Holocene glacial oscillations in Bransfield Basin as revealed by siliceous microfossil assemblages. Antarctic Science, 10: 269-285.

Bartsch, A., 1989. Die Eisalgenflora des Weddellmeeres (Antarktis): artenzusammensetzung und biomasse sowie Ökophysioliogie ausgewählter Arten. Berichte Polarforschung, 63: 259-294.

Brovkin, V. et al., 2002. Carbon cycle, vegetation and climate dynamics in the Holocene: experiments with the CLIMBER-2 model. Global Biogeochemical Cycles, 16: 1139, doi:10.1029/2001GB001662.

Buffen, A., Leventer, A., Rubin, A. and Hutchins, T., 2007. Diatom assemblages in surface sediments from the northwestern weddell Sea, Antarctic Peninsula. Marine Micropaleontology, 62: 7-30.

Cremer, H., Roberts, D., McMinn, A., Gore, D. and Melles, M., 2003. The Holocene diatom flora of marine bays in the Windmill Islands, East Antarctica. Botanica Marina, 46: 82-106.

Crosta, X., Crespin, J., Billy, I. and Ther, O., 2005. Major factors controlling Holocene $d^{13}C_{org}$ changes in a seasonal sea-ice environment, Adélie Land, East Antarctica. Global Biogeochemical Cycles, 19: GB4029, doi:10.1029/2004BG002426.

Crosta, X., Debret, M., Denis, D., Courty, M.A. and Ther, O., 2007. Holocene long- and short-term climate changes off Adélie Land, East Antarctica. Geochemistry, Geophysics, Geosystems, 8: doi:10.1029/2007GC001718, 1-15.

Crosta, X., Denis, D. and Ther, O., 2008. Sea ice seasonality during the Holocene, Adelie Land, East Antarctica. Marine Micropaleontology, 66: 222-232.

Cunningham, W.L. and Leventer, A., 1998. Diatom assemblages in surface sediments of the Ross Sea: relationship to present oceanographic conditions. Antarctic Science, 10: 134-146.

Denis, D. et al., 2006. Seasonal and subseasonal climate changes recorded in laminated diatom ooze sediments, Adélie Land, East Antarctica. The Holocene, 16: 1137-1148.

Doucette, G.J. and Fryxell, G.A., 1985. Thalassiosira antarctica (Bacillariophyceae): vegetative and resting stage ultrastructure of an ice-related marine diatom. Polar Biology, 4: 107-122.

Fryxell, G.A., Doucette, G.J. and Hubbard, G.F., 1981. The genus *Thalassiosira*: the bipolar diatom *T. antarctica* Comber. Botanica Marina, 24: 321-335.

Fryxell, G.A., Kang, S.-H. and Reap, M.E., 1987. AMERIEZ 1986: phytoplankton at the Weddell Sea ice edge. Antarctic Journal of the United States, 22: 173-175.

Fryxell, G.A. and Kendrick, G.A., 1988. Austral spring microalgae across the Weddell Sea ice edge; spatial relationships found along a northward transect during AMERIEZ 83. Deep-Sea Research Part A - Oceanographic Research Papers, 35: 1-20.

Gersonde, R. and Wefer, G., 1987. Sedimentation of biogenic siliceous particles in Antarctic waters from the Atlantic sector. Marine Micropaleontology, 11: 311-322.

Gleitz, M., Bartsch, A., Dieckmann, G.S. and Eicken, H., 1998. Composition and succession of sea ice diatom assemblages in the eastern and southern Weddell Sea, Antarctica. In: M.P. Lizotte and K.R. Arrigo (Editors), Antarctic sea ice biological processes, interactions, and variability. Antarctic Research Series. American Geophysical Union, Washington, D.C., pp. 107-120.

Gleitz, M., Grossmann, S., Scharek, R. and Smetacek, V., 1996. Ecology of diatom and bacterial assemblages in water associated with melting summer sea ice in the Weddell Sea, Antarctica. Antarctic Science, 8: 135-146.

Goosse, H. and Fichefet, T., 1999. Importance of ice-ocean interactions for the global ocean circulation: a model study. Journal of Geophysical Research - Oceans, 104: 23337-23355.

Hasle, G.R., 1973. Some marine plankton genera of the diatom family Thalassiosiraceae. Beiheft zur Nova Hedwigia, 45: 1-68.

Hasle, G.R. and Heimdal, B.R., 1968. Morphology and distribution of the marine centric diatom *Thalassiosira antarctica* Comber Journal of the Royal Microscopical Society, 88: 357-369.

Hemer, M.A. and Harris, P.T., 2003. Sediment core from beneath the Amery Ice Shelf, East Antarctica, suggests mid-Holocene ice-shelf retreat. Geology, 31: 127-130.

Heroy, D.C., Sjunneskog, C. and Anderson, J.B., 2008. Holocene climate change in the bransfield Basin, Antarctic Peninsula: evidence from sediment and diatom analysis. Antarctic Science, 20: 69-87.

Krebs, W.N., Lipps, J.H. and Burckle, L.H., 1987. Ice diatom floras, Arthur Harbor, Antarctica. Polar Biology, 7: 163-171.

Leventer, A., 1991. Sediment trap diatom assemblages from the northern Antarctic Peninsula region. Deep-Sea Research, 38: 1127-1143.

Leventer, A. et al., 2006. Marine sediment record from the East Antarctic margin reveals reveals dynamics of ice sheet recession. GSA Today, 16(12): doi:10.1130/GSAT01612A.1.

Leventer, A. et al., 1996. Productivity cycles of 200-300 years in the Antarctic Peninsula region: Understanding linkages among the sun, atmosphere, oceans, sea ice, and biota. Geological Society of America Bulletin, 108: 1626-1644.

Leventer, A. and Dunbar, R., 1987. Diatom Flux in Mcmurdo Sound, Antarctica. Marine Micropaleontology, 12: 49-64.

Lowry, R., 2008. Concepts and Applications of Inferential Statistics. http://faculty.vassar.edu/lowry/webtext.html (accessed 18th September 2008).

Maddison, E.J., 2006. Seasonally Laminated Late Quaternary Antarctic Sediments. Cardiff University, unpublished PhD thesis.

Maddison, E.J., Pike, J., Leventer, A. and Domack, E.W., 2005. Deglacial seasonal and sub-seasonal diatom record from Palmer Deep, Antarctica. Journal of Quaternary Science, 20: 435-446.

Maddison, E.J. et al., 2006. Post-glacial seasonal diatom record of the Mertz Glacier Polynya, East Antarctica. Marine Micropaleontology, 60: 66-88.

Masson, V. et al., 2000. Holocene climate variability in Antarctica based on 11 ice-core isotopic records. Quaternary Research, 54(3): 348-358.

Opsteegh, J.D., Haarsma, R.J., Selten, F.M. and Kattenberg, A., 1998. ECBILT: a dynamic alternative to mixed boundary conditions in ocean models. Tellus, 50A: 348-367.

Palmisano, A.C. and Sullivan, C.W., 1982. Physiology of sea ice diatoms. 1. Response of three polar diatoms to a simulated summer-winter transition. Journal of Phycology, 18: 489-498.

Pearce, R.B. et al., 1998. A lamina-scale SEM-based study of a late Quaternary diatom-ooze sapropel from the Mediterranean Ridge, ODP Site 971. In: K.-C. Emeis, A.H.F. Robertson, C. Richter and et-al. (Editors), Proceedings of ODP, Scientific Results, 160. College Station, TX (Ocean Drilling Program), pp. 333-348.

Peters, E. and Thomas, D.N., 1996a. Prolonged darkness and diatom mortality. I: Marine Antarctic species. Journal of Experimental Marine Biology and Ecology, 207: 25-41.

Peters, E. and Thomas, D.N., 1996b. Prolonged nitrate exhaustion and diatom mortality: a comparison of polar and temperate *Thalassiosira* species. Journal of Plankton Research, 18: 953-968.

Pike, J. and Kemp, A.E.S., 1996. Preparation and analysis techniques for studies of laminated sediments. In: A.E.S. Kemp (Editor), Palaeoclimatology and Palaeoceanography from Laminated Sediments. Geological Society of London, Special Publication 116, pp. 37-48.

Renssen, H., Goosse, H., Fichefet, T., Masson-Delmotte, V. and Koç, N., 2005. Holocene climate evolution in the high-latitude Southern Hemisphere simulated by a coupled atmosphere-sea ice-ocean-vegetation model. The Holocene, 15: 951-964.

Schweitzer, P.N., 1995. Monthly averaged polar sea ice concentration. U. S. Geological Survey Digital Data Series.

Scott, P., McMinn, A. and Hosie, G., 1994. Physical Parameters Influencing Diatom Community Structure in Eastern Antarctic Sea-Ice. Polar Biology, 14: 507-517.

Smetacek, V. et al., 1992. Early spring phytoplankton blooms in ice platelet layers of the southern Weddell Sea, Antarctica. Deep-Sea Research Part A - Oceanographic Research Series, 39: 153-168.

Smith, A.E. and Morris, I., 1980. Pathways of carbon assimilation in phytoplankton from the Antarctic Ocean. Limnology and Oceanography, 25: 865-872.

Sommer, U., 1991. Comparative nutrient status and competitive interactions of two Antarctic diatoms (*Corethron criophilum* and *Thalassiosira antarctica*). Journal of Plankton Research, 13: 61-75.

Stickley, C.E. et al., 2005. Deglacial ocean and climate seasonality in laminated diatom sediments, Mac.Robertson Shelf, Antarctica. Palaeogeography, Palaeoclimatology, Palaeoecology, 227: 290-310.

Taylor, F. and Leventer, A., 2003. Late Quaternary palaeoenvironments in Prydz Bay, East Antarctica: interpretations from marine diatoms. Antarctic Science, 15: 512-521.

Taylor, F. and McMinn, A., 2001. Evidence from diatoms for Holocene climate fluctuation along the East Antarctic margin. Holocene, 11(4): 455-466.

Taylor, F. and McMinn, A., 2002. Late Quaternary diatom assemblages from Prydz Bay, eastern Antarctica. Quaternary Research, 57: 151-161.

Taylor, F., McMinn, A. and Franklin, D., 1997. Distribution of diatoms in surface sediments of Prydz Bay, Antarctica. Marine Micropaleontology, 32: 209-229.

Taylor, F. and Sjunneskog, C., 2002. Postglacial marine diatom record of the Palmer Deep, Antarctic Peninsula (ODP Leg 178, Site 1089), 2, diatom assemblages. Paleoceanography, 17: DOI 10.1029/2000PA000564.

Villareal, T.A. and Fryxell, G.A., 1983. Temperature effects on the valve structure of the polar diatoms *Thalassiosira antarctica* and *Porosira glacialis*. Polar Biology, 2: 163-169.

Watanabe, K., 1988. Sub-ice microalgal strands in the Antarctic coastal fast ice area near Syowa Station. Japanese Journal of Phycology, 36: 221-229.

Zielinski, U. and Gersonde, R., 1997. Diatom distribution in Southern Ocean surface sediments (Atlantic sector): Implications for paleoenvironmental reconstructions. Palaeogeography, Palaeoclimatology, Palaeoecology, 129: 213-250.

Résumé :
L'Holocène a été marqué par une variabilité plurimillénaire, ponctuée par une variabilité millénaire rapide. L'étude d'enregistrements à forts taux de sédimentation couplée à une approche multi-proxy s'avère indispensable pour comprendre la dynamique de la machine climatique au cours de l'Holocène à travers tous ses compartiments climatiques: cryosphère, océan, banquise, atmosphère et biosphère. Nous avons appliqué ce type d'approche multi-échelle et multi-proxy à deux enregistrements marins de la marge continentale Est Antarctique afin d'appréhender les variations climatiques d'une échelle plurimillénaire à séculaire au cours de l'Holocène dans l'environnent singulier de la zone marginale des glaces. Cette étude a permis de caractériser la réponse des différents compartiments climatiques en Antarctique aux variations d'ordre plurimillénaire à millénaire et de documenter la cohérence spatiale de ces changements à l'échelle de l'Antarctique grâce à une comparaison modèle-donnée. Cette approche a permis de souligner les forçages climatiques intervenant à l'échelle du forçage orbital et de documenter les connections inter sous-systèmes climatiques, mettant en lumière le rôle clé de la banquise. A l'échelle sub-Milankovitch, les compartiments climatiques affichent aussi des réponses synchrones mais les facteurs forçant restent à éclaircir.

Mot-clés : Paléoclimatologie, Holocène, Antarctique, Océan Austral, marqueurs sédimentologiques, paléontologiques, radio-isotopiques et biogéochimiques.

Abstract:
The present Holocene interglacial period was affected by long-term and rapid millennial short-term climatic changes. Multi-proxy high-resolution studies are crucial to better understand the climatic system via all the sub-systems involved: crysophere, ocean, sea ice, atmosphere, and biosphere. A multi-scale and multi-proxy approach on two high resolution marine sediment cores off East Antarctica allowed us to provide accurate reconstructions of Milankovitch and sub-Milankovitch climatic variability of the sea ice zone. We characterized the response of climatic sub-systems to long- and short-term climatic changes and documented the spatial coherence of these changes over Antarctic thanks to coupled model-data comparison. This study highlights the forcing factors involved at Milankovitch timescales, the relationships linking the different climatic components and particularly the key role played by sea ice in the Earth climate. Forcing factors acting at the sub-Milankovitch timescales are less clear although sub-systems components display synchronous response.

Key-words: Paleoclimatology, Holocene, Antarctic, Southern Ocean, sedimentological, paleontological, radio-isotopic and biogeochemical tracers.

~2008~